University of Alberta

Rehabilitation and Repair of Reinforced Concrete Short Columns with External Steel Collars

by

Jianhua Liu ©

A thesis submitted to the Faculty of Graduate Studies and Research

in partial fulfillment of the requirements for the degree of Doctor of Philosophy

in

Structural Engineering

Department of Civil and Environmental Engineering

Edmonton, Alberta, Canada

Fall 2008

Your file Votre référence
ISBN: 978-0-494-46364-2
Our file Notre référence
ISBN: 978-0-494-46364-2

ABSTRACT

A rehabilitation and repair technique with external steel collars was investigated for reinforced concrete short columns through experiment and finite element analysis.

Ten cantilever short columns, including two control columns without steel collars and eight rehabilitated columns confined externally by steel collars, have been constructed and tested under combined axial and lateral loading. Parameters considered in the experimental program include collar spacing, collar stiffness, longitudinal reinforcement ratio, axial compression index, pretension of collar bolts, and shear span-to-depth ratio. One control column was tested to failure and then repaired to study the feasibility of using external steel collars on previously damaged columns. The experimental results have shown excellent improvements in the ductility, strength, and energy dissipation capacity of the columns due to the presence of the collars. Three-dimensional finite element models were developed using the finite element program ABAQUS Explicit to further investigate the behaviour of these externally confined columns. Experimental results and finite element analysis have shown that this rehabilitation technique has great promise as an effective procedure for rehabilitation of deficient reinforced concrete short columns.

Research was also conducted with other existing analytical approaches and an improved sectional strength model was proposed for reinforced concrete columns with external steel collars. Finally, design guidelines were proposed for the rehabilitation of reinforced concrete columns along with design examples to illustrate the design guidelines.

ACKNOWLEDGEMENTS

I would like to express my utmost and sincere gratitude to my research advisors—Professors Robert G. Driver and Adam S. Lubell, for their warm guidance, patience, support, detailed and constructive comments, and encouragement throughout the research. I can not imagine better advisors and mentors for my Ph.D. Thanks are also extended to my dissertation committee, Profs. Robert Loov (University of Calgary), Jozef Szymanski, and Peter Schiavone for their valuable suggestions and advice. Some of their comments on my thesis will motivate me for further exploration in the field of structural rehabilitation.

The helpful discussions with Professors Gilbert Grondin, Roger Cheng, Alaa Elwi, Mohamed Al-Hussein, Vivek Bindiganavile, and Dongyang Li are gratefully acknowledged. The technical assistance of the staff of the I. F. Morrison Structural Engineering Laboratory, Larry Burden and Richard Helfrich, during the experimental part of this research was invaluable. The author is also thankful to the numerous graduate students who provided assistance in one way or others. Especially Ian MacPhedran, Zhangcheng Hao, Zoulong Chou, Xiaoyan Deng, Ming Jin, Armin Erfanian, Munawar Hussain, Mahbuba Begum, Anjan Bhowmick, Minyoung Kim, Vincent Guo, Honglan Miao, Xia Jin, Hua Jing, Dong Liu, Jianmin Zhang, Brent Prickett, Jonah Shishkin, James Chapman, Mohammad Behbahanifard, Jiang Shao, Georg Josi, Ved Sharma, Bing Song and Peter Song.

I also want to express my gratitude to the staff in the Civil & Environmental Engineering Department at University of Alberta. They offered me tremendous help during my graduate study, especially Dale Lathe, Anne Jones, Anita Mueller, Lorraine Grahn, and Peter Altobelli.

Heartful thanks also given to many friends I met in Edmonton for their unselfish help and constant parental encouragement, David and Kathy Gottlob, Bob and Wilma Korthuis, William and Olive Brandenbarg, and Trudy Schatz.

Last but not least, I want to extend my deepest gratitude to my family especially to my wife—Yi Yang and my parents, for their love, unlimited patience, encouragement and constant support.

TABLE OF CONTENTS

LIST OF TABLES

LIST OF FIGURES

LIST OF ABBREVIATIONS AND NOTATIONS

Abbreviations

ACI	American Concrete Institute
ASCE	American Society of Civil Engineers
ASTM	American Society for Testing and Materials
C. O. V.	Coefficient of Variation
CSA	Canadian Standards Association
CV	Column identifier
FEA	Finite Element Analysis
FRP	Fibre Reinforced Polymer
HSS	Hollow Structural Sections
kg	kilogram
kN	kiloNewton
LVDTs	Linear Variable Displacement Transformers
mm	millimetre
MCFT	Modified Compression Field Theory
MPa	MegaPascal

Notations

A_e	Effective shear resisting area, typically taken as 80% A_g
A_{ef}	Effective cross-sectional area of external FRP

A_g	The gross cross-sectional area of the column
A_h	Cross-sectional area of hoop or spiral reinforcement
A_{ps}	Cross-sectional area of the external presstressing strand/wire
A_s	Total longitudinal reinforcement area
A_{sc}	Cross-sectional area of steel collar
A_{sh}	Total cross-sectional area of transverse reinforcement (including crossties) within spacing s
A_t	Total tensile longitudinal reinforcement area
A_v	Total cross-sectional area of transverse steel at section within spacing s
a	Depth of concrete compression zone
a_g	Maximum aggregate size
B_j	Short principal diameter of elliptical jacket
b	Width of rectangular cross section
b_w	Effective concrete web width
C	A coefficient related to the elastic bending moment of the collar
c_1	Factor in calculation of concrete compressive stress in Chapter 5
c_2	Factor in calculation of concrete compressive stress in Chapter 5
c_3	Factor in calculation of concrete compressive stress in Chapter 5
D	Overall section depth or gross diameter for circular column
D'	Distance between centers of peripheral hoop for the confined core

D_j	The outside diameter of the circular jacket, or long principal diameter of elliptical jacket
d	Distance from the extreme compression fibre to the centroid of the longitudinal tension reinforcement
d_f	Depth of FRP in the direction of load
d_{sc}	Effective shear depth for steel collar
d_v	Effective shear depth
$d\varepsilon_v^{\ p}$	Plastic volumetric strain rate
$d\gamma^p$	Plastic deviatoric strain rate
E_c	Secant modulus of elasticity of concrete
E_{co}	Initial concrete tangent modulus
E_{FD}	The energy absorbed by frictional dissipation
E_I	Internal energy including both elastic and plastic strain energy
E_j	The modulus of elasticity of jacket
E_{KE}	The kinetic energy
E_s	Modulus of elasticity of steel
E_{sc}	Secant modulus of external steel collar calculated from collar pressure and lateral strain
E_{total}	Total energy in the system
E_V	The energy absorbed by viscous dissipation
E_W	The energy of external forces

F_p Pretension applied to the each collar bolt

F_i The axial tensile force in the collar during i th stage of the plastic analysis

F_y The axial yield force of the collar element at the location where the next hinge will form during a specific analysis stage

f_c Stress of unconfined concrete at strain ε

$f_c^{'}$ Specified compressive strength of concrete based on standard cylinders

$f_c^{''}$ Peak compressive stress of the Todeschini curve

f_{cc} Stress of confined concrete at strain ε_{cc}

$f_{cc}^{'}$ Peak stress of the confined concrete of the columns

$f_{ccsg}^{'}$ Peak stress of the confined concrete of the columns consideration of strain gradient effects within the cross-section

$f_{co}^{'}$ Strength of the unconfined concrete

f_{esc} Effective stress of external steel collars

f_j Yield strength of external jacket

f_{je} Effective strength of external jacket

$f_l^{'}$ The effective lateral confining pressure

f_{pi} Initial stress in the external presstressing strand/wire

f_{py} Yield strength of the external presstressing strand/wire

f_{sh} Stress of the transverse reinforcement

$f_t^{'}$ Tensile strength of concrete, taken as $f_t^{'} = 0.1 f_c^{'}$ for normal strength concrete

f_u Ultimate strength of steel

f_y Yield strength of steel or shear reinforcement

f_{yh} Specified yield strength of the transverse reinforcement

f_{yj} Yield strength of external steel jacket

f_{ysc} Yield strength of external steel collar

G_F Fracture energy of concrete

H Height of column subjected to double curvature, equals to twice the height for column in single curvature

H_1 Distance to the point of application of lateral from the base of the column

H_2 Distance to the point of application of vertical load from the column base

H_3 Distance between two pin connections of the vertical loading assembly

h Section depth of the column in the direction of shear force

h_c Cross-sectional dimension of the column core

h_x Spacing of longitudinal reinforcement in the cross-section

I_{sc} Moment of inertia of external steel collar

K Confinement efficiency factor

K_{dist} Confinement distribution effectiveness factor related to the spacing and thickness of collars along the longitudinal axis of column

K_{eff} Confinement effectiveness factor related to the amount of confined core cross-section due to the concrete spalling

K_{sg} Confinement effectiveness factor related to the strain gradient effect at the cross-section

K_y Elastic secant stiffness at first yield of the specimen

k Factor to calculate shear strength contribution from concrete considering ductility level

k_1 Empirical constant used in confinement concrete model proposed by Triantafillou *et al.* (2006)

k_2 Empirical constant used in confinement concrete model proposed by Triantafillou *et al.* (2006)

k_n Factor to calculate minimum shear reinforcement in CSA/A23.3-04

k_p Factor to calculate minimum shear reinforcement in CSA/A23.3-04

M Applied moment at the column section

M_f Factored moment

M_i The bending moment in the collar during i th stage of plastic analysis

M_p The plastic bending moment of the collar element at the location where the next hinge will form during a specific analysis stage

M_m Modified moment at the critical section

$M_{\max,esa}$ Maximum moment from equivalent rectangular stress block sectional analysis

$M_{\max,\exp}$	Average maximum moment from experiment in the push and pull directions
$M_{\max,lsa}$	Maximum moment from layered sectional analysis
M_u	Factored moment at the critical section
n_l	Number of longitudinal bars that are laterally supported by the corner of hoops or by hooks of seismic crossties
P	Axial compressive load applied to the column
P_f	Factored axial load applied to the column
P_0	Theoretical nominal axial capacity of the column without eccentricity
$P_{\max,esa}$	Maximum axial load from equivalent rectangular stress block sectional analysis
$P_{\max,lsa}$	Maximum axial load from layered sectional analysis
P_u	Factored axial compressive load applied to the column
R	Horizontal force applied to the column
R_d	The ductility-related force reduction factor for base shear
r	Ratio between the rotation induced displacement and the total displacement of the column in the experiment
r_c	Radius at the corners of rectangular section
s	Centre-to-centre spacing of transverse reinforcement
s_1	FRP anchor spacing in x direction
s_2	FRP anchor spacing in y direction

s'	Clear spacing between steel collars
s_p	Centre-to-centre spacing of external prestressing strand/wire
s_{sc}	Centre-to-centre spacing of steel collars
s_x	Spacing requirement in CSA/A23.3-04 for the transverse reinforcement
s_z	Crack spacing parameters
s_{ze}	Equivalent crack spacing parameters
t	The thickness of steel collar parallel to column longitudinal axis
t_f	Thickness of FRP
t_j	Thickness of external jackets
u_1	Elongation of the longitudinal bars in the footing
u_2	Elongation of the longitudinal bars in the footing
V	Shear force at the column section
V_1	Load level for the first five cycles in the experimental program
V_c	Shear strength contribution from concrete
V_{cf}	Final concrete shear strength contribution at high displacement ductility
V_{ci}	Initial concrete shear strength contribution at low displacement ductility
V_{df}	Final shear strength for high displacement ductility
$V_{esa,flexure}$	Lateral force corresponding to flexural strength from equivalent rectangular stress block sectional analysis
$V_{esa,shear}$	Shear strength from equivalent rectangular stress block sectional analysis
V_f	Factored shear demand

V_i Initial shear strength for low displacement ductility

V_j Shear strength contribution from external jackets

$V_{lsa,flexure}$ Lateral force corresponding to flexural strength from layered sectional analysis

$V_{lsa,shear}$ Shear strength from layered sectional analysis

$V_{\max}$ Peak lateral force

$V_{\max,aci}$ Peak lateral force from ACI318-05

$V_{\max,csa}$ Peak lateral force from CSA/A23.3-04

$V_{\max,esa}$ Maximum lateral force from equivalent rectangular stress block sectional analysis, which is taken as the smaller value of $V_{esa,flexure}$ and $V_{esa,shear}$

$V_{\max,\exp}$ Average peak lateral force from experiment in the push and pull directions

$V_{\max,\exp,push}$ Peak lateral force from experiment in the push direction

$V_{\max,fea}$ Peak lateral force from finite element analysis

$V_{\max,lsa}$ Maximum lateral force from layered sectional analysis, which is taken as the smaller value of $V_{lsa,flexure}$ and $V_{lsa,shear}$

$V_{\max,response}$ Peak lateral force from Response 2000 program

$V_{\max,mc}$ Peak lateral force from moment-curvature sectional flexural analysis

$V_{\max,stm}$ Peak lateral force from strut-and-tie model

$V_{\max n}$ The normalized shear strength

V_n Nominal shear strength

V_p	Shear strength contribution from axial compressive load
V_{pc}	Shear strength enhancement in concrete induced by external prestressing strand/wire
V_{pr}	Shear strength contribution from external prestressing strand/wire
V_{ps}	Shear strength enhancement in shear reinforcement induced by external prestressing strand/wire
V_r	Factored shear strength
V_s	Shear strength contribution from shear reinforcement
V_{sc}	Shear strength contribution from external steel collar
V_{sf}	Final shear strength contribution from internal shear reinforcement at high displacement ductility
V_{si}	Initial shear strength contribution from internal shear reinforcement at low displacement ductility
V_{sj}	Shear strength contribution from external steel jacket
V_y	Estimated shear force corresponding to the first yield of the longitudinal bars ignoring influence of collars
V_u	Factored shear force at the critical section
w	The thickness of steel collar perpendicular to column longitudinal axis
w_c	Crack width
w_{ccr}	Critical crack width
w_i'	The i th clear distance between adjacent longitudinal bars

α	Inclination angle of vertical loading assembly
α_1	Ratio of average stress in rectangular compression block to the specified concrete strength
β	Factor accounting for the shear resistance of cracked concrete used in CSA/A23.3-04
β_1	A coefficient to calculate the depth of equivalent rectangular stress block, ratio of the depth of the equivalent stress block to the depth of the neutral axis
γ	Equivalent viscous damping ratio
γ_c	Density of concrete
Δ	Total displacement at the horizontal loading position
Δ_1	Lateral displacement at the vertical loading position
Δ_2	Lateral displacement at the horizontal loading position
Δ_{axial}	Collar deflection due to axial elongation of the adjacent sides
Δ_{bend}	Collar deflection from bending
Δ_i	Total collar deflection up to the i th stage of plastic analysis
Δ_{max}	Maximum displacement at each displacement-control loading level
Δ_n	Collar deflection at the n th stage of plastic analysis
$\Delta_{n\,total}$	Total collar deflection up to the n th stage of plastic analysis
Δ_u	Ultimate displacement
Δ_R	Rotation induced displacement

Δ_y	Average yield displacement in the push and pull directions
Δ_{yc}	Control yield displacement in conducting the test
Δ_{yt}	Modified average test yield displacement in the push and pull directions
Δ_{yt+}	Modified test yield displacement in the push direction
Δ_{yt-}	Modified test yield displacement in the pull direction
Δ_t^*	Modified average test displacement in the first cycle
Δ_{t+}^*	Modified test displacement in the first cycle in push direction
Δ_{t-}^*	Modified test displacement in the first cycle in pull direction
Δ_{c+}^*	Control displacement in the first cycle in push direction in conducting test
Δ_{c-}^*	Control displacement in the first cycle in pull direction in conducting test
Δ_c^*	Average control displacement in the first cycle in conducting test
ε	Strain of concrete
ε_0	Average longitudinal strain of concrete cylinders at peak stress
ε_c'	Strain corresponding to the peak concrete compressive stress
ε_{fe}	The effective strain in FRP jacket
ε_{cc}	Strain of the confined concrete
ε_{cc}'	Strain at peak stress of confined concrete
ε_{co}'	Strain at peak stress of unconfined concrete
ε_{cu}	Ultimate concrete compressive strain
ε_{esc}	Effective axial strain of the external steel collar

ε_{lat}	Lateral strain of the external collar
$\varepsilon_{lat\,n}$	The average lateral strain at the end of i th stage of plastic analysis
ε_{nom}	Engineering (nominal) strain in ABAQUS modeling
ε_{true}	True strain in ABAQUS modeling, calculated from $\varepsilon_{true} = \ln(1+\varepsilon_{nom})$
ε_u	Strain of steel at ultimate stress
ε_x	Longitudinal strain of at the mid-height of the cross-section
η	Factor in calculation of concrete compressive stress in Chapter 5
θ	Angle of diagonal crack in concrete column measured from the longitudinal axis of column; the direction of the average principal compression with respect to the longitudinal axis
θ_R	Rotation angle of at the interface between the column and footing in the experiment
μ	Displacement ductility
μ_c	Control displacement ductility used in conducting the test
ξ	Reduction factor for effective compressive strength of the diagonal compression strut that accounts for the influence of flexural ductility
ρ	Longitudinal reinforcement ratio, calculated from $\rho = A_s / A_g$
ρ_{eff}	The effective transformed content of FRP into equivalent steel content
ρ_w	Tensile longitudinal reinforcement ratio, calculated from $\rho_w = A_t / A_g$
ρ_v	Volumetric ratio of spiral steel to core concrete
σ	Stress of concrete or steel

σ_{active}	Active confining pressure
σ_h	The equivalent uniform confining pressure
σ_{lu}	The confining pressure at failure
$\sigma_{\max}$	Maximum confining pressure can be developed by the collar
σ_n	The incremental (additional) collar pressure during n th stage of the plastic analysis
σ_{nom}	Engineering (nominal) stress in ABAQUS modeling
$\sigma_{passive}$	Passive confining pressure
σ_{total}	Total confining pressure
σ'_{total}	Total equivalent confining pressure
σ_{true}	True stress in ABAQUS modeling, calculated from $\sigma_{true} = \sigma_{nom}(1+\varepsilon_{nom})$
ν_c	Poisson's ratio of concrete at a given level of axial strain
ν_{co}	Initial Poisson's ratio of concrete
ϕ	Angle of the fibre reinforced polymer ply or internal friction angle of concrete; material strength reduction factor to calculate factored strength
ϕ_c	Concrete material strength reduction factor
ϕ_p	Reduction factor for the shear contribution from axial compressive load
ϕ_s	Steel material strength reduction factor
ψ	Dilation angle of concrete
ψ'	Factor in calculating shear strength contribution of shear reinforcement

CHAPTER 1 INTRODUCTION

1.1 Introduction

In most parts of the world, the building stock and the civil infrastructure are aging and in constant need of maintenance, repair and upgrading. Moreover, much of our building infrastructure was constructed prior to significant advances in earthquake engineering. With the development of the knowledge about seismic action and re-zoning of seismic activity, many reinforced concrete structures built before the 1970s in regions of high seismic risk are in need of upgrading. The design codes used at that time did not fully account for the seismic load effect and did not contain stringent detailing requirements to ensure ductile behaviour, which is critical to prevent structural collapse under sustained seismic loading. As a result, many structures in regions of high and moderate seismicity have been rendered "seismically deficient" by modern standards and are therefore in urgent need of rehabilitation. In these regions, the major part of the seismic threat to human life and property comes from those old existing structures. Situations unrelated to seismic performance, such as deterioration and damage of materials, adding more floors to existing structures, or changing the function of the structures, can also render the original structure deficient. Although a method of rehabilitation for many types of deficiencies is discussed in this report, the emphasis is on seismic rehabilitation.

Columns are critical elements in any structural system and their performance during a seismic event can dominate the overall outcome. Existing reinforced concrete building columns can be particularly vulnerable due to various design and detailing deficiencies. Deficiencies that often characterize the old existing reinforced concrete frame structures include: (1) insufficient transverse reinforcement to confine the column core and to restrain buckling of longitudinal reinforcement; (2) inadequate lap splices located immediately above floor levels where inelastic actions may be concentrated with large flexural demand; (3) insufficient shear strength to develop the column flexural capacity, or the potential degradation of column shear strength with increasing flexural ductility demand; (4) inadequate column strength to develop a strong-column, weak-beam mechanism; and (5) deficient beam-to-column joint dimensions and details.

Recent earthquakes have highlighted the urgency and importance of rehabilitating seismically deficient structures to achieve an acceptable level of performance. In earthquakes such as the 1933 Long Beach earthquake, 1940 El Centro earthquake, 1971 San Fernando earthquake, 1989 Loma Prieta earthquake, 1994 Northridge earthquake, and 1995 Kobe earthquake, severe damage was observed in poorly detailed structures and some even collapsed, demonstrating the vulnerability of these systems. In order to prevent greater loss from the many similar buildings in stock, rehabilitation is required to improve their seismic performance.

1.2 Rehabilitation Techniques

Different rehabilitation techniques have been developed over the years, and rehabilitation with steel collars is one of them.

1.2.1 General

Seismic rehabilitation has emerged as a major topic in earthquake engineering and has become a prominent research field that receives considerable emphasis throughout the world, especially in countries with significant seismic risk (CEB-FIB 2003). Over the past 20 years, many research projects have been carried out on the rehabilitation of existing structures, and significant advancements have been made in the research and development of innovative materials and technologies for improving the seismic performance of existing structures through rehabilitation processes. Many rehabilitation techniques have been proposed, studied, and implemented, but some are extremely costly and require invasive work that is highly disruptive to the building occupants. Ideally, an effective rehabilitation technique shall possess such characteristics as being easy to implement, minimizing disruption to the use of the structure, not requiring highly specialized skills, minimizing labour costs, and resulting in efficient performance.

Rehabilitation can be achieved, in part, by reducing the load effects input to the existing structure, or by improving the strength, stiffness, and/or ductility of the structure. Rehabilitation techniques fall under two main categories: structural system-level rehabilitation and member-level rehabilitation (Moehle 2000; Bai and Hueste 2003). Installation of structural systems, such as adding structural walls, damping devices, base isolators, steel braces, or steel shear plates, has an impact on the overall structural response to earthquakes. It involves global modifications to the whole structural system so that the design demand, often represented by target displacement, on the existing structural system is less than its capacity. The second approach is a member-level approach, such as the use of concrete, fibre-reinforced polymer composite, or steel jacketing, to improve the performance of individual deficient elements such as columns, beams, and walls. In this approach, the objective is to increase the strength and deformation capacity of the deficient components so that they can reach their designated performance level (Moehle 2000).

1.2.2 Rehabilitation by Steel Confinement Collars

Considering the various factors such as effectiveness, amount of time and material involved, and the disruption of the use and operation of the structure, a simple and effective, minimally intrusive rehabilitation scheme using steel plate shear walls and steel collars has been proposed by Hussain and Driver (2001) and Driver *et al.* (2001), as shown in Figure 1-1.

Research on steel plate shear walls conducted at the University of Alberta and elsewhere has confirmed the technical and economical attributes that make the steel plate shear wall system desirable as a lateral load resisting system, which has been used in some new structures. Those attributes include superior ductility, robust resistance to degradation under severe cyclic loading, and high capacity of energy dissipation. Driver *et al.* (2001) proposed that steel plate shear walls can also be used to rehabilitate deficient reinforced concrete frame structures as well as new structures. The concept is to take advantage of

the high strength, high ductilility, and high energy dissipation capacity of the steel plate shear wall to improve the performance of existing deficient reinforced concrete frame structures in strength/ductility/energy dissipation.

There are some challenges that arise due to the use of steel plate shear walls in reinforced concrete frame structures, however, such as the connection between the concrete and steel, the ductility incompatibility between ductile steel plate shear walls and non-ductile concrete columns, and the fact that the tension field of the steel shear panel induces a high shear demand on the neighbouring columns. In order to solve these problems, an external steel collar system has been proposed for the existing frame columns by Hussain and Driver (2001, 2003, 2005a, 2005b). The external steel collars perform multi-functions in the rehabilitation system. Besides providing a means of connecting the steel to the concrete, they also enhance the strength and improve the ductility of the concrete columns. Steel collars were also found to be effective on their own as a rehabilitation scheme.

Hussain and Driver (2001, 2003, 2005a, 2005b) conducted experimental and analytical research on collared columns under concentric axial loading, as well as under axial and lateral loading where the flexural behaviour of the rehabilitated system was the focus. The rehabilitation method, using external steel collars as the confinement elements, was shown to be an effective rehabilitation method and benefits in both strength and ductility were demonstrated. The external steel collars used in the research were cut from steel hollow structural sections, as shown in Figure 1-2. Welding was needed in the fabrication and assembly of the collars, however, which made the process somewhat complicated, time consuming, and costly. Hence, a relatively simple, economical alternative was developed as a solid steel collar cut from thick steel plates that requires no welding, as shown in Figure 1-3. Chapman and Driver (2006) studied reinforced concrete columns rehabilitated with solid steel collars under concentric and eccentric axial loading and reported significant enhancement in both the strength and ductility of the columns.

1.2.3 Collar Application to Short Columns

Seismic rehabilitation of existing structures is often focussed on enhancing the ability to develop highly ductile flexural hinges in the frame under cyclic load input. However, in many cases columns also need to be capable of resisting cyclic shear. Cases where shear may be influential occur in short columns that are incorporated into structural systems either purposely or as a result of structural changes not considered in the original design. Examples include short columns in parking facility frames where storey levels vary, columns between window and other openings, and columns shortened by masonry infills, as shown in Figure 1-4. A typical case is a column whose clear height is reduced by stiff structural elements that limit the deformation of the column over a portion of its length (Woodward and Jirsa 1984). It has also been pointed out (Driver *et al.* 2001) that deficient reinforced concrete frames can be rehabilitated by installing thin vertical steel plates to create a hybrid steel plate shear wall, a condition that can induce high local shears on the columns.

Although Hussain and Driver (2001, 2003, 2005a, 2005b) studied the behaviour of collared reinforced concrete columns under axial load or combined lateral and axial loads, all columns were relatively slender columns with a shear span-to-depth ratio greater than 2.5. Previous research has shown that although the flexural capacity of a column can be estimated with good accuracy, the shear capacity can be difficult to predict. Failure of existing reinforced concrete columns in shear usually takes place at low deformations and is associated with a large and sudden drop in lateral and axial load resistance. Moreover, the shear strength of a column subject to cyclic lateral load tends to degrade faster than its flexural strength. The risk of premature shear failure remains in existing reinforced concrete columns that do not meet current earthquake-resistant design criteria (Lynn *et al.* 1996; Jaradat *et al.* 1998; Kim *et al.* 2001; Lehman *et al.* 2004; Biskinis *et al.* 2004). Since the brittle shear mode failure normally gives no warning, it should be avoided in the design and rehabilitation of concrete columns. Hence, research on the behaviour of collared reinforced concrete short columns under combined axial and cyclic lateral loading is needed.

1.3 Objectives and Scope

An ongoing research program at the University of Alberta is directed at understanding the performance of the proposed rehabilitation scheme for reinforced concrete columns using external steel collars. Experimental and analytical studies in earlier phases of the overall research program have already shown that steel collars provide an effective rehabilitation method for reinforced concrete slender columns (Hussain and Driver 2001, 2003, 2005a, 2005b; Chapman and Driver 2006). Improvements in both strength and member ductility were demonstrated for concentric and eccentric axial loading conditions, and under simulated seismic loading that led to plastic hinging and eventual flexural failure.

The current study was developed to further the understanding of the external steel collar rehabilitation scheme, with specific focus on the behaviour of reinforced concrete short columns. Research was conducted on the rehabilitation and repair of seismically deficient reinforced concrete short columns with steel collars under combined axial and cyclic lateral loading through analytical and experimental approaches. Design guidelines on the rehabilitation of deficient reinforced concrete frame columns are also proposed. This research also adds some experimental data to the general research pool on the behaviour of reinforced concrete short columns that may benefit other research, including the calibration of damage models.

The overall goal of this research was to capture the effectiveness of this rehabilitation method so that it can be applied in practice through rehabilitation and repair approaches. The objective was to propose a strength model and guidelines that can be adopted in the rehabilitation design of concrete columns with external steel collars. To achieve this objective, five items were established in the research scope:

(1) Evaluate through experiment the feasibility of and benefits resulting from the rehabilitation technique with external steel collars applied to short columns;

(2) Experimentally investigate the main parameters affecting the performance of collared reinforced concrete short columns;

(3) Study the rehabilitation technique with external steel collars on reinforced concrete short columns through finite element (numerical) simulation, including a parametric analysis;

(4) Perform analyses on collared reinforced concrete short columns adopting different analytical approaches, such as code provisions and a strut-and-tie model, and propose a strength model suitable for use in design or evaluation; and

(5) Outline the general design guidelines for a practical rehabilitation scenario, using examples to demonstrate their application.

The current research includes three main phases. In phase one, the behaviour of collared reinforced concrete short columns under simulated seismic loading was studied experimentally. In phase two, analytical studies on the behaviour of collared reinforced concrete short columns under simulated seismic loading were conducted through finite element simulation and with some conventional computational approaches. In phase three, design guidelines were developed to assist practicing design engineers in conducting a rehabilitation design of deficient reinforced concrete columns with external steel collars.

1.4 Format and Organization

This report is organized into eight chapters, and this section provides an overview of the remaining content.

Chapter 2 presents a literature review on previous experimental and numerical studies on the behaviour of reinforced concrete short columns, including rehabilitated columns. Shear strength models for columns are reviewed. Concrete confinement models are also presented.

Chapter 3 outlines the experimental program, which is focussed on reinforced concrete short columns with external steel collars that are subjected to combined axial and cyclic lateral loading. The results of the experimental program are presented in Chapter 4, where the effects of the test parameters are discussed and conclusions are drawn from comparisons among the specimens.

In Chapter 5, a finite element modelling approach is adopted for the study of the behaviour of collared reinforced concrete short column. After validation of the finite element model with the experimental results, a parametric study is conducted.

Other analytical approaches are adopted to predict the behaviour of collared reinforced concrete short column in Chapter 6, including the CSA/A23.3-04 and ACI318-05 code provisions, software Response 2000, and a strut-and-tie model. A strength model is proposed to predict the shear and flexural capacities of collared reinforced concrete columns.

Chapter 7 presents design guidelines for the rehabilitation of deficient reinforced concrete columns with external steel collars. Consideration is given to flexural and axial strengthening, as well as shear strengthening. Design examples are provided to illustrate the application of the design guidelines.

Chapter 8 summarizes the conclusions drawn from the current experimental and analytical studies. Recommendations for future research are also presented.

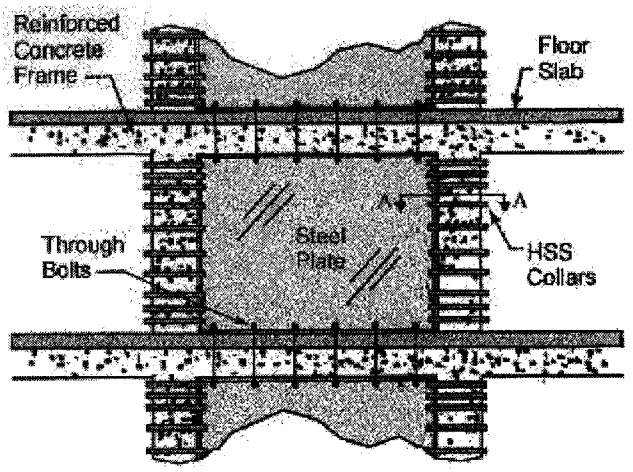

Figure 1-1 Rehabilitation of reinforced concrete frame using steel plate shear wall with steel collar connections (adapted from Driver *et al.* 2001)

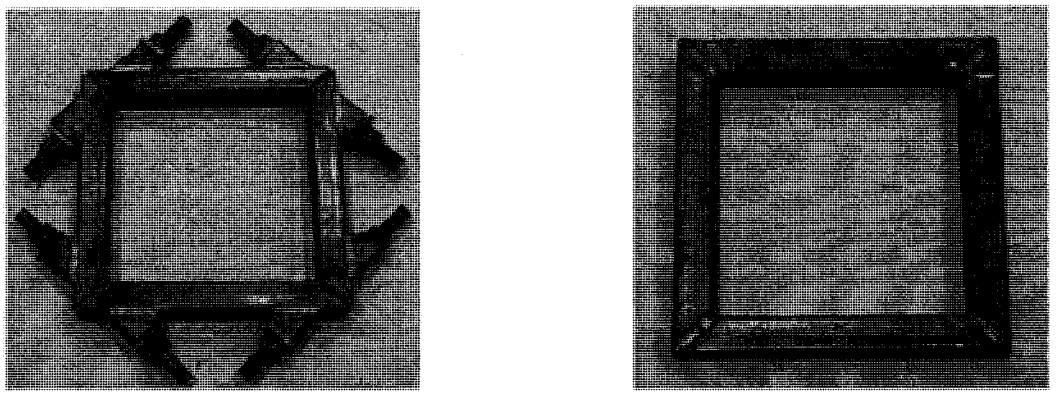

(a) Bolted steel HSS collars (b) Welded steel HSS collars

Figure 1-2 Steel hollow structural section (HSS) collars

(Hussain and Driver 2005b)

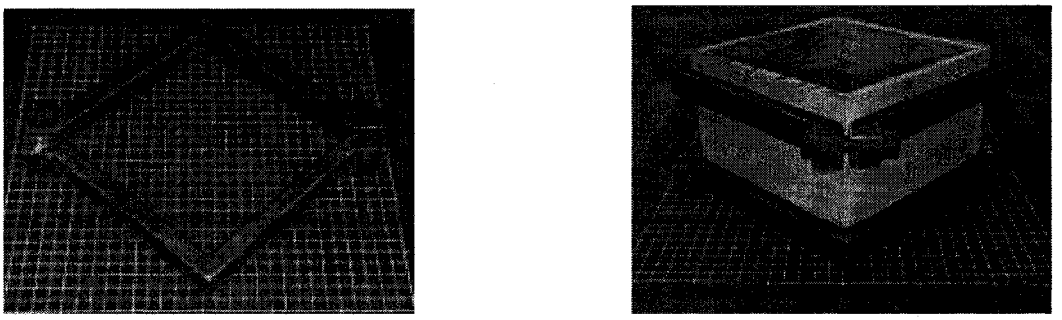

(a) Plan (b) Elevation

Figure 1-3 Bolted solid steel collars

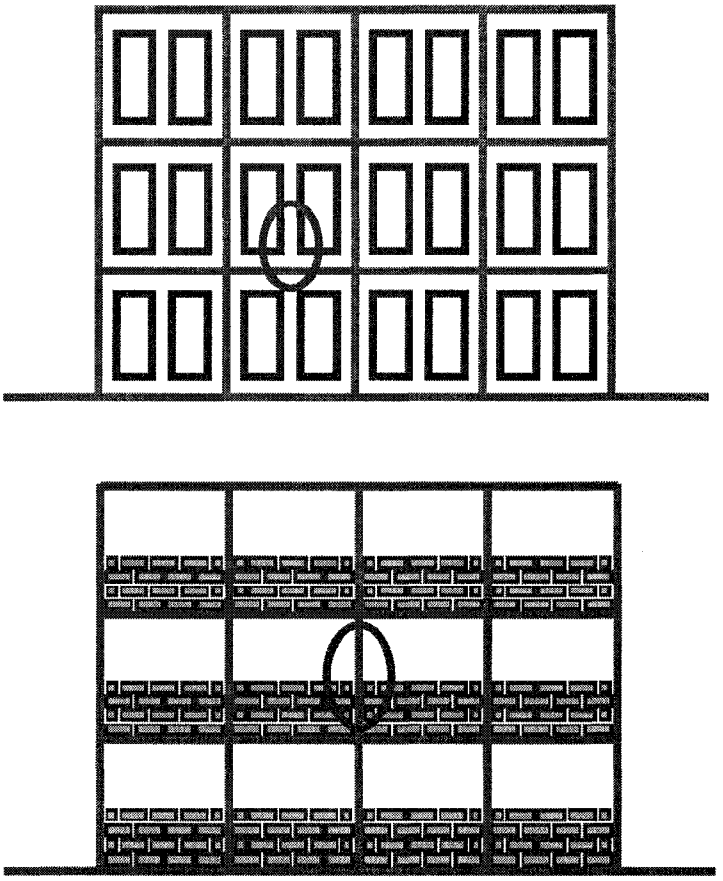

Figure 1-4 Reinforced concrete short columns

CHAPTER 2 LITERATURE REVIEW

2.1 Introduction

Severe damage and even collapse of non-ductile reinforced concrete frames during past earthquakes have demonstrated the potential vulnerability of these systems and the need for effective rehabilitation schemes. Over the past two decades, various rehabilitation techniques have been proposed and implemented. Previous research has shown that although the moment capacity of frame members can generally be estimated with good accuracy, the shear capacity can be difficult to predict. Shear deficiency can sometimes lead to a brittle and sudden shear failure, and short columns can be particularly vulnerable. This chapter summarizes key research pertaining to the behaviour of normal strength reinforced concrete short columns as well as different rehabilitation techniques intended to improve the shear behaviour of as-built columns. Some prominent shear strength models are also summarized in this chapter.

The understanding and knowledge of the shear transfer mechanisms in various types of concrete structural elements has progressed significantly. The main types of shear transfer are: (1) Shear stress in the uncracked concrete; (2) crack interface shear transfer; (3) dowel action; (4) arch action; (5) shear reinforcement (ACI-ASCE Committee 426, 1974). The ASCE-ACI Committee 445 on Shear and Torsion (1998) pointed out another mechanism, residual tensile stresses transmitted directly across cracks. Opinions vary about the relative importance of each mechanism in the total shear strength, resulting in different models for the prediction of shear strength. As for the shear reinforcement, in addition to the shear it carries directly, it aids several other kinds of shear transfer mechanisms. That is, when an inclined crack crosses the shear reinforcement, the reinforcement can contribute significantly to the capacity of the member by increasing or maintaining the shear transferred through crack interface interlock, dowel action of longitudinal reinforcing bars, and arch action, by the restriction of the widening of the crack (ACI-ASCE Committee 426, 1974).

Columns are critical elements in any structural building system and their performance during a seismic event can dominate the overall performance of the structure since single column failures can lead to additional failures and potentially result in total building collapse. Previous research showed that shear-dominated behaviour is most common in columns having shear span-to-depth ratio less than 2.5 (Woodward 1980; Ghee *et al.* 1989; Wong *et al.* 1993; Priestley *et al.* 1994a; 1994b; Jaradat *et al.* 1998). The shear span-to-depth ratio, referred to herein as the "aspect ratio" for simplicity, is calculated as $M/(VD)$, where M is the moment at the critical section, V is the shear force at the critical section, and D is the overall dimension of the cross-section parallel to the shear. The columns are made more vulnerable to damage when their spans are shortened by structural elements that are stiff and hence limiting the deformation of the column over a portion of its length, such as those adjacent to balcony parapets or masonry infill. This is known as the "short column" effect and it tends to make columns less ductile. If the structure contains both short and long columns, the load will be concentrated in the shorter columns due to their higher flexural stiffness. Hence, short columns are often

damaged in earthquakes due to this effect. In reinforced concrete members, it is desirable to ensure higher shear capacity than the corresponding flexural capacity in order to develop the relatively ductile flexural failure mode according to capacity design philosophy. As a result, study of the various parameters that influence the shear behaviour of reinforced concrete columns is necessary.

The research on shear strength has developed from the early truss model to modified truss models. The modified truss model includes the strut-and-tie models, and includes models with Compression Field Theory or Modified Compression Field Theory to describe the stress–strain response. The early truss model approximated the shear behaviour of reinforced concrete members by neglecting tensile stress in the diagonally cracked concrete and by assuming the shear would be carried by diagonal compressive stresses in the concrete. The diagonal compressive stresses were assumed to incline at 45° to the longitudinal axis (ASCE-ACI Committee 445 on Shear and Torsion, 1998).

The ASCE-ACI Committee 445 on Shear and Torsion (1998) presented a thorough review of the historical development of shear capacity models for reinforced concrete. Truss models were used as conceptual tools in the analysis and design of reinforced concrete beams for shear postulated independently by Ritter in 1899 and Mörsch in 1902. Mörsch later extended the use of truss models to torsion in 1920 and 1922. In the truss model, a reinforced concrete beam can be idealized as a parallel chord truss with compression diagonals inclined at 45° with respect to the longitudinal axis of the beam after it cracks due to diagonal tensile stress. The diagonal compressive concrete stresses push apart the top and bottom faces of the member, while the tensile stresses in the shear reinforcement pull them together. Equilibrium requires these two effects to be equal. According to the truss model, the shear capacity is reached when the shear reinforcement yields, or when the concrete compression diagonals crush, which is usually prevented by setting an upper limit to the maximum average shear stress in design code provisions. This approach is conservative due to the choice of inclination of the compression diagonals measured from the longitudinal axis as 45°.

The ASCE-ACI Committee 445 on Shear and Torsion (1998) also pointed out that Talbot has concluded the shear strength varies with the amount of reinforcement and length-to-depth ratio of the beam as early as 1909. Short, deep beams give higher shear strength results than long slender ones, and beams with a high percentage of reinforcement give higher results than beams with a small amount of reinforcement.

Different from the classical truss model, later research and practice led to the modified truss models that added a concrete contribution in the tension term of the shear reinforcement capacities, assuming either 45° or a variable angle of inclination of the diagonals. The inclination of the truss diagonals is allowed to deviate from 45° within certain limits based on the theory of plasticity (ASCE-ACI Committee 445 on Shear and Torsion, 1998).

2.2 Experimental Research on Short Reinforced Concrete Columns

Many reinforced concrete structures built in high seismic regions before the 1970s are considered deficient due to reinforcing details that do not ensure ductile member response under severe seismic loading. It is important to identify the particular structural deficiency of the existing structure during the evaluation process in order to select an appropriate means of rehabilitation. Reported in this section are experimental studies of the behaviour of short reinforced concrete columns with normal strength concrete under combined axial compression and lateral loading. The aspect ratio of the short column is set as around 2.5 in this thesis.

Jirsa *et al.* (1980) studied the influence of load history on the shear behaviour of short reinforced concrete columns through tests of 18 specimens simulating a short column between stiff floors. The columns had a cross-section of 300×300 mm and an overall height of 910 mm with two end blocks to facilitate loading and maintain end restraint. The internal longitudinal and transverse reinforcement were designed to represent the typical practice in column design at that time. The nominal strength of the concrete was 35 MPa, with values ranging from 30 to 41 MPa. The geometry and reinforcement was kept constant throughout the experimental program but the loading history was different. In each case the lateral deformations were applied to a given level of multiples of yield displacement for three reversals and then the deformation was increased or the deformation path was changed. The following lateral deformation and axial load histories were considered: (1) No axial load with unidirectional or bidirectional lateral deformation path; (2) Constant compressive or tensile axial loads with unidirectional or bidirectional lateral deformation path; (3) Alternate tensile or compressive axial loads with unidirectional or bidirectional lateral deformation path. Based on the tests, the researchers concluded that the load history affects the rate of stiffness and strength degradation. Bidirectional lateral histories in which the deformations were applied alternately in each direction produced a slightly more rapid degradation than unidirectional loadings. Constant compressive axial load appeared to accelerate shear deterioration. Constant axial tension decreased shear deterioration but substantially reduced the shear capacity and the stiffness. Alternating axial tension and compression produced results similar to that of constant compression.

Woodward (1980) tested 11 short reinforced concrete columns, each representing a column bounded by large framing members that restrain end rotation. The columns were subjected to slowly-applied cyclic displacements of the upper end relative to the lower end to simulate the action of a building column subjected to seismic excitation. The overall geometry of the specimen was kept unchanged. The test column was 910 mm in overall height with a 300×300 mm cross-section and 25 mm clear cover to the tie reinforcement, which was a 2/3-scale model of a prototype column 1370 mm in overall height with a 460×460 mm cross-section and 38 mm of clear cover. The amount of longitudinal and transverse reinforcement relative to each other was changed to study the effect of the ratio of shear capacity to flexural capacity on the member behaviour. Constant compressive axial load with a value of approximately 50 percent of the axial load at balanced strain conditions for each column was applied. Diagonal (in plan) lateral

displacement was applied to produce biaxial displacement. Three cycles of reversed displacement were applied along each diagonal at each displacement level. Test results showed that the shear capacity of a short column is largely dependent on the capacity of the concrete to resist shear force before inclined cracking develops. After cracking, the shear resistance of the column was strongly related to the effectiveness of aggregate interlock along the inclined cracks. In the short columns tested, there was a lower limit on the amount of transverse reinforcement that was required before an increase in the maximum lateral load of the column was observed. Varying the amount of transverse reinforcement while remaining below this limit did not cause a proportionate increase in the shear capacity. No single parameter uniquely determined the behaviour of these short columns, but there existed a hierarchy of parameters that affect the column behaviour to different degrees.

Kokusho *et al.* (1986) conducted an experimental study of aseismic shear behaviour of reinforced concrete columns under high axial load. A total of 18 scaled-down specimens simulating the low storey columns in a 25-storey building were tested. Three shear span-to-depth ratios, 1.0, 1.5, and 2.0, and five axial force ratios were examined. Three of the specimens had little shear reinforcement. The cross-section of all specimens was 200×200 mm. The axial compressive load was applied first and kept constant, and monotonic loading of lateral displacement was applied later until the rotation angle of the columns reached a prescribed limit. Test results showed that the ultimate shear strength of the column increases with an increase of the axial compressive force if the axial compression index is not greater than 0.4, but under higher axial compressive load the ultimate strength increases little because compressive failure of the concrete occurs. The axial compression index is calculated from $P/\left(f_c^{'}A_g\right)$, where P is the axial compressive load applied to the column, $f_c^{'}$ is the compressive strength of concrete, and A_g is the gross cross-sectional area of the column. Tests showed that the greater the aspect ratio, the larger the deformation capacity, and the lower the amount of shear reinforcement, the lower the deformation at shear failure. It was suggested that in order to maintain aseismic integrity in columns subjected to a high axial compressive load, an effective arrangement of shear reinforcement is required so that every corner and alternate longitudinal bar has lateral support.

Kobayashi *et al.* (1986) performed an experimental study on the ultimate shear strength of reinforced concrete columns subjected to bi-directional lateral loads. All the specimens had a 150×150 mm cross-section and an aspect ratio of 2.0. Test results indicated that ultimate shear strength under bi-directional lateral load was lower than that under uni-directional lateral load.

Ghee *et al.* (1989) tested 25 circular columns under axial load and cyclic lateral inelastic displacement. The columns, tested as simple vertical cantilevers, had a diameter of 400 mm, which was considered to provide approximately one-third scale models of typical bridge columns. The target 28-day compressive strength of concrete was 30 MPa. Results indicated that the shear strength was dependent on the axial compression index, the column aspect ratio, the amount of transverse spiral reinforcement, and the

displacement ductility factor, μ . At low displacement ductility, a summation of a concrete contribution to shear strength plus a 45° truss mechanism involving the transverse spiral reinforcement and the diagonal concrete compression struts could be used to predict the column shear capacity. The researchers pointed out that the then current U.S. and New Zealand code design equations for the concrete contribution were found to be very conservative. At displacement ductilities, μ , of $\mu > 2$, the shear strength degraded gradually with increasing ductility, and the inclination of the diagonal compression struts of the truss mechanism to the longitudinal axis decreased. Based on the test results, the researchers proposed design equations relating the degradation of shear strength to the displacement ductility factor.

Wong *et al.* (1993) tested sixteen 400 mm diameter circular cantilever columns with an aspect ratio of 2.0 and different transverse spiral reinforcement ratios ranging from 0.4% to 2.5% to investigate the strength and stiffness of shear-resisting mechanisms under various displacement patterns and axial compressive load intensities. All test columns had a longitudinal reinforcement ratio of $\rho = 3.2\%$, where ρ is the total longitudinal reinforcement area, A_s, divided by the gross cross-sectional area of the column, A_g. Three levels of axial compressive load were applied: 0, $0.19 f_c' A_g$, and $0.39 f_c' A_g$. Four types of lateral displacement patterns were studied: uniaxial and three patterns of biaxial loading. Test results showed that elastic shear deformations in short circular columns with small or no axial compressive load were significant. In comparison with the uniaxial displacement pattern, biaxial displacement pattern (one cycle consisted of North-South path followed by an East-West path) resulted in more severe degradation of stiffness and strength and, in turn, also energy dissipation. However, the reduction of initial shear strength and ductility capacity of short columns subjected to a biaxial displacement history was not significant. The value of the ultimate displacement was, on average, less than that obtained in identical units subjected to a uniaxial loading history. Axial compressive load increased shear strength enhancement, but tended to decrease the ductility. Strength loss in columns subjected to a large axial compressive load was sudden and without warning, mainly due to the development of a wedge mechanism formed by the crossed diagonal cracks and axial compressive load. Assessments in ACI 318-89 of shear carried by the concrete were conservative at low ductility levels. All test specimens satisfying ACI 318-89 code requirements for non-seismic shear strength developed a displacement ductility of four or higher even under the most severe displacement patterns.

Lynn *et al.* (1996) constructed eight full-scale specimens typical of pre-1970s reinforcement detailing practice. The specimens were subjected to constant axial compressive load and increasing cyclic lateral displacement increments until failure. All columns were 456×456 mm in cross-section and 2940 mm in overall height with two stiff and strong ends that enforced double curvature in the columns. Normal weight aggregate concrete with compressive strengths ranging from 26 to 33 MPa was used and the axial compressive load was either $0.12 f_c' A_g$ or $0.35 f_c' A_g$. It was observed that those columns that reached the calculated flexural strength before the calculated shear strength exhibited a relatively ductile response, while those that did not reach the flexural strength exhibited brittle failure. Loss of axial load capacity (failure of the specimen) occurred at or after

significant loss of lateral force resistance. Axial load failure occurred soon after the loss of lateral force resistance when the response was governed by shear. Axial load resistance was maintained until eventually shear failure occurred when the response was initially governed by lap-splice deterioration and axial compressive loads were small. Axial load capacity was maintained to relatively large displacement levels when the response was predominantly flexural.

Jaradat *et al.* (1998) investigated the flexural and shear performance of old existing columns for the purpose of seismic assessment and rehabilitation design through the testing of eight reduced-scale circular specimens. All the specimens had a diameter of 250 mm, while the aspect ratios ranged from 2.0 to 3.5. The compressive strengths of concrete were 26 MPa and 29 MPa for two different batches of concrete. All specimens were subjected to constant axial compressive load and increasing cyclic lateral displacement with three cycles at each level. It was found that increasing the amount of longitudinal reinforcement resulted in shear failure in the short specimens due to the increase in the shear demand required to develop the flexural strength. In the specimens that had flexure-dominated failures, greater amounts of longitudinal reinforcement resulted in less pinching in the hysteresis curves. A decrease in the aspect ratio resulted in an increase in the column shear demand. Specimens with larger aspect ratios dissipated more energy and experienced less pinching in the hysteresis curves. Increasing the splice length at the column base resulted in a slight increase in column strength and a delay in the onset of splice degradation.

2.3 Confinement of Reinforced Concrete Columns

The benefit of confinement to strength and ductility can be shown when the concrete stress approaches the uniaxial capacity and the volume of the concrete increases due to the internal cracking. Enclosing confining elements exert reaction pressure to the core concrete, which in turn increases its strength and ductility. Extensive research on the confinement of reinforced concrete columns to enhance strength and ductility has been conducted over the years. Confinement can be provided through such mechanisms as internal reinforcement, external reinforcement, external jackets (made of concrete, steel, or fibre reinforced polymers, etc.), or external prestressing. The structural behaviour of reinforced concrete columns can be improved through the confinement provided to the concrete core and the lateral support provided to the longitudinal bars. Numerous analytical models have been proposed to predict the stress-strain behaviour of confined concrete, accounting for the confinement effect exhibited through different confining systems. Though these models showed reasonable accuracy through validation with experimental results, there appears to be little consensus as to a specific confinement model that yields accurate results consistently. Discussions of only a few recent confinement studies from the literature are presented in the following sections. A more complete review can be found in Hussain and Driver (2005b) and Chapman and Driver (2006).

2.3.1 Confinement Models

Hussain and Driver (2005b) and Chapman and Driver (2006) presented detailed reviews of existing confinement models in previous phases of this research program. Only the more recent additions to the literature are presented here.

Triantafillou *et al.* (2006) conducted an experimental study of confined cylinders and short rectangular columns with textile-reinforced mortar jackets, and proposed a confinement model through the introduction of experimentally-derived jacket effectiveness coefficients. The typical approach assuming that the confined strength and ultimate strain depend on the confining stress at failure was adopted as follows:

$$\frac{f_{cc}^{'}}{f_{co}^{'}} = 1 + k_1 \left(\frac{\sigma_h}{f_{co}^{'}} \right)^m \qquad [2\text{-}1a]$$

$$\varepsilon_{cc}^{'} = \varepsilon_{co}^{'} + k_2 \left(\frac{\sigma_h}{f_{co}^{'}} \right)^n \qquad [2\text{-}1b]$$

$$\sigma_h = k_e \frac{(b+h)}{bh} t_j f_{je} \qquad [2\text{-}1c]$$

$$k_e = 1 - \frac{(b-2r_c)^2 + (h-2r_c)^2}{3bh} \qquad [2\text{-}1d]$$

where $f_{cc}^{'}$ is the peak stress of confined concrete, $f_{co}^{'}$ is the unconfined concrete material strength. σ_{lu} is the confining pressure at failure, $\varepsilon_{cc}^{'}$ is the confined concrete strain at peak stress, $\varepsilon_{co}^{'}$ is the unconfined concrete strain at peak stress, k_1, and k_2 are empirical constants and can be derived experimentally. m and n are taken as 1 for simplicity to assume that the relationship between confined strength and ultimate strain and their unconfined counterparts is linear. b and h are the section dimension of the column, r_c is the radius at corners of rectangular section. t_j and f_{je} are the thickness and effective strength of jackets.

Yan and Pantelides (2006) proposed a confinement model based on plasticity theory using the William-Warnke five-parameter concrete model and the Pantazopoulou-Mills theory of degradation of concrete elastic modulus. The Popovics concrete model for hardening behaviour and the Saenz model for softening behaviour were applied in the formulation. The confinement model was implemented adopting an incremental approach

to account for the variable fibre reinforced polymer (FRP) confinement and dilation behaviour with the axial loading history. The model was verified using medium scale and large scale tests of FRP-confined concrete compression members with bonded FRP jackets or post-tensioned FRP shells and showed good agreement with experimental results.

2.3.2 Confinement Study by Hussain and Driver (2005b)

Through their literature review, Hussain and Driver (2005b) pointed out that the existing available confinement models lack an explicit flexural stiffness parameter for the confining element and most of those models were developed under the assumption of constant confining pressure. Hence, they may be unable to predict the behaviour of concrete confined by external steel collars because of the significant flexural stiffness that these collars possess. Hussain and Driver (2005b) conducted finite element studies of collared reinforced concrete columns to establish confining behaviour of the collars in terms of average confining pressure versus average lateral strain. The average confining pressure was obtained by dividing the total force in the connection elements (the outrigger elements between the concrete surface nodes and the external steel collars nodes) located in a strip by the strip area. The average lateral strain was obtained by dividing the average horizontal displacements of the concrete surface nodes by half the width of the column. The axial and flexural stiffnesses of the external steel collars were incorporated into the proposed model. The active confining pressures applied through prestressing the collar bolt connections were generated by applying a negative temperature change to the corner bolts of the collars.

After obtaining the average confining pressure versus average lateral strain relationships, the lateral strain was related to the axial strain, and the confining pressure was related to the axial stress through a confinement model. While the available existing confinement model dealt with constant confining pressure, an incremental-iterative procedure was required since the confining pressure under external steel collars was variable through the loading history. Hence, the analysis was performed in increments of axial load and in each increment a constant confining pressure was assumed. As the process repeated, the entire stress versus strain curve of the confined concrete was traced.

2.3.3 Confinement Study by Chapman and Driver (2006)

Based on the work presented by Hussain and Driver (2005b), Chapman and Driver (2006) proposed a procedure to determine the confining pressures induced by the collars through a simplified plastic analysis that eliminates the need for finite element modelling. The predicted load history was partially extended into the descending branch of column response after the peak load. The approach was distinct from other models because of the simple, yet effective, behavioural modelling of the collars based on a generalized plastic analysis. The plastic analysis allowed both the axial stiffness and flexural stiffness of the collars to be incorporated into the confinement model and provided representative confining pressures that increase as the column was loaded. Moreover, the model can be used with or without active confinement. The model was applied to 17 concentrically

loaded columns with external steel collars and good agreement was achieved between experimental and predicted column axial load–axial strain histories. The analytical model presented by Chapman and Driver (2006) is used in Chapter 6 to predict the stress versus strain response of the collared concrete columns tested as part of this research project.

The first step for the general procedure of this model is the development of independent behavioural representations for the steel collar and the confined concrete based on a simple rational approach. Once these independent relationships have been established, an equilibrium confining pressure can be calculated based on displacement compatibility, which expresses the interaction between the two elements. Then an idealized relationship between the collar lateral deflection and confining pressure is developed that is independent of the concrete behaviour. This assumed uniform confining pressure is then modified to the equivalent uniform confining pressure through the introduction of a confinement efficiency factor to represent the effects of collar spacing and confinement effectiveness. A revised confinement effectiveness factor that accounts for the axial strain gradient across the column cross-section could be included if the column is not concentrically loaded. Once the equivalent uniform confining pressure is obtained, the peak stress of confined concrete is calculated according to equations for constant confining pressure. An incremental iterative approach is used that assumes a constant confining pressure within each small increment. Finally, the established unconfined concrete stress–strain relationship is modified to apply to confined concrete. The procedure requires the axial strain in the column as an input value. As the axial strain is incremented, points along the confined concrete stress–strain curve are formulated. Within each increment, initial values for unknown parameters are assumed and iteration is performed until convergence is reached.

A solution strategy was presented by Chapman and Driver (2006) that outlines the detailed steps required to generate the stress versus strain history of concrete columns confined with external steel collars, summarized as follows:

[Step 1] Plastic analysis of the external steel collars themselves produces intermediate values of an idealized uniform confining pressure, σ_n, using Eq. 2-2, and resulting lateral strains at the centre of the collar segments, $\varepsilon_{lat\,n}$, corresponding to the formation of plastic hinges using Eqs. 2-3a through 2-3f. A maximum value of collar pressure, $\sigma_{\max}$, is also calculated using Eq. 2-4 that limits the level of passive confining pressure, $\sigma_{passive}$, that can be generated by the collar system.

[Step 2] The equilibrium passive confining pressure, $\sigma_{passive}$, can be calculated from Eq. 2-5a, which includes four variables (ε_{cc}, υ_c, E_c, E_{sc}) determined as follows:

1. The concrete axial strain, ε_{cc}, is an input variable that is incremented upward to generate the load history.
2. The secant Poisson's ratio, υ_c, is calculated from Eq. 2-5b. The value of σ_h in Eq. 2-5c is taken as the total equivalent confining pressure, σ_{total}'.

3. The concrete secant modulus, E_c, is the ratio between concrete stress and strain f_{cc}/ε_{cc} taken at $40\%f_c^{'}$.
4. The collar secant modulus, E_{sc}, is the ratio between collar pressure and lateral strain $\sigma_{collar}/\varepsilon_{lat}$, and is calculated from the curve generated in Step 1 once the value of column lateral strain is known.

[Step 3] The equivalent uniform confining pressure, $\sigma_{total}^{'}$, based on the total confining pressure ($\sigma_{active}+\sigma_{passive}$) can be calculated from Eqs. 2-6a and 2-6b, using values for the confinement efficiency factor, K, from Eqs. 2-6c to 2-6e.

[Step 4] The peak confined concrete strength, $f_{cc}^{'}$, and strain at peak stress, $\varepsilon_{cc}^{'}$, are calculated from Eqs. 2-7a and 2-7b, respectively.

An iterative process is used because the variables υ_c, E_c, and E_{sc} are all functions of confining pressure. Initially, values for the unconfined concrete properties (υ_{co} and E_{co}) and the starting value of E_{sc} (before the first plastic hinge forms) are used for the unknowns. Next, the values for equilibrium passive confining pressure, $\sigma_{passive}$, and peak confined concrete strength, $f_{cc}^{'}$, are calculated according to Eqs. 2-5a and 2-7a, respectively. The values for υ_c, E_c, and E_{sc} are then updated. Iterations (Steps 2 to 4) are performed until convergence is achieved. This process is readily executed using a spreadsheet.

[Step 5] The confined concrete stress, f_{cc}, at each increment of axial strain, ε_{cc}, is calculated using Eqs. 2-8a to 2-8d.

[Step 6] The process (Steps 2 to 5) is repeated with increasing levels of axial strain, ε_{cc}.

$$\sigma_n = \frac{-\left(\frac{\sum F_i th}{F_y^2}+\frac{th^2}{CM_p}\right)+\sqrt{\left(\frac{\sum F_i th}{F_y^2}+\frac{th^2}{CM_p}\right)^2-\left(\frac{th}{F_y}\right)^2\left[\left(\frac{\sum F_i}{F_y}\right)^2+\frac{\sum M_i}{M_p}-1.0\right]}}{0.5\left(\frac{th}{F_y}\right)^2} \qquad [2\text{-}2]$$

$$\varepsilon_{lat\,n} = \frac{2\Delta_{n\,total}}{h} \qquad [2\text{-}3a]$$

$$\Delta_{n\,total} = \sum_{i=1}^{n-1} \Delta_i + \Delta_n \qquad [2\text{-}3b]$$

$$\Delta_n = \Delta_{bend} + \Delta_{axial} \qquad [2\text{-}3c]$$

$$\Delta_1 = \Delta_{bend} + \Delta_{axial} = \frac{\sigma_n th^4}{720 E_{sc} I_{sc}} + \frac{\sigma_n th^2}{4 A_{sc} E_{sc}} \qquad [2\text{-}3d]$$

$$\Delta_2 = \Delta_{bend} + \Delta_{axial} = \frac{\sigma_n th^4}{320 E_{sc} I_{sc}} + \frac{\sigma_n th^2}{4 A_{sc} E_{sc}} \qquad [2\text{-}3e]$$

$$\Delta_3 = \Delta_{bend} + \Delta_{axial} = \frac{\sigma_n th^4}{120 E_{sc} I_{sc}} + \frac{\sigma_n th^2}{4 A_{sc} E_{sc}} \qquad [2\text{-}3f]$$

$$\sigma_{\max} = \sum_{n=1}^{3} \sigma_n \qquad [2\text{-}4]$$

$$\sigma_{passive} = \frac{\upsilon_c \varepsilon_{cc}}{\frac{1}{E_{sc}} + \frac{(1-\upsilon_c)}{E_c}} \qquad [2\text{-}5a]$$

$$\upsilon_c = \upsilon_{co}\left[C_1\left(\frac{\varepsilon_{cc}}{\varepsilon_{cc}'}\right) + 1\right] \le 0.5 \qquad [2\text{-}5b]$$

$$C_1 = 1.914\left(\frac{\sigma_h}{f_{co}'}\right) + 0.719 \qquad [2\text{-}5c]$$

$$\sigma_{total}' = K\sigma_{total} \qquad [2\text{-}6a]$$

$$\sigma_{total} = \sigma_{passive} + \sigma_{active} \qquad [2\text{-}6b]$$

$$K = K_{dist} K_{eff} \qquad [2\text{-}6c]$$

$$K_{dist} = \frac{t}{s'} \leq 1.0 \qquad [2\text{-}6d]$$

$$K_{eff} = \frac{\left(h - 0.5s'\right)^2}{h^2} \qquad [2\text{-}6e]$$

$$f_{cc}' = f_{co}' \left[2.254 \sqrt{1 + \frac{7.94\sigma_{total}'}{f_{co}'}} - 2\frac{\sigma_{total}'}{f_{co}'} - 1.254 \right] \qquad [2\text{-}7a]$$

$$\varepsilon_{cc}' = \varepsilon_{co}' \left[1 + 5\left(\frac{f_{cc}'}{f_{co}'} - 1 \right) \right] \qquad [2\text{-}7b]$$

$$f_{cc} = \frac{f_{cc}' xr}{r - 1 + x^r} \qquad [2\text{-}8a]$$

$$r = \frac{E_{co}}{E_{co} - E_c'} \qquad [2\text{-}8b]$$

$$E_c' = \frac{f_{cc}'}{\varepsilon_{cc}'} \qquad [2\text{-}8c]$$

$$x = \frac{\varepsilon_{cc}}{\varepsilon_{cc}'} \qquad [2\text{-}8d]$$

where σ_n is the incremental (additional) collar pressure during the nth stage of the plastic analysis, F_i is the axial tension force in the collar during ith stage of the plastic analysis, t is the thickness of the collar beam element (along the column longitudinal axis), h is the length of the collar beam element and the column width, F_y and M_p are

the axial yield force and plastic bending moment of the collar element at the location where the next hinge will form during a specific analysis stage, C is a coefficient related to the elastic bending moment and is equal to 12 initially (stage $n=1$) , and eight after the first plastic hinge has formed (stage $n=2$ or $n=3$). M_i is the bending moment in the collar during ith stage of the plastic analysis. $\varepsilon_{lat\,n}$ is the average lateral strain at the end of each analysis stage, $\Delta_{n\,total}$ is the total collar deflection at the end of each analysis stage, which is calculated by adding deflections from previous analysis stages, Δ_i , to the deflection during the current stage, Δ_n, which itself includes components from bending, Δ_{bend} , and axial elongation of the adjacent sides, Δ_{axial}. E_{sc} is the secant modulus of the collar, I_{sc} and A_{sc} are the moment of inertia and cross-sectional area of the collar, respectively. $\sigma_{\max}$ is the maximum collar pressure that can be developed by that collar and the collar pressure remains constant at this maximum value as the collar beam element continues to deflect outward. This is the limit of the passive confining pressure the collar can provide to the concrete, $\sigma_{passive}$. ν_c is the secant Poisson's ratio of concrete at the applied axial strain, ε_{cc} is the axial strain for confined concrete. σ_h is the uniform confining pressure imposed on the concrete surface in the two directions orthogonal to the original uniaxial strain. E_c is the secant modulus of the concrete. ν_{co} and $\varepsilon_{cc}^{'}$ are the initial Poisson's ratio and strain at the peak stress of confined concrete. $f_{co}^{'}$ is the unconfined concrete material strength. $\sigma_{total}^{'}$ is the equivalent uniform confining pressure, which is calculated from the total confining pressure σ_{total} through the confinement efficiency factor K. σ_{active} is the active confining pressure due to bolt pretensioning. The confinement efficiency factor K involves a semi-empirical distribution factor that spreads the confinement stress at the collar level over the height of the column K_{dist}, which is related to the clear spacing of the collar, $s^{'}$, and the collar thickness, t. The factor K_{eff} provides a penalty to the confining pressure for areas of the column cross-section that are ineffectively confined where spalling takes place. A revised confinement effectiveness factor considering strain gradient effect factor as well may be included in this confinement efficiency factor if the column is not concentrically loaded. $f_{cc}^{'}$ is the peak stress of confined concrete, $\varepsilon_{co}^{'}$ is the unconfined concrete strain at peak stress, f_{cc} is the general value for confined concrete stress, and E_{co} is the initial concrete tangent modulus.

2.4 Column Rehabilitation Techniques

Column failures have caused the most significant failures of reinforced concrete structures. To prevent the column failure mechanism during earthquakes, columns should never be the weakest components in the whole structure. As a result, column rehabilitation is often critical to the seismic performance of a rehabilitated structure. Clearly, it would be desirable if speedy, economic, effective, and simple strengthening techniques were available. Practical methods available for strengthening existing

reinforced concrete columns include adding concrete jackets, steel jackets, FRP jackets, external prestressing wires, strands, or belts, and steel collars. Previous research on these rehabilitation techniques as applied to normal strength reinforced concrete columns under combined axial compression and lateral loading are reviewed in this section.

2.4.1 Concrete Jackets

Bett *et al.* (1988) tested three short columns under constant axial compressive load and reversed cyclic lateral loads. All three test specimens had a cross-section of 304×304 mm and an overall height of 912 mm, which gives an aspect ratio of 1.5, and were constructed with normal weight concrete and deformed reinforcement according to typical practice of column design in the 1950s and early 1960s. Two columns were strengthened with shotcrete jackets before testing. One specimen was strengthened with a shotcrete jacket only. The other, however, had the same basic shotcrete jacket plus longitudinal bars at each midface connected by supplementary cross ties inserted through drilled holes in the column and cemented with epoxy adhesive. The third column was repaired after being tested to failure. Test results showed that the specimen representing an existing column performed poorly under cyclic lateral deformations exceeding 0.5 percent drift. The rehabilitated specimens demonstrated improved behaviour. The modification of the rehabilitation through providing additional midface longitudinal bars in the jacket connected by cross-ties grouted with epoxy adhesive did not significantly affect the column's stiffness or strength under monotonic loading, but it did improve the stability of strength and stiffness response under cycles of reversed lateral displacement exceeding 2 percent drift.

Rodriguez and Park (1994) reported the results of an experimental study of the improvement in seismic behaviour of reinforced concrete columns repaired and/or rehabilitated by concrete jacketing. The tests consisted of both as-built control columns typical of those constructed prior to the 1970s and columns rehabilitated by concrete jacketing with added longitudinal and transverse reinforcement. The cross-section of the columns was 350×350 mm. A stub was present at the mid-height of each specimen to represent a portion of the beams oriented in the two perpendicular directions and the slab at the beam–column joint. The concrete jacketing consisted of a 100 mm thickness of additional reinforced concrete, with eight or 12 new longitudinal reinforcing bars and new square or octagonal transverse reinforcement. Results of the simulated seismic load tests showed that the strength and stiffness of the jacketed columns were as high as three times those of the as-built control columns, and very good ductility and energy dissipation were observed in the jacketed columns. However, this technique of rehabilitation was found to be labour-intensive and time-consuming.

Fukuyama *et al.* (2000) conducted tests of eight specimens to study the effectiveness of jacketing with reinforced concrete, steel plates or carbon fibre sheets in enhancing the shear strength and ductility of deficient columns. The overall column height of all specimens was 900 mm and the original cross-section was 350×350 mm. Two specimens represented the restored columns: one specimen was rehabilitated with a reinforced concrete jacket, and the cross-section was enlarged by the placement of high-fluidity

concrete and welded wire fabric; the other specimen was repaired by adding new longitudinal reinforcing bars along the buckled longitudinal reinforcing bars and adding steel plates along the perimeter of the column with the gap between the steel plate and original concrete grouted with high-fluidity concrete. Two specimens were rehabilitated by replacing the cover concrete with new concrete and shrinkage-compensating mortar. Both specimens were jacketed with steel plates along the perimeter of the original existing column, with two layers of carbon fibre sheets, and with preformed carbon fibre reinforced polymer (CFRP) plates and the gap between the preformed CFRP plates and column concrete was filled with shrinkage-compensating mortar. Cyclic shear force was applied to the column while the axial compressive load was kept constant at $0.3f_c^{'}A_g$. Test results demonstrated that the shear strength and ductility of the repaired columns can be restored to a performance level that exceeds that of the pre-damaged columns. The shear strength of columns having rehabilitated cover concrete with shrinkage-compensating mortar was restored back to the original performance level. The displacement ductility of jacketed columns with steel plates, carbon fibre sheets or preformed CFRP plates was enhanced substantially.

Takiguchi and Abdullah (2001) tested six columns with inadequate shear strength that had been rehabilitated with circular or square ferrocement jackets containing four to six layers of wire mesh. The cross-section of the specimens was 120×120 mm and 600 mm in overall height, with two end blocks. Cement slurry was used as infill mortar and for the ferrocement jacket. Constant axial compressive load and cyclic lateral load were applied to all the specimens. Test results indicated that all strengthened columns showed extremely stable and ductile response, regardless of the amount of axial compressive load and strengthening scheme.

2.4.2 Steel Jackets

Priestley *et al.* (1994a, 1994b) investigated the effectiveness of steel jackets for rehabilitating columns with inadequate shear strength. Eight circular columns with diameter of 610 mm and six rectangular columns with cross-section of 406×610 mm were constructed to simulate the critical moment-to-shear ratio of typical squat bridge columns. Columns were constructed with aspect ratio of 2 or 1.5. Circular jackets and elliptical jackets were used for rehabilitating the circular and rectangular columns, respectively. Both rehabilitated circular and rectangular columns were tested with steel jackets over the full length. All test specimens were subjected to a standard cyclic loading pattern, which consisted of an initial force-controlled stage, followed by displacment control after first yield of the longitudinal reinforcement was attained. The test results of 14 large-scale model columns under constant axial compressive load and cyclic shear in double curvature showed that the steel jacketed columns developed stable hysteresis loops with much higher load-carrying capacities and ductilities. Test results indicated that steel jacketing of circular columns by circular steel jackets, and of rectangular columns by elliptical steel jackets, was extremely effective in enhancing shear strength and flexural ductility of shear-deficient columns; the brittle shear failure that occurred in the as-built models, simulating the existing columns, was completely prevented by steel

jacket rehabilitation. Simple analytical shear strength models were developed based on the experimental results.

Aboutaha *et al.* (1996) investigated the use of rectangular steel jackets for strengthening typical building columns with inadequate lap splices designed and constructed in the 1950s and 1960s in the United States. A total of 11 large columns were tested including four as unrehabilitated control specimens. Six of the seven rehabilitated columns were rehabilitated with solid steel jackets, with and without adhesive anchor bolts used to stiffen the steel jacket and improve confinement of the splice, and the other column was rehabilitated with steel collars made of channel sections. The rectangular solid steel jackets were prefabricated in two L-shaped panels in plan and assembled around the column, and the ends of these two L-shaped panels were fillet welded together over the full height of the steel jacket. The steel collars were made of four C4×7.25 steel channels. The channels were connected at the column corners using half-inch diameter A325 bolts. The gap between the steel jacket or steel collar and the concrete column was filled with non-shrink cementitious grout. Anchor bolts were installed in pre-drilled holes in the concrete using an adhesive compound to connect the jacket to the concrete column. Anchor bolts were provided only on one side of the column rehabilitated with steel channel collars to assess their benefit. The following variables were examined: concrete strength, width of column, number and location of adhesive anchor bolts, spacing between adhesive anchor bolts, and height of steel jackets. The test results demonstrated that such columns can be effectively rehabilitated with thin rectangular steel jackets augmented by a small number of adhesive anchor bolts. Rehabilitated columns showed significant improvements in cyclic loading performance, but the column rehabilitated with steel channel collars experienced an early splice failure during the test, and ultimately showed only a small improvement in strength and ductility over the unrehabilitated column. Hence, no further tests were conducted on steel channel collars. Design recommendations were proposed to rehabilitate the lap-splice deficient columns with rectangular steel jackets based on these test results and a simple analytical model.

Xiao and Wu (2003) proposed using partially stiffened steel jackets to rehabilitate square or rectangular reinforced concrete columns. Five one-third scale model columns were tested under a constant axial compressive load of $0.3f_c^{'}A_g$ and cyclic lateral force in a double-curvature condition. All the columns had an overall height of 1016 mm with a cross-section of 254×254 mm and aspect ratio of 2. The reinforcement details simulated existing columns built based on pre-1971 design codes. Four of the five columns were rehabilitated using partially stiffened steel jackets. To rehabilitate an existing column, relatively thin steel plates were welded to form a rectilinear jacket for shear strength enhancement, and additional confinement elements (stiffeners) with various configurations were welded to the potential plastic hinge regions at the column ends to ensure a ductile behaviour. From the tests, the rehabilitation method was found to be very effective for improving the seismic behaviour of existing deficient columns. All three model columns rehabilitated by rectilinear steel jackets with stiffeners developed excellent hysteretic behaviour with ultimate drift ratios exceeding 8%. However, the specimen rehabilitated with a welded steel jacket without stiffeners for shear strength enhancement was not able to develop satisfactory ductility.

Saiidi *et al.* (2004) conducted four 0.3-scale model column tests on a shake table. One specimen represented an as-built control column and the other three were rehabilitated with jackets, of which one was fabricated with steel, one with glass fibre reinforced polymer (GFRP), and the third with carbon fibre reinforced polymer (CFRP). The cross-section of all columns was an irregular octagon, with constant width and variable depth over the flares (*i.e.*, tapered columns). The cross-section of the oval steel jacket varied along the height to follow the column profile. The space between the jacket and the original column was filled with a high-strength and low-shrinkage pressurized grout The GFRP and CFRP fabrics were installed directly onto the columns and followed the column shape. Then, a thin layer of epoxy was applied to the fabrics. The jacket thickness was designed to resist the difference between the shear demand and the original column capacity using the provisions of the U.S. Federal Highway Administration Rehabilitation Manual (FHWA 1995) assuming a 45° shear crack angle. The behaviour of the column rehabilitated by a steel jacket was compared with those of the two columns rehabilitated by FRP jackets and the as-built control column. Test results indicated that all the jackets accomplished their primary goal of enhancing the shear strength and the displacement ductility capacity of the columns. The jackets changed the mode of failure from shear/flexural failure to flexural failure. The seismic performance of the steel-jacketed column was similar to that of the columns with FRP jackets.

2.4.3 FRP Jackets

Advanced composite materials have been applied to the rehabilitation of reinforced concrete columns due to the many advantages of the material, such as light weight, and high stiffness and strength-to-weight ratios. The concept of confinement systems utilizing FRP materials was first developed in Japan during the early 1980s as a structural rehabilitation alternative to steel systems. Later using carbon fibres and epoxy resin as the FRP constituents, rehabilitation applications extended for building and bridge columns, and chimneys. Several composite jacketing and wrapping systems have been developed and validated in laboratory or field conditions.

Priestley and Seible (1995) reported an experimental investigation of circular and rectangular columns rehabilitated with fibreglass/epoxy composite jackets. The column cross-section was 610 mm diameter or 730×489 mm, with aspect ratios ranging from 1.5 to 2.0. Test results showed that the composite material bonded to the external surfaces of columns, with the fibres running primarily in the transverse direction, provides a similar action to internal transverse reinforcement in restraining the opening of diagonal tension cracks and hence in enhancing shear strength. Rehabilitated columns maintained stable hysteresis behaviour up to much higher ductility levels than achieved for as-built control columns. A model of shear enhancement provided by composite material jackets was developed. In the experimental program, one of the as-built circular columns that had previously been tested and had failed in shear was repaired and re-tested to investigate the feasibility of repairing the badly damaged columns with composite material jackets. The repaired column was able to maintain its strength with a larger ductility level than that of the original column.

Xiao and Ma (1997) investigated a prefabricated composite jacketing system for rehabilitating reinforced concrete columns. The rehabilitation system consists of a series of prefabricated E-glass fibre reinforced composite cylindrical shells with slits. When a column was rehabilitated, the shells were opened and clamped around the column in sequences with their slits staggered. Adhesive was applied to bond the shells to each other and to the column to form a continuous jacket. Three half-scale model columns with a diameter of 610 mm and an overall height of 2440 mm were tested with aspect ratio of 2. One was tested under the as-built condition and two others were tested after being rehabilitated using prefabricated composite jacketing. Constant axial compressive load and cyclic horizontal load were applied to the model columns. Test results indicated that rehabilitated columns demonstrated improved behaviour over that of the as-built column. The researchers reported that using prefabricated composite jacketing can delay the failure, significantly improve the hysteretic response, and increase displacement ductility.

Xiao *et al.* (1999) tested three half-scale circular columns under cyclic shear in double curvature and constant axial compressive load to study the rehabilitation effectiveness of two similar prefabricated composite jacketing methods for enhancing seismic shear resistance of short circular columns. All specimens had the same cross-section of 610 mm diameter and were 1830 mm tall with two end blocks, hence with aspect ratio of 1.5. All specimens were subjected to a number of lateral cyclic loads while the axial compressive load was maintained constant. The test results validated the rehabilitation design approach proposed by the research. The full-height prefabricated glass fibre reinforced composite jackets prevented completely the shear failure and converted the poor hysteretic behaviour as observed for the as-built column into a ductile and stable performance. The difference of the response between the individual shell jackets and the continuous shell jacket was small. Besides improving the hysteretic performance and ductility, the use of prefabricated composite jacketing for rehabilitating existing columns did not have much influence on the stiffness, nor did it cause a dramatic enhancement in the flexural strength of the columns.

Ma *et al.* (2000) conducted a full-scale test of a parking structure column rehabilitated with carbon fibre reinforced composites under constant axial compressive load and cyclic shear force and moment. The column had a 410×410 mm cross-section and an overall height of 2340 mm, giving an aspect ratio of 2.875 due to the double-curvature condition. The rehabilitated column developed a stable flexural behaviour with excellent ductility and energy dissipation capacity. Premature failure due to brittle shear failure or lap-splice degradation was prevented through the rehabilitation.

Li and Sung (2003, 2004) tested three 0.4-scale reinforced concrete circular bridge columns that were 1750 mm in overall height and 760 mm in diameter with aspect ratio of 2.3. The columns were rehabilitated with carbon fibre reinforced composite jacketing. A constant axial compressive load of $0.147 f_c' A_g$ and cyclic horizontal load were applied to the cantilever columns. Test results showed that the rehabilitation significantly improved the seismic performance of the reinforced concrete columns in terms of

strength, ductility and energy dissipation capacity. The failure mode of the column changed from shear failure to flexural failure since composite jacketing enhanced the shear capacity significantly.

Galal *et al.* (2005) tested seven reinforced concrete short columns under combined cyclic lateral load and constant axial compressive load, rehabilitated with CFRP or GFRP jackets. The cross-section of all the specimens was 305×305 mm, and the overall height was 915 mm. The aspect ratio was 1.5 and nominal conrete compressive strength was 25 MPa. Test results showed that anchoring of the FRP jackets to the columns was very effective in increasing the shear strength and energy dissipation capacity of the short columns.

2.4.4 External Prestressing

Frangou *et al.* (1995) investigated a rehabilitation technique involving post-tensioning metal strips around the column (by using standard strapping machines used in the packaging industry) and subsequently securing them in place by metal clips. Two groups of tests were conducted including 18 cylindrical specimens of 100 mm diameter and 200 mm in height tested axially in compression, and 28 prisms of 100×100 mm cross-section and 200 mm in overall length tested in bending. Test results demonstrated that this simple and economical technique was successful in effectively strengthening the specimens and preventing brittle shear failure.

Budek *et al.* (2002) tested nine model concrete bridge columns using prestressing strand as transverse reinforcement. Five of these columns with an aspect ratio of 2.0 were tested quasi-statically to examine shear behaviour at two axial compressive load levels and incorporating either single-wire or seven-wire transverse reinforcement. The observed response of the tested columns indicated that more stable and enhanced strength and ductility can be attained as compared with conventionally reinforced columns. Energy dissipation capacity was also improved. Moderate volumetric ratios of high-strength wire provided satisfactory performance under shear-critical conditions.

Saatcioglu and Yalcin (2003) investigated external prestressing of reinforced concrete columns for improved seismic shear strength. This technology consists of external prestressing of columns in the transverse direction by means of individual hoops that consist of prestressing strands and specially designed anchors. Seven full-scale columns were tested under constant axial compressive load and incrementally increased lateral displacement reversals. The columns had either a circular section with a diameter of 610 mm or a square section with a cross-section of 550×550 mm. The aspect ratios were 2.43 and 2.70 for circular and square columns, respectively. The columns were designed to represent pre-1970s design practice. Two columns were tested without any rehabilitation and were used as control columns. One square and four circular columns were rehabilitated by external prestressing prior to testing. This technique provided active and passive lateral confinement against the lateral expansion of the concrete under compression. It also provided a clamping force in reinforcement splice locations to improve the bond between the steel and concrete. In shear-critical columns, transverse

prestressing must be overcome before the concrete can develop diagonal tension caused by the shear; thereore, prestressing improved the shear resistance of the column. The tests demonstrated significant enhancement in lateral drift capacity: from 1% in shear-critical control columns up to 5% in rehabilitated columns. The results showed that the seismic rehabilitation strategy by external prestressing was very effective in enhancing the seismic behaviour of the existing reinforced concrete columns.

Nesheli *et al.* (2004) proposed a new seismic rehabilitation technique through prestressed external aramid fiber belts. Five shear-critical reinforced concrete square columns with an aspect ratio of 1.5 (750 mm in overall height and 250 mm in depth with two stubs at the top and bottom of the column) and inadequate steel hoops were rehabilitated and tested under reversed cyclic lateral load and constant axial compressive load. The aramid fiber belts used were two-ply, where each ply had a width of 17 mm, a thickness of 0.612 mm, and a cross-sectional area of 10.4 mm^2. Two values of spacings of aramid fibre belts (200 mm or 65 mm), and two levels of prestressing (half or one-third of the tensile strength of the aramid fiber material) were considered in the experimental program. Test results showed that the proposed rehabilitation technique was a highly effective rehabilitation method for reinforced concrete columns with inadequate shear resistance or poor bond strength. Brittle shear failure was prevented while energy dissipation capacity and displacement ductility were improved.

2.4.5 Steel Collars

Hussain and Driver (2001, 2003, 2005a, 2005b) conducted experimental and analytical research on collared columns under concentric axial loading, as well as under axial and flexural-dominant lateral loading. Eleven square columns (300×300×1500 mm) were tested under concentrical loading, consisting of two control columns with conventional internal transverse reinforcement (with either closely or widely spaced transverse hoops) and nine rehabilitated collared columns with external hollow structural section (HSS) collars. All eleven columns had the same longitudinal reinforcement details, but the nine collared columns were intentionally designed not to have internal transverse reinforcement in the test region. Different collar sizes and spacings were studied as well as two different collar corner connections (bolted or welded). As shown in Table 2-1, the peak load and peak strain of collared columns were greatly enhanced from the control columns with conventional internal transverse reinforcement. Experiments showed that collared columns exhibited significant improvement over the control columns in terms of strength and ductility due to the confinement provided through external collars. The performance of the collared columns was also investigated under combined axial and cyclic lateral loading. Nine columns (300×300×2100 mm; with aspect ratios of 2.5 and 6.3) were tested under constant axial compressive load and reversed cyclic lateral load, with five cycles being applied at each displacement level. Among the nine columns, one was a control column with conventional internal transverse reinforcement, while the other eight were rehabilitated columns with external welded HSS collars and no internal transverse reinforcement in the test region. The effects of collar spacing, collar size, axial compression index, and aspect ratio were studied. As shown in Table 2-2, the peak moment and peak drift of collared columns were greatly enhanced from the control

column with conventional internal transverse reinforcement. All the collared columns exhibited more ductile behaviour under severe cyclic loading than the control column. Less concrete spalling was observed during the test of the collared columns than for the control columns. Stable hysteresis loops with significant energy dissipation were obtained for collared columns. Columns with the larger aspect ratio had improved strength retention, energy dissipation, and ductility. The rehabilitation method was shown to be effective and benefits in both strength and ductility were demonstrated.

The external steel collars used in the research conducted by Hussain and Driver (2005b) were fabricated from hollow structural sections. A relatively simple alternative fabrication technique was developed to use solid steel collars cut from plates, as shown in Figure 1-3. Chapman and Driver (2006) studied reinforced concrete columns under concentric and eccentric axial loading rehabilitated with solid steel collars and obtained significant enhancement results in both strength and ductility compared to control columns without collars. A total of 14 square columns (300×300×1500 mm) were tested under axial compressive loading, with seven columns being loaded eccentrically. The same arrangement of internal reinforcement as used by Hussain and Driver (2005b) was maintained in this experimental program in order to facilitate direct comparisons. Four different collar spacings, two different collar sizes, two different end conditions, three different pretension levels in the collar bolts, and four different eccentricities were studied, as shown in Table 2-3. Columns with external collars showed significant improvements in both strength and ductility compared with conventionally reinforced columns through the development of passive confining pressure, as shown in Figure 2-1. Eccentrically loaded specimens generally had lower axial strength enhancement than equivalent concentrically loaded specimens, as shown in Table 2-3.

2.5 Numerical Analysis

Most of the studies on the shear behaviour of reinforced concrete columns reported in the literature are based on either experimental results and/or empirical formulae. There appears to be relatively fewer finite element analysis-based investigations. Reported in this section is a partial summary of the research using the finite element analysis approach for examining the behaviour of reinforced concrete columns, specifically pertaining to columns with normal strength concrete likely to show shear-dominant behaviour under combined axial and lateral loading.

Ignatakis *et al.* (1989) conducted parametric analyses of reinforced concrete short columns under axial and shear loading using the finite element method. A finite element program RECONFIN was developed for the analytical representation of the nonlinear behaviour of concrete, steel reinforcement, and their mechanical interaction up to failure. Triangular elements were used for the concrete, while the steel reinforcement was represented by one-dimensional elements connected to the concrete elements with nonlinear linkage spring elements. A smeared cracking model was used with the nonlinear two-dimensional incremental constitutive law for concrete. Four main parameters that influence the behaviour were studied: aspect ratio, magnitude of the axial compressive load, concrete strength, and relative amounts of longitudinal and transverse

reinforcement. Twelve models of columns were analyzed and reported, and the relatively accurate modelling indicated the reliability of the analytical tool. It emphasized that short columns should be avoided if possible, especially in seismic areas, due to the explosive diagonal cracking observed experimentally and analytically, and because design and detailing procedures so far have not been able to provide adequate ductility and energy dissipation capacity to short columns. However, the analysis can only simulate the response up to failure without post-peak response.

Chung and Ahmad (1995) developed a nonlinear finite element model to predict the complete load–deflection response of shear-critical reinforced concrete members. The nonlinear finite element model employed a biaxial stress–strain constitutive relationship for concrete based on an equivalent uniaxial approach and a simplified bilinear stress-strain relationship for the reinforcing steel. The deflection incremental approach based on the secant stiffness was used. Numerical predictions were evaluated against some experimental results and showed good agreement, including the post-peak displacement-softening behaviour. Simulation of shear behaviour of columns was not reported although the shear behaviour of some available deep beam experiments was used to verify the model.

Lee *et al.* (1999) reported simulations of cyclically loaded reinforced concrete columns using the finite element program FEAP, where a plastic-damage concrete constitutive model and a steel model including the constitutive relations of isotropic and kinematic hardening, and Baushinger effect, are used along with a bond-slip model. The plastic-damage concrete constitutive model includes material hardening and softening, stiffness degradation and stiffness recovery on crack closing. The numerical simulation of a single column test specimen under cyclic horizontal displacement and constant vertical force loads showed good results compared to the experimental results. However, the two damage variables included in the plastic-damage model, one for tensile damage and the other for compressive damage, are difficult to obtain without proper experimental data.

Parent and Labossière (2000) presented a finite element analysis study of reinforced concrete columns confined with composite materials based on the use of a bar element by considering the global constitutive law. All the constituents of the reinforced concrete column confined with composite materials were included in the global constitutive law. After calculation of the strain at any point on the section using the global constitutive law in the integration process of the stiffness matrix, stress can be calculated using the individual stress–strain relationship of the material, and the failure load can be obtained. However, the model only predicted the ultimate load under a constant axial force and the lateral displacement. The post-peak response and neither second-order effects nor damage models were included.

Maekawa and An (2000) conducted finite element analyses of the shear failure and ductility of reinforced concrete columns using the WCOMD-SJ finite element code. The smeared crack approach, including distributed fixed multi-directional cracks, was adopted. The reinforced concrete model was developed by combining the constitutive law of concrete and that of reinforcement, consisting of tension stiffness, compression and a

shear transfer model. The analytical simulation was verified to be able to estimate the failure with reasonable accuracy when the expected failure mode is shear. The concrete exhibits different post-cracking nonlinearity in both tension and shear at different parts of the member, however, and shows brittleness when located in zones without reinforcement. Hence, it was concluded by the researchers that any finite element model should include both the reinforced concrete and plain concrete zone without reinforcement, which increased the complexity in formulating the model.

Bentz (2000) developed the nonlinear sectional analysis program Response 2000, which incorporates the MCFT relationships. Response 2000 is a program providing a layered sectional analysis to determine the shear stress distribution throughout the cross-section and to obtain the behaviour of reinforced concrete elements subjected to shear. The program accepts any cross-section that is subjected to any combination of axial load, moment or shear. It also includes a method to integrate the sectional behaviour for simple prismatic beam segments to obtain full-member behaviour. One of the assumptions embedded in the program is that plane sections remain plane. While it is a reasonable assumption for relatively slender members, it is not so accurate for short span members where a direct load-carrying strut may exist. It can calculate an entire moment–shear interaction diagram for a cross-section. The program can also evaluate the load–deflection properties and anticipated cracking for members.

Bentz (2001) used two implementations of the Modified Compression Field Theory (MCFT) to model the behaviour of six shear-dominant reinforced concrete columns tested at the University of California at San Diego (UCSD): the finite element program TRIX97 (Vecchio 1989) and the sectional analysis program Response 2000. The finite element program, uses a secant stiffness based approach in the element principal direction to determine the element stiffness matrix, and iteration approach was adopted to generate convergence. The finite element program underestimated the displacement characteristics, though produced a good estimate of the failure load. The Response 2000 software, discussed in Section 2.3, gave conservative results due to the lack of compatibility between cross-sections, which prevented redistribution of the compression.

Dowell and Parker (2001) performed finite element analyses of the as-built and seismically rehabilitated reinforced concrete bridge columns tested at UCSD using the general-purpose finite element program ABAQUS (HKS 1996) along with ANACAP-U (ANATECH 1997) concrete and steel material models. Concrete was modelled as a three-dimensional continuum with strain-hardening and softening as well as tension cut-off. A fixed angle smeared crack approach was adopted. It also considered the reduction of shear stress accumulation and shear stiffness through shear shedding and lowering the initial shear modulus. Although the analysis showed similar failure mode and shape of the load-displacement response as the tests, only 77% to 83% of the maximum measured shear force level was attained in the simulation, probably due to the fixed orthogonal crack angles adopted in the concrete plasticity model.

Hussain and Driver (2001) conducted a finite element study of the strength and ductility of externally confined rectangular and square concrete columns using the program

ABAQUS/Standard. Eight-node continuum elements with reduced integration were used for the concrete. Both vertical reinforcement and the ties, when present, were modelled by two-node three-dimensional truss elements. The collars were modelled using two-node beam elements with six degrees of freedom at each node. The external confining beam elements were not connected to continuum elements directly but instead through the introduction of truss element outriggers. The concrete material model used a smeared crack approach with tension stiffening based on fracture energy cracking criteria. The compressive material curve used in the analyses for the concrete included a straight line descending branch. The concrete material model consists of an isotropically hardened yield surface which is active when the stress is dominantly compressive and an independent "crack detecting surface" which determines if a point fails by cracking. The model was found to be reasonably accurate through verification studies based on their testing program, although in most cases the failure mode was primarily flexural.

Ožbolt and Li (2001) carried out finite element analyses of the benchmark columns tested at UCSD with the special purpose finite element code MASA, a finite element code based on the microplane model and a smeared crack concept. The analysis uses an incremental iterative solution procedure based on the constant initial or secant stiffness matrix approaches. Eight-node brick elements were used for concrete with reinforcement represented by truss or beam elements. Perfect bond between reinforcement and concrete was assumed. Monotonic pushover analyses and cyclic loading analyses were conducted. The comparisons of the analytical results with the experimental data show that the model can predict the observed failure mechanism with good agreement. Some numerical problems encountered, however, made it difficult to exactly reproduce the load-displacement response and decreased the computational efficiency.

Girard and Bastien (2002) used the finite element program CLEF to analyze reinforced concrete columns under cyclic loads. Three-dimensional three-node bar elements were used for reinforcement with an elasto-plastic constitutive law and positive hardening. Concrete was modelled with three-dimensional 20-node solid elements. The concrete constitutive law consists of a hypoelastic model, with consideration of loading path and stress history-dependent material properties. The concept of an equivalent uniaxial stress-strain relationship was adopted and compression and tension softening were included, taking into account of the compressive strength of concrete and the confinement level. The steel-concrete interface was also considered using a special bar element in some cases. While the nonlinear finite element simulation compared well against the experimental results, one of the modeling difficulties, as pointed out by the authors, was the choice of the parameter value for the interface constitutive law which must be obtained through specific testing.

Lee and Elnashai (2002) performed inelastic seismic analysis of reinforced concrete bridge piers using the finite element analysis program ADAPTIC, including flexure-shear-axial interaction. Strain hardening of reinforcement was taken into account in the constitutive relationships. A modified stress-strain relationship for concrete in compression was derived that included the confinement effect. Test specimens of short square columns dominated by shear were used to verify the finite element model and

showed good agreement. However, the shear stiffness transition model needed for the development of the shear-axial interaction was related to the axial force level and shear deformation and, hence, was difficult to obtain.

Parvin and Wang (2002) proposed a highly complex nonlinear finite element model for FRP jacketed circular columns to study the behaviour under combined axial and cyclic lateral loadings. The nonlinear FEA software MARC was used. The concrete was modelled with three-dimensional eight-node brick elements. The nonlinear behaviour of the confined concrete material was simulated by employing the Mohr-Coulomb yield criterion combined with an isotropic hardening rule. The steel bars were modelled with three-dimensional truss elements. The FRP jacket was modelled as three-dimensional thin shell elements. Perfect bond between reinforcement and concrete was assumed. Both monotonic and cyclic loading were considered in the modelling. Validations of the proposed numerical models with columns tested have been conducted and showed good correlation.

Yamakawa *et al.* (2004) carried out nonlinear analyses of reinforced concrete columns using a fibre model considering both flexural displacement and shear distortion. The flexural deformation is based on a conventional fibre model. The shear model, however, is based on an explicit definition of the shear force–distortion relationship of a reinforced concrete member, consisting of a concentrated translational spring of zero dimensions located at each member end. The relationship between the lateral displacement and shear force of the column was obtained by combining the flexural deformation and shear distortion. However, due to the nonlinearity, repeated calculations are needed to achieve convergence.

2.6 Codified Shear Strength of Reinforced Concrete Columns

The models discussed in this section deal with monotonic load only and do not decrease shear strength with extra displacement ductility. The ACI code presents two sets of equations for calculating the sectional shear strength of reinforced concrete. These are herein categorized as the simplified method and the detailed method. The ACI 318-05 sectional design approach for shear is based on a parallel chord truss model with constant 45° inclination diagonals supplemented by a concrete contribution. For non-prestressed members subject to axial compression and shear reinforcement perpendicular to the axis of member, the SI equivalent equations in ACI 318-05 are shown below:

ACI 318-05 Simplified Method:

$$V_n = V_c + V_s \qquad [2\text{-}9a]$$

SI equivalent equation of ACI 318-05 Eq. 11-4:

$$V_c = 0.167\left(1 + 0.0725 P_u / A_g\right)\sqrt{f_c'}\, b_w d \qquad [2\text{-}9b]$$

ACI 318-05 Eq. 11-15:

$$V_s = \frac{A_v f_y d}{s} \qquad [2\text{-}9c]$$

ACI 318-05 Detailed Method:

$$V_n = V_c + V_s \qquad [2\text{-}10a]$$

SI equivalent equation of ACI 318-05 Eq. 11-5:

$$V_c = \left(0.158\sqrt{f_c'} + 17.2\rho_w \frac{V_u d}{M_m} \right) \cdot b_w d \qquad [2\text{-}10b]$$

SI equivalent equation of ACI 318-05 Eq. 11-7:

$$V_c \le \left(0.29\sqrt{f_c'} \cdot \sqrt{1 + 0.29 P_u / A_g} \right) \cdot b_w d \qquad [2\text{-}10c]$$

ACI 318-05 Eq. 11-15:

$$V_s = \frac{A_v f_y d}{s} \qquad [2\text{-}10d]$$

where (ACI 318-05 Eq. 11-6):

$$M_m = M_u - \frac{P_u (4D - d)}{8} \qquad [2\text{-}10e]$$

where V_n is the nominal shear strength, V_c is the shear contribution from the concrete, V_s is the shear contribution from the shear reinforcement, P_u is the factored axial compressive load, A_g is the gross cross-sectional area, f_c' is the compressive strength of the concrete, b_w is the effective width of the section, d is the distance from the extreme compression fibre to the centroid of the longitudinal tension reinforcement, A_v is the total cross-sectional area of the shear reinforcement within a distance s of the critical section, f_y is the yield stress of the shear reinforcement, s is the spacing of the shear reinforcement, ρ_w is the reinforcement ratio of the longitudinal tension reinforcement, V_u and M_u are the factored shear force and moment at the critical section, M_m is the modified moment calculated from Eq. 2-10e, and D is the overall depth of the cross-section.

Many empirical formulae have been proposed for shear strength, typically based on experimental study of the shear behaviour of the reinforced concrete members. With respect to the various empirical formulae, considerable differences exist as a result of the uncertainty in assessing the influence of complex parameters in a simple formula, and the relatively poor representation of some parameters in limited test data. These issues limit the validity of empirical formulas and increase the necessity for rational models and theoretically justified relationships. To this end, Vecchio and Collins (1986) proposed a modified compression field theory (MCFT) to include a rationale for determining the tensile stresses in the diagonally cracked concrete with variable strut inclination of the truss model.

MCFT (Vecchio and Collins 1986) treats the cracked concrete as a new type of concrete material with its own stress–strain characteristics related to the original concrete and reinforcement characteristics. It takes into account the overall load–deformation responses of elements by considering uniaxial tension response of the reinforcement with a bilinear stress–strain constitutive law and the tension or compression response of the concrete in the direction of the corresponding principal stresses and principal strains. Principal stresses and strains are assumed coincident, and transformation between member axes and principal axes directions are made according to Mohr's circle. In the MCFT, the compressive response of cracked concrete is affected by the magnitude of the principal tensile strain in the perpendicular direction. The equilibrium equations, compatibility relationships, and constitutive relationships are formulated in terms of average stresses and average strains over a length which includes several cracks. Variability in the angle of inclination of the compression struts and the strain-stiffening effects are taken into consideration, as well as the tensile stress of the concrete. Tensile strength of concrete is an important aspect during the development of cracking. In turn, it is important for the prediction of deformations and the durability of concrete. Other characteristics such as bond between reinforcement and concrete, the concrete contribution to the shear and torsion capacities are also closely related to the tensile strength of concrete. Concrete in tension is assumed to be linear–elastic until cracking occurs, after which the average tensile strength decays as a function of the cracking strength and the tensile strain. Local stress conditions at crack locations are also considered in the model, including the maximum interface shear stress capacity due to aggregate interlock.

MCFT is capable of predicting the response of reinforced concrete elements subjected to shear and axial loads, and this more rational unified approach has been adopted in a number of codes and standards for the shear design provisions. The shear design equations stipulated in both CSA-A23.3-94 and CSA-A23.3-04 are based on MCFT and provide both a simplified and a general method of shear design. The major difference between the simplified method and general method is the way that the shear carried by the concrete is calculated. CSA-A23.3-94 gave tabular values to the parameters to calculate the shear carried by concrete, and the simplified method has no direct relationship with the general method. In CSA-A23.3-04, the general method adopts a unified continuous equation to calculate the shear carried by the concrete, and the simplified method is directly derived from the general method with some logical

assumptions (Bentz and Collins 2006). An iterative solution technique may be required to obtain the response of sections subject to shear, bending, and axial load using the general method in CSA-A23.3-04.

CSA-A23.3-04 Clause 11.3 includes the general and simplified approaches for the shear contribution. The nominal shear strength (of a non-prestressed member) can be obtained through the following general form:

$$V_n = V_c + V_s = \beta\sqrt{f_c'}\,b_w d_v + \frac{A_v f_y d_v \cot\theta}{s} \qquad [2\text{-}11a]$$

A23.3-04 Eq. 11-11:

$$\beta = \frac{0.40}{(1+1500\varepsilon_x)} \cdot \frac{1300}{(1000+s_{ze})} \qquad [2\text{-}11b]$$

A23.3-04 Eq. 11-12:

$$\theta = 29 + 7000\varepsilon_x \qquad [2\text{-}11c]$$

A23.3-04 Eq. 11-13 for nonprestressed member:

$$\varepsilon_x = \frac{M_f/d_v + V_f + 0.5P_f}{2E_s A_t} \qquad [2\text{-}11d]$$

where V_n is the nominal shear strength, V_c is the shear contribution from the concrete, V_s is the shear contribution from the shear reinforcement, β is a factor accounting for shear resistance of cracked concrete, f_c' is the compressive strength of the concrete, b_w is the effective width of the section, d_v is the effective shear depth, A_v is the total cross-sectional area of the shear reinforcement, f_y is the yield stress of the shear reinforcement, θ is the direction of the average principal compression with respect to the longitudinal axis, s is the longitudinal spacing of the shear reinforcement, ε_x is the longitudinal strain calculated at the mid-height of the cross-section resulting from the direct shear force, axial force, moment, and prestressing force, if applicable, s_{ze} is the effective crack spacing related to the basic crack spacing and coarse aggregate sizes, E_s is the modulus of elasticity of reinforcement, and A_t is the area of non-prestressed tension reinforcement.

The equivalent crack spacing parameter, s_{ze}, is taken as 300 mm for sections containing at least the minimum shear reinforcement. Otherwise, it is computed from $s_{ze} = \frac{35 s_z}{15 + a_g}$,

where s_z is the crack spacing parameter, taken as d_v or as the maximum distance between layers of distributed longitudinal reinforcement, whichever is less, and a_g is the maximum aggregate size.

CSA-A23.3-04 Clause 11.3.6.3 outlines the simplified method that can be used for cases where the specified yield strength of the longitudinal steel reinforcement does not exceed 400 MPa and the specified concrete strength does not exceed 60 MPa. In these cases, θ can be taken as 35° and β as 0.18, for sections containing at least the minimum shear reinforcement. β should be calculated from $\beta = (230)/(1000 + d_v)$ for other cases.

CSA-A23.3-04 includes the provisions for strut-and-tie model, with details on proportioning the strut, ties, and node regions. ACI 318-05 also provide an appendix on strut-and-tie models. Structural members can be divided into portions called B-regions and D-regions, with the term B standing for "beam" or "Bernoulli" and the term D standing for "discontinuity," "disturbance," or "details." The axial strain distribution in the cross-section of a B-region is linear and the beam can be designed using sectional analysis with conventional flexural theory with the plane section assumption. The plane section assumption of flexural theory is not good where linear distribution of axial strains is a poor assumption. Marti (1985), Schlaich *et al.* (1987), and Collins and Mitchell (1997) extended the uniformly inclined diagonals truss model to strut-and-tie models that can be applied to D-region design. A strut-and-tie model consisting of concrete compression struts, steel tension ties, and nodal zones can be used to simulate the behaviour of D-regions, where the strain distribution is significantly nonlinear along the depth of the cross-section. This approach allows the designer to develop an understanding of the loading transfer behaviour of reinforced concrete columns in addition to predicting the ultimate capacity. The D-region is normally assumed to extend one member depth each way from the discontinuity according to St. Venant's principle, which suggests that localized effect of a disturbance will be diminished over a distance about one member depth away from the disturbance.

A strut-and-tie model is a system of forces in equilibrium with a given set of loads, which provides a lower bound estimate of the strength of the structure according to the lower bound theorem of plasticity. Although many models can be constructed that meet the equilibrium requirements, according to MacGregor and Bartlett (2000), the model with the fewest and shortest ties is the best. The loads will try to follow the path involving the fewest forces and resulting in the least deformation, since the tensile ties are more deformable than the compression struts. Crack patterns may also assist in selecting the best strut-and-tie model since the compression strut will roughly follow the compressive stress trajectory or the crack direction.

2.7 Other Shear Strength Models

Besides the design practices documented by the codes and standards, there exist many empirical shear models derived from experimental research. Shear strength models have been proposed by researchers mostly based on experimental studies on reinforced

concrete members. Several recent models have incorporated some prominent features such as the concept of shear strength degradation with increasing ductility demand. Instead of assigning a fixed quantity to the concrete contribution, those models typically introduce an equation derived from experimental observations that reflects the fact that the concrete contribution to the shear capacity degrades with increasing deformation ductility. The positive performance-enhancing capabilities of steel or FRP confinement systems have also been documented in experimental and analytical studies conducted in the past. A brief summary of the prominent shear strength models for normal strength reinforced concrete columns under combined axial compression and lateral loading are presented in this section.

2.7.1 Ghee *et al.* (1989)

Ghee *et al.* (1989) conducted tests on 25 small-scale short circular columns under axial load and cyclic lateral inelastic displacement. Test results showed that existing design equations were conservative for initial shear strength. They also indicated that the shear strength depends on the axial load level, the column aspect ratio, the amount of shear reinforcement, and the flexural displacement ductility factor. A model considering the influence of flexural ductility on shear strength was proposed to calculate the initial shear strength applicable for low flexural ductility and final shear strength applicable for ductile flexural designs. The shear capacity model equation takes the following form:

$$V_i = V_{ci} + V_{si} = 0.37\left(\frac{2}{M/(VD)}\right)\left(1+3\frac{P}{f_c' A_g}\right)\sqrt{f_c'}\cdot A_e + \frac{\pi}{2}A_h f_{sh}\frac{D'}{s} \qquad [2\text{-}12a]$$

$$V_{df} = V_{cf} + V_{sf} \qquad [2\text{-}12b]$$

where

$$V_{cf} = 18.5\rho_v\sqrt{f_c'}\cdot A_e \le 0.185\sqrt{f_c'}\cdot A_e \qquad [2\text{-}12c]$$

and

$$V_{sf} = \frac{\pi A_h f_y D'}{2s}\frac{\sqrt{1-\psi'}}{\psi'} \le \frac{2.15\pi A_h f_y D'}{2s} \qquad [2\text{-}12d]$$

$$\psi' = \frac{\rho_v f_y}{\xi f_c'} \qquad [2\text{-}12e]$$

where V_i is the initial shear strength, V_{ci} and V_{si} are the shear forces carried by the concrete shear-resisting mechanism, V_c, and the truss mechanism involving shear reinforcement, V_s, at a displacement ductility, μ, less than 2, M and V are the moment

and shear force at that section, D is the gross column diameter, P is the axial load on the column, f_c' is the cylinder compressive strength of concrete, A_g is the gross cross-sectional area of the column, A_e is the effective shear area that can be taken as $0.8A_g$, A_h is the area of the hoop or spiral bar, f_{sh} is the stress in the hoop or spiral reinforcement, D' is the diameter of the confined core, s is the spacing of the hoops or the pitch of the spiral reinforcement along the longitudinal axis, V_{df} is the final shear strength at a high displacement ductility, μ, V_{cf} and V_{sf} are equivalent to V_{ci} and V_{si} but at a high displacement ductility, μ, ρ_v is the volumetric ratio of hoop or spiral reinforcement to core volume, f_y is the yield strength of the hoop or spiral reinforcement, ψ' is a mechanical reinforcement ratio defined by Eq. 2-12e, ξ is a reduction factor for effective compressive strength of the diagonal compression strut that accounts for the influence of flexural ductility, with a value of $\xi = 0.2$ at a ductility of $\mu = 6$.

Although proposals for degraded shear strength and the form of the shear strength versus flexural ductility relationship were developed, they require verification by further testing. The tests should establish the shear strength of circular columns at axial load ratios outside the comparatively narrow range investigated in the original test program. Other factors that may also affect the results, such as bi-directional lateral displacement and double bending, need further investigation as well.

2.7.2 Priestley *et al.* (1994a)

Priestley *et al.* (1994a) proposed a set of shear strength equations for circular and rectangular columns. The approach relates shear strength to flexural ductility, and considers the nominal concrete and axial load contribution to shear strength separately. The nominal shear strength, V_n, is given by an additive equation of the form:

$$V_n = V_c + V_s + V_p \qquad [2\text{-}13a]$$

where V_c is the concrete shear contribution, consisting primarily of aggregate interlock and dowel action effects, resulting from flexure alone in the absence of axial load, V_s is the shear carried by the shear reinforcement using a truss analogy with diagonals 30° from the vertical, and V_p is the shear capacity provided by axial load through arching action.

The concrete shear contribution is determined as follows:

$$V_c = k\sqrt{f_c'}A_e \qquad [2\text{-}13b]$$

where k is a factor from 0.29 for $\mu \leq 2$ to 0.1 for $\mu \geq 4$, $f_c^{'}$ is the cylinder compressive strength of concrete, A_e is the effective shear area that can be taken as $0.8A_g$, and A_g is the gross cross-sectional area of the column.

For the contribution from shear reinforcement, different equations are adopted for circular and rectangular columns.

For circular columns:

$$V_s = \frac{\pi}{2}\frac{A_h f_y D^{'}}{s}\cot 30^\circ = 0.865\pi\frac{A_h f_y D^{'}}{s} \qquad [2\text{-}13c]$$

For rectangular columns:

$$V_s = \frac{A_v f_y D^{'}}{s}\cot 30^\circ = 1.73\frac{A_v f_y D^{'}}{s} \qquad [2\text{-}13d]$$

where A_h is the cross-sectional area of one leg of a hoop or of the spiral reinforcement, f_y is the yield strength of shear reinforcement, $D^{'}$ is the diameter of the confined core, which is the distance between centres of the peripheral hoop or spiral reinforcement, A_v is the total cross-sectional area of shear reinforcement at a section, s is the spacing of hoop or pitch of spiral reinforcement along the longitudinal axis.

The shear contribution provided by axial load can be calculated from:

$$V_p = P(D-a)/H \qquad [2\text{-}13e]$$

where P is the axial load applied to the column, D is the section depth or column diameter, H is the height of the column subjected to reversed bending (hence, for a cantilever column it is twice the column height), and a is the depth of the concrete compression zone at the critical section.

If steel jackets are used to enhance the shear strength of a column, another term V_{sj} can be added to Eq. 2-13a in addition to the V_s term, which can be calculated through the following equations:

For circular jackets:

$$V_{sj} = \frac{\pi}{2}\frac{t_j^{\,2} f_{yj}(D_j - t_j)\cot 30^\circ}{t_j} = 0.865\pi t_j f_{yj}(D_j - t_j) \qquad [2\text{-}13f]$$

where t_j is the steel jacket thickness, f_{yj} is the yield strength of the jacket steel, and D_j is the outside diameter of the steel jacket.

For the strong direction of elliptical steel jackets:

$$V_{sj} = 3.46 t_j f_{yj} (D_j - t_j) \left[1 - \left(1 - \frac{\pi}{4} \right) \frac{B_j}{D_j} \right] \qquad [2\text{-}13g]$$

and for the weak direction of elliptical steel jackets:

$$V_{sj} = 3.46 t_j f_{yj} (B_j - t_j) \left[1 - \left(1 - \frac{\pi}{4} \right) \frac{D_j}{B_j} \right] \qquad [2\text{-}13h]$$

where B_j and D_j are the short and long principal diameters of elliptical jacket, respectively.

Tests of 14 large-scale columns were conducted by the authors to determine the appropriateness of the proposed shear strength model. Half of the specimens represented "as-built" columns and the remaining were rehabilitated with steel jackets. This model was proven to be considerably less conservative than the ACI 318-89 design provisions in predicting the shear strength of all columns for low levels of ductility.

Unlike some approaches for shear design that incorporate effects for the column aspect ratio and longitudinal reinforcement ratio, the concrete mechanism in this model does not account for these factors, although it is logical that the shear strength is greater for columns with smaller aspect ratios. It is also reasonable that a smaller longitudinal reinforcement ratio will result in a decrease in the strength of the concrete shear resisting mechanism due to three aspects. First, dowel action from the longitudinal reinforcement will be smaller if there are fewer numbers of smaller diameter bars. Second, the crack distribution will be more concentrated resulting in fewer and more widely spaced cracks, which, in turn, results in a decrease in the strength of the concrete aggregate interlock mechanism. Third, the smaller compression zone resulting from the reduced longitudinal steel ratio will, in turn, reduce the compression zone shear transfer.

2.7.3 Priestley and Seible (1995)

Priestley and Seible (1995) proposed a simple mathematical formula to account for the shear enhancement provided by external composite jackets besides the concrete and shear reinforcement contributions.

For circular jackets:

$$V_j = \frac{\pi}{2} t_j f_j D \cot\theta \qquad [2\text{-}14a]$$

For rectangular jackets:

$$V_j = 2t_j f_j h \cot\theta \qquad [2\text{-}14b]$$

where V_j is the shear strength enhancement by the external composite material jackets, t_j is the jacket thickness, and the jacket stress, f_j, used corresponds to a maximum strain of 0.004, i.e., $f_j = 0.004E_j$. D is the jacket diameter for a circular column, and h is the section depth in the direction of the shear force for a rectangular section. The angle θ is measured between the column axis and the diagonal tension crack and a value of $\theta = 35^\circ$ has been suggested as appropriate for design work.

2.7.4 Mirmiran *et al.* (1998)

Mirmiran *et al.* (1998) proposed a formula to calculate the shear strength of a hybrid concrete column made of concrete-filled fibre reinforced polymer (FRP) tube. It is generally assumed that the external tube acts as a continuous array of shear stirrups. If the tube is made of $\pm\phi$ angle plies and if the angle of the shear failure plane is assumed to be θ, the shear resistance by the tube, V_j, is given by:

$$V_j = \frac{\pi t_j f_j (D_j - t_j)\cos\phi}{2\tan\theta} \qquad [2\text{-}15]$$

where t_j is the thickness of the tube, f_j is the strength of the plies in the direction of the fibres, and D_j is the diameter of the whole cross-section.

Eq. 2-15 is derived based on the assumption that the load is transferred to the tube without the occurrence of slippage. If, however, slippage occurs, the tube will not work as effectively. In that case, the above equation will provide a less accurate estimate of the shear strength.

2.7.5 Xiao and Wu (2003)

Xiao and Wu (2003) introduced an improved steel jacketing method to rehabilitate square or rectangular reinforced concrete columns. Relatively thin steel plates were welded to form a rectilinear jacket that was supplemented with stiffeners of various kinds. This rehabilitation approach recognized the beneficial effect of the flexural stiffness of the stiffeners on the development of confining pressure, and hence the shear strength enhancement, as discussed in Section 2.4.2. In the prediction of the shear strength of the rehabilitated column, the researchers assumed that the total shear strength is composed of concrete, existing shear reinforcement, and additional jacket shear-strength contributions, an approach proposed by Priestley *et al.* (1994), given by

$$V_n = V_c + V_s + V_{sj} \quad [2\text{-}16a]$$

where, for simplicity, V_c and V_s can be calculated based on the ACI 318 shear-strength design equations. The steel jacket strength contribution is obtained through assuming a 45° truss mechanism and considering the jacket to be a series of independent hoops with both thickness and spacing of t_j, and its shear strength enhancement V_{sj} can be simply estimated as:

$$V_{sj} = 2t_j h f_{yj} \quad [2\text{-}16b]$$

where h is the cross-sectional dimension of column parallel to the shear force, and f_{yj} is the yield strength of the jacket steel.

The above equations were verified through comparison between the prediction and observed experimental results.

2.7.6 Saatcioglu and Yalcin (2003)

Saatcioglu and Yalcin (2003) performed full-scale experimental research on a method of seismic rehabilitation of shear deficient concrete columns. The rehabilitation technology consists of prestressing external individual hoops that consist of prestressing strands and specially designed anchors, as discussed in Section 2.4.4. A design procedure was proposed, including a shear strength model. According to the authors, the contribution of transverse prestressing to the concrete shear resistance may be expressed as follows:

$$V_{pc} = 2A_{ps} f_{pi} \frac{h}{s_p} \quad [2\text{-}17a]$$

where V_{pc} is the shear strength enhancement in the concrete introduced by external prestressing, A_{ps} is the area of strand used to prestress the column in the transverse direction, f_{pi} is the initial stress in the prestressing strand, h is the column cross-sectional dimension parallel to the shear force, or the diameter of a circular section, and s_p is the spacing of external prestressing hoops.

Prestressing strands also acts as additional shear reinforcement, providing extra enhancement for column shear resistance. This is expressed as:

$$V_{ps} = 2A_{ps}\left(f_{py} - f_{pi}\right)\frac{h}{s_p} \quad [2\text{-}17b]$$

where V_{ps} is the enhancement in shear resistance provided by the shear reinforcement introduced by external prestressing, and f_{py} is the yield strength of the prestressing strand material.

The total shear resistance enhancement provided by prestressing, V_{pr}, can be written as:

$$V_{pr} = V_{pc} + V_{ps} = 2A_{ps}f_{py}\frac{h}{s_p} \qquad [2\text{-}17c]$$

The nominal shear capacity of a reinforced concrete column, V_n, rehabilitated by external prestressing consists of contributions from concrete, V_c, internal shear reinforcement, V_s, and external prestressing, V_{pr}:

$$V_n = V_c + V_s + V_{pr} \qquad [2\text{-}17d]$$

The authors conducted an experimental study to validate the proposed shear strength model and achieved reasonably good results.

2.7.7 Galal *et al.* (2005)

Galal *et al.* (2005) proposed a procedure to predict the shear response of short reinforced concrete rectangular columns rehabilitated using anchored and unanchored FRP jackets. In their model, the nominal shear capacity, V_n, is equal to the sum of the contributions of four mechanisms: concrete, V_c, axial load, V_p, shear reinforcement, V_s, and FRP, V_j:

$$V_n = V_c + V_p + V_s + V_j \qquad [2\text{-}18a]$$

The degradation of the shear strength of an axially and laterally loaded short column with respect to its displacement ductility is explicitly given. The model assumes that with the increase of lateral displacement ductility, μ, after reaching $\mu = 2$, the concrete and axial load contribution decreases to one-third at $\mu = 4$ and drops to zero at $\mu = 6$:

$$V_n = \frac{1}{3}(V_c + V_p) + V_s + V_j \quad \text{for } \mu = 4 \qquad [2\text{-}18b]$$

$$V_n = V_s + V_j \quad \text{for } \mu = 6 \qquad [2\text{-}18c]$$

$$V_c = 0.3\sqrt{f'_{cc}}A_e \qquad [2\text{-}18d]$$

$$V_p = \frac{PD}{H} \qquad [2\text{-}18e]$$

$$V_s = \frac{A_v f_y d}{s} \qquad [2\text{-}18f]$$

$$V_j = 0.95(2t_f)(\varepsilon_{fe} E_j) d_f \qquad [2\text{-}18g]$$

where $f_{cc}^{'}$ is the confined compressive strength of concrete, A_e is the area of the effectively confined concrete core, P is the axial load on the column, D is the total depth of the column cross-section, H is the height of the column subjected to reversed bending (hence in double curvature, for a cantilever column, it is twice the column height), d is the column section depth to the tensile steel, A_v, f_y, and s are the total cross-sectional area, yield strength, and spacing, respectively, of the transverse reinforcement. The term $2t_f$ is the total thickness of FRP sheets (*i.e.*, for two opposite sides), ε_{fe} is the design strain for FRP ($\varepsilon_{fe} = 0.004$ for unanchored FRP sheets and $\varepsilon_{fe} = 0.006$ for anchored FRP sheets), E_j is the Young's modulus of the FRP composite material, and d_f is the depth of the FRP in the direction of load.

This method adopted the limits from ACI 318 for the total shear strength where more than one type of shear reinforcement is used, with minor modifications:

$$V_s + V_j \leq 0.66\sqrt{f_{cc}^{'}}\, bd \qquad [2\text{-}18h]$$

where b is the width of the column.

To calculate the confined concrete compressive strength, $f_{cc}^{'}$, at the design strain, ε_{fe}, of the FRP, the Mander *et al* model (1988) was applied at a constant lateral confining pressure using an effective transformed confinement content for the steel ties and FRP, provided that ε_{fe} is larger than the yield strain of the steel ties:

$$\frac{f_{cc}^{'}}{f_{co}^{'}} = 2.254\sqrt{1 + 7.94\frac{f_l^{'}}{f_{co}^{'}}} - 2\frac{f_l^{'}}{f_{co}^{'}} - 1.254 \qquad [2\text{-}18i]$$

where $f_{co}^{'}$ is the unconfined concrete compressive strength, and $f_l^{'}$ is the effective lateral confining pressure:

$$f_l^{'} = K\rho_{eff} f_y \qquad [2\text{-}18j]$$

where K is the confinement effectiveness coefficient:

$$K = \frac{A_{ef}/bd}{\left(1-\frac{A_v}{bd}\right)} \qquad [2\text{-}18k]$$

with:

$$A_{ef} = b_c d_c - \sum_{i=1}^{n} \frac{\left(w_i'\right)^2}{6}\left(1-\frac{s_1}{2b}\right)\left(1-\frac{s_2}{2d}\right) \qquad [2\text{-}18l]$$

such that b and d are: (a) in the case of no FRP, the core dimensions to centrelines of the perimeter ties in the x and y directions, respectively; and (b) in the case of FRP jacket, the width b and the total depth D of the column, respectively.

In Eq. 2-18l, w_i' is the ith clear distance between adjacent longitudinal bars, and s_1 and s_2 are the lesser of the transverse hoop reinforcement and FRP anchor spacing in the x and y directions, respectively. ρ_{eff} is the effective transformed confined content, transforming the FRP sheets at strain ε_{fe} into an equivalent steel content having the same steel yield strength, and is given by:

$$\rho_{eff} = \frac{A_v}{sd} + \frac{2t_f}{d} \cdot \frac{\varepsilon_{fe} E_j}{f_y} \qquad [2\text{-}18m]$$

Comparisons between the analytical predictions and experimental results showed reasonable correlation, with the theoretical results overestimating the experimental capacities slightly. The difference was attributed to the interaction between flexure and shear, which was not included in the analysis.

2.8 Summary

The focus of the current research includes the study of the behaviour of collared reinforced concrete short columns under combined axial and cyclic lateral loading. Various rehabilitation techniques, such as concrete jacketing, composite material jacketing, steel jacketing, external prestressing, and steel collars, have been studied by previous researchers. Previous research on the behaviour of existing and rehabilitated reinforced concrete columns with normal strength concrete under combined axial compression and lateral loading are reported in this chapter and some prominent shear strength models are also summarized.

Table 2-1 Collared columns under concentric loading (Hussain and Driver 2005b)

Specimen	Concrete compressive strength	Collar cross-section *	Spacing on centres	Corner connection	Peak load	Peak strain
	MPa	mm × mm × mm	mm		kN	
C00A	34.4	Ties 10M	267	—	3475	0.0035
C00B	35.0	Ties 15M	70	—	3342 /3419**	0.0034 /0.035**
C01	37.9	HSS 51×51×6.35	122	Bolted	4874	0.0300
C02	38.4	HSS 76×51×6.35	122	Bolted	5283	0.0356
C03	37.8	HSS 76×51×6.35	122	Bolted	6093	0.0350
C04	37.8	HSS 76×51×6.35	170	Bolted	4135	0.0034
C05	36.4	HSS 76×51×6.35	95	Bolted	6600	0.0430
C06	34.8	HSS 51×51×6.35	122	Welded	6409	0.0359
C07	47.0	HSS 76×51×6.35	122	Welded	8882	0.0283
C08	52.8	HSS 102×51×6.35	122	Welded	9802	0.0318
C09	36.3	HSS 76×51×6.35	170	Welded	5123	0.0267

* C00A and C00B refer to the conventional 10M and 15M internal transverse reinforcement; others show dimensions that are perpendicular and parallel to the column longitudinal axis and the wall thickness of the HSS collars, respectively.

** Presented for two distinct load peaks observed for specimen C00B.

Table 2-2 Collared columns under combined axial and lateral loading (Hussain and Driver 2005b)

Specimen	Concrete compressive strength	Collar cross-section *	Spacing on centres	Axial load	Location of lateral load	Peak moment	Drift at peak
	MPa	mm × mm × mm	mm	kN	mm	kN·m	%
CL0	32.7	Ties 15M	70	1470 /720 **	1900	216.50	8.00
CL1	12.3	HSS 76×51×6.35	101	0	1900	235.47	10.10
CL2	15.9	HSS 76×51×6.35	151	720	1900	276.92	8.80
CL3	15.4	HSS 76×51×6.35	101	720	1900	300.96	10.45
CL4	32.7	HSS 51×51×6.35	101	720	1900	296.84	8.91
CL5	26.3	HSS 76×51×6.35	101	0	750	207.42	4.53
CL6	32.6	HSS 76×51×6.35	151	720	0	282.93	4.66
CL7	35.4	HSS 76×51×6.35	101	720	720	296.90	6.31
CL8	35.3	HSS 51×51×6.35	101	720	720	296.48	5.67

* CL0 refers to the conventional 15M internal transverse reinforcement; others show dimensions that are perpendicular and parallel to the column longitudinal axis and the wall thickness of the HSS collars, respectively.

** Two levels of axial load applied to specimen CL0.

Table 2-3 Collared columns under concentric and eccentric loading (Chapman and Driver 2006)

Specimen	Collar cross-section **	Spacing on centres	Avg. bolt P/T load	Initial load eccentricity	End condition	Peak load	Peak strain
	mm × mm	mm	kN	mm		kN	
C00A*	Ties 10M	267	—	0	Fixed	3475	0.0035
C00B*	Ties 15M	70	—	0	Fixed	3342 /3419***	0.0034 /0.035***
CE01	50×38	122	25	0	Fixed	5200	0.0344
CE02	50×38	95	25	0	Fixed	6500	0.0203
CE03	50×38	170	25	0	Fixed	3905	0.0104
CE04	50×38	122	25	0	Fixed	5607	0.0275
CE05	50×38	122	144	0	Fixed	5950	0.0189
CE06	40×50	122	25	0	Fixed	5516	0.0219
CE07	50×38	122	25	30	Pinned	2997	0.0138
CE08	50×38	122	25	60	Pinned	2276	0.0154
CE09	50×38	122	25	10	Pinned	3861	0.0276
CE10	50×38	122	25	0	Pinned	4490	0.0248
CE11	50×38	95	25	30	Pinned	3415	0.0267
CE12	50×38	170	25	30	Pinned	2744	0.0073
CE13	50×38	122	135	30	Pinned	3695	0.0137
CE14	40×50	122	25	30	Pinned	3171	0.0104

* Non-collared column tested by Hussain and Driver (2005b) with concrete compressive strength of 34.4 MPa and 35.0 MPa, while all other columns have the concrete compressive strength of 31.7 MPa.

** C00A and C00B refer to the conventional 10M and 15M internal transverse reinforcement; others show dimensions that are perpendicular and parallel to the column longitudinal axis, respectively.

*** Presented for two distinct load peaks observed for specimen C00B.

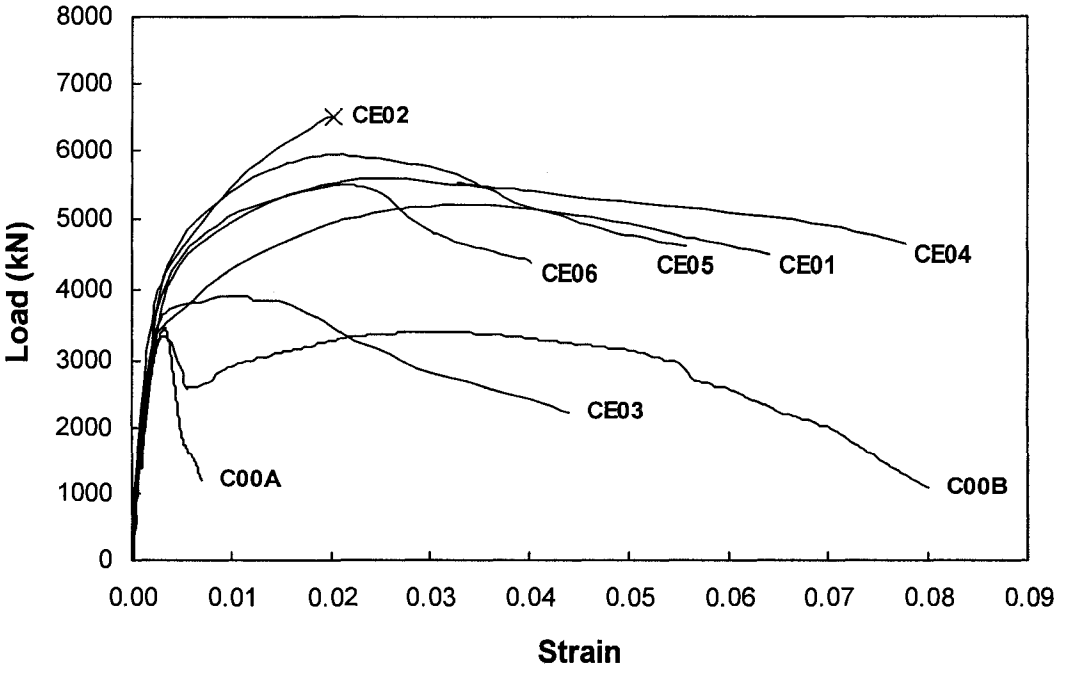

Figure 2.1 Axial load versus axial strain for concentrically loaded specimens (adapted from Chapman and Driver 2006)

CHAPTER 3 EXPERIMENTAL PROGRAM

3.1 Introduction

To complement previous research conducted at the University of Alberta on collared reinforced concrete slender columns under axial and combined axial and lateral loading, a testing program was designed to investigate the strength, ductility, and overall response of collared reinforced concrete short columns subjected to combined axial and cyclic lateral loading. The principal parameters considered in the test program are: collar spacing, collar size/stiffness, longitudinal reinforcement ratio, axial compression ratio, pretension of collar bolts, and shear span-to-depth ratio. A description of the test specimens, material properties, test set-up, instrumentation, and loading procedures are presented in this chapter.

3.2 Description of Test Specimens

To simplify discussions about the various test specimens, a notation consisting of a three-part identifier is used. The general form of the notation is: CVx, where "C" stands for Column, "V" means the test is to study the behaviour of the short column (to distinguish from previous phases of the overall research program), and "x" is a serial number from 1 to 8 for collared columns, "0A" or "0B" for the control specimens (without collars), or "0AR" for the repaired specimen after the initial test of specimen CV0A. The character "A" indicates that the ties were widely spaced and "B" indicates closely spaced ties.

3.2.1 Specimen Design

The test specimens were designed as cantilever columns with a short shear span to create a high shear-to-moment ratio at the critical cross-section and thereby might encourage shear-dominant behaviour. Based on a review of available test results, a shear span-to-column-depth ratio, referred to herein as the "aspect ratio" for simplicity, of less than 2.5 is needed to develop shear-dominant behaviour (Woodward 1980; Ghee *et al.* 1989; Wong *et al.* 1993; Priestley *et al.* 1994a, 1994b; Jaradat *et al.* 1998). Ten full-scale column specimens (CV0A, CV0B and CV1 to CV8) were designed with 400×400 mm cross-sections and an overall height of 800 mm. The aspect ratios, $M/(VD)$, selected were 1.63 and 0.88, where M is the moment at the critical section (*i.e.*, at the column base), V is the shear force at the critical section, and D is the section dimension (400 mm). The tests also included control columns with conventional transverse reinforcement. One control column (CV0B) was designed to meet the seismic requirements of both CSA-A23.3-04 and ACI 318-05, whereas the other (CV0A) had only nominal tie reinforcement to meet the gravity load provisions. Eight specimens (CV1 to CV8) were rehabilitated with external steel collars, and a post-damage repaired and rehabilitated specimen (CV0AR) was used to determine whether a damaged column can be salvaged after an earthquake. All specimens except one were subjected to compressive axial loads, because the presence of compressive axial loads would appear

to be more representative of the loads generally present on a column in a structure in service. Details of the test specimens are shown in Table 3-1.

The test specimens were constructed with a footing to allow foundation influence or interaction to be monitored, as well as to facilitate the connection to the laboratory strong floor. All the specimens had 1600×1000×570 mm footings that were anchored to the strong floor by four prestressed 50 mm diameter high strength threaded rods. An additional constraint system was used to prevent any sliding of the footing under large horizontal loads during the test.

The 28-day compressive strengths of the concrete in the footings and columns were both targeted at 30 MPa. The mix design for the column concrete was conducted according to the mix design manual authored by Kosmatka *et al.* (2002) and published by Canadian Portland Cement Association (2002) and was batched in the laboratory. Concrete used for the footings was ready-mix. Concrete required for the test specimens was exposed to neither chlorides nor freezing and thawing, so it pertains to an "N" class of exposure. As such, air-entrainment was not required. The slump was targeted at around 80 mm. A nominal maximum size aggregate of 20 mm was used along with Type 10 cement. Mix proportions for the test columns are shown in Table 3-2. However, water was adjusted based on laboratory experience due to the varying moisture contents of the aggregates during mixing at different times.

3.2.2 Internal Reinforcement Details

In order to capture the shear capacity of the column, the flexural design strength was set higher than the flexural demand corresponding to the anticipated shear capacity based on ACI 318-02 and CSA-A23.3-94 (current editions at the time the specimens were designed) without considering the shear contribution from the steel collars or the cyclic loading condition. A high longitudinal reinforcement ratio of ten 25M longitudinal bars (3.13%) was therefore adopted in this test program for all the columns, except one with ten 20M bars (1.88%). All columns met the seismic requirement of longitudinal reinforcement ratio range of 1% and 6%. All the longitudinal bars were weldable deformed bars due to their need to be welded to the top bearing plate. Diagrams of a typical specimen (CV1) before the assembly of external steel collars, including the reinforcement details, are shown in Figures 3-1 and 3-2. The rebar cage set in the form is presented in Figure 3-3. Since there was no splicing of the longitudinal bars, the code requirement of lap splices being permitted only within the centre half of the member length was met. The longitudinal bars were extended into the footing with 90° 400 mm long hooks. Specimens CV1 to CV8 had external steel collars, and in order to study the effect of the collars separately, no internal transverse reinforcement was provided in the test regions of these columns. For the control columns—CV0A and CV0B—conventional transverse reinforcement was chosen as 10M ties with spacings of 400 mm and 100 mm, respectively. The former spacing meets the gravity load design criteria and the latter the seismic plastic hinge requirements of both CSA-A23.3-04 and ACI 318-05. Gravity load design requires that the vertical spacing of the transverse reinforcement not exceed 16 longitudinal reinforcement diameters, 48 transverse reinforcement diameters, or the

smallest dimension of the compression member. The seismic provisions require that the vertical spacing of the transverse reinforcement not exceed one-quarter of the smallest dimension of the compression member, six times the diameter of the smallest longitudinal reinforcement, or s_x, defined as follows:

$$s_x = 100 + \left(\frac{350 - h_x}{3} \right) \qquad [3\text{-}1]$$

where h_x is the horizontal spacing between longitudinal bars that are laterally supported by seismic hoops or crosstie legs; here h_x was 122 mm on two sides and 73 mm on the other two sides. It shall not exceed the greater of 200 mm or one-third of the core dimension in that direction, and shall not be more than 350 mm.

The minimum permissible areas of transverse reinforcement are set by Eqs. 3-2 and 3-3 from CSA-A23.3-04 and Eqs. 3-4 and 3-5 from ACI 318-05:

$$A_v = 0.2 k_n k_p \frac{A_g}{A_{ch}} \frac{f_c'}{f_y} s h_c \qquad [3\text{-}2]$$

$$A_v = 0.09 \frac{f_c'}{f_y} s h_c \qquad [3\text{-}3]$$

$$A_v = 0.3 s h_c \frac{f_c'}{f_y} \left(\frac{A_g}{A_{ch}} - 1 \right) \qquad [3\text{-}4]$$

$$A_v = 0.09 s h_c \frac{f_c'}{f_y} \qquad [3\text{-}5]$$

where $k_n = n_l/(n_l - 2)$, $k_p = P_f/P_0$, n_l is the total number of longitudinal bars in the column cross-section that are laterally supported by the corner of hoops or by hooks of seismic crossties, P_f is the maximum factored axial load for earthquake loading cases, P_0 is nominal axial resistance at zero eccentricity, A_v is the total cross-sectional areas of the transverse reinforcement (including crossties) within the spacing s and perpendicular to dimension h_c, s is the spacing of the transverse reinforcement measured along the longitudinal axis of the column, h_c is the dimension of the concrete core of the rectangular section measured perpendicular to the direction of the hoop bars to the outside of the peripheral hoop, f_c' is the specified compressive strength of concrete, f_y is the specified yield strength of the transverse reinforcement, A_g is the gross cross-sectional area of the column, which is 160 000 mm^2, and A_{ch} is the cross-sectional

area of the core of the column measured out-to-out of the transverse reinforcement, which is 115 600 mm^2.

The transverse reinforcement was detailed with seismic hooks, *i.e.*, 135° hooks with an extension length of at least six bar diameters. The internal transverse reinforcement for specimen CV0A and CV0B, shown in Figure 3-4, did not extend into the footings. The column reinforcement cages were tied to the footings before the concrete of the footings was cast. Four pieces of 10M bars were welded to the column longitudinal bars near the top to secure the positions of these bars during assembly, as shown in Figure 3-3. All vertical reinforcing bars had a 90° hook at the footing base and the top end passed through drilled holes in a square steel top bearing plate. The bars were then welded to the steel plate to ensure adequate anchorage of the vertical steel over the short shear span, as shown in Figure 3-5.

3.2.3 Steel Collars

Steel collars used in some previous phases of this research program were made from Hollow Structural Sections (HSS) with bolted or welded corner connections. These configurations tend to be somewhat difficult to fabricate, especially when welding is required, necessitating special quality control procedures. Some collars were welded in the shop and then threaded over the columns from the top, which is not applicable to a real rehabilitation scenario. In order to standardize and simplify the fabrication and installation of steel collars, a new type of collar was developed for this test program and another, where collared columns were tested axially (Chapman and Driver 2006). These collars, shown in Figure 3-6, consist of two "L" shaped pieces cut from a 50 mm thick steel plate in a commercial fabrication shop using a conventional computer controlled oxy-gas cutting table and the pieces are connected using high strength structural bolts. Standard 25.4 mm (1 in.) diameter ASTM A490 high strength structural bolts were used in these tests. This fabrication process, making use of common equipment and completely eliminating the need for welding, is cost–effective.

The collars were installed in an alternating orientation sequence by rotating each successive collar 90° about the column axis, balancing the possible effect aroused by the restraint difference between the rigid corner and bolted corner. The collar cross-section is 30×50 mm (the second dimension against column face and parallel to the longitudinal axis of the column), except the collars of column CV8 had a larger cross-section of 50×50 mm to assess the effect of increased collar stiffness. The clear spacing between the collars is 100 mm (for most specimens), 150 mm, or 45 mm. The clear spacing between the top of the footing and the bottom of the first layer collar is equal to one-half of the spacings above.

The bolts connecting the steel collars for all of the columns except column CV7 were tightened to be just snug with the column, while a significant pretension force was applied to the bolts for column CV7. The pretension was measured by an annular bolt load cell to study the potential benefits of active confining pressure. The pretension was applied to the bolts through five incremental steps.

3.2.4 Specimen Preparation

Fabrication and testing was conducted in the I. F. Morrison Structural Engineering Laboratory at the University of Alberta. Casting of the columns and footings was done in two stages. Two footings were cast at the same time, as shown in Figure 3-7, using the same batch of commercial ready mix concrete. After the footing concrete had partially cured, the two corresponding columns were cast using separate batches of concrete (due to the small capacity of the mixer) prepared in the laboratory, as shown in Figure 3-8. The construction joint between the footing and column was roughened and cleaned up before casting the column concrete. At least eight standard 150×300 mm cylinders were cast for each batch of concrete used for the footings or columns, as per the requirement of ASTM standard C192-02 (ASTM Standard C192. 2002), to characterize the material properties. Four cylinders were tested to measure the strength evolution with time and at least three were used to obtain the strength of the concrete at the time of testing of the columns. Curing conditions for the cylinders and test specimens were identical to ensure representative results. The specimens and cylinders were moist-cured under polyethylene sheets for a total of seven days after casting and cured under ambient laboratory conditions thereafter.

To investigate the feasibility of repairing badly damaged columns using external steel collars, one of the failed control columns was retested after being repaired. The specimen CV0AR was the repaired specimen from the damaged control column (CV0A) using epoxy mortar and external collars. Before the application of repair, a visual investigation of the condition of the damaged specimen needs to be conducted, to evaluate the feasibility of repair. It should be pointed out that for specimen CV0A the internal transverse reinforcement did not fracture, the longitudinal reinforcing bars were essentially straight, and the column axis was still close to vertical due to the small lateral displacement applied to the specimen during the whole test, indicating the feasibility of repair. The repair process involves surface preparation, assembling of a form, mixing and application of mortar, and curing.

The first step in the repair of CV0A was to remove the weak, deteriorated soft concrete using a hand-held pneumatic chisel. Then the specimen was brushed and blown to eliminate superficial dust. Four strain gauges were installed on the longitudinal reinforcement at the same positions as original specimen CV0A. A total of 16 strain gauges were also attached on collar 1 and collar 2. After the preparation of the specimen, a form was constructed as shown in Figures 3-9(a). Styrofoam was used as the form work for casting the epoxy mortar as well acting as collar spacers. Special tapes were attached to cover the inside of the Styrofoam spacers and collars. One side of the tape is wax coated, which will make a very smooth surface of the repaired specimen and the easy removal of the Styrofoam spacers. External braces using threaded rods and HSS short columns were applied to provide confinement and support during the pouring of the epoxy mortar.

The epoxy mortar used has a volumetric mix ratio of 10:2:1 for fine sand: Part A (Resin): Part B (Hardener). Epoxy part A and part B was mixed using a low-speed drill with custom stirring attachment. Fine sand was added while stirring. Mixing continued for at least five minutes after all the fine sand was added. Then some water was sprayed on the specimen to wet the surface before pouring the mortar. All mortar was cast within 45 minutes of mixing. At the end of application, excess epoxy mortar was removed from the specimen surface before it hardened. Then epoxy mortar was cured in the laboratory for one week under ambient temperature conditions as shown in Figure 3-9(b).

In order to mount the clinometers on the control specimens CV0A and CV0B to obtain curvature distribution along the column, four bars were pre-embedded for each control column at the height of 75 mm, 225 mm, 375 mm, and 525 mm measured from the column footing interface in the east side. The position of clinometers can be seen from Figures A-1 and A-3. For other columns, clinometers were mounted at the external collars.

3.3 Material Mechanical Properties

The physical properties of the concrete in the columns and footings were obtained by standard concrete cylinder tests, as per ASTM standard C469-02 (ASTM Standard C469. 2002), conducted at 7- and 28-days, as well as on the day of or one day before the testing of the respective column. The mean compressive strengths, $f_c^{'}$, the standard deviations, and corresponding ages of concrete at the time of the testing of the cylinder (on the day/one day before the testing of the respective column) are given in Table 3-3. The stress versus strain curve for each cylinder was plotted, and the secant method to $40\% f_c^{'}$, as specified in CSA-A23.3-04 Clause 8.6.2.1, was used to obtain the modulus of elasticity E_c for the concrete, which is also reported in Table 3-3. As mentioned in the Explanatory Notes of Clause 8.6.2.3 in CSA-A23.3-04, the value of E_c varies markedly depending on the concrete strength, the concrete density, and the type of coarse aggregate, and is affected by the aggregate fraction in the mix, the modulus of elasticity of the aggregates, and the loading rate. Its value will generally be between 80 and 120% of the values specified in CSA-A23.3-04 Clauses 8.6.2.2 and 8.6.2.3. The modulus of elasticity for the concrete of the columns used in this experimental program was found to be around 85% of the values specified in Clause 8.6.2.2, around 87% of the values specified in Clause 8.6.2.3., and around 82% of the value obtained adopting the ACI318-05 modulus of elasticity equation $E_c = 0.043\gamma_c^{1.5}\sqrt{f_c^{'}}$, where γ_c is the density of the concrete. The slightly lower than average values are typical of concretes made with aggregates from central Alberta.

All reinforcing bars conformed to standard CSA-G30.18. Three tension coupons were tested for each rebar size, where all bars of given size were from the same heat of steel, as specified in Table 3-4. Tension coupon tests were conducted to get the key material properties. Figure 3-10 shows the mean stress versus strain curves for the reinforcing bars and steel collars. The mean yield stress, modulus of elasticity, ultimate stress, and strain

at ultimate stress are listed in Table 3-4. The mean yield stress, modulus of elasticity ultimate stress, and strain at ultimate stress are static values and are the average of three values from the coupon stress-strain curves. The mean stress-strain curves are constructed by taking the average of the stress and strain from these three coupon tests. If one of the tests terminated earlier, then the remaining part of the curve will be the average of the remaining two coupon test results. All tension tests were carried out as per ASTM standard A370-02 (ASTM Standard A370. 2002).

Specimen CV0A was initially tested in the same manner as the other specimens and the damaged specimen was then repaired with epoxy mortar and external steel collars. A low-viscosity moisture-insensitive epoxy adhesive, including resin and hardener, was used with fine sand to make the mortar. Six 51×51×51 mm cubes were made to determine the material properties of the mortar. The stress versus strain curves are shown in Figure 3-11. The mean ultimate stress, modulus of elasticity, and strain at ultimate stress were found to be 40.0 MPa, 3251 MPa, and 0.026, respectively.

3.4 Test Set-up

The test set-up includes three prominent features: column base fixing system (footing), horizontal loading assembly and its reaction system, and vertical loading assembly and its reaction system. The schematic loading set-up is shown in Figure 3-12, and Figure 3-13 shows a photograph thereof.

All the specimen footings were levelled using a high strength plaster material underneath and then anchored to the strong floor by four prestressed 50 mm diameter high strength threaded rods. The prestressing force applied to each rod was about 500 kN. The anchor rod prestressing set-up is shown in Figure 3-14. An additional constraint system consisting of Dywidag rods, nuts, and double channel beams was used to prevent sliding of the footing under the large horizontal loads applied during the test. This arrangement can be seen in Figures 3-13 and 3-15.

The horizontal load is applied to the specimens by two double-acting hydraulic jacks in parallel mounted on a reaction frame. The jacks, mounted adjacent to each other at the same elevation, were connected to the reaction frame through a pin-connection assembly. A yoke assembly was used to connect the other end of these two jacks to create a single applied force. The force application system was then connected to a loading arm (see Figure 3-15) with an integral clamp plate on the column (specimen) side. A load cell was installed between the yoke and loading arm to measure the single load output. A common oil pumping valve was used for the two jacks to ensure that the same fluid pressure was maintained. Clamp plates and four high-strength threaded rods were used to clamp the specimen and were designed to provide a means of loading in the two opposite directions. Figures 3-16 and 3-17 show the schematic set-up of the horizontal loading assembly and Figure 3-15 shows a photograph. Two different shear-spans were tested in this program, which required the adjustment of the horizontal load assembly.

A vertical load, simulating the gravity load on the column, was provided by a single jack connected to an overhead reaction beam. Pin connections were used to accommodate lateral displacement of the column specimens. A brace system was used at the top pin of the vertical load jack to carry any horizontal component of the applied load, as shown in Figure 3-18.

3.5 Instrumentation

Five types of measuring devices were used to monitor the performance of the specimens during testing: load cells, strain gauges, clinometers, LVDTs, and mechanical dial gauges. Horizontal and vertical loads were measured with load cells on the loading rams. One annular bolt load cell measured the load in the bolt of the second (from the bottom) layer collar.

Electrical resistance strain gauges were attached to both the longitudinal reinforcement and the collars. In the collars, the strain gauges were installed in pairs, one on the side of the collar and the other on the top with the centre of the strain gauge 5 mm away from the inner edge, providing as much distance between them as possible to better capture the flexural behaviour of the collar cross-section. All collared columns had eight strain gauges installed on the bottom two layers of collars, except specimen CV3 (with the narrowest spacing of steel collars) where the first and the third layer of collars from the bottom were instrumented. Previous researchers (*e.g.*, Hussain and Driver 2005b) revealed that a discrete rotation develops at the base of the column due to the penetration of axial strains in the tensile longitudinal reinforcement into the footing that was accentuated by bond deterioration between the steel and concrete during extreme cyclic loading. In order to capture these additional fixed-end rotations, strain gauges were installed at two levels below the surface of the footing to obtain an estimate of the strain and strain gradient in the reinforcing bars in the footing for specimens CV0B, CV1, and CV4.

Clinometers measured the collar rotations to aid in the characterization column curvature. The angle of the horizontal loading assembly changed slightly as the specimens underwent lateral movement. This angle change was monitored by a clinometer to ensure that acceptably small rotations were maintained. The horizontal load was not adjusted for this angular change since the change was negligible, as discussed in Chapter 4, Section 4.3.

The horizontal displacement of the column was measured with linear variable displacement transformers (LVDTs) at the height of application of the horizontal load. Additional LVDTs at the top and bottom pin of the vertical load hydraulic jack permitted a resolution of horizontal and vertical load components from the nominally vertical jack. In order to monitor the possible slip of the footing, a dial gauge was installed to measure the displacement relative to the floor. Figure 3-19 shows the instrumentation details for specimen CV1.

3.6 Loading Procedure

The vertical load was applied initially to achieve the desired axial compression index and then kept constant throughout the remainder of the test. The axial compression index is calculated from $P/\left(f_c^{'}A_g\right)$, where P is the axial compressive load, $f_c^{'}$ is the measured compressive strength of concrete, and A_g is the gross cross-sectional area of the column. For all the columns except column CV6, the axial compression index was 30%, while no axial compressive load was applied to column CV6.

The sequence for horizontal loading is shown in Figure 3-20 and is similar to that used by Ghee *et al.* (1989), except that instead of controlling the test solely based on the estimated force V_y that results in the theoretical yield moment developing at the base of the column, it was also controlled based on real-time observations of the behaviour of the test specimen in the first cycle. For all the tests, the first five cycles of horizontal loading were load controlled to 0.75 V_y, and the remaining were displacement controlled. For the weakly reinforced control specimen CV0A, the initially damaged specimen CV0AR, and specimen CV5 (with the smaller aspect ratio giving rise to a very high value of calculated V_y), the initial five-cycle load control values were intentionally reduced to around half of the calculated V_y. This modification was invoked to prevent the possible sudden failure of these specimens during the first series of five cycles.

The estimation of the yield force, V_y, is very important for performing this test. It is defined herein as the lateral force corresponding to the yield moment of the column, which is taken as the point of first yield of the vertical tensile steel, considering the combined effects of axial compression and bending, and is based on measured material properties with unconfined concrete strength ignoring influence of collars. The measured material properties include longitudinal bar yield stress and strain, concrete cylinder stress versus strain curve, concrete compressive strength, and modulus of elasticity. It was found that the concrete stress versus strain curves from the standard cylinder tests fit well with the stress versus strain relationship proposed by Todeschini *et al.* (1964), especially before reaching the ultimate strength. In obtaining the stress versus strain relationship, the maximum stress and the strain at this maximum stress were taken as suggested by MacGregor and Bartlett (2000) as shown in Eqs. 3-7 and 3-8. Therefore, the concrete stress was calculated from the strain using the following relationships (Todeschini *et al.* 1964):

$$f_c = \frac{2f_c^{''}\left(\frac{\varepsilon}{\varepsilon_c^{'}}\right)}{1+\left(\frac{\varepsilon}{\varepsilon_c^{'}}\right)^2} \qquad [3\text{-}6]$$

$$f_c^{''} = 0.9f_c^{'} \qquad [3\text{-}7]$$

$$\varepsilon_c' = 1.71 f_c'/E_c \qquad [3\text{-}8]$$

where f_c is the compressive stress of the concrete at strain ε, f_c'' is the peak compressive stress of the Todeschini curve, ε is the strain of concrete, ε_c' is the strain corresponding to the peak concrete compressive stress, and f_c' is the compressive strength of the concrete.

In the calculation of the column compressive force and moment corresponding to the yield force, V_y, the concrete compression zone is divided into ten rectangular layers of equal area. The concrete in tension is neglected.

The values of V_y for all columns were calculated using the trial-and-error sectional analysis procedure assuming strain compatibility, but in order to avoid the possible sudden failure for columns CV0A and CV0AR, the first five-cycles of these two columns were conducted at a lower load value. For column CV5, the value of V_y was very large due to the smaller shear-span, and a lower value was also adopted in the initial five cycles, and this lower value was chosen to be the same as the values used other collared columns, CV1, CV2, CV3, CV4, CV6, CV7, and CV8.

As shown in Figure 3-20 (a), the yield displacement at the point of application of the horizontal load, Δ_y, is defined using the first full cycle by extrapolating straight lines from the origin through the peaks of the lateral load versus displacement curve at $\pm 0.75 V_y$ to the points defined as $\pm V_y$. The average of the values in the positive and negative directions is taken as the yield displacement, Δ_y, for both directions. The displacement ductility factor, μ, is defined as the ratio of the actual maximum displacement, Δ_{max}, at the point of application of the horizontal load to the yield displacement, Δ_y. The subsequent loading sequence consists of five displacement controlled cycles to displacement ductilities $\mu = 1.5$, 2, 4, 6, and so on. The test is continued until significant degradation of the specimen strength is observed. It is to be noted that although this procedure was used for controlling the test, the values of Δ_y were re-evaluated after the test program was complete when the behaviour of specimens rehabilitated in this way was better understood. This re-evaluation, discussed in Chapter 4, led to displacement ductilities considered to be representative of the behaviour of the specimens. As a means of clarification, the value of Δ_y used specifically for controlling the tests is hereafter designated as Δ_{yc}.

Table 3-1 Summary of the test specimen configurations

Specimen	Aspect ratio	Collar cross-section*	Collar centre-centre spacing**	Axial compres-sion index	Longitudinal reinforcement ***	P/T in collar bolt
	M/(VD)	mm × mm	mm	$P/(f_c' A_g)$	Bars, ρ***	(kN)
CV0A	1.63	—	400	0.3	Ten 25M,3.13%	—
CV0AR	1.63	30×50	150	0.3	Ten 25M,3.13%	10
CV0B	1.63	—	100	0.3	Ten 25M,3.13%	—
CV1	1.63	30×50	150	0.3	Ten 25M,3.13%	9
CV2	1.63	30×50	200	0.3	Ten 25M,3.13%	12
CV3	1.63	30×50	95	0.3	Ten 25M,3.13%	12
CV4	1.63	30×50	150	0.3	Ten 20M,1.88%	12
CV5	0.88	30×50	150	0.3	Ten 25M,3.13%	11
CV6	1.63	30×50	150	0	Ten 25M,3.13%	11
CV7	1.63	30×50	150	0.3	Ten 25M,3.13%	144
CV8	1.63	50×50	150	0.3	Ten 25M,3.13%	13

* Dimensions are perpendicular and parallel to the column longitudinal axis, respectively

** CV0A and CV0B values refer to the centre-to-centre spacing of conventional 10M internal transverse reinforcement (see Fig. 3-4 for arrangement)

*** Longitudinal reinforcement ratio, ρ , is the total longitudinal reinforcement area, A_s, divided by the gross cross-sectional area of the column, A_g, $\rho = A_s / A_g$

Table 3-2 Mix proportions for the test columns

Unit weight (kg/m^3)			
Water	**Cement**	**Fine aggregate**	**Coarse aggregate**
205	471	726	992

Table 3-3 Properties of concrete

Specimen	Footing concrete		Column concrete				
	Mean strength f'_c (MPa)	Standard deviation (MPa)	Mean strength f'_c (MPa)	Standard deviation (MPa)	Strain at peak stress ε'_c	Secant modulus of elasticity E_c (MPa)	Age of concrete (Days)
CV0A	28.9	0.27	26.3	1.12	0.0025	19 700	35
CV0AR	28.9	0.42	26.6	2.00	0.0029	20 700	56
CV0B	28.6	0.31	26.9	0.74	0.0023	18 200	27
CV1	41.1	1.00	33.3	0.88	0.0029	22 800	84
CV2	37.7	0.48	25.5	0.43	0.0026	20 700	27
CV3	37.6	1.13	22.0	0.50	0.0024	18 000	33
CV4	28.6	0.48	30.8	1.12	0.0028	22 000	123
CV5	26.2	0.30	29.5	0.36	0.0028	19 900	39
CV6	40.6	0.08	31.5	1.65	0.0027	23 700	125
CV7	29.2	0.07	29.1	0.40	0.0028	21 400	132
CV8	26.8	0.68	27.4	0.68	0.0026	20 000	27

* Compressive strength of concrete on the day or one day before the column tests.

Table 3-4 Properties of rebar and collar steel

Steel type	Size	Specimen	Yield stress f_y (MPa)	Modulus of elasticity E_s (MPa)	Ultimate stress f_u (MPa)	Strain at ultimate stress ε_u
Rebar	10 M	CV0A, 0AR, 0B	406	185 000	649	0.137
	20 M	CV4	441	201 000	618	0.124
	25 M (order 1)	CV1, 6, 7	453	195 000	641	0.124
	25 M (order 2)	CV0A, 0AR, 0B, 2, 3, 5, 8	383	190 000	535	0.166
Collar	order 1	CV0AR, 1, 2, 4, 5, 6, 7	309	200 000	470	0.163
	order 2	CV3*, 8	272	209 000	456	0.157

* Collar order 1 is used for the first layer of collars in CV3.

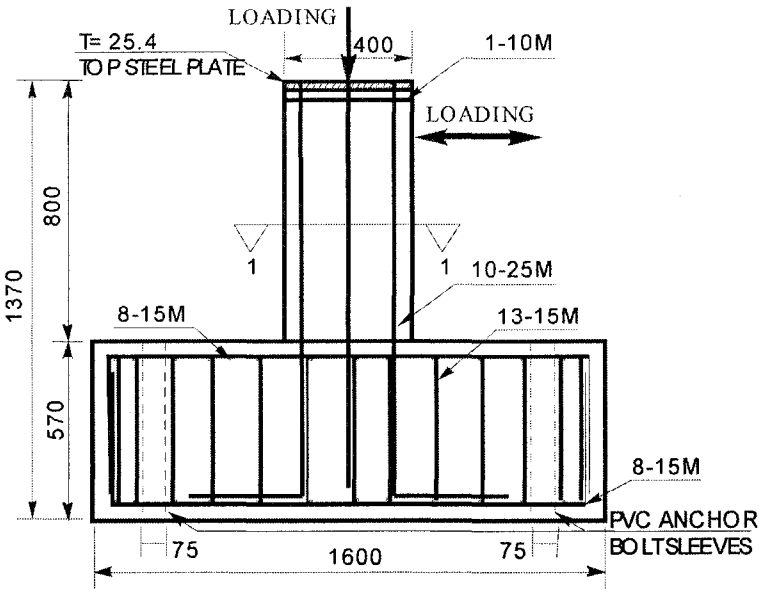

(a)

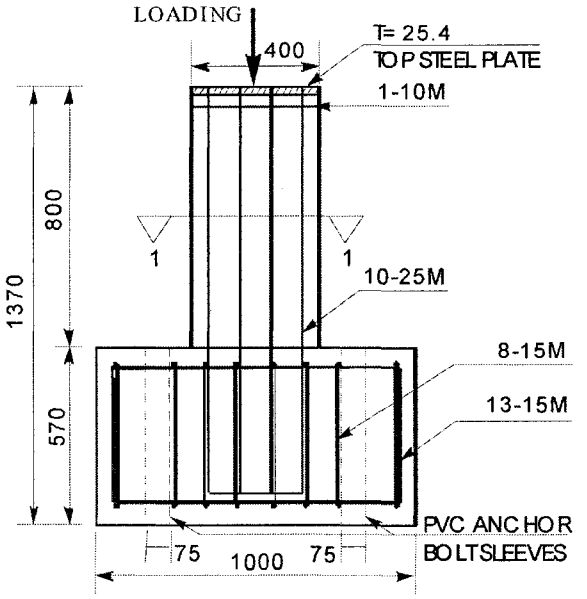

(b)

Figure 3-1 Specimen internal reinforcement details (specimen CV1) (elevation)
(a) footing long side direction; and (b) footing short side direction

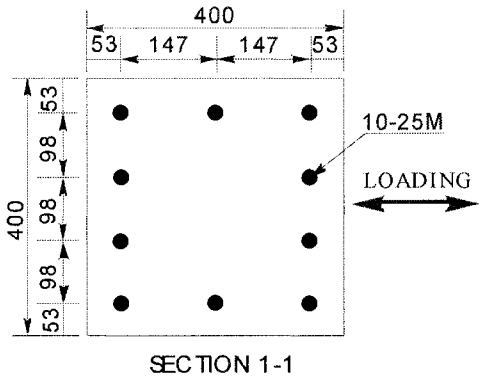

Figure 3-2 Specimen internal reinforcement details (specimen CV1) (plan)

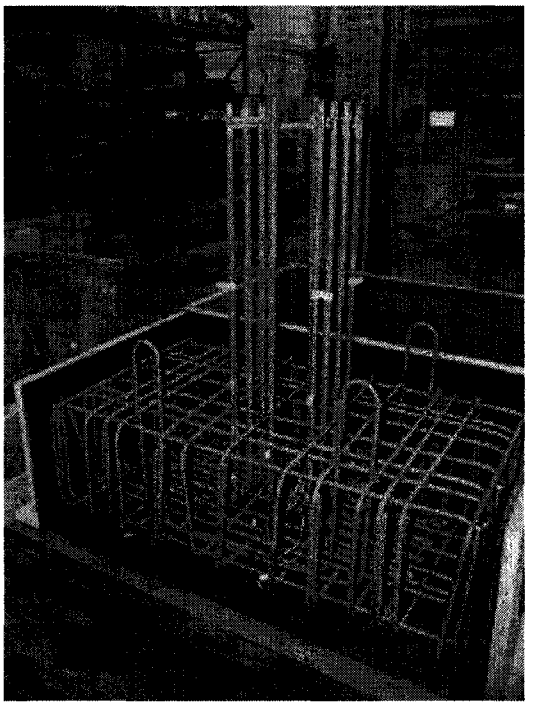

Figure 3-3 Rebar cage set in form

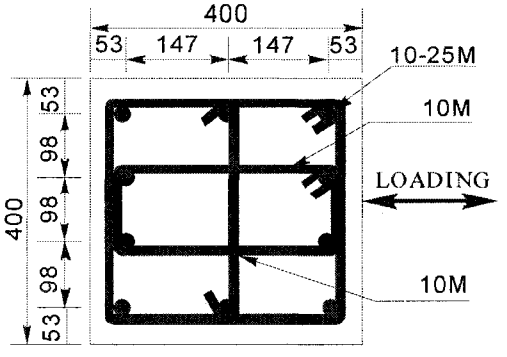

Figure 3-4 Internal transverse reinforcement detail for specimens CV0A and CV0B (plan)

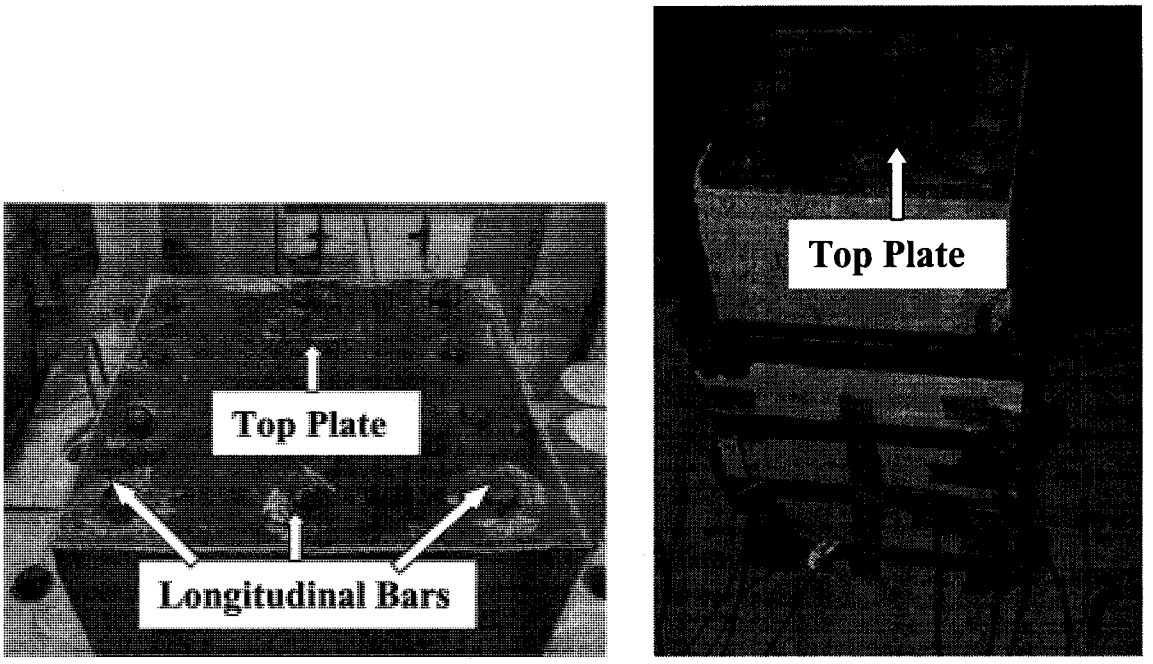

(a) (b)

Figure 3-5 Welded top plate: (a) before welding; (b) after welding

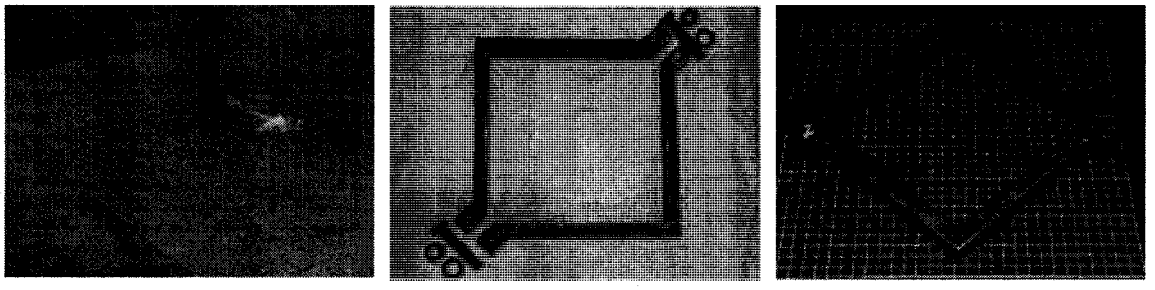

(a) (b) (c)

Figure 3-6 Steel collars: (a) during cutting; (b) exploded view; and (c) assembled view

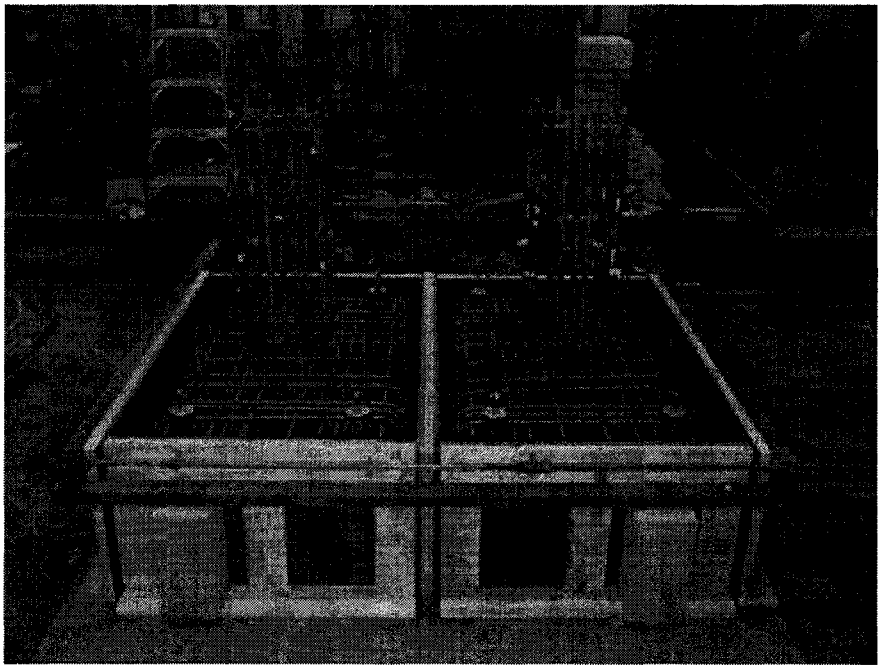

Figure 3-7 Two specimens ready for concrete casting of footings

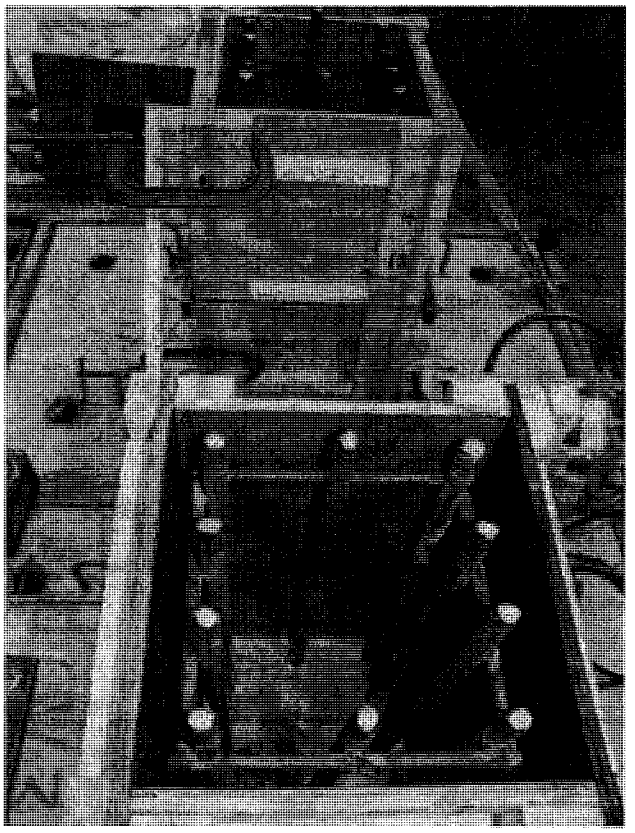

Figure 3-8 Two columns ready for concrete casting

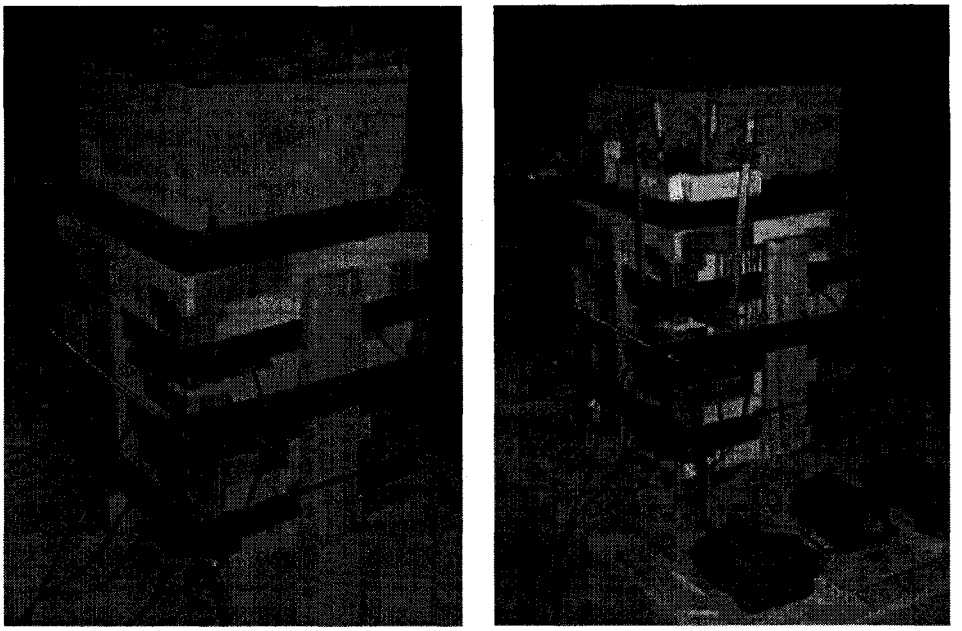

(a) Form and brace system for grout repair (b) After epoxy mortar grout

Figure 3-9 Repair of damaged specimen

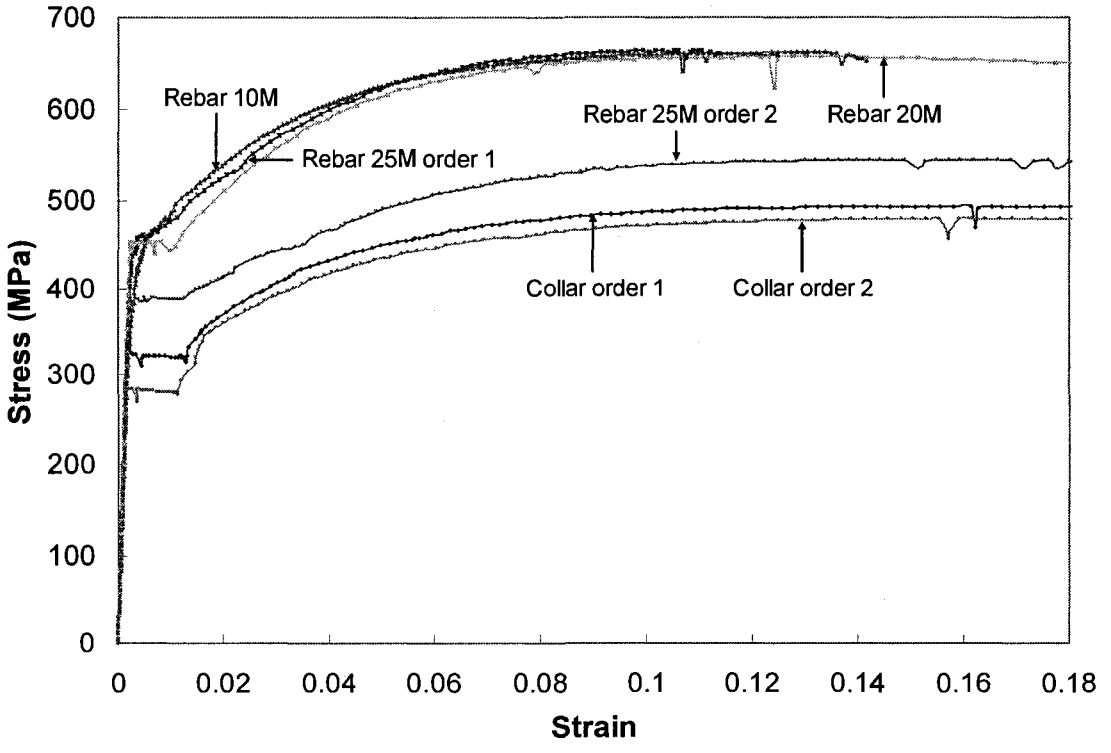

Figure 3-10 Stress versus strain curves for rebar and collar steel

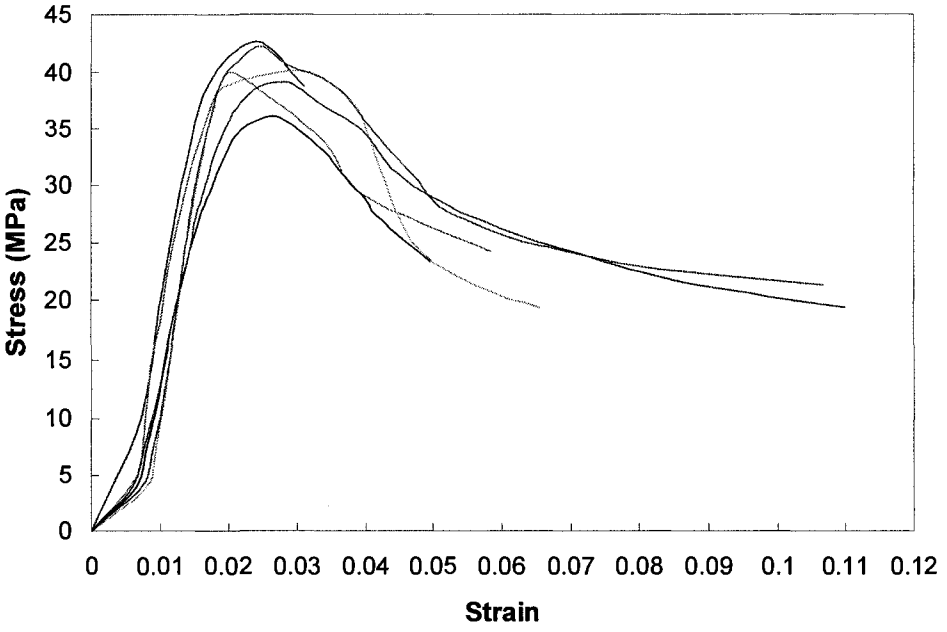

Figure 3-11 Epoxy mortar stress versus strain curves

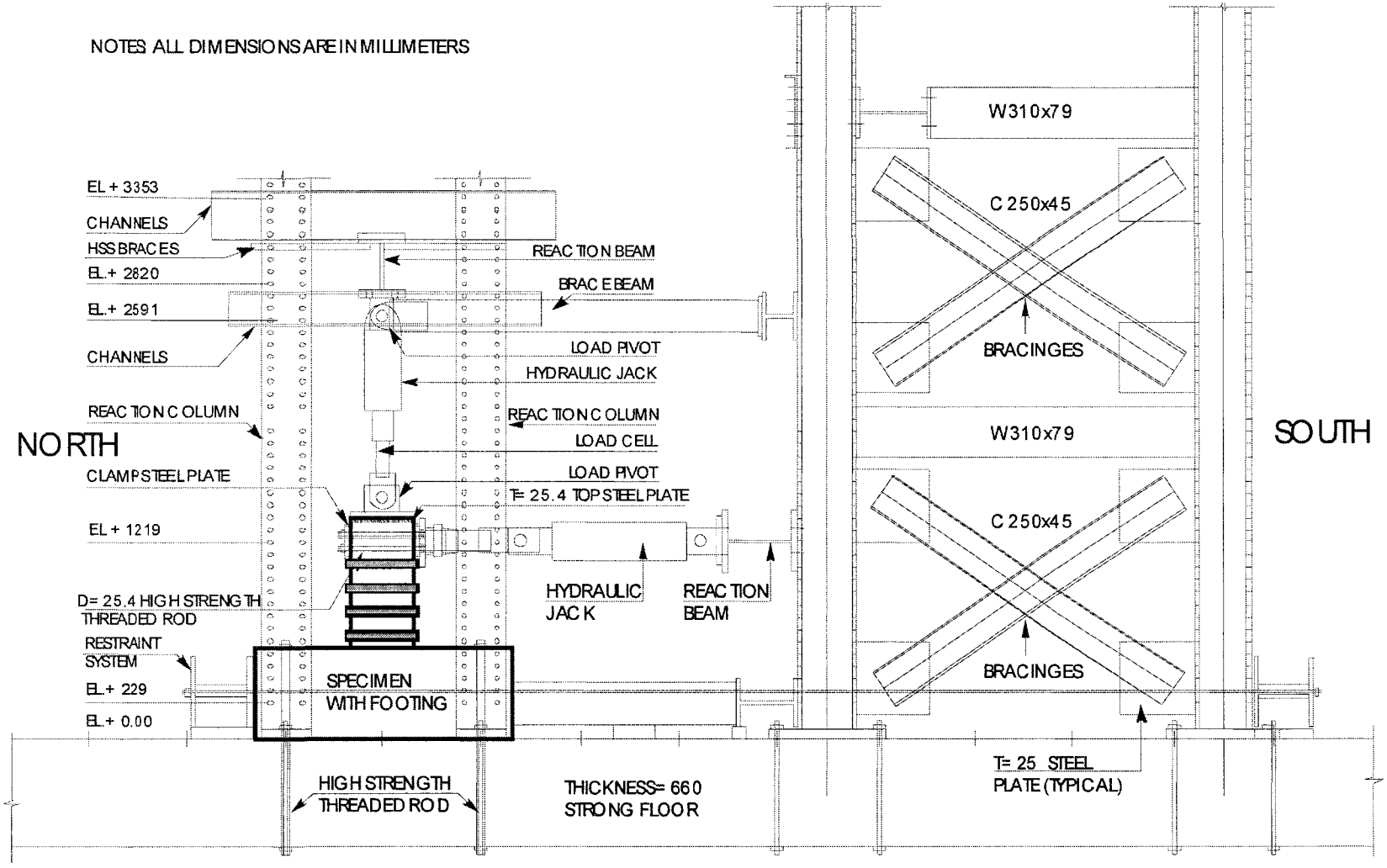

Figure 3-12 Test set-up schematic

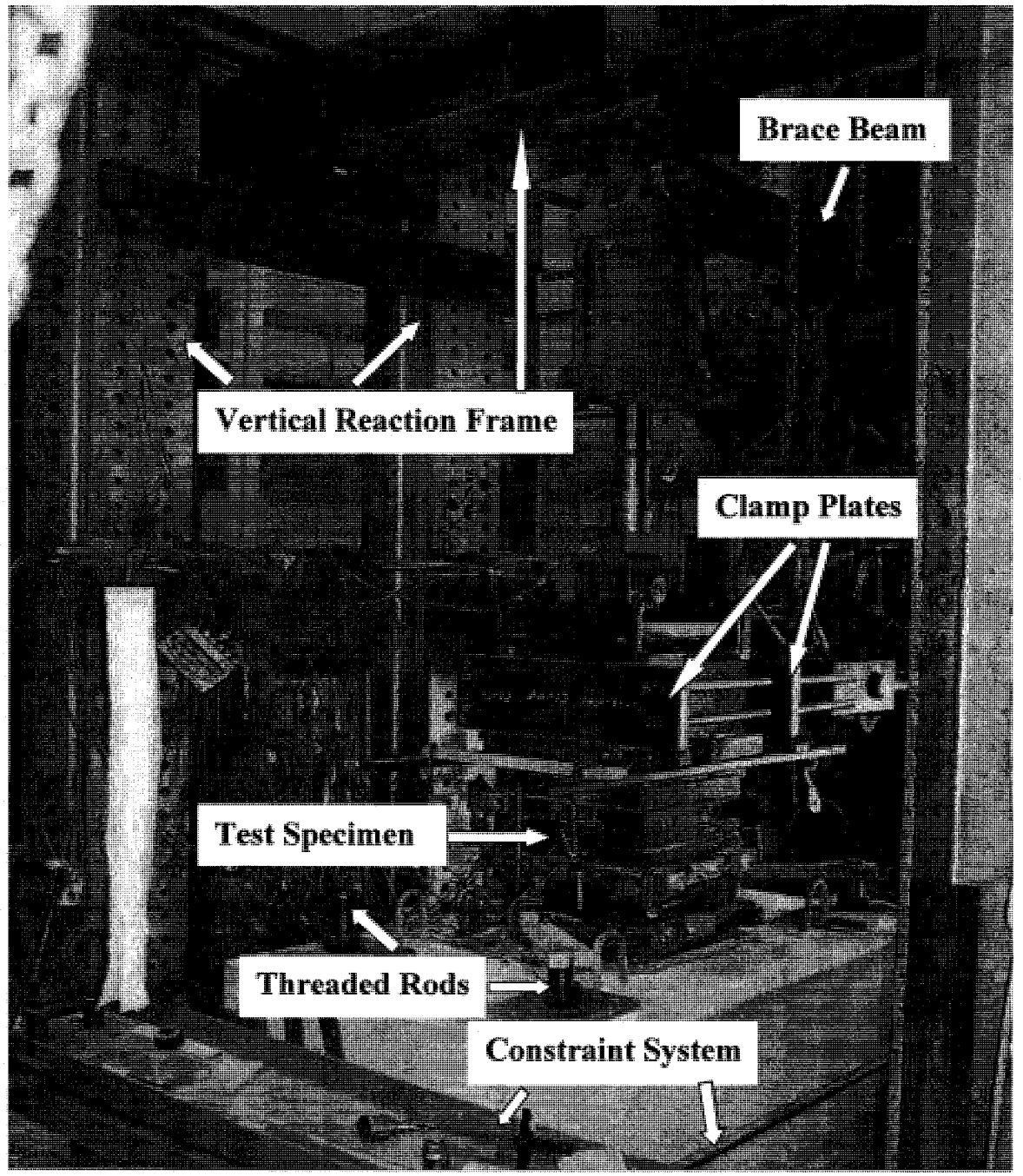

Figure 3-13 Test set-up

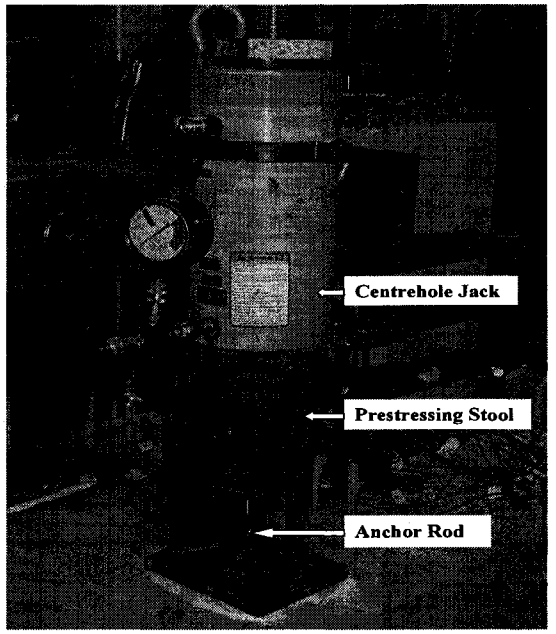

Figure 3-14 Anchor rod prestressing set-up

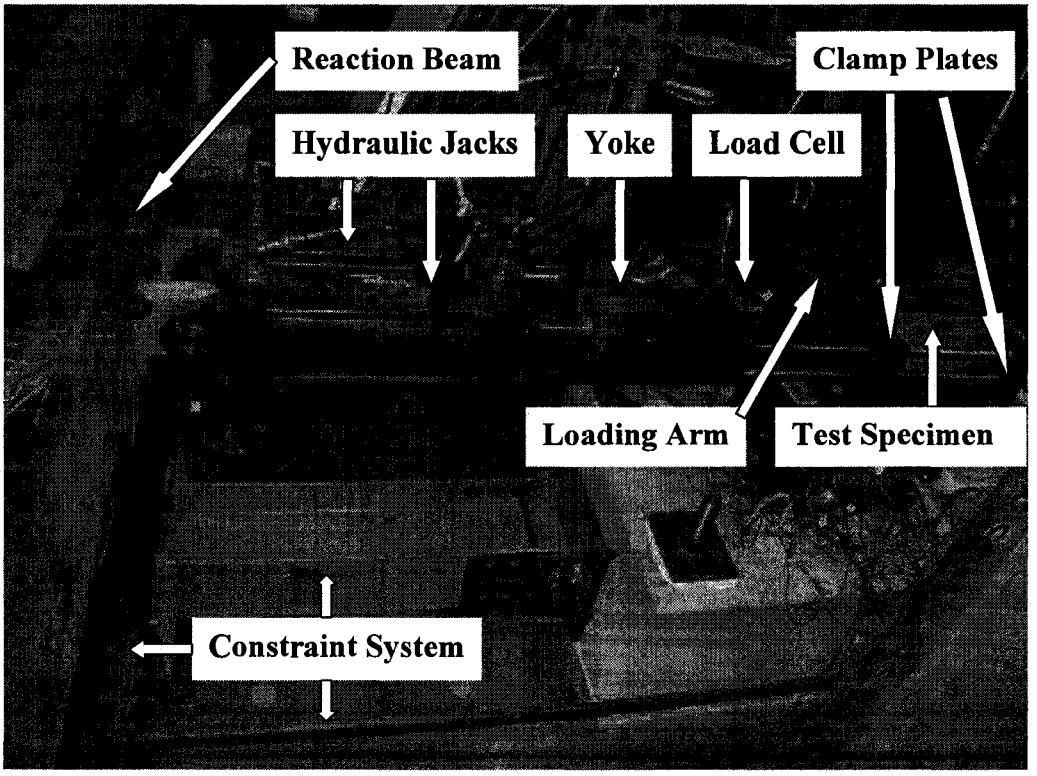

Figure 3-15 Constraint system and horizontal loading assembly (reverse angle as compared to Figure 3-13)

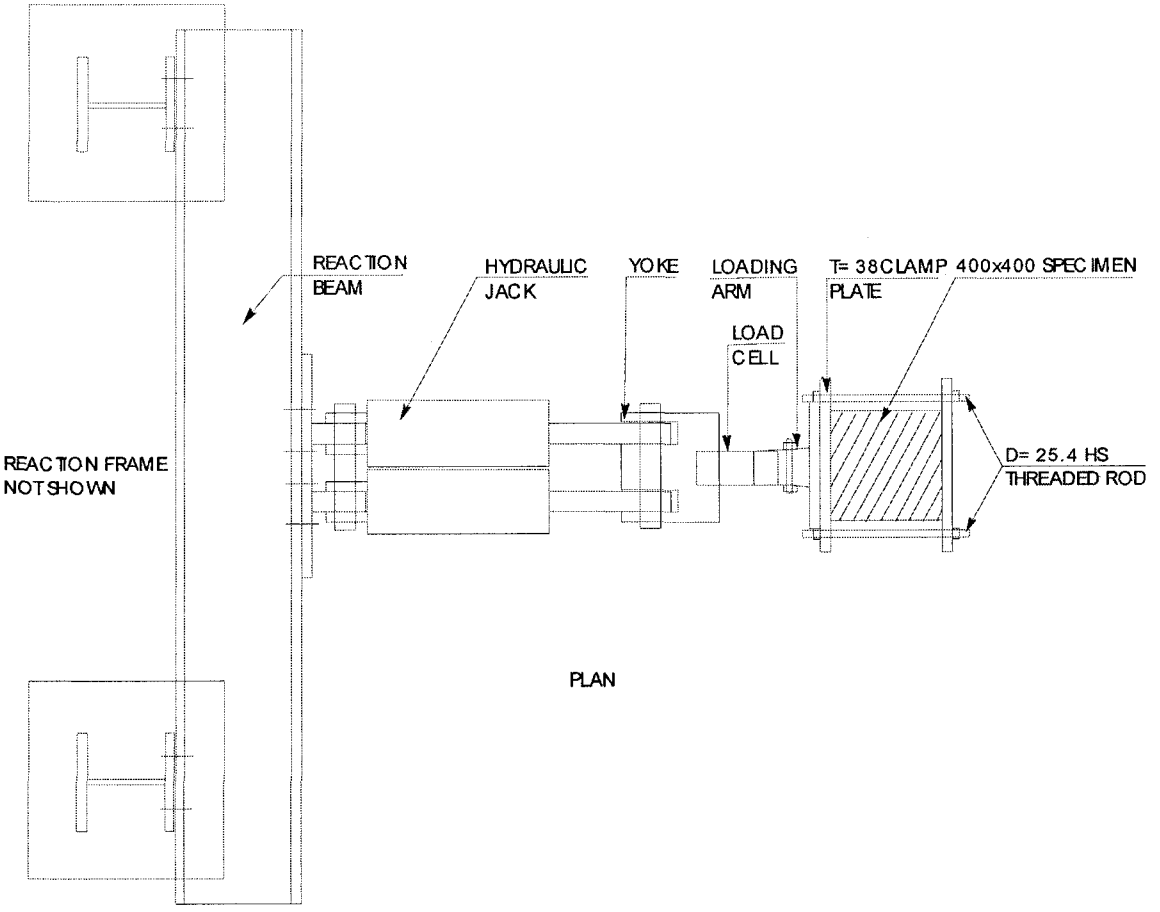

Figure 3-16 Horizontal loading assembly schematic (plan)

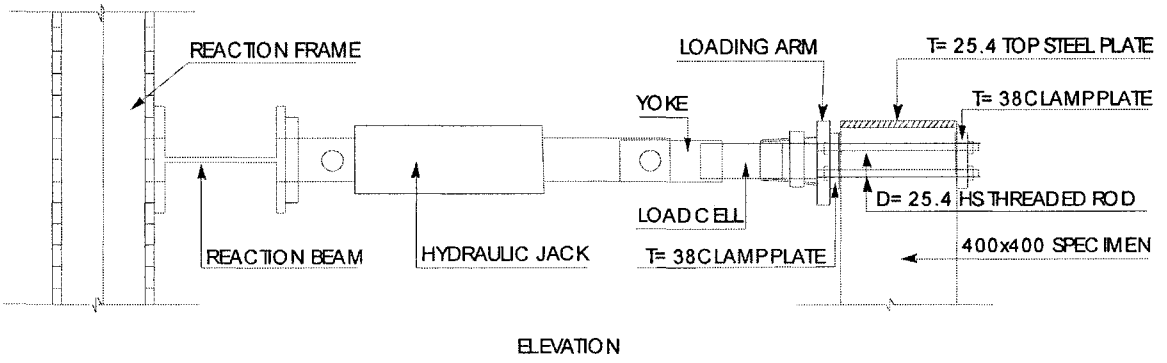

Figure 3-17 Horizontal loading assembly schematic (elevation)

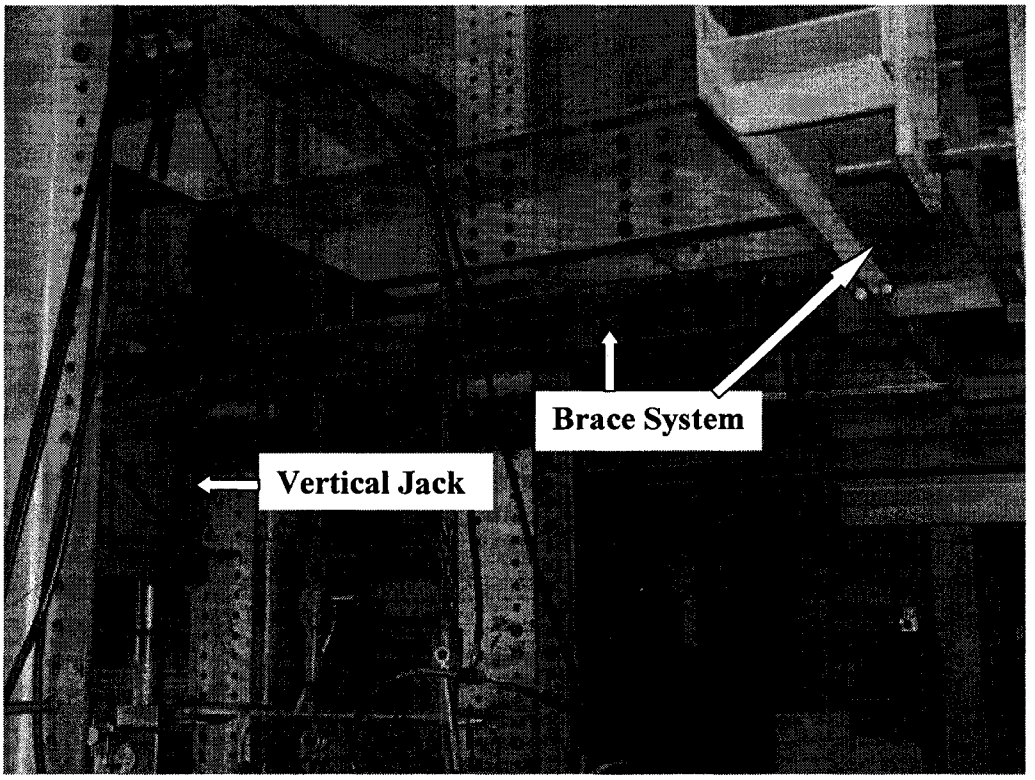

Figure 3-18 Brace system for vertical jack

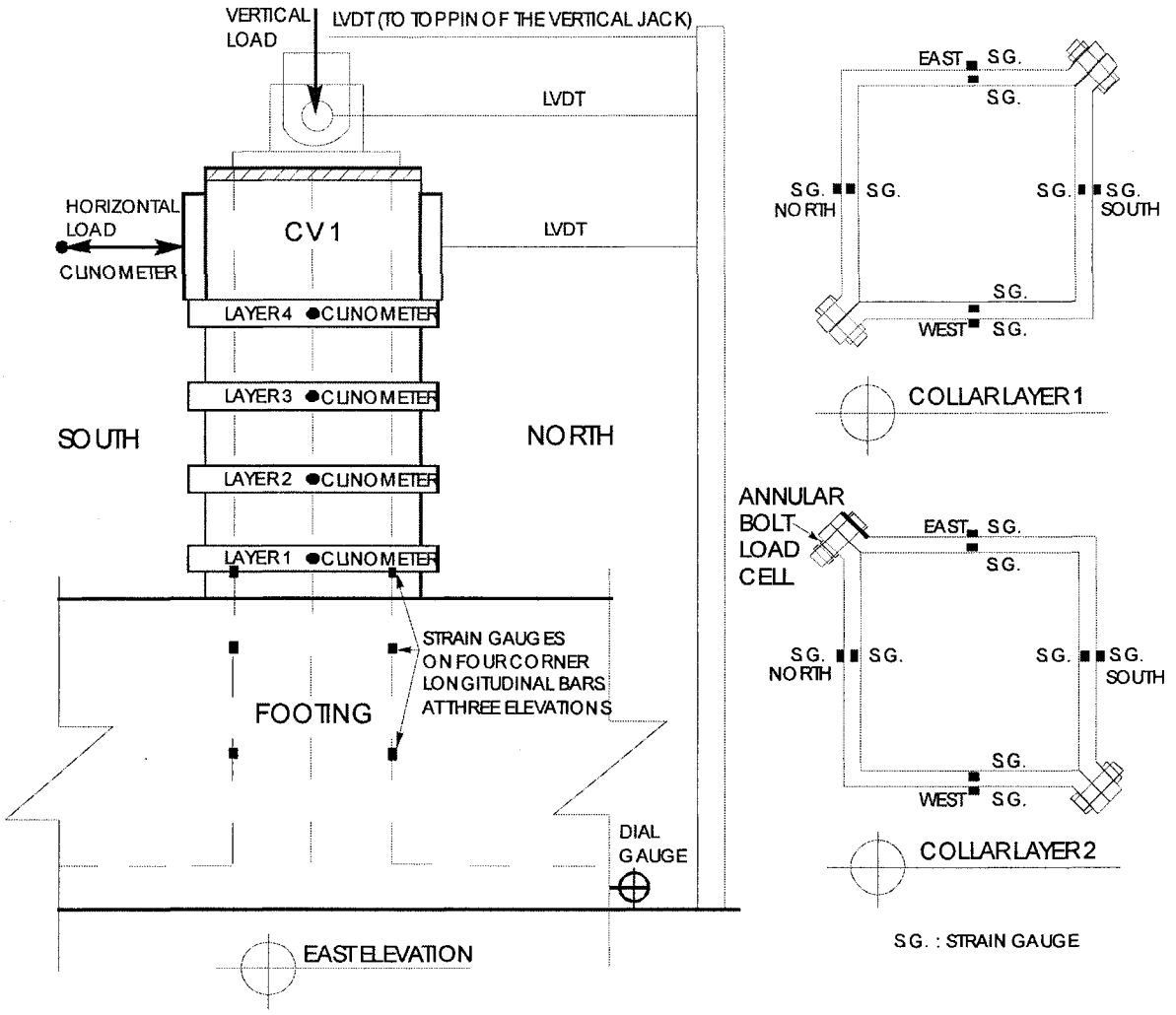

Figure 3-19 Instrumentation details schematic (specimen CV1)

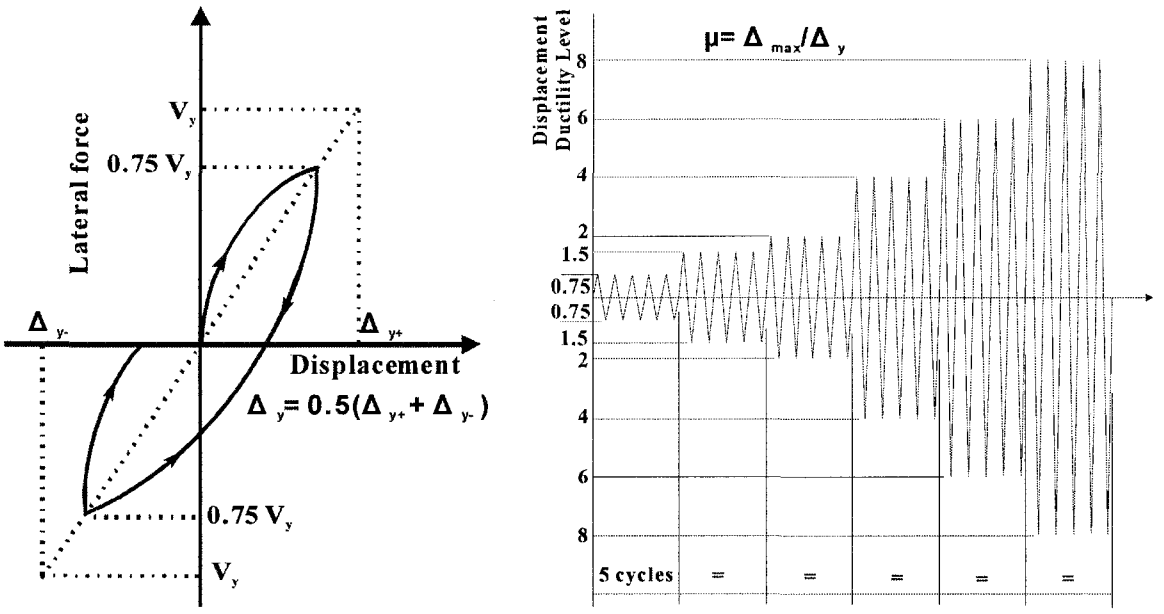

(a) Definition of yield displacement (b) Typical displacement sequence

Figure 3-20 Sequence of imposed displacements for test specimens

CHAPTER 4 DISCUSSIONS OF TEST RESULTS

4.1 Introduction

For convenience, in the following discussion the numbering of the layers of collars and gaps between collars are defined so that from the bottom to the top of the column, the number increases. That is, the first layer of collar near the footing is given the number 1 and the second layer (above) is given the number 2. Similarly, the gap between the footing and the first layer of collar is given the number 1 and the gap between the first and the second layers of collar is given the number 2.

The loading scheme is described in detail in Chapter 3; a brief summary of the aspects central to the discussion in this chapter is provided here for convenience. The direction of loading is defined as follows: the "push" direction relates to column deflection toward the north in the test set-up (see Figure 3-12), while the "pull" direction relates to southward column deflection. In tables, the loading direction is shown with the sign "+" for "Push to the North" and the sign "-" for "Pull to the South". One complete cycle consists of a push-half-cycle followed by a pull-half-cycle, starting and ending at the initial vertical column alignment. Five cycles were implemented at each force or displacement level according to the loading protocol described in Chapter 3, Section 3.6. The axial load, if applicable, was applied initially before any lateral loads and then kept constant throughout the remainder of the test. The axial compressive load was established using an axial compression index value of 0.3 (as shown in Table 3-1), based on the measured concrete strength. Lateral loading was applied under force-control up to 75 percent of the force corresponding to the estimated first yield of the longitudinal reinforcement, followed by displacement-controlled loading thereafter. For specimens CV0A, CV0AR and CV5, reduced peak force levels were utilized for the initial five cycles to reduce the chance of an early sudden failure. The analysis related to displacement ductility in this chapter is based on the value determined from the plot after the completion of the test.

4.2 General Observations

This section provides a general description of the behaviour of each specimen during testing. When conducting the test, the load–displacement hysteresis was plotted in real time to provide a graphical insight into the behaviour of each specimen and a way to control the test. The number of cycles sustained by each specimen at each control displacement ductility level, μ_c, is given in Table 4-1. Since the first five force-control cycles of specimens CV0A, CV0AR, and CV5 were conducted at loads lower than 0.75 times the estimated yield force, and hence resulted in a much smaller control displacement in conducting the test. However, the control displacement levels shown in Table 4-1 are just for convenience in the test, not the final displacement ductility levels. Also for specimen CV6, the final cycle of loading was conducted at displacement level 7, instead of 8 because of the stroke limit of the horizontal LVDTs.

Application of lateral load and displacement consisted of a series of cycles of imposed inelastic displacement, with maximum excursions that ranged from ±12 mm (CV0A) to

±75 mm (CV6). The columns were pushed and pulled far beyond their flexural yield points, to levels that in most cases probably exceeded the maximum displacements expected in an earthquake.

The external steel collars were bolted in place, directly on the surface of the square columns without creating stress concentrations at the corners, which might lead to crushing and damage of the concrete. Visible crack patterns indicated that a combination of diagonal cracking and concrete crushing in the flexural compression region was the dominant failure mode for all the test specimens, as was evident by inclined cracks of increasing distribution and widths after yield of the longitudinal bars. Generally, at later loading stages, the shape of the hysteretic loops became increasingly "pinched" toward the origin and the strength and stiffness of the specimens deteriorated somewhat more rapidly. A larger number of inclined cracks were visible in both directions, indicating more damage. At the end of the test, spalling of concrete cover was extensive in the bottom region of each column. The angle of the most severe diagonal cracking, measured from the longitudinal axis, was 32° to 42° for each specimen, except for CV7 which was 49°, and with an average of 37°, as shown in Table 4-2.

The observed mode of failure was ductile failure after yielding of the longitudinal bars took place except for CV4, which failed by longitudinal bar rupture. The strains in the longitudinal bars of all the columns, except specimens CV0A and CV5, were well above the yield strain of the bars at the peak applied load, while the longitudinal bars in specimen CV0A and CV5 just barely reached the yield strain. Ductile failure occurs when the column develops its flexural strength but ultimately fails due to the widening of the diagonal cracks, leading to a more rapid degradation of strength than flexural strength under repeated reversal of loading. The primary damage zone concentrated in the lower part of each specimen in gap 2, with the formation of a plastic hinge and crushing of concrete. At this location, the combination of shear force and curvature is close to maximum, while the critical section at the base was constrained by the footing which makes the failure zone move upward and away from it. Significant flexural horizontal cracks developed at the column-footing interface. Also, failure was delayed substantially by the presence of the collars—even after the formation of diagonal cracks—and the diagonal cracks developed at a relatively higher load than in the control columns. This resulted from the confinement effect provided by the external collars.

Even though the concrete crushed in the flexural compression region at the base of the column and three 20M longitudinal reinforcing bars on the south side of specimen CV4 ruptured in tension during the tests, no slippage of the collars was observed during the experiments. Collars deformed plastically outward to some degree, indicating substantial confinement was being provided to the concrete. The collar legs on the north and south sides (the push and pull direction of the lateral load) deformed more than the west and east sides because of increased concrete dilation at the extreme compression fibre locations. At the end of each test, the steel collars were removed and the column was examined visually. No concrete spalling occurred directly under the collars. The steel collars allowed a more gradual degradation of strength at failure, as compared to the control columns without collars.

4.2.1 Specimen CV0A

Specimen CV0A represents an existing column with typical transverse reinforcement designed for gravity loads, but with seismic hooks. The first five cycles were controlled by lateral load levels of 280 kN, 60% of the typical load used for collared columns, and this much lower load was used to avoid brittle failure during the first cycle. The control yield displacement used for conducting the test was 1.59 mm, as shown in Table 4-3. The remaining groups of cycles were controlled by increasing the lateral displacement to levels of 1.5, 2, 4, 6, and 8 times this control yield displacement.

Hairline diagonal cracks were first found during cycle 7 at each side extending from a height of 300 mm to 250 mm from the column base, but they closed fully after unloading. No new cracks initiated until cycle 14. At cycle 16, cracks emerged at the west and east sides extending from the bottom of the column to the height of the lateral loading position, as shown in Figures 4-1(a). These cracks grew progressively larger and wider in the later cycles, and were oriented at approximately 32° (from the longitudinal axis) at the east side and 40° at the west side during the push direction half-cycle, and 28° at the east side and 32° at the west side during the pull direction half-cycle. Minor concrete cover spalling started at cycle 20 at the east and west sides of column, and concrete crushing was found at the bottom of the four corners at cycle 21. From cycle 21, concrete crushing was observed at the interface between the south and north sides of the column and footing. The test was terminated after cycle 27 due to the substantial degradation of strength.

All the longitudinal bars and one layer of transverse reinforcement were visible at the end of the test after removing the loose concrete, as shown in Figures 4-1(b). All the longitudinal bars showed some degree of local bending, especially the four corner bars. Most bending happened in the region of 150 mm to 300 mm height from the footing surface. The exposed transverse tie remained in place without any apparent loosening or slippage. This good performance can be attributed to the seismic hook and a corner tie located at every longitudinal bar. No crack was found in the footing.

4.2.2 Specimen CV0AR

The repaired specimen CV0AR was tested after the completion of the repairs of the damaged control specimen CV0A. Similar to the test of CV0A, the first five cycles were controlled by a lower lateral load level. Here this load was taken as 243 kN, half of the load used in the other collared column tests. The control yield displacement used for conducting the test was 3.09 mm as shown in Table 4-3. The remaining groups of cycles were controlled by increasing the lateral displacement to levels of 1.5, 2, 4, 6, 8, 10, 12, 14, 16, and 18 times this control yield displacement.

A hairline crack was first detected during cycle 6 at the southwest corner, which closed after unloading. No new cracks initiated until cycle 16, when they developed at the west and east sides between the collars. These cracks grew wider in the later cycles, and were

oriented at approximately 37° (from the longitudinal axis) at the east side and 31° at the west side during the push direction half-cycle, and 32° at the east side and 38° at the west side during the pull direction half-cycle. At cycle 17, a crack was found at the interface between the south side of the column and footing. At cycle 22, a crack was found at the interface between the north side of the column and footing. After cycle 31, cracks at the interface between the south and north side of the column and footing got wider, as shown in Figure 4-2(a). Very minor concrete cover spalling started at the east side of the column at cycle 34 and at the west side of column at cycle 36. Concrete crushing was found at the interface between the column at the north side and the footing during cycle 38, and at the interface between the column at the south side and the footing at cycle 49. After cycle 45, wider cracks, concrete bulging, and more cover spalling were found, especially after cycle 51.

As observed by Hussain and Driver (2005b) and others, cracks were found in the footing due to the extension of the longitudinal bars of the column below the footing surface and the resulting bond failure. These cracks appeared as early as cycle 17 at the west side, but did not occur at the east side until cycle 33. The cracks extended 400 mm and 500 mm from the top into the footing at the east and west sides, respectively. Most of the concrete spalling happened in gap 2, although some occurred in gaps 1 and 4. At the south side of the column, the concrete bulged out about 10 mm in gap 2, while it bulged out about 25 mm at the north side in gaps 1 and 2, but the concrete was intact.

The middle longitudinal bars at the east and west sides, and the four longitudinal bars at the north side of the column became visible in gap 2 after removal of the loose concrete at the end of the test. The middle rebar at the east side became partially visible in gap 4. The collars deformed, especially the south and north legs of collars 1 and 2, as shown in Figure 4-2(b). Connection bolts for collars 1 and 2 also deformed plastically.

4.2.3 Specimen CV0B

Specimen CV0B was detailed according to CSA-A23.3-04 and ACI 318-05. The first five cycles were controlled by a lateral load level of 486 kN, control yield displacement used for conducting the test was 5.72 mm as shown in Table 4-3. The remaining groups of cycles were controlled by increasing the lateral displacement to levels of 1.5, 2, 4, and 6 times this control yield displacement.

Hairline diagonal cracks were first found during cycle 3 at the east, west and north sides extending from the height of 490 mm to 235 mm from the column base, but they closed after unloading. More hairline cracks emerged after cycle 4 at four sides. At cycle 6, cracks developed at the interface between the column at the south and north sides and the footing, and the concrete showed softening indicating the forthcoming crushing and spalling. These cracks grew wider in the later cycles, and were oriented at approximately 37° (from the longitudinal axis) at the east side and 33° at the west side during the push direction half-cycle, and 40° at the east side and 38° at the west side during the pull direction half-cycle. Very minor concrete cover spalling started at the west side at cycle 9 and at the east side at cycle 13. Some crushing were observed at the bottom of northeast

and northwest corners at cycle 11 and at the bottom of southeast and southwest corners at cycle 12. Diagonal cracks were apparent at cycle 16, as shown in Figure 4-3(a). After that wider cracks, concrete bulging and more cover spalling were found, especially after cycle 19.

Cracks were found in the footing due to the extension of the longitudinal bars of the column below the footing surface and the resulting bond failure. Cracks in footing were found as early as the cycle 15 at the east and west sides. These cracks extended 500 mm into the footing at the east and west sides. Most of the cover spalling happened in the region of 150 mm and 300 mm height from the footing surface at the east and west sides. No crack or spalling was found underneath the loading clamp plate. The concrete around the longitudinal bars spalled and left the bars unbonded. All the longitudinal bars and five layers of transverse reinforcement became visible after removing the loose concrete at the end of the test as shown in Figures 4-3(b). All the longitudinal bars showed some degree of local bending, especially the four corner bars. Most bending happened in the region of 150 mm to 320 mm height from the footing surface. All the exposed transverse ties remained in place without any apparent loosening or slippage, except the third layer tie expanded out and loosened slightly at the southeast corner.

4.2.4 Specimen CV1

Specimen CV1 was considered to be the base case specimen from which all the testing parameters were varied. The first five cycles were controlled by a lateral load level of 486 kN, control yield displacement used for conducting the test was 4.43 mm as shown in Table 4-3. The remaining groups of cycles were controlled by increasing the lateral displacement to levels of 1.5, 2, 4, 6, and 8 times this control yield displacement.

Approximately 35° (from the longitudinal axis) hairline diagonal cracks were first observed at the east and west sides as early as cycle 2. More cracks occurred after cycle 6. These cracks get wider in the later cycles, and were oriented at approximately 35° (from the longitudinal axis) at the east side and 35° at the west side during the push direction half-cycle, and 30° at the east side and 37° at the west side during the pull direction half-cycle. At cycle 13, some minor concrete crushing was observed at the interface between the column and the footing; however, very little concrete crushing in collar gaps was observed up to cycle 18, a ductility level of 4, which is commonly used for the design of new reinforced concrete structures in seismic zones.

The test was terminated after cycle 30 with maximum control displacement ductility of 8 due to the strength deterioration and visible damage. Most of the damage occurred in gaps 2 and 3 at the east and west sides, and the interface between the column at the south and north sides and the footing. Some damages were found in gap 3 at the east and west sides.

Specimen CV1 exhibited vertical cracks at location coincident with the locations of the longitudinal bars as shown in Figure 4-4(a), an observation also found by Lynn *et al.* (1996), Aboutaha and Machado (1999). Longitudinal cracks at the middle of the east and

west sides were found in cycle 14, which initiated considerable concrete crushing after cycle 20, and it extended from above collar 1 to below collar 4. In the middle of the west side, there was a vertical crack along the middle longitudinal bar.

None of the longitudinal bars ruptured. The middle longitudinal bars at the east and west sides became visible between collar 1 and collar 4 as shown in Figures 4-4(b), two longitudinal bars at southwest and northeast corners became visible between collars 1 and 2, and the longitudinal reinforcing bar at the northwest corner became visible between collar 1 and collar 3 after removal the loose concrete at the end of the test and these bars bent at the portion of gap 2. No crack was found in the footing. All collars deformed, especially collars 1 and 2. The connection bolts for collars, however, did not show much deformation.

4.2.5 Specimen CV2

Specimen CV2 was different from specimen CV1 in that the collar centre-to-centre spacing was 200 mm instead of 150 mm. The first five cycles were controlled by a lateral load level of 486 kN, control yield displacement used for conducting the test was 5.85 mm as shown in Table 4-3. The remaining groups of cycles were controlled by increasing the lateral displacement to levels of 1.5, 2, 4, and 6 times this control yield displacement.

Hairline diagonal cracks were first found during cycle 1 at four sides in gap 2 and gap 3 but all these cracks were closed after unloading except two cracks at the east and west sides. More hairline cracks developed after cycle 7 at the east and west sides. These cracks became wider in the later cycles, and were oriented at approximately 37° (from the longitudinal axis) at the east side and 40° at the west side during the push direction half-cycle, and 41° at east side and 31° at the west side during the pull direction half-cycle. Very minor concrete cover spalling started at the middle of the west side above and below collar 2 at cycle 7, at the interface between the column at the south and north sides and the footing at cycle 13, and at the middle of east side below collar 2 at cycle 22. Concrete crushing was found at the interface between the column at the south and north sides and the footing at cycle 13. After cycle 16, wider cracks, concrete bulging, and more cover spalling were found, especially after cycle 22. Similar as specimen CV1, vertical cracking at locations coincident with the locations of the longitudinal bars was observed as shown in Figure 4-5(a).

Cracks were found in the footing at the east and west sides, extending 560 mm from the top into the footing. Most of the concrete cover spalling happened in gap 2, middle part of gap 3, corners of gap 1 at the east and west sides, and the interface between the column at the south and north sides and the footing. No crack or spalling was developed underneath the loading clamp plate. At the south side of the column, the concrete bulged out about 20 mm in gap 2, while it bulged out about 30 mm at the north side in gap 2. The shear displacement and bulging was very apparent as shown in Figure 4-5(b). Cracks also extended 180 mm from the top of collar 3 to upper part of the column on the east, west and north sides.

The middle and southeast corner longitudinal bars became visible in gap 2, and the northeast corner longitudinal bar became visible in gap 1, and two longitudinal bars at southwest corner and northeast corner became visible in gaps 1 and 2, and the middle longitudinal rebar at the west side became visible in gaps 2 and 3 after removing the loose concrete at the end of the test. Very apparent deformation was found for all the collars especially the south and north legs of collars 1 and 2. The connection bolts of collar 1 also experienced bending.

4.2.6 Specimen CV3

Specimen CV3 was different from specimen CV1 in that the collar centre-to-centre spacing was 95 mm instead of 150 mm. The first five cycles were controlled by a lateral load level of 486 kN, control yield displacement used for conducting the test was 7.04 mm as shown in Table 4-3. The remaining groups of cycles were controlled by increasing the lateral displacement to levels of 1.5, 2, 4, 6, 8, and 10 times this control yield displacement.

Hairline diagonal cracks were first found during cycle 1 at the east and west sides in gap 3, gap 4 and gap 5, and during cycle 2 at the north side but most cracks diminished after unloading. No new cracks occurred until cycle 12 at the west side. These cracks grew wider in the later cycles, and were oriented at approximately 36° (from the longitudinal axis) at the east side and 36° at the west side during the push direction half-cycle, and 41° at the east side and 39° at the west side during the pull direction half-cycle. Very minor concrete cover spalling started at the middle of the west side in gap 3 at cycle 12, at the interface between the column at the south and north sides and the footing at cycle 17, and at the middle of east side in gap 4 at cycle 17. Some concrete crushing was found at the interface between the column at the south and north sides and the footing at cycle 17. The column retained very good integrity even at the displacement level of 4. Only after cycle 22, wider cracks, concrete bulging, and more cover spalling were found. Most of the cover spalling happened in gap 2, middle part of gap 3, in gap 4, a little in gap 5 at the east and west sides, in gap 2 and some in gap 3 at the south and north sides. However the bottom collar had direct contact with the footing at large displacement levels, causing some concrete damage at the footing. At the end of the test, although large displacement was applied, the specimen was still in good condition without much damage as shown in Figure 4-6(a). From collar 3 to above, no crack or spalling was found at south side. Bulging was not apparent, and only a little happened at the south and north sides below collar 3. Concrete cover damaged at the north side and west side in gap 1, also the concrete cover was damaged at the interface between the column and footing as shown in Figures 4-6(b).

Cracks in the footing were found at the east and west sides, extending 460 mm and 500 mm from the top into the footing, respectively. Three longitudinal bars became visible in gap 2 at the west side, the middle longitudinal rebar became visible in gap 3 at the east side, and the northwest corner longitudinal reinforcing bar became visible in gap 2 after removing the loose concrete at the end of the test. Apparent collar

deformation was found for collar 2 especially the south and north sides. The connection bolts of collar 1 were also bent.

4.2.7 Specimen CV4

The difference between specimens CV4 and CV1 were that CV4 had ten 20M longitudinal bars while all the other specimens had ten 25M longitudinal bars, hence CV4 had a longitudinal reinforcement ratio 1.88% instead of 3.13%. The first five cycles were controlled by a lateral load level of 486 kN, control yield displacement used for conducting the test was 5.14 mm as shown in Table 4-3. The remaining groups of cycles were controlled by increasing the lateral displacement to levels of 1.5, 2, 4, 6, 8, and 10 times this control yield displacement.

A hairline flexural crack was first found at the north side in gap 2 during cycle 2 but closed after unloading. No new cracks developed until cycle 4 at the west, east and north sides, and later on south side. These minor cracks remained small in the later cycles until cycle 16, grew progressively and were oriented at approximately 30° (from the longitudinal axis) at the east side and 29° at the west side during the push direction half-cycle, and 34° at the east side and 33° at the west side during the pull direction half-cycle. The column showed very good integrity even at the displacement level of 4 and 6. Very minor concrete cover spalling started at the middle of the west side in gap 3 at cycle 16 as shown in Figures 4-7(a), at the interface between the column at the south and north sides and the footing at cycle 17, and at the middle of the east side in gap 2 at cycle 25. Some concrete crushing was found at the interface between the column at the south and north sides and the footing at cycle 22. More spalling and crushing were found at the southwest corner in gap 2. The longitudinal bar at the southwest corner became visible in gap 2 during the pull direction of cycle 31. This bar buckled during the push direction of cycle 32 and fractured during cycle 33. Another longitudinal bar also fractured along with a big "bang" noise was heard and the lateral load dropped a lot at the same time. During the pull direction of cycle 33, another big "bang" was heard and the lateral load dropped a lot. The test was stopped at the end of cycle 34 with the fracture of the longitudinal bars.

Observations at the end of the test showed that, most of the cover spalling happened in gap 2 and some in gap 1 at the south and north sides. While the east and west sides experienced very minor damage below collar 2. Three longitudinal bars on the south side fractured as shown in Figures 4-7(b), and eight bars were visible in gap 2 except two middle bars on the east and west sides. Cracks in footing were found at the east and west sides, extending 470 mm from the top into the footing. Apparent collar deformation was found for collars 1 and 2 especially the south and north sides. No apparent deformation was found on the connection bolts of the collars.

4.2.8 Specimen CV5

Smaller shear span (350 mm instead of 650 mm for others) was used for specimen CV5, and it resulted in repositioning of the horizontal loading assembly and the measuring

instruments. The first five cycles were controlled by a lateral load level of 486 kN, the control yield displacement used for conducting the test was 1.19 mm as shown in Table 4-3. The remaining groups of cycles were controlled by increasing the lateral displacement to levels of 1.5, 2, 4, 6, 8, 10, and 12 times this control yield displacement.

No crack was found until cycle 7 in the pull direction half-cycle, and there was a minor crushing at the northwest corner directly under the loading clamp plate. Diagonal cracks developed at the east side above collar 2 and on the west side in gap 2 during the push direction of cycle 11. At cycle 12, more cracks appeared in gap 2 on four sides. Cracks were found in the footing, and these cracks extended 220 mm into the footing at cycle 13 and extended 450 mm into the footing at cycle 21. The column showed very good integrity with narrow cracks and no crushing and spalling until the displacement ductility level of 2.26. Load values from the bolt load cell and strains in collars were very small up to cycle 15, indicating that not much concrete expansion and hence less confinement provided to the concrete. Later the cracks grew wider but no more new cracks formed. These cracks grew progressively, and were oriented at approximately 30° (from the longitudinal axis) at the east side and 45° at the west side during the push direction half-cycle, and 30° at the east side and 45° at the west side during the pull direction half-cycle. Minor concrete cover spalling was found at the bottom of the column at the south and north sides at cycle 21. Some concrete cover spalling on the east and west side in gap 2 was found at cycle 23. No new cracks developed until cycle 26, but some concrete cover spalling occurred in east and west sides especially in the west side as shown in Figures 4-8(a), and wider crack on the north side. During cycle 33, deep holes were found below collar 2 resulting from the concrete spalling on the east and west sides.

Observations at the end of the test showed that most of the concrete cover spalling happened in gap 2 on the east and west sides, and the interface between the column and footing especially at four corners. Six longitudinal bars on the east and west sides were visible in gap 2. The portion in gap 2 had been significantly bulged out showed very apparent shear displacement on the south and north sides. And the bottom part of the column below collar 1 also bulged out a little bit. Cracks were found to extend 480 mm from the top into the footing, as shown in Figure 4-8(b). Very apparent deformation of collars, especially on the south and north sides, can be seen corresponding to the concrete bulging at these two sides. All four collar connection bolts deformed.

4.2.9 Specimen CV6

No axial compressive load was applied to the test of specimen CV6. The first five cycles were controlled by a lateral load level of 486 kN, control yield displacement used for conducting the test was 10.87 mm as shown in Table 4-3. The remaining groups of cycles were controlled by increasing the lateral displacement to levels of 1.5, 2, 4, 6, and 7 times this control yield displacement. The lateral displacement level 7 was used because of the stroke limit of the linear variable displacement transformers (LVDTs).

Hairline diagonal cracks occurred during cycle 1 at all four sides in gap 2 and gap 3. More cracks in the subsequent cycles were found. These cracks grew progressively, and

were oriented at approximately 35° (from the longitudinal axis) at the east side and 45° at the west side during the push direction half-cycle, and 41° at the east side and 45° at the west side during the pull direction half-cycle. Cracks were found to extend 330 mm from the top into the footing during cycle 6, indicating significant extension of the longitudinal bars when no axial compression loads were applied. Minor concrete cover spalling was found at the interface between the column and the footing during cycle 6. More and wider cracks were found in the later loading and the cracks in the footing extend further from the top into the footing side, which was 400 mm deep during cycle 7. Concrete cover spalling was first seen on the west side in gap 2 during cycle 13 and on the east side in gap 2 during cycle 17, as shown Figure 4-9(a). Cracks in the footing were about 2.5 mm wide during cycle 17 and extended to 470 mm deep and 3 mm wide during cycle 18. More concrete cover spalling was observed at later cycles. The portion of gap 2 on the south and north sides bulged out significantly during cycle 22.

Specimen CV6 developed much damage at lateral displacement level of 6. But in order to study whether the collars will slip under significant spalling of concrete, test was continued further to the lateral control displacement level of 7 to extensive damage. No collar slippage was observed during the whole test even under significant concrete spalling as shown in Figures 4-9(b).

Observations at the end of the test showed the column experienced much damage on all four sides up to collar 4. Longitudinal bars had bent, especially the eight bars on the south and north sides, and they were visible from the bottom of the footing to collar 4. Cracks extended 490 mm from the top into the footing on the east and west sides, and extended 200 mm into the footing on the north side. All the collars deformed especially the collars 1, 2 and 3 on the south and north sides, but no apparent deformation was found in the connection bolts.

4.2.10 Specimen CV7

Unlike other specimens with snug-tight connection bolts at the start of the test, connection bolts in specimen CV7 were prestressed to provide some active confinement from the start of the test. The bolt pretension was applied through five steps, alternately at two corners from collar 1 to collar 4, to prevent pretension loss and initial corner concrete damage. All the bolts were pretensioned to 144 kN (about 35% of the specified minimum tensile strength of the ASTM A490 bolts) and stopped when very minor concrete damage was found at the corners. The first five cycles were controlled by a lateral load level of 486 kN, control yield displacement used for conducting the test was 4.13 mm as shown in Table 4-3. The remaining groups of cycles were controlled by increasing the lateral displacement to levels of 1.5, 2, 4, 6, 8, and 10 times this control yield displacement.

The pretension applied to the bolts delayed the occurrence of the cracks. Hairline diagonal crack was first found during cycle 6 in gap 2 and gap 3 and the crack closed after unloading. A crack in the footing was found at the top during the pull direction of cycle 12. The crack extended 370 mm from the top into the footing, then extended to 400 mm during cycle 16, and extended 490 mm into the footing during cycle 23. Strain

readings were very small for collars up to cycle 23, as can be validated that no deformation was visible in the collars. Cracks developed at the interface between the column at the south and north sides and the footing during cycle 15, and these cracks closed after unloading. During cycle 18, very minor concrete cover spalling was found at the interface between the column at the south and north sides and the footing, and during cycle 27, minor concrete cover spalling was found at the interface between the column at the east and west sides and the footing. Cracks remained very small after unloading until cycle 21, after which a few cracks became a little wider. These cracks grew progressively, and were oriented at approximately 50° (from the longitudinal axis) at the east side and 50° at the west side during the push direction half-cycle, and 49° at the east side and 45° at the west side during the pull direction half-cycle. The column showed very good integrity condition with narrow cracks and no crushing and spalling until the control displacement ductility level of 8.

The observations at the end of test showed that, most of the concrete cover spalling happened in gap 2 on the east and west sides and the interface between column and the footing on the south and north sides. Other regions were still in good conditions, as shown in Figures 4-10(a). Four corner longitudinal bars were visible in gap 2. Cracks extended 500 mm into the footing on the east side, 480 mm on the west side and 270 mm on the north side. All the collars deformed especially collars 1 and 2 on the south and north sides as shown in Figure 4-10(b). All the connection bolts deformed especially those in the collars 1 and 2.

4.2.11 Specimen CV8

Specimen CV8 had a larger size of collars with cross-section of 50×50 mm instead of 30×50 mm. The first five cycles were controlled by a lateral load level of 486 kN, control yield displacement used for conducting the test was 5.33 mm as shown in Table 4-3. The remaining groups of cycles were controlled by increasing the lateral displacement to levels of 1.5, 2, 4, 6, 8, and 10 times this control yield displacement.

Hairline diagonal cracks occurred during cycle 1 in gap 2 and gap 3, but closed after unloading. A few more cracks were found after cycle 6. These cracks grew progressively, and were oriented at approximately 39° (from the longitudinal axis) at the east side and 40° at the west side during the push direction half-cycle, and 40° at the east side and 30° at the west side during the pull direction half-cycle. The column showed very good integrity with narrow cracks and no crushing and spalling until the displacement level of 4 as shown in Figures 4-11(a). Cracks were found at the interface between the column at the south and north sides and the top of the footing during cycle 18, which extended 400 mm from the top into the footing during cycle 23. Very minor concrete cover spalling was found on the east and west sides during cycle 17. During cycle 20, cracks became wider especially on the north side. A little more concrete cover spalled on the west side and at the interface between the column at the north side and footing.

Minor damage was found even at the end of the test, as shown in Figure 4-11(b). Observation at the end of the test shows that most of the concrete cover spalling

happened in gap 2, middle portion of gaps 3 and 4 on the east side, and gap 2, middle portion of gaps 3 and 4 on the west side, and the interface between the column the south and north sides and the footing. Apparent concrete bulge happened in gap 2 on the south and north sides, showing shear displacement. Four longitudinal bars on the south side and the northwest corner bar were visible in gap 1. The middle longitudinal bars on the east and west sides were visible in gaps 2 and 3. Cracks extended 500 mm from the top into the footing on the east and west side and 80 mm on south side. No apparent deformation can be observed for all the collars and connection bolts.

4.3 Hysteresis Response

Specimen performance can be evaluated based on the peak lateral force, moment capacity, deformability, rate of strength degradation, and hysteretic behaviour. Hysteretic characteristics are very important for structures under earthquake action. Cyclic behaviour introduces incremental cracking that involves opening and closing of cracks, as well as bond destruction that shows pinching in the hysteresis loop. Similar unloading and reloading paths for successive loading cycles indicates little degradation, while the extent of the pinching nature of a hysteretic response can be examined when the unloading path passes near the origin. Pinching reflects the sliding shear displacement at the through-depth cracks (along with dowel action of the longitudinal reinforcement), and represents the degradation not only of the strength but also the energy dissipation capacity of the hinge region. It is caused by the interaction of shear force and axial force with the opening and closing of the cracks.

Because the axial compressive load was applied through pinned connections, the horizontal and vertical components of the axial compressive load contribute increasingly to the moment at the critical section of the column at large lateral displacements. The lateral force discussed below accounts for the deformed geometry, lateral loads, and axial loads within the system. When the top of the column moved laterally, both the vertical and horizontal load assemblies became inclined. However, the largest horizontal load assembly rotation, measured by clinometer during the test, was 3.2° for all the tests except CV3 it was 3.9°. Hence, the rotation of horizontal jack was assumed negligible. Therefore, as shown in Figure 4-12, the moment, M, at the critical column section (at the base) and the equivalent applied lateral force, V, in the test are determined as follows:

$$M = R \cdot H_1 + P\sin\alpha \cdot H_2 + P\cos\alpha \cdot \Delta_1 \qquad [4\text{-}1]$$

$$V = M/H_1 \qquad [4\text{-}2]$$

$$\tan\alpha = \Delta_1/H_3 \qquad [4\text{-}3]$$

where R is the total force in the horizontal hydraulic jacks; P is the force in the vertical hydraulic jack; Δ_1 is the lateral displacement at the vertical loading point; α is the inclination angle of the vertical loading assemblies; H_1 and H_2 are the vertical distances from the base of the column to the horizontal and vertical loading positions, respectively

(H_2 equals the height of the column plus the height of the load pivot, as defined in Figure 3-12); and H_3 is the vertical distance between the pin connections at opposite ends of the vertical loading assembly. Both H_2 and H_3 are the same for all the test specimens, while H_1 is the same for all test specimens except specimen CV5, which was tested with a smaller shear span. Although all three of these heights varied from the original values at the start of the test along with the movement of the column, the change was small and can be neglected without inducing much difference to the final calculation.

The lateral force–displacement hysteresis loops for all the test specimens are shown in Figures 4-13 to 4-23. The graphs are drawn to the same scale for all columns to facilitate comparisons. The first quadrant of the graph shows the behaviour of column when pushed in the north direction and the third quadrant is when pulled in the south direction.

In general, at later loading stages the shape of the loops became increasingly "pinched" toward the origin and the strength and stiffness of the specimen deteriorated at an increased rate. The experiments showed that collared columns have stable hysteresis behaviour with enhanced strength and ductility compared to columns without collars. The collared system also maintained its integrity under repetitive reverse cyclic loading with large displacement amplitudes.

The behaviour of specimen CV0A under the imposed cyclic deformations and axial loads is presented as a lateral force–displacement hysteresis loop in Figure 4-13. It can be seen that the deformation ability of this specimen is very small. The very narrow lateral force–displacement hysteresis loops indicate poor energy dissipation capacity, which is validated further in Section 4.8. Rapid strength degradation is apparent after reaching the peak load.

As shown in Figure 4-14, specimen CV0AR exhibited stable hysteresis behaviour and the long, wide hysteresis loops show the substantially improved energy dissipation capacity of this specimen after the repair. The hysteretic behaviour of specimen CV0B—with closely spaced ties—is shown in Figure 4-15, where it can be seen that the deformation capacity, although greater than CV0A—with widely spaced ties—is considerably less than the severely damaged and repaired (collared) specimen CV0AR. Figure 4-16 shows that specimen CV1 (the base case) exhibited excellent hysteretic behaviour. For specimen CV2, with wide collar spacing, the hysteresis loops shown in Figure 4-17 are not as stable as for specimen CV1, but still much better than the control specimen CV0A. The response of specimen CV3 with closely spaced collars, shown in Figure 4-18, indicates significantly more stable force–displacement characteristics up to a displacement of more than 60 mm.

The stable response of specimen CV4, with smaller longitudinal bars and hence lower longitudinal reinforcement ratio, can be seen in Figure 4-19. Specimen CV5 has a smaller shear-span, and the hysteresis behaviour is shown in Figure 4-20. The hysteresis loops are very tall and narrow due to the dramatically reduced deformation capacity and

increased strength, and significant degradation of strength can be found in cycles beyond a lateral displacement of about 5 mm, along with pinching of the hysteresis loops.

Specimen CV6 had no axial compressive load applied and, as shown in Figure 4-21, significant lateral force degradation occurred at a displacement around 75 mm. Severe pinching can be seen in the hysteresis loops. Satisfactory response for specimen CV7, which had collars with prestressed bolts, was obtained as shown in Figure 4-22. The hysteresis loops are wide and stable with much less pinching. From Figure 4-23 it can be concluded that specimen CV8, with thicker collars, also showed stable hysteresis characteristics with good deformation capacity.

Hysteretic performance of concrete columns is sometimes compared using the moment–drift response instead of the lateral force-displacement response, where lateral drift, expressed in percentage, is defined as the lateral displacement at the point of application of the horizontal load (Δ_2) divided by the vertical distance from the base of the column to the horizontal loading position (H_1):

$$Drift = \Delta_2 / H_1 \times 100\% \qquad [4\text{-}4]$$

where H_1 is 650 mm for all the test specimens except specimen CV5, where it is 350 mm. These response curves have also been generated and they lead to similar conclusions to those above. Complete moment–drift response curves for all of the tests can be found in Appendix B and the ultimate drift ratios achieved are discussed later in this chapter.

4.4 Comparison of Envelope Curves

A load–deformation envelope for each column was obtained by connecting the peak load for the initial hysteresis loop obtained at each displacement level. These curves reveal clearly when the peak value is reached and how stable the post-peak hysteretic behaviour is. The lateral force–displacement envelopes for the test specimens are shown in Figure 4-24, where it can be seen that the collared columns, as compared to the control columns, exhibited increased peak lateral force values and the peak value was maintained for larger displacements. In general, a stable response was obtained through the use of external steel collars.

The moment–drift envelope curves have also been generated and they lead to similar conclusions to those above. Complete moment–drift response curves for all of the tests can be found in Appendix B.

4.5 Displacement Ductility

As pointed out by Priestley *et al.* (1994a), although in reinforced concrete frame design, plastic hinges will normally be located at the ends of beams, column plastic hinges at the base of the structure are required to complete the plastic deformation mechanism. Special consideration is needed when plastic hinges form in the columns, so the rotation and

deformation capacities—and hence the displacement ductility—of the column are very important factors in the post-elastic design of columns.

Displacement ductility, μ, is defined as the ratio of the ultimate lateral displacement of the specimen, Δ_u, to the yield displacement of the specimen, Δ_y. Thus:

$$\mu = \Delta_u / \Delta_y \qquad [4\text{-}5]$$

Challenges in calculating representative displacement ductilities for specimens arise because of the different methods for defining the yield displacement. Two alternatives are discussed in the Section 4.5.1.

4.5.1 Modified Yield Displacement

Yield displacement is a critical parameter in calculating the displacement ductility of the test specimens. Before conducting the tests, a section analysis was performed to predict the flexural yield strength ignoring possible strength increase due to collars. 75% of this value was used as guidance for the first five load control cycles along with close visual observation of the load versus displacement curve during the test (similar to the approach adopted by Saatcioglu and Baingo 1999). The value used was close to 486 kN, except that for specimen CV5 (short shear span) it was about 860 kN. For consistency, the load level of 486 kN was also used for the first five load control cycles in the test of CV5, but load levels of 280 kN and 243 kN were used in conducting the tests of specimens CV0A and CV0AR, respectively, in an attempt to avoid possible failure in the initial cycles if a load level 486 kN was used. Hence, the control yield displacements used for the purpose of conducting these three tests were smaller than they should have been, so an initial modification was performed to these three tests to obtain the modified test displacements. Modification was done through linear extrapolation from displacement of the first cycle at the load of 280 kN and 243 kN to 486 kN for Specimens CV0A and CV0AR as the modified test displacement of the first cycle, and through linear extrapolation from displacement of the first cycle at the load of 486 kN to 860 kN for Specimens CV5 as the modified test displacement of the first cycle. The modified test yield displacement are 2.75 mm for specimen CV0A, 6.19 mm for specimen CV0AR, and 2.1 mm for specimen CV5, as shown in Table 4-3. In the table, V_1 is the load level for the first five cycles of the test, Δ^*_{c+} is the control displacement in the first cycle in push direction in conducting test, Δ^*_{c-} is the control displacement in the first cycle in pull direction in conducting test, Δ^*_c is the average of the push and pull control displacements of the first cycle, Δ_{yc} is the control yield displacement in conducting the test, Δ^*_{t+} is the modified test displacement in the first cycle in push direction, Δ^*_{t-} is the modified test displacement in the first cycle in pull direction, Δ_t^* is the modified average test displacement in the first cycle, Δ_{yt+} is the modified test yield displacement in the push direction, Δ_{yt-} is the modified test yield displacement in the pull direction, and Δ_{yt} is the

modified average test yield displacement in the push and pull directions. The modified test yield displacement, Δ_{yt}, is obtained through the extrapolation from the first cycle results and is calculated as 1.33 times Δ_t^*.

After the test, however, modification of the yield displacement was conducted to obtain a more representative value for comparisons of the test lateral force–displacement envelopes. There are several ways to modify the yield displacement. Discussed in the following are those methods used by Lacobucci *et al.* (2003), Youakim and Ghali (2003), Hosseini *et al.* (2005), Memon and Sheikh (2005), all of which involve an attempt to develop an idealized bilinear curve taking into consideration the peak lateral forces.

One method is the first cycle trendline method, using the test results from the first cycle to find the trendline and obtain the yield displacement. The lateral displacement corresponding to the peak lateral force $V_{max,exp}$ on this trend line is defined as the yield displacement. Yield displacements were obtained in push and pull directions separately using the same procedure. The calculation was shown schematically in Figure 4-25.

Another method is the secant line method, also used by Lacobucci *et al.* (2003), Youakim and Ghali (2003), Hosseini *et al.* (2005), Memon and Sheikh (2005), that involves the construction of the envelope of the whole test. The yield displacement represents the lateral displacement corresponding to the peak lateral force $V_{max,exp}$ on a secant line connecting the origin and a point at $65\%V_{max,exp}$, or $75\%V_{max,exp}$ (recommendations by different authors) on the envelope curve. Push and pull direction were considered separately. The method is shown schematically in Figure 4-26.

Considering the fact that the first trendline was based on the test result in the first cycle instead of randomly choosing 65% or 75%, here the first cycle trendline method was adopted and the modified yield displacement, Δ_y, for each specimen obtained by this method is listed in Table 4-4.

4.5.2 Ultimate Displacement and Drift

In order to provide a criterion of comparison of the ductility and a failure criterion, the concept of ultimate displacement is normally used by researchers. It is reasonable to assume that some degradation can be tolerated in the lateral force capacity of a column due to potential redundancies in the system and possible redistribution of resisting forces among other components. The ultimate displacement is typically defined as the displacement corresponding to where the lateral force resistance drops to 80% or 90% of its peak value. Saatcioglu and Baingo (1999) used 80%, Lacobucci *et al.* (2003) used 80% and 90%, Youakim and Ghali (2003) used 80%, Li and Sung (2004) used 80%, Hussain and Driver (2005b) used 90%, Memon and Sheikh (2005) used 80% and 90%.

Herein, the 90% rule is used to calculate the ultimate displacement from the envelope, as shown in Figures 4-35 and 4-36. The ultimate drift is then calculated as the ultimate

displacement divided by the corresponding shear span. The values of ultimate displacement and drift for all the test specimens are shown in Table 4-5. The values of ultimate displacement and drift are calculated separately in the push and pull directions for the convenience of calculating the displacement ductility in the push and pull directions separately in Section 4.5.3.

4.5.3 Ductility Levels

Values of displacement ductility, μ, based on the first cycle trendline method are shown in Table 4-4. The average of the displacement ductilities in the push and pull directions were calculated for later discussion and comparison in Section 4.12 and Section 4.13.

In general, the collared columns have greater ductility than the control columns. The collared column with a wide collar spacing (CV2) had less ductility than those with narrower collar spacings (CV1 and CV3). The collared column with a smaller longitudinal reinforcement ratio and smaller bars (CV4) had higher ductility than the collared column with a larger longitudinal reinforcement ratio (CV1). The specimen with the smaller aspect ratio (CV5) had less ductility than the specimen with the larger aspect ratio (CV1), and the collared column with pretensioned bolts (CV7) had more ductility than the equivalent collared column with snug-tight bolts (CV1). The specimen with the larger size of collars (CV8) showed a higher ductility level than the specimen with the smaller collars (CV1). Although the axial load index had a significant effect on the lateral force capacity, it had a minimal effect on the displacement ductility, as can be seen in Tables 4-4 and 4-6 by comparing specimens CV6 with no axial load applied and CV1 with an axial load index of 0.3. This phenomenon was also observed by Ahn *et al.* (2000) for column specimens regardless of concrete strength.

4.6 Normalized Peak Lateral Force

Shown in Table 4-6 are the peak lateral force and corresponding moment of each specimen in the push and pull directions. The average peak lateral force and moment are also calculated and listed in this table. Note that there are slight differences of peak lateral forces and moments between the push and pull directions that arose partly because of the small fluctuation in the axial load, less than 2% in all the tests, and partly due to the slight differences in the relative amplitudes of the displacements applied.

To account for the variation of the strength of the concrete from specimen to specimen, the maximum lateral force was normalized by the square root of the concrete compressive strength, using procedures similar to other researchers (Woodward and Jirsa 1984; Ghee *et al.* 1989; Priestley *et al.* 1994a, 1994b; Lynn *et al.* 1996):

$$V_{\max n} = \frac{V_{\max,\exp}}{A_g \sqrt{f_c'}} \qquad [4\text{-}6]$$

where $V_{max\,n}$ is the normalized peak lateral force, $V_{max,exp}$ is the average peak lateral force, A_g is the gross cross-sectional area of the column, which is the same for all the specimens in the present study, and $f_c^{'}$ is the compressive strength of concrete on the test day or one day before the test day. This dimensionless normalized peak value permits direct comparisons of results, regardless of the variation in $f_c^{'}$.

The normalized peak lateral force for each specimen is listed in Table 4-6. Comparing the normalized peak values in Table 4-6, it is seen that all collared columns experienced normalized peak lateral forces higher than those resisted by both CV0A and CV0B, with the exception of specimen CV6. The slight decrease in capacity of CV6 is attributed to the absence of an axial compressive load, which has been found to be beneficial to the capacity for reasonable axial load levels (*e.g.*, Woodward and Jirsa 1984). Neglecting specimen CV5, which had a smaller shear span, the greatest benefits in capacity over the control columns were achieved by prestressing the bolts (CV7) and reducing the collar spacing (CV3). Increasing the flexural stiffness of the collars (CV8) had a relatively small benefit in capacity, supporting the observation based on numerical studies that there is an optimal collar stiffness beyond which the column strength benefits tend to diminish rapidly (Hussain and Driver 2001). This was also observed in the parametric study discussed in Chapter 5, Section 5.4.

4.7 Initial Effective Stiffness K_y

Stiffness is an important aspect of the behaviour of columns loaded laterally. Excessive stiffness enhancement through rehabilitation will result in attracting extra force that might be a concern. Hence, it is worthwhile to calculate the effective stiffness of the collared columns as well as the control columns. Xiao *et al.* (1993), Priestley *et al.* (1994a, 1994b), Xiao *et al.* (1999), and Ahn *et al.* (2000) calculated the elastic secant stiffness at first yield of all the specimens tested, whereas Su and Zhu (2005) used the ultimate shear force divided by the yield displacement to calculate the initial stiffness. Lacobucci *et al.* (2003) and Memon and Sheikh (2005) used the slope of the secant line connecting the origin and a point at 65% $V_{max,exp}$ as the initial effective stiffness, while Youakim and Ghali (2003), Hosseini *et al.* (2005) used the slope of the secant line connecting the origin and a point at 75% $V_{max,exp}$ as the initial effective stiffness. Another approach is calculation of the slope for the first cycle trendline.

Herein, the slopes using the first cycle trendline method were calculated and shown in Tables 4-7. The calculation of initial effective stiffness K_y, taken as the slope of trendline of the first cycle, is shown schematically in Figure 4-25. Similar to findings reported by Xiao *et al.* (1999) and Sauce *et al.* (2004) that rehabilitating existing as-built columns with prefabricated composite jackets did not increase the stiffness significantly, the rehabilitated column with external collars also did not increase the initial effective stiffness. This shows that this system can be more advantageous than full height steel jacketing, which often stiffens the column and thus results in attracting excessive force. It

is worthwhile to point out that the initial effective stiffness discussed here relates to the yield displacement, and can not reflect the post-peak behaviour. The smaller value of stiffness can also be expected due to the relatively larger yield displacement of the collared columns as shown in Table 4-3. The first cycle for CV0A was conducted with an artificially low force, hence the trendline of this first cycle resulted in a higher stiffness than that had high force were adopted due to the degradation at high load.

4.8 Energy Dissipation Characteristics

The degree of energy dissipation is an important indicator of the performance of the column. The energy dissipation characteristics of the columns are influenced by various factors including the yield displacement, the axial load, and the number of load cycles applied. The structure is expected to dissipate significant energy input due to ground motion. The energy absorption capacity is a measure of the ability of a structure to survive a large number of inelastic cycles during an earthquake. This section discusses the energy dissipation capacity for the control columns and collared columns in terms of four measures: energy dissipated per cycle, cumulative energy dissipated, total energy dissipated, and equivalent viscous damping ratio.

4.8.1 Energy Dissipated Per Cycle

The energy dissipated in a loading cycle can be considered as the area enclosed by the lateral force–displacement hysteresis loop corresponding to that cycle. Wider and more stable hysteresis loops indicate higher energy dissipation. The energy dissipated per cycle for each specimen is shown in Figure 4-27 to Figure 4-37.

As expected, the energy dissipated in the first cycle at a certain displacement level is more than that in each of the remaining four cycles. At the same ductility level, the energy dissipation in a cycle gradually decreases due to the degradation in strength and stiffness. The extent of decrease is in good agreement with the degradation of the strength as depicted as percentage reduction between the first and fifth cycle in Table 4-8. All the columns dissipated very little energy during the cycles at initial loading levels, since they behave essentially in a near-elastic manner. It can be seen that a jump of the energy dissipated occurs after Cycle 16, which corresponds to the ductility level of 4—the ductility which is commonly used for the design of new reinforced concrete structures in seismic zones.

4.8.2 Cumulative Energy Dissipated versus Cycle Number

As used by many other researchers, Nanni and Norris (1995), Driver *et al.* (2001), Su and Zhu (2005), Hussain and Driver (2005b), Galal *et al.* (2005), cumulative energy dissipated by each test specimen was presented to show the energy dissipation capacity of the specimen. After calculating the energy dissipated in each cycle, the cumulative energy dissipated was then calculated by summing the energy dissipated in consecutive cycles throughout the test. Figure 4-38 shows the cumulative energy dissipated versus cycle number for all the test specimens. The figure show that collared columns far

out-performed the control columns. As expected, the energy dissipated in the first 16 cycles is very small because less inelastic behaviour occurred in the initial loading stages.

4.8.3 Total Energy Dissipated

Apart from enhancing the strength and ductility, the rehabilitation techniques would preferably also achieve significant levels of energy dissipation. As mentioned by Li and Sung (2003), the total energy dissipated, which serves as an index of the energy dissipation characteristics of the system, was calculated and compared among the specimens.

The energy dissipation characteristics of the specimens can be evaluated in terms of total energy dissipated at the end of the tests or at failure. The total energy dissipated is determined by summing the energy dissipated in each cycle up to a certain displacement level. The ultimate displacement was obtained first through the 90% rule on the envelope curve discussed in Section 4.5.2. The displacement level, which has a larger than ultimate displacement in the first cycle of this displacement level, was then determined. The energy dissipated was then added in all the cycles up to the displacement level right before this displacement level. The total energy dissipated by each test specimen is given in Figure 4-39. For Specimens CV0A, CV0AR, and CV5, smaller displacement increments were used since low forces were adopted in the first five cycles. Hence, five additional cycles of loading were conducted for specimens CV0A, 20 additional cycles were conducted for CV0AR, and ten additional cycles were conducted for CV5 compared the typical five cycles at each displacement level of 0.75, 1.5, 2, 4, 6, and so on. Energy dissipated in those additional cycles was included in the calculation of the total energy dissipated. It was found that the collared columns generally had better energy dissipation characteristics than the control columns, CV0A and CV0B, 32 kN·m and 134 kN·m, respectively, except the column with a reduced aspect ratio, CV5 (50 kN·m), was lower than CV0B. Rehabilitated specimen CV0AR showed improved energy dissipation (758 kN·m) capacity compared to the original control specimen. The reference specimen, CV1, dissipated 295 kN·m. By comparison, the total energy dissipated by the column with a reduced collar spacing, CV3, was significantly higher (694 kN·m), the total energy dissipated by the column with a wider collar spacing, CV2, was lower (252 kN·m), the total energy dissipated by the column with a reduced aspect ratio, CV5, was lower (50 kN·m), the total energy dissipated by the column with prestressed collar bolts, CV7, was higher (351 kN·m), the total energy dissipated by the column without axial compressive load applied, CV6, was lower (185 kN·m), and the total energy dissipated by the column with larger collars, CV8, was higher (485 kN·m).

4.8.4 Equivalent Viscous Damping Ratio

It is useful to compare the energy dissipation capacity of the test specimen with that of the ideal elastic-plastic hysteretic response. Ghobarah *et al.* (1996), Chopra (2001), Fischer and Li (2003), Hussain and Driver (2005b), Moretti and Tassios (2006) indicated using equivalent viscous damping ratio to measure the pinching of the hysteretic loop and the energy dissipation capacity of the specimens. The most common method for defining

equivalent viscous damping is to equate the energy dissipated in a hysteresis cycle of the real specimen and an equivalent viscous system. The definition of the equivalent viscous damping ratio γ is shown schematically in Figure 4-40 adapted from Ghobarah *et al.* (1996). It was taken as the ratio of the dissipated energy in a cycle to 2π times the strain energy measured at the peak of an equivalent linear elastic system.

The comparison of the variation of the equivalent viscous damping ratio for each test specimen with the drift ratio is shown in Figure 4-41. In general, collared column exhibited increasing ratio with the increase of drift ratio. The change of the specimen behaviour after rehabilitation was evident from the increase in the equivalent viscous damping of specimens CV1 to CV8 and CV0AR compared to control specimen CV0A. The relative lower value of the ratio for specimen CV0A can also be explained as that the pinching in the hysteretic response shown in Figure 4-13.

4.9 Curvature Distribution Along the Column Height.

Using the experimental data obtained from the clinometers mounted on the specimens, the average curvature between each two adjacent clinometers was determined as the difference in measured rotations divided by the vertical distance between the clinometers. Since the clinometers were attached to the collars for collared columns and pre-embedded bars for control columns, the clinometer heights varied on the different specimens, as shown in Table 4-9. No. 1, No. 2, No. 3, and No. 4 refer to the clinometer order from the column base. Portion 1, Portion 2, Portion 3, Portion 4 refer to the gap between the column base and clinometer No. 1, between clinometer No. 1 and No. 2, between clinometer No. 2, and No. 3, between clinometer No. 3 and No. 4. The curvature was plotted at the mid-point of the corresponding portion along the column height. From the test observations, most of the curvature happened at the bottom portion of the column. The curvature distribution along the first 500 mm column height for each specimen in the push and pull directions of loading under different displacement levels are found in Figures 4-42 to 4-52. Different scales were used in the horizontal curvature axis for each specimen for clarity. Control displacement level values show the order of the curvature curves as they move from left to right along the horizontal line with arrow for the Push curves. The Pull curves are dashed and the Push curves are solid.

The distribution of the curvature along the column height showed apparent symmetry in the push and pull directions. Curvature is typically small at the top of the column and is much larger in the bottom part of the column after the load-displacement behaviour becomes inelastic. The concentration of curvatures in the end regions of the columns became apparent especially after the lateral force exceeded the initial flexural yield of the longitudinal bars, indicating a relatively large inelastic rotation in these regions. The pattern of curvature distribution along the column height at different displacement levels can serve as a good experimental basis for the assessment of the plastic hinge length. For all the test specimens, the plastic hinge was concentrated in the bottom half of the column.

Curvature distribution along the column height also shows that specimens such as CV0A, CV2, and CV5 could not develop large inelastic curvatures due to the larger portion of

sliding shear deformation. As the load-displacement behaviour of specimen CV5 was strongly dominated by shear instead of flexure due to the small aspect ratio, the curvature was very small in comparison with the other specimens. Specimen CV5 failed by shear eventually and the load-carrying capacity dropped rapidly after reaching the peak load. Near the end of the test, more concrete spalling and crushing happened than encountered in the previous test cycles, and the unevenly distributed damage made the originally parallel collars inclined to different extents, despite the fact that slipping did not occur. This type of damage reveals itself in apparently erratic and large curvature at later stages of the test.

4.10 Capacity Degradation

Specimen strength and stiffness degradation occurs due to the widening of cracks, yielding of reinforcement, and spalling and crushing of the cover concrete during the later stages of loading in the test. One indication of desirable cyclic behaviour is the stability of the hysteresis loops, that is, the tendency for the loops to achieve the same peak lateral force in subsequent cycles at a given displacement level. Woodward and Jirsa (1984) suggested that the degree of degradation can be quantified as the percentage reduction of peak lateral force from the first to last cycles at each displacement level. Table 4-8 presents the percentage reduction at each test displacement level with five cycles for each of the cyclic tests. The percentage reduction targeted as a comparison of the fifth cycle to the first.

The test displacement values shown in Table 4-8 were the modified test displacements shown in Table 4-3. The test displacement levels were adjusted for CV0A, CV0AR and CV5 from the control displacement as shown in Table 4-3. For CV0A, the test displacement levels are 0.86, 1.15, 2.3, 3.45, and 4.6 from the modified test displacement, but only test displacement levels 1.15 and 2.3 were included in Table 4-8 for the percentage losses, intended to keep close to the typical 1.5 and 2 levels. For CV0AR, the test displacement levels are 0.75, 1, 2, 3, 4, 5, 6, 7, 8, and 9, but only test displacement levels 1, 2, 4, 6, and 8 were included in Table 4-8 for the percentage losses, intended to keep close to the typical 1.5, 2, 4, 6, and 8 levels. For CV5, the test displacement levels are 0.85, 1.13, 2.26, 3.39, 4.52, 5.65, and 6.78 from the modified test displacement, but only test displacement levels 1.13, 2.26, 4.42, and 5.65 were included in Table 4-8 for the percentage losses, intended to keep close to the typical 1.5, 2, 4, and 6 levels.

As can be seen from Table 4-8, control columns (CV0A and CV0B) generally exhibited a larger percentage reduction in lateral force capacity than collared columns CV0AR, CV1, CV2, CV3, CV4, CV7, and CV8. Table 4-8 also indicates that the strength degradation was minor at lower levels of displacement and increased with the increase of the maximum displacement for all collared column specimens. The specimen with a smaller aspect ratio (CV5) had larger capacity degradation than the corresponding specimen with the larger aspect ratio (CV1) from the low to high displacement levels between these two specimens. The specimen without axial compressive load (CV6) exhibited similar degradation to specimen CV1 at low displacement levels, but had significantly higher degradation during the large displacement cycles. However, this latter point can be

attributed largely to the fact that specimen CV6 was intentionally loaded to very high displacement levels—even though the column should have been deemed as failed because the lateral force had already dropped much lower than 90% of the peak load—in order to study whether collar slippage would occur under severe concrete spalling and crushing.

Specimen CV7 (with pretensioned bolts) showed much less degradation than specimen CV1 (with snug-tight bolts), with fewer and smaller cracks developing in CV7 due to the larger confinement provided to the concrete. Specimen CV2 (with the widest collar spacing) showed a degradation of more than 20% at large displacement levels and about 10% for the initial displacement levels, whereas CV3 (with the narrowest spacing) exhibited a reduction of less than about 10% for all displacement levels. Specimen CV8 (with the larger collar stiffness) showed slightly less degradation (around 10% for all displacement levels) than specimen CV1 (more than 10% at higher displacement levels). In general, collar configurations that provide higher degrees of confinement slowed the degradation in capacity from initial to later cycles.

4.11 Rotation-Induced Displacement

Previous researchers (*e.g.*, Hussain and Driver 2005b) revealed that a discrete rotation develops at the base of the column due to the penetration of axial strains in the tensile longitudinal reinforcement into the footing. In order to capture these additional fixed-end rotations, strain gauges were installed at two levels below the surface of the footing to obtain an estimate of the strain and strain gradient in the reinforcing bars in the footing for specimens CV0B, CV1, and CV4.

The rotation-induced displacement is the displacement at the lateral loading position induced specifically by the equivalent rotation at the interface between the footing and column. The rotation is created by the different elongations of the longitudinal bars in the footing. The elongation can be deduced approximately from the strain readings recorded by strain gauges installed on the four corner longitudinal bars at two different levels in the footing. The rotation-induced displacement can be calculated according to the procedure shown in Figure 4-53. A linear strain distribution, ε, was assumed along the longitudinal bars in the footing. Integration of the strain distribution is used to obtain the elongation of the longitudinal bars u_1 and u_2 between the top of the footing and the zero strain position. Differential elongation of the longitudinal bars resulted in the rotation at the interface between the footing and column. This rotation θ_R, in turn, introduced a displacement, Δ_R, at the lateral loading position, with an elevation of H_1 from the interface between the footing and column. Once the rotation-induced displacement, Δ_R, is obtained, the ratio between this displacement and the total displacement (the recorded lateral displacement measured by LVDT in the experiment) $r = \frac{\Delta_R}{\Delta}$, can be calculated accordingly. The displacement for the case where the interface between the footing and column is assumed to be fixed without rotation, as in the finite element models described in Chapter 5, can be obtained by subtracting the rotation-induced displacement from the

total displacement, $(\Delta - \Delta_R)$. Hence, the relationship between r and $(\Delta - \Delta_R)$ can be determined throughout the test. Figure 4-54 shows this relationship for specimen CV1. Similar relationships were obtained for specimens CV0B and CV4 from the above procedure. It is found that the ratio r changes with $(\Delta - \Delta_R)$, and hence the total displacement. For simplicity, and recognizing the approximate nature of this analysis, the ratio has been taken as a constant value of 10% of the total displacement.

4.12 Effect of Various Parameters on Specimen Behaviour

Six parameters were varied in the test specimens as shown in Table 3-1: collar spacing, longitudinal reinforcement ratio (and bar size), aspect ratio, axial compression index, bolts pretension, and collar stiffness (flexural and axial). This section evaluates the effects of these parameters through comparisons of the behaviour of the test specimens. The influences of these parameters are evaluated using comparisons of similar specimens tested under identical loading conditions, but with only one difference among them.

4.12.1 Effect of Collar Spacing

The importance of close spacing of internal transverse reinforcement has been well established in past studies. Decreased tie spacing increases the deformation levels at which capacity can be maintained. For external collars, which can be considered as one kind of external transverse reinforcement, different collar spacing also shows some influences on the behaviour of specimens. Three different centre-to-centre spacings were used: Specimen CV1 has a centre-to-centre collar spacing of 150 mm, specimen CV2 has a larger spacing of 200 mm, and specimen CV3 has the smallest spacing of 95 mm. In order to study the effect of collar spacing on the performance of the collared columns under cyclic loading, the results of specimen CV2 are compared with those of specimens CV1 and CV3.

The specimen with the widest spaced collars (CV2) had more spalling and crushing than specimens with a narrower spacing of collars (CV3 and CV1). The specimen with the smallest spacing, CV3, exhibited a higher normalized peak lateral force (1.01) than the specimen with moderate spacing, CV1 (0.88), and the specimen with the widest spacing of collars, CV2 (0.90), while CV1 and CV2 had similar normalized peak lateral force, as shown in Table 4-6.

Examination of the displacement ductility from Table 4-4 indicates that specimen CV3 attained a displacement ductility, μ, 40% higher than specimen CV1, 46% higher than specimen CV2. Furthermore, the ultimate drift for specimen CV3 is 111% higher than specimen CV1 and 87% higher than specimen CV2, as shown in Table 4-5. From Table 4-8, the percentage reduction at each displacement level for specimen CV3 is much less than that for specimens CV1 and CV2, which can also be deduced from the stability of the hysteresis of the lateral force–displacement curves and envelope curves. It is also apparent that the total energy dissipated by the specimen CV3 is 2.4 times that by specimen CV1 and 2.8 times that by specimen CV2, as can found from Figure 4-39. In addition, specimen CV3 showed a much lower initial effective stiffness compared to

specimens CV1 and CV2 due to the larger yield displacement, as demonstrated by Table 4-7.

Based on the results of specimens CV1, CV2, and CV3, it is clear that decreased collar spacing improved the overall behaviour of the specimen. Increase of peak lateral force, reduction of rate of degradation, increase of the deformability, improvement of energy dissipation capacity, and more stable hysteretic response are expected by decreasing of the collar spacing, although at some point the benefits of further decreases will diminish.

4.12.2 Effect of Longitudinal Reinforcement Ratio

As found also by Woodward and Jirsa (1984), degradation of the shear capacity of reinforced concrete columns did not seem to be a function of the amount of transverse reinforcement only. The longitudinal reinforcement ratio and longitudinal bar diameter also have an effect on the shear capacity and its degradation. The diameter of the longitudinal bar will affect the bond strength and bond degradation of the column, while the longitudinal reinforcement ratio will affect the capacity and failure mode through the relative strength of flexure and shear.

Two different longitudinal reinforcement ratios were adopted in an attempt to study its effect. Specimen CV1 was constructed with ten 25 M bars, which makes the longitudinal reinforcement ratio 3.13%, while specimen CV4 had ten 20 M bars, with which the longitudinal reinforcement ratio is 1.88%.

The hysteresis loops for specimens CV1 and CV4 are very similar, as shown in Figure 4-16 and Figure 4-19. The change in shape (pinching) of the hysteretic loops is another indication of strength degradation. Also three longitudinal bars fractured under low-cycle fatigue in specimen CV4, while no longitudinal bar fracture happened in specimen CV1 and other specimens.

Based on capacity design principles, the maximum shear force demand, V, on a column is a function of the moment capacity, M, of the end sections (where plastic hinges are designed and detailed to occur) and the shear span, H_1. Between specimens CV1 and CV4, specimen CV4 had a lower shear force input because of the reduced column end moment capacity due to ten 20 M longitudinal reinforcing bars, while the shear spans for CV1 and CV4 both had an aspect ratio of 1.63. Both specimens had no internal transverse reinforcement, and the same size of external collars with the same spacing. Thus, the shear force capacity would be expected to be close since there would be similar axial strain in the reinforcement if both are close to flexural yield. However, the shear force demand is lower for CV4 than CV1, and the result is that specimen CV4 shows better ductility than specimen CV1. All these aspects were validated in the test and can be found from the following comparisons.

Specimen CV1, with a higher longitudinal reinforcement ratio, exhibited 9% higher normalized peak lateral force (0.88) than the specimen with a smaller longitudinal reinforcement ratio CV4 (0.81), as shown in Table 4-6.

Examination of the displacement ductility from Table 4-4 indicates that specimen CV4 attained a displacement ductility 69% higher than specimen CV1. Furthermore, the ultimate drift for specimen CV4 is 61% higher than CV1, as shown in Table 4-5. From Table 4-8, the percentage reduction in lateral force at each displacement level for specimen CV4 is much less than that for specimen CV1, which can also be found from the stability of the hysteresis of the lateral force–displacement curves and envelope curves. The total energy dissipated by specimen CV4 is 1.4 times that by specimen CV1, as can found from Figure 4-39. In addition, specimen CV4 showed a lower initial effective stiffness compared to CV1, as demonstrated by Table 4-7.

Based on the results of specimens CV1 and CV4, it is clear that a lower longitudinal reinforcement ratio improved the overall behaviour of the collared column. Reduction of rate of degradation, increase of the deformability, improvement of energy dissipation capacity, and more stable hysteretic response but slightly less strength is found with the decrease in the longitudinal reinforcement ratio.

4.12.3 Effect of Aspect Ratio

Two aspect ratios of 1.63 and 0.88 were studied. Specimen CV5 has a shear-span of 350 mm, while specimen CV1 and others had a shear-span of 650 mm, which make the aspect ratios 0.88 and 1.63, respectively. As would be expected, decreasing the aspect ratio caused a higher shear demand under the same moment, which caused a different failure pattern. In order to study the effect of shear-span on the performance of the collared columns, the results of specimen CV1 are compared with specimen CV5.

Specimen CV5 had the greater shear force input of these two columns due to the reduced shear span. Both columns had no internal transverse reinforcement and the same size of external collars with the same spacing. But the shear force demand is lower for CV1 than CV5 and the result is that specimen CV1 would be expected to show better ductility than specimen CV5, which is validated by the following comparisons.

Specimen CV5, with the smaller shear-span and hence a smaller aspect ratio, exhibited 56% higher normalized peak lateral force (1.37) than the specimen with larger shear-span and hence a larger aspect ratio, CV1 (0.88), as shown in Table 4-6.

Examination of the displacement ductility from Table 4-4 indicates that specimen CV1 attained a displacement ductility 26% higher than specimen CV5. Furthermore, the ultimate drift for specimen CV1 is 87% higher than CV5, as shown in Table 4-5. Kokusho *et al.* (1986) also found that a greater aspect ratio specimen led to a larger deformation capacity. From Table 4-8, the percentage reduction at each displacement level for column CV1 is much less than that for specimen CV5, which can also be found from the stability of the hysteresis of the lateral force-displacement curves and envelope curves. Also, the total energy dissipated by the specimen CV1 is 5.9 times that by specimen CV5 as can found from Figure 4-39. In addition, specimen CV1 showed a

much lower initial effective stiffness compared to specimen CV5, as demonstrated by Table 4-7.

Based on the results of specimens CV1 and CV5, it is clear that larger aspect ratio improved the overall behaviour of the collared column, as would be expected. Reduction of rate of degradation, increase of the deformability, improvement of energy dissipation capacity, more stable hysteretic response, and less strength (although less demand as well) are found with increasing aspect ratio.

4.12.4 Effect of Axial Compression Index

On specimen CV1 an axial compressive load of $0.3 f_c^{'} A_g$ was applied, which is slightly lower than the balanced failure axial load in the column ignoring influence of collars, while specimen CV6 had no axial compressive load applied. As pointed out by Saatcioglu (1996), most columns in building practice are subjected to moderate levels of axial compression, ranging from 20% to 40% of their concentric capacities. Hence, one type of axial compression index was chosen as 0.3. As shown in Figures 4-16 and 4-21, the lateral force-displacement curves of CV1 and CV6 illustrate that the presence of the axial compressive load increases the peak lateral force of the specimen. This effect was expected, since past research has shown that the presence of an axial compressive load less than that at balanced strain conditions increases the capacity compared to the same section with no axial compressive load (Woodward and Jirsa 1984; Kokusho *et al.* 1986). Kokusho *et al.* (1986) also found that the ultimate strength of the column generally increases with an increase of the axial compressive load if the axial compression index is not greater than 0.4, but for greater than 0.4, the ultimate strength shows little increase because compressive crushing failure of concrete occurs. The axial compressive load tends to control the inclined crack width and can help to maintain aggregate interlock along the crack and keep the shear interface transfer capacity and thus contribute to the capacity of the column.

In order to study the effect of the variation of axial compressive load on the behaviour of the collared columns, the results of specimens CV1 and CV6 are compared with respect to the peak lateral force, deformability, energy dissipation, and strength degradation.

Specimen CV1, with axial compressive load of $0.3 f_c^{'} A_g$, exhibited 31% higher normalized peak lateral force (0.88) than specimen CV6, without axial compressive load (0.67), as shown in Table 4-6. Examination of the displacement ductility from Table 4-4 indicates that specimen CV6 attained ductility almost the same as specimen CV1. This phenomenon has also been found by Ahn *et al.* (2000), who showed that there was no significant change in the ductility capacity with increasing axial compressive load for the column specimens regardless of concrete strength.

Similar to findings by Saatcioglu and Baingo (1999) and Melek and Wallace (2004), the deformability of the column was reduced due to a higher axial compressive load. Specimen CV1 developed an ultimate drift of 5.04%, while specimen CV6 developed 8.69%, as shown in Table 4-5. In addition, specimen CV6 showed a much lower initial

effective stiffness compared to specimen CV1 due to larger yield displacement, as demonstrated by Table 4-7.

The total energy dissipated by specimen CV6 is 0.6 times that dissipated by CV1, as shown in Figure 4-39. The effect of axial compression index might also be examined referring to the percentage reduction of lateral load at different displacement levels as a guide to behaviour. The specimen without axial compressive load (CV6) exhibited similar degradation to specimen CV1 at low displacement levels, but had significantly higher degradation during the large displacement cycles.

Based on the results of specimens CV1 and CV6, it is clear that an increase of the axial compression index and hence the axial compressive load will increase the peak lateral force, but reduce the deformability, while resulting in no significant change in the displacement ductility.

4.12.5 Effect of Pretension of Bolts

There are two types of confinement: active and passive. Concrete can be considered as actively confined when some externally applied action induces the transverse stress, while passive confinement is the case when the confining stresses develop as a result of the transverse expansion of the concrete. In the present test program, specimen CV7 was tested to study the effectiveness of active confinement. Specimens CV7 and CV1 were similar except that the collar connection bolts in specimen CV7 were pretensioned to about 35% (this value was limited to prevent severe crushing of the concrete in the vicinity of the collar connection) of the specified minimum tensile strength of standard high strength structural bolts (ASTM A490), while the bolts were fastened to a snug-tight condition in specimen CV1.

The test of specimen CV7 provides some information in assessing the effectiveness of active confinement. As observed during the test, fewer cracks and damage occurred in specimen CV7 and they emerged at a much later stage. Specimen CV7 remained intact until a larger displacement level during the test. The specimen with pretensioned bolts (CV7) had less spalling and crushing than specimen (CV1). This proved the effectiveness of active confinement in restraining cracking and improving crack stability as observed by Hussain and Driver (2005b) and Chapman and Driver (2006).

The hysteresis loops for specimens CV1 and CV7 are similar, as shown in Figure 4-16 and Figure 4-22, except that there is slightly more pinching in Figure 4-16 and more stable hysteresis loop as shown in Figure 4-22. The change in shape (pinching) of the hysteretic loops is another indication of strength degradation.

Specimen CV7, with pretension in the connection bolts at the start of the test exhibited 20% higher normalized peak lateral force (1.06) than the specimen CV1 with snug-tight connection bolts (0.88), as shown in Table 4-6.

Examination of the displacement ductility from Table 4-4 indicates that specimen CV7 attained a ductility 4% higher than specimen CV1. Furthermore, the ultimate drift for specimen CV7 is also 4% higher than specimen CV1, as shown in Table 4-5. From Table 4-8, the percentage reduction at each displacement level for specimen CV7 is much less than that for specimen CV1, which can also be found from the stability of the hysteresis of the lateral force–displacement curves and envelope curves. The total energy dissipated by the specimen CV7 is 1.2 times that by specimen CV1, as can found from Figure 4-39. In addition, specimen CV1 showed a slightly lower initial effective stiffness compared to specimen CV7, as demonstrated by Table 4-7.

Based on the results of specimens CV1 and CV7, it is clear that active confinement improved the overall behaviour of the collared column. Increase of peak lateral force, reduction of rate of degradation, increase of the deformability, improvement of energy dissipation capacity, and more stable hysteretic response are found with the application of the active confinement.

4.12.6 Effect of Collar Stiffness

Specimens CV1 and CV8 are identical except that specimen CV1 has a smaller size external collar, the cross section of which is 30×50 mm, while it is 50×50 mm for collars in specimen CV8. The collar stiffness (both flexural and axial stiffness) and the transverse reinforcement volumetric ratio increases with the increase of the size of the collars, while keeping other parameters unchanged. In order to study the effect of the size of collars, and hence the stiffness of collars, on the performance of the collared columns under cyclic loading, the results of specimen CV1 are compared with those of specimen CV8.

As observed during the test, fewer cracks and less damage occurred in specimen CV8 and it remained intact until a larger displacement level during the test. The hysteresis loops for specimens CV1 and CV8 are similar, but those of specimen CV8 are more stable than specimen CV1 and there is slightly more pinching in specimen CV1, as can be seen in Figure 4-16 and Figure 4-23. This proved the effectiveness of the increase of collar stiffness in reducing damage and increasing confinement as observed by Hussain and Driver (2005b) and others.

Specimen CV8, with the larger size of external collars and hence larger collar stiffness, exhibited 5% higher normalized peak lateral force (0.92) than the specimen CV1, with the smaller size of external collars and hence smaller collar stiffness (0.88), as shown in Table 4-6.

Examination of the displacement ductility from Table 4-4 indicates that specimen CV8 attained a ductility 56% higher than specimen CV1. Furthermore, the ultimate drift for specimen CV8 is 50% higher than specimen CV1, as shown in Table 4-5. From Table 4-8, the percentage reduction at each displacement level for specimen CV8 is much less than that for specimen CV1, which can also be found from the stability of the hysteresis of the lateral force–displacement curves and envelope curves. The total energy dissipated by the

specimen CV8 is 1.6 times that by specimen CV1, as can found from Figure 4-39. In addition, the specimen CV8 showed a slightly lower initial effective stiffness compared to specimen CV1 due to the larger yield displacement, as demonstrated by Table 4-7.

Based on the results of specimens CV1 and CV8, it is clear that increasing the size, and hence the stiffness, of external collars improved the overall behaviour of the collared column. Reduction of the rate of degradation, increase of the deformability, more stable hysteretic response, improvement of energy dissipation capacity, and increase of strength are found with the increase of collar size.

4.13 Comparison of Control Columns and Collared Columns

4.13.1 Control Columns CV0A and CV0B

Specimens CV0A and CV0B are identical in all respects except that specimen CV0A had internal transverse reinforcement spaced at 400 mm, and the internal transverse reinforcement was spaced at 100 mm for specimen CV0B.

Control column CV0B, with the closer spacing of internal transverse reinforcement, exhibited 20% higher normalized peak lateral force (0.85) than the control column CV0A, with wider spacing (0.71), as shown in Table 4-6.

Examination of the displacement ductility from Table 4-4 indicates that specimen CV0B attained a ductility (4.57) just 9% higher than that of specimen CV0A (4.21). Specimen CV0A, the control column satisfying the CSA-A23.3-04 and ACI 318-05 code requirements for non-seismic shear strength, also developed a ductility capacity of 4.21, and previous research has obtained similar results. For example, when Wong *et al.* (1993) studied the response of circular reinforced concrete columns to multi-directional seismic attack and found that all test units satisfying code requirements for non-seismic shear strength developed a displacement ductility of four or more under different patterns of loading. Another reason for the high displacement ductility for CV0A is due to the low force adopted in conducting the first five cycles of loading. If the first cycle was conducted to a higher load level than currently used, the stiffness of the first cycle will reduce due to the degradation of the load-displacement response. Hence, the trendline of the first cycle will also have a smaller initial stiffness. Then this trendline will intersect the horizontal maximum load line at a larger displacement. Calculation of the displacement ductility with this larger displacement results in a smaller ductility. So under current first cycle trendline, the displacement ductility is larger than it might be if larger load used in conducting the first cycle load.

Furthermore, the ultimate drift for specimen CV0B is 140% higher than CV0A, as shown in Table 4-5. From Table 4-8, the percentage reduction at each ductility level for specimen CV0B is slightly less than that for specimen CV0A, which can also be found from the stability of the hysteresis of the lateral force-displacement curves and envelope curves. The total energy dissipated by the specimen CV0B is 4.2 times that by specimen CV0A, as can found from Figure 4-39. In addition, specimen CV0B showed

lower initial effective stiffness compared to specimen CV0A due to the larger yield displacement, as demonstrated by Table 4-7.

Based on the results of specimens CV0A and CV0B, it is clear that a decrease of the spacing of internal transverse reinforcement improved the overall behaviour of the column. Reduction of rate of degradation, increase of the deformability, more stable hysteretic response, improvement of energy dissipation capacity, and increase of strength are found with a decrease of the spacing of internal transverse reinforcement.

4.13.2 Control Columns and Collared Columns

The effectiveness of the rehabilitation technique using external collars can be quantified based upon the differences in the behaviour between collared columns and control columns, as well as the visual observations during the test. This can be done by comparing the following measures: damage pattern, lateral force–displacement response envelopes, displacement ductility, ultimate drift, normalized strength, strength degradation, and total energy dissipation.

For the collared columns (CV0AR, CV1, CV2, CV3, CV4, CV5, CV6, CV7, and CV8), most of the damage occurred between the first and second layer collars at the east and west sides and the interface between the column and footing at the south and north sides, while the control columns (CV0A and CV0B) had a wider range of damage. No slippage of the collars was observed during the test for all the collared columns even under severe spalling and crushing of cover concrete.

The lateral force-displacement responses of the collared columns are compared with those of the control columns and shown in Figures 4-13 to 4-23. Envelopes are shown in Figure 4-24. It can be seen that the control columns behaved in a more brittle way compared to the collared columns. This behaviour is clear from the more abrupt drop in the strength shortly after the peak force value due to extensive spalling and crushing of concrete. The collared columns exhibited a more ductile behaviour through the formation of a stable hinge in the columns. From the lateral force-displacement envelopes, the collared columns have a long segment of a post-peak plateau evident of better ductile behaviour. Stable hysteresis loops are preferred because ductile and stable behaviour is critical at seismic hinges to prevent structural collapse under sustained loading. Under moderate to strong ground motion earthquakes, the behaviour of the structure is no longer dominated by the elastic properties. Of greater importance are the inelastic properties, which are substantially improved by this rehabilitation technique.

All collared columns exhibited 14% to 93% higher normalized peak lateral force than the control column CV0A except CV6, with a slightly (6%) lower value than CV0A due to the absence of axial compressive load. Collared column CV4 exhibited slightly (5%) lower normalized peak lateral force than control column CV0B due to the smaller longitudinal reinforcement ratio, as shown in Table 4-6. The normalized peak lateral force reached by collared column CV6 is 21% lower than that of control column CVB due to the absence of axial compressive load.

Examination of the displacement ductilities from Table 4-4 indicates that all collared columns attained ductilities 7% to 122% higher than the control column CV0A, and all collared columns also have 16% to 105% higher ductility than control column CV0B except specimen CV5, with slightly (4%) lower ductility than CV0B due to the smaller aspect ratio.

Furthermore, control column CV0A failed at a very small drift ratio, with an ultimate drift of 1.74%. Control column CV0B has a higher ultimate drift of 4.19%, while the ultimate drift for collared columns are generally higher and as high as 10.61% for specimen CV3, except specimen CV5 is only 2.69% as shown in Table 4-5. The ultimate drift ratios for all the collared columns are much higher than the control column CV0A (54% to 508% higher). All the collared columns achieved much higher ultimate drifts than control column CV0B, except that specimen CV5 is 36% lower than specimen CV0B due to the smaller aspect ratio. This shows that the high drift deformation capacity of the collared column is beneficial to the structure under earthquake ground motion.

From Table 4-8, the percentage reduction at each displacement level for collared columns are less than that for control columns CV0A and CV0B except specimens CV5 and CV6, which can also be found from the stability of the hysteresis of the lateral force-displacement curves and envelope curves.

The total energy dissipated by the collared reinforced concrete columns is 1.6 to 23.7 times that dissipated by control column CV0A. The total energy dissipated by the collared columns is 1.4 to 5.7 times that dissipated by control column CV0B except specimen CV5 is 0.4 times that of CV0B due to the smaller aspect ratio, as can found from Figure 4-39. In addition, due to the larger yield displacement, the collared column showed a lower initial effective stiffness compared to specimen CV0A except specimen CV5, but are very close to control column CV0B, as demonstrated by Table 4-7.

The experimental results presented above demonstrated that, for the same specimen size and longitudinal reinforcing bars, collared columns tend to exhibit higher normalized peak lateral force and displacement ductility, greater energy dissipation, and more stable hysteresis loops with less degradation. The overall behaviour of the collared column was therefore much improved over the control columns.

It is worthwhile to reiterate that no internal transverse reinforcement was present in the collared column tests. In a rehabilitation scenario, any existing hoops can only further benefit the behaviour of collared columns.

4.14 Repair of Damaged Specimen

To investigate the feasibility of repairing badly damaged columns using external steel collars, one of the failed control columns was retested after being repaired. The repair of a reinforced structural concrete component of a building should restore it to a structural

condition consistent with the intended use for the defined service life. The study of the effectiveness of repair of damaged specimens has also been attempted by Priestley and Seible (1995), Lacobucci *et al.* (2003), Li and Sung (2003), and Memon and Sheikh (2005). Epoxy mortar was used to reinstate the specimen integrity before the addition of external steel collars.

The specimen CV0AR, repaired from the damaged control column (CV0A) using epoxy mortar and external collars, had little spalling and crushing and remained in good, intact condition after the test. Hysteresis loops for the original and repaired specimens are shown in Figures 4-13 and 4-14. The repaired specimen showed more stable hysteretic response than the original control specimen. Examination of the ductility from Table 4-4 indicates that the repaired specimen attained ductility 64% higher than the original control specimen. Much better deformability—more than four times ultimate drift ratio of specimen CV0A—can be seen from Table 4-5. Furthermore, it can be found from Table 4-6 that the normalized peak lateral force of repaired specimen CV0AR increased 28% from the original specimen CV0A. Repaired specimen CV0AR also showed much higher energy dissipation capacity than the original specimen CV0A, as shown in Figure 4-39, with a total dissipated energy of 23.7 times that by the original specimen although those additional cycles of loading in CV0AR would contribute significantly to the enhancement of the total energy dissipated. Much less strength degradation at each level is shown in Table 4-8. In addition, the repaired specimen showed a lower initial effective stiffness compared to original specimen due to the larger yield displacement, as demonstrated by Table 4-8.

The repaired specimen CV0AR demonstrated significant improvement in ductility, deformability, energy dissipation, and enhancement in strength than the original control column CV0A after the proper repair and rehabilitation. The test results show that external steel collars and epoxy grout were sufficient to fully compensate for the previous damage and can indeed increase the ductility and strength after proper repair and rehabilitation. The fact that the repaired specimen was superior to the original control specimen shows that repair with epoxy grout and steel collars in field application holds promise as a means for practitioners to restore the damaged column back to functionality quickly after an earthquake. Clearly, quality control in this rehabilitation technique is critical since the benefits stem not only from the collars, but also through the grouting technique. Further study is required to fully characterize how and when this technique could be used.

Comparisons can also be made between the repaired collared column CV0AR and the base case collared column CV1. Hysteresis loops for specimens CV0AR and CV1 are shown in Figures 4-14 and 4-16. The repaired collared column showed more stable hysteretic response than the base case collared column. Examination of the ductility from Table 4-4 indicates that specimen CV0AR attained ductility 25% higher than specimen CV1. Specimen CV0AR showed better deformability—55% higher ultimate drift ratio than CV1—can be seen from Table 4-5. Furthermore, it can be found from Table 4-6 that the normalized peak lateral force of repaired specimen CV0AR is slightly higher than that of the base case collared column CV1. Repaired specimen CV0AR also

showed much higher energy dissipation capacity than specimen CV1, as shown in Figure 4-39, with a total dissipated energy of 2.57 times that by CV1 although those additional cycles of loading in CV0AR would contribute significantly to the enhancement of the total energy dissipated. Much less strength degradation at each level is shown in Table 4-8. In addition, the repaired specimen showed a lower initial effective stiffness compared to base case collared column due to the larger yield displacement, as demonstrated by Table 4-7. The test results indicate that external steel collars and epoxy grout can rehabilitate specimens and exhibit behaviour as good as an undamaged collared column.

4.15 Summary

An experimental program of the seismic rehabilitation and repair of short columns with steel collars was conducted. Test results demonstrated the effectiveness of steel collars for improving the performance of reinforced concrete short columns under cyclic reversals of horizontal loading even when no internal ties were present. In general, collared columns showed ductile response with stable hysteresis loops and exhibited significantly improved energy dissipation capacity over the control columns without collars. The repaired specimen demonstrated significantly improved ductility, deformability, energy dissipation, and enhancement in strength over the original control column. These observations validate the feasibility and effectiveness of this rehabilitation technique. The following conclusions can be drawn from this experimental study:

(1) The experimental results of the collared reinforced concrete columns and control columns demonstrated that, for the same specimen size and longitudinal reinforcing bars, collared reinforced concrete columns exhibited higher strength and displacement ductility, greater energy dissipation, and more stable hysteresis loops with less degradation. The overall behaviour of the collared reinforced concrete column was much improved over the control columns due to the significant confinement the collars provide.

(2) The external steel collars were bolted in place, directly on the surface of the square columns without creating stress concentrations at the corners, which might lead to crushing and damage of the concrete. No rounding of the corners at a certain radius was needed as in other rehabilitation techniques such as FRP jacketing. No slippage of the collars was observed during the tests of collared columns, even when severe spalling and crushing of cover concrete took place between them, implying the combined action of the concrete and steel collars had been achieved. The feature of no slippage is beneficial for seismic rehabilitation.

(3) The rehabilitated reinforced concrete columns with external steel collars enhanced the displacement ductility, and provided sufficient shear strength to the extent that brittle shear failure modes are converted to a more ductile failure mode. Ductile failures beyond a displacement ductility of four were observed, although longitudinal reinforcing bar fracture was observed in one specimen under low-cycle fatigue.

(4) In general, collared reinforced concrete columns attained a much higher ultimate drift ratio, showed improved deformability, and exhibited much better energy dissipation capacity under cyclic loading than the control columns without collars, all features that are beneficial to structural performance in an earthquake. Collared reinforced concrete columns showed very ductile response with stable hysteresis loops and gradual post-peak degradation. All collared reinforced concrete columns exhibited 14% to 93% higher normalized peak lateral force than the control column with internal conventional transverse reinforcement spaced at 400 mm (CV0A), except the collared reinforced concrete column without axial compressive load exhibited 6% lower normalized peak lateral force. All collared reinforced concrete columns attained ductilities 7% to 122% higher than CV0A. Furthermore, the ultimate drift ratios for all the collared reinforced concrete columns were 54% to 508% higher than column CV0A. It was also found that the total energy dissipated by the collared reinforced concrete columns was 1.6 to 23.7 times that dissipated by CV0A.

(5) Decreasing the centre-to-centre collar spacing from 200 mm to 95 mm improved the overall behaviour of the collared reinforced concrete column with less concrete spalling and crushing, including a 10% increase in normalized peak lateral force, a 46% increase in displacement ductility, an 87% enhancement in drift ratio, and 2.8 times of energy dissipated.

For collared reinforced concrete columns, decreasing the longitudinal reinforcement ratio from 3.13% to 1.88% reduced the normalized peak lateral force by 9%, but reached 69% higher displacement ductility. The ultimate drift also improved by 61% and the energy dissipated increased by 43%.

Increasing the aspect ratio of the collared reinforced concrete column from 0.88 to 1.63 exhibited a 36% decrease in the normalized peak lateral force, but gained 26% in displacement ductility and 87% in the ultimate drift ratio, with 5.9 times of energy dissipated.

Collared reinforced concrete column CV1, with an axial compressive load of $0.3f_c^{'}A_g$, exhibited a 31% enhancement in normalized peak lateral force, but a 42% decrease in the ultimate drift compared with the collared reinforced concrete column without axial compressive load (CV6). The total energy dissipated by specimen CV6 is 0.6 times that dissipated by CV1, while the displacement ductilities are similar.

Comparison between the collared reinforced concrete column with a pretension of 35% of the minimum specified tensile strength applied to the connection bolts (CV7) and the equivalent collared reinforced concrete column with snug-tight connection bolts (CV1) showed that prestressing the bolts provided an increase of 20% in the normalized peak lateral force and a 19% enhancement in the energy dissipation, but with only a marginal increase in displacement ductility and ultimate drift ratio.

The collared reinforced concrete column with a large size of external collars (50×50 mm) and hence a larger collar stiffness (CV8) exhibited a 5% higher normalized peak lateral

force than the equivalent collared reinforced concrete column with a smaller size of external collars (30×50 mm) and hence smaller collar stiffness (CV1). With the larger collars the displacement ductility increased by 56% and the ultimate drift enhanced by 50%, while the total energy dissipated increased by 64%.

Epoxy mortar injection followed by installation of collars proved to be a promising repair method that is easy to implement and quick to serve its function. The 30% enhancement in the normalized peak lateral force of specimen CV0AR, 57% in the displacement ductility, 347% in the ultimate drift ratio, and 23.7 times the energy dissipated as compared to the original control column (CV0A) showed that proper repair to the initially damaged reinforced concrete columns can achieve good performance. The similar normalized peak lateral force attained by specimen CV0AR, 25% enhancement in the displacement ductility, 55% increase in the ultimate drift ratio, and 2.6 times the energy dissipated as compared to the base case collared column (CV1) indicate that external steel collars and epoxy grout can rehabilitate specimens and exhibit behaviour as good as an undamaged collared column.

Table 4-1 Number of cycles sustained by specimens

Specimen	Number of cycles sustained											
	V=0.75V_y	Control displacement ductility, μ_c										Total
		1.5	2	4	6	8	10	12	14	16	18	
CV0A	5*	5	5	5	5	2						27
CV0AR	5*	5	5	5	5	5	5	5	5	5	3	53
CV0B	5	5	5	5	1							21
CV1	5	5	5	5	5	5						30
CV2	5	5	5	5	4							24
CV3	5	5	5	5	5	5	1					31
CV4	5	5	5	5	5	5	3					33
CV5	5*	5	5	5	5	5	5	1				36
CV6	5	5	5	5	5	1**						26
CV7	5	5	5	5	5	5	2					32
CV8	5	5	5	5	5	5	1					31

* The first five force control cycles for specimens CV0A, CV0AR, and CV5 were conducted at loads lower than 75%V_y, which resulted in a smaller test displacement in conducting the test. Hence, the control displacement levels, which are based on these control displacements, for these three specimens are just a designation of displacement level for convenience in the test, not the final displacement ductility.

** This cycle was performed at a control displacement ductility level of 7 instead of the specified ductility level of 8 due to the stroke limit of the horizontal LVDTs.

Table 4-2 Principal crack inclination measured from longitudinal axis (in degrees)

Specimen	Push direction			Pull direction			Average
	East side	West side	Average	East side	West side	Average	
CV0A	32	40	36	28	32	30	33
CV0AR	37	31	34	32	38	35	35
CV0B	37	33	35	40	38	39	37
CV1	35	35	35	30	37	34	34
CV2	37	40	39	41	31	36	37
CV3	36	36	36	41	39	40	38
CV4	30	29	30	34	33	34	32
CV5	30	45	38	30	45	38	38
CV6	35	45	40	41	45	43	42
CV7	50	50	50	49	45	47	49
CV8	39	40	40	40	30	35	37

Table 4-3 Modified test displacement values

Specimen	Control displacement values used in conducting test (mm)					Modified test displacement values (mm)						
	V_1 (kN)	Δ_{c+}^*	Δ_{c-}^*	Δ_c^*	Δ_{yc}	V_1 (kN)	Δ_{t+}^*	Δ_{t-}^*	Δ_t^*	Δ_{yt+}	Δ_{yt-}	Δ_{yt}
CV0A	280	1.17	1.21	1.19	1.59	486	2.03	2.10	2.07	2.71	2.80	2.75
CV0AR	243	2.24	2.40	2.32	3.09	486	4.48	4.80	4.64	5.97	6.40	6.19
CV0B	486	5.08	3.50	4.29	5.72	486	5.08	3.50	4.29	6.77	4.67	5.72
CV1	486	3.34	3.30	3.32	4.43	486	3.34	3.30	3.32	4.45	4.40	4.43
CV2	486	4.40	4.38	4.39	5.85	486	4.40	4.38	4.39	5.87	5.84	5.85
CV3	486	5.21	5.35	5.28	7.04	486	5.21	5.35	5.28	6.95	7.13	7.04
CV4	486	3.89	3.82	3.85	5.14	486	3.89	3.82	3.85	5.18	5.10	5.14
CV5	486	1.12	0.66	0.89	1.19	860	1.98	1.17	1.57	2.64	1.56	2.10
CV6	486	8.22	8.08	8.15	10.87	486	8.22	8.08	8.15	10.96	10.78	10.87
CV7	486	3.48	2.71	3.10	4.13	486	3.48	2.71	3.10	4.64	3.62	4.13
CV8	486	4.16	3.83	4.00	5.33	486	4.16	3.83	4.00	5.55	5.11	5.33

Table 4-4 Modified yield displacement, Δ_y, and displacement ductility, μ, by the first cycle trendline

Specimen	Δ_u (mm)		Δ_y (mm)		Displacement ductility (μ)		
	Push (+)	Pull (-)	Push (+)	Pull (-)	Push (+)	Pull (-)	Average
CV0A	12.15	10.52	2.83	2.55	4.30	4.13	4.21
CV0AR	47.51	53.81	6.81	7.84	6.98	6.86	6.92
CV0B	27.18	27.27	5.72	6.21	4.75	4.39	4.57
CV1	31.64	33.86	5.00	7.14	6.33	4.75	5.54
CV2	38.52	35.27	6.08	8.22	6.34	4.29	5.31
CV3	74.22	63.65	8.51	9.37	8.72	6.80	7.76
CV4	59.17	46.32	5.10	6.51	11.60	7.11	9.36
CV5	9.64	9.17	2.73	1.75	3.54	5.25	4.39
CV6	57.58	55.37	8.91	11.79	6.46	4.70	5.58
CV7	34.46	33.89	5.48	6.45	6.29	5.25	5.77
CV8	47.31	51.21	5.78	6.51	8.18	7.86	8.02

Table 4-5 Ultimate displacement, Δ_u, and ultimate drift at push and pull directions

Specimen	Δ_u (mm)		Ultimate drift				
	Push (+)	Pull (-)	Push (+) (%)	Pull (-) (%)	Average (%)	/CV1	/CV0A
CV0A	12.15	10.52	1.87	1.62	1.74	0.35	1.00
CV0AR	47.51	53.81	7.31	8.28	7.79	1.55	4.47
CV0B	27.18	27.27	4.18	4.20	4.19	0.83	2.40
CV1	31.64	33.86	4.87	5.21	5.04	1.00	2.89
CV2	38.52	35.27	5.93	5.43	5.68	1.13	3.25
CV3	74.22	63.65	11.42	9.79	10.61	2.10	6.08
CV4	59.17	46.32	9.10	7.13	8.11	1.61	4.65
CV5	9.64	9.17	2.75	2.62	2.69	0.53	1.54
CV6	57.58	55.37	8.86	8.52	8.69	1.72	4.98
CV7	34.46	33.89	5.30	5.21	5.26	1.04	3.01
CV8	47.31	51.21	7.28	7.88	7.58	1.50	4.35

Table 4-6 Average peak lateral force, $V_{max,exp}$, normalized peak lateral force $V_{max\,n}$, and peak moment, $M_{max,exp}$

Specimen	f_c' (MPa)	Peak lateral force $V_{max,exp}$ (kN)				$V_{max\,n}$*	Peak moment $M_{max,exp}$ (kN.m)		
		Push (+)	Pull (-)	Difference (%)	Average		Push (+)	Pull (-)	Average
CV0A	26.3	599	567	5.25	583	0.71	389	369	379
CV0AR	26.6	700	795	13.61	748	0.91	455	517	486
CV0B	26.9	675	730	8.04	702	0.85	439	474	457
CV1	33.3	791	838	5.88	815	0.88	514	545	529
CV2	25.5	701	747	6.61	724	0.90	455	485	470
CV3	22.0	746	774	3.78	760	1.01	485	503	494
CV4	30.8	689	752	9.09	721	0.81	448	489	468
CV5	29.5	1161	1227	5.77	1194	1.37	406	430	418
CV6	31.5	555	654	17.69	604	0.67	361	425	393
CV7	29.1	889	944	6.20	916	1.06	578	614	596
CV8	27.4	731	804	9.97	767	0.92	475	523	499

*$V_{max\,n}=V_{max,exp}/\left(A_g\sqrt{f_c'}\right)$ and A_g =160 000 mm^2 for all the test specimens.

Table 4-7 Initial effective stiffness K_y

Specimen	Initial effective stiffness from the first cycle trendline method (kN/mm)			
	Push (+)	Pull (-)	Average	/CV0A
CV0A	212	222	217	1.00
CV0AR	103	101	102	0.47
CV0B	125	118	121	0.56
CV1	158	117	138	0.64
CV2	115	91	103	0.47
CV3	88	83	85	0.39
CV4	135	115	125	0.58
CV5	426	703	564	2.60
CV6	62	55	59	0.27
CV7	162	146	154	0.71
CV8	126	123	125	0.58

Table 4-8 Percentage reduction in lateral force between the first and the fifth cycles

Specimen	$1.5\Delta_{yt}$		$2\Delta_{yt}$		$4\Delta_{yt}$		$6\Delta_{yt}$		$8\Delta_{yt}$	
	Push (+)	Pull (-)	Push (+)	Pull (-)	Push (+)	Pull (-)	Push (+)	Pull (-)	Push (+)	Pull (-)
CV0A*	6	18	16	21						
CV0AR*	7	11	10	13	4	8	5	7	12	8
CV0B	12	14	11	12	20	21				
CV1	7	4	11	9	19	12	13	20	30	27
CV2	12	14	12	9	10	16				
CV3	10	9	7	6	6	9	6	10	9	11
CV4	7	8	6	2	7	6	7	5	5	12
CV5*	14	12	9	12	20	22	32	33		
CV6	12	10	9	12	22	27	74	81		
CV7	6	8	6	10	5	7	7	4	11	17
CV8	10	13	8	12	10	7	8	11	9	12

* The first five force control cycles for specimens CV0A, CV0AR, and CV5 were conducted at loads lower than 75%V_y, which resulted in a smaller control displacement in conducting the test. Hence, the test displacement levels, which are based on these control displacements, were adjusted.

Table 4-9 Height of clinometers from the base of column

Specimen	Height of clinometers (mm)				Height for average curvature* (mm)			
	No. 1	No. 2	No. 3	No. 4	Portion 1	Portion 2	Portion 3	Portion 4
CV0A	75	225	375	525.0	37.5	150.0	300.0	450.0
CV0AR	50	200	350	474.3	25.0	125.0	275.0	412.2
CV0B	75	225	375	525.0	37.5	150.0	300.0	450.0
CV1	100	250	400	500.0	50.0	175.0	325.0	450.0
CV2	—	75	275	475.0	—	37.5	175.0	375.0
CV3	115	210	305	469.3	57.5	162.5	257.5	387.2
CV4	50	200	350	474.3	25.0	125.0	275.0	412.2
CV5	50	200	—	474.3	25.0	125.0	—	337.2
CV6	50	200	350	474.3	25.0	125.0	275.0	412.2
CV7	50	200	350	474.3	25.0	125.0	275.0	412.2
CV8	50	200	350	474.3	25.0	125.0	275.0	412.2

* Relative curvature at each portion is calculated.

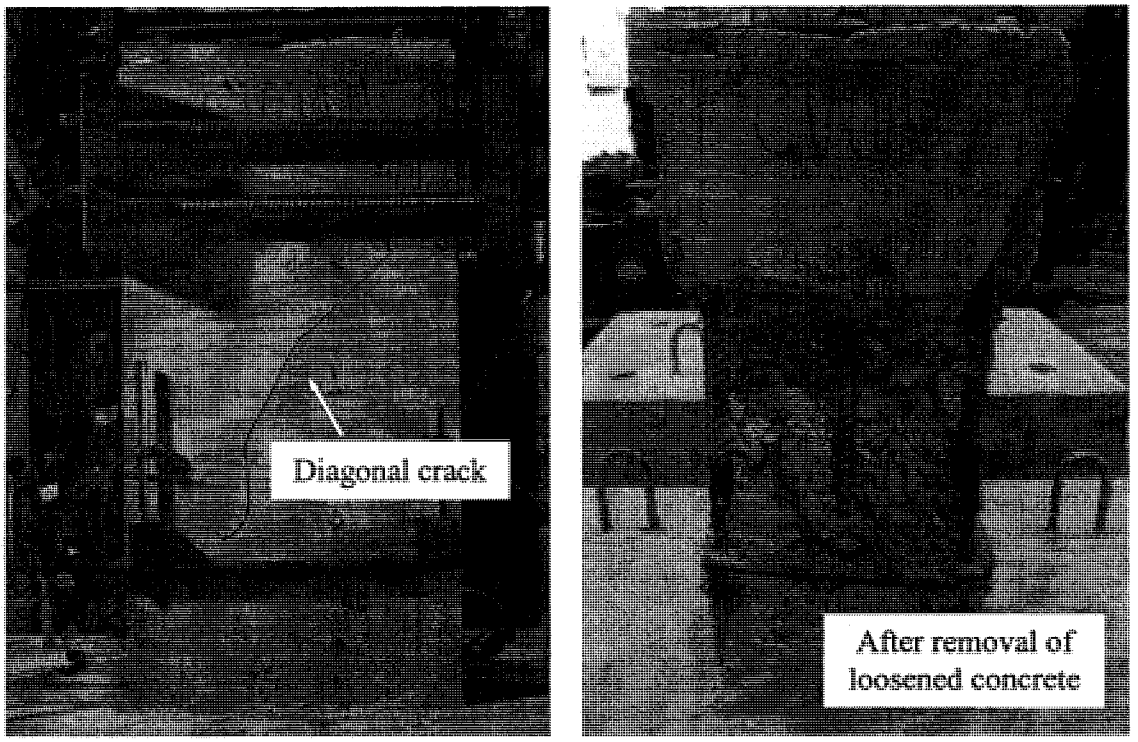

(a) Cracks at cycle 16 (μ =2.3) (b) At the end of the test

Figure 4-1 Specimen CV0A

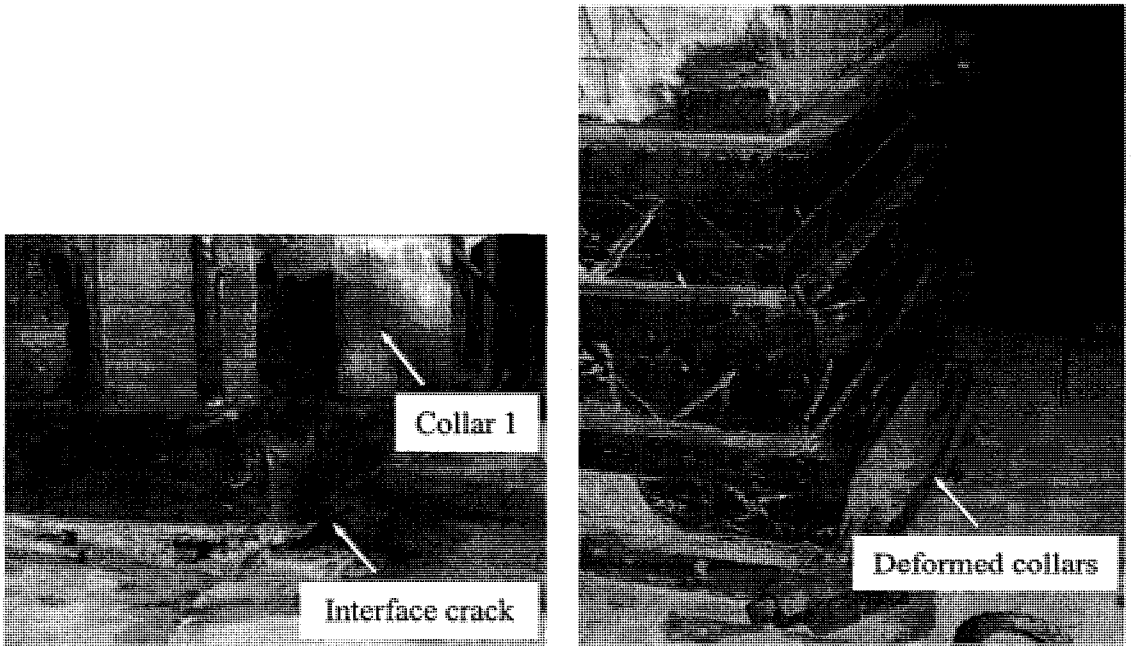

(a) Wide crack at the interface (b) Bulge of collars

Figure 4-2 Specimen CV0AR

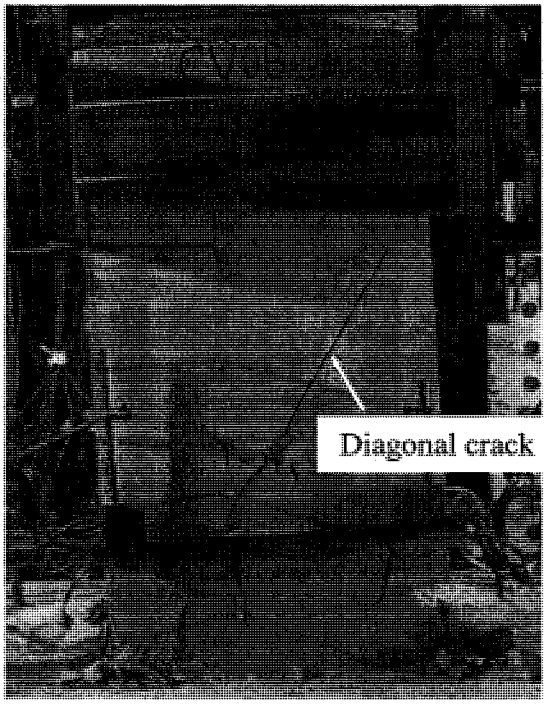

(a) Cracks at cycle 16 (μ =4)

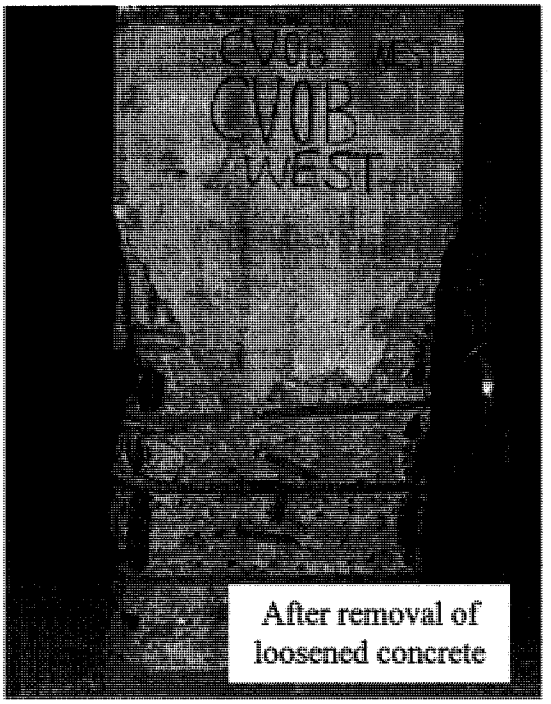

(b) At the end of the test

Figure 4-3 Specimen CV0B

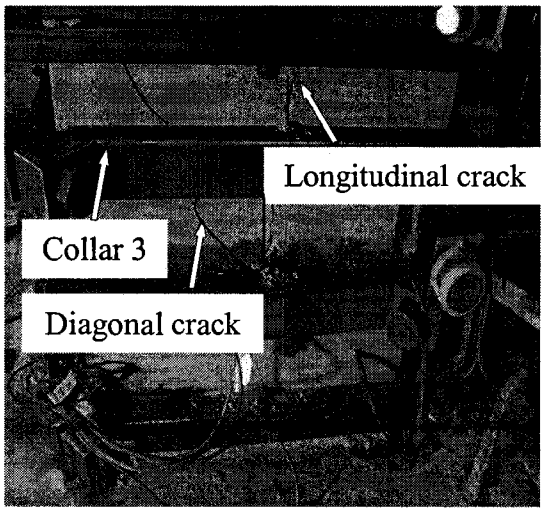

(a) Cracks at cycle 16 (μ =4)

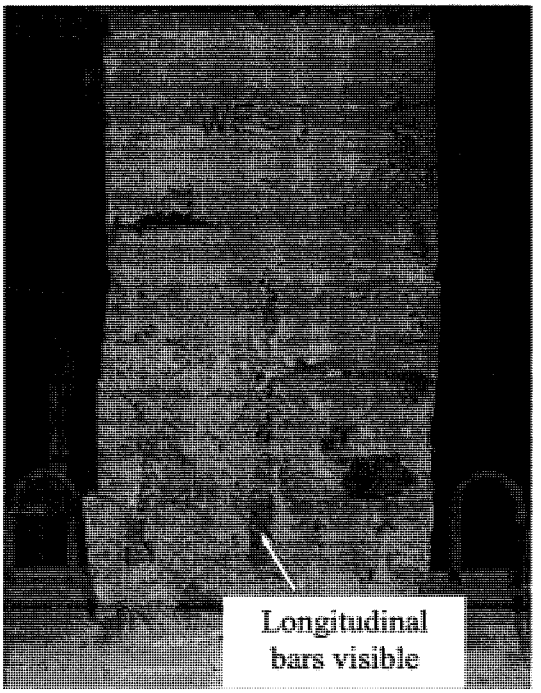

(g) At the end of the test

Figure 4-4 Specimen CV1

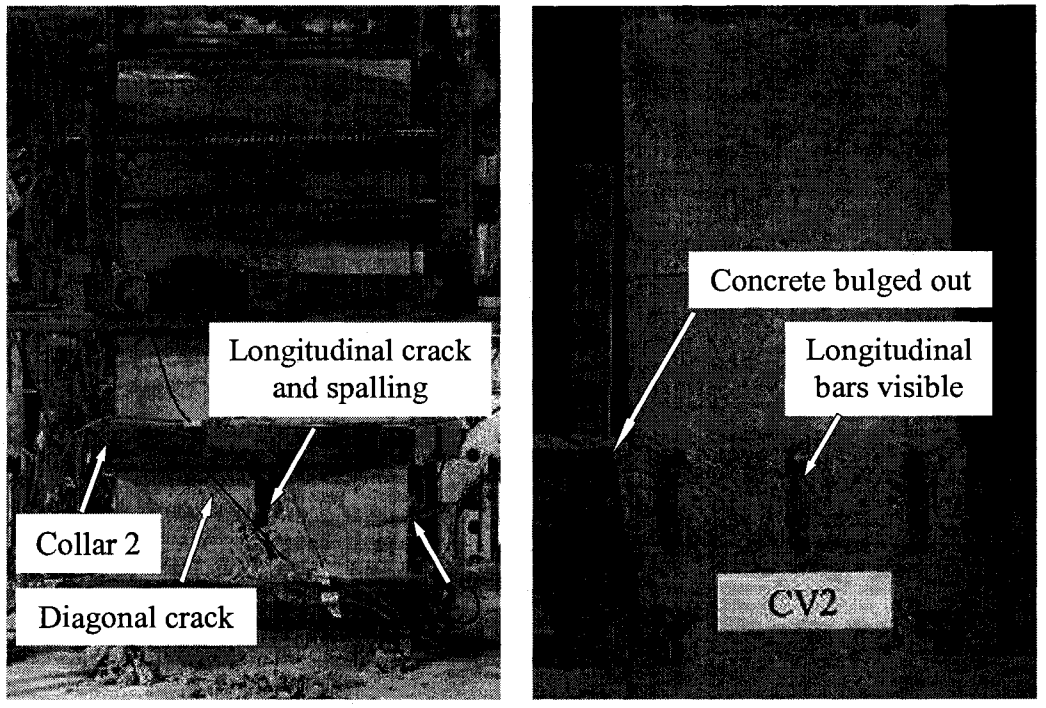

(a) Diagonal and longitudinal cracks (b) At the end of test

Figure 4-5 Specimen CV2

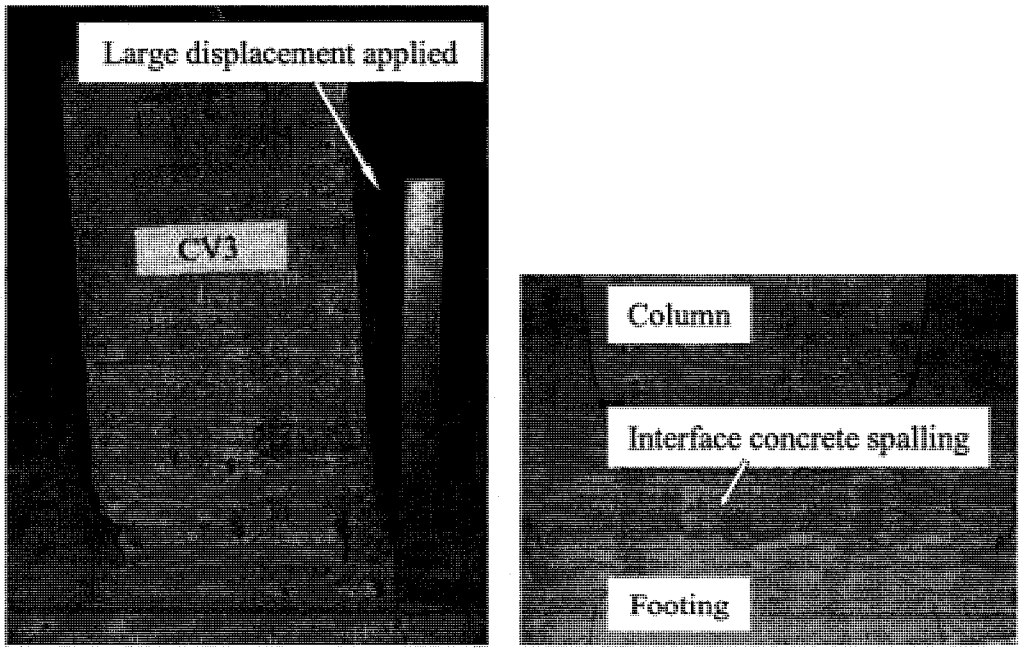

(a) Column sustained large displacement (b) Damage at the interface

Figure 4-6 Specimen CV3

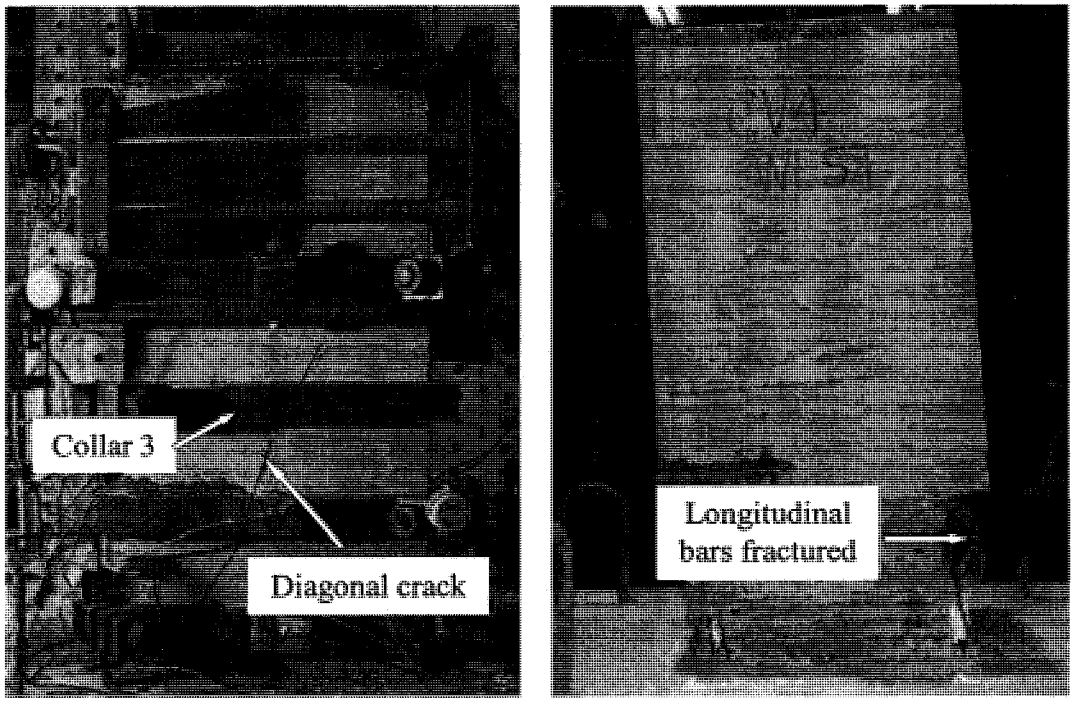

(a) Cracks at cycle 16 (μ =4) (b) At the end of the test

Figure 4-7 Specimen CV4

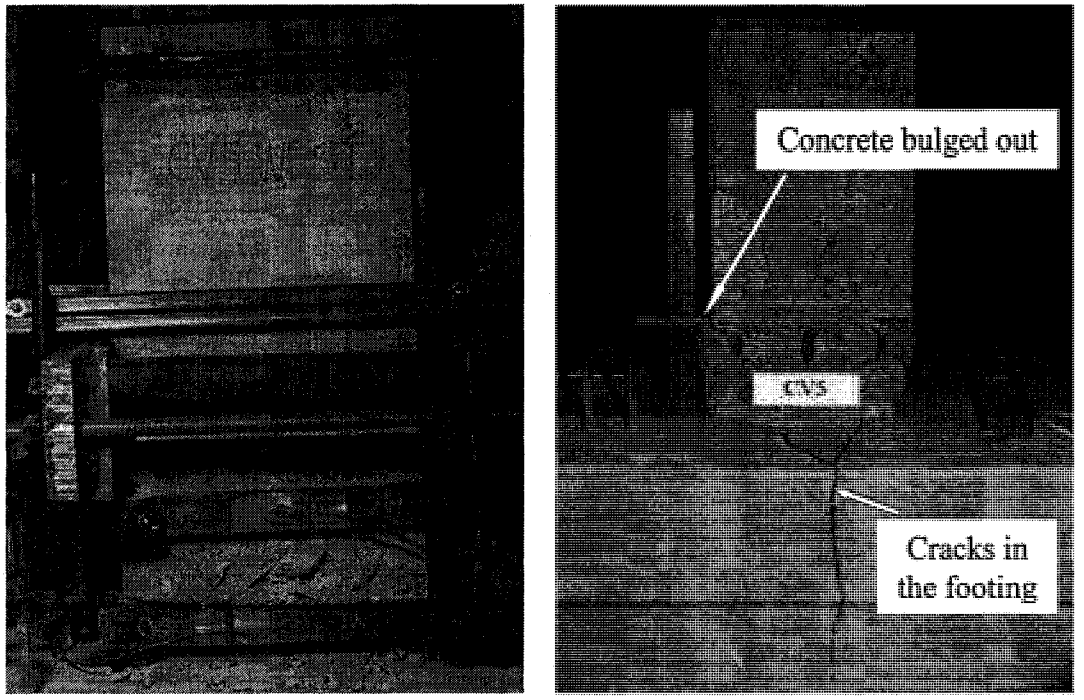

(a) Damage at cycle 26 (μ =4.52) (b) At the end of the test

Figure 4-8 Specimen CV5

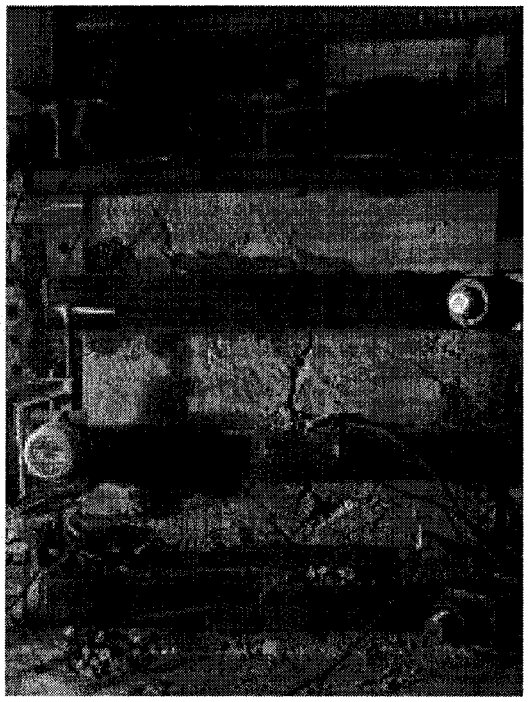

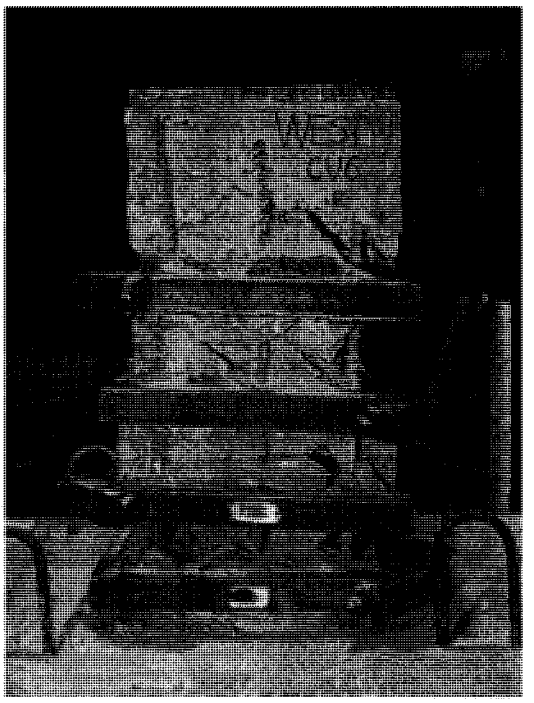

(a) Cracks at cycle 16 (μ =4) (b) No collar slippage after significant spalling

Figure 4-9 Specimen CV6

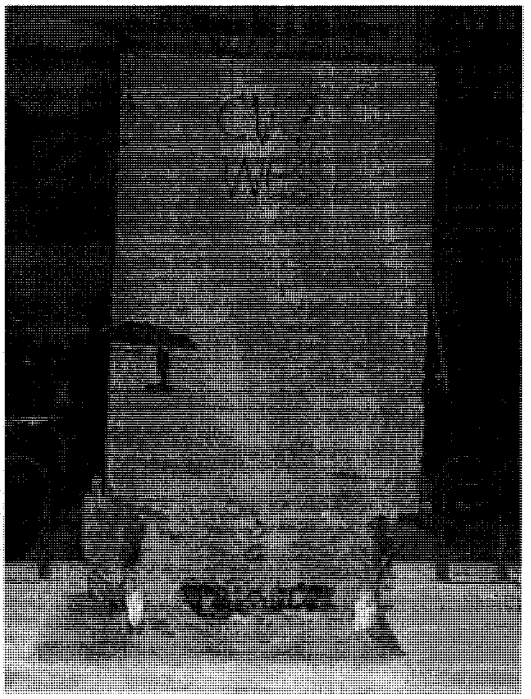

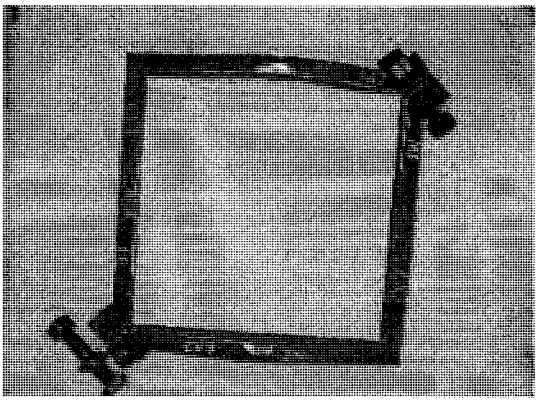

(a) Minor damage even at the end of the test (b) Collar deformation (collar 1)

Figure 4-10 Specimen CV7

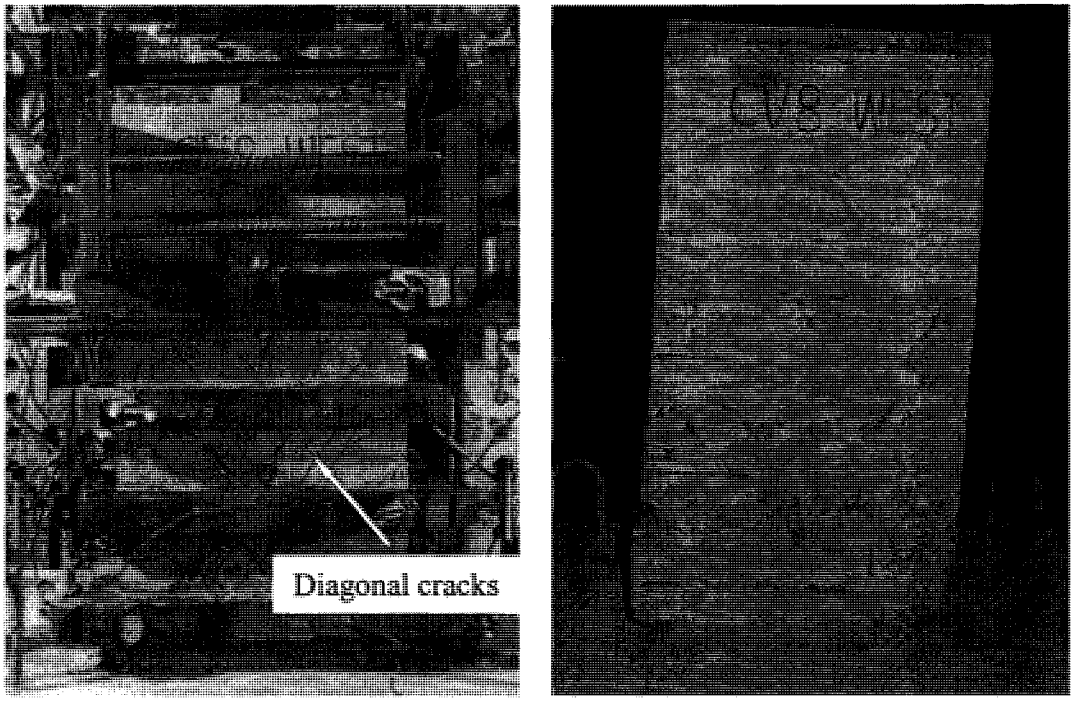

(a) Cracks at cycle 16 (μ =4) (b) Minor damage even at the end of the test

Figure 4-11 Specimen CV8

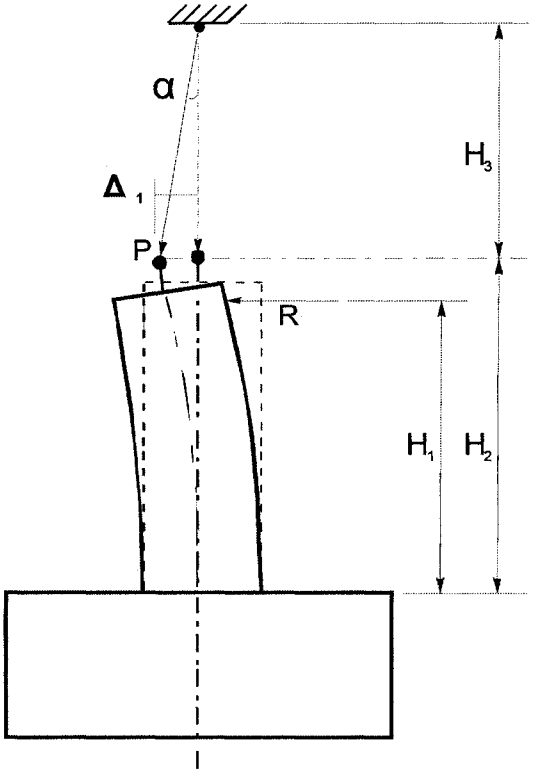

Figure 4-12 Lateral force calculation schematic

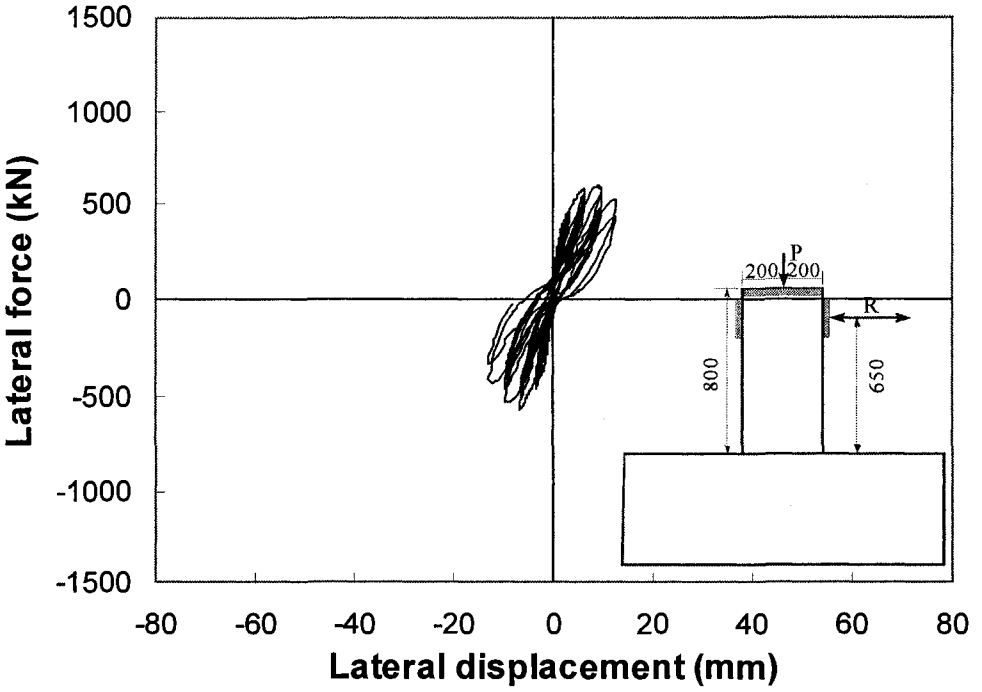

Figure 4-13 Lateral force–displacement hysteresis loops for specimen CV0A

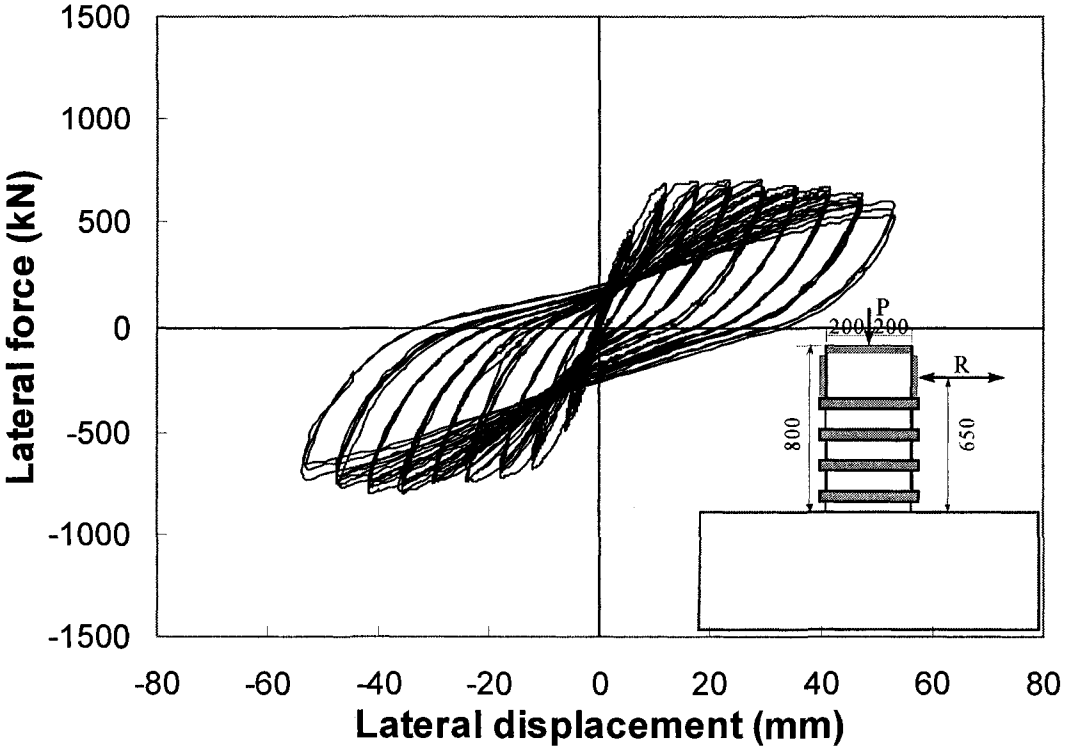

Figure 4-14 Lateral force–displacement hysteresis loops for specimen CV0AR

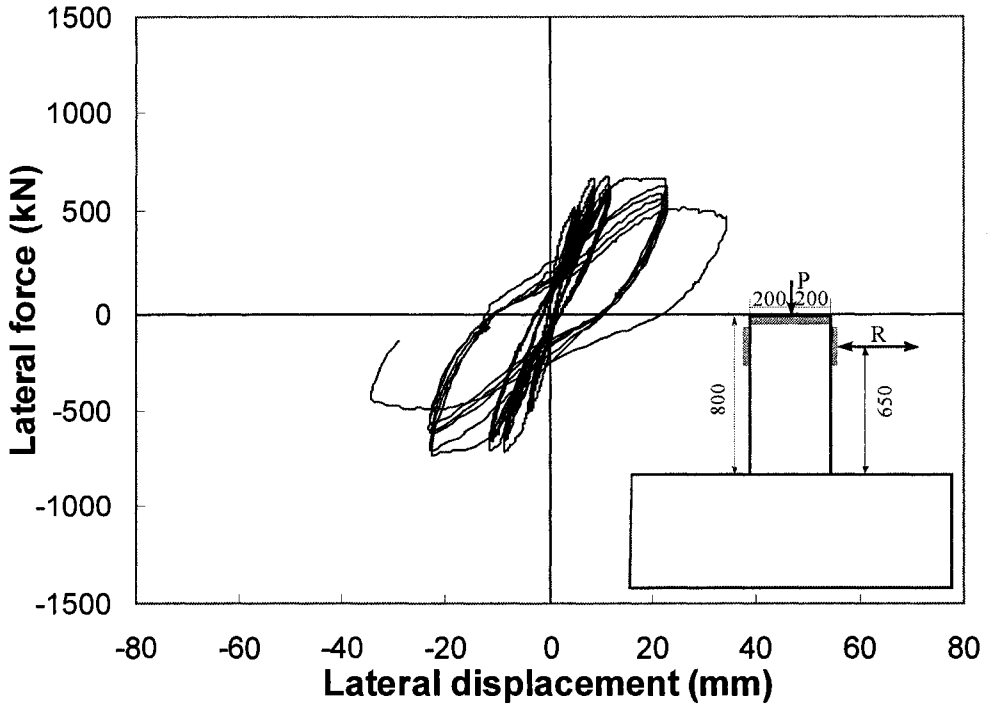

Figure 4-15 Lateral force–displacement hysteresis loops for specimen CV0B

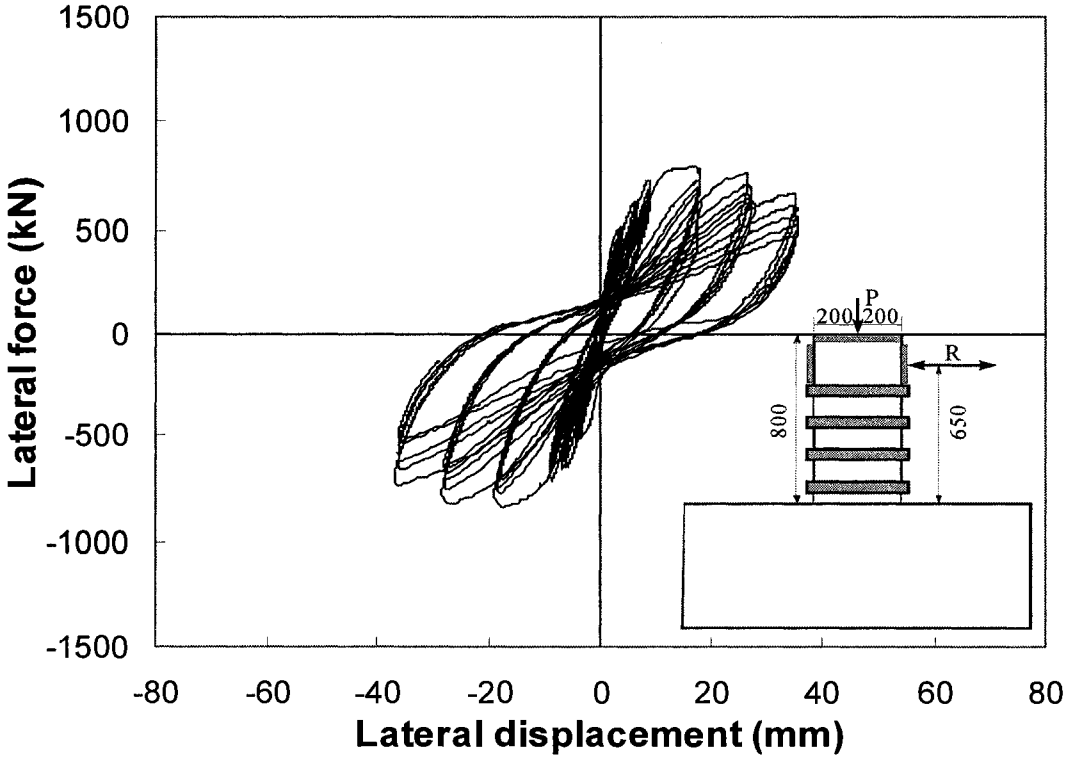

Figure 4-16 Lateral force–displacement hysteresis loops for specimen CV1

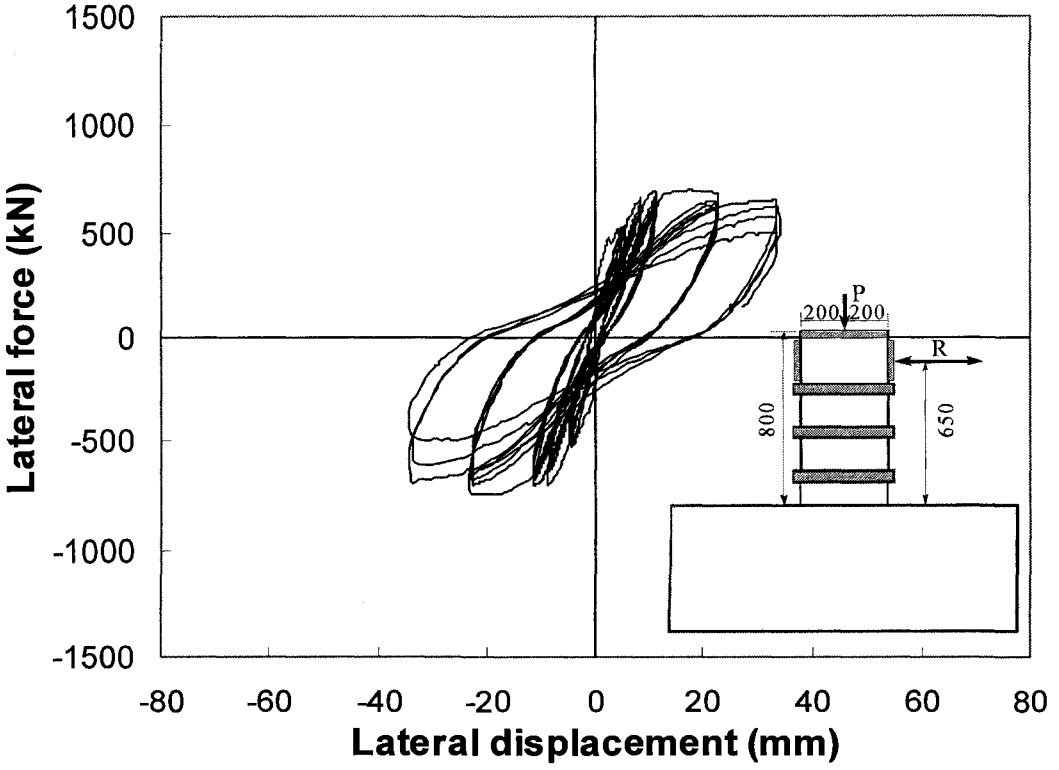

Figure 4-17 Lateral force–displacement hysteresis loops for specimen CV2

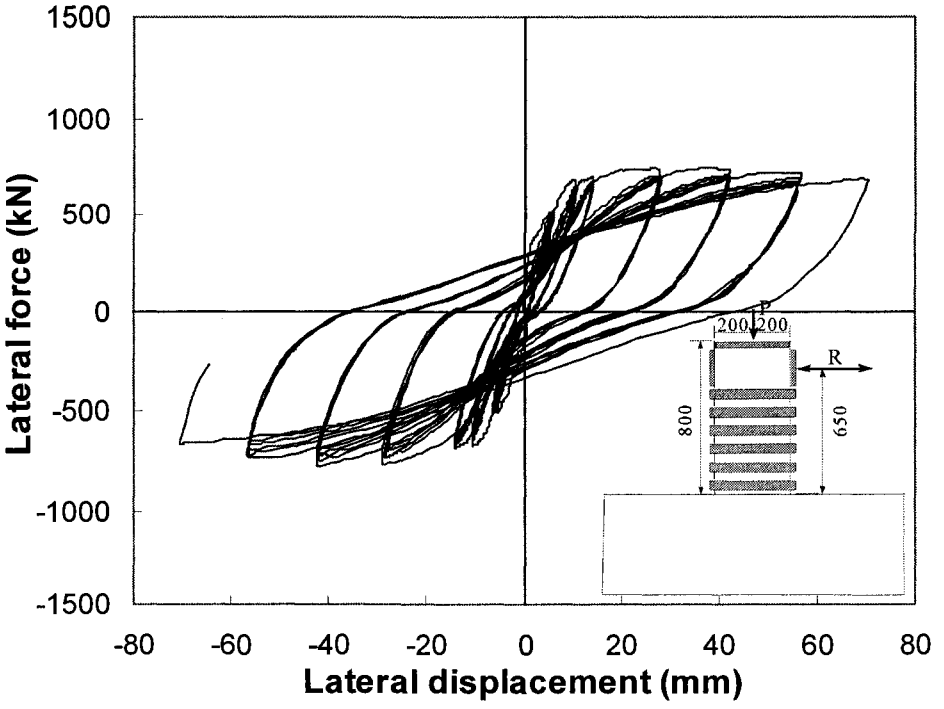

Figure 4-18 Lateral force–displacement hysteresis loops for specimen CV3

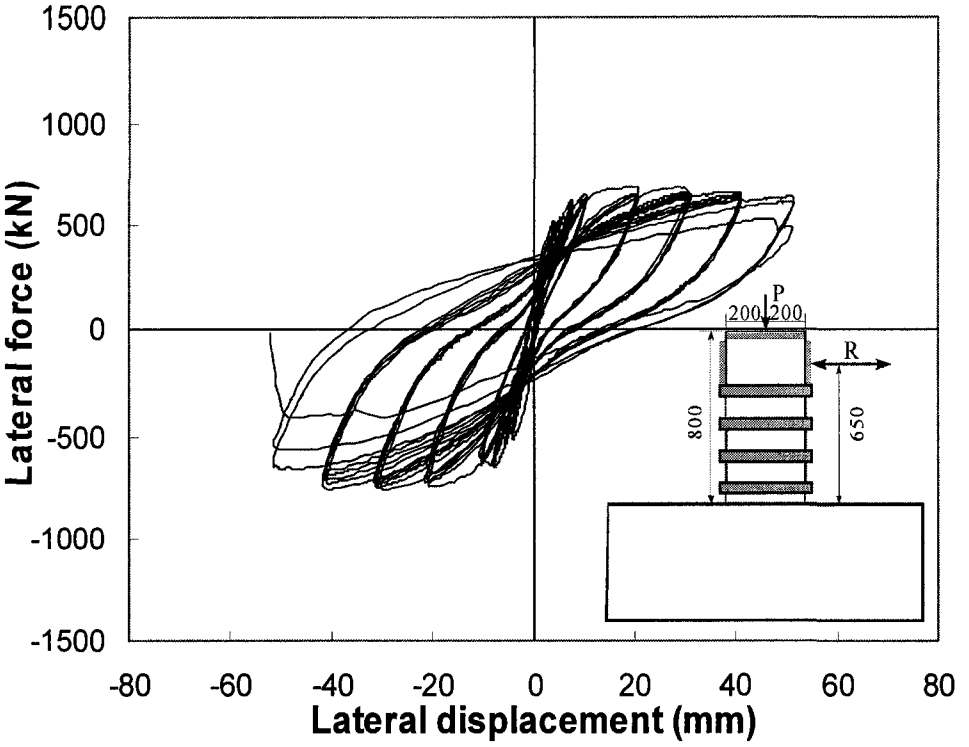

Figure 4-19 Lateral force–displacement hysteresis loops for specimen CV4

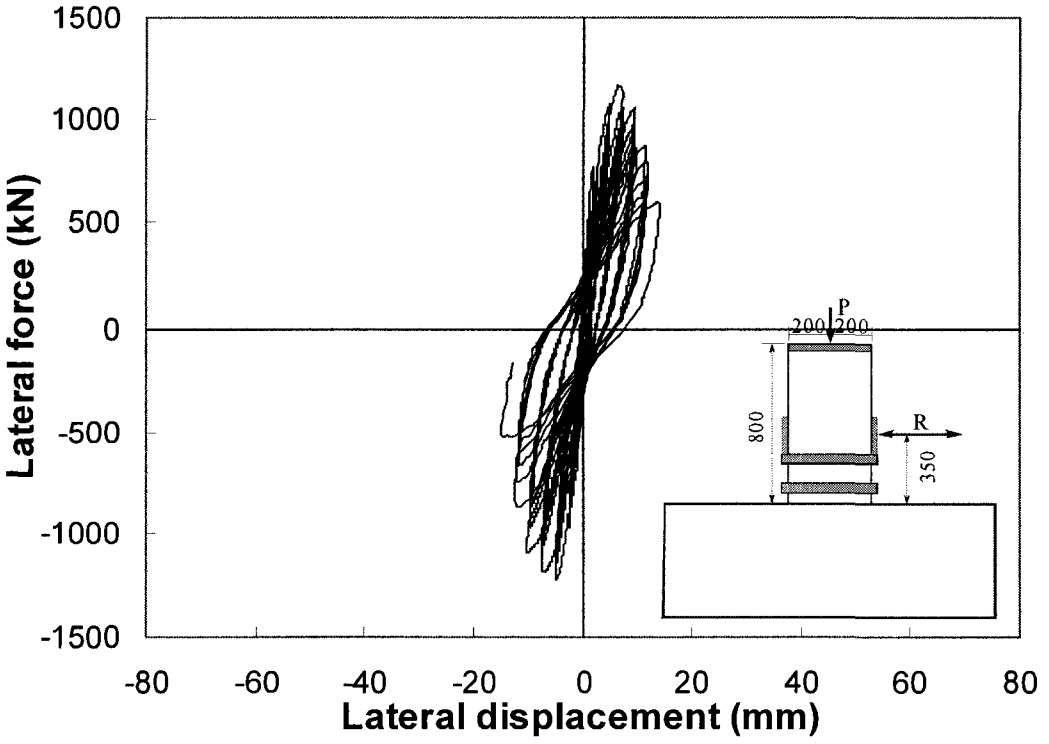

Figure 4-20 Lateral force–displacement hysteresis loops for specimen CV5

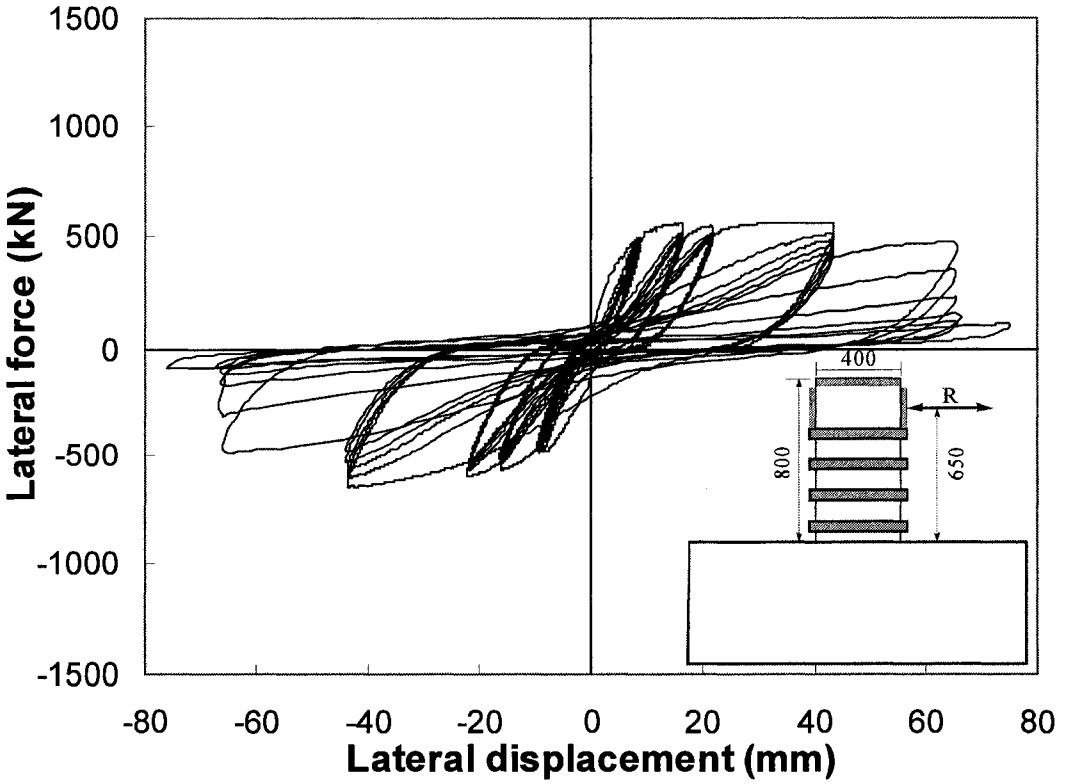

Figure 4-21 Lateral force–displacement hysteresis loops for specimen CV6

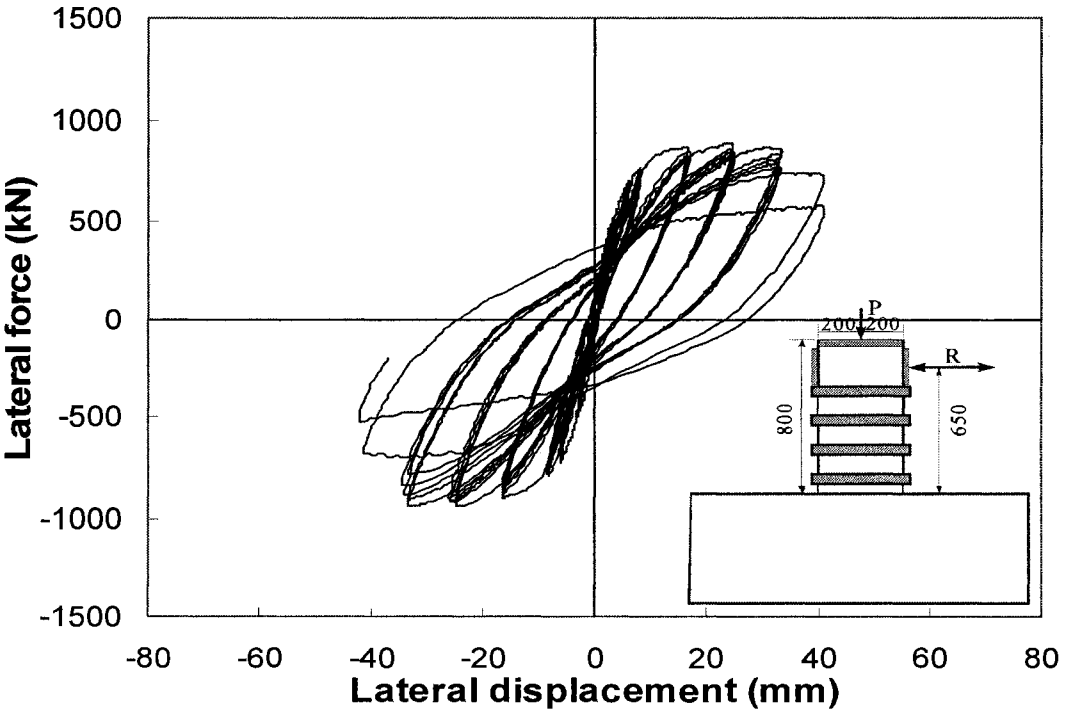

Figure 4-22 Lateral force–displacement hysteresis loops for specimen CV7

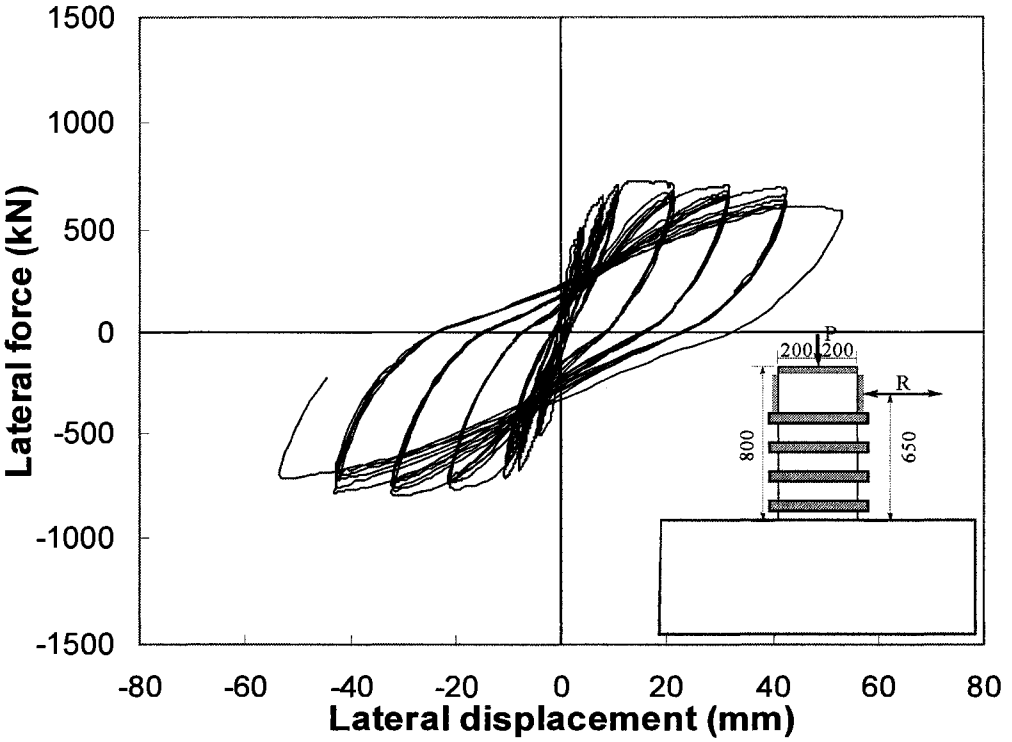

Figure 4-23 Lateral force–displacement hysteresis loops for specimen CV8

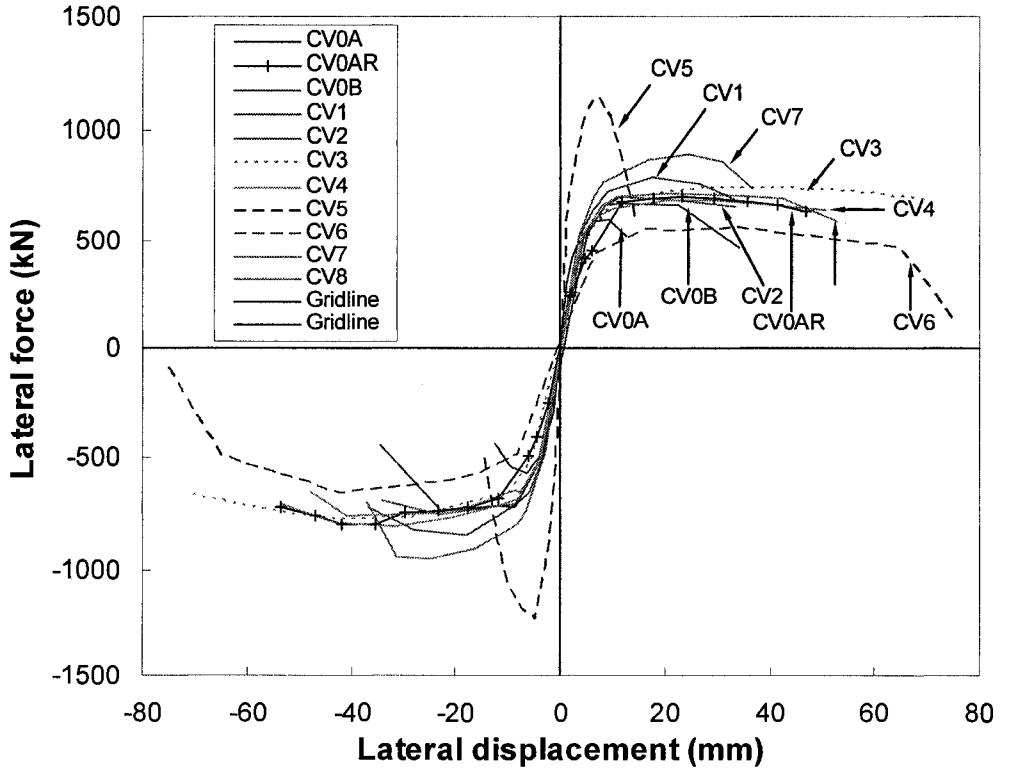

Figure 4-24 Lateral force–displacement envelopes for test specimens

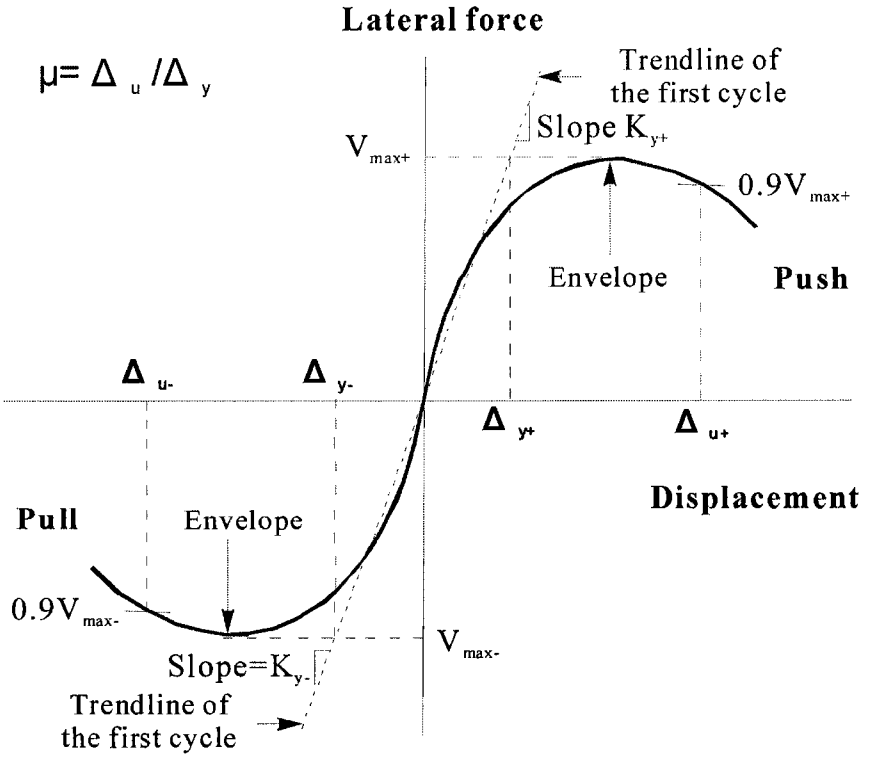

Figure 4-25 Displacement ductility by first cycle trendline method

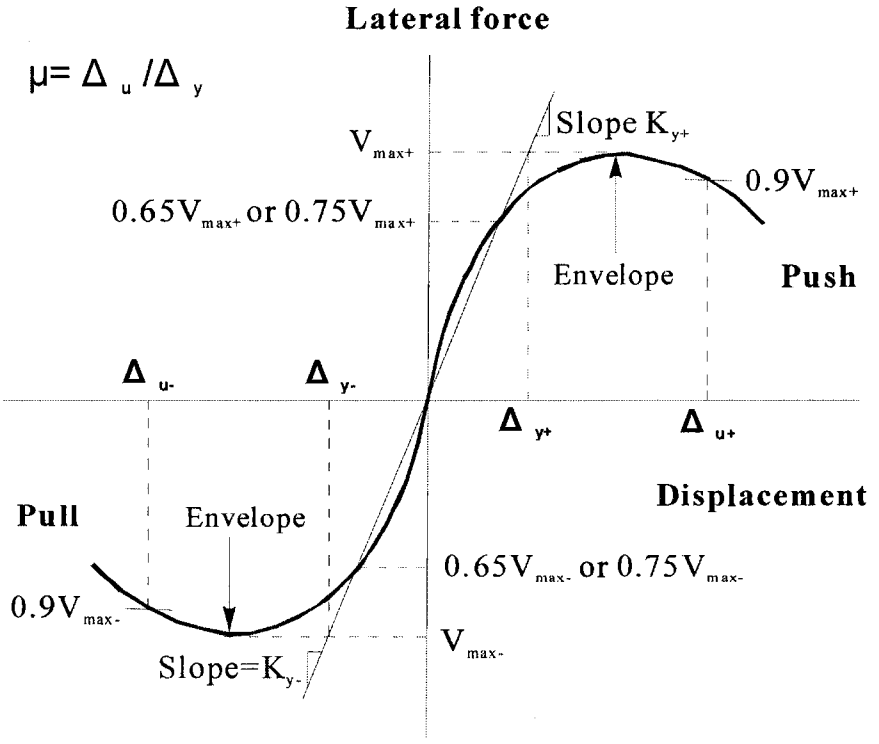

Figure 4-26 Displacement ductility by 65% V_{max} or 75% V_{max} secant line method

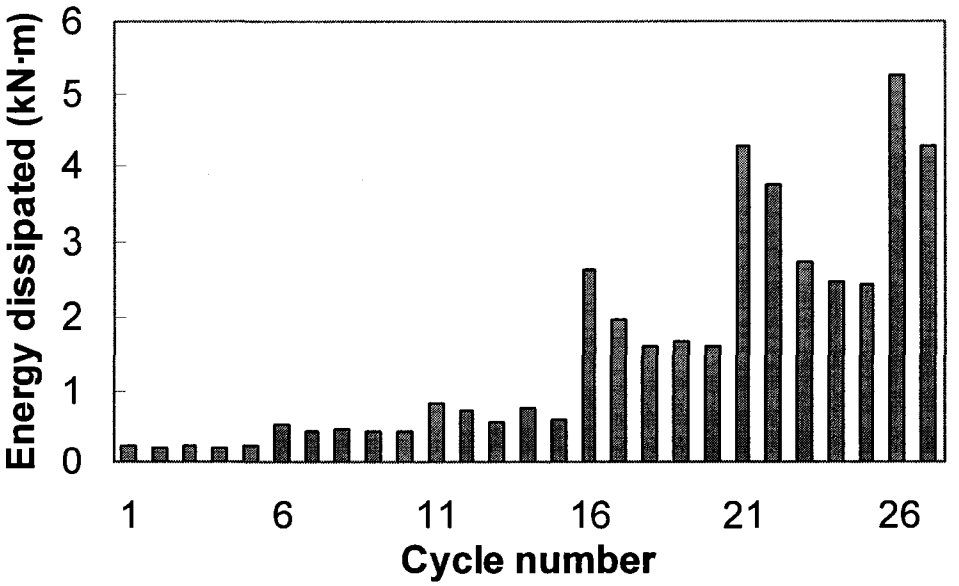

Figure 4-27 Energy dissipated during each cycle by specimen CV0A

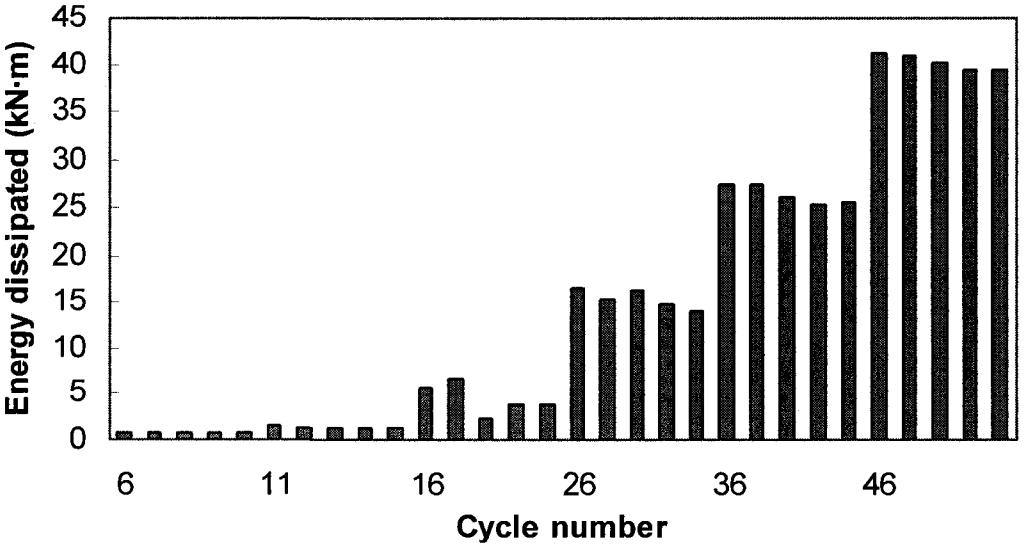

Figure 4-28 Energy dissipated during each cycle by specimen CV0AR

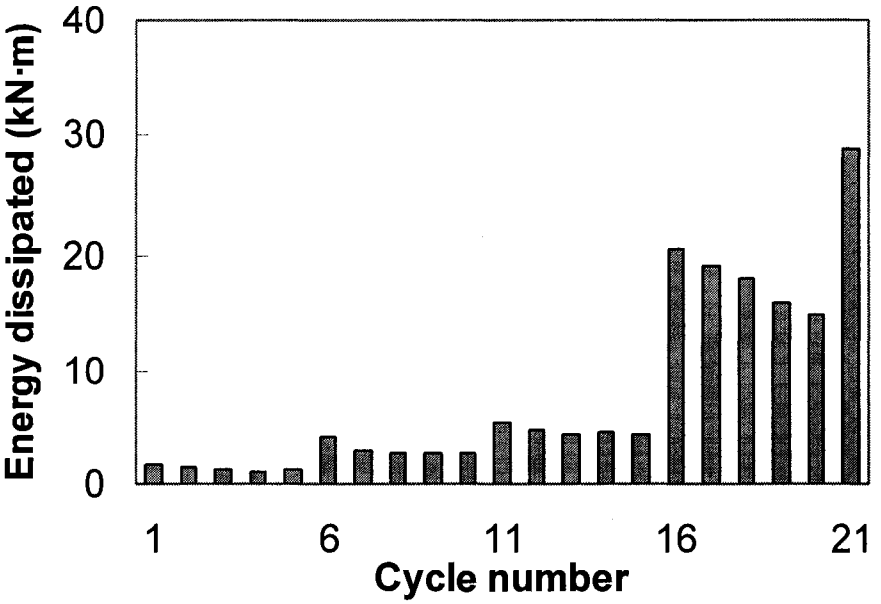

Figure 4-29 Energy dissipated during each cycle by specimen CV0B

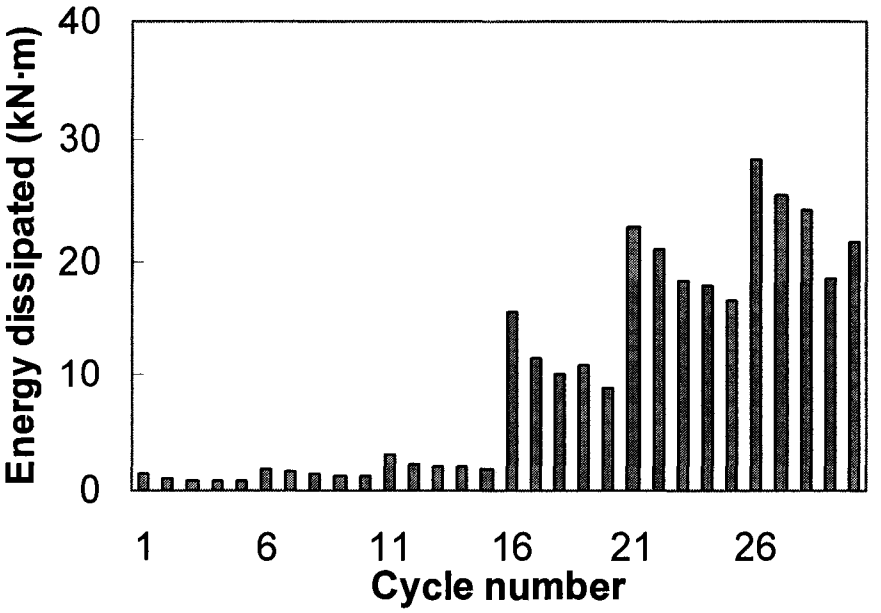

Figure 4-30 Energy dissipated during each cycle by specimen CV1

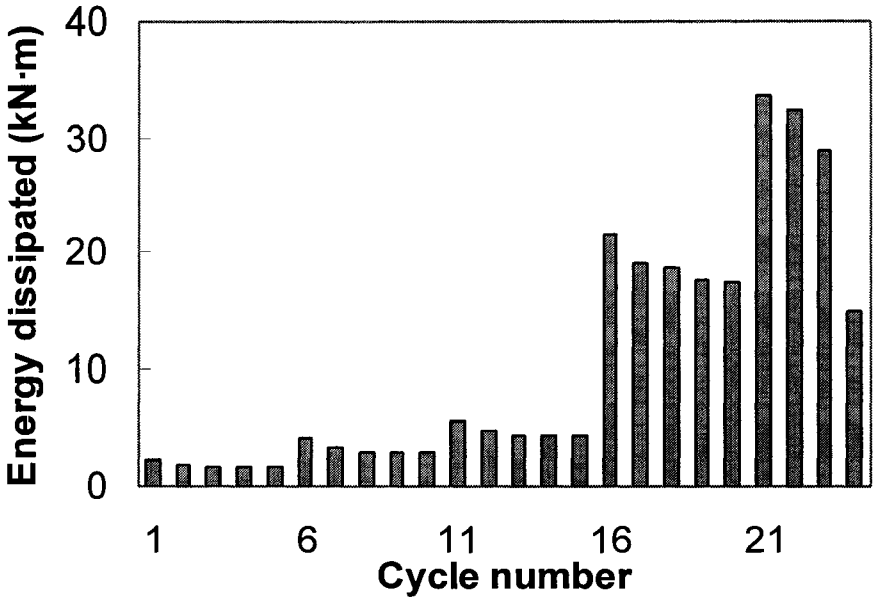

Figure 4-31 Energy dissipated during each cycle by specimen CV2

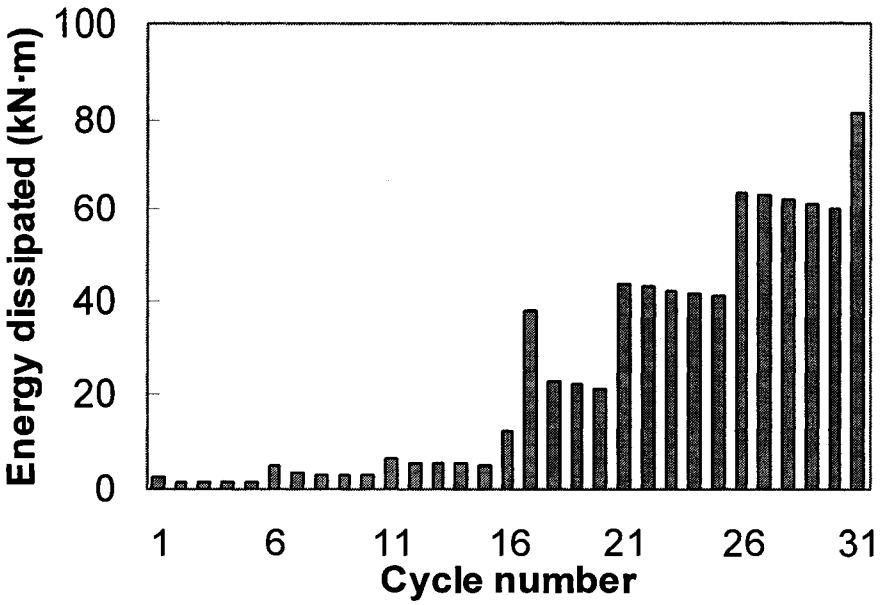

Figure 4-32 Energy dissipated during each cycle by specimen CV3

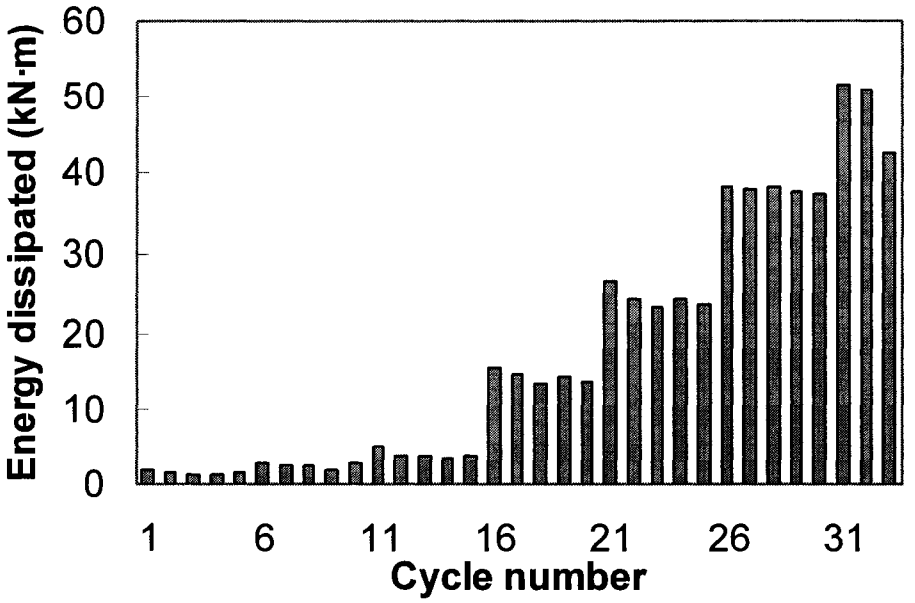

Figure 4-33 Energy dissipated during each cycle by specimen CV4

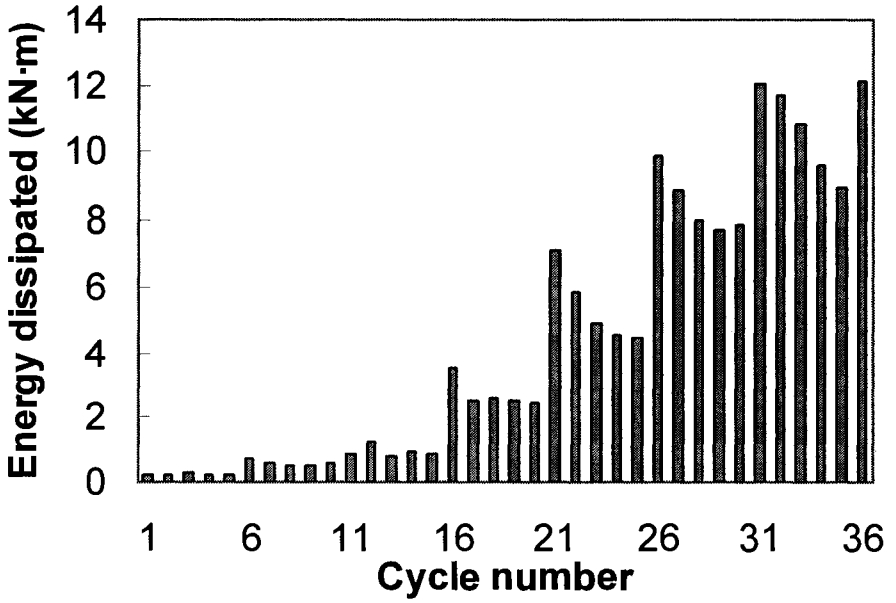

Figure 4-34 Energy dissipated during each cycle by specimen CV5

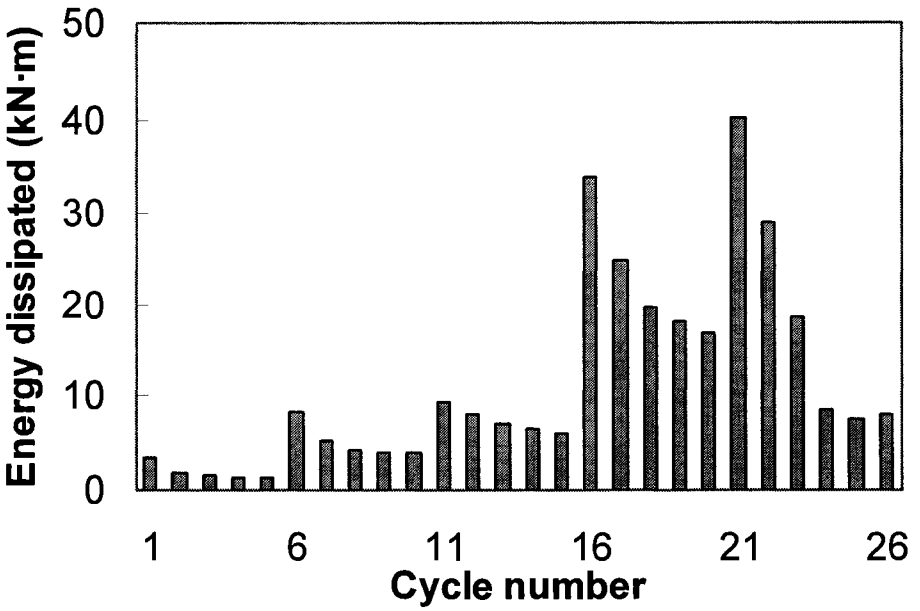

Figure 4-35 Energy dissipated during each cycle by specimen CV6

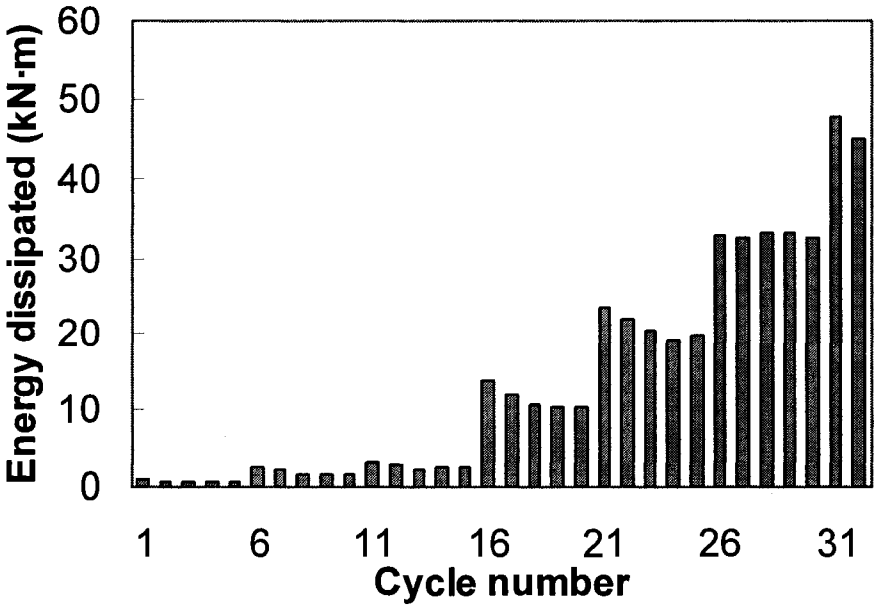

Figure 4-36 Energy dissipated during each cycle by specimen CV7

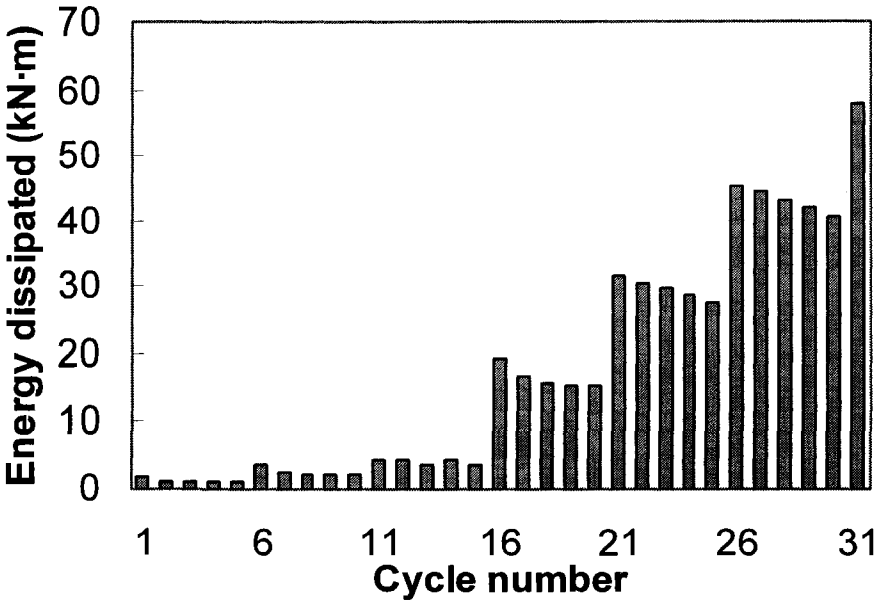

Figure 4-37 Energy dissipated during each cycle by specimen CV8

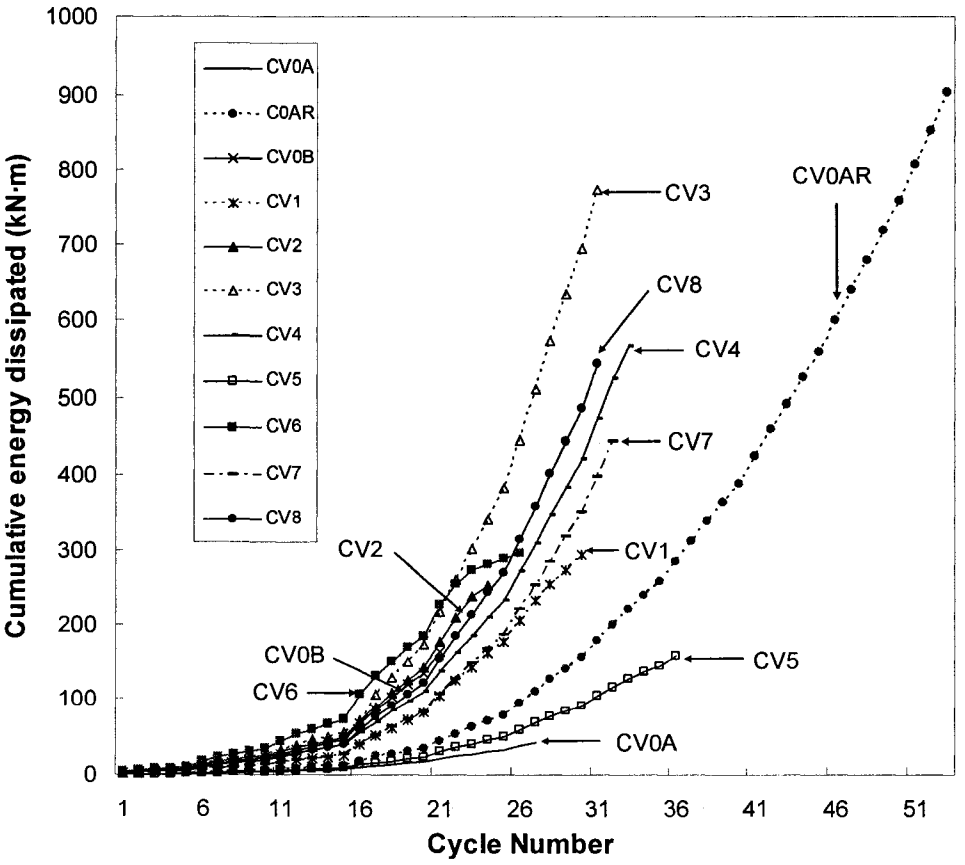

Figure 4-38 Cumulative energy dissipated versus cycle number

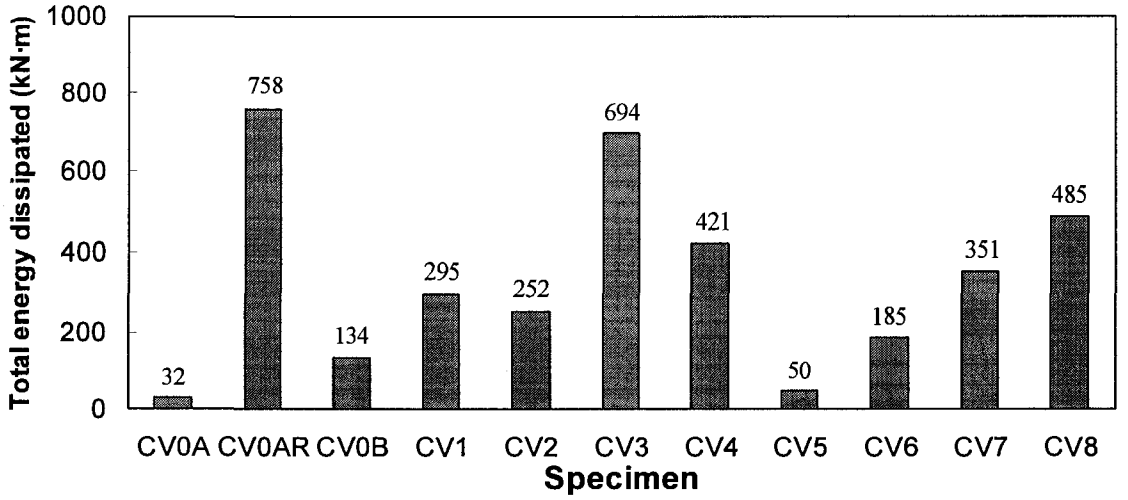

Figure 4-39 Total energy dissipated

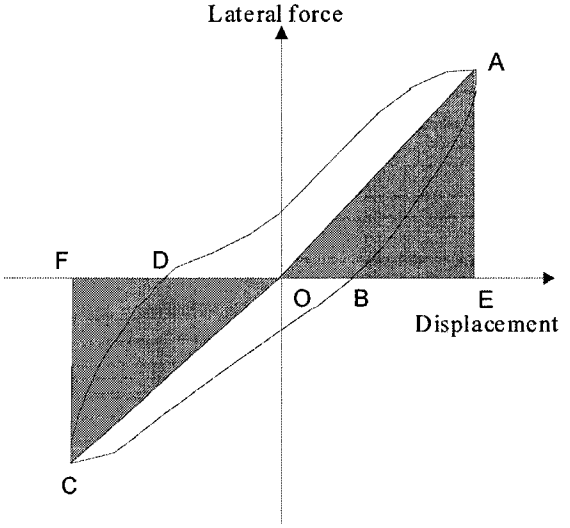

$$\gamma = \frac{1}{2\pi} \cdot \frac{area(ABCDA)}{area(\Delta OAE + \Delta OCF)}$$

Figure 4-40 Equivalent viscous damping ratio γ (adapted from Ghobarah *et al.* 1996)

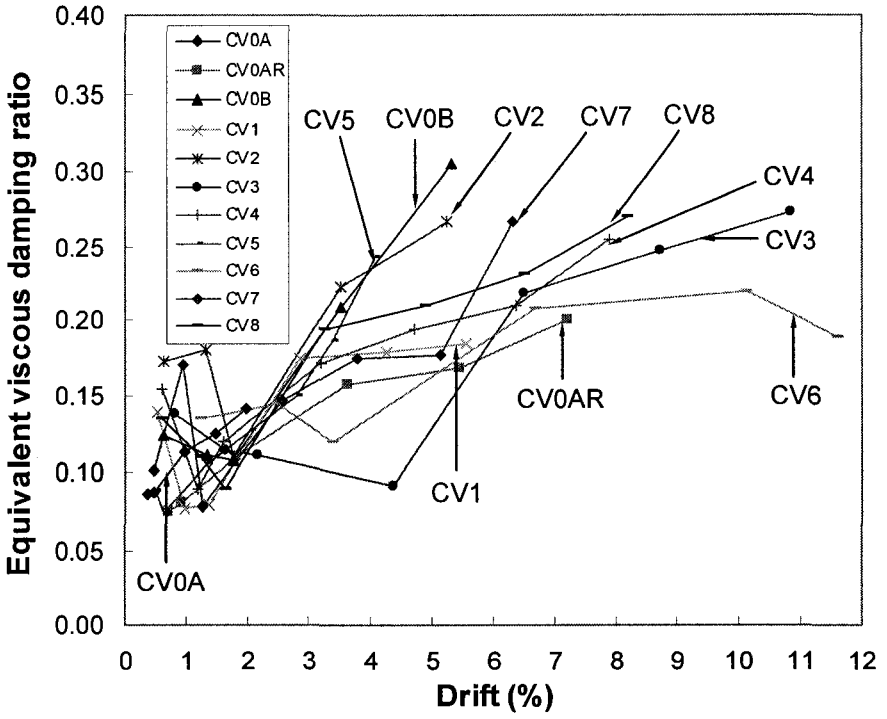

Figure 4-41 Equivalent viscous damping ratios

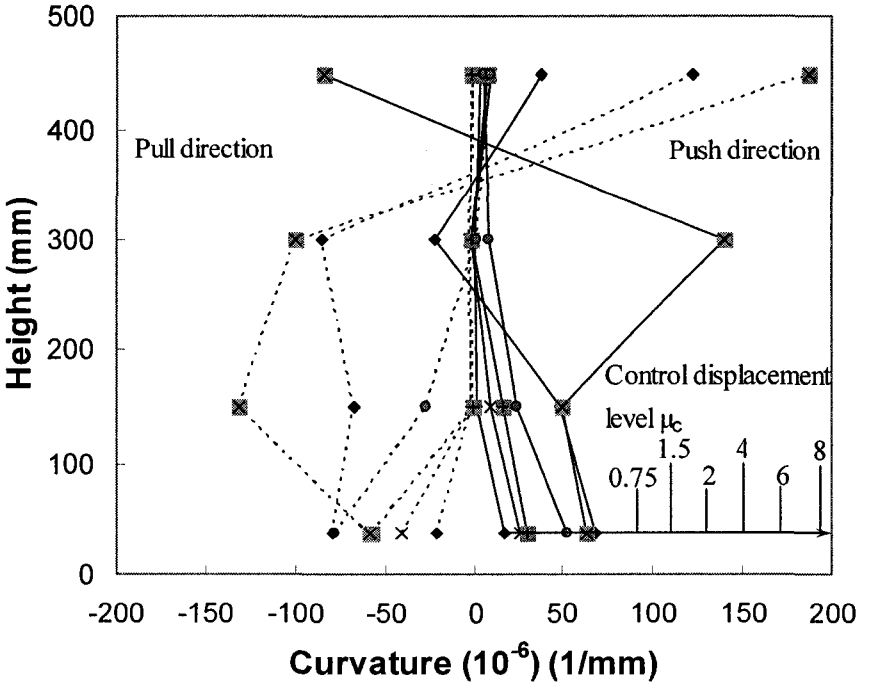

* Dashed curves are in pull direction and solid curves are in push direction
* Control displacement level μ_c of 0.75, 1.5, 2, 4, 6, etc. show the order of the curvatures as they move from left to right in the push direction

Figure 4-42 Curvature distribution along height for specimen CV0A

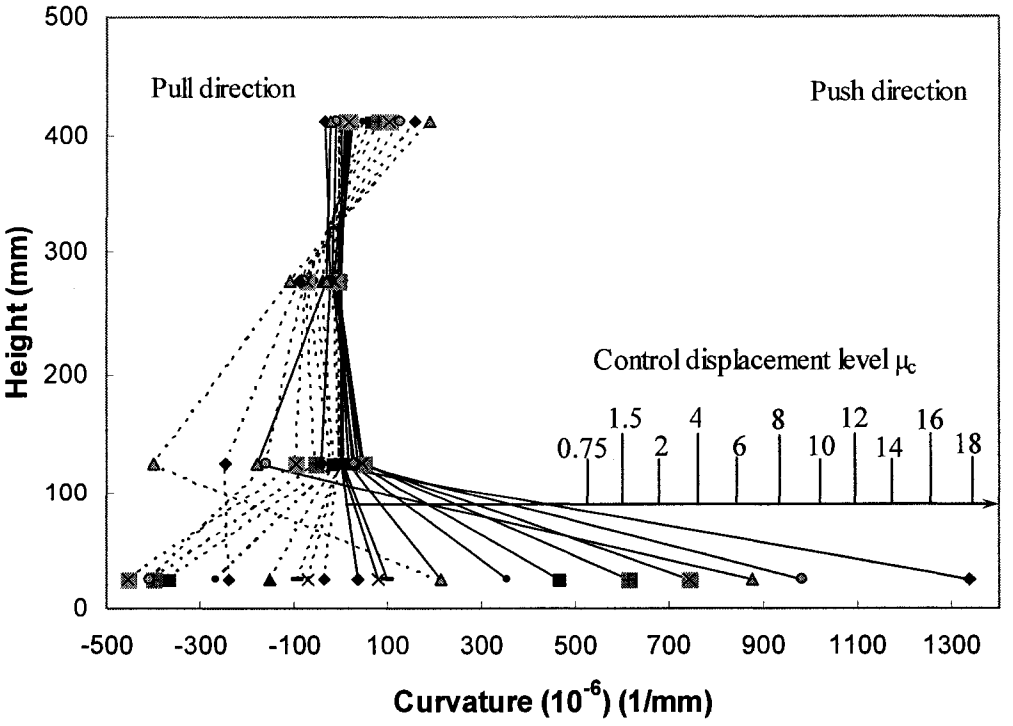

Figure 4-43 Curvature distribution along height for specimen CV0AR

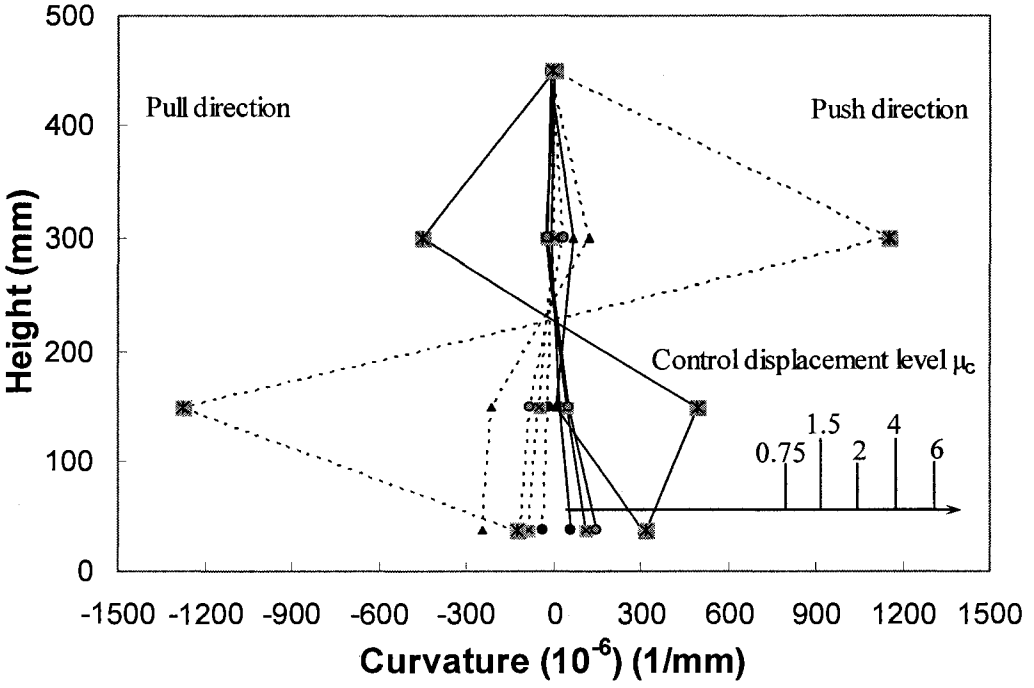

Figure 4-44 Curvature distribution along height for specimen CV0B

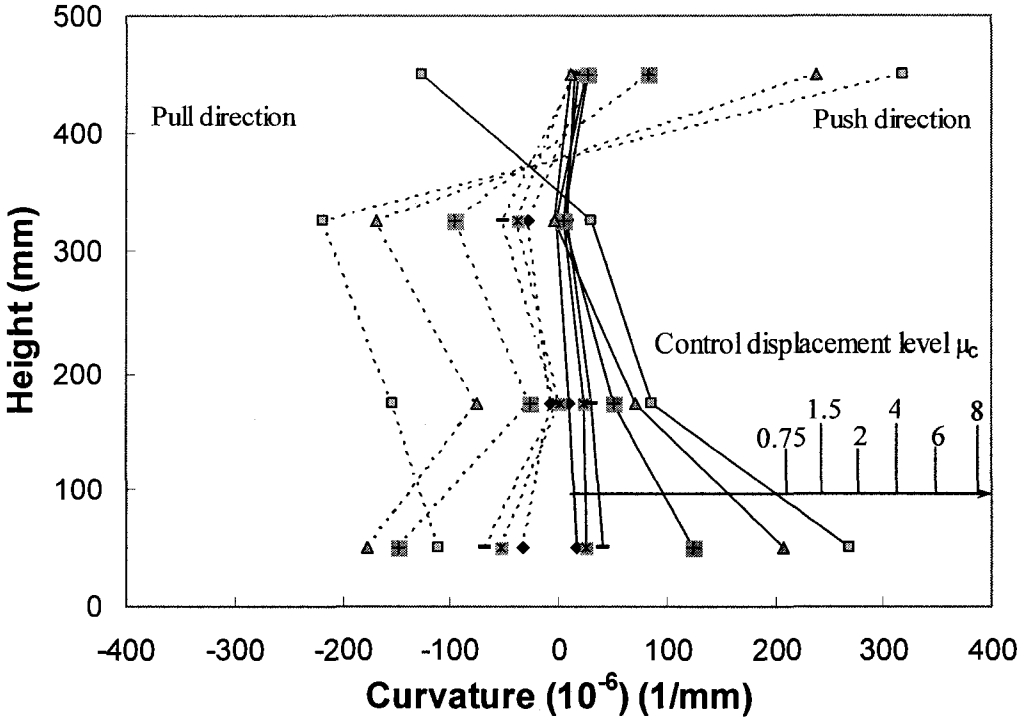

Figure 4-45 Curvature distribution along height for specimen CV1

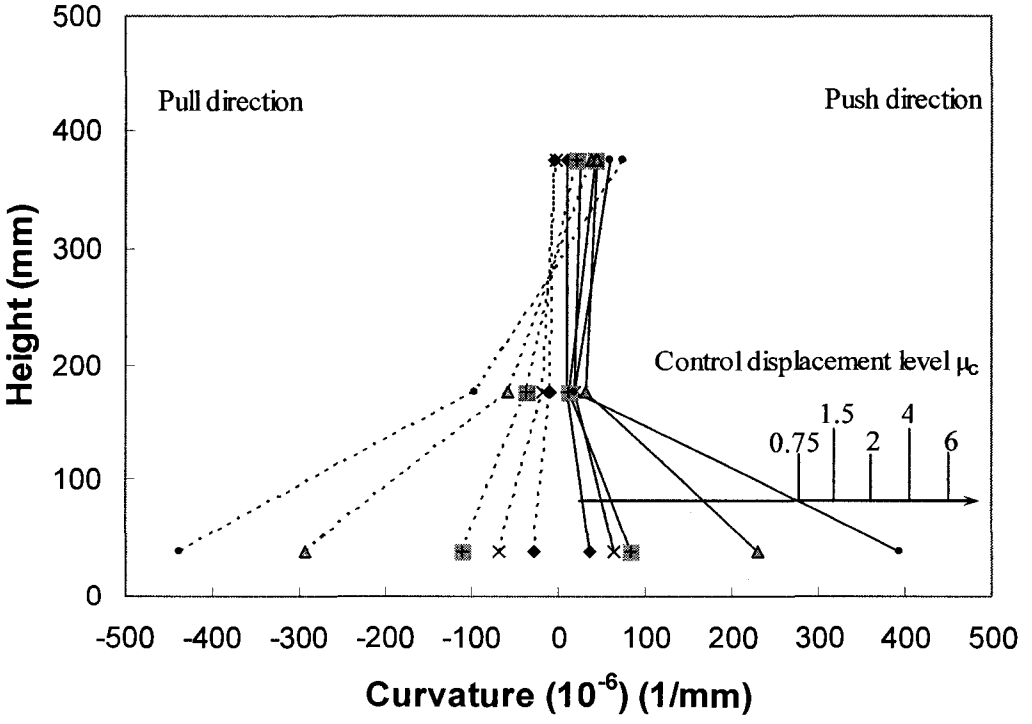

Figure 4-46 Curvature distribution along height for specimen CV2

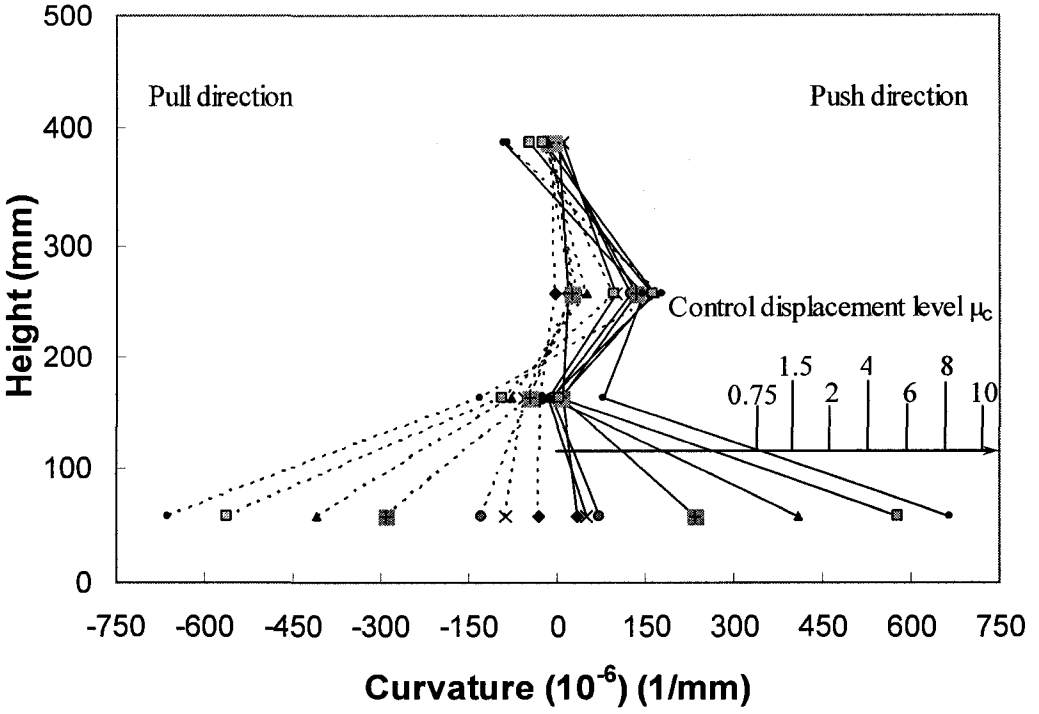

Figure 4-47 Curvature distribution along height for specimen CV3

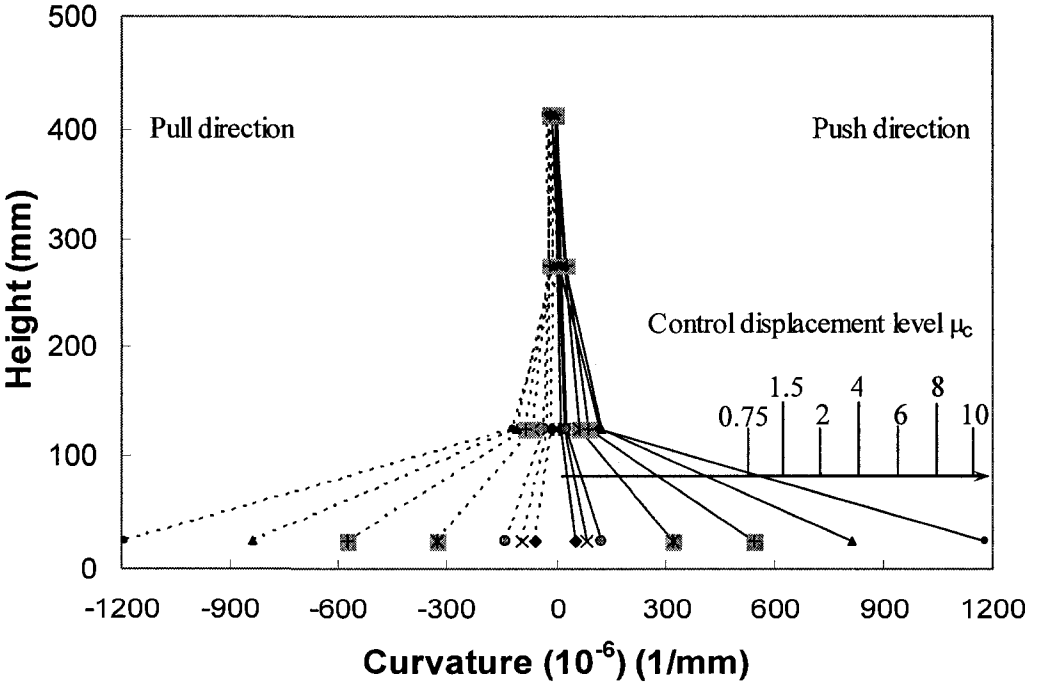

Figure 4-48 Curvature distribution along height for specimen CV4

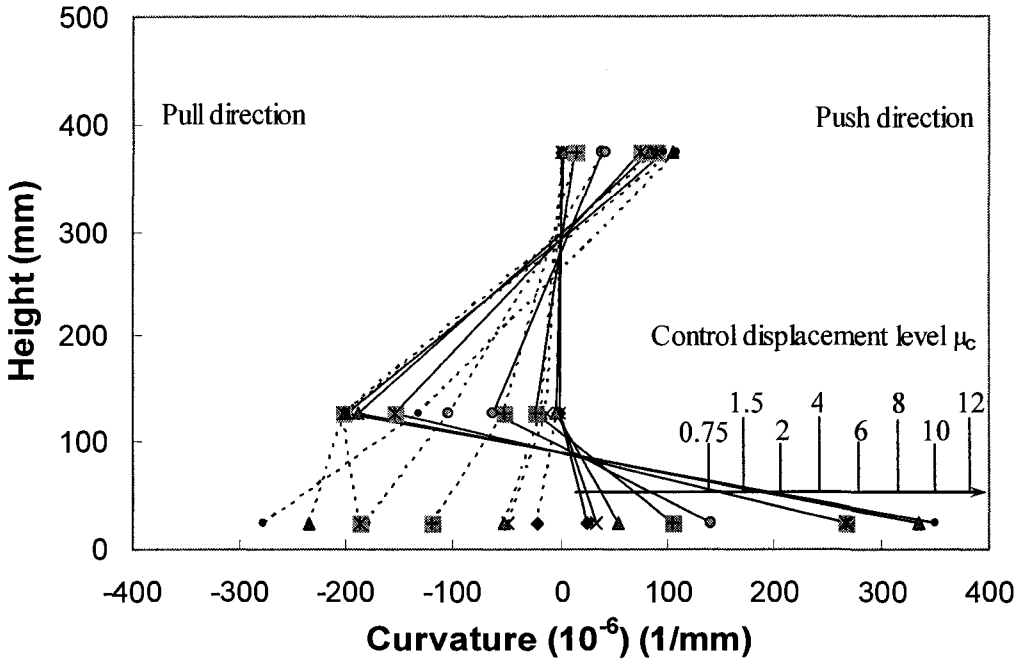

Figure 4-49 Curvature distribution along height for specimen CV5

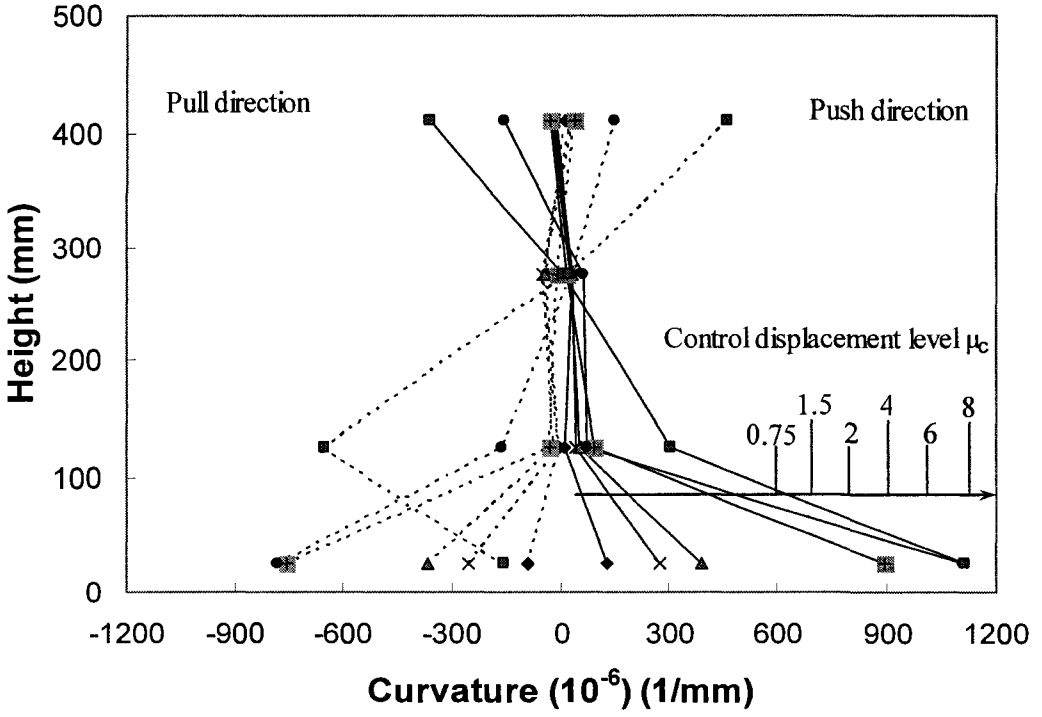

Figure 4-50 Curvature distribution along height for specimen CV6

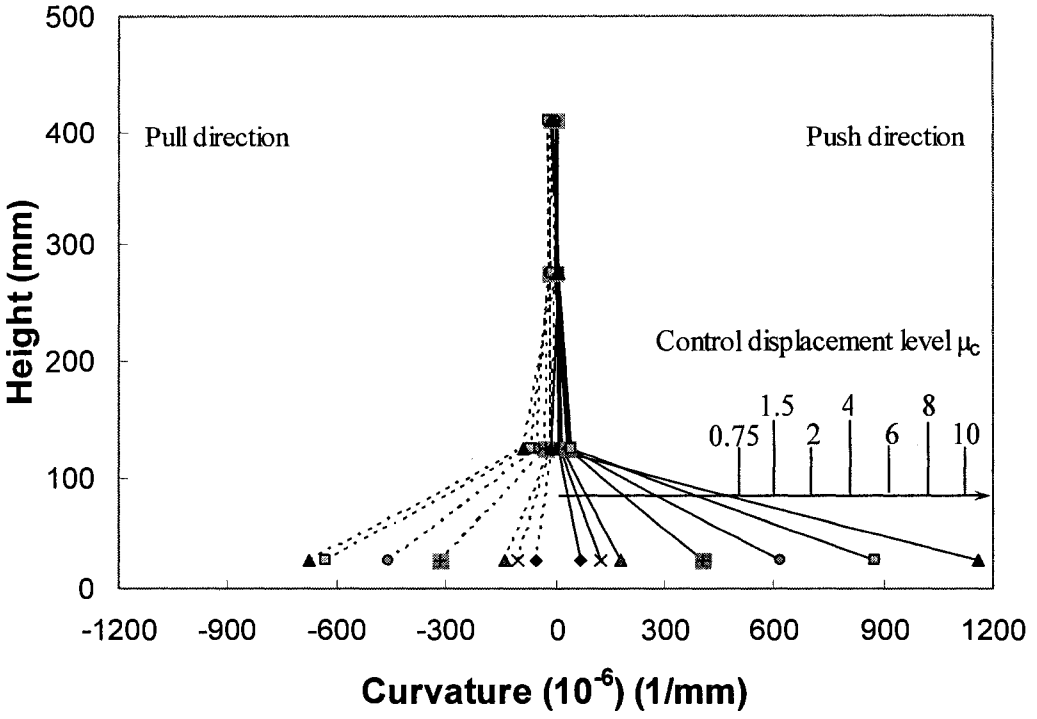

Figure 4-51 Curvature distribution along height for specimen CV7

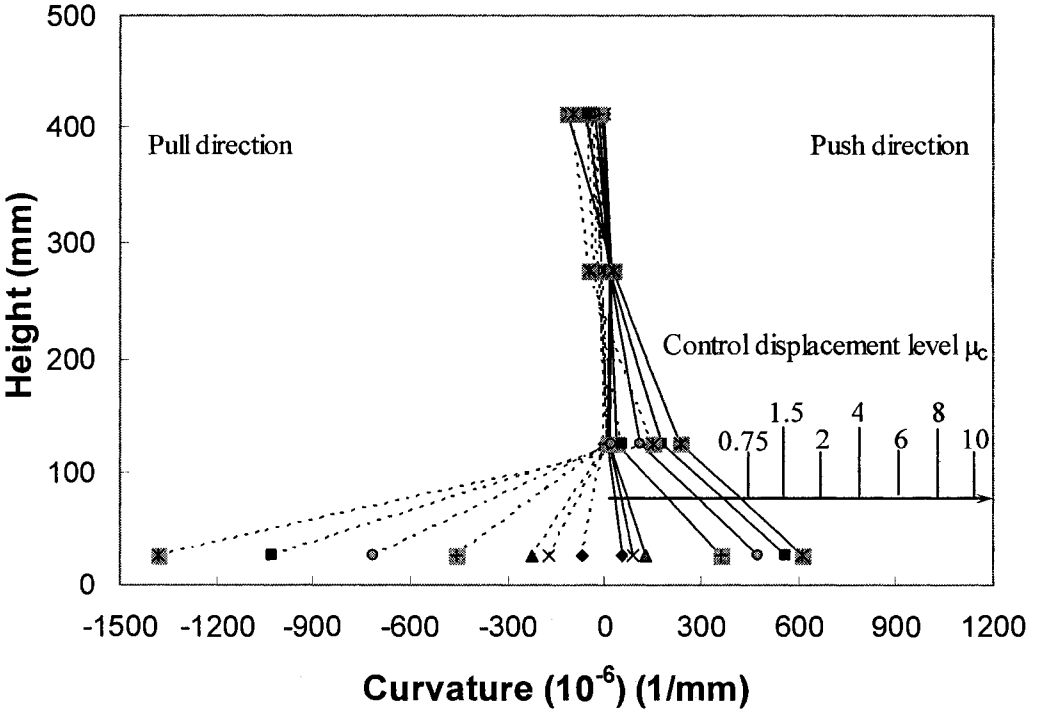

Figure 4-52 Curvature distribution along height for specimen CV8

u_1 and u_2 are longitudinal bar elongations in the footing

d_1 and d_2 are distance from the strain origin to the lower strain gauges

Δ_R: Rotation induced displacement

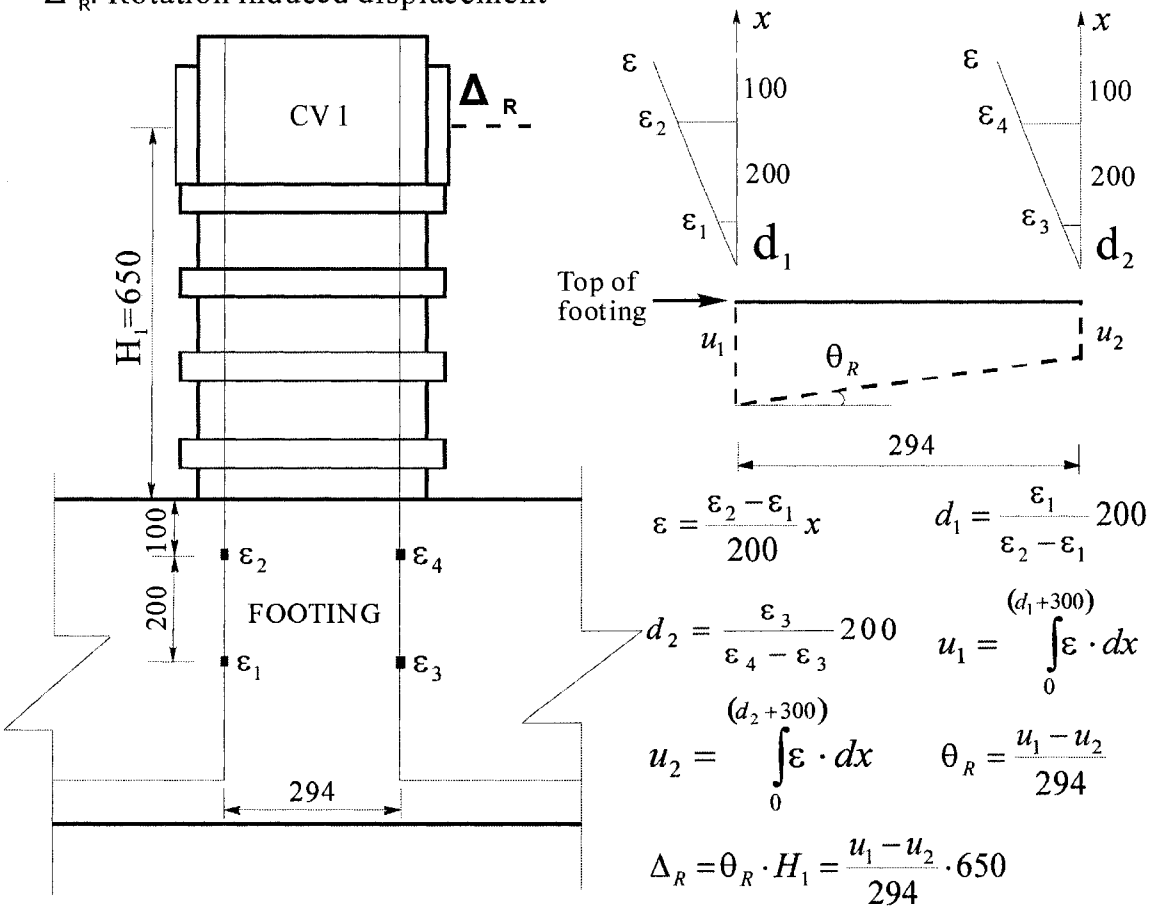

Figure 4-53 Calculation of the rotation-induced displacement

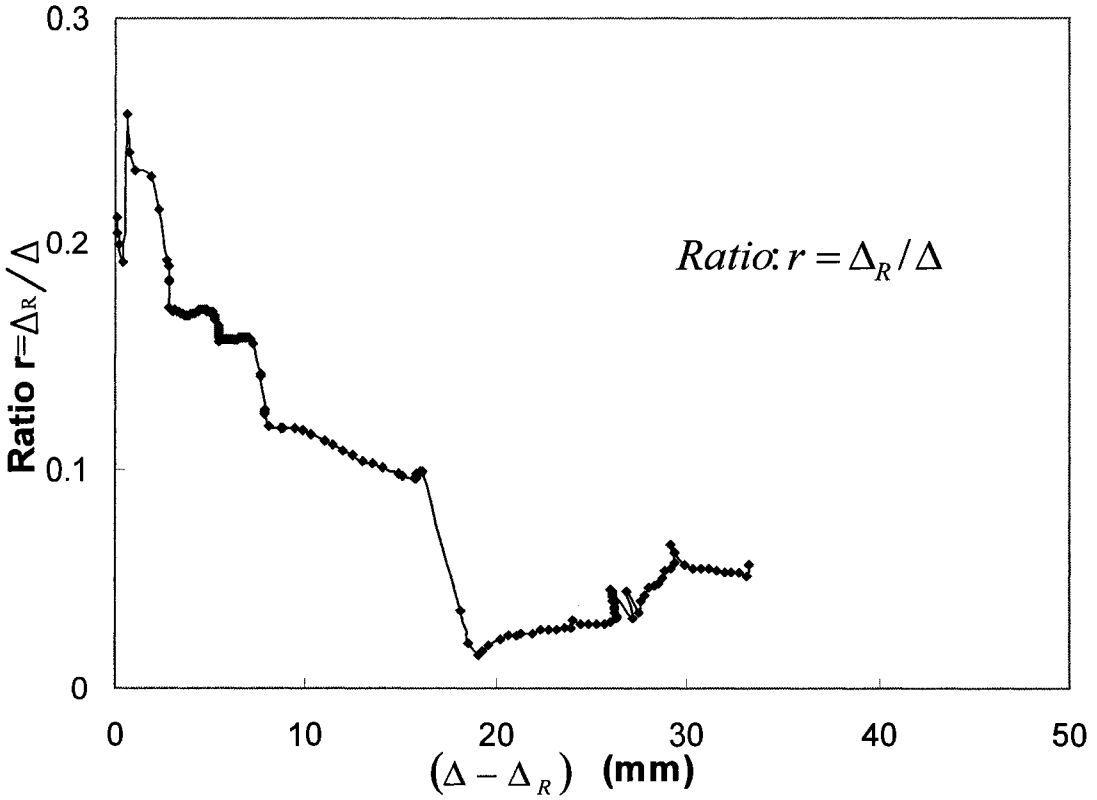

Figure 4-54 Relationship between r and $(\Delta - \Delta_R)$ for specimen CV1

CHAPTER 5 FINITE ELEMENT ANALYSIS

5.1 Introduction

While it is valuable to conduct large-scale tests on reinforced concrete columns with collars, as presented in Chapters 3 and 4, it is not practical to consider the full range of geometric dimensions, loading conditions, or other parametric variations that may be encountered in practice. It is also convenient if a numerical model is available for the design or evaluation of such members. It is therefore necessary to conduct numerical simulations of the reinforced concrete columns rehabilitated with external steel collars from the experimental program, to aid in development and validation of a proposed simplified modelling technique.

The process of developing analytical predictions of the behaviour of reinforced concrete structures is relatively complex due to the presence of the reinforcement, nonlinear concrete behaviour under multi-axial stress states including cracking, stress transfer across cracked concrete sections, and stiffness and strength degradation under cyclic loading. Analytical studies through empirical mathematical formulae and/or numerical finite element simulation are important techniques for research on reinforced concrete structures. These techniques can be used to reproduce experimental results and they also allow the study of additional design parameters in a more efficient and less expensive manner than additional full-scale laboratory testing.

As reported in Chapters 3 and 4, external steel collars have been proven to be effective in the rehabilitation and repair of deficient reinforced concrete short columns under combined axial and cyclic lateral loading in an experimental program conducted at the University of Alberta. Numerical analysis using the finite element method was conducted to simulate the response of the control columns and collared columns tested. A finite element model capable of matching the overall lateral force–displacement envelope of the experimental results for short collared columns was developed. The validated model was then used to conduct parametric studies to explore further aspects of collared column behaviour.

5.2 Finite Element Model

Three-dimensional finite element models were developed to simulate the envelope response of collared reinforced concrete short columns under combined axial and cyclic lateral loading using the commercial finite element program ABAQUS Version 6.4 (ABAQUS 2003). The ABAQUS program has two main analysis modules: Standard and Explicit. These two modules use different solution strategies for solving nonlinear quasi-static and dynamic problems: ABAQUS/Standard uses an implicit strategy with an iterative equation solver to solve a large set of equations and approach the solution through successive equilibrium cycles, while ABAQUS/Explicit uses a nonlinear explicit dynamic formulation and determines the solution by explicitly advancing the state of the model over small time increments without iteration (ABAQUS 2003).

The dynamic explicit method was originally developed to analyze high-speed dynamic events in which inertia plays a dominant role in the solution, such as short-duration blast loading. This would be extremely computationally costly to analyze using an implicit solver. Later, it was found that ABAQUS/Explicit is also very efficient for solving highly nonlinear quasi-static structural response, including structural elements that exhibit material property degradation near failure (ABAQUS 2003).

The finite element analysis in this study was initially performed with the static implicit method in ABAQUS/Standard in order to simulate the tests on collared reinforced concrete columns, which were conducted under quasi-static conditions. However, material degradation often led to severe convergence difficulties in the implicit analysis program functions such as the concrete cracking model, where tensile cracking often caused the material stiffness to become negative. Extensive concrete cracking made it difficult to trace the load-deformation envelope relationship accurately after the peak load due to these convergence problems. Other researchers have also reported convergence problems during implicit finite element modelling. For example, Cofer *et al.* (2002) reported that solution convergence could not be achieved beyond initial cracking when modelling typical reinforced concrete bridge columns. Rusinowski (2005) also identified convergence problems in using ABAQUS/Standard for two-way concrete slabs with openings because the analyses were sensitive to the discrete change of stiffness encountered at the slab opening. For this reason, ABAQUS/Explicit was adopted for use in the finite element analysis for this study.

5.2.1 Solution Strategy

ABAQUS/Explicit uses a central difference rule to integrate the equations of motion explicitly through time, using the kinematic conditions at one increment to calculate the kinematic conditions at the next increment (ABAQUS 2003). Applying the explicit dynamic procedure to quasi-static problems requires special considerations since the static solution is a long-time process, which requires an excessive number of small time increments if analyzed at its natural time scale. The event needs to be accelerated in some way to obtain a computationally efficient solution. However, the introduction of large accelerations will change the characteristics of the problem into one of dynamics, where the influence of inertial forces must be considered. If the loading speed is increased to a point where inertia plays a prominent role in the solution, the results will be quite different from the quasi-static solution. Hence, the solution strategy should include techniques to model the process in the shortest computation time period, while ensuring the influence of inertial forces on the predicted response remain insignificant.

Energy history must be studied to evaluate whether the proper simulation of quasi-static behaviour is achieved using ABAQUS/Explicit. For quasi-static behaviour, the work applied by the external forces should be nearly equal to the internal energy of the system, and kinetic energy should be maintained within a small fraction (typically 5% to 10%) (ABAQUS 2003) of its internal energy throughout most of the process, as shown schematically in Figure 5-1. The energy equation can be stated as follows:

$$E_I + E_V + E_{KE} + E_{FD} - E_W = E_{total} = CONSTANT \qquad [5\text{-}1]$$

where E_I is the internal energy (both elastic and plastic strain energy), E_V is the energy absorbed by viscous dissipation, E_{KE} is the kinetic energy, E_{FD} is the energy absorbed by frictional dissipation, E_W is the energy (work) of external forces, and E_{total} is the total energy in the system, normally taken as a constant value. Eq. 5-1 can be used to assess the suitability of the quasi-static simulation by comparing the internal energy with the work by external forces, as well as the ratio of kinetic energy to internal energy (ABAQUS 2003).

One method to simulate the quasi-static process using a dynamic explicit solution is to increase the loading rate so that the same physical event occurs in less time, as long as the solution remains nearly the same as the true static solution and the dynamic effects remain insignificant. For efficiency and accuracy, quasi-static analyses require the application of loading that is as smooth as possible, as shown in Figure 5-2. Generally, a smooth loading history will produce smooth load-deformation results, although certain loading rates and energy proportions may result in somewhat oscillatory or "noisy" results. Hence, a smooth amplitude function (termed "smooth step" in ABAQUS) was used to define the loading rate to ensure accuracy of the analysis. Mass scaling enables an analysis to be performed computationally efficiently without artificially increasing the rate of loading. However, the solution time reduction associated with the mass scaling technique is a function of the square root of the mass scaling factor, whereas the time reduction associated with the loading rate is proportional to the loading rate scaling factor (ABAQUS 2003). A loading rate of 1 mm/s and a mass scaling factor of 500 were used in the finite element analyses in this research, chosen based on the energy balance and the economy of the solution time for the whole system.

5.2.2 Geometric Modelling and Element Selection

The large footing for each column specimen was heavily reinforced to avoid local failure prior to achieving failure within the column. This failure condition was confirmed through visual observation during the experiments. The behaviour of the column itself is the main focus of the research; hence, only the column was modelled in the finite element analysis and the nodes on the bottom surface of the column are restrained against translation in all directions. The results from the analysis were later modified, as discussed in Section 5.3.2, to simulate the boundary condition of some rotation at the base that was present during the experiment.

The sensitivity of the numerical solution to element size was examined to check the mesh objectivity. Mesh sensitivity studies were conducted to find a reasonable mesh that would provide accurate results within a minimal computational time. Four different meshes were used for specimen CV1 (number of concrete elements in length×width×height of the column): 8×8×18, 10×10×18, 16×16×32, and 20×20×32. These meshes are denoted as coarser, coarse, fine, and finer meshes, respectively. The results, shown in Figure 5-3, indicate that the coarse mesh (10×10×18) can capture the overall behaviour and the peak

load with significantly less computation time than finer meshes (total analysis CPU time 47 minutes instead of 78 minutes) and, hence, the 10×10×18 mesh was adopted to model all other collared columns in this study. The mesh configuration for the finite element model is shown in Figure 5-4 for the case of specimen CV1, the typical collared reinforced concrete column in the experimental program. CV1 is also the reference column for the parametric study presented in Section 5.4.

Standard elements in ABAQUS/Explicit (Version 6.4) were used in the model. Eight-node continuum elements with reduced integration (C3D8R) were used to model the concrete. Each node has three translational degrees of freedom. Reduced integration elements were used to minimize concerns about shear locking under applied moment and to reduce analysis time, while still producing results similar to elements using full integration (ABAQUS 2003).

A comparison study was conducted to determine the suitability of different element types to represent the internal reinforcement, including truss elements (T3D2) and beam elements (B31). Truss elements can carry axial compression and tension, but cannot resist bending moment. Conversely, beam elements can carry axial compression and tension, as well as shear and bending moment. It was found that models with beam elements used to represent the reinforcement provided better agreement with the test capacities than models using truss elements, as shown in Table 5-1. Mean values for the ratio of the experimental peak lateral force in the push half-cycle to analytical peak lateral force were 1.05 and 1.13 using beam elements and truss elements, respectively. The coefficients of variation were almost the same for the two cases, with values of 0.13 and 0.12, respectively. Hence, internal reinforcement, modelled using two-node three-dimensional beam elements (B31), was included in the form of embedded discrete elements within the column. Similar practice was adopted by Saito and Higai (2001) using beam elements to model the internal reinforcement in the FEA of reinforced concrete columns under cyclic loading. Perfect bond between reinforcement and concrete was assumed. This assumption has been adopted by many researchers when modelling reinforced concrete columns, such as Chung and Ahmad (1995), Dowell and Parker (2001), Girard and Bastien (2002), and Noguchi and Uchida (2004). Darwin (1991) also pointed out that 15 of the 24 models in a survey of finite element analysis research on reinforced concrete structures assumed perfect bond between the reinforcing steel and the concrete. Beam elements representing the vertical reinforcing bars were connected directly to the nodes of the concrete elements, and to the nodes of the top plate and bottom boundary nodes. The internal ties in columns CV0A, CV0B, and CV0AR were also modelled with beam elements and the nodes were attached to the centrelines of the longitudinal bars.

Steel collars, including the connection bolts and the collar flanges (*i.e.*, the projecting end parts of the steel collar with holes through which the connection bolts pass), were also modelled with two-node, three-dimensional beam elements (B31) to account for bending under concrete expansion. The beam element nodes for the steel collars were placed at the centreline of the steel collars, as shown in Figure 5-4. No relative sliding was observed between the steel collars and the adjacent concrete during the tests, so a multi-point constraint (MPC) type BEAM was imposed between concrete nodes and

adjacent nodes on the steel collars to constrain the displacement and rotation at the first node (concrete node) to the displacement and rotation at the second node (external steel collar node). These constraints prevented relative movement between the steel collar and concrete. This technique also ensured that outward deformations of the steel collars were consistent with the lateral expansion of the concrete, even under extreme displacements.

The steel top plate was modelled with C3D8R (8-node, reduced integration) continuum elements. The two lateral loading plates were modelled as rigid bodies, each with a reference node, where the reference nodes correspond to either the lateral loading or displacement measurement position in the experiment.

5.2.3 Loading

Monotonic pushover analyses were conducted by pushing each model towards the north direction (see Figure 3-12), which corresponds to the push half-cycle direction in the experimental program. Initially, the axial compressive load, if applicable, was applied to the top steel bearing plate of the column through a uniformly distributed pressure and was kept constant during the pushover analysis. Since the pressure load is perpendicular to the bearing plate surface, as the column bends and the top surface slopes the axial compression is no longer vertical. However, the maximum inclination angle for all the columns modelled is less than 5°, hence the error in load magnitude associated with this inclination is neglected. Then, monotonic pushover loading in the "push direction" was conducted using a displacement boundary condition approach, by increasing the lateral displacement at the central node of the lateral loading plate. This displacement-controlled loading technique permitted simulation of the post-peak behaviour. The lateral displacement was targeted by setting the maximum displacement applied to the node equal to the maximum displacement level attained in the experiment. The central node was chosen as the reference node of the rigid surface of the lateral loading plate, simulating the experiment condition of evenly distributed loading over the entire loading plate. The pretension force applied to the steel collar bolts in specimen CV7 was generated in ABAQUS by applying a negative temperature change to the bolt as the initial load step of the analysis. The behaviour of the collared reinforced concrete columns is described in terms of the lateral force versus reference node displacement relationship, as well as the peak lateral force, and general observations.

5.2.4 Material Properties

The finite element models were constructed with material components of concrete, steel reinforcing bars, and steel collars. The material properties for each component were established using relevant cylinder or coupon test results from the experimental program described in Chapter 3.

5.2.4.1 Concrete

Under low confining pressures, plain concrete shows relatively brittle behaviour, with cracking in tension and crushing in compression. In ABAQUS, concrete can be modelled

with a smeared cracking model or a damaged plasticity model. The smeared cracking concrete model is based on a damaged elastic formulation and consists of the crack detecting surface and propagating a number of micro-cracks. It involves the modification of the stress and material stiffness after the occurrence of cracks (ABAQUS 2003). This model has convergence problems when extensive cracks exist (Cofer *et al.* 2002), which is the case in the current modelling of collared reinforced concrete columns.

The concrete damaged plasticity model was utilized in this research, including both concrete compression hardening and tension stiffening definitions. This model can overcome the convergence problems of the smeared crack approach and can capture the concrete behaviour and failure modes. The damaged plasticity model in ABAQUS is a continuum, plasticity-based damaged model for concrete under low confining pressures proposed by Lubliner *et al.* (1989). This model is an isotropic damage model where cracking is indirectly considered. This model uses a non-associated plastic flow rule to describe the plastic strain increments. There are five parameters that need to be defined to solve the yield and plastic flow functions: dilation angle, flow potential eccentricity indicating the rate at which the plastic flow function approaches the asymptote, ratio of initial equibiaxial compressive strength to uniaxial compressive strength, viscosity parameter, and the ratio of the second stress invariant on the tensile meridian to the second stress invariant on the compressive meridian (ABAQUS 2003). The dilation angle for concrete is defined under this model to identify the plastic strain direction relative to the gradient of the yield surface.

Dilation is the increase of volume relative to the initial state caused by deformation. The basic parameter to account for volume increase is the dilation angle. The widely accepted definition of dilation is the change in volume that is associated with shear distortion of an element in the material (Lubliner *et al.* 1989, Nielsen 1999, Park *et al.* 2001). According to this definition, the dilation angle, ψ, is found from the ratio of volumetric strain rate, $d\varepsilon_v^{\,p}$, to the shear strain rate, $d\gamma^p$, as follows:

$$\sin\psi = \left(d\varepsilon_v^{\,p}\right)/\left(d\gamma^p\right) \qquad [5\text{-}2a]$$

where the superscript p means plastic.

According to Park *et al.* (2001), a dilation angle can be defined for establishing the flow rule. If the dilation angle is equal to the internal friction angle, ϕ, that is $\psi = \phi$, then the flow rule is associative, meaning that plastic straining occurs normal to the yield surface and that there is a volumetric expansion of the material with increasing plastic strains. However, if $\psi < \phi$, the flow rule is non-associative and there will be less volumetric expansion as compared to the associated flow rule. Clearly, if ψ is zero, there will be no volumetric expansion. The internal friction angle is usually set at 36° to 45° for most structural concretes (Goodman 1989). Nielsen (1999) used a value of 37° as the internal friction angle for concrete.

Lin and Li (2003) proposed a simplified relationship between the internal friction angle and concrete compressive strength as follows:

$$\phi = 36 + 1\left(f_c^{'}/35\right) \leq 45 \qquad [5\text{-}2b]$$

where $f_c^{'}$ is the uniaxial concrete compressive strength.

With the available information, the internal friction angle of concrete was taken as about 37° for all concrete used in the current research program, which had uniaxial compressive strengths between 25 and 33 MPa. The dilation angle should be less than the internal friction angle for a non-associated flow rule, and it should decrease with an increase of confinement stress. However, there is no well-defined, widely accepted way of calculating the dilation angle. The dilation angle can be measured experimentally by measuring changes in volume as plastic deformations take place. However, this angle can be affected by the constituents of the concrete—such as size, shape or gradation of aggregates—and can vary among different concrete specimens from the same batch. In two example models described by Lubliner *et al.* (1989), the dilation angles were chosen to be 15° and 32°. In the ABAQUS Example reference (ABAQUS 2003), the damaged plasticity model was used with a dilation angle of 36.31° for the model of the Koyna concrete dam. A dilation angle of 15° was used in the analysis of composite columns under concentric loading by Begum *et al.* (2004). Since experimental determination of this parameter was not considered to be feasible, a value of 36° is used for the dilation angle in concrete with very small confinement stresses, and then a smaller value can be considered for concrete subject to the confinement provided by the external steel collars. A sensitivity study was conducted adopting three configurations of dilation angle for the concrete. The first case used a dilation angle of 36° for all concrete. Another case used a dilation angle of 15° for concrete at the steel collar elevations and 36° for all other concrete. The third case used a dilation angle of 15° for all concrete. Table 5-2 provides comparisons of peak lateral force among models with these three dilation angle configurations. It was found that the second case, with a dilation angle of 15° for concrete at the steel collar elevations along with 36° for the remaining concrete, captured the peak lateral force well and resulted in the lowest coefficient of variation in the test-to-predicted strength ratios. Therefore, this dilation angle configuration was used in the finite element analyses conducted in this research.

The concrete compression model includes both elastic and inelastic parts. The elastic limit is chosen as the stress corresponding to $0.3\,f_c^{'}$. The modulus of elasticity, E_c, was obtained from the test program, with values shown in Table 3-3. The concrete inelastic compressive stress–strain function in uniaxial compression was defined using a double exponential model (Barr and Lee 2003):

$$f(\varepsilon) = c_1\left(e^{-c_2\varepsilon} - e^{-c_3\varepsilon}\right) \qquad [5\text{-}3a]$$

where c_1, c_2, and c_3 are constants controlling the shape of the $f(\varepsilon)$ curve, with c_1 significantly influencing the peak value of $f(\varepsilon)$, c_2 significantly influencing the tail-end of $f(\varepsilon)$ and also the peak, and c_3 impacting the initial shape of the $f(\varepsilon)$ curve. These parameters are defined as follows:

$$c_1 = f_c' \Big/ \left(\eta^{\frac{1}{1-\eta}} - \eta^{\frac{\eta}{1-\eta}} \right) \qquad [5\text{-}3b]$$

$$c_2 = \ln\eta / \left[\varepsilon_{co}' (\eta - 1) \right] \qquad [5\text{-}3c]$$

$$c_3 = \eta c_2 \qquad [5\text{-}3d]$$

where f_c' and ε_{co}' are the peak concrete stress and corresponding strain obtained from concrete cylinder tests. The value of η represents the type of the response, varying from brittle to elastic-plastic. As $\eta \to 1$, this model exhibits a very deep (brittle) post-peak curve, while an elastic-plastic curve is manifested with $\eta \to \infty$. In this study, $\eta = 10$ was used, similar to the value selected by Begum *et al.* (2004) that resulted in reasonably accurate modelling results compared to test results under confined conditions.

Table 5-3 shows that the use of other compressive concrete models, such as the Todeschini curve (Todeschini *et al.* 1964) and the Barr and Lee (2003) model with $0.6 f_c'$ as the elastic limit, resulted in peak lateral force predictions similar to those obtained with the Barr and Lee (2003) model with $0.3 f_c'$ as the elastic limit. However, the Barr and Lee (2003) model with $0.3 f_c'$ as the elastic limit was reported to be suitable for predicting the post-peak descending branch of concrete cylinder test curves in compression and has been adopted previously by others, such as Begum *et al.* (2004). Hence, this model was selected for the current finite element study.

Figure 5-5 shows a typical concrete cylinder test curve and the corresponding concrete compression hardening curve used as ABAQUS input data for specimen CV1.

The tensile strength of concrete is relatively low and it is common practice to neglect it in strength calculations of structural concrete members. However, this is not always possible; *e.g.,* the shear resistance of a column without shear reinforcement depends on tensile stresses in the concrete. Also, the effect of tensile stresses in concrete should be taken into account when the overall load–displacement relationship of a member is desired, including the post-peak behaviour, as in the current case. Thus, in modelling the collared reinforced concrete columns with the finite element method, the effects of tension softening and tension stiffening become important and a realistic model should be used in the analysis.

The stiffness contribution of the concrete in tension between the cracks in reinforced concrete is called the tension stiffening effect. It is related to the crack distribution, the tensile capacity of the intact concrete between the cracks, and the interaction between the reinforcement and the concrete (Massicotte *et al.* 1988).

The tension stiffening behaviour can be described by defining a fracture energy curve, post-cracking tensile stress–strain curve, or stress–crack width curve. As shown in Figure 5-6, ABAQUS/Explicit permits three ways of specifying the tension stiffening behaviour of concrete: defining the fracture energy needed for crack formation, the stress–strain relationship with identification of the strain at which the tensile strength drops to zero, or the stress–crack width relationship. To explore the implications of this choice, all three methods are used to simulate the tests conducted in the experimental program.

Similar to the fracture energy value of 331 N/m for the concrete with $f_c^{'}$ of 40 MPa used by Li *et al.* (2002), a fracture energy of 300 N/m is used in the analysis with the tension stiffening defined through the fracture energy curve. In the definition of tension stiffening with a post-crack tensile stress-strain curve, the curve is obtained by defining two pairs of stress-strain data. One pair represents the peak tensile stress and zero strain condition, while the other represents the total strain at which the tensile stress normal to a crack will be zero. The total strain is a multiple of the strain at a crack. The actual value of strain at concrete crack for normal strength concrete is near to 0.0003. It is reasonable to assume that the stress reduces linearly to zero at a total strain of about 10 times the crack strain (ABAQUS 2003). Hence, the total strain when the tensile stress drops to zero is taken as 0.003 in the analysis. The final method is the case of defining the tension stiffening with the stress-crack width curve. According to MacGregor and Bartlett (2000), the tensile strength of concrete varies between 8 and 15% of the compressive strength, depending on the type of aggregate, the compressive strength itself, and the presence of a compressive stress transverse to the tensile stress. It may also be affected by the test method used to determine the tensile strength. In this study, the uniaxial tensile strength of concrete is assumed to be 10% of the uniaxial compressive strength for normal strength concrete. The 10% rule was also used by Begum *et al.* (2004). The interaction between the concrete and reinforcement—the so-called tension stiffening effect—is considered through modifying the crack width, and hence the post-cracking stress–displacement relationship of the concrete as follows (Li *et al.* 2002):

$$\sigma = f_t^{'}\left\{1-\exp\left[-\left(\frac{0.05}{w_c / w_{ccr}}\right)^{1.3}\right]\right\} \qquad [5\text{-}4]$$

where $f_t^{'}$ is the tensile strength of concrete, taken as $f_t^{'} = 0.1 f_c^{'}$ for normal strength concrete, w_c is the crack width, and w_{ccr} is the critical crack width when tensile strength is assumed to be zero. In this study, 1.5 mm is used for the critical crack width, identical to the value used by Begum *et al.* (2004) for normal strength concrete.

Table 5-4 provides comparisons of the peak lateral force for different tension stiffening definitions adopted in the analysis. The comparisons show that similar results are obtained when appropriate fracture energy or stress–crack width relationships are chosen, as discussed above, but poorer agreement with test results is obtained using the stress–strain relationship model. For the finite element simulations in this research, the stress–displacement curve following the stress–crack width relationship proposed by Li *et al.* (2002) (Eq. 5-4) was adopted for the analysis. This model was adopted because of its simplicity in expressing the stress-crack width relationship for reinforced concrete under uniaxial tension with a single continuous expression and the good results shown in Table 5-4.

Figure 5-7 shows the tension stiffening relationship used for concrete for the analysis of specimen CV1. Note that no direct or indirect tensile tests were completed in the experimental program.

The Poisson's ratio of concrete, ν_c, under uniaxial compressive stress varies from about 0.15 to 0.22 for normal strength concrete. Darwin (1991) pointed out that the value of Poisson's ratio plays a minor role in the accurate representation of reinforced concrete after summarizing the finite element research on both flexural-type and shear-type reinforced concrete members. Hence, in the current study, the Poisson's ratio of concrete was taken as 0.2.

5.2.4.2 Reinforcing Bars, Steel Collars, and Loading Plate

Tension coupon tests were conducted to obtain the average material properties for the steel reinforcing bars and the steel plates used to fabricate the collars. No tension coupon tests were completed for the top loading plate; as the material properties of this item have little influence on the column behaviour, the steel collar material properties were used. In all cases, the engineering stress and strain data obtained in the coupon tests were used to calculate the corresponding true stress and strain data for input into the ABAQUS material model. The steel reinforcement and the external collars were both modelled as isotropic elasto-plastic material satisfying the von Mises yield criterion.

The relationship between the true strain, ε_{true}, and engineering (nominal) strain, ε_{nom}, can be expressed as follows:

$$\varepsilon_{true} = \ln(1 + \varepsilon_{nom}) \qquad [5\text{-}5]$$

The relationship between the true stress, σ_{true}, and engineering (nominal) stress, σ_{nom}, is:

$$\sigma_{true} = \sigma_{nom}(1 + \varepsilon_{nom}) \qquad [5\text{-}6]$$

The stress versus plastic strain curve in Figure 5-8 was used as the plastic portion of the reinforcement material definition in the analysis input file. It is converted from the

material test data into the appropriate input format for ABAQUS as described above. The Poisson's ratio for steel was taken as 0.3.

5.3 Finite Element Analysis Results

Finite element analysis and experimental results were compared in terms of general observations, including crack patterns, and the peak lateral forces of the collared reinforced concrete columns. The overall shapes of the lateral force versus displacement relationships from the quasi-static pushover analysis were also examined in comparison with load–deformation envelope curves from the cyclic tests.

5.3.1 General Observations

In conducting each laboratory test, the loads were applied very slowly. To ensure that the quasi-static loading condition was also met in the numerical analyses, the energy histories of external work, internal energy, and kinetic energy were set as output items. Figure 5-9 shows the external work, internal energy, and kinetic energy curves for specimen CV1, confirming that kinetic energy was negligible compared to the internal energy and external work. The internal energy was identical to the external work during the whole process. These relationships confirm that the quasi-static loading condition requirements were met for the specimen CV1 analysis. Similar results were obtained for the other specimens modelled.

Figure 5-10(a) illustrates the deformed shape of specimen CV1 with a displacement amplification scale factor of 2.0 at the end of the analysis (still under load) and Figure 5-10(b) shows the test specimen at the end of the cyclic test (unloaded) after undergoing the same peak displacement in the final excursion. Similar deformed shapes were obtained from the analysis and test, and similar results were obtained for the other specimens modelled.

In the numerical analyses, all the specimens except specimens CV0A and CV5 reached their peak load after the yielding of longitudinal bars, the same behaviour as observed in the experiments. For all the specimens except CV0A and CV5, the mean value of the ratio of load at first yield to peak load is 78% from the experiments, with a coefficient of variation of 0.10, while in the numerical analyses, the mean and coefficient of variation are 84% and 0.12, respectively. Specimens CV0A and CV5 experienced longitudinal bar yielding immediately after the peak load in both the experiments and analyses.

The crack pattern can be found from the ABAQUS analysis results using the concrete damaged plasticity model. The maximum principal (tensile) strain vector plot is shown in Figure 5-11 for specimen CV1. The crack plane can be indirectly determined from the direction of maximum principal plastic strain since the analysis uses the assumption that cracking initiates at locations where the tensile equivalent plastic strain is greater than zero and the maximum principal plastic strain is positive (*i.e.* tensile). Furthermore, the analysis assumes that the direction of the principal plastic strain is parallel to the direction of the vector normal to the crack plane (ABAQUS 2003). Hence, through the

visualization of the maximum principal tensile plastic strain direction (arrowed line, Figure 5-11), the crack plane can be constructed normal to this arrowed line. In turn, the angle between the crack plane and the longitudinal axis of the specimen can be calculated. For specimen CV1, an angle of 36° was obtained from the finite element analysis, which is close to the value of 35° measured on the test specimen in the push direction for the major diagonal crack. Other specimens provided similar correlation of angles between analysis and test specimens.

For the control columns, especially the column with less transverse reinforcement (CV0A), the cracking and crushing of concrete extend from the bottom half to the upper part of the test regions. For collared columns, most of the damage was found to be restricted to the bottom half of the test regions. Figure 5-12 shows the vector plot of the maximum principal tensile strain for column CV0A. As indicated in ABAQUS (2003), the crack initiates at locations where the tensile equivalent plastic strain is greater than zero and the maximum principal plastic strain is positive (*i.e.* tensile). It can be seen from Figure 5-12 that quantitatively more maximum principal tensile strain vectors are present in CV0A than in CV1 (Figure 5-11) at the end of the analysis, indicating more cracks are formed in CV0A than in CV1. These analysis results are similar to the observations in the experiments.

5.3.2 Lateral Force versus Displacement Relationships

In order to present the analytically determined lateral force–displacement relationships for the specimens, an equivalent lateral force was determined. This approach was taken in an attempt to include, in a simple way, the impact on the lateral behaviour of the vertical load acting on the displaced column. The equivalent lateral force is taken as the horizontal reaction plus the additional lateral force that would generate the same contribution to base moment as the vertical load (similar to Eqs. 4-1 and 4-2). The reaction force was taken at the node where the displacement boundary condition was applied. This node is at the same position as the lateral loading position and at the same height as the deflection measurement in the experiment.

The base of the column was assumed to be fully restrained in the analysis, but since the longitudinal bars in the experiment extended into the footing, as shown in Figure 3-1, deformations of these bars introduced a discrete rotation at the column base. Measurements from strain gauges affixed to the column longitudinal bars embedded in the footing indicate unequal elongations among those longitudinal bars, implying a discrete base rotation. This rotation affects the lateral displacement at the lateral loading position. The rotation-induced displacement is found through the interpretation of the strain readings from the longitudinal bars in the experiments. Based on the data from the strain gauges installed on the longitudinal bars on specimen CV1, CV4, and CV0B, the ratio between the rotation-induced displacement and the total horizontal displacement recorded by linear variable displacement transformers (LVDTs) varies with the change of the applied displacement. For simplicity, and recognizing the approximate nature of this analysis, the ratio has been taken as a constant value of 10%, which is a simplification directly from the test results. A detailed discussion about the rotation-induced

displacement is reported in Chapter 4, Section 4.11. In order to compare with the experimental results appropriately, the displacements presented in the analysis results were modified with a 10% increase to account for the rotation-induced displacements. The displacements presented, therefore, are the total displacements obtained by adding the rotation-induced displacement to the applied displacement.

For comparison of the measured peak lateral force with the pushover analysis results, the peak lateral force in the push direction from the hysteresis curve envelope was used for consistency. Table 5-5 shows that the mean and coefficient of variation of the experimental-to-numerical peak lateral force ratio are 1.05 and 0.13, respectively, indicating that the finite element model captures the peak force with reasonable accuracy. The numerical simulations yielded accurate predictions of the peak lateral force for specimens CV0AR, CV1, CV3, CV4, and CV8 (test-to-numerical ratios from 0.99 to 1.06). However, the simulations overestimated the peak lateral forces for specimens CV0B and CV6 and underestimated them for specimens CV0A, CV2, CV5, and CV7. For specimen CV2, with the widest collar spacing, the analysis underestimated the peak lateral force significantly (by 22% of the experimental load). For specimen CV6, with no vertical load, the analysis overestimated the peak lateral force significantly (by 24%). There is no apparent trend in underestimation or overestimation with respect to specimen configuration parameters examined in this study.

The predicted lateral force–displacement curves for the control column and collared column models are shown in Figures 5-13 through 5-23. The curves are all plotted to the same scale to facilitate comparisons among them. Analyses showed good agreement with the experimental results in the ascending portion of the lateral force–displacement envelope curves for all the specimens except specimen CV0AR. Some perturbation of the analytical results towards the end of the analysis can be observed in most cases due to the extensive propagation of crack-induced damage, which led to numerical instability and poor results in the later stages of analyses. The rapid strength degradation at large displacements observed in several of the experiments was generally not captured in the finite element analyses. The curves for specimens CV3 and CV6 (especially for CV3) actually tended to increase near the end of the curves. This might be due to the originally small space between the lowest collar and the footing was reduced because of the hinge formation and large rotation at the base of CV3 at large lateral displacements, hence causing the bottom collar to have direct contact with the footing and hence contributing to the strength gain in the numerical model. The post-peak behaviour for specimen CV7 in the analysis was not as stable and ductile as that obtained in the experimental program, partly because the influence from the pretension of the bolts was not sufficiently captured in the analysis. Additional discussion of bolt pretension influence is presented in the parametric study in Section 5.4. The analysis model of specimen CV0AR, the repaired specimen CV0A, captured the peak force very well, but the initial part of the load-displacement curve was much stiffer than the one obtained from the experimental results. The stiffer behaviour in the analysis was partly due to the less stiff epoxy mortar material in the test compared to concrete, which was ignored during the analysis. The epoxy mortar, used to repair the damaged specimen, had a modulus of elasticity of 3250 MPa, only about one-sixth that of the concrete in the specimen (20 700 MPa).

Table 5-6 shows comparisons between displacement data from the experiments and from the finite element analyses (including the approximate discrete base rotation adjustment, as discussed previously) at first yield of the longitudinal bars and at the peak lateral force. First yield of longitudinal bars was determined by comparing the strain of the longitudinal bars with their yield strain for both the experiments and analyses. The mean value and coefficient of variation of the ratio of the experiment-to-analysis displacement values corresponding to first yield of longitudinal bars were 1.24 and 0.44, respectively. This indicates that the longitudinal bars yielded at larger displacement levels in the experiments than in the analyses for most columns. The strength degradation of columns CV3 and CV6 were not captured in the analysis and the longitudinal bars yielded in the analysis at significantly larger displacement levels than in the experiments. The mean value and coefficient of variation of the ratio of experiment-to-analysis displacement values at the peak lateral force were 1.34 and 0.56, respectively, also indicating that the peak force was attained in the analyses at smaller displacement levels than in the experiments. In general, somewhat stiffer lateral load–displacement responses were observed from the analyses compared to the experimental results, although the overall trends and shapes of the lateral load–displacement curves from analyses were similar to the experimental responses. Stiffer analytical predictions compared to experimental results were also reported by Cofer *et al.* (2002) in the finite element analysis of reinforced concrete columns using ABAQUS. The longitudinal bars in columns CV0A and CV5 were found to yield after reaching the peak lateral force, which is consistent with the findings from experiments, indicating shear failure.

Although there are several factors that may contribute to the higher modelled stiffness, given the constraints and testing conditions performed in the experimental program, the following seven possible fundamental causes of the discrepancies are proposed: (1) inaccuracies in the modelled material properties because of possible variation of material properties between the column specimens and the cylinders or coupons; (2) possible geometric imperfections in the specimens that were not taken into account in the numerical analyses; (3) perfect bonding was assumed between the concrete and reinforcement in the numerical simulation, while bond-slip between reinforcement and concrete may exist in the experiments; (4) differences resulting from pushover analysis in the model and cyclic loading in the tests (cyclic loads were applied to the specimens in the test with five cycles at each displacement level, while the numerical simulation used monotonic loading without consideration of the additional specimen damage incurred due to repeated cracking under load reversal); (5) simplification of the material model with the assumption of tensile strength at 10% of the compressive strength of concrete; (6) lack of consideration of shrinkage on cracking performance; and (7) simplified representation of cracking in the model.

5.4 Parametric Study

Comparisons between analytical and experimental results reported in Section 5.3 demonstrated the effectiveness of the finite element model in simulating the overall behaviour of collared reinforced concrete columns and in achieving good correlation for

the peak lateral force. In order to extend the range of application of the rehabilitation with external steel collars, and to allow development of an empirical design model for strength (presented in Chapter 6), a parametric study was conducted using the validated finite element model that focused exclusively on the peak lateral force capacity. The following parameters were the major variables studied: column geometry, external steel collar spacing, longitudinal reinforcement ratio, shear span-to-depth ratio, pretension of collar bolts, axial compression index, concrete compressive strength, and external steel collar stiffness. The longitudinal reinforcement ratio, ρ, is the total longitudinal reinforcement area, A_s, divided by the gross cross-sectional area of the column, A_g. That is, $\rho = A_s / A_g$. The shear span-to-depth ratio, herein referred to as the "aspect ratio" for simplicity, is calculated as $M/(VD)$, where M is the moment at the critical section, taken at the base of the column, V is the shear force at the critical section, and D is the overall dimension of the cross-section parallel to the shear. The axial compression index is calculated from $P/(f_c' A_g)$, where P is the axial compressive load and f_c' is the measured uniaxial compressive strength of concrete.

Two sizes of column geometry were considered in the parametric study: 400×400 mm square columns with an overall height of 800 mm and 600×600 mm square columns with an overall height of 1225 mm. Only the 400×400 columns were studied in the experimental program. The parametric study was performed with a variation of one parameter at a time, while keeping all other aspects unchanged. For the 400×400×800 mm columns, specimen CV1 was taken as the reference collared column in the parametric study for convenience, with variations of the parameters reported in the following paragraphs. Similarly, for the 600×600×1225 mm columns, the reference collared column has the following features (identical to CV1 except for the shear span): 30×50 mm external steel collar with centre-to-centre spacing of 150 mm, concrete compressive strength of 33.3 MPa, ten 25 M longitudinal bars, shear span of 1100 mm, no pretension applied to the collar connection bolts, and axial compression index of 0.3.

Variations of parameters studied are shown in Tables 5-7 and 5-8 for the 400×400×800 mm columns and 600×600×1225 mm columns, respectively. The layout of the ten longitudinal bars is similar to Figure 3-2. The set of five aspect ratios for the 400×400×800 mm columns corresponds to shear spans of 225 mm, 375 mm, 525 mm, 650 mm, and 750 mm. The set of five aspect ratios for the 600×600×1225 mm columns corresponds to the shear spans of 500 mm, 650 mm, 800 mm, 950 mm, and 1100 mm.

The smallest and largest dimensions of external steel collar, considered to define the practical range, were taken as 20 mm and 80 mm, respectively, for all columns. In the study of isolated collar stiffness, however, dimensions outside of these limits were also considered to extend the data further. Parametric analyses were also conducted on collar dimensions within this range to investigate the influence of external steel collar stiffness.

In the experimental program, the following ranges of parameters were studied: three collar centre-to-centre spacings (95 mm, 150 mm, and 200 mm); two longitudinal reinforcement ratios (1.88% and 3.13%, corresponding to ten 20 M and ten 25 M

longitudinal bars); two aspect ratio (0.875 and 1.625, corresponding to shear spans of 350 mm and 650 mm); two axial compression indices (0.0 and 0.3); two levels of bolt pretensions (10 kN for snug-tight condition and 144 kN for pretensioned bolts); and two collar sizes (30×50 mm, and 50×50 mm); as shown in Table 3-1. The concrete compressive strength ranged from 22 MPa to 33 MPa.

As shown in Figure 5-24, the peak lateral force tended to decrease with an increase in the spacing of the steel collars, as expected, but the reduction of the peak lateral force with increasing collar spacing was not as significant for the 600×600×1225 mm columns as it was for the 400×400×800 mm columns. This may be due to differences in the ratio between collar spacing and the column cross-sectional dimensions, which were smaller for the 600×600×1225 mm columns studied compared to the 400×400×800 mm columns, and hence the reduction in the confinement is less. The 600×600×1225 mm column with a collar spacing of 250 mm reached a very slightly larger peak lateral force than the column with a collar spacing of 200 mm for some reason. In the experimental study, peak lateral forces were normalized with respect to the square root of the concrete compressive strength, as discussed in Chapter 4, Section 4.6. Specimen CV3, with the narrowest spacing (centre-to-centre spacing of 95 mm), exhibited a 15% higher normalized peak lateral force (1.01) than that of the specimen CV1 (0.88), which had a moderate centre-to-centre collar spacing of 150 mm. The normalized peak lateral force of CV3 was also 12% higher than that of specimen CV2 (0.90) with the widest spacing of collars (centre-to-centre spacing of 200 mm). CV1 has a slightly smaller normalized peak lateral force than CV2, which might be due to the normalization with respect to concrete compressive strength since CV1 had a much greater concrete compressive strength than CV2. Lamanna *et al.* (2001) and Sheikh (2002) also reported that flexure capacity decreases with the increase of the shear reinforcement spacing. For reinforced concrete members with internal shear reinforcement of constant bar configuration, the shear strength decreases with the increase of the spacing of shear reinforcement (ASCE-ACI Committee 445, 1998).

From Figure 5-25, it can be determined that the peak lateral force tends to increase with an increase in the longitudinal reinforcement ratio. However, after a certain longitudinal reinforcement ratio, 3.13% for 400×400×800 mm columns and 4.17% for 600×600×1225 mm columns, the peak lateral force reduced. After checking the strain of the longitudinal bar, it was found that the longitudinal bars did not yield at the peak lateral force in 400×400×800 mm columns with a longitudinal reinforcement ratio of 3.13%, and they slightly exceeded the yield strain for 600×600×1225 mm columns with a reinforcement ratio of 4.17%. Hence, the reduction is due to the higher enhancement of the flexural capacity relative to the shear capacity with more flexural reinforcement that resulted in shear governing the failure. In the experimental study, specimen CV1, with a longitudinal reinforcement ratio of 3.13%, exhibited a 9% higher normalized peak lateral force than that of specimen CV4 with a smaller longitudinal reinforcement ratio of 1.88%, as shown in Table 4-6. It is well know that the flexural capacity increases with the increase in the longitudinal reinforcement. ACI-ASCE Committee 426 (1974) reported that shear strength of reinforced concrete members drops with the decrease of the longitudinal reinforcement. Kani (1966) also reported that the percentage of longitudinal

reinforcement has an influence, whereby the shear strength increases when the longitudinal reinforcement ratio increases.

The influence of aspect ratio on the peak lateral force is illustrated in Figure 5-26. With an increase of aspect ratio, the peak lateral force decreases. This trend was also found in the experimental study between specimens CV1 and CV5. In the experimental study, specimen CV5 with a smaller aspect ratio (0.875) exhibited a 56% higher normalized peak lateral force than specimen CV1 with a larger aspect ratio (1.625), as shown in Table 4-6. ACI-ASCE Committee 426 (1974) reported that the aspect ratio is an important parameter for the shear strength of reinforced concrete members. Kani (1966) reported the same trend that the shear strength decreases with the increase of the aspect ratio for a series of shear test.

Figure 5-27 shows that the magnitude of the pretension force applied to the steel collar bolts affects the peak lateral force to a certain degree. In the numerical model, the specimen with a pretension force of 143 kN in the collar bolts only exhibited 8% higher peak lateral force than the specimen without pretension in the collar bolts. However, the influence of this parameter in the numerical model was not as significant as the influence observed in the experiments, as shown in Figures 4-16 and 4-22. In the experimental study, specimen CV7 with a pretension force of 144 kN in the collar bolts at the start of the test exhibited 20% higher normalized peak lateral force than specimen CV1 with a pretension force of 9 kN in the collar bolts (snug-tight condition), as shown in Table 4-6 (the results in Figure 5-27 are not normalized to account for concrete material strength). This indicates that the effect of the pretension force was not sufficiently captured in the analysis. With the increase of the pretension force of the shear reinforcement, the flexural capacity should also be increased due to the increased confinement. Saatcioglu and Yalcin (2003) investigated external lateral prestressing of concrete columns and reported improved shear strength and deformability.

The effect predicted by the finite element model of the axial compression index on the peak lateral force is shown in Figure 5-28. With an increase of the axial compression index, the peak lateral force also increased, but there was a declining influence as the axial compression index increased. For the columns with the external collars of 30×50 mm, in the analysis, the specimen with an axial compression index of 0.3 exhibited 29% higher peak lateral force than the specimen with an axial compression index of 0.0, though both predicted flexural failure. In the experimental study, specimen CV1 with an axial compression index of 0.3 exhibited 31% higher normalized peak lateral force than the specimen CV6 with an axial compression index of 0.0, as shown in Table 4-6. Abrams (1987) conducted experiments and reported that with the increase of axial compression the flexural capacity of reinforced concrete columns increase. Gupta and Collins (2001) reported that shear strength increases as the compression-shear loading ratio increases after testing a series of 24 reinforced concrete members subjected to varying levels of axial compression.

Figure 5-29 shows the influence on peak lateral force for collared columns of concrete compressive strength. With an increase in the concrete compressive strength, the peak

lateral force also increased, as expected. This parameter was not explicitly studied in the experimental program as the specified concrete compressive strength was targeted as the same value for all specimens, and the variation of actual strengths was minimal. Note that although concrete compressive strengths up to 80 MPa have been used in the analyses, the CSA-A23.3-04 design standard only permits the use of concrete strengths up to 64 MPa for determining the shear strength contribution of concrete (*i.e.* $\sqrt{f_c'} \leq 8$ MPa). It is well known that the flexure capacity increases with the increase of concrete compressive strength. ACI-ASCE Committee 426 (1974) reported that contribution from concrete to the shear strength of reinforced concrete member increases with the increase of concrete compressive strength.

The influence of the collar stiffness (both axial stiffness and flexural stiffness) on the peak lateral force was studied through the modelling of a series of collar sizes, as shown in Figure 5-30. The axial stiffness relates to the cross-sectional area of the collar A_{sc}, while the flexural stiffness relates to the moment of inertia of the collar I_{sc}. With an increase of the collar dimension parallel to the column longitudinal axis (hence, an increase of collar stiffness), the peak lateral force increased, with declining influence as the collar stiffness increased. This phenomenon can also be seen in Figures 5-28 and 5-29. For the same axial compression index or concrete compressive strength, the peak lateral force increased when the collar size increased from 20×20 mm to 80×80 mm, but the enhancement of peak lateral force from 70×70 mm to 80×80 mm was smaller than the enhancement from 20×20 mm to 30×50 mm. The specimens CV1 and CV8 in the experimental program also validated this parametric study observation of the effect of the collar stiffness. Specimen CV8 with 50×50 mm collars attained 5% higher normalized peak lateral force than the specimen CV1 with 30×50 mm collars. Hussain and Driver (2005b) also reported that flexural capacity increases with the increase of axial and/or flexural stiffness of the steel collar.

Finite element analysis was also conducted to study the isolated effects of the collar axial stiffness and flexural stiffness on the peak lateral force of the collared column. The collar cross-section was selected to facilitate changes in axial stiffness while keeping moment of inertia constant and vice versa. In some cases, collar dimensions beyond the range that might be considered as the practical dimensions (20—80 mm) were used to establish the trend. Also through finite element parametric study, it suggests that the ratio between the bigger dimension of the collar cross-section and the smaller dimension should be less than 3 to ensure effectiveness and efficiency of the collar as well as the practicality of construction. The effect of the collar axial stiffness was studied for four sets of moment of inertia: 112500, 225000, 520833, and 1250000 mm^4. The effect of the collar flexural stiffness was studied for seven sets of cross-sectional area: 300, 400, 500, 800, 1000, 2000, and 3000 mm^2. For the same cross-sectional area, the moments of inertia were selected such that each successive data point was generated using a moment of inertia that was four times the previous one. Both the 400×400×800 mm columns and 600×600×1225 mm columns were modelled. Figure 5-31 shows the peak lateral force versus the cross-sectional area of collar. It is clear from this figure that with an increase of collar cross-sectional area, the peak lateral forces increases. Moreover, there exists an

axial stiffness beyond which the peak lateral force is not enhanced for the 400×400×800 mm columns, an observation made also by Hussain and Driver (2001). The trend also exists for the 600×600×1225 mm columns, but could be at a much higher collar axial stiffness than for 400×400×800 mm columns, since the confining effect for the same collar cross-section will be different for each column cross-section. Figure 5-32 shows the peak lateral force versus the collar moment of inertia. It can be seen that with the increase of moment of inertia, the peak lateral forces increase, but at a small rate and even decreases for small collar cross-sectional area. Comparing Figures 5-31 and 5-32 indicates that the collar cross-sectional area and, hence, axial stiffness has a greater influence on the peak lateral force of the collared column than the moment of inertia and, hence, the flexural stiffness.

Among the columns in the parametric study, most columns experienced longitudinal bar yielding before reaching the peak lateral force. A few exceptions were columns with small size of external steel collar: 400×400×800 columns with external steel collar of 20×20 and concrete compressive strength of 20 MPa and 30 MPa, axial compression index of 0.0, 0.1, and 0.2; and columns with external steel collar of 20×30, 20×40 30×20, 30×30, 40×20. Other exceptions were columns with external steel collars of 30×50, but with smaller shear spans of 225 mm, 350 mm, and 525 mm, or collar spacings of 250 mm and 300 mm, or with longitudinal reinforcement ratio of 3.13%. The strains of steel collars at the peak lateral force of those columns that experiencing longitudinal bar yielding after the peak lateral force are in the range of 200 to 800 microstrain. There are many factors that might affect the external steel collar strain at the peak lateral force, including the concrete compressive strength, column aspect ratio, axial compression index, longitudinal reinforcement ratio, and flexural capacity. At this stage of research, it is not possible to develop a general model to predict collar strain for a given set of applied loads and member geometry.

5.5 Summary

Laboratory experiments have been shown to be very useful in understanding the behaviour of collared reinforced concrete columns. However, it is costly and time consuming to perform experiments with multiple variations of geometry and loading conditions in practice. Hence, it is desired to develop reliable and efficient analytical methods to predict the behaviour. In this chapter, three-dimensional nonlinear finite element models were described that simulate the response of collared reinforced concrete columns under cyclic loading using the commercial finite element program ABAQUS/Explicit. The finite element models were validated against the experimental results. The finite element models were also used to study the influence of various design parameters on collared reinforced concrete columns through a parametric study.

Comparisons were made between the pushover finite element model developed using ABAQUS/Explicit and the experimental results. Although the analytical models generally overestimated the column lateral stiffness in the initial part of the test and did not fully capture the post-peak range, they predicted the peak lateral force of collared reinforced concrete columns under combined axial and lateral loading with reasonable

accuracy. For the columns studied in the experimental program, the mean experiment-to-analysis capacity ratio was 1.05, with a coefficient of variation of 0.13.

Parametric studies were conducted with emphasis placed on the capacity predicted by the finite element model. The studies showed that with an increase of external steel collar spacing, the peak lateral force typically decreased. With increases of the axial compression index, the longitudinal reinforcement ratio, or the concrete compressive strength, the peak lateral force increased. Increasing the aspect ratio resulted in a decrease in the peak lateral force. A pretension force applied to the steel collar bolts did increase the peak lateral force of the collared reinforced concrete column; however, the extent of the increase observed in the tests was not fully reflected in the analytical results. With an increase of the collar axial and flexural stiffness, the peak lateral force increased, but the enhancement drops and the peak lateral force reaches a limit after certain value. The axial stiffness of the external collars appears to be a more important parameter for increasing the strength of collared columns than the flexural stiffness.

Table 5-1 Peak lateral force using beam elements (B31) or truss elements (T3D2) for the reinforcement

Specimen	$V_{max,exp,push}$ (kN)	Beam element B31		Truss element T3D2	
		$V_{max,fea}$ (kN)	$V_{max,exp,push}/V_{max,fea}$	$V_{max,fea}$ (kN)	$V_{max,exp,push}/V_{max,fea}$
CV0A	599	526	1.14	506	1.18
CV0AR	700	693	1.01	597	1.17
CV0B	675	754	0.90	646	1.05
CV1	791	768	1.03	757	1.04
CV2	701	544	1.29	523	1.34
CV3	746	701	1.06	673	1.11
CV4	689	700	0.99	711	0.97
CV5	1161	1027	1.13	922	1.26
CV6	555	689	0.81	612	0.91
CV7	889	769	1.16	708	1.26
CV8	731	708	1.03	664	1.10
	Mean		**1.05**		**1.13**
	C. O. V.		**0.13**		**0.12**

Table 5-2 Peak lateral force for different concrete dilation angle models

Specimen	$V_{max,exp,push}$ (kN)	36°		36°/15°*		15°	
		$V_{max,fea}$ (kN)	$V_{max,exp,push}/V_{max,fea}$	$V_{max,fea}$ (kN)	$V_{max,exp,push}/V_{max,fea}$	$V_{max,fea}$ (kN)	$V_{max,exp,push}/V_{max,fea}$
CV0A	599	526	1.14	526	1.14	461	1.30
CV0AR	700	885	0.79	693	1.01	640	1.09
CV0B	675	754	0.90	754	0.90	543	1.24
CV1	791	967	0.82	768	1.03	684	1.16
CV2	701	699	1.00	544	1.29	492	1.42
CV3	746	941	0.79	701	1.06	751	0.99
CV4	689	803	0.86	700	0.99	684	1.01
CV5	1161	1242	0.93	1027	1.13	775	1.50
CV6	555	812	0.68	689	0.81	612	0.91
CV7	889	924	0.96	769	1.16	667	1.33
CV8	731	907	0.81	708	1.03	654	1.12
	Mean		**0.88**		**1.05**		**1.19**
	C. O. V.		**0.14**		**0.13**		**0.16**

* Dilation angle of 15° for concrete at the external steel collar elevation along with 36° for concrete outside of the external steel collar elevation.

Table 5-3 Peak lateral force for different concrete compression hardening models

Specimen	$V_{max,exp,push}$ (kN)	Todeschini curve		Barr and Lee model with $0.3f_c'$ as elatic limit		Barr and Lee model with $0.6f_c'$ as elatic limit	
		$V_{max,fea}$ (kN)	$V_{max,exp,push}/V_{max,fea}$	$V_{max,fea}$ (kN)	$V_{max,exp,push}/V_{max,fea}$	$V_{max,fea}$ (kN)	$V_{max,exp,push}/V_{max,fea}$
CV0A	599	517	1.16	526	1.14	532	1.13
CV0AR	700	680	1.03	693	1.01	724	0.97
CV0B	675	730	0.92	754	0.90	752	0.90
CV1	791	728	1.09	768	1.03	761	1.04
CV2	701	528	1.33	544	1.29	553	1.27
CV3	746	768	0.97	701	1.06	781	0.96
CV4	689	674	1.02	700	0.99	682	1.01
CV5	1161	903	1.29	1027	1.13	1017	1.14
CV6	555	679	0.82	689	0.81	686	0.81
CV7	889	694	1.28	769	1.16	741	1.20
CV8	731	675	1.08	708	1.03	724	1.01
	Mean		**1.09**		**1.05**		**1.04**
	C. O. V.		**0.15**		**0.13**		**0.13**

Table 5-4 Peak lateral force for different concrete tension stiffening models

Specimen	$V_{max,exp,push}$ (kN)	Fracture energy model		Stress–strain model		Li *et al.* model stress-crack width	
		$V_{max,fea}$ (kN)	$V_{max,exp,push}/V_{max,fea}$	$V_{max,fea}$ (kN)	$V_{max,exp,push}/V_{max,fea}$	$V_{max,fea}$ (kN)	$V_{max,exp,push}/V_{max,fea}$
CV0A	599	518	1.15	495	1.21	526	1.14
CV0AR	700	691	1.01	650	1.08	693	1.01
CV0B	675	746	0.90	730	0.92	754	0.90
CV1	791	705	1.12	706	1.12	768	1.03
CV2	701	558	1.25	437	1.60	544	1.29
CV3	746	763	0.98	738	1.01	701	1.06
CV4	689	678	1.02	664	1.04	700	0.99
CV5	1161	1020	1.14	1002	1.16	1027	1.13
CV6	555	674	0.82	668	0.83	689	0.81
CV7	889	714	1.24	674	1.32	769	1.16
CV8	731	705	1.04	680	1.08	708	1.03
	Mean		**1.06**		**1.12**		**1.05**
	C. O. V.		**0.13**		**0.18**		**0.13**

Table 5-5 Peak lateral force between experiment and analysis

Specimen	f_c' (MPa)	$V_{max,exp,push}$ (kN)	$V_{max,fea}$ (kN)	$V_{max,exp,push}/V_{max,fea}$
CV0A	26.3	599	526	1.14
CV0AR	26.6	700	693	1.01
CV0B	26.9	675	754	0.90
CV1	33.3	791	768	1.03
CV2	25.5	701	544	1.29
CV3	22.0	746	701	1.06
CV4	30.8	689	700	0.99
CV5	29.5	1161	1027	1.13
CV6	31.5	555	689	0.81
CV7	29.1	889	769	1.16
CV8	27.4	731	708	1.03
Mean				**1.05**
C. O. V.				**0.13**

Table 5-6 Displacement at first yield of longitudinal bars and at peak lateral force

Specimen	Displacement at first yield of longitudinal bars (mm)			Displacement at peak lateral force (mm)		
	Experiment	Analysis	Experiment /Analysis	Experiment	Analysis	Experiment /Analysis
CV0A	8.15	4.02	2.03	9.19	4.42	2.08
CV0AR	10.67	7.71	1.38	35.24	55.77	0.63
CV0B	6.65	3.94	1.69	22.78	16.42	1.39
CV1	4.31	4.22	1.02	17.78	10.26	1.73
CV2	6.34	5.66	1.12	23.03	8.65	2.66
CV3	7.07	15.23	0.46	42.26	71.43	0.59
CV4	5.86	3.73	1.57	29.60	50.98	0.58
CV5	3.63	4.74	0.77	4.68	6.34	0.74
CV6	4.81	11.80	0.41	42.18	74.74	0.56
CV7	5.84	4.46	1.31	20.15	11.15	1.81
CV8	7.58	4.07	1.86	31.69	15.70	2.02
Mean			**1.24**			**1.34**
C. O. V.			**0.44**			**0.56**

Table 5-7 Parameter variations for 400×400×800 mm columns

Parameters	**Values considered**
Collar centre-to-centre spacing, mm	100, 150, 200, 250, 300
Longitudinal reinforcement ratio, Bars, ρ	Ten 10M-0.63%, Ten 15M-1.25%, Ten 20M-1.88%, Ten 25M-3.13%, Ten 30M-4.38%
Aspect ratio, M/(VD)	0.5625, 0.9375, 1.3125, 1.625, 1.875
Pretension force in collar bolt, kN	0, 41, 83, 122, 143
Axial compression index, $P/(f_c'A_g)$	0.0, 0.1, 0.2, 0.3, 0.4, 0.5, 0.6, 0.7
Concrete Compressive strength, MPa	20, 30, 40, 50, 60, 70, 80
Collar dimension, mm	20, 30, 40, 50, 60, 70, 80

Table 5-8 Parameter variations for 600×600×1225 mm columns

Parameters	**Values considered**
Collar centre-to-centre spacing, mm	100, 150, 200, 250, 300
Longitudinal reinforcement ratio, Bars, ρ	Ten 15M-0.56%, Ten 25M-1.39%, Ten 30M-1.94%, Ten 35M-2.78%, Ten 45M-4.17%
Aspect ratio, M/(VD)	0.8333, 1.0833, 1.3333, 1.5833, 1.8333
Pretension force in collar bolt, kN	0, 41, 83, 122, 143
Axial compression index, $P/(f_c'A_g)$	0.0, 0.1, 0.2, 0.3, 0.4, 0.5, 0.6, 0.7
Concrete Compressive strength, MPa	20, 30, 40, 50, 60, 70, 80
Collar dimension, mm	20, 30, 40, 50, 60, 70, 80

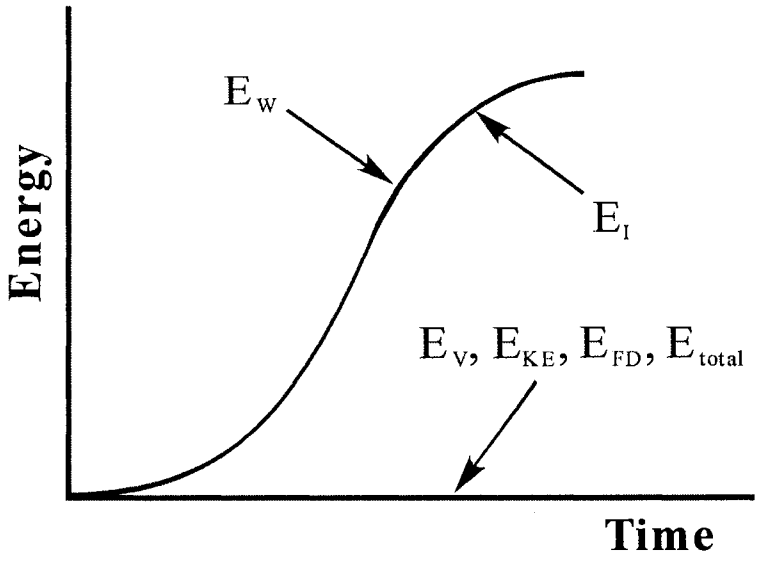

Figure 5-1 Energy history for quasi-static simulation

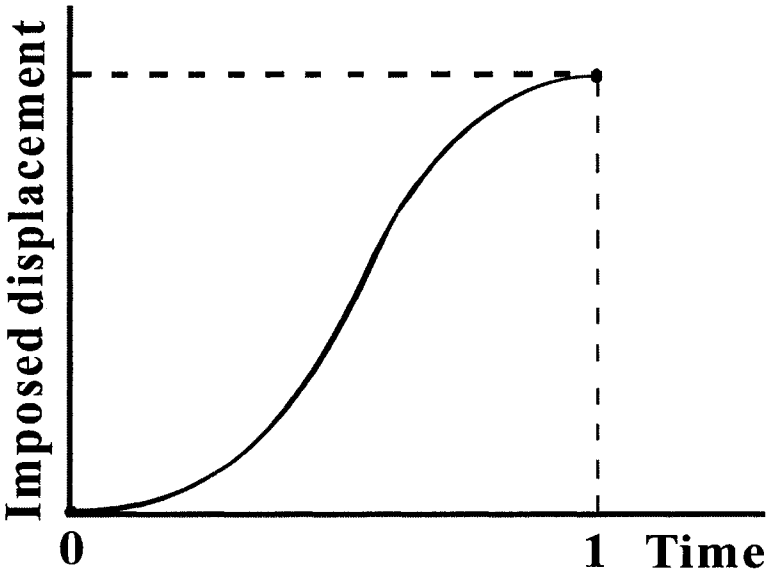

Figure 5-2 Amplitude of displacement controlled loading using smooth step definition

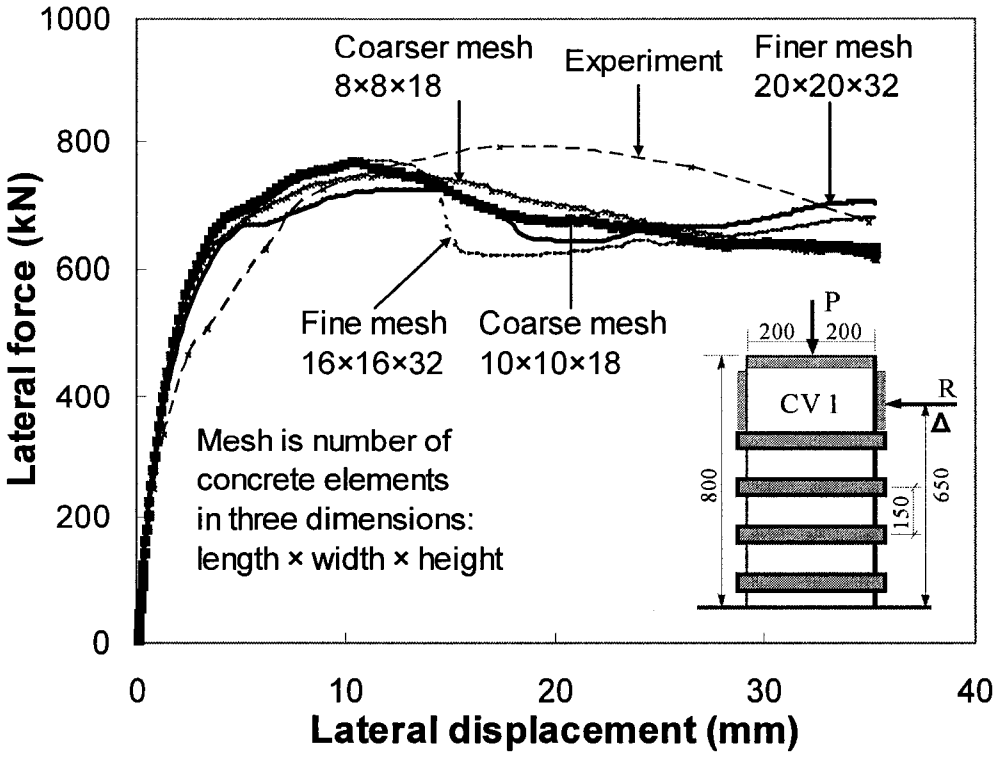

Figure 5-3 Mesh sensitivity study comparison

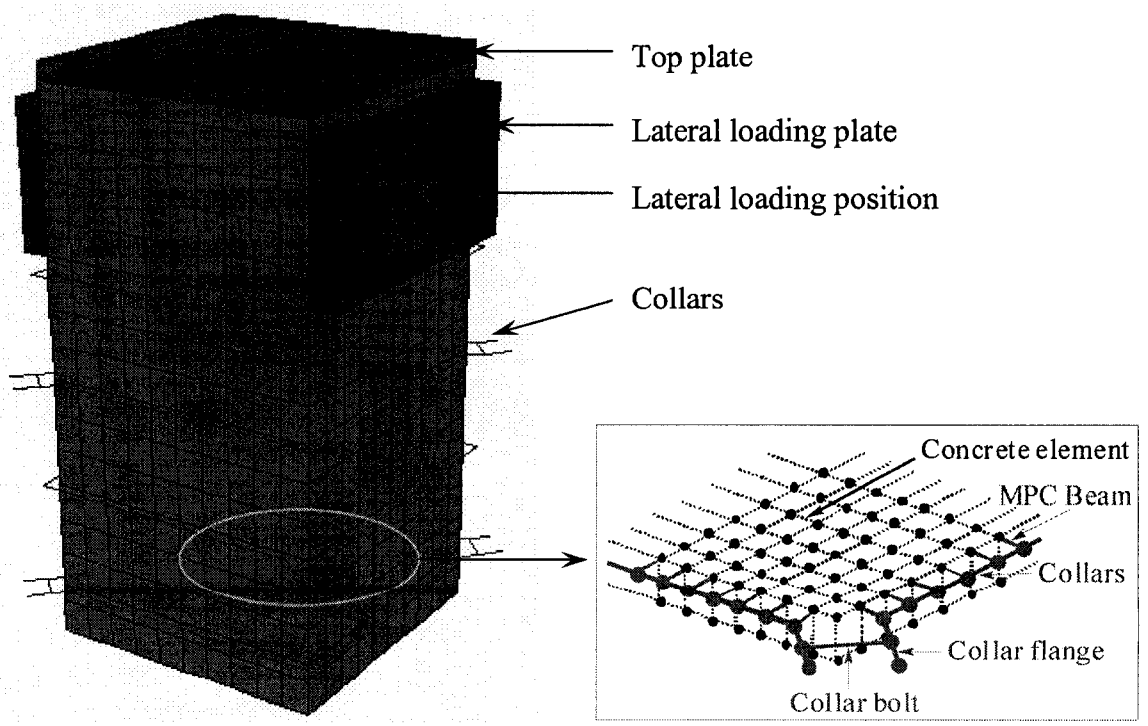

Figure 5-4 Finite element model mesh (1/4 cross-section inset)

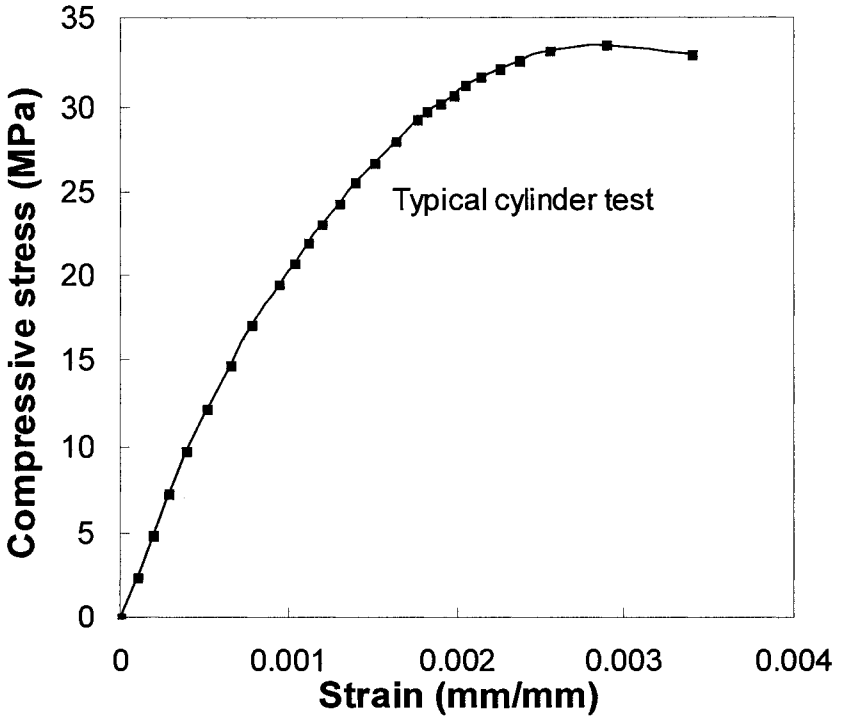

(a)

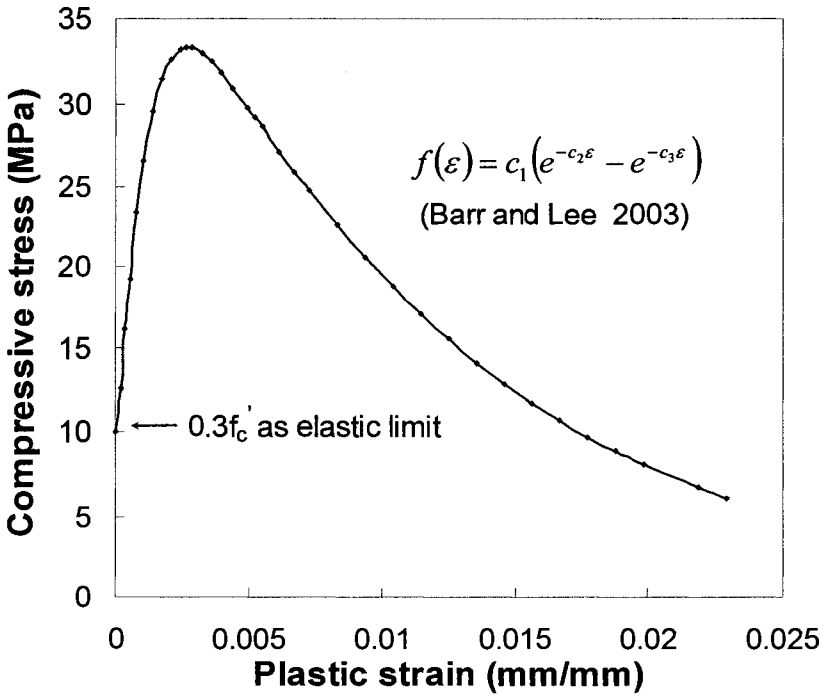

(b)

Figure 5-5 Specimen CV1 (a) typical concrete cylinder test curve, and (b) concrete compression hardening model used in ABAQUS

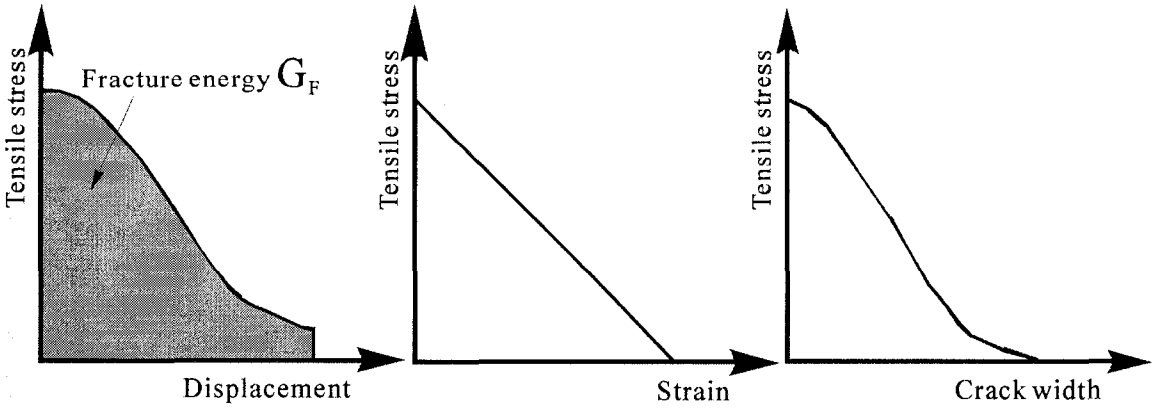

Figure 5-6 Concrete tension stiffening definitions available in ABAQUS

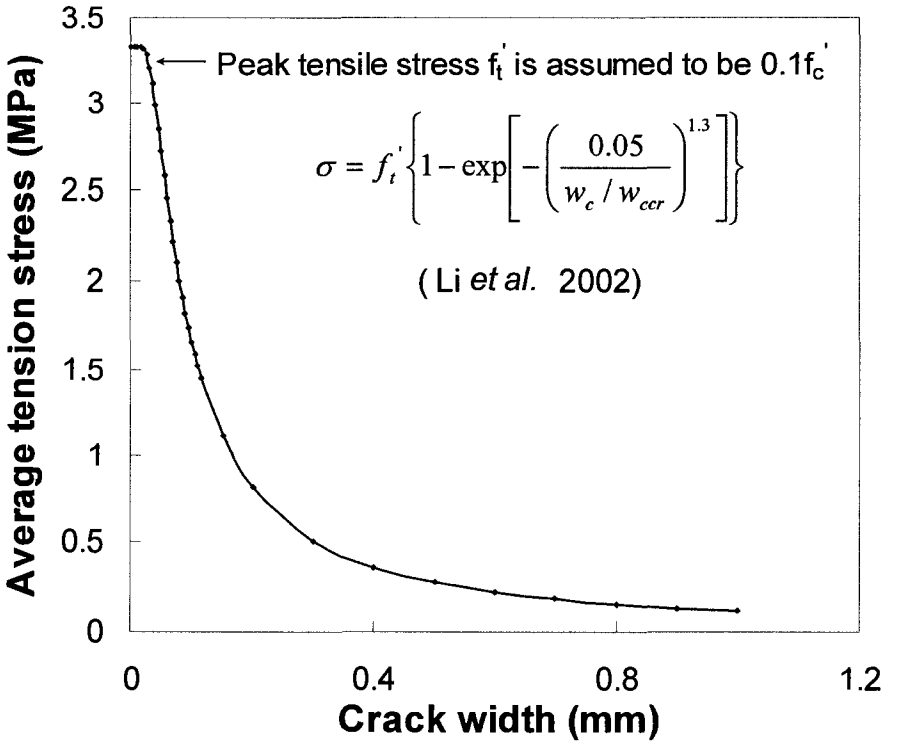

Figure 5-7 Concrete tension stiffening model used in ABAQUS for specimen CV1

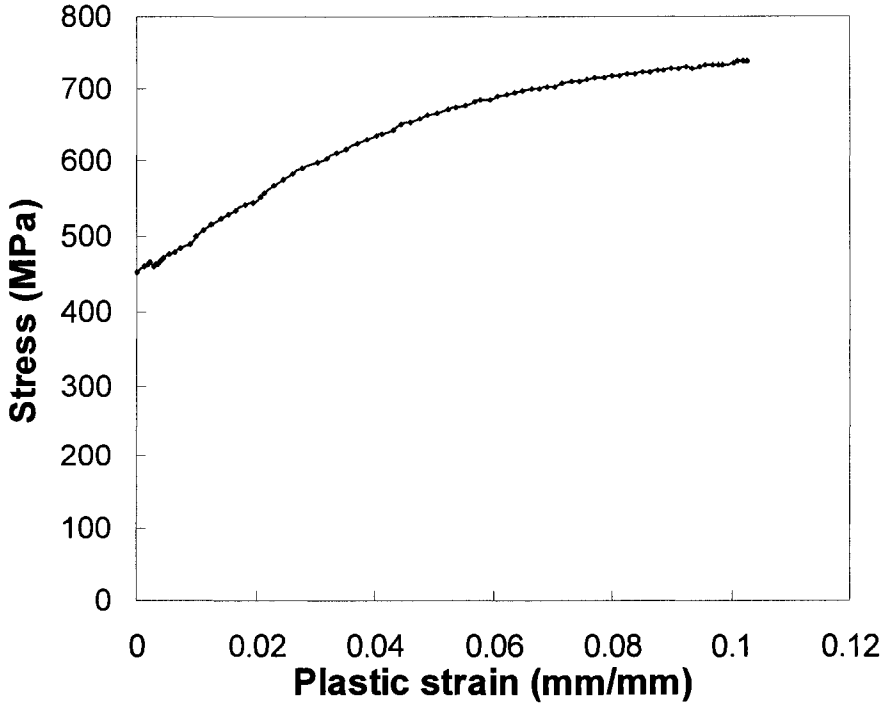

Figure 5-8 Stress–plastic strain relationship for longitudinal bars used in ABAQUS for specimen CV1

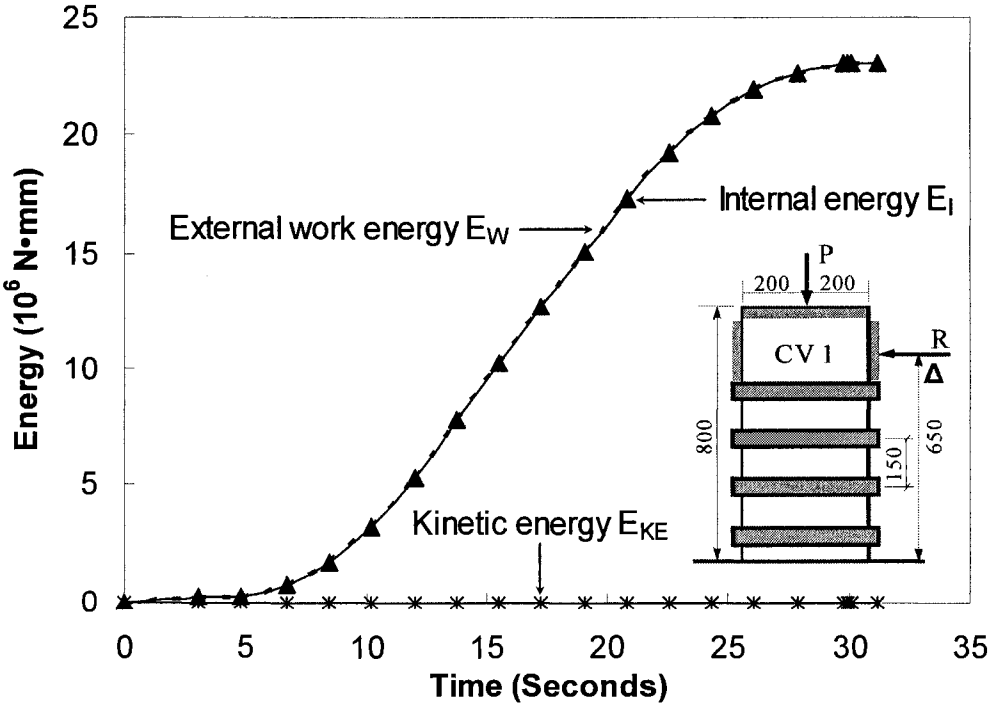

Figure 5-9 Energy curves from ABAQUS analysis of specimen CV1

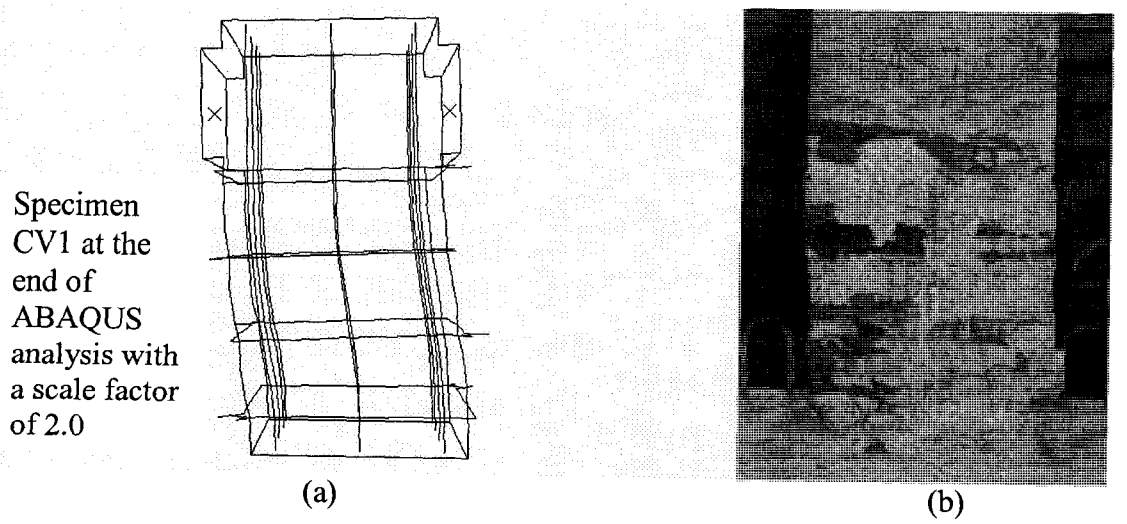

Figure 5-10 Deformed shape of specimen CV1 from (a) analysis and (b) experiment

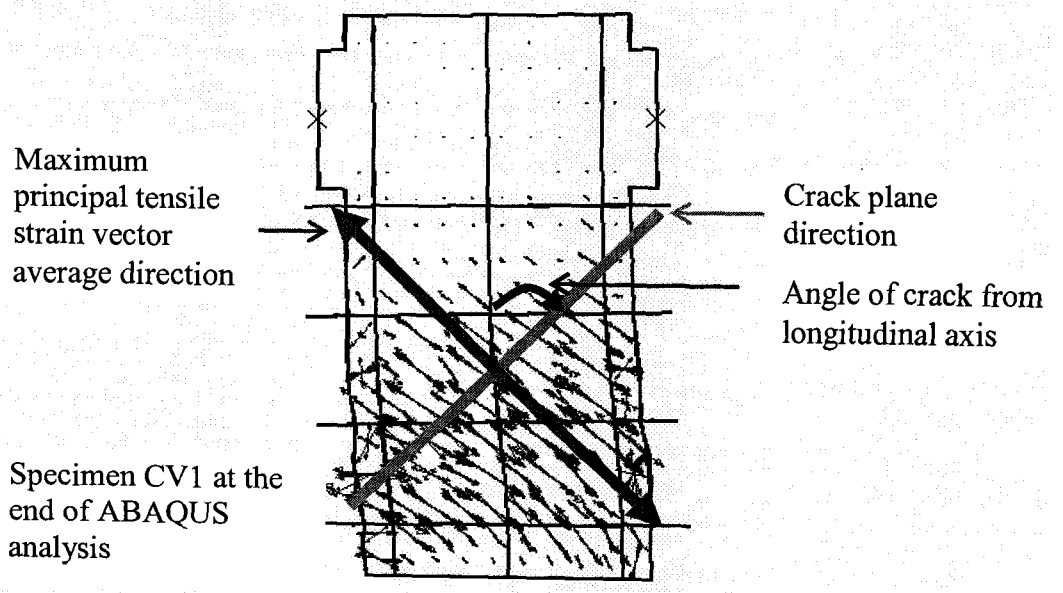

Figure 5-11 Vector plot of maximum principal tensile strain and crack plane direction for specimen CV1

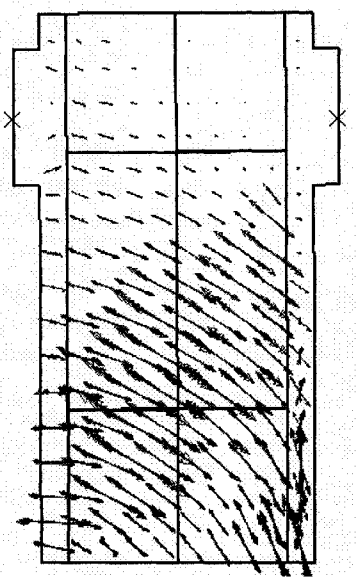

Figure 5-12 Vector plot of maximum principal tensile strain for specimen CV0A

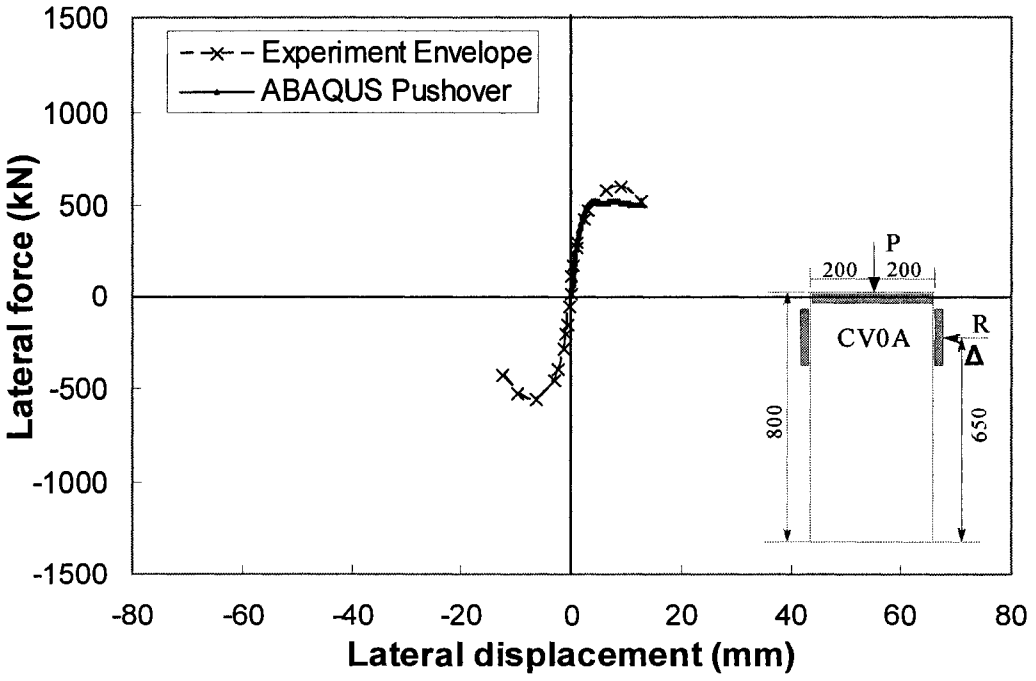

Figure 5-13 Lateral force–displacement curves from analysis and experiment for specimen CV0A

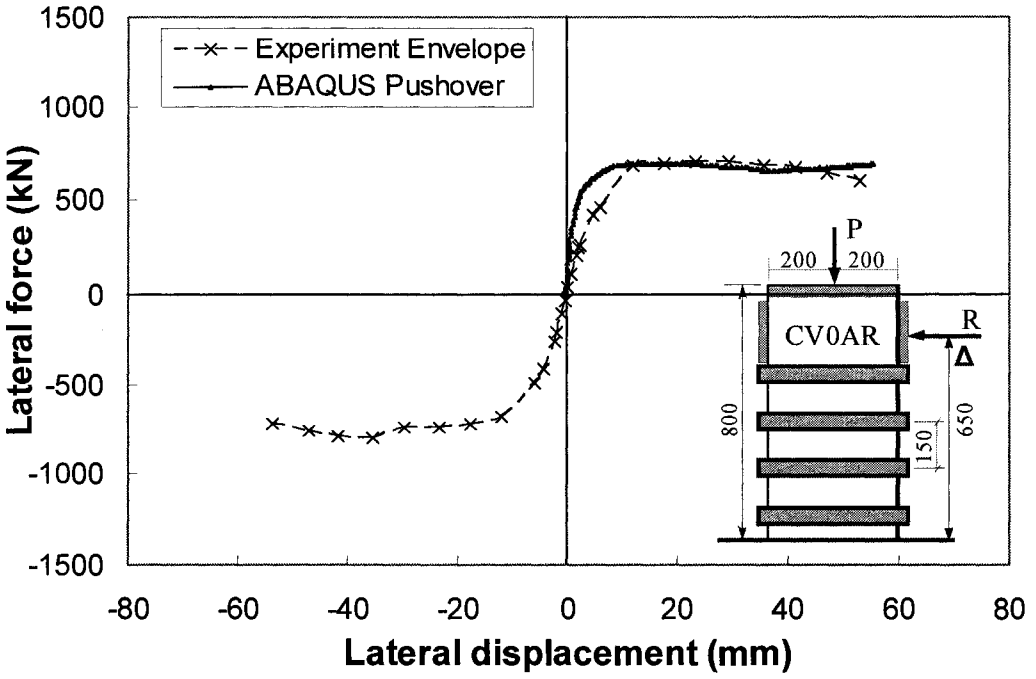

Figure 5-14 Lateral force–displacement curves from analysis and experiment for specimen CV0AR

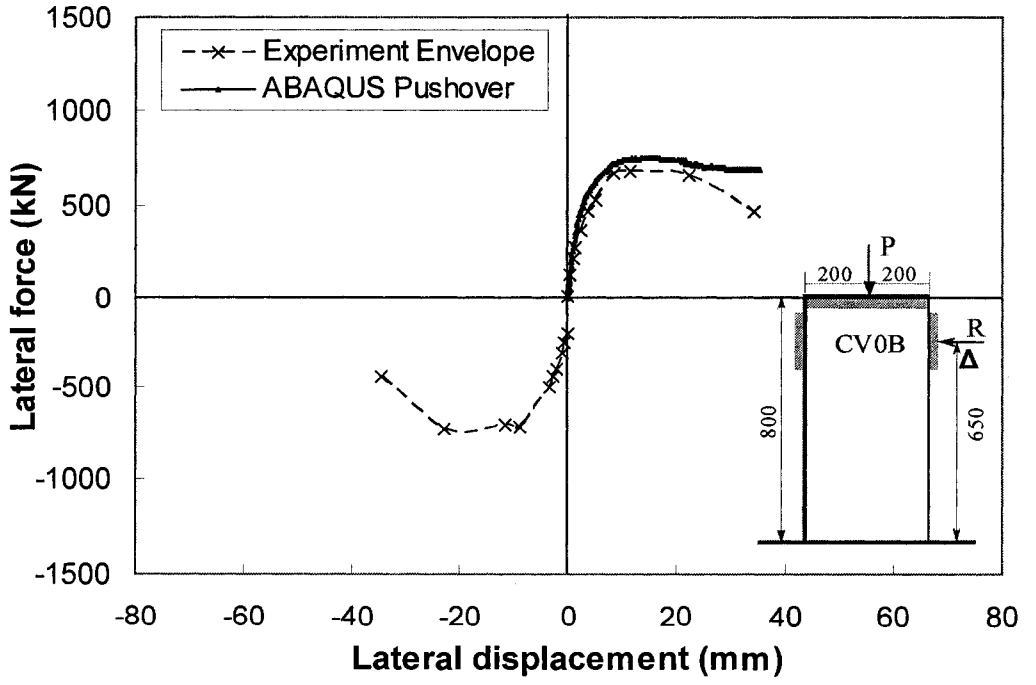

Figure 5-15 Lateral force–displacement curves from experiment and analysis for specimen CV0B

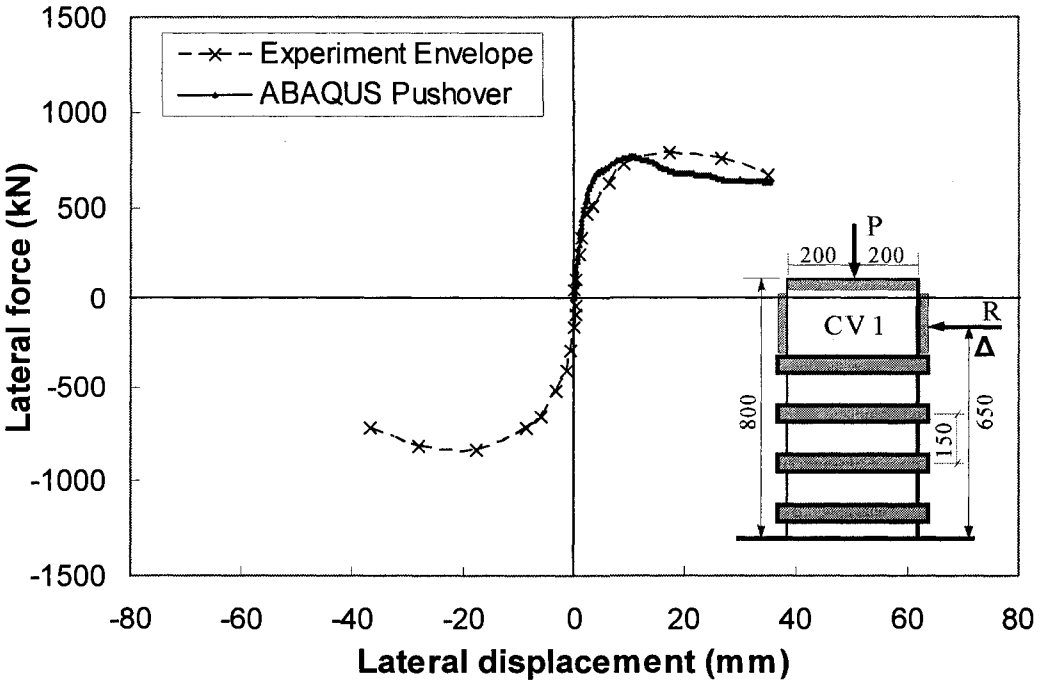

Figure 5-16 Lateral force–displacement curves from experiment and analysis for specimen CV1

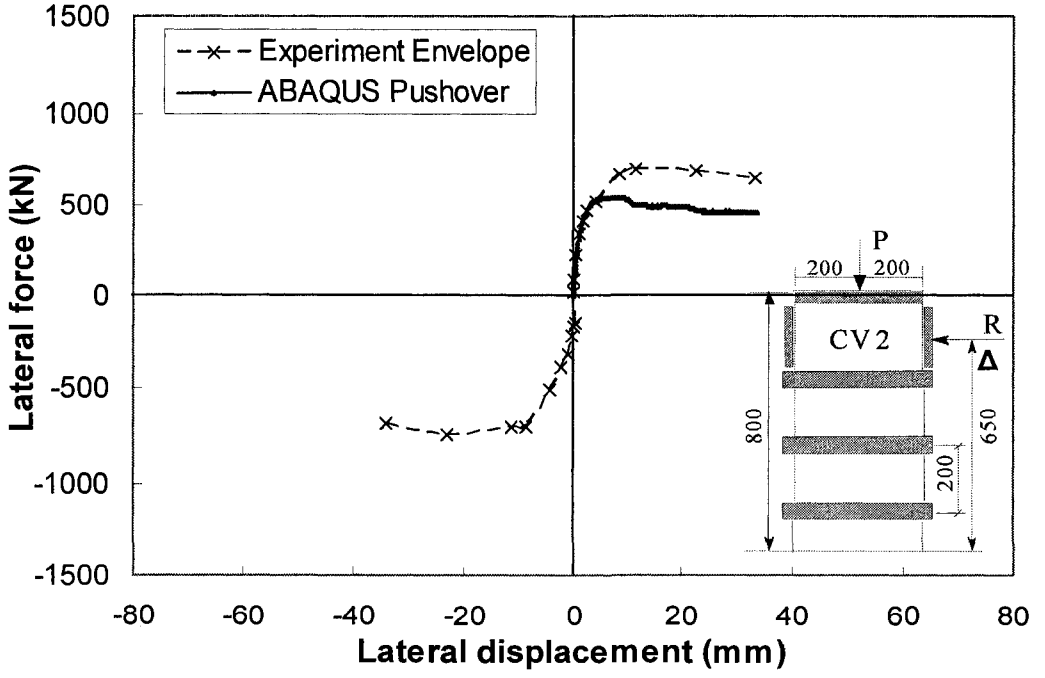

Figure 5-17 Lateral force–displacement curves from experiment and analysis for specimen CV2

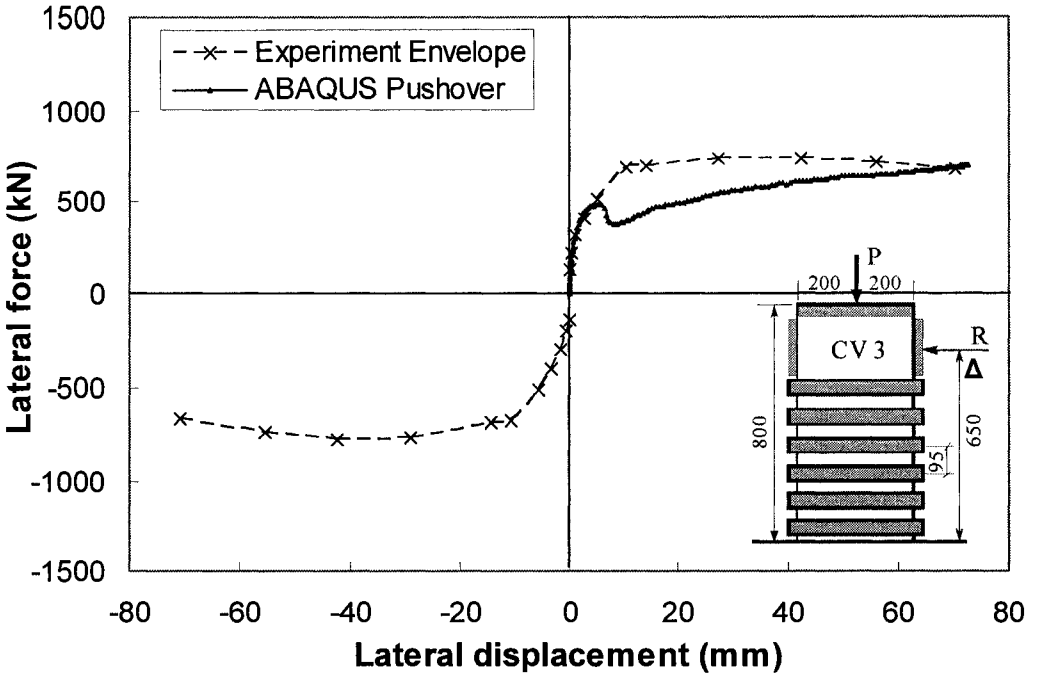

Figure 5-18 Lateral force–displacement curves from experiment and analysis for specimen CV3

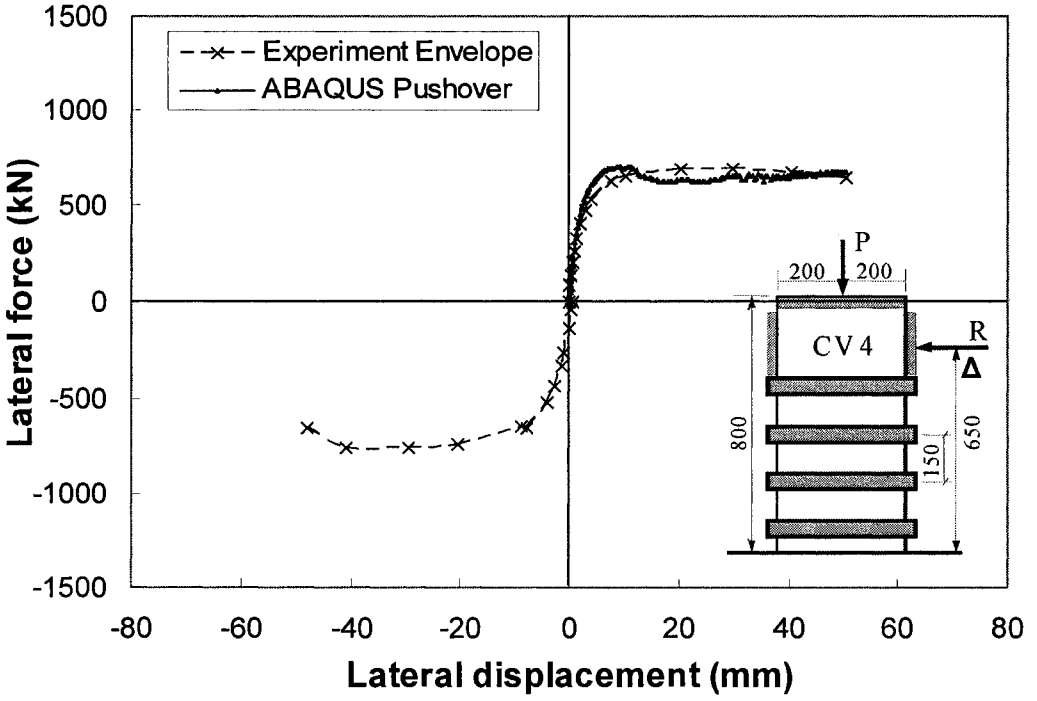

Figure 5-19 Lateral force–displacement curves from experiment and analysis for specimen CV4

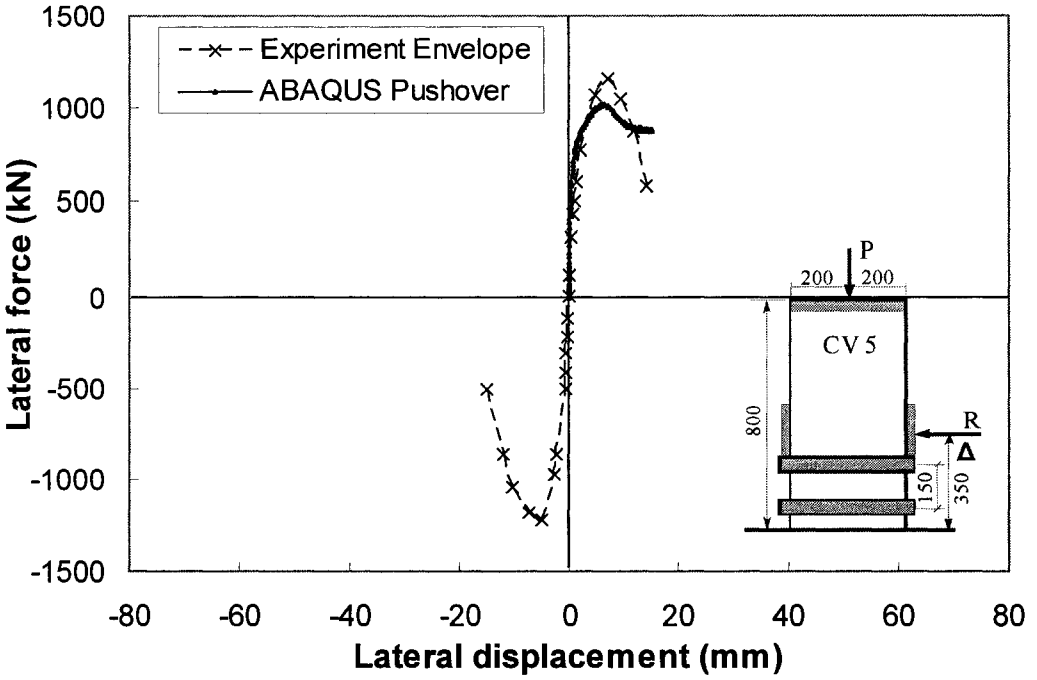

Figure 5-20 Lateral force–displacement curves from experiment and analysis for specimen CV5

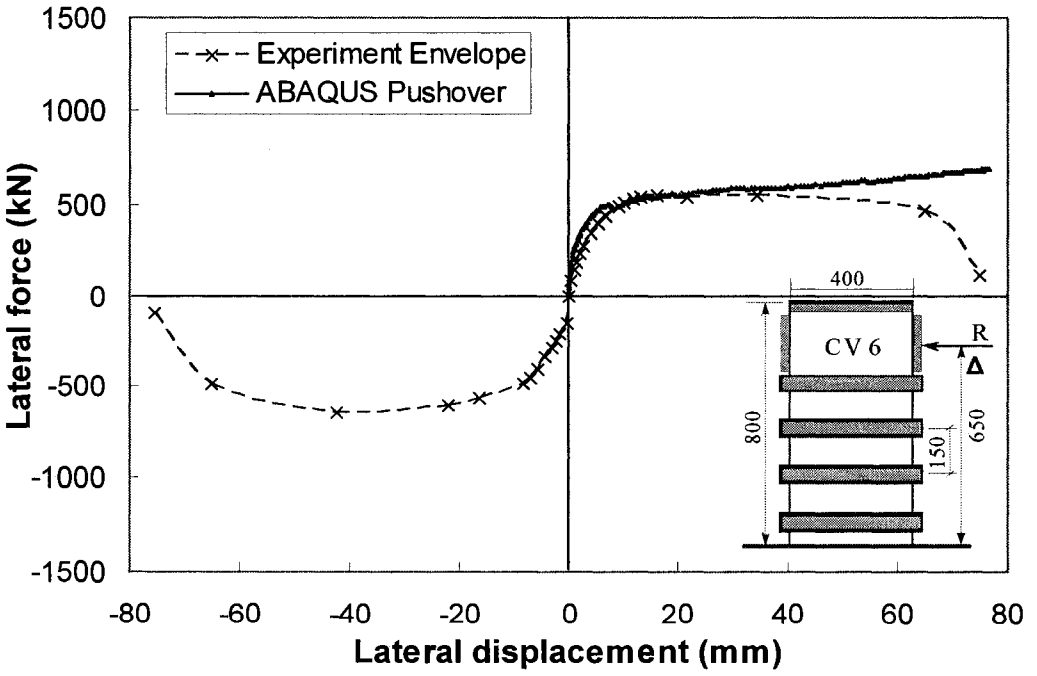

Figure 5-21 Lateral force–displacement curves from experiment and analysis for specimen CV6

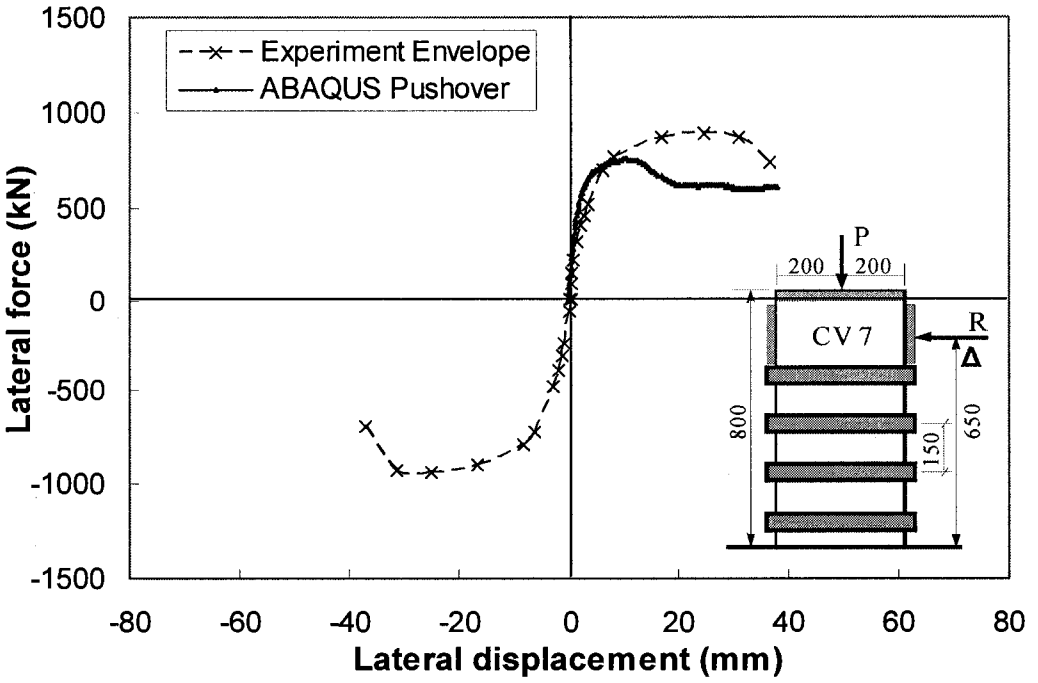

Figure 5-22 Lateral force–displacement curves from experiment and analysis for specimen CV7

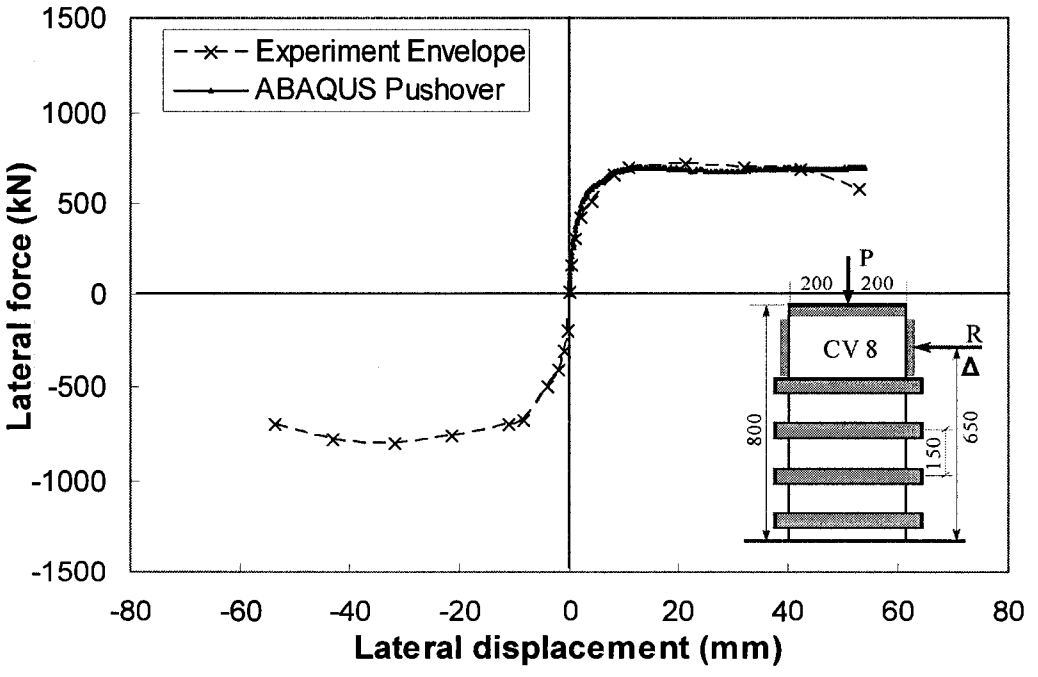

Figure 5-23 Lateral force–displacement curves from experiment and analysis for specimen CV8

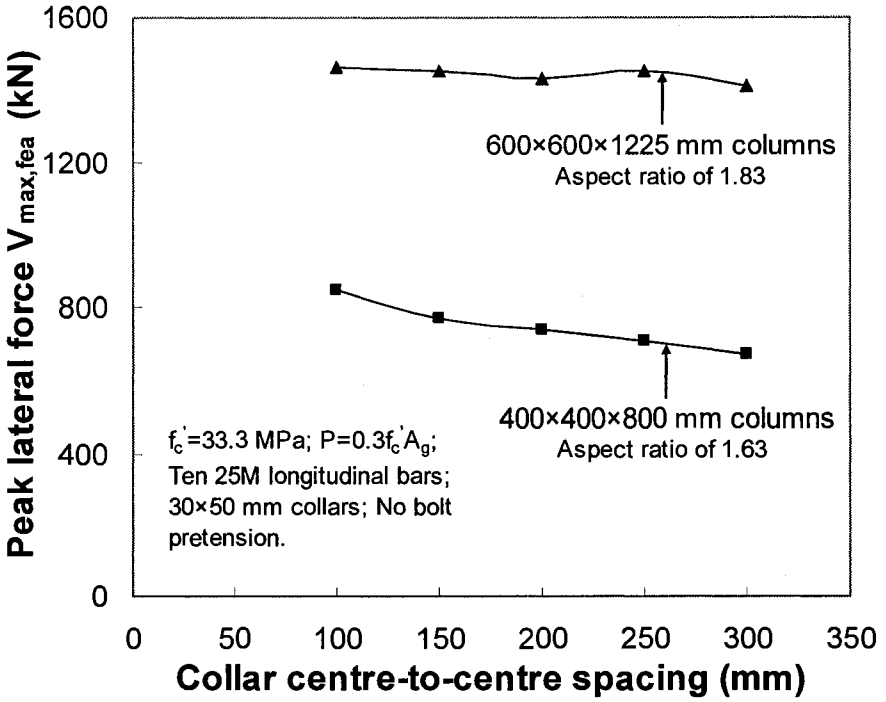

Figure 5-24 Parametric study—different external collar spacings

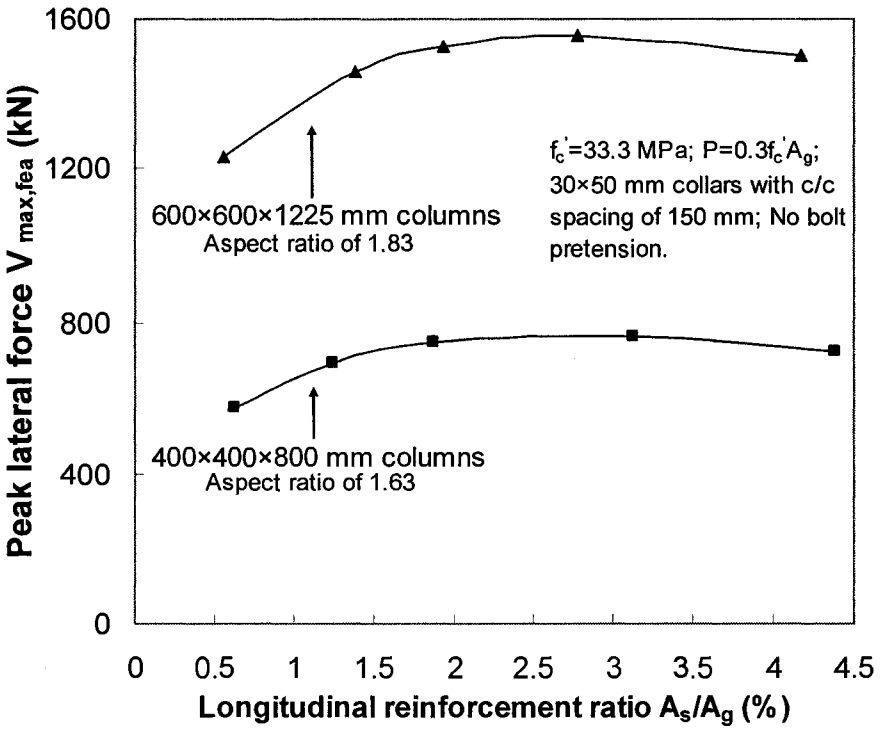

Figure 5-25 Parametric study—different longitudinal reinforcement ratios

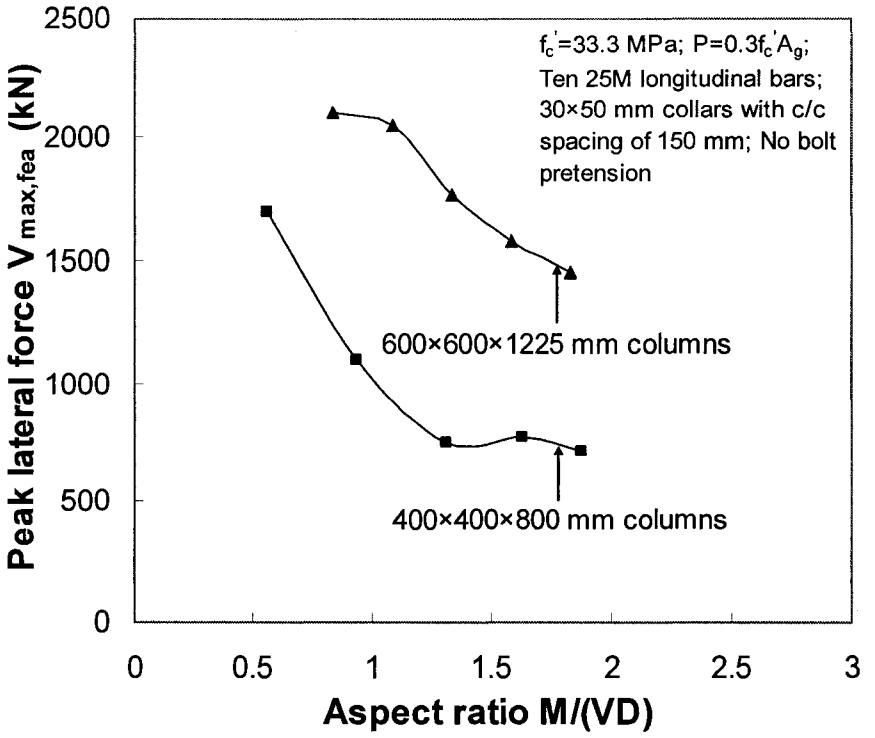

Figure 5-26 Parametric study—different aspect ratios

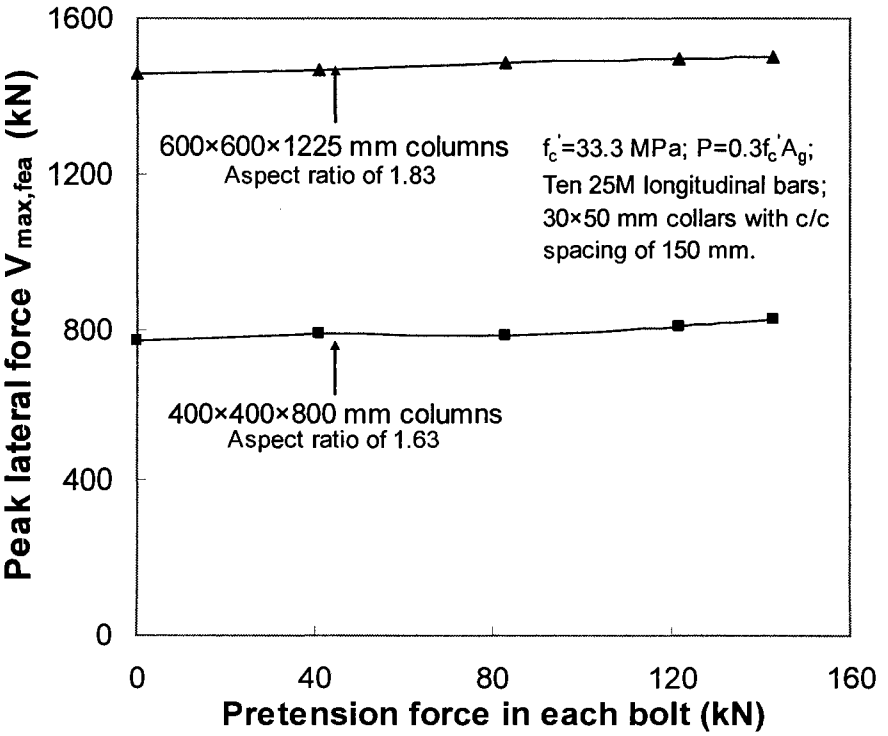

Figure 5-27 Parametric study—different pretension forces applied to collar bolts

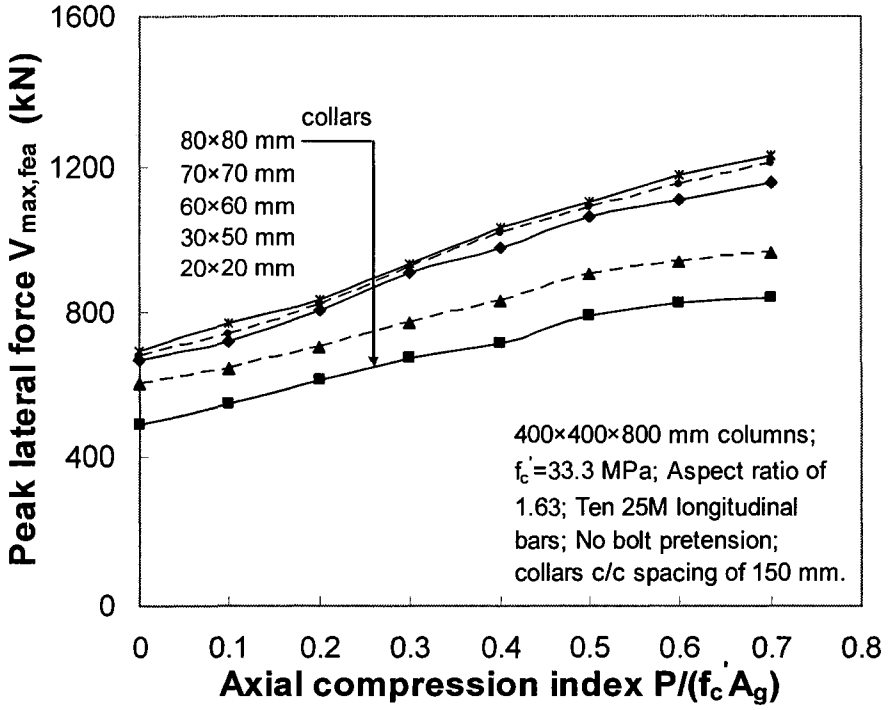

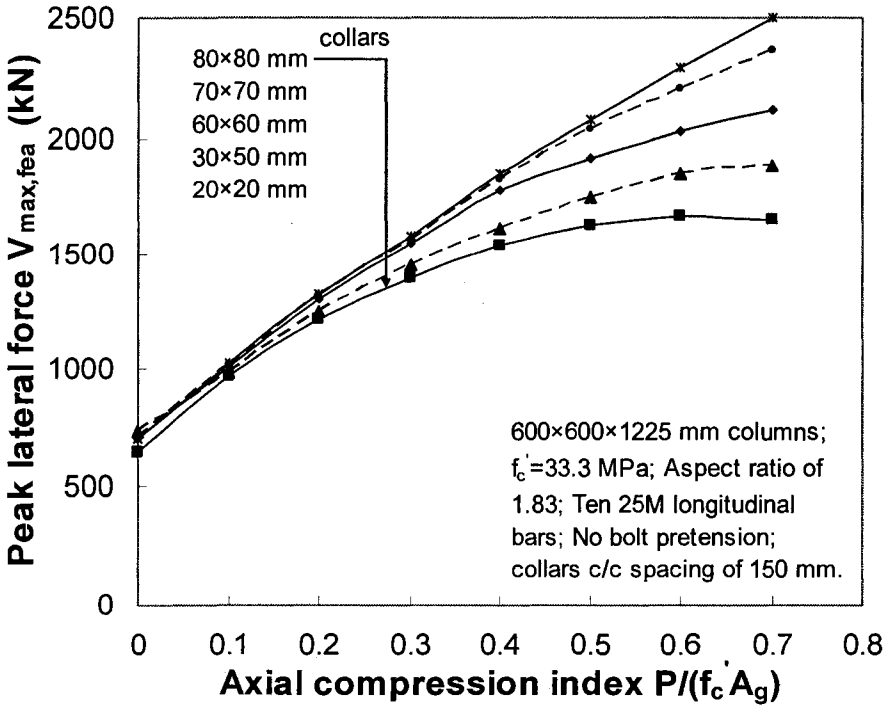

Figure 5-28 Parametric study—different axial compression indices

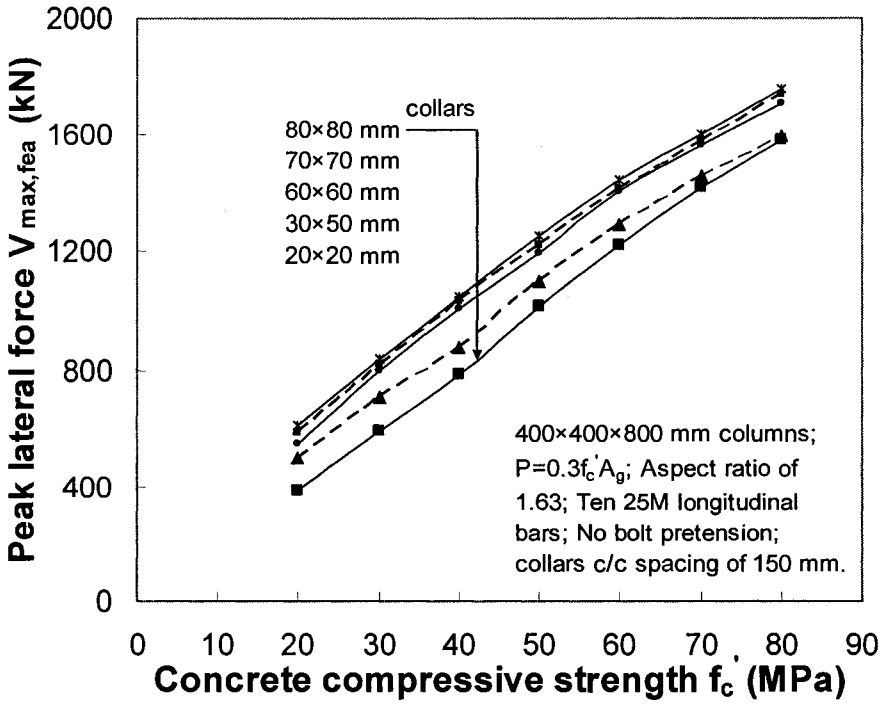

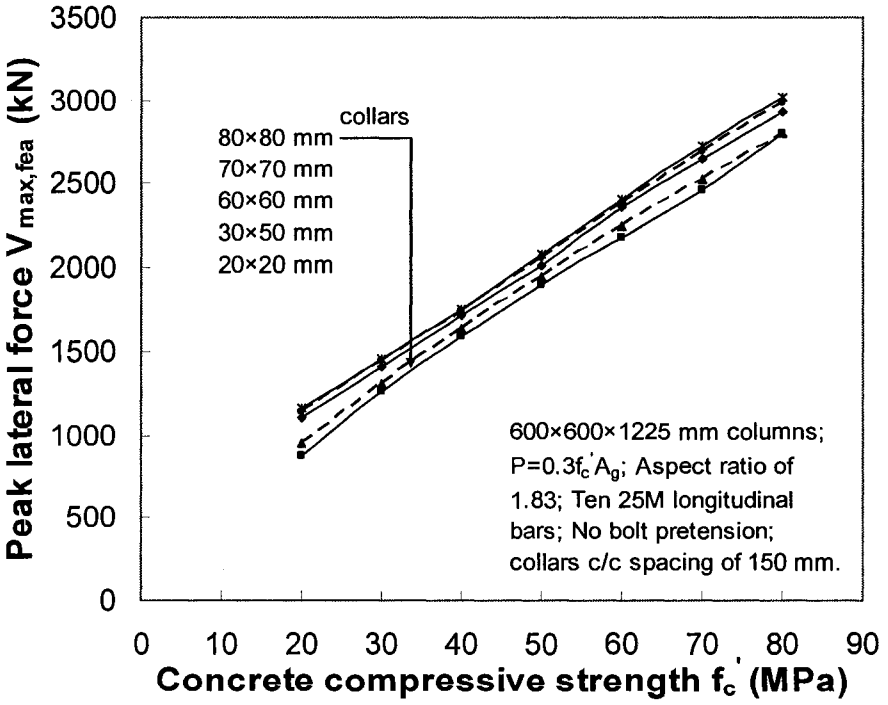

Figure 5-29 Parametric study—different concrete compressive strengths

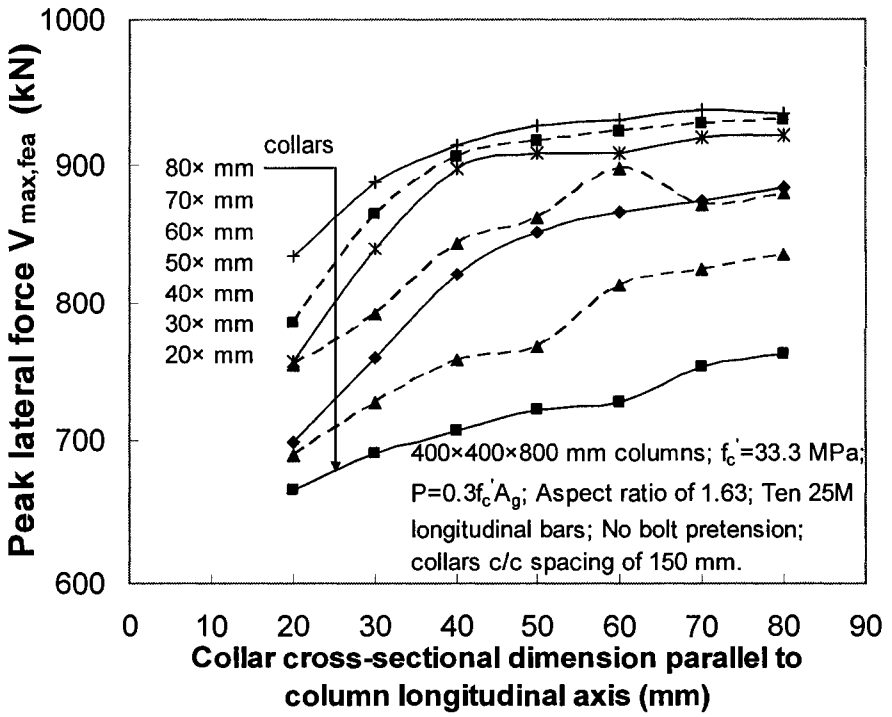

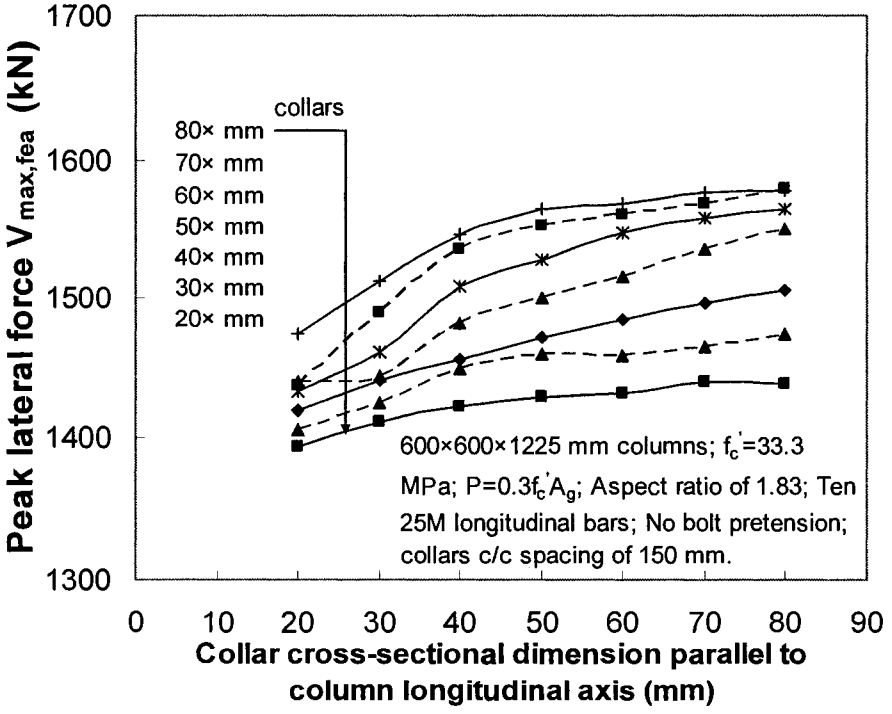

Figure 5-30 Parametric study—different collar sizes

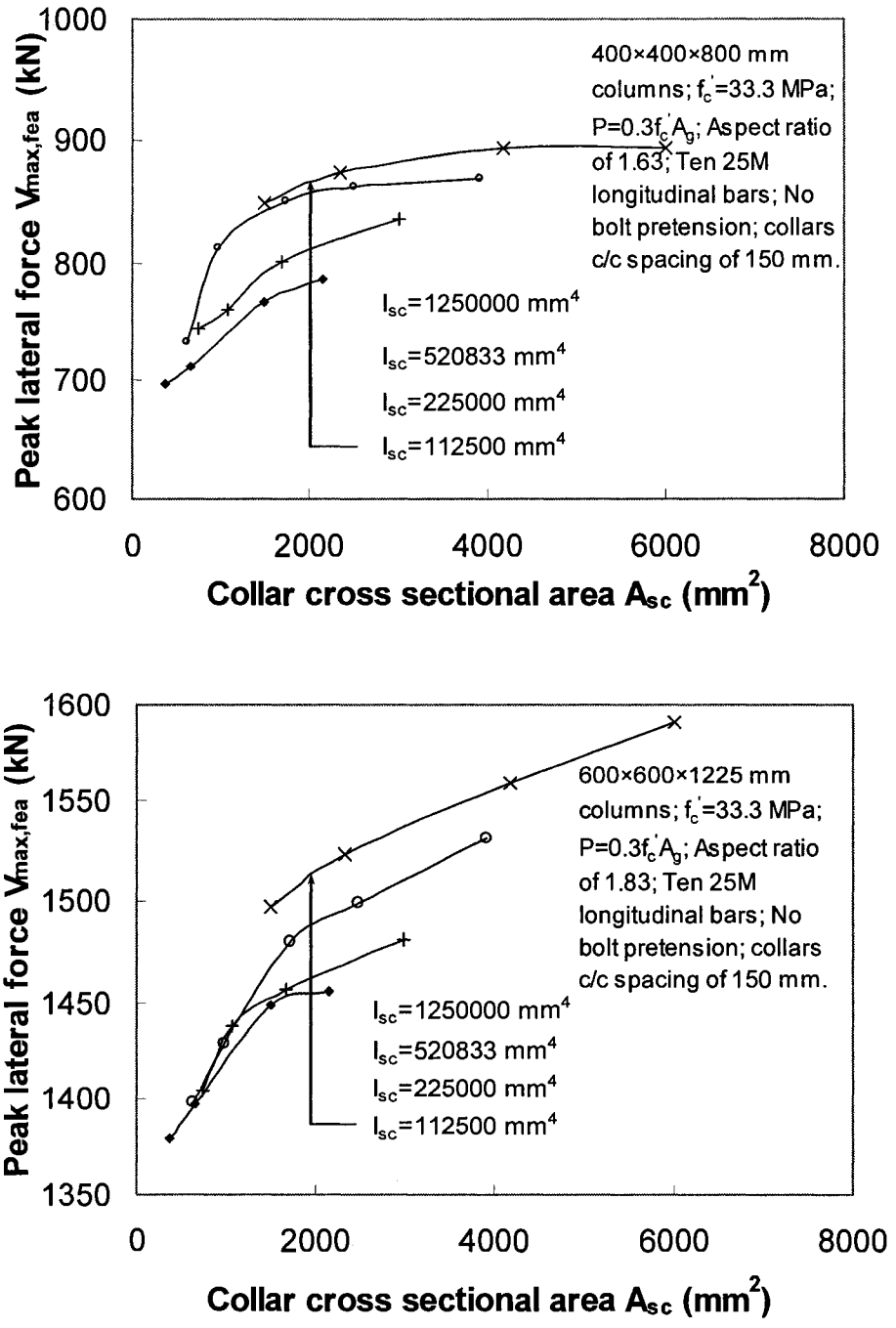

Figure 5-31 Parametric study— isolated effect of collar axial stiffness

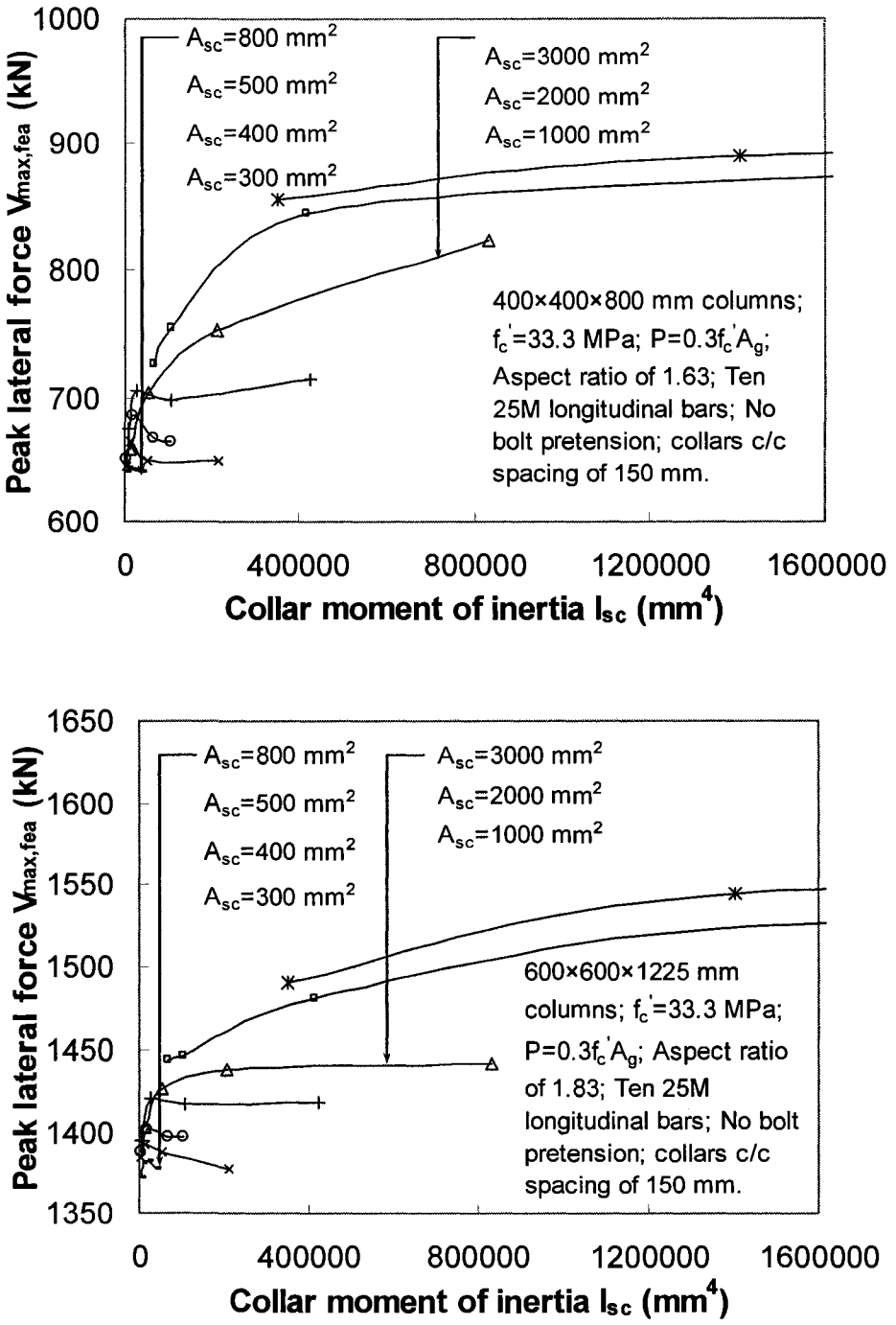

Figure 5-32 Parametric study— isolated effect of collar flexural stiffness

CHAPTER 6 ANALYTICAL APPROACHES

6.1 Introduction

In this chapter, the abilities of various simple analytical tools to predict the peak lateral force capacity of collared reinforced concrete short columns are investigated. Existing analytical tools utilized include the CSA-A23.3-04 and ACI 318-05 design codes with both sectional shear and flexure models, the software Response 2000, and the strut-and-tie modelling technique for full-member response. An improved sectional shear and flexural model is proposed and calibrated against the experimental and finite element analysis results presented in Chapters 4 and 5. Comparisons are focused exclusively on the peak lateral force capacity.

6.2 Published Sectional Analysis Models

Available published sectional analysis models, including the flexure and shear model, are more appropriate for concrete members with aspect ratios greater than about 2.5. It has long been recognized that the average shear stress at failure for members with aspect ratios smaller than 2.5 is larger than in slender members with large aspect ratios (ASCE-ACI Committee 445, 1998). When sectional analysis models, instead of strut-and-tie models, are applied to columns with aspect ratios smaller than 2.5, they usually result in an underestimation of the member shear strength (MacGregor and Bartlett 2000, Kani 1979). However, strength degradation under cyclic loading encountered in the experiment is not considered in the sectional analysis model, which may partially offset the shear strength underestimation from the analysis. Hence, sectional analysis models are applied to predict the peak lateral force for the collared columns in the experimental program.

6.2.1 CSA-A23.3-04 and ACI 318-05 Code Equations

The sectional shear models from CSA-A23.3-04 and ACI 318-05 were utilized to predict the shear strength of the collared reinforced concrete columns. The "General Method" in CSA-A23.3-04 and the detailed method in ACI 318-05 were used, and those models were described in Chapter 2, Section 2.6. For CSA-A23.3-04, an iterative solution approach was adopted to obtain the nominal shear strength. For both the CSA and ACI cases, the external steel collars of the collared columns were treated similar to traditional internal shear reinforcement, by utilizing the cross-sectional area of the steel collar, A_{sc}, and the yield strength of the steel collar, f_{ysc}, in place of A_v and f_y in Eqs. 2-9c and 2-11a. Using the yield stress for the collars, however, seems inappropriate since the collars did not actually yield by the time the peak lateral force was reached in the tests, a discrepancy that is addressed in Section 6.4. For the repaired collared column, CV0AR, shear contributions from both the internal shear reinforcement and the external steel collar were calculated separately and then were combined by direct summation.

Sectional analyses were also conducted to obtain the peak lateral forces corresponding to the flexural capacity of the columns. The sectional analysis was based on measured

material properties and an assumed concrete compressive strain at the extreme fibre, ε_{cu}, of -0.0035 in the CSA-A23.3-04 sectional flexure model, while the value of -0.003 is used in the ACI 318-05 model. Equivalent rectangular stress blocks using the respective formulations from each code are used for calculation of the concrete contribution on the flexural compression side. The strength of concrete in tension was neglected.

Material properties were presented in the discussion of the experimental program in Chapter 3, Section 3.3. Measured material properties for the reinforcement include the longitudinal bar yield stress and yield strain. Strain hardening was neglected. Measured concrete properties included the concrete compressive strength.

Galal *et al.* (2005) used confined concrete strength to calculate the concrete shear contribution for columns rehabilitated with external fibre reinforced polymer (FRP). Hence, for collared columns, unconfined concrete strength and confined concrete strengths were both considered within the CSA-A23.3-04 and ACI 318-05 sectional shear and flexure models.

The confined concrete strength was obtained adopting a procedure proposed by Chapman and Driver (2006) and was adapted in Chapter 2, Section 2.3.3. The approach first determines the confining pressures induced by the collars through a simplified plastic analysis. For the confined model, analysis results are reported that include or omit consideration of strain gradient effects within the cross-section. The gradient in axial strains that occurs across a cross-section affects the confinement efficiency by reducing the effective confined area and hence the average confined concrete strength. This phenomenon was reported by Parvin and Wang (2001) through experimental tests and numerical analyses of FRP-jacketed square concrete columns under eccentric loading, where the effects of various eccentricities and FRP jacket thicknesses were investigated. The results from Parvin and Wang (2001) showed that the strain gradient decreases the rehabilitation efficiency of the FRP jacket for concrete columns. For columns experiencing low axial force and flexural dominated by bar yielding, if the extreme fibre of the cross-section has a compressive strain of ε_{cu}, the average compressive strain over the compression zone is $0.5\varepsilon_{cu}$. Further considering that only part of the overall section may be in compression when a strain gradient exists over the cross-section, the average compressive strain for the whole section is smaller than $0.5\varepsilon_{cu}$. To account for the lower average strain, an additional reduction factor of $K_{sg} = 0.33$ was introduced in the calculation of the confinement efficiency factor when the cross-section experiences a strain gradient, K, as discussed in Chapter 2, Section 2.3.3, if strain gradient to be considered.

The final predicted capacity and governing mode of failure were determined by comparing the predicted strengths from the two modes of failure—flexural or shear—with the lower value governing. These predicted capacities were used to determine the ratio of the experimental peak lateral force to the predicted peak lateral force.

The peak lateral force comparisons between the experimental results and predictions from the CSA-A23.3-04 and ACI 318-05 sectional models are summarized in Tables 6-1 through 6-3 using unconfined concrete strength or confined concrete strength, with the confined concrete strength either including or omitting the consideration of the strain gradient effect at the cross-section. The magnitude of $V_{\max,\exp}$ represents the average of the peak lateral forces reached for the push and pull cycles in each laboratory test. $V_{\max,csa}$ and $V_{\max,aci}$ are the peak lateral force predicted by CSA-A23.3-04 and ACI 318-05, respectively. $f_c^{'}$ is the unconfined concrete strength, while $f_{ccsg}^{'}$ and $f_{cc}^{'}$ are the confined concrete strength considering and omitting the strain gradient effect at the cross-section, respectively. The coefficients of variation of the ratios between the experiment and prediction with CSA-A23.3-04 are consistently smaller than with ACI 318-05 although the mean values are close, indicating that the prediction with CSA-A23.3-04 is more consistent than with ACI 318-05. In both code predictions, CV0A and CV5 are governed by the shear capacity, while the others are governed by flexural capacity, which is consistent with the experimental results where the longitudinal bars yielded after reaching the peak load for CV0A and CV5. Both code equations are extremely conservative for the column with little shear reinforcement (specimen CV0A). The CSA-A23.3-04 and ACI 318-05 sectional models also predicted shear failure for specimen CV0A, but the predicted shear capacities according to CSA-A23.3-04 and ACI 318-05 were 30% and 40% lower, respectively, than the experimentally obtained maximum lateral force. The mean and coefficient of variation of the experimental to CSA-A23.3-04 sectional prediction ratios were 1.28 and 0.07 with unconfined concrete strength, 1.23 and 0.07 with confined concrete strength considering the strain gradient, and 1.15 and 0.10 with confined concrete strength omitting the strain gradient effect. The mean and coefficient of variation of the experimental to ACI 318-05 prediction ratios were 1.29 and 0.12 with unconfined concrete strength, 1.25 and 0.13 with confined concrete strength considering the strain gradient, and 1.19 and 0.15 with confined concrete strength omitting the strain gradient effect. It shows that better predictions were obtained with the confined concrete strength omitting the strain gradient effect than with the other two types of concrete strength.

The assumption that plane sections remain plane, neglect of strain hardening, and the exclusion of the shear strength contribution from the direct strut action results in an underestimation of the peak lateral force of short columns. But the strength degradation under cyclic load is not considered in the code model predictions, which might offset the strength underestimation somewhat.

6.2.2 Response 2000

The nonlinear sectional analysis program Response 2000 (Bentz 2000) adopts the modified compression field theory (Vecchio and Collins 1986, 1988) to obtain the behaviour of reinforced concrete elements subjected to combinations of axial, flexural and shear loading. The actual properties of the materials as summarized in Chapter 3, Section 3.3 were used. The tensile capacity of the concrete was taken as 10% of the peak compressive strength of the concrete. Measured material properties for the reinforcement

include longitudinal bar yield stress and yield strain. Strain hardening was neglected. Response 2000 solves shear and flexural response simultaneously. Results reported in this study represent the lateral force corresponding to the peak load, not necessarily the lateral force corresponding to a shear failure.

The peak lateral force comparisons between experimental results and predictions by Response 2000 are shown in Tables 6-1 through 6-3, using the unconfined concrete strength, and confined concrete strength including or omitting the strain gradient effect. $V_{\max,response}$ is the peak lateral force predicted by Response 2000. The Response 2000 program predicted flexural failure for all the specimens except CV0A. The peak lateral forces obtained from Response 2000 were generally lower than the peak lateral forces reached in the tests. The mean and coefficient of variation of the experimental to Response 2000 prediction ratios were 1.32 and 0.09 with unconfined concrete strength, 1.25 and 0.08 with confined concrete strength considering the strain gradient, and 1.21 and 0.09 with confined concrete strength omitting the strain gradient effect. Thus, better predictions were obtained with the confined concrete strength omitting the strain gradient effect than with the other two representations of concrete strength. The general conservatism of the program is partly the result of the plane section assumption of the program and the exclusion of the shear strength contribution from the direct strut action. Lack of strain hardening also makes the predictions conservative. Since the aspect ratios of the column specimens in this research program were quite small, it was likely that there was significant direct strut action rather than a uniform diagonal stress field. Thus, sectional approaches such as Response 2000 are conservative. Bentz (2001) also reported conservative results when modelling shear-dominant columns tested at the University of California at San Diego with Response 2000. However, it can be seen that the coefficient of variation is small compared to that of the ACI 318 predictions, indicating better consistency.

6.3 Strut-and-Tie Model

According to Schlaich *et al.* (1987) and MacGregor and Bartlett (2000), the following procedure can be adopted to predict the strength of discontinuity ("D") regions with a strut-and-tie model: (1) select an appropriate strut-and-tie model to transmit the applied forces from boundary to boundary of the D-region; (2) calculate the force in the struts and ties in terms of the external applied force; (3) check the stresses in the individual strut and tie members and the nodes against the allowable stresses; (4) the lowest external load leading to the failure of the weakest elements (compression struts, tension ties, or nodal zones) is the predicted failure load. For statically indeterminate truss models, an estimate of relative stiffness of the members will be needed to determine the force capacity of the truss model. The struts, ties, and nodal zones all have finite dimensions with stress limits. According to the strut-and-tie model provisions in CSA-A23.3-04, the maximum compressive strength of a concrete strut is also affected by the component of the tensile strain in the perpendicular direction.

Strut-and-tie models were developed for each collared column in the test program. The models incorporated the two traditional mechanisms of compression fans and

compression fields reported by MacGregor and Bartlett (2000). The layouts of the strut-and-tie models for each specimen are presented in Figures 6-1 through 6-3. The strut-and-tie model provisions in CSA-A23.3-04 were adopted to set the allowable limits.

The peak lateral force comparisons between the experimental results and the strut-and-tie model predictions are listed in Tables 6-1 through 6-3, using unconfined concrete strength, as well as confined concrete strength either considering or omitting the strain gradient effect. $V_{max,stm}$ is the peak lateral force predicted by the strut-and-tie model. The mean and coefficient of variation of the experimental to strut-and-tie model prediction ratios were, respectively, 1.53 and 0.10 with unconfined concrete strength, 1.47 and 0.11 with confined concrete strength considering the strain gradient, and 1.36 and 0.14 with confined concrete strength omitting the strain gradient effect. Again, better predictions were obtained with the confined concrete strength omitting the strain gradient effect than with the other two representations of concrete strength. These analyses indicate that the failure is related to yielding of the longitudinal reinforcement, and the typical limiting element is the longitudinal reinforcement. In the test, all the specimens except the control column with widely spaced shear reinforcement (CV0A) and the collared column with the smaller aspect ratio (CV5) experienced longitudinal bars yielding before the peak lateral force was reached. The conservative results are expected due to the lower bound nature of this modelling approach. Neither tension stiffening in the concrete nor strain hardening in the longitudinal reinforcement was considered, which contributed to the conservatism of the strut-and-tie model strength predictions.

6.4 Proposed Strength Model

For practitioners, it is convenient to adopt a simple to understand, simple to implement analytical model to evaluate the capacity of columns rehabilitated with external steel collars. Among the models discussed above, the sectional strength models in CSA-A23.3-04 or ACI 318-05 appear to be a good basis to follow. However, improved consideration of the confinement provided by the external steel collar shall be considered. Hence, a new strength model is proposed to evaluate the peak lateral capacities of columns with external steel collars. The proposed model is based on the format of the code sectional equations, but considers the confined concrete strength and effective strain of the steel collar. Similar to other researchers who considered the effects of external jackets as being equivalent to an increased quantity of stirrups, the effect of each external steel collars is also simplified as an equivalent stirrup with a large cross-sectional area. The model was developed and validated for columns subjected to various combinations of axial, moment and shear. Validation utilized the results of the eccentrically loaded column tests conducted by Chapman and Driver (2006), tests on collared columns under combined axial and lateral loading reported by Hussain and Driver (2005b), the current experimental investigation, and the finite element studies reported in Chapter 5 Section 5.4.

Sectional shear analysis in the proposed model was performed using a modified version of the CSA-A23.3-04 general method. The proposed shear model is described in Section 6.4.1.

The sectional flexural analysis was based on measured material properties and an assumed concrete compressive strain at the extreme fibre, ε_{cu}, of -0.0035, equal to the value adopted in the CSA-A23.3-04 sectional flexure model. Two methods were investigated for calculation of the concrete compression in the sectional analysis: layered sectional analysis and equivalent rectangular stress block sectional analysis, described in Sections 6.4.2 and 6.4.3, respectively. Equivalent rectangular stress block sectional analysis obtained marginally better quality predictions for the collared columns studied in the current test program than layered sectional analysis, but showed similar predictions for 400×400×800 mm columns and worse predictions for 600×600×1225 mm columns in the parameter study. Hence, equivalent stress block sectional analysis is recommend over layered sectional approach for columns with a similar small cross-section as 400×400×800 mm columns.

The confined concrete stress-strain relationship was obtained adopting a procedure proposed by Chapman and Driver (2006) and was adapted in Chapter 2, Section 2.3.3. Since predictions using confined concrete strength but omitting strain gradient effects resulted in improved results compared to analysis with unconfined concrete strength or confined concrete strength including the strain gradient effect for the current experimental program, only confined concrete strength omitting strain gradient effect is used in this section to perform sectional flexural and shear analysis.

The predicted capacity and governing mode of failure were determined by comparing the predicted strengths from the two modes of failure—flexural or shear—with the lower value governing. These predicted capacities were used to determine the ratios of the experimental or finite element analytical peak lateral force to the predicted peak lateral force.

6.4.1 Shear Strength

For the "General Method" in CSA-A23.3-04, described in Section 2.6, an iterative solution approach was adopted to obtain the nominal shear strength, which is the summation of contributions from the concrete and internal shear reinforcement. In the proposed model, the external steel collars were treated similarly to traditional internal shear reinforcement, with A_{sc} representing the cross-sectional area of the steel collar. The stress in the steel collar legs is found as the product of the effective collar strain, ε_{esc}, and the modulus of elasticity, E_{sc}. Hence, while Eqs. 2-11b through 2-11d of the general method remain unchanged, Eq. 2-11a is replaced by:

$$V_n = V_c + V_s + V_{sc} = \beta\sqrt{f'_{cc}}\,b_w d_v + \frac{A_v f_y d_v \cot\theta}{s} + \frac{A_{sc}\varepsilon_{esc}E_{sc}d_{sc}\cot\theta}{s_{sc}} \qquad [6\text{-}1]$$

A23.3-04 Eq. 11-11:

$$\beta = \frac{0.40}{(1+1500\varepsilon_x)} \cdot \frac{1300}{(1000+s_{ze})} \qquad [2\text{-}11b]$$

A23.3-04 Eq. 11-12:

$$\theta = 29 + 7000\varepsilon_x \qquad [2\text{-}11c]$$

A23.3-04 Eq. 11-13 for non-prestressed member:

$$\varepsilon_x = \frac{M_f/d_v + V_f + 0.5P_f}{2E_s A_t} \qquad [2\text{-}11d]$$

where V_n is the nominal shear strength, V_c is the shear contribution from the concrete, V_s is the shear contribution from the internal shear reinforcement, V_{sc} is the shear contribution from the external steel collars, β is a factor accounting for shear resistance of cracked concrete, $f_{cc}^{'}$ is the confined compressive strength of concrete omitting the strain gradient, b_w is the effective width of the section, d_v is the effective shear depth, A_v is the total cross-sectional area of the internal shear reinforcement, f_y is the yield stress of the internal shear reinforcement, θ is the direction of the average principal compression with respect to the longitudinal axis, s is the longitudinal spacing of the internal shear reinforcement, A_{sc} is the total cross-sectional area of the steel collar, ε_{esc} is the effective strain of external steel collars, E_{sc} is the modulus of elasticity of the external steel collars, d_{sc} is the effective shear depth for the steel collars, and it can be taken equal to d_v in order to align with the longitudinal reinforcement of the truss model, s_{sc} is the centre-to-centre spacing of steel collars, ε_x is the longitudinal strain calculated at the mid-height of the cross-section resulting from the direct shear force, axial force, moment, and prestressing force, if applicable, s_{ze} is the effective crack spacing related to the basic crack spacing and coarse aggregate sizes, M_f is the moment at the cross-section, P_f is the axial force applied at the member cross-section (with compression taken negative), E_s is the modulus of elasticity of the longitudinal reinforcement, and A_t is the area of non-prestressed tension reinforcement.

In the current test program, all longitudinal bars in the collared columns had yielded before reaching the peak lateral force except those in specimen CV5. The strains at the peak lateral force in the steel collars of the columns considered in the finite element analysis parametric study discussed in Section 5.4 are in the range of 200 to 800 microstrain. There are many factors that might affect the collar strain at the peak lateral force, such as concrete compressive strength, aspect ratio, axial compression index, longitudinal reinforcement ratio, and so on. It is difficult to predict this value without enough experimental validation for finite element analysis. Hence, at the current stage of

research, the steel collar strain at the peak lateral force is simply taken as 500 microstrain from the tests.

For columns with internal shear reinforcement, such as the repaired collared column, CV0AR, shear contributions from both the internal shear reinforcement and the external steel collars were calculated separately and then were combined by direct summation.

Similar to the "General Method" in CSA-A23.3-04, a maximum nominal shear capacity is defined as follows to prevent a strut crushing mode in the concrete diagonals:

$$V_n \leq 0.25 f_{cc}^{'} b_w d \qquad [6\text{-}2]$$

where d is the distance from the extreme compression fibre to the centroid of the longitudinal tension reinforcement. It is noted that this maximum value will sometimes govern for collar sizes expected to be used in practice, in effect reducing the influence of the approximated collar strain used in Eq. 6-1.

6.4.2 Layered Sectional Analysis for Flexure

In layered sectional analysis, the concrete compression zone is divided into ten parts of equal thickness along the compression depth. The concrete in tension is neglected. The trial-and-error procedure to determine the flexural capacity is as follows and was carried out with the aid of a spreadsheet:

[Step 1] A concrete compression depth is initially assumed for which the concrete strain in each layer is to be determined. The concrete strain is assumed to possess a linear distribution at the critical section, with the extreme fibre compression strain, ε_{cu}, of -0.0035. Strain compatibility is assumed between the concrete and bars at their interface;
[Step 2] The average value of concrete strain across each layer is used to calculate a corresponding concrete stress for the layer using the stress-strain relationship; the tensile or compressive stresses of the reinforcing bars are calculated from the strains obtained in Step 1 using the measured material properties;
[Step 3] The compressive force in each layer of the concrete compressive zone is calculated as the stress in that layer multiplied by the area of the layer, adjusted by the area of any reinforcing bars present in that layer, as required; the tensile or compressive forces in the reinforcing bars are calculated by multiplying the bar area by the corresponding bar stress;
[Step 4] The moment incurred due to each individual compressive and tensile force is then calculated as the force times the moment arm to the column centroid;
[Step 5] The total column axial force is obtained by the summation of the forces obtained in Step 3;
[Step 6] The axial force equilibrium of the whole section is checked and if equilibrium is not satisfied, a new concrete compression depth, and hence a new linear strain distribution, is selected (Step 1) and the steps above are repeated;

[Step 7] The moment on the whole section is obtained by the summation of the individual moments calculated in Step 4;
[Step 8] The corresponding equivalent lateral force, $V_{lsa,flexure}$, is obtained by dividing the column moment by the shear span.

Shear strength from layered sectional analysis, $V_{lsa,shear}$, is obtained from shear strength model discussed in Section 6.4.1, $V_{\max,lsa}$, the maximum lateral force from layered sectional analysis, hence, is taken as the smaller value of $V_{lsa,flexure}$ and $V_{lsa,shear}$.

6.4.3 Equivalent Rectangular Stress Block Sectional Analysis for Flexure

In sectional analysis with an equivalent rectangular stress block, similar to equations in CSA-A23.3-04 are used and concrete in tension is neglected. Similar to the layered sectional analysis, a trial-and-error procedure is adopted. The difference is that the total concrete compression force is determined through the equivalent rectangular stress block of uniform stress instead of implementing a summation of the effects from multiple layers, each with its own uniform stress value. The corresponding equivalent lateral force, $V_{esa,flexure}$, is obtained by dividing the predicted flexural capacity by the shear span. Shear strength from equivalent rectangular stress block sectional analysis, $V_{esa,shear}$, is obtained from shear strength model discussed in Section 6.4.1, $V_{\max,esa}$, the maximum lateral force from equivalent rectangular stress block sectional analysis, hence, is taken as the smaller value of $V_{esa,flexure}$ and $V_{esa,shear}$. This procedure was also carried out with the aid of a spreadsheet.

6.4.4 Capacities Based on the Proposed Model

Comparisons between experimental results and evaluations by the proposed strength model are shown in Tables 6-4 through 6-6, using the confined concrete strength omitting the strain gradient effect. Nominal values are discussed in this chapter. For specimens in the current test program, the effectiveness of the proposed model is demonstrated through the test-to-predicted ratio of maximum lateral applied force. For the specimens under eccentric loading tested by Chapman and Driver (2006), the test-to-predicted ratio of maximum axial load was evaluated. In this case, the predicted maximum axial load values from layered sectional analysis and equivalent rectangular stress block sectional analysis, $P_{\max,lsa}$, and, $P_{\max,esa}$, were evaluated by increasing the axial load and maintaining the moment equal to the axial load multiplied by the eccentricity. For the specimens under combined axial and lateral loading tested by Hussain and Driver (2005b), the peak moment values from layered sectional analysis and equivalent rectangular stress block sectional analysis, $M_{\max,lsa}$, and, $M_{\max,esa}$, were evaluated and compared against the corresponding test values.

As shown in Table 6-4, the proposed strength model obtained reasonably accurate results compared to the experimental results from Chapman and Driver (2006), with small

coefficients of variation for sectional analyses: 0.05 and 0.09. However, the layered sectional analysis underestimated the peak axial load and hence corresponding column moment, while the equivalent rectangular stress block sectional analysis overestimated it, with mean values of the strength ratios of 1.07 and 0.86, respectively. The peak moments for the specimens tested by Hussain and Driver (2005b) were underestimated by both sectional analyses, as shown in Table 6-5, with mean values of the strength ratios of 1.28 and 1.25, and coefficients of variation of 0.12 and 0.13, indicating that the effect of confinement was not accounted for sufficiently.

From Table 6-6, it was found that the proposed strength model gives predictions of the peak lateral force below the test values and finite element results for all specimens in the current test program except for the column with the smaller aspect ratio (CV5). The mean and coefficient of variation of the experimental to proposed strength model ratios are 1.16 and 0.07 for layered sectional analysis, and 1.13 and 0.05 for equivalent rectangular stress block sectional analysis. The mean and coefficient of variation of the finite element analysis to proposed strength model ratios are 1.13 and 0.14 for layered sectional analysis, and 1.10 and 0.13 for equivalent rectangular stress block sectional analysis. The ratios between the finite element analysis results and the corresponding proposed model evaluations showed larger variation than the ratios between the experimental results and proposed model evaluations.

Tables 6-7 and 6-8 show a summary of the comparisons between the finite element analysis results and the proposed model evaluations for the 400×400×800 mm and 600×600×1225 mm columns considered in the parametric study. Detailed values are shown in Appendix C. For the 400×400×800 mm columns in Table 6-7, specimen CV1 was taken as the reference standard case with variations of parameters as reported in the table. Thus, the reference case has 30×50 mm external steel collars with centre-to-centre spacing of 150 mm, concrete compressive strength of 33.3 MPa, ten 25M longitudinal bars, shear span of 650 mm, no pretension applied to the collar connection bolts, and axial compression index of 0.3. Similarly, for the 600×600×1225 mm columns in Table 6-8, the reference standard case has features identical to CV1 except for the shear span: 30×50 mm external steel collar with centre-to-centre spacing of 150 mm, concrete compressive strength of 33.3 MPa, ten 25M longitudinal bars, shear span of 1100 mm, no pretension applied to the collar connection bolts, and axial compression index of 0.3. Parameters considered include collar centre-to-centre spacing, longitudinal reinforcement ratio, aspect ratio, bolt pretension, axial compression index, concrete compressive strength, and collar stiffness.

For the 400×400×800 mm columns, with a total of 130 cases considered, the proposed model obtained reasonably accurate results, with the mean of the ratio between the finite element result and model evaluation ranging from 0.99 to 1.15, and coefficient of variations typically ranging from 0.01 to 0.19 with some values as high as 0.32. Also, from the detailed results provided in Appendix C, no apparent trend was found in terms of the ratio between the finite element result and the prediction from the proposed model for variation of several parameters: aspect ratio, bolt pretension, and collar stiffness. The ratio between the finite element result and prediction from the proposed model was found

to increase for increases in collar spacing, concrete compressive strength, and axial compression index. The finite element to model ratio decreases with the increase of longitudinal reinforcement ratio. For 600×600×1225 mm columns, the quality of the predictions of the proposed model compared to the finite element results were less satisfactory. The mean of the ratio between the finite element result and model prediction ranges from 1.06 to 1.58, with typical results in the range of 1.30 to 1.40. The coefficient of variations ranges from 0.00 to 0.17 with some values as high as 0.24. Also as shown in Appendix C, similar trends occur between the studied parameters and the finite element result to model prediction values. In addition to the results reported in Tables 6-7 and 6-8, several sets of additional analyses were conducted where more than one parameter was simultaneously changed from the standard reference case. When variations in axial compression index or concrete compressive strength were introduced, the influence of steel collar sizes including 20×20, 60×60, 70×70, and 80×80, were studied, with the results provided in Appendix C. For both column sizes, the model evaluation is less accurate for the parameters of concrete compressive strength and the axial compression index compared to the other parameters, especially for cases with small steel collars. From the values of the mean and coefficient of variation of the ratios between the finite element analysis results and model evaluations as shown in Tables 6-7 and 6-8, in general, the quality of the model evaluation using the layered sectional analysis approach were similar or better to results with the equivalent rectangular stress block sectional analysis approach. Also, the model evaluations are closer to the finite element results for the 400×400×800 mm columns than the 600×600×1225 mm columns. No shear capacity prediction is limited by concrete crushing (*i.e.* $V_n \leq 0.25 f_{cc}^{'} b_w d$) except for 400×400×800 mm columns with concrete compressive strength of 20 MPa and external steel collar of 60×60 mm, 70×70 mm, and 80×80 mm.

More accurate predictions of the steel collar contribution and confined concrete strength, especially with respect to shear capacity, are required to improve the proposed model. However, the proposed model represents an initial step towards a simplified design approach for external steel collars around reinforced concrete columns.

6.5 Results Comparisons of Analytical Approaches Considered

In general, the CSA-A23.3-04 and ACI 318-05 sectional models and the proposed strength model use simple formulae and, hence, avoid the complexity that might be involved in the Response 2000 program and the strut-and-tie models. The flexural analysis methods from the codes and from the Response 2000 program obtained lower than experimental peak lateral force predictions for most cases, but the under-estimation is not as significant as those encountered when using strut-and-tie models. The mean value and coefficient of variation of the test to prediction capacity ratios obtained with CSA-A23.3-04 is smaller than those with ACI 318-05. Also both CSA-A23.3-04 and ACI 318-05 sectional models overestimated the strength of CV5, the collared column with small aspect ratio.

The proposed strength model provided predictions with reasonable accuracy, though generally below the actual strength of the test specimens and the predicted strength from

the finite element model. The test to predicted capacity ratios and corresponding coefficients of variation of both the proposed equivalent rectangular stress block sectional analysis and the layered sectional analysis were better compared to the ACI 318-05 approach, and similar to the CSA-A23.3-04 approach. Equivalent rectangular stress block sectional analysis was considered to give marginally better quality predictions for the collared columns studied in the current test program than layered sectional analysis, but showed similar predictions for 400×400×800 mm columns and worse predictions for 600×600×1225 mm columns in the parameter study. Hence, equivalent stress block sectional analysis is recommend over layered sectional analysis approach for columns has a similar small cross-section as 400×400×800 mm columns. While some additional research is warranted to further refine the proposed model, as discussed in Section 6.4.4, the proposed strength model can be adopted for predicting the peak lateral force of collared reinforced concrete column.

6.6 Summary

Sectional strength models from CSA-A23.3-04 and ACI 318-05, along with the Response 2000 program and strut-and-tie models were used to evaluate the capacities of column specimens tested as part of this research project. Comparisons were made between the predicted strengths and the experimental results. A new strength model for collared concrete columns with a square cross-section has been proposed. This model determines the peak lateral force the column can carry as the lower value of the flexural capacity and shear strength, with the shear strength determined from summation of contributions from the concrete mechanism and shear reinforcement truss mechanism. Predictions from the proposed model were compared with experimental results as well as the columns from the finite element parametric study discussed in Chapter 5, Section 5.4, and other results from earlier experimental program on collared columns under eccentric axial loading or combined axial and lateral loading. The proposed strength model generally provided predictions below the actual strength of the test specimens and the predicted strength from the finite element model for the effects of collar spacing and collar stiffness, bolt pretension, longitudinal reinforcement ratio, aspect ratio, axial compression index, concrete compressive strength. Of the two flexural analysis approaches studied in the proposed model, the layered sectional analysis approach was considered to be marginally better for 600×600×1225 mm columns, but equivalent rectangular stress block sectional analysis was considered to give marginally better quality predictions for the collared columns studied in the current test program than layered sectional analysis, and showed similar predictions for 400×400×800 mm columns. Further research is required, however, to generalize and validate this strength model since it is based on limited experimental data and the finite element parametric study reported in Chapter 5. Additional experimental validations are needed for parameters beyond the ranges considered.

Table 6-1 Peak lateral force comparisons between experimental results and evaluations with unconfined concrete strength

Specimen	f_c' (MPa)	$V_{max,exp}/V_{max,csa}$	$V_{max,exp}/V_{max,aci}$	$V_{max,exp}/V_{max,response}$	$V_{max,exp}/V_{max,stm}$
CV0A	26.3	1.42	1.67	1.46	1.79
CV0AR	26.6	1.26	1.26	1.24	1.52
CV0B	26.9	1.18	1.18	1.36	1.42
CV1	33.3	1.14	1.16	1.14	1.37
CV2	25.5	1.24	1.24	1.25	1.50
CV3	22.0	1.38	1.38	1.50	1.66
CV4	30.8	1.36	1.37	1.33	1.67
CV5	29.5	1.30	1.09	1.28	1.25
CV6	31.5	1.15	1.15	1.23	1.45
CV7	29.1	1.35	1.38	1.49	1.63
CV8	27.4	1.28	1.28	1.26	1.54
Mean		**1.28**	**1.29**	**1.32**	**1.53**
C. O. V.		**0.07**	**0.12**	**0.09**	**0.10**

Table 6-2 Peak lateral force comparisons between experimental results and evaluations with confined concrete strength considering strain gradient*

Specimen	f_{ccsg}' (MPa)	$V_{max,exp}/V_{max,csa}$	$V_{max,exp}/V_{max,aci}$	$V_{max,exp}/V_{max,response}$	$V_{max,exp}/V_{max,stm}$
CV0A	26.3	1.42	1.67	1.46	1.79
CV0AR	30.3	1.21	1.22	1.19	1.44
CV0B	26.9	1.18	1.18	1.36	1.42
CV1	37.1	1.11	1.13	1.11	1.31
CV2	27.3	1.22	1.22	1.20	1.46
CV3	28.1	1.29	1.30	1.27	1.51
CV4	34.5	1.31	1.32	1.29	1.57
CV5	33.2	1.15	1.01	1.25	1.19
CV6	35.2	1.14	1.14	1.22	1.45
CV7	38.3	1.26	1.29	1.26	1.60
CV8	33.0	1.21	1.22	1.19	1.43
Mean		**1.23**	**1.25**	**1.25**	**1.47**
C. O. V.		**0.07**	**0.13**	**0.08**	**0.11**

* The confined concrete strength was obtained including the consideration of strain gradient effects within the cross-section (see Section 2.3.3).

Table 6-3 Peak lateral force comparisons between experimental results and evaluations with confined concrete strength omitting strain gradient*

Specimen	f_{cc}' (MPa)	$V_{max,exp}$ /$V_{max,csa}$	$V_{max,exp}$ /$V_{max,aci}$	$V_{max,exp}$ /$V_{max,response}$	$V_{max,exp}$ /$V_{max,stm}$
CV0A	26.3	1.42	1.67	1.46	1.79
CV0AR	37.7	1.14	1.16	1.14	1.31
CV0B	26.9	1.18	1.18	1.36	1.42
CV1	45.1	1.05	1.08	1.06	1.20
CV2	31.8	1.17	1.18	1.14	1.37
CV3	43.1	1.15	1.18	1.19	1.24
CV4	42.4	1.22	1.25	1.23	1.39
CV5	41.0	0.94	0.96	1.23	1.08
CV6	43.2	1.12	1.13	1.20	1.45
CV7	54.3	1.16	1.19	1.19	1.46
CV8	43.8	1.12	1.14	1.13	1.24
Mean		**1.15**	**1.19**	**1.21**	**1.36**
C. O. V.		**0.10**	**0.15**	**0.09**	**0.14**

* The confined concrete strength was obtained omitting the consideration of strain gradient effects within the cross-section (see Section 2.3.3).

Table 6-4 Peak lateral force comparisons between experimental results by Chapman and Driver (2006) and proposed model evaluations*

Specimen	Eccentricity (mm)	$P_{max,exp}$ (kN)	$P_{max,lsa}$ (kN)	$P_{max,esa}$ (kN)	$P_{max,exp}$ /$P_{max,lsa}$	$P_{max,exp}$ /$P_{max,esa}$
CE07	30	2997	2895	3645	1.04	0.82
CE08	60	2276	2192	2783	1.04	0.82
CE09	10	3861	3606	5006	1.07	0.77
CE10	0	4490	4171	4512	1.08	1.00
CE11	30	3415	3071	4299	1.11	0.79
CE12	30	2744	2759	2956	0.99	0.93
CE13	30	3695	3180	4293	1.16	0.86
CE14	30	3171	2868	3515	1.11	0.90
Mean					**1.07**	**0.86**
C. O. V.					**0.05**	**0.09**

* Specimens under eccentric axial loading tested by Chapman and Driver (2006).

Table 6-5 Peak lateral force comparisons between experimental results by Hussain and Driver (2005b) and proposed model evaluations*

Specimen	$M_{max,exp}$ (kN·m)	$M_{max,lsa}$ (kN·m)	$M_{max,esa}$ (kN·m)	$M_{max,exp}/M_{max,lsa}$	$M_{max,exp}/M_{max,esa}$
CL1	235	177	175	1.33	1.34
CL2	277	187	181	1.48	1.53
CL3	301	197	211	1.53	1.43
CL4	297	239	243	1.24	1.22
CL5	207	195	205	1.06	1.01
CL6	283	241	249	1.17	1.14
CL7	297	246	254	1.21	1.17
CL8	296	244	248	1.21	1.20
Mean				**1.28**	**1.25**
C. O. V.				**0.12**	**0.13**

* The specimens under combined axial and lateral loading tested by Hussain and Driver (2005b).

Table 6-6 Peak lateral force comparisons between experimental/finite element analysis results and proposed model evaluations*

Specimen	$V_{max,exp}$ (kN)	$V_{max,fea}$ (kN)	$V_{max,lsa}$ (kN)	$V_{max,esa}$ (kN)	$V_{max,exp}/V_{max,lsa}$	$V_{max,exp}/V_{max,esa}$	$V_{max,fea}/V_{max,lsa}$	$V_{max,fea}/V_{max,esa}$
CV0AR	748	693	635	657	1.18	1.14	1.09	1.05
CV1	815	768	770	777	1.06	1.05	1.00	0.99
CV2	724	736	625	622	1.16	1.16	1.18	1.18
CV3	760	846	607	664	1.25	1.14	1.39	1.27
CV4	721	700	567	584	1.27	1.23	1.23	1.20
CV5	1194	1027	1157	1157	1.03	1.03	0.89	0.89
CV6	604	689	539	538	1.12	1.12	1.28	1.28
CV7	916	769	745	789	1.23	1.16	1.03	0.97
CV8	767	708	652	688	1.18	1.12	1.09	1.03
Mean					**1.16**	**1.13**	**1.13**	**1.10**
C. O. V.					**0.07**	**0.05**	**0.14**	**0.13**

* The specimens under combined axial and lateral loading in the current test program.

Table 6-7 Peak lateral force comparisons between finite element analysis results and proposed model evaluations for 400×400×800 mm columns with parameter variations

Parameters	**Values considered**	**Mean, coefficient of variation of $V_{max,fea}$ / $V_{max,\,lsa}$**	**Mean, coefficient of variation of $V_{max,fea}$ / $V_{max,\,esa}$**
Collar centre-to-centre spacing, mm	100, 150, 200, 250, 300	1.00, 0.05	1.00, 0.03
Longitudinal reinforcement ratio, Bars, ρ	Ten 10M-0.63%, Ten 15M-1.25%, Ten 20M-1.88%, Ten 25M-3.13%, Ten 30M-4.38%	1.15, 0.22	1.13, 0.21
Aspect ratio, M/(VD)	0.5625, 0.9375, 1.3125, 1.625, 1.875	1.01, 0.16	1.13, 0.32
Pretension force in collar bolt, kN	0, 41, 83, 122, 143	1.01, 0.02	0.99, 0.01
Axial compression index, $P/(f_c'A_g)$	0.0, 0.1, 0.2, 0.3, 0.4, 0.5, 0.6, 0.7	1.12, 0.14	1.10, 0.11
Concrete compressive strength, MPa	20, 30, 40, 50, 60, 70, 80	1.05, 0.17	1.06, 0.19
Collar dimension, mm	30×20, 30×30, 30×40, 30×50, 30×60, 30×70, 30×80	1.05, 0.05	1.03, 0.05

Table 6-8 Peak lateral force comparisons between finite element analysis results and proposed model evaluations for 600×600×1225 mm columns with parameter variations

Parameters	**Values considered**	**Mean, coefficient of variation of $V_{max,fea}$ / $V_{max,\,lsa}$**	**Mean, coefficient of variation of $V_{max,fea}$ / $V_{max,\,esa}$**
Collar centre-to-centre spacing, mm	100, 150, 200, 250, 300	1.33, 0.01	1.36, 0.03
Longitudinal reinforcement ratio, Bars, ρ	Ten 15M-0.56%, Ten 25M-1.39%, Ten 30M-1.94%, Ten 35M-2.78%, Ten 45M-4.17%	1.06, 0.17	1.12, 0.12
Aspect ratio, M/(VD)	0.8333, 1.0833, 1.3333, 1.5833, 1.8333	1.19, 0.11	1.19, 0.12
Pretension force in collar bolt, kN	0, 41, 83, 122, 143	1.33, 0.00	1.31, 0.03
Axial compression index, $P/(f_c'A_g)$	0.0, 0.1, 0.2, 0.3, 0.4, 0.5, 0.6, 0.7	1.49, 0.15	1.58, 0.17
Concrete compressive strength, MPa	20, 30, 40, 50, 60, 70, 80	1.31, 0.07	1.54, 0.24
Collar dimension, mm	30×20, 30×30, 30×40, 30×50, 30×60, 30×70, 30×80	1.33, 0.01	1.35, 0.02

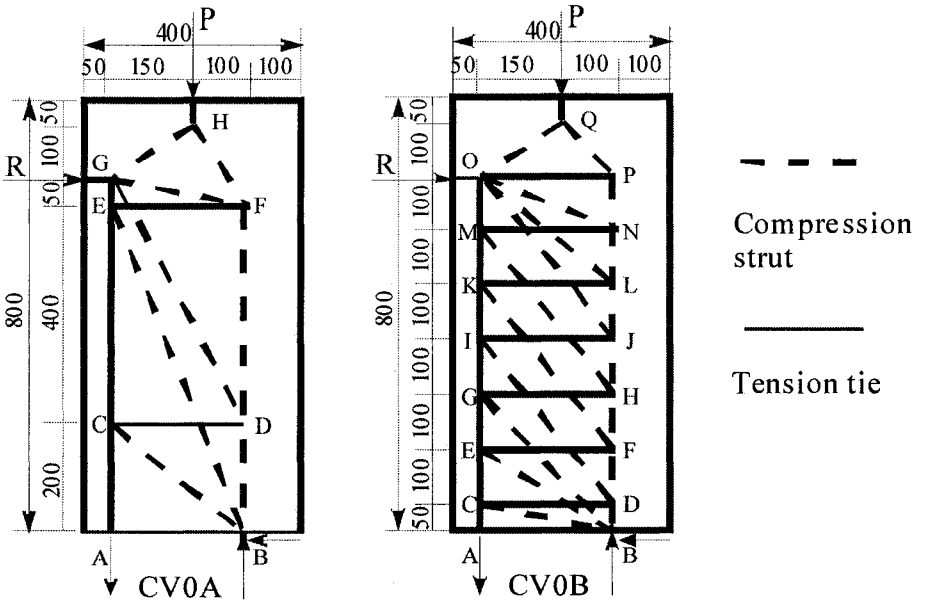

Figure 6-1 Strut-and-tie models for specimens CV0A and CV0B

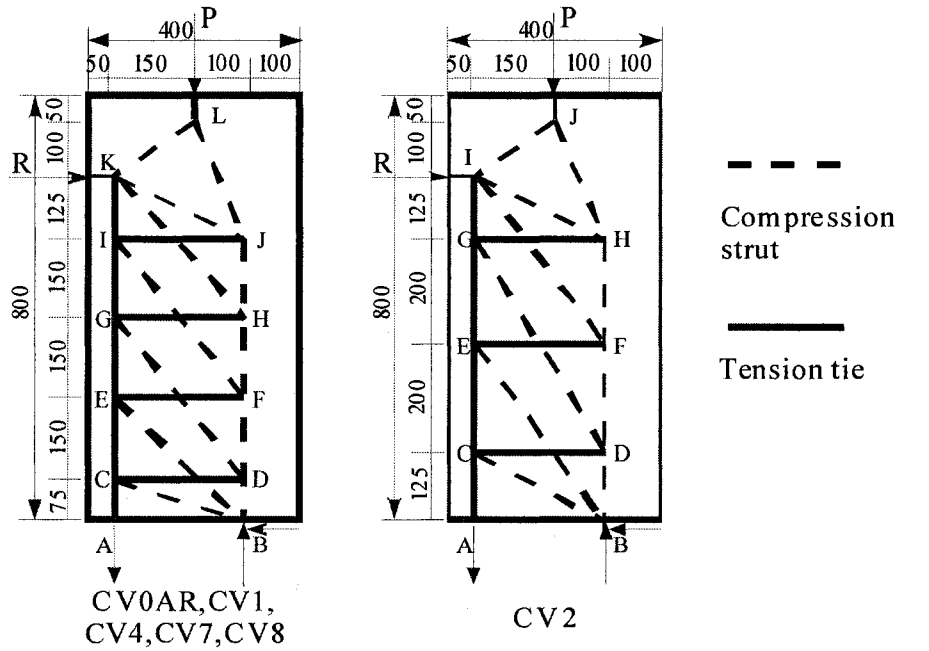

Figure 6-2 Strut-and-tie models for specimens CV0AR, CV1, CV2, CV4, CV7, and CV8

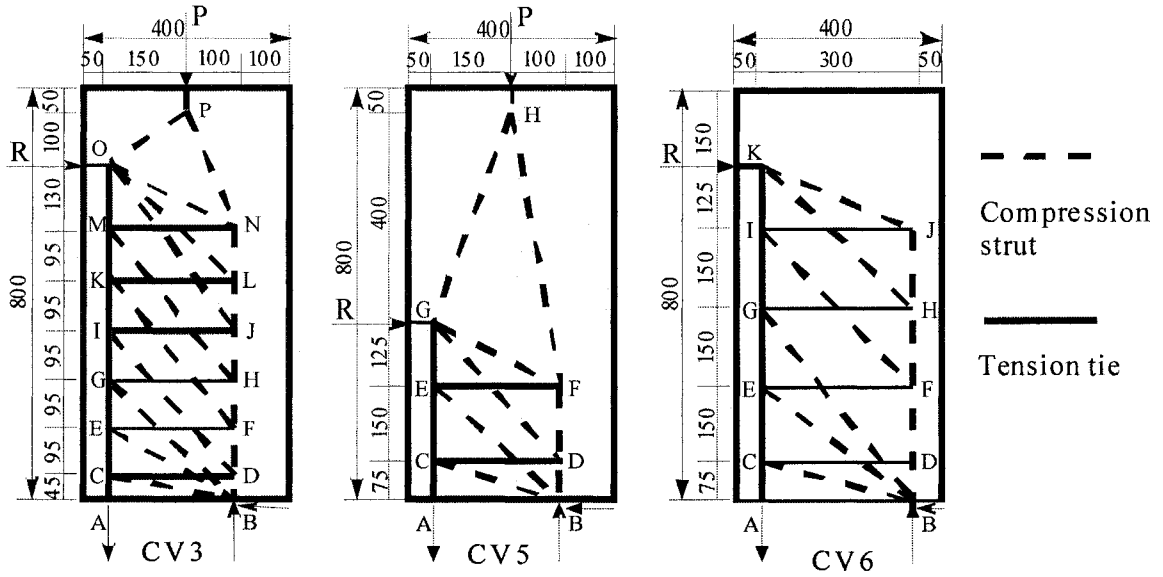

Figure 6-3 Strut-and-tie models for specimens CV3, CV5 and CV6

CHAPTER 7 DESIGN GUIDELINES

7.1 Introduction

Responses of as-built and rehabilitated reinforced concrete short columns were examined through experimental and analytical research. From the evaluation of the results of the current experimental and analytical investigation and previous studies conducted by Hussain and Driver (2005b) and Chapman and Driver (2006), it was concluded that external steel collars can provide effective rehabilitation of columns under axial concentric or eccentric loading, and combined axial and lateral loading. Based on the current research and available knowledge on the steel collar system, general guidelines for the design of external steel collars for rehabilitation or strengthening of reinforced concrete columns were developed. The guidelines consider flexural, axial, and shear performance for columns with external steel collars. The guidelines are based on existing sectional reinforced concrete design provisions from CSA-A23.3-04 and ACI 318-05, as discussed in Chapter 6, and on limit states design principles. Implementation of the guidelines is illustrated through design examples in this chapter.

7.2 Rehabilitation and Strengthening Design Goal

When selecting the rehabilitation method, the goal or objective of the rehabilitation should be defined to reflect the desired structural performance criteria. When seismic rehabilitation is performed for a column, the rehabilitation goals usually include improvements in strength and ductility. According to limit states design philosophy, the ultimate limit state criterion is established to ensure that the load effects are smaller than the strength of the structure. Serviceability limit states are to ensure that the structure can fulfill its function satisfactorily under service loads. In the case of seismic rehabilitation, the enhancement of ductility may be the overriding criterion. The rehabilitation and strengthening should also follow limit states design philosophy. A flowchart to describe the rehabilitation design goal is shown in Figure 7-1. However, only the ultimate limit state is discussed in the current study.

Rehabilitation with external steel collars can satisfy the limit states design philosophy if designed according to available experimental and analytical research guidelines. A design methodology and design equations for determining the required dimensions and spacing of the steel collars are needed to form guidelines in fulfilling those design requirements. For non-seismic application of strengthening, the intent is to provide enough confinement to increase the axial strength, and/or shear strength (besides confinement, the collars provide shear reinforcement), and/or flexural strength. The design basis for seismic rehabilitation is that reliable response in terms of strength and ductility should be ensured, even at relatively high ductility levels. Considerations shall also be given to the ease of rehabilitation construction and post-rehabilitation maintenance, as well as overall rehabilitation economy.

7.3 Rehabilitation and Strengthening Design Guidelines

Overall and detailed procedures are discussed along with assumptions and scope in this section.

7.3.1 Overall Rehabilitation and Strengthening Procedures

A flowchart for the overall rehabilitation and strengthening of structures is provided as Figure 7-2 and briefly described below.

[Step 1] Rehabilitation need. Evaluate the existing structure to determine the current performance and compare with the desirable performance, to identify deficient members in need of rehabilitation.

[Step 2] Rehabilitation method. Select an appropriate rehabilitation method and determine the materials to be used. Factors that should be considered in selecting the rehabilitation method include: the current performance status of the existing structure determined through detailed inspection and evaluation; the performance requirements of the structure; the effectiveness of the rehabilitation method with respect to the required performance improvements; the construction and erection constraints of the structure; the viability of the execution of the rehabilitation work; the impact of the rehabilitation work on the surrounding environment; the disruption of the use, occupancy, and operation of the existing structure; and the economy and ease of maintenance after rehabilitation.

[Step 3] Rehabilitation design. Perform the rehabilitation design, and provide detailed specifications and construction method requirements. Rehabilitation design shall be conducted to ensure adequate flexural strength, axial compression capacity, shear resistance, and ductility capacity.

[Step 4] Rehabilitation implementation. Implement the rehabilitation according to the design.

7.3.2 General Assumptions and Scope

In this chapter, it is assumed that the appropriate evaluation of an existing structural member has been completed and the use of external steel collars is selected as the preferred rehabilitation method. The following design discussion concentrates on and is applicable to columns with square cross-section. The design procedure determines the required dimensions and spacing of the external steel collars needed for the appropriate rehabilitation of reinforced concrete columns under a given applied load.

Chapman and Driver (2006) tested one specimen to simulate an existing building column in a rehabilitation scenario. An axial preload was introduced to the deficient column before applying the steel collars, with a magnitude corresponding to the axial compression index of 0.50. After collars were installed, the specimen was loaded to failure in the usual manner under increasing axial load. Test results showed that installing

external collars on a column already under significant preload resulted in similar strength and ductility to a column where the collars were installed prior to the application of any axial load. Therefore, it is appropriate to assume that initial strains in the section at the time of rehabilitation with steel collars can be ignored. This assumption is similar to the recommendations by Bisby and Williams (2004) for rehabilitation of concrete structures with external FRP wrapping. Similar assumptions were made for flexure and shear strengthening.

The rehabilitation guideline proposed focuses on strength rehabilitation only. Other considerations might be taken into account, such as corrosion of steel under exposure to certain environments, like alkalinity/acidity. It might also need to be checked for fire-resistance rating since steel loses strength under high temperature. Hence, reasonable rehabilitation limits might be applied to prevent the rehabilitated columns/beams from failure due to fire and other environmental effects. Special surface treatment to protect the steel collars from corrosion might also be required.

7.3.3 Collar Spacing

Requirements for minimum area of steel collars and maximum spacing can be taken similar to the current minimum tie reinforcement requirements in CSA-A23.3-04: Clause 7.6.5 for compression members, Clause 11.2.8 for minimum shear reinforcement, and Clause 21.4.4 for transverse reinforcement for ductile moment-resisting frame members subjected to flexure and significant axial load. Clause 7.6.5.1 states that "In compression members, all non-prestressed longitudinal bars of sizes 30M or smaller shall be enclosed by ties having a diameter of at least 30% of that of the largest longitudinal bars." Clause 7.6.5.2 states that "Tie spacing shall not exceed the smallest of: (a) 16 times the diameter of the smallest longitudinal bars or the smallest bar in a bundle; (b) 48 tie diameters; (c) the least dimension of the compression member; and (d) 300 mm in compression members containing bundled bars." Clause 11.2.8.2 states that "where shear reinforcement is required by Clause 11.2.8.1 or by calculation, the minimum area of shear reinforcement shall be such that $A_v = 0.06\sqrt{f_c'}\frac{b_w}{f_y}s$", where A_v is the area of shear reinforcement within a distance s, f_c' is the compressive strength of concrete, b_w is the minimum effective web width, f_y is the specified yield strength of reinforcement, and s is the spacing of the shear reinforcement measured along the longitudinal axis. Clause 21.4.4 is discussed in Chapter 3, Section 3.2.2.

Experimental studies showed that collared columns exhibit improved behaviour in terms of strength and ductility compared to the control column without collars, for collar centre-to-centre spacing up to 200 mm (half of the square column cross-sectional dimension). Finite element analyses were also conducted for columns having centre-to-centre spacing larger than half of the square column cross-sectional dimension (up to 75% of the cross-sectional dimension). In these cases, stable response was achieved which demonstrates that use of spacings larger than half of the square column cross-sectional dimension spacing is promising. Hence, with currently available

information, the maximum spacing of steel collars can be taken as 75% of the smaller cross-sectional dimension of the column. Finite element analysis suggested that a proposed practical range of collar sizes of 20 to 80 mm in each dimension is reasonable, since beneficial effects from smaller collar dimensions is limited and larger collars do not continue to bring increasing strength improvement. Also, the finite element parametric study suggests that the ratio between the bigger dimension of the collar cross-section and the smaller dimension should be less than 3 to ensure effectiveness and efficiency of the collar as well as the practicality of construction. The bigger dimension is preferred to be oriented parallel to column axis to increase the directly contacted area.

7.3.4 Flexural and Axial Rehabilitation

The safety of the rehabilitated structure shall be verified by confirming that the flexural and axial load-carrying capacities are greater than the flexural and axial load effects acting on the structure. According to experimental and analytical studies conducted by Hussain and Driver (2005b) and by Chapman and Driver (2006), the flexural and axial load-carrying capacities and the deformation capability were improved through the rehabilitation with external steel collars.

The flexural and axial capacities of a column with external steel collars are determined through cross-sectional analysis at the ultimate limit state, including the confining effect of the steel collars. The confined concrete stress-strain relationship is used in the ultimate state analysis to obtain the axial load versus moment interaction diagram for the rehabilitated reinforced concrete columns. The confinement model, proposed by Chapman and Driver (2006), was discussed in Chapter 2, Section 2.3 neglecting strain gradient effects within the cross-section. The axial load versus moment interaction diagram is referred to herein as the P-M interaction diagram. Elastic–perfectly plastic stress-strain relationships are assumed for both the longitudinal reinforcement and the external steel collars. Those curves, along with the following assumptions, form the basis for the ultimate limit state analysis of collared reinforced concrete columns. An equivalent rectangular compressive stress block was used for concrete in the analysis.

(1) Design calculations are based on measured geometric dimensions, internal reinforcement details, and the material properties of the existing column to be rehabilitated.

(2) Plane sections remain plane after loading so that a linear strain distribution exists across the column cross-section.

(3) There is no relative slip between the external steel collars and the concrete. This assumption has been verified through the experimental observations in the current study and results reported by Hussain and Driver (2005b) and by Chapman and Driver (2006).

(4) Strain compatibility exists between the concrete and longitudinal reinforcement through a perfect bond model.

(5) Initial strains in the concrete and internal reinforcement at the time of strengthening can be ignored. This assumption was also suggested by Bisby and Williams (2004) for rehabilitation of concrete structures with FRP wraps.

(6) Strength degradation and corrosion of steel reinforcement are ignored. This assumption was also adopted by Nezamian *et al.* (2004) for rehabilitation design of concrete bridge piers with externally applied FRP.

A trial-and-error procedure for collar size and spacing is adopted to evaluate flexural and axial rehabilitation design alternatives. A flowchart for the rehabilitation design for flexural and axial strength is shown in Figure 7-3 and briefly described below.

[Step1] Determine the factored axial and flexural loading requirements: M_f and P_f. Slenderness effects should be considered where appropriate.

[Step2] Select a collar size, $w \times t$, and collar centre-to-centre spacing, s_{sc}, to meet the requirement of the tie reinforcement for compression members, Clause 7.6.5 in CSA-A23.3-04, where $A_v = 2 \times w \times t$ and $s = s_{sc}$. w and t are the dimensions perpendicular and parallel to the longitudinal axis of the column, respectively. This minimum reinforcement requirement normally gives very small collar dimensions. The minimum practical dimension is suggested as 20×20 mm in order to achieve the benefit from collars obtained in the finite element parametric study.

[Step 3] For the parameters $w \times t$ and s_{sc} selected at Step 2, determine the confined concrete compressive strength, $f_{cc}^{'}$, from the relationship proposed by Chapman and Driver (2006) and adapted in Chapter 2, Section 2.3 as Eqs. 2-2 to 2-8, omitting the strain gradient in the cross-section in the calculation of the confinement efficiency factor.

[Step 4] Perform an equivalent rectangular stress block sectional analysis to construct the P–M interaction diagram.

[Step 5] Check whether (M_f, P_f) falls inside the enclosed region of the P–M interaction diagram, in which case the size and spacing of the steel collars are acceptable. Otherwise, a smaller spacing, s, or larger collar size, $w \times t$, must be selected at Step 3 until (M_f, P_f) falls inside the enclosed region. The first collar should be spaced away from the ends by half of the typical spacing used in the middle portion.

The procedure to construct the P–M interaction diagram is similar to that adopted for conventional practice for the design of reinforced concrete columns, as documented in MacGregor and Bartlett (2000). In the case of collared columns, the confined concrete compressive strength, $f_{cc}^{'}$, is used in place of the unconfined compressive strength, $f_c^{'}$. Material resistance factors are taken as those suggested in the CSA-A23.3-04 code provisions, that is, $\phi_s = 0.85$ and $\phi_c = 0.65$ for reinforcing steel and concrete,

respectively. $\phi_{sc} = 0.85$ is used for the steel collars. The upper limit of $0.80P_0$, where P_0 is the concentrically loaded column capacity, is used to account for accidental axial load eccentricities. The factored concentrically loaded column capacity can be found from $P_0 = \phi_c \alpha_1 f_c^{'}(A_g - A_s) + \phi_s A_s f_y$, where A_g is the gross cross-sectional area of the column, A_s is the total longitudinal reinforcement area, and α_1 is the ratio of average stress in rectangular compression block to the specified concrete strength. The design interaction diagram represents the failure surface of the collared column. Only loading points falling inside the interaction diagram represent safe combinations of applied axial load and moment, and hence are acceptable. (The resistance factors recommended in this paragraph are believed to be reasonable for this application based on experience with reinforced concrete structural members. It is emphasized that although a reliability study is beyond the scope of this research, it would be required to assess fully the adequacy of the values selected.)

The interaction diagram for a collared column will move toward higher combined axial load and moment combinations than the original column at the failure state, as shown in the Section 7.4.1, Example 1, indicating the effect of the external steel collar system in enhancing the capacity.

7.3.5 Shear Rehabilitation

The shear rehabilitation design of a reinforced concrete column with external steel collars should ensure that the shear capacity exceeds the shear demand on the column. In order to extend the limited experimental results into more general circumstances, an empirical shear strength model for the rehabilitated column with external steel collars was proposed in Chapter 6, Section 6.4. The empirical shear strength model was derived from a parametric study using finite element analysis and verified through experimental results on short column CV5 that failed in shear.

According to capacity design philosophy in seismic shear rehabilitation of a frame member, over-strength shall be taken into account to obtain the probable moment strength used to determine the maximum shear force that can be imparted to the member. CEB-FIB (2003) suggests that the shear capacity of a rehabilitated column should exceed the shear force corresponding to the flexural capacity of the column, with consideration of over-strength due to reinforcement strain hardening by 25%. CSA-A23.3-04 Clause 21.4.5.1 stipulates that "A column shall have a factored shear resistance that exceeds...the design shear force determined from consideration of the maximum forces...using the maximum probable moment strength...". MacGregor and Bartlett (2000) pointed out that the probable moment strength can be determined by replacing the f_y with 1.25 f_y since the average yield strength of the longitudinal bars tends to be greater than f_y. Hence, the over-strength factor applied to the nominal moment capacity is taken as 1.25 in the current study. This over-strength factor is also applied to the moment capacity after consideration of flexural strength increase due to confinement is applied.

The design for shear rehabilitation of the reinforced concrete columns is based on the modified truss model for sectional shear, similar to the model commonly used for conventional reinforced concrete columns. A summation approach of contributions from concrete, internal shear reinforcement, and external steel collars was adopted. The design procedure for this model requires a trial-and-error solution technique with different collar spacing and collar size to predict the capacity and compare with the demand. A flowchart describing the design sequence for shear strength rehabilitation is shown in Figure 7-4 and the procedure is summarized as follows:

[Step 1] Calculate the shear demand at the critical section. Shear demand is calculated from the nominal moment demand by dividing the moment demand by the shear span and then multiplying by the over-strength factor 1.25.

[Step 2] Calculate A_v and s according to CSA-A23.3-04 Clause 11.2.8 requirements of minimum shear reinforcement, $A_v = 0.06\sqrt{f_c'}\frac{b_w}{f_y}s$. Then choose the size of steel collars $w \times t$ (the second dimension is parallel to the longitudinal axis of the column) and spacing s_{sc}, with $2 \times w \times t = A_v$ and $s_{sc} = s$. Alternatively, a set of s_{sc} and $w \times t$ values can be estimated to start the iteration, with a check that they conform to the minimum shear reinforcement requirements.

[Step 3] Using the spacing s_{sc} and $w \times t$ from Step 2, determine the shear contribution from the external steel collar, V_{sc}, using Eqs. 6-1 and 6-2, and Eqs. 2-11b through 2-11d discussed in Chapter 6, Section 6.4.

[Step 4] Calculate the factored shear strength, $V_r = \phi_c V_c + \phi_s V_s + \phi_{sc} V_{sc}$, and compare this factored shear strength with the factored shear force, V_f.

The shear strength of the rehabilitated column is determined by adding the contribution of the external steel collars to the contributions from the concrete and the internal shear reinforcement (if applicable) as described in Chapter 6. The term d_{sc} is the effective shear depth for the steel collar, and in order to align with the longitudinal reinforcement of the truss model, it can be taken as the same as d_v, which is the effective shear depth, taken as the greater of $0.9d$ or $0.72h$, while d is the distance from the extreme compression fibre to centroid of longitudinal tension reinforcement, and h is the section depth of the column in the direction of shear force. The maximum allowable shear contributions from the internal shear reinforcement and external steel collars are described by the following expression: $V_s + V_{sc} \leq 0.66\phi_c\sqrt{f_c'}bd$. Material resistance factors are taken as those suggested in the CSA-A23.3-04 code provisions, that is, $\phi_s = 0.85$ and $\phi_c = 0.65$ for steel and concrete, respectively. The factor of $\phi_{sc} = 0.85$ is assumed in the calculation of the factored shear contribution from the steel collars.

[Step 5] If $V_r \geq V_f$, then the spacing and size of the steel collars determined at Step 2 are acceptable. Otherwise, a smaller spacing s_{sc} or larger size $w \times t$ must be selected at Step 2. The first collar should be spaced from the ends at a distance of half the typical spacing used in the middle portion.

The influence of the axial-shear interaction was already incorporated in the proposed empirical shear strength model since the model was formed out of the analysis of columns under shear loading with and without axial loading. The effect of axial load is explicitly included in Eq. 2-11 d, which in turn is considered in the shear capacity in Eq. 6-1.

7.4 Rehabilitation Design Examples

Three design examples for rehabilitation of reinforced concrete frame members (*i.e.*, columns and beams) with external steel collars are presented to illustrate the design guidelines proposed in Section 7.3.

7.4.1 Example 1-Flexural and Shear Rehabilitation of Column

Details of the column to be rehabilitated are shown in Figure 7-5, including the geometry, reinforcement details and loading condition. The design yield strength of reinforcement is 400 MPa, and the design compressive strength for concrete is 25 MPa. The modulus of elasticity for the longitudinal reinforcement and the steel used for the collars is $E_s = 200\,000$ MPa. The secant modulus of the concrete is taken as $E_c = 22\,500$ MPa. The column is subject to combined axial and lateral loads, with the factored gravity load of $0.3 f_c^{'} A_g$, which is 1200 kN. A 200 kN factored lateral load is applied at the mid-height of the column. The maximum moment at the critical section, which is the end of the column, is 300 kN·m.

The factored flexural resistance of the existing column is calculated to be 246 kN·m from sectional analysis of the column with the coexisting axial load, and assuming the extreme compressive strain of concrete reaches -0.0035. The factored resistance of the existing column under pure axial load is 2736 kN, obtained from $P_0 = \phi_c \alpha_1 f_c^{'}\left(A_g - A_s\right) + \phi_s A_s f_y$ and setting the upper limit as $0.80 P_0$. The factored shear resistance is 108 kN, calculated from Eqs. 2-11a to 2-11d, $V_r = \phi_c V_c + \phi_s V_s$, where V_c and V_s are the contributions to the shear capacity from the concrete and internal shear reinforcement. The existing column is assumed to have been constructed before strict requirements were introduced on shear reinforcement details. Such a column would typically have widely spaced internal shear reinforcement, hence, the internal shear reinforcement contribution can be neglected for a conservative estimate of original capacity. Thus, V_s can be taken as 0 kN.

Rehabilitation design procedure:

Initial evaluation of the flexural, axial and shear capacity of the column showed that this column is deficient in flexural as well as shear strength; hence, rehabilitation is required. The use of steel collars is evaluated as a technique to enhance the flexural and shear strength. The design procedure is described as follows:

[Step 1] Determine the factored flexural and axial requirements of the column: $M_f = 300$ kN·m, and $P_f = 1200$ kN. Perform a sectional analysis to obtain the P–M interaction diagram for the original column. It is found that the flexural and axial demands with the coordinates (M_f, P_f) of (300, 1200) fall outside the region enclosed by the interaction diagram, as shown in Figure 7-6.

[Step 2] Choose the size and spacing of the steel collars as 20×20 mm and 200 mm, respectively, according to the criteria described in Section 7.3.2: the dimension of 20 mm is larger than 30% of the largest longitudinal bars 25M (7.5 mm), and the spacing of 200 mm is smaller than the least of 16 times the diameter of the smallest longitudinal bars (400 mm), 48 tie diameter (480 mm), and the least cross-sectional dimension of the column (400 mm).

[Step 3] Calculate $f_{cc}^{'}$ according to the analytical model discussed in Chapter 2, Section 2.3 Eqs. 2-2 to 2-8. A value of $f_{cc}^{'} = 26.6$ MPa is obtained.

[Step 4] Perform an equivalent rectangular stress block sectional analysis to obtain a capacity point in the P–M interaction diagram for the column with the proposed collar configuration and corresponding confined concrete strength of $f_{cc}^{'} = 26.6$ MPa, as shown in Figure 7-6. It is found that the flexural and axial demands with the coordinates (M_f, P_f) of (300, 1200) falls outside the region enclosed by the interaction diagram for the proposed collar configuration selected at Step 2.

[Step 5]: To enhance the strength increase from the external steel collar scheme, the size and spacing of the steel collars was modified to reduce the collar spacing and increase the collar cross-sectional dimensions. Modify the size and spacing of the steel collars by using 30×50 mm steel collar spaced at 150 mm. Repeat Step 3 and obtain $f_{cc}^{'} = 36.3$ MPa, and repeating Step 4 shows that the flexural and axial demands are within the region enclosed by the interaction diagram as shown in Figure 7-6.

Finally, 30×50 mm steel collar spaced at 150 mm are the chosen size and spacing for flexural and axial rehabilitation.

Shear rehabilitation design procedure:

Note that the influence of the axial-shear interaction was already incorporated in the proposed shear strength model discussed in Chapter 6, Section 6.4, since this model was formed out of the analysis of columns under shear loading with and without axial loading.

The effect of axial load is explicitly included in Eq. 2-11d, which in turn is considered in the shear capacity in Eq. 6-1.

[Step 1] Since the column in this example has already been rehabilitated in flexure, the factored shear demand for this seismic rehabilitation is calculated assuming a flexural over-strength factor of 1.25 is applied to the flexural strength considering the confinement provided by the 30×50 mm steel collars spaced at 150 mm, hence $V_f = 261$ kN is obtained.

[Step 2] From the above flexural and axial rehabilitation design, 30×50 mm steel collars spaced at 150 mm were selected as the first trial size and spacing of the collars for the shear rehabilitation design. This collar size and spacing also meet the minimum shear reinforcement requirement according to CSA-A23.3-04 Clause 11.2.8.

[Step 3] Determine the shear contribution from the external steel collar, V_{sc}, and calculate the factored shear strength using the shear model proposed in Chapter 6, Section 6.4 Eqs. 6-1 to 6-2, and Eqs. 2-11b to 2-11d, with the effective strain of the steel collars taken as 500 microstrain and $V_r = 578$ kN is obtained.

[Step 4] Comparison between this factored peak lateral force and the factored shear force shows that $V_r \geq V_f$, hence the chosen size and spacing are acceptable. Therefore, 30×50 mm steel collars spaced at 150 mm are chosen as the size and spacing for the shear rehabilitation.

The final layout of the steel collars for the column rehabilitation is shown in Figure 7-7.

7.4.2 Example 2-Shear Rehabilitation of Columns in a Three-Story Building

Abou-Elfath and Ghobarah (2000) investigated the seismic performance of a three-storey nonductile reinforced concrete building rehabilitated using concentric steel bracing. The selected building was designed for gravity loads according to the 1963 ACI 318 code (Abou-Elfath and Ghobarah 2000). The concrete strength is 21 MPa and the reinforcing steel yield strength is 300 MPa. Dimensions and reinforcement details for interior and exterior beams and columns are shown in Figure 7-8. A typical elevation and plan of the building is shown in Figure 7-9. Transverse reinforcements (both ties and stirrups) with 90° hooks are assumed to be U.S. No. 3 bars spaced at 400 mm for interior columns and spaced at 300 mm for exterior columns. Concrete clear cover is assumed to be 20 mm for the columns. The design live load for the building is taken as 2.4 kN/m^2 and the ground snow load is taken as 1.6 kN/m^2, assuming the building is located in Vancouver.

Abou-Elfath and Ghobarah (2000) pointed out that the ratio of the ultimate base shear capacity to the weight of the existing building determined using a pushover analysis was 0.15. The ratio of the ultimate base shear to the weight for a similar building in the Vancouver area is 0.23 according to NBCC 1995. The base shear design value provided by Abou-Elfath and Ghobarah (2000) was based on importance and foundation factors of

unity and a reduction factor $R = 1$ (NBCC 1995) for a nonductile structure. Hence, according to Abou-Elfath and Ghobarah (2000), rehabilitation is needed to increase the lateral load resistance capacity of the original columns to a value higher than the NBCC 1995 design lateral load. Abou-Elfath and Ghobarah (2000) proposed rehabilitation with concentric steel bracings and studied different bracing layouts. In the current study, the nonductile frame columns were considered to be rehabilitated with external steel collars. A check on the flexural rehabilitation needs and consideration of the shear corresponding to the collar-enhanced flexural failure mode would ordinarily be needed in this type of rehabilitation application. However, since no detailed flexural requirement information was available in the report by Abou-Elfath and Ghobarah (2000), only shear rehabilitation is considered in the current example.

For the external steel collar rehabilitation option in this study, the modulus of elasticity of the steel collars, E_{sc}, is assumed to be 200 000 MPa. Only columns in the first floor are considered in this example. For interior columns, the factored axial compressive load is found to be 1057 kN, which is about $0.31 f_c' A_g$. For exterior columns, the factored axial compressive load is 561 kN, which is about $0.30 f_c' A_g$.

The shear contribution from concrete, axial compressive load, internal shear reinforcement, and steel collars can be obtained using the empirical shear model reported in Chapter 6.

$$V_n = V_c + V_s + V_{sc} \qquad [7\text{-}1]$$

$$V_r = \phi_c \cdot V_c + \phi_s \cdot V_s + \phi_{sc} \cdot V_{sc} \qquad [7\text{-}2]$$

$$V_r = 0.65 \cdot V_c + 0.85 \cdot V_s + 0.85 \cdot V_{sc} \qquad [7\text{-}3]$$

In the original column, a shear resistance of $0.15W$ is provided by the shear capacity contribution from the concrete (V_c) and the internal stirrups (V_s). The rehabilitated column must provide a greater shear resistance than $0.23W$ from the V_c, V_s, and collar (V_{sc}) components. Thus, the required V_{sc} can be determined through the ratio:

$$\frac{0.85 \cdot V_{sc}}{0.65 \cdot V_c + 0.85 \cdot V_s} \geq \frac{0.23W - 0.15W}{0.15W} \qquad [7\text{-}4]$$

By rearranging Eq. 7-4, one can obtain:

$$0.85 \cdot V_{sc} \geq 0.53 \cdot (0.65 \cdot V_c + 0.85 \cdot V_s) \qquad [7\text{-}5]$$

where V_n and V_r are the nominal and factored shear capacities, respectively, of a reinforced concrete column rehabilitated with external steel collars, which is equal to the

sum of the contributions from the concrete, V_c, the internal shear reinforcement, V_s, and the external steel collars, V_{sc} (this contribution does not exist before rehabilitation), and W is the weight of the structure.

For an interior column:

$$0.85 \cdot \frac{A_{sc}\varepsilon_{esc}E_{sc}d_{sc}\cot\theta}{s_{sc}} \geq 0.53 \cdot (0.65 \cdot V_c + 0.85 \cdot V_s) \qquad [7\text{-}6]$$

$$\frac{A_{sc}}{s_{sc}} \geq 3.39 \text{ mm} \qquad [7\text{-}7]$$

where A_{sc} is the cross-sectional area of the collar, ε_{esc} is the effective strain of the steel collar taken as 500 microstrain in the current study, E_{sc} is the modulus of elasticity of the steel collars, d_{sc} is the effective shear depth for the steel collars, θ is the direction of the average principal compression with respect to the longitudinal axis, and s_{sc} is the spacing of the external steel collars.

Possible collar configurations that satisfy this requirement include 30×30 mm steel collars spaced at 250 mm; 20×30 mm steel collars spaced at 175 mm; and 20×20 mm steel collars spaced at 100 mm.

For an exterior column:

$$0.85 \cdot \frac{A_{sc}\varepsilon_{esc}E_{sc}d_{sc}\cot\theta}{s_{sc}} \geq 0.53(0.65 \cdot V_c + 0.85 \cdot V_s) \qquad [7\text{-}8]$$

$$\frac{A_{sc}}{s_{sc}} \geq 2 \text{ mm} \qquad [7\text{-}9]$$

Possible configurations include: 20×30 mm steel collars spaced at 225 mm; and 20×20 mm steel collars spaced at 150 mm.

Select 20×30 mm steel collars with a centre-to-centre spacing of 175 mm for interior columns and 225 mm for exterior columns for this example. With the selected collar configuration, the shear strength and flexure strength of the interior collared column and the exterior collared column must be checked with the proposed strength model discussed in Chapter 6, Section 6.4. Assuming a flexure over-strength factor of 1.25 (applied to the rehabilitated flexural capacity), the required shear capacity corresponding to the flexural strength of the interior collared column is 159 kN. The shear strength of the collared interior column is 300 kN, hence, the relatively ductile flexural failure mode governs. Similarly, required minimum shear strength of the exterior collared column accounting

for flexural overstrength is 74 kN. The provided shear strength of the collared exterior column is 131 kN, hence, the relatively ductile flexure failure mode governs. Thus, 20×30 mm steel collars are used for both interior and exterior columns but with different centre-to-centre spacing: 175 mm and 225 mm for interior and exterior columns, respectively. The layout for the steel collars for the rehabilitation design is shown in Figure 7-10.

7.4.3 Example 3-Shear Rehabilitation of Beam

Although the guidelines discussed in Section 7.3 pertain to the rehabilitation of columns, external steel collars may also be considered for rehabilitation of beams. A similar design principle can be adopted for rehabilitation of beams subjected to combined flexural, axial and shear demands. The rehabilitated member should target a more ductile failure mode than brittle shear failure.

Duong *et al.* (2007) studied the behaviour of a shear-critical reinforced concrete building frame under reversed cyclic lateral loads. A single-bay, two-storey, reinforced concrete frame with shear-critical beams was constructed and tested until significant shear damage occurred in the first floor beam. Dimensions and reinforcement details for the beams and columns in the tested frame are shown in Figure 7-11. Axial load of 420 kN was applied during the tests. The beams were then repaired with five carbon fibre reinforced polymer (CFRP) strips that were wrapped fully around each beam. Each strip was 150 mm wide and equally spaced along the length of the beam. An overlap of 75 mm was used for all the CFRP strips at the top surface. The rehabilitated frame was then retested to failure. The peak shear force in the original first-storey beam was estimated to be 202 kN using the CSA-A23.3-04 code provisions, while the peak shear force for the rehabilitated first-storey beam was found to be at least 264 kN. Thus, an enhancement of 62 kN in the shear capacity was reported due to the introduction of the CFRP strips.

In this design example, an alternative rehabilitation system with external steel collars is investigated, with a similar target minimum enhancement to the nominal beam shear capacity of 62 kN. Note that since measured capacities from the experimental test are compared in this example, all load and resistance factors are taken as unity. The modulus of elasticity of the steel collars, E_{sc}, is assumed to be 200 000 MPa in this study, as shown in Figure 7-12.

The shear contribution from steel collars can be obtained using the empirical shear model reported in Chapter 6, Section 6.4 Eqs. 6-1 to 6-2, and Eqs. 2-11b to 2-11d:

$$\frac{A_{sc}\varepsilon_{esc}E_{sc}d_{sc}\cot\theta}{s_{sc}} \geq (264-202) = 62\,\text{kN} \qquad [7\text{-}10]$$

$$\frac{A_{sc}}{s_{sc}} \geq 1.99\,\text{mm} \qquad [7\text{-}11]$$

Possible collar configurations include: 20×20 mm steel collars spaced at 200 mm and 20×30 mm steel collars spaced at 300 mm. Considering the suggestion based on the currently available information that spacings be no greater than 75% of the smaller cross-sectional dimension of the primary member, 20×20 mm steel collars spaced at 200 mm is selected for beam shear rehabilitation for this example. Hence, a total of eight steel collars are needed for the first storey beam. The proposed layout for the steel collar rehabilitation option is shown in Figure 7-12. The procedure to determine collars for strengthening of the second storey beam would be similar.

7.5 Summary

The design guidelines presented in this chapter were developed by a combination of experimental and analytical results in previous chapters and existing practices for the design of reinforced concrete frame members. The design methodology was illustrated by three design examples. They are generically applicable to rehabilitation of reinforced concrete columns or beams.

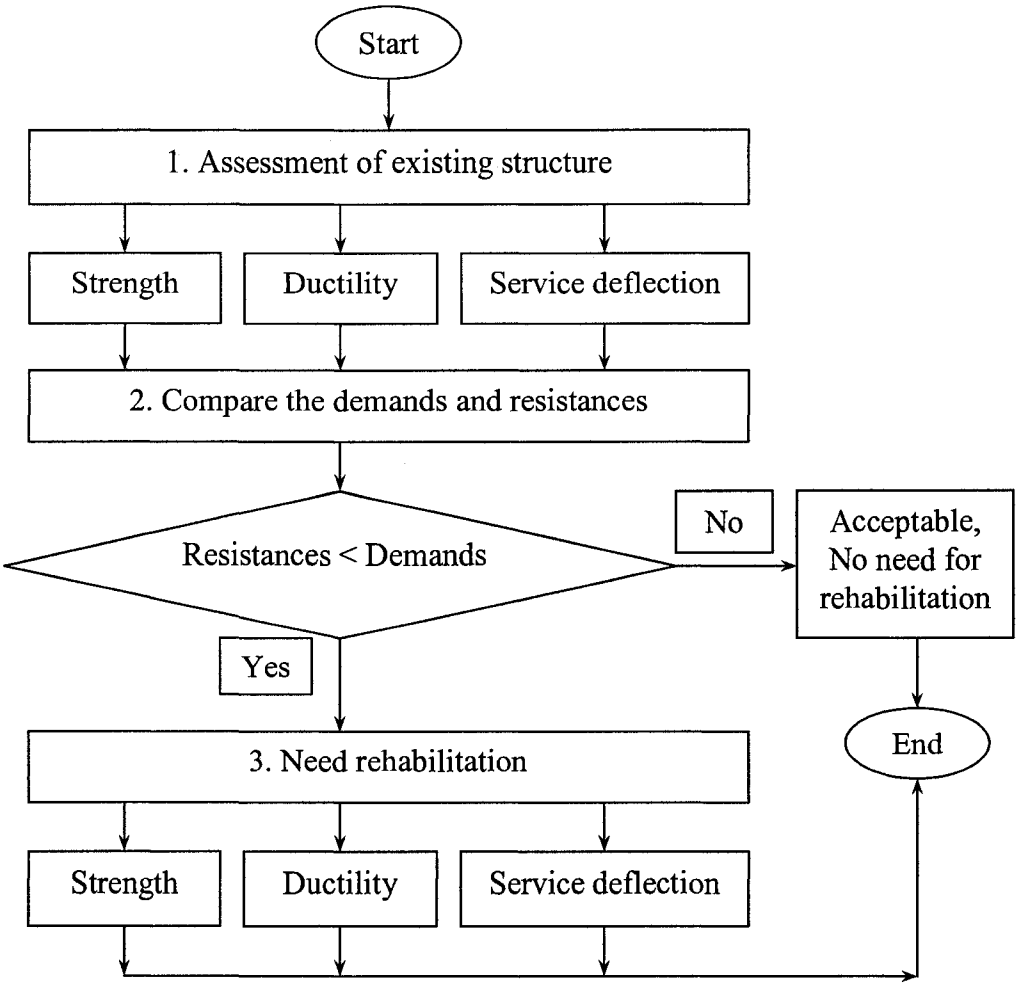

Figure 7-1 Rehabilitation design goal flowchart

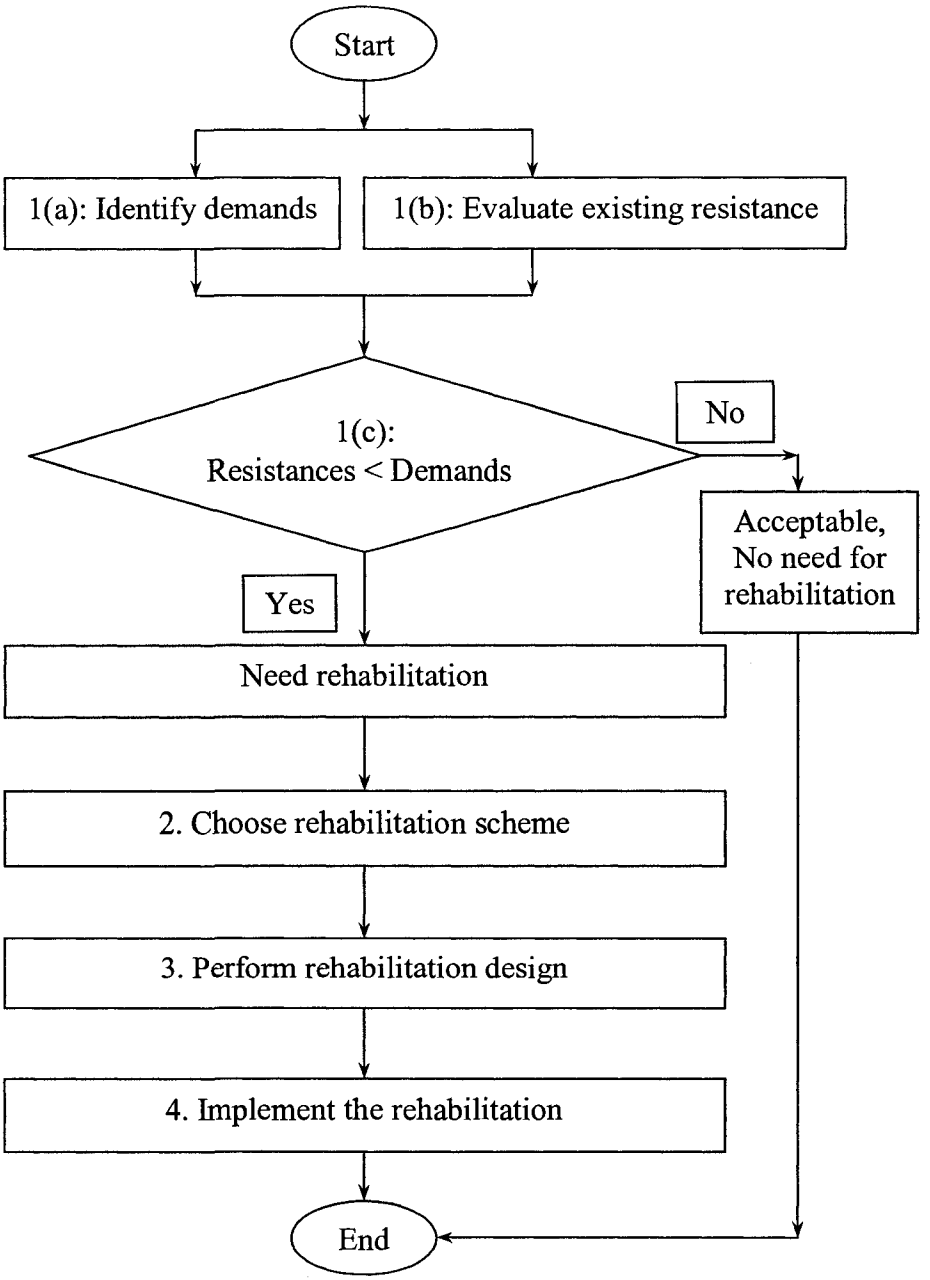

Figure 7-2 Overall rehabilitation procedures flowchart

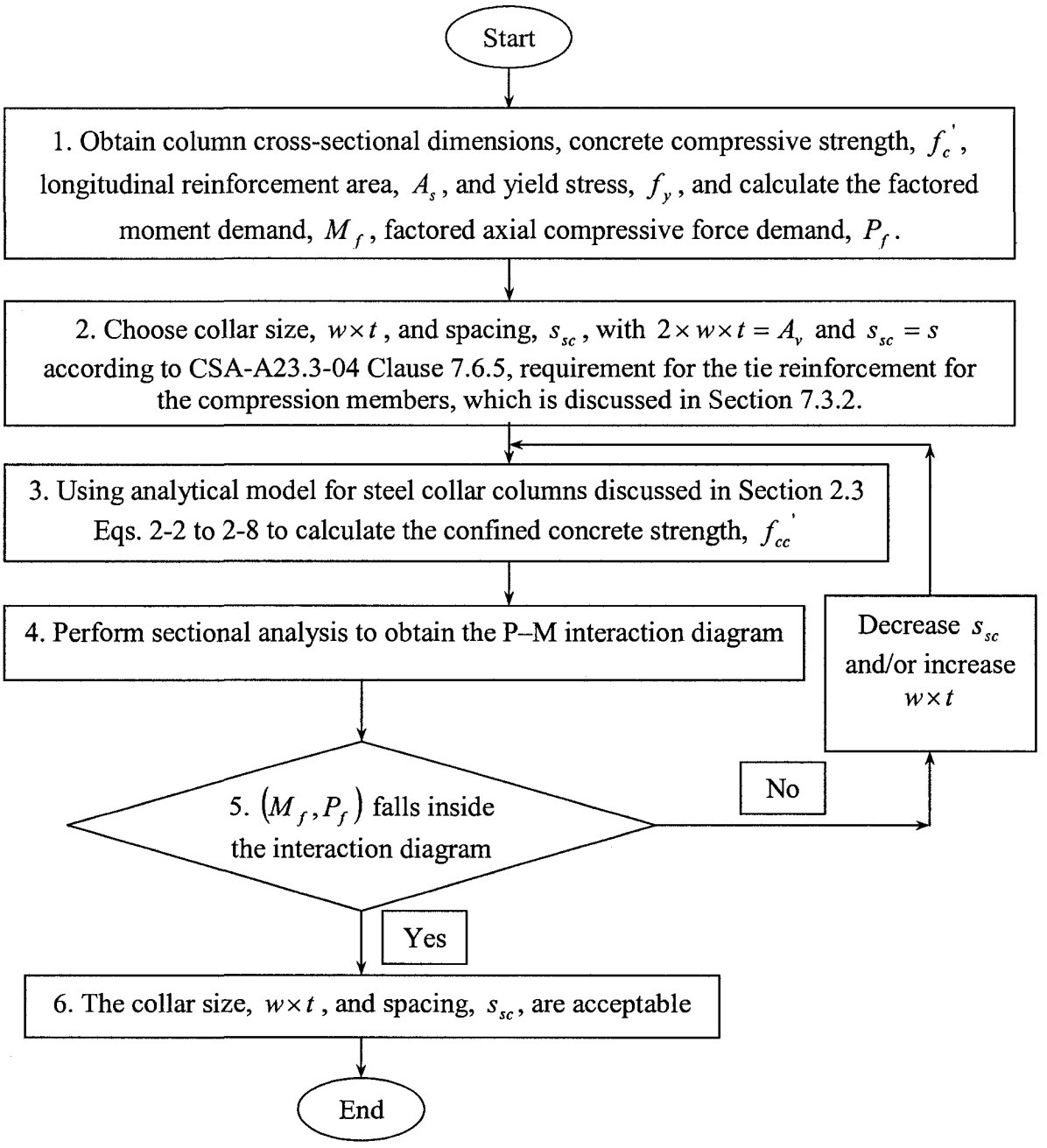

Figure 7-3 Proposed flexural and axial rehabilitation design flowchart

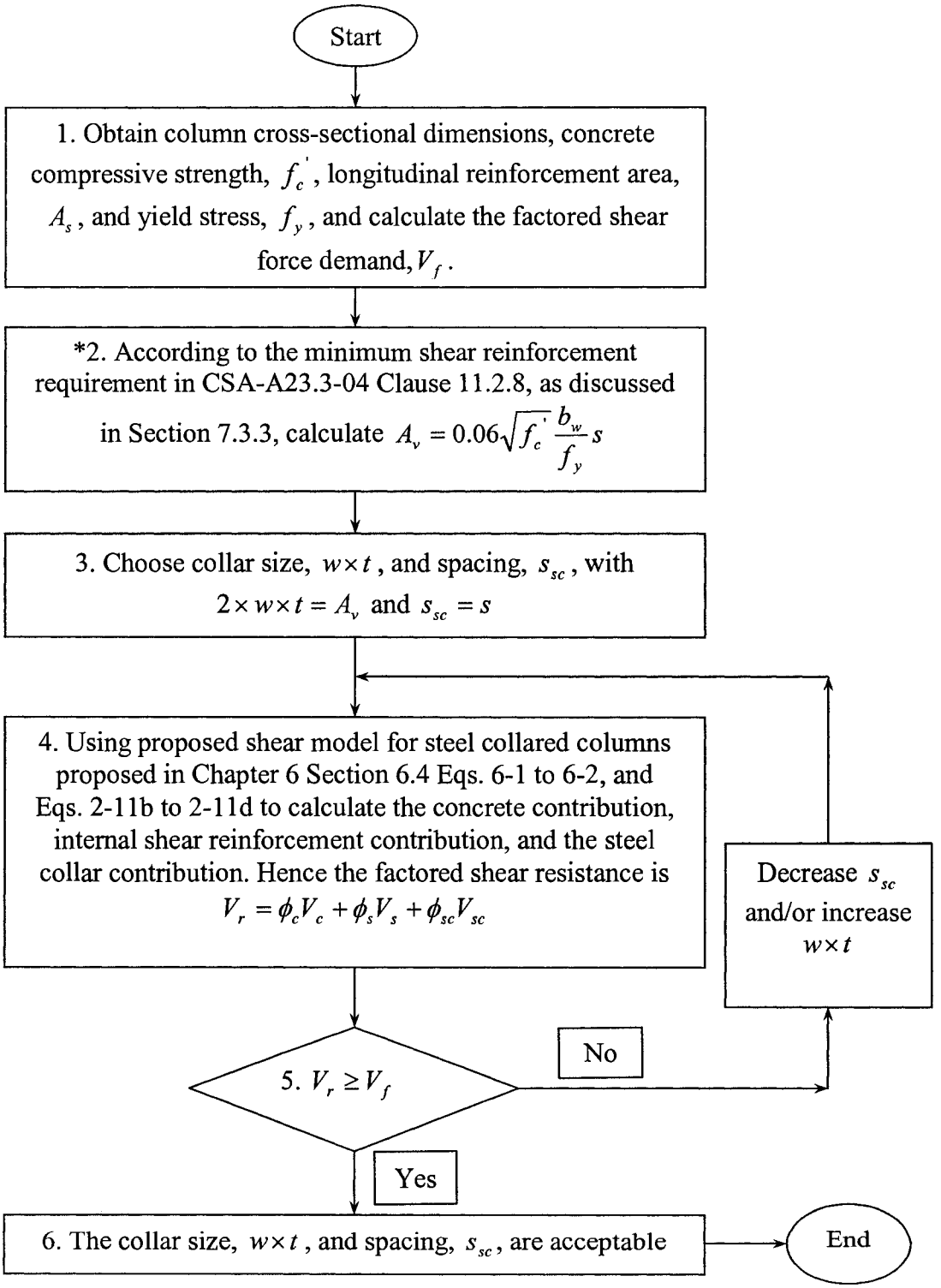

* Alternatively, a set of s_{sc} and $w \times t$ can be estimated to start the iteration, and with a check the minimum shear reinforcement.

Figure 7-4 Proposed shear rehabilitation design flowchart

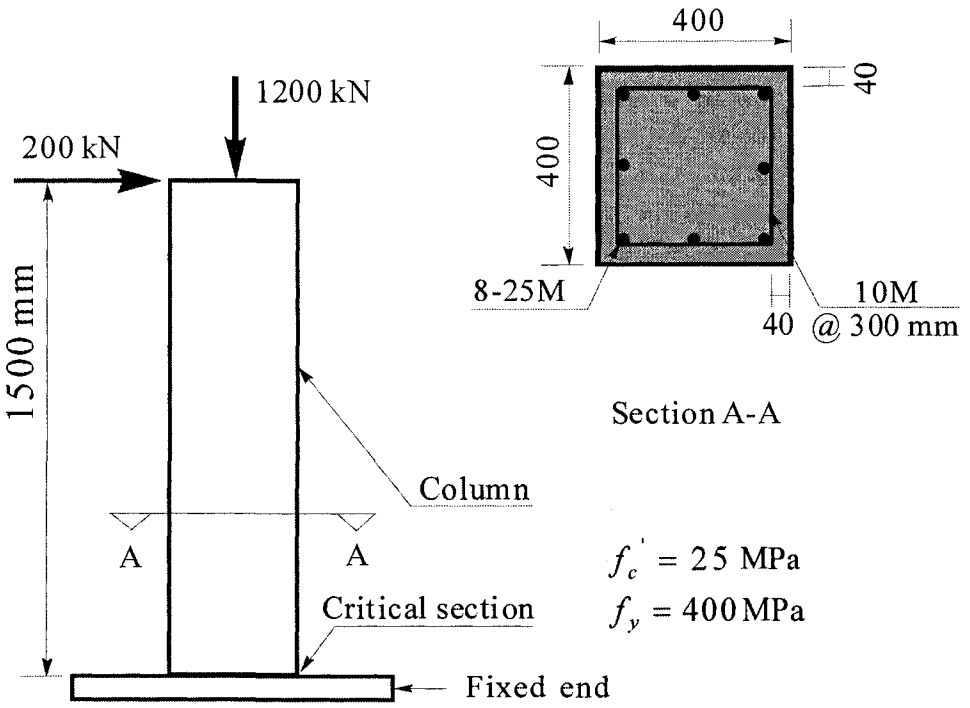

Figure 7-5 Details for design example 1 column

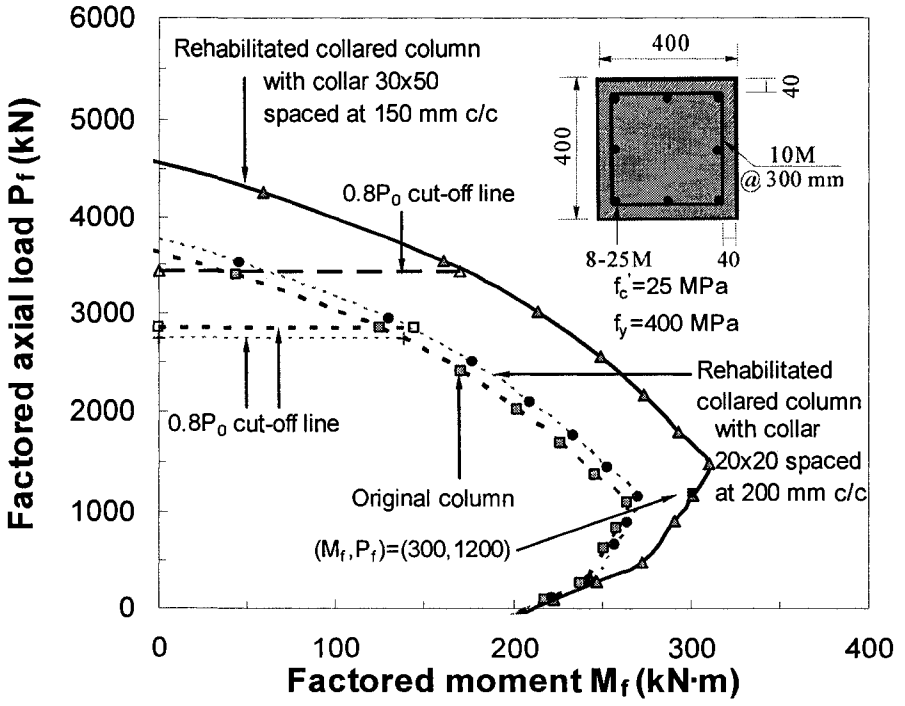

Figure 7-6 The axial-moment (P–M) interaction diagram for the example 1 column

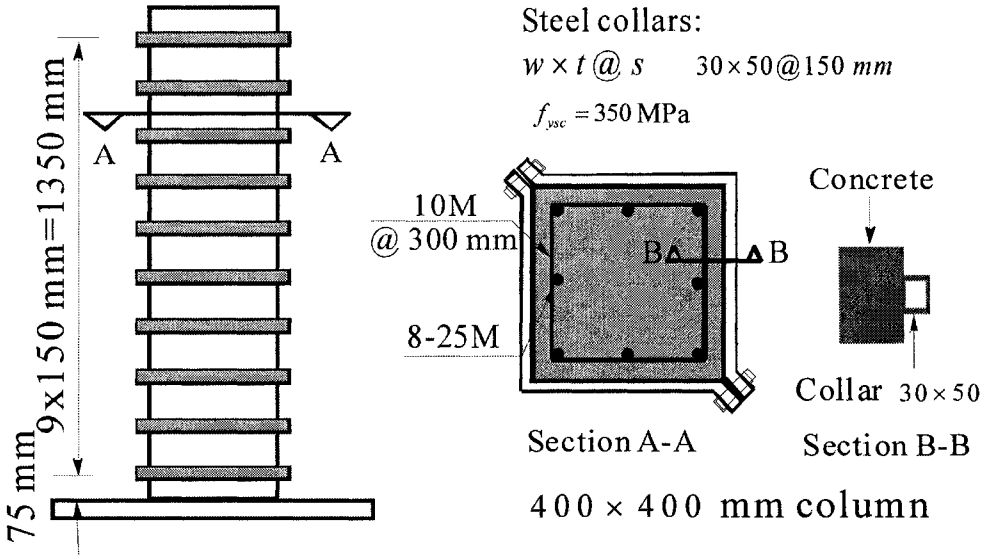

Figure 7-7 Steel collar layout for design example 1

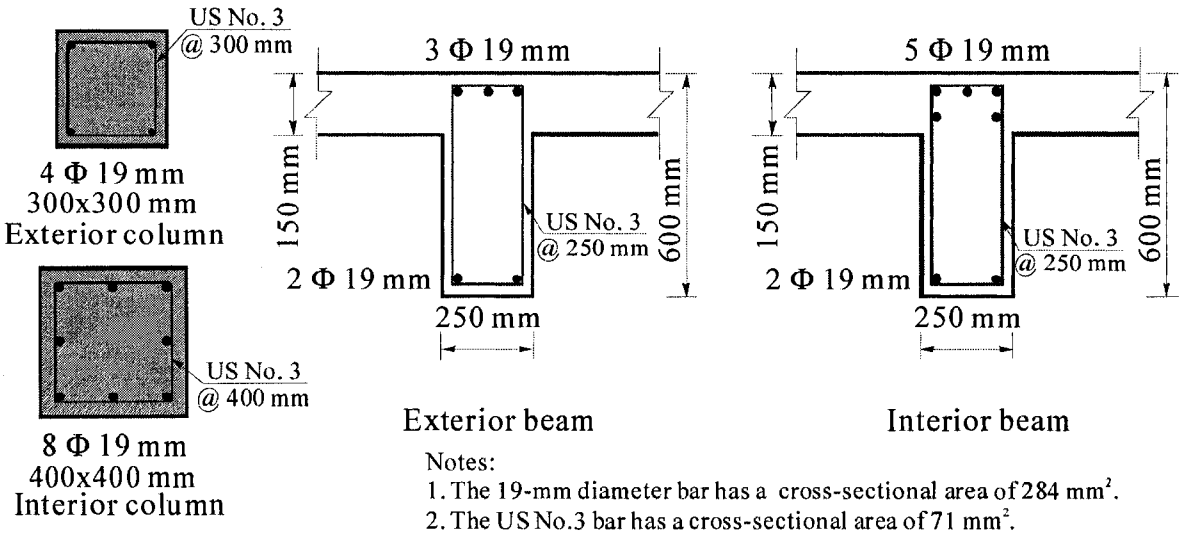

Notes:
1. The 19-mm diameter bar has a cross-sectional area of 284 mm^2.
2. The US No.3 bar has a cross-sectional area of 71 mm^2.

Figure 7-8 Details of columns and beams for design example 2 (adapted from Abou-Elfath and Ghobarah 2000)

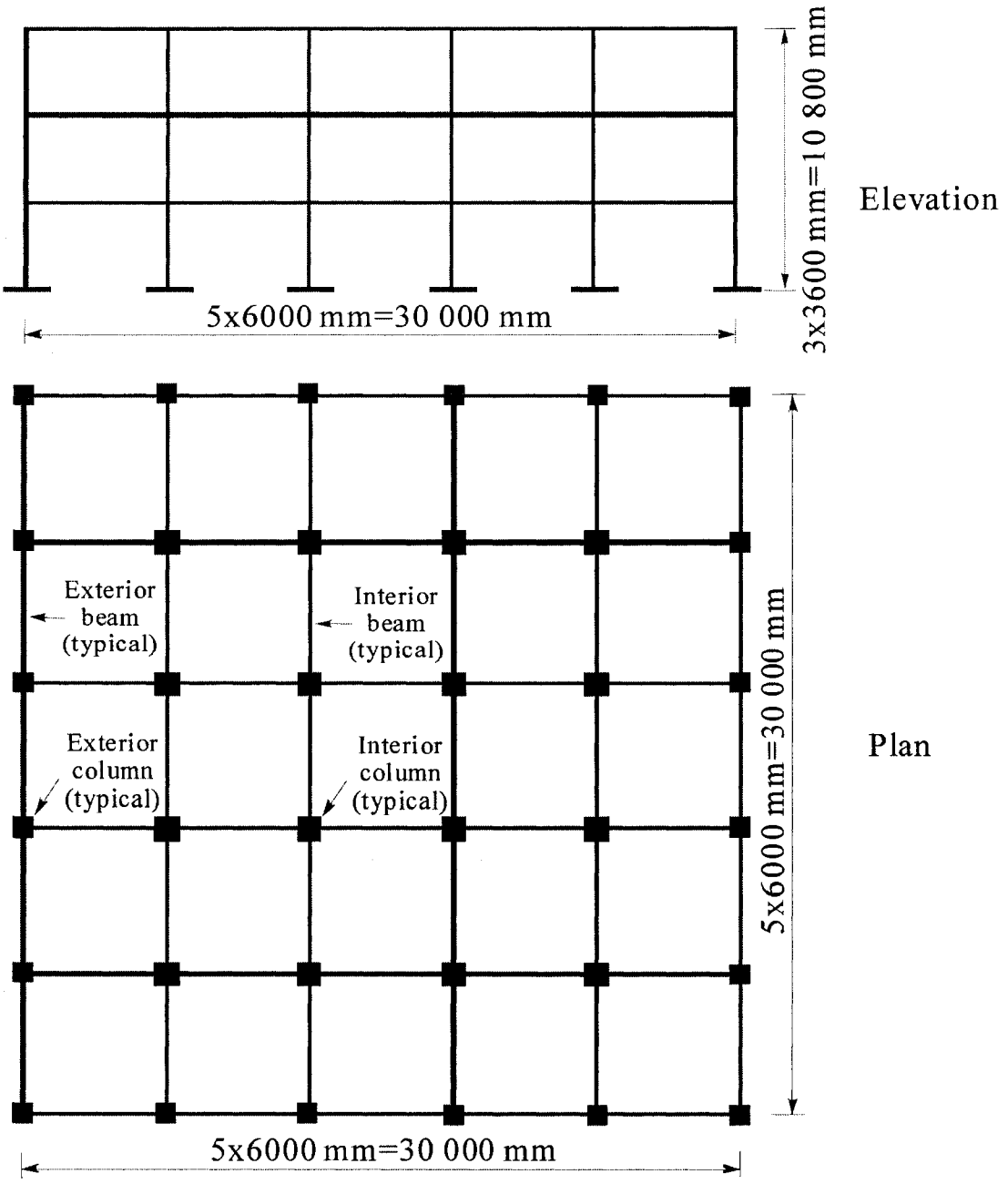

Figure 7-9 Dimension of the 3-story office building for design example 2

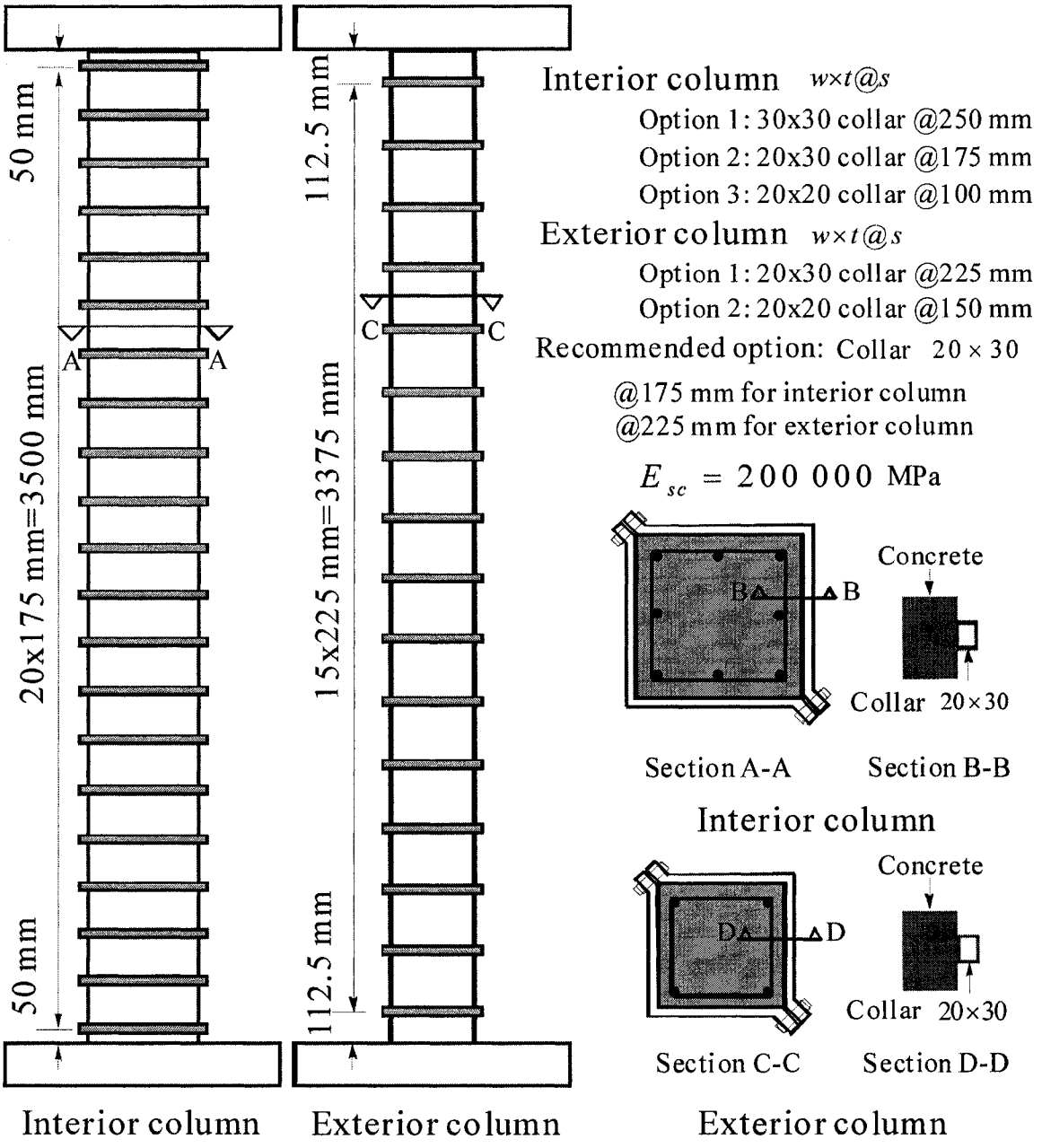

Figure 7-10 Steel collar layout for design example 2

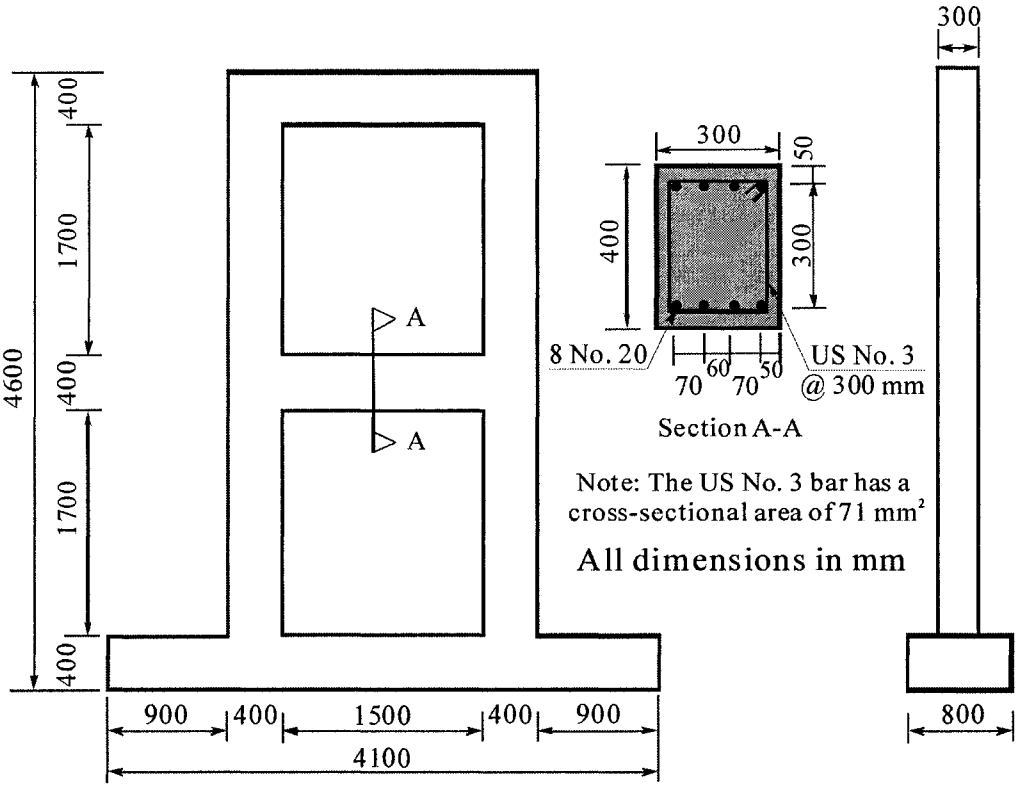

Figure 7-11 Details of design example 3 (adapted from Duong *et al.* 2007)

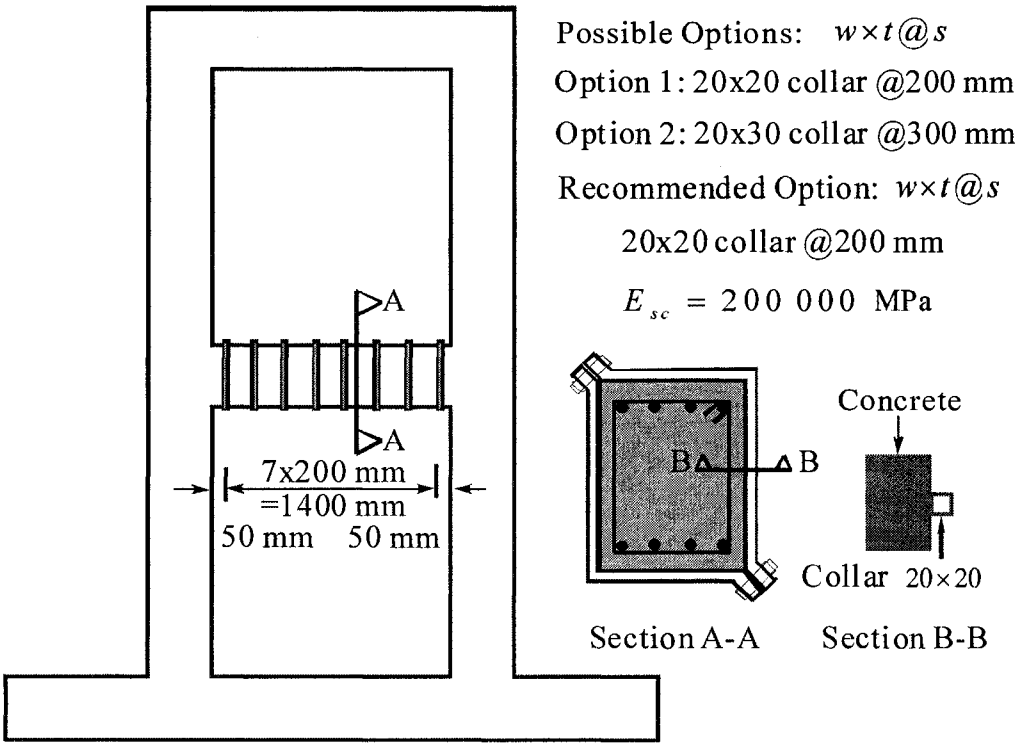

Figure 7-12 Steel collar layout for design example 3

CHAPTER 8 SUMMARY, CONCLUSIONS, AND RECOMMENDATIONS

8.1 Summary

The objective of the ongoing research at the University of Alberta is to evaluate the effectiveness of the proposed rehabilitation scheme for deficient reinforced concrete frame columns with external steel collars. This proposed rehabilitation scheme has been demonstrated to be a promising rehabilitation solution through research examining the behaviour of collared reinforced concrete columns under concentric and eccentric axial loading, and under combined axial and flexural-dominant lateral loading.

In the current study, the behaviour of reinforced concrete short columns was studied experimentally and analytically. An experimental program involving construction and eleven tests on ten full-scale reinforced concrete short columns was conducted. The primary parameters studied in the experiments include collar spacing, collar size/stiffness, longitudinal reinforcement ratio, axial compression index, pretension of collar bolts, and shear span-to-depth ratio. Pseudo-seismic force and gravity force were used to simulate the conditions of earthquake loading. Three-dimensional nonlinear finite element models were established with ABAQUS/Explicit program and were validated with the experimental results. The finite element models were also used to study how the behaviour of the collared reinforced concrete short columns was influenced by various parameters through a parametric study. Research was conducted to examine the peak lateral force of the collared reinforced concrete columns with other conventional computation approaches, such as CSA-A23.3-04 and ACI 318-05 code provisions, Response 2000 program, and strut-and-tie model. A new strength model for columns with external steel collars was proposed based on the current and prior test data and results from the validated finite element model. Finally, design guidelines were proposed for the rehabilitation of reinforced concrete frame columns using the proposed strength model.

8.2. Conclusions

Based on both the experimental and analytical study of the behaviour of collared reinforced concrete short columns, along with previous research results, this rehabilitation technique is shown to be effective for seismic rehabilitation of deficient reinforced concrete columns. Conclusions can be drawn from the experimental and analytical study as follows.

8.2.1 Experimental Behaviour of Collared Columns

Experimental results showed that external steel collars, with significant flexural and axial stiffness, provide significant confinement to the existing concrete columns. The collars were demonstrated to improve the strength of the existing (unrehabilitated) columns, and to enhance the ductility and energy dissipation capacity of the columns.

The external steel collars were bolted in place, directly on the surface of the square columns. Unlike other rehabilitation techniques, no rounding of the corners at a certain

radius was needed prior to installation. The viability of using pretensioned collar bolts was demonstrated.

Collared reinforced concrete columns subject to combined axial and cyclic lateral loading experienced less damage than control columns without collars, and remained intact at much larger imposed displacements. No slippage of the collars was observed during the tests of collared columns, even when severe spalling and crushing of cover concrete took place between them, implying the composite action between concrete and steel collars has been achieved. This feature is beneficial for seismic rehabilitation.

In general, collared reinforced concrete columns attained much higher ultimate drift ratio, showed improved deformability, and exhibited much better energy dissipation capacity under cyclic loading than control columns without collars, which are beneficial to the structure prone to earthquake. Collared reinforced concrete columns showed impressive ductile response with stable hysteresis loops and gradual post-peak degradation. All collared reinforced concrete columns exhibited 14% to 93% higher normalized peak lateral force than the control column with internal conventional transverse reinforcement spaced at 400 mm (CV0A) except the collared reinforced concrete column without axial compressive load exhibited 5% lower normalized peak lateral force. All collared reinforced concrete columns attained ductility 7% to 122% higher than this control column (CV0A). Furthermore, the ultimate drift ratios for all the collared reinforced concrete columns were 54% to 508% higher than this control column (CV0A). It was also found that the total energy dissipated by the collared reinforced concrete columns was 1.6 to 23.7 times that dissipated by the control column without collars (CV0A). The repaired specimen demonstrated significantly improved ductility, deformability, energy dissipation, and enhancement in strength over the original control column. These observations validate the feasibility and effectiveness of this rehabilitation technique.

Decreasing the centre-to-centre collar spacing from 200 mm to 95 mm improved the overall behaviour of the collared reinforced concrete column with less concrete spalling and crushing, including 12% increase in normalized peak lateral force, 46% increase in displacement ductility, 87% enhancement in drift ratio, and 2.8 times the energy dissipated.

For collared reinforced concrete columns, decreasing the longitudinal reinforcement ratio from 3.13% to 1.88% reduced the normalized peak lateral force by 9%, but increased the displacement ductility by 69%, the ultimate drift ratio by 61% and the energy dissipated by 43%.

Increasing the aspect ratio of the collared reinforced concrete column from 0.88 to 1.63 resulted in a 56% decrease in normalized peak lateral force, but an increase in displacement ductility by 26%, the ultimate drift ratio by 87%, and the energy dissipated by 490%.

The collared reinforced concrete column with axial compression load of $0.3f_c^{'}A_g$ (CV1) exhibited a 31% enhancement in normalized peak lateral force, but a 42% decrease in the

ultimate drift ratio compared to the collared reinforced concrete column without axial compressive load (CV6). The total energy dissipated by specimen CV6 is 0.6 times that dissipated by CV1, while the displacement ductilities are similar.

Comparison between collared reinforced concrete column with pretension applied to the connection bolts (CV7) and collared reinforced concrete column with snug-tight connection bolts (CV1) showed that an increase of 20% in the normalized peak lateral force, 19% enhancement in the energy dissipation, but only marginal increase in displacement ductility and ultimate drift ratio. The bolt pretension was at 35% of the minimum specified tensile strength of the bolt.

Collared reinforced concrete column CV8 with a larger size of external collars (50×50 mm) and hence large collar stiffness exhibited 5% higher normalized peak lateral force than the collared reinforced concrete column CV1 with smaller size of external collars (30×50 mm) and hence smaller collar stiffness. The displacement ductility of column CV8 was increased by 56% and the ultimate drift ratio enhanced by 50%, while the total energy dissipated increased by 64% from column CV1.

Epoxy mortar injection followed by installation of collars proved to be a promising repair method that is easy to implement and quick to serve its function. A 28% enhancement in the normalized peak lateral load, 64% enhancement in displacement ductility, and 22.7 times increase in energy dissipated was obtained in CV0AR compared to the original control column before rehabilitation (CV0A). This level of enhancement showed that proper repair to an initially damaged reinforced concrete column with epoxy mortar and external steel collars can achieve good performance. CV0AR was similar in final configuration to the base case collared column (CV1). The similar normalized peak lateral force attained by specimen CV0AR, 25% enhancement in the displacement ductility, 55% increase in the ultimate drift ratio, and 1.6 times increase the energy dissipated as compared to the base case collared column (CV1) indicates that external steel collars and epoxy grout can rehabilitate specimens and exhibit behaviour as good as an undamaged collared column.

The experimental results of the collared reinforced concrete columns and columns without collars demonstrated that, for the same specimen size and longitudinal reinforcing bars, collared reinforced concrete columns exhibited higher peak lateral force, displacement ductility, greater energy dissipation, and more stable hysteresis loops with less degradation. The overall behaviour of the collared reinforced concrete column was much improved from columns without collars due to the existence of external steel collars.

8.2.2 Analytical Behaviour of Collared Columns

Analytical behaviour of collared column has been studied from finite element analysis and other analytical approaches.

8.2.2.1 Finite Element Analysis

Comparisons between a pushover finite element model developed using ABAQUS/Explicit and the experimental results showed that the model offered a reasonably reliable analytical tool that was capable of capturing the major performance characteristics of collared reinforced concrete columns under combined axial and lateral loading. Although the finite element models generally overestimated the column lateral stiffness in the initial part of the test and did not fully catch the post-peak degradation, it was shown that the proposed model was capable of predicting the peak lateral force with reasonable accuracy. For the columns studied, the mean experiment-to-analysis capacity ratio was 1.05, with a coefficient of variation of 0.13.

Parametric studies showed that with the increase of external steel collar spacing, the peak lateral force decreased and more brittle behaviour in the post-peak region was observed. With increased axial compression load, longitudinal reinforcement ratio, or concrete compressive strength, the peak lateral force also increased but a less ductile and less stable response with faster post-peak degradation was found. The influence of the aspect ratio on the behaviour of the collared reinforced concrete column was that increasing the aspect ratio resulted in a decrease of the peak lateral force but with a more ductile response. Pretension force applied to the steel collar bolts was observed to affect the overall behaviour of the collared reinforced concrete column during the experimental program. However, this influence was not apparent in the finite element analysis parametric study for unknown reasons. Increases in the axial or the flexural stiffness of the collars influenced the strength of the collared reinforced concrete column but to different extents. Influence of those two factors, however, tended to reach a limit after some values.

8.2.2.2 Analytical Approaches

Comparisons were made between the predicted strengths according to various analytical models with the peak lateral force values for the test specimens. Codes CSA-A23.3-04 and ACI 318-05, software Response 2000, and the strut-and-tie methods were examined. All models typically provided conservative results for most cases, but unconseravtive predictions occurred for the column with small aspect ratio (CV5) by codes CSA-A23.3-04 and ACI 318-05.

A new strength model for collared reinforced concrete columns was proposed. The proposed model is based on the format of the code sectional equations for shear and flexure, but considers the confined concrete strength and effective strain of external steel collars. The final predicted capacity and governing mode of failure were determined as the lower value of predicted strength for the flexural or shear capacities. The flexural model used a layered sectional approach with concrete confinement according to a procedure that was proposed by Chapman and Driver (2006) and discussed in Chapter 2, Section 2.4.3. The shear strength model used a composition approach for the contributions of concrete and truss mechanisms. Capacity predictions using the proposed model were compared with specimen test results from three collared column

experimental programs conducted at the University of Alberta as well as columns from the parametric study conducted using the developed finite element model. The model was in reasonable agreement with the test results. More accurate prediction of the steel collar contribution and confined concrete strength are required to improve the proposed model. However, the proposed model represents an initial step towards a simplified design approach for external steel collars around reinforced concrete columns.

8.3 Recommendations for Future Research

Based on the findings from current research, the following major research areas are recommended for future work.

8.3.1 Experimental Research

1. Additional full scale laboratory tests should be conducted on collared reinforced concrete columns with other geometry of steel collars to confirm the results obtained from the finite element parametric study.

2. Systematic experimental study of column with shear failure in the absence of flexural yielding and under monotonic loading is needed in order to further validate the proposed shear capacity model. In the current study, most specimens had longitudinal bars which yielded prior to final failure. The cyclic loading also resulted in degradation of the shear capacity with increased cycles and increased specimen deformation, and thus the ability to predict the monotonic shear capacity of a short collared column is uncertain. Furthermore, the proposed shear strength model included an effective strain term with assumed value, which requires further assessment. Hence additional tests on specimen with shear-critical behaviour under monotonic loading are needed.

3. An experimental study should be initiated to investigate the behaviour of collared reinforced concrete columns under other loading conditions, such as biaxial lateral loading, and variable axial loading. Actual seismic action usually involves biaxial lateral movement in a random pattern of horizontal displacement, rather than the uniaxial lateral movement considered in the present research (Jirsa *et al.* 1980; Kobayashi *et al.* 1986). Previous research demonstrated that in comparison with uniaxial displacement paths, biaxial displacements lead to more severe degradation of stiffness and strength and hence also energy dissipation (Jirsa *et al.* 1980; Kobayashi *et al.* 1986; Wong *et al.* 1993). In general, the ultimate strength under biaxial lateral loading was lower than that under uniaxial lateral loading. Even if a column was designed to be flexural-critical under uniaxial lateral loads, shear failure might occur when the column is subjected to biaxial lateral loads. Most previous research on reinforced concrete columns subject to seismic action has been conducted under constant axial load and a lateral monotonic or cyclic displacement or force. However, as pointed out by Esmaeily and Xiao (2004), in some earthquakes the strong vertical motion has played a significant role in the damage of the reinforced concrete structures. The vertical force due to the vertical ground motion is not necessarily proportional to the horizontal loading nor remains constant. Research using columns subject to variable axial loads is needed. The performance of collared reinforced

concrete columns subjected to a combination of variable axial load and various levels of lateral load reversing cycles need to be studied.

4. All previous research on the collared reinforced concrete columns has dealt exclusively with columns having square cross-sections. In order to generalize the conclusions of those studies, columns with rectangular (unsymmetric) cross-section should be investigated. It is anticipated that the behaviour of a rectangular cross-section cannot be adequately represented by the results obtained from a square section. This is especially true for the shear capacity of a rectangular cross-section loaded in some arbitrary diagonal direction.

5. One of the main concerns about the seismic performance of as-built reinforced concrete frame column has been the insufficient development length of vertical reinforcement at lap-splice regions at the bottom of columns. Insufficient splices may result in loss of column strength and stiffness, and strength degradation resulted from bond deterioration between the reinforcement bars and the surrounding concrete, causing premature failure of the structure. (Melek and Wallace 2004, Valluvan *et al.* 1993) Rehabilitation techniques, such as use of steel angles and straps or ties with grout and welding the lap spliced bars, improved the performance of the specimens with short lap-splice. Failure can be prevented if the confinement in the fracture surface provides an adequate clamping pressure so that the bar forces can be transferred. Valluvan *et al.* (1993) tested twelve specimens to examine two approaches for strengthening column splices. Aboutaha *et al.* (1996) indicated that using steel jackets is an effective method for improving the cyclic response of columns with compression lap splices. Ghosh and Sheikh (2007) studied seismic upgrade with carbon fibre-reinforced polymer of columns containing lap-spliced reinforcing bars. Study on the rehabilitation of those deficient columns with inadequate lap splices using external collars should be conducted.

6. Tests are required for reinforced concrete frames rehabilitated with steel collars and infill steel plate shear wall panels to evaluate the effectiveness of the combined rehabilitation system. Previous experiments have applied external lateral loads directly to the column rather than applying external loads to the collars. There is concern that if a steel plate shear wall panel is connected directly to the steel collars the rehabilitation effectiveness of each collar may be reduced due to corresponding changes in confinement provided by the steel collars.

7. Future experimental programs should seek to determine the appropriate dilation angle for concrete for use in the finite element simulations of collared reinforced concrete columns. Modeling results tend to be very sensitive to selected dilation angle, however, Values used by other researchers are not consistent and there is no widely accepted simple way to experimentally obtain the value for this parameter. Targeted experiments need to be conducted to enhance the understanding of this parameter and lead to simpler techniques to arrive at an appropriate value.

8.3.2 Analytical Research

1. Perfect bond was assumed between the reinforcement and concrete in conducting finite element analysis of the collared reinforced concrete columns. This is a reasonable and widely accepted practice for pushover analysis under monotonic loading. Cyclic loading, however, may influence the reinforcement-concrete interface behaviour. As the number of cycles increases, the bond strength might decreases significantly. This was evidenced in the current investigation by the observation of cracks along the longitudinal bars during the experiments. The use of the perfect bond assumption in the current analytical investigation may have contributed to the overestimation of lateral stiffness in the models. In order to improve the analytical models, a realistic interfacial bond-slip model between the concrete and longitudinal reinforcement needs to be studied instead of assuming perfect bond. It is expected that an interface element with bond-slip relationship that considers the degradation due to cyclic loading can better capture the general behaviour of collared columns through finite element analysis.

2. Degradation of response due to the cyclic loading in the tests was not considered when performing pushover numerical analysis. This resulted in higher modelled stiffness than the tests. Hence, further work to simulate reverse-cyclic loading during modelling is needed, including incorporation of the mechanical properties of the materials under reversed cyclic loading conditions.

3. Sectional flexural analysis based on a moment-curvature approach has been conducted with the confined concrete stress-strain relationships. However, additional study is required on methods to better model the confinement level introduced by the external steel collars under axial and lateral cyclic loading, including the effect of strain gradients.

4. Research to establish the reliability factors is needed, such as the resistance factors for concrete and steel, lateral force reduction factors for use in seismic design, to obtain more efficient and reliable design guidelines.

5. Since inelastic deformations generated during seismic response are not limited to flexural deformation, and increased portion of shear displacement in the total displacement will lead to increased ductility demand, which in turn will affect the overall behaviour. Hence, to better understanding the behaviour of collared reinforced concrete columns, decomposition of the total displacement into shear and flexural displacement components should be performed, and to assess the interaction between the shear and flexural behaviour through either experimental or analytical efforts.

6. Further study on the effective strain of steel collars is needed to validate the proposed shear strength model, and to relate the effective strain to various parameters, such as aspect ratio, longitudinal reinforcement ratio, axial compression index, concrete compressive strength, and steel collar dimension/spacing.

REFERENCES

ABAQUS, Inc. 2003. *ABAQUS/Explicit Version 6.4 Theory Manual & User's Manual*, Pawtucket, R. I., USA.

Abrams, D.P. 1987. Influence of Axial Force Variation on Flexural Behavior of Reinforced Concrete Columns. *ACI Structural Journal*, V.84, No.2:246-254.

Aboutaha, R.S., Engelhardt, M.D., Jirsa, J.O. and Kreger, M.E. 1996. Retrofit of Concrete Columns with Inadequate Lap Splices by the Use of Rectangular Steel Jackets. *Earthquake Spectra,* V.12, No.4:693-714.

Aboutaha, R.S. and Machado, R.I. 1999. Seismic Resistance of Steel-Tubed High-Strength Reinforced-Concrete. *ASCE Journal of Structural Engineering,* V.125, No.5:485-494.

Abou-Elfath, H. and Ghobarah, A. 2000. Behaviour of Reinforced Concrete Frames Rehabilitated with Concentric Steel Bracing. *Can. J. Civ. Eng.,* V.27:433-444.

ACI Committee 318. 2005. Building Code Requirements for Structural Concrete (ACI 318-05) and Commentary (ACI 318R-05). American Concrete Institute, Farmington Hills, Michigan.

ACI-ASCE Committee 426. 1974. The Shear Strength of Reinforced Concrete Members ACI 426R-74) (Reapproved 1980). *Proceedings, ASCE*, V100, No. ST8, August 1974, pp.:1543-1591

Ahn, J.M., Lee, J.Y., Bahn, B.Y., and Shin, S.W. 2000. An Experimental Study of the Behaviour of High-Strength Reinforced Concrete Columns Subjected to Reversed Cyclic Shear Under Constant Axial Compression. *Magazine of Concrete Research,* Vol.52, No.3:209-218.

ANATECH, Inc. 1997. *ANACAP User's and Theory Manual Version 2.5.*

ASCE-ACI Committee 445. 1998. Recent Approaches to Shear Design of Structural Concrete. *ASCE Journal of Structural Engineering,* V.124, No.12:1375-1417.

ASTM Standard A370. 2002. Standard Test Methods and Definitions for Mechanical Testing of Steel Products. (ASTM Standard A370-02). ASTM International, West Conshohocken, PA.

ASTM Standard C192. 2002. Standard Practice for Making and Curing Concrete Test Specimens in the Laboratory. (ASTM Standard C192-02). ASTM International, West Conshohocken, PA.

ASTM Standard C469. 2002. Standard Test Method for Static Modulus of Elasticity and Poisson's Ratio of Concrete in Compression. (ASTM Standard C469-02). ASTM International, West Conshohocken, PA.

Bai, J. and Hueste, M. B. 2003. Seismic Rehabilitation for Reinforced Concrete Building Structures. *Consequence-Based Engineering (CBE) Institute Final Report.* Texas A&M University. August 2003.

Barr, B. and Lee, M. K. 2003. Modelling the Strain-Softening Behaviour of Plain Concrete Using A Double-Exponential Model. *Magazine of Concrete Research*, V.55, No.4:343-353.

Begum, M., Elwi, A.A., and Driver, R.G. 2004. Numerical Simulation of The Behaviour of Partially Encased Composite Columns. *Proceedings of Canadian Society for Civil Engineering Annual Conference*, June 2-5, 2004, Saskatoon, Saskatchewan, Canada.

Bentz, E.C. 2000. Sectional Analysis of Reinforced Concrete Members. *Ph.D. Dissertation,* Department of Civil Engineering, University of Toronto:318pp.

Bentz, E.C. 2001. Analysis of UCSD Columns by Modified Compression Field Theory. *Finite Element Analysis of Reinforced Concrete Structures,* American Concrete Institute (ACI) SP-205:145-168.

Bentz, E.C. and Collins, M.P. 2006. Development of the 2004 Canadian Standards Association (CSA) A23.3 Shear Provisions for Reinforced Concrete. *Can. J. Civ. Eng.*, V.33:521-534.

Bett, B.J., Klingner, R.E., and Jirsa, J.O. 1988. Lateral Load Response of Strengthened and Repaired Reinforced Concrete Columns. *ACI Structural Journal*, V.85, No.5:499-508.

Biskinis, D.E., Roupakias, G.K., and Fardis, M.N. 2004. Degradation of Shear Strength of Reinforced Concrete Members with inelastic Cyclic Displacement. *ACI Structural Journal,* V.101, No.6:773-783.

Bisby, L.A. and Williams, B.K. 2004. An Introduction to FRP Strengthening of Concrete Structures. *ISIS Educational Module 4,* ISIS Canada, A Canadian Network of Centres of Excellence. February 2004.

Budek, A.M., Prestley, M.J.N., and Lee, C.O. 2002. Seismic Design of Columns with High-Strength Wire and Strands as Spiral Reinforcement. *ACI Structural Journal*, V.99, No.5:660-670.

Canadian Standards Association. CSA/A23.3-04. Design of Concrete Structures. Mississauga, Ontario, Canada.

Canadian Standards Association. CSA/G30.18–M92. Billet-Steel Bars for Concrete Reinforcement. Rexdale, Ontario, Canada.

Canadian Standards Association. CSA/G40.21-04 Structural Quality Steels. Mississauga, Ontario, Canada.

CEB-FIB. 2003. FIB Bulletin 24: Seismic Assessment and Retrofit of Reinforced Concrete Buildings. International Federation for Structural Concrete. Lausanne, Switzerland.

Chapman, J.R. and Driver, R.G. 2006. Behaviour of Collared Concrete Columns Under Concentric and Eccentric Loads. *Structural Engineering Report 263*, Department of Civil & Environmental Engineering, University of Alberta. January 2006. 140 pp.

Chopra, A.K. 2001. Dynamics of Structures-Theory and Application to Earthquake Engineering (*Second Edition*). Prentice Hall, Inc.

Chung, W. and Ahmad, S.H. 1995. Analytical Model for Shear Critical Reinforced Concrete Members. *ASCE Journal of Structural Engineering*, V.121, No.6:1023-1029.

Cofer, W.F., Zhang, Y., and McLean, D.I. 2002. A Comparison of Current Computer Analysis Methods for Seismic Performance of Reinforced Concrete Members. *Finite Elements in Analysis and Design,* Vol.38: 835-861.

Collins, M.P. and Mitchell, D. 1997. Prestressed Concrete Structures, Response Publications, Canada, 1997.

Darwin, D. 1991. Reinforced Concrete. *Finite Element Analysis of Reinforced Concrete Structures II, Proceedings of the International Workshop,* New York, New York, June 2-5, 1991:203-232.

Dowell, R.K. and Parker, D.R. 2001. Finite Element Analysis of UCSD Shear Columns. *Finite Element Analysis of Reinforced Concrete Structures,* American Concrete Institute (ACI) SP-205:121-144.

Driver, R.G., Grondin, G.Y., Behbahanifard, M., and Hussain, M.A. 2001. Recent Developments and Future Directions in Steel Plate Shear Wall Research. *Proc., North American Steel Construction Conference*, May, Ft. Lauderdale, FL, USA.

Duong, K.V., Sheikh, S.A., and Vecchio, F.J. 2007. Seismic Behavior of Shear-critical Reinforced Concrete Frame: Experimental Investigation. *ACI Structural Journal,* V.104, No.3:304-313.

Esmaeily, A. and Xiao, Y. 2004. Behavior of Reinforced Concrete Columns under Variable Axial Loads. *ACI Structural Journal,* V.101, No.1:124-132.

Federal Highway Administration (FHWA). 1995. *Seismic Retrofitting Manual for Highway Bridges.* Publication No. FHWA-RD-94-052, Department of Transportation Research and Development, Turner-Fairbank Highway Research Center, Mclean, Va.

Fischer, G. and Li, V.C. 2003. Deformation Behavior of Fiber-Reinforced Polymer Reinforced Engineered Cementitious Composite (ECC) Flexural Members under Reversed Cyclic Loading Conditions. *ACI Structural Journal,* V.100, No.1:25-35.

Frangou, M., Pilakoutas, K., and Dritsos, S. 1995. Structural Repair/Strengening of RC Columns. *Construction and Building Materials,* Vol. 9, No. 5: 259-266.

Fukuyama, K., Higashibata, Y., and Miyauchi, Y. 2000. Studies on Repair and Strengthening of Damaged Reinforced Concrete Columns. *Cement & Concrete Composites,* Vol.22:81-88.

Galal, K., Arafa, A. and Ghobarah, A. 2005. Retrofit of RC Square Short Columns. *Engineering Structures,* V.27: 801-813.

Ghee, A.B., Priestley, M.J.N., and Paulay, T. 1989. Seismic Shear Strength of Circular Reinforced Concrete Columns. *ACI Structural Journal,* V.86, No.1:45-59.

Ghobarah, A., Aziz, Tarek.S., and Biddah, Ashraf. 1996. Seismic Rehabilitation of Reinforced Concrete Beam-Column connections. *Earthquake Spectra,* V.12, No.4:761-780.

Ghosh, K.K. and Sheikh, S.A. 2007. Seismic Upgrade with Carbon Fiber-Reinforced Polymer of Columns Containing Lap-Spliced Reinforcing Bars. *ACI Structural Journal,* V.104, No.2:227-236.

Girard, C. and Bastien, J. 2002. Finite-Element Bond-Slip Model for Concrete Columns under Cyclic Loads. *ASCE Journal of Structural Engineering,* V.128, No.12:1502-1510.

Goodman, R.E. 1989. Introduction to Rock Mechanics 2nd Edition. John Wiley & Sons Inc., New York, USA.

Gubbins, J. 2002. Strut Action in Columns Subject to Seismic Loading. *M. Eng. Report,* Department of Civil Engineering and Applied Mechanics, McGill University, Montreal, QC, Canada. March 2002: 137pp.

Gupta, P.R. and Collins P.C. 2001. Evaluation of Shear Design Procedures for Reinforced Concrete Members under Axial Compression. *ACI Structural Journal,* V.98, No.4:537-547.

Hibbit, Karlson and Sorenson. 1996. *ABAQUS User's and Theory Manual, Version 5.6* Pawtucket, R. I., USA.

Hosseini, A., Khaloo, A.R., and Fadaee, S. 2005. Seismic Performance of High-Strength Concrete Square Columns Confined with Carbon Fiber Reinforced Polymers (CFRPs). *Can. J. Civ. Eng.,* V.32:569-578.

Hussain, M.A. and Driver, R.G. 2001. Finite Element Study on the Strength and Ductility of Externally Confined Rectangular and Square Concrete Columns. *Proceedings of Canadian Society for Civil Engineering Annual Conference*, May 30-June 2, 2001, Victoria, British Columbia, Canada.

Hussain, M.A. and Driver, R.G. 2003. Behaviour of Externally Confined Reinforced Concrete Columns under Extreme Lateral Cyclic Loading. *Proceedings of 1st Conference on Response of Structures to Extreme Loading*, August 3-6, 2003, Toronto, Ontario, Canada.

Hussain, M.A. and Driver, R.G. 2005a. Experimental Investigation of External Confinement of Reinforced Concrete Columns by HSS Collars. *ACI Structural Journal*, V.102, No.2:242-251.

Hussain, M.A. and Driver, R.G. 2005b. Seismic Rehabilitation of Reinforced Concrete Columns through Confinement by Steel Collars. *Structural Engineering Report 259*, Department of Civil & Environmental Engineering, University of Alberta. May 2005.

Ignatakis, C.E., Stavrakakis, E.J., and Penelis, G.G. 1989. Parametric Analysis of Reinforced Concrete Columns under Axial and Shear Loading Using the Finite Element Method. *ACI Structural Journal,* V.86, No.4:413-418.

Jaradat, O.A., McLean, D.I., and Marsh, M.L. 1998. Performance of Existing Bridge Columns under Cyclic Loading---Part 1: Experimental Results and Observed Behavior. *ACI Structural Journal,* V.95, No.6:695-704.

Jirsa, J.O., Maruyama, K., and Ramirez, H. 1980. The Influence of Load History on the Shear Behavior of Short RC Columns. *Proceedings of the Seventh World Conference on Earthquake Engineering*, Istanbul, Turkey :339-346.

Kani, G.N.J. 1966. Basic Facts Concerning Shear Failure. *ACI Journal, Proceedings,* V.63, No.6:675-692.

Kani, M.W., Huggins, M.W., and Wiltkopp, P.F. 1979. *Kani on Shear in Reinforced Concrete*. Department of Civil Engineering, University of Toronto, Toronto, Ontario, Canada.

Kim, J.K., Kim, I.H., Lim, H.W., Lee, J.H., and Lee, J.H. 2001. Cyclic Loading Test of Bridge Pier Models Without Seismic Detailing. *The Eighth East Asia-Pacific Conference on Structural Engineering and Construction*, Singapore, Singapore: Paper No.:1308.

Kobayashi, K., Kokusho, S., Takiguchi, K., Ishi, H., Munakata, M., and Sato, K. 1986. Experimental Study on the Ultimate Shear Strength of Reinforced Concrete Column under Bi-directional Horizontal Forces. *Report of the Research Laboratory of Engineering Materials*, Tokyo Institute of Technology. Number 11, 1986, Nagatsuta, Yokohama 227, Japan.

Kokusho, S., Matsuzaki, Y., Takiguchi, K., Wada, A., Hayashi, S. Fukuhara, M., Kobayashi, K., and Aoki, T. 1986. Study of Aseismic Shear Behavior of Reinforced Concrete Column under High Axial Load. *Report of the Research Laboratory of Engineering Materials*, Tokyo Institute of Technology. Number 11, 1986, Nagatsuta, Yokohama 227, Japan.

Kosmatka, S.H., Kerkhoff, B., Panarese, W., MacLeod, N.F., and McGrath, R.J. 2002. Design and Control of Concrete Mixtures. *7th Canadian Edition.* Canadian Portland Cement Association. Ottawa, Ontario, Canada.

Lacobucci, R.D., Sheikh, S.A., and Bayrak, O. 2003. Retrofit of Square Concrete Columns with Carbon Fiber-Reinforced Polymer for Seismic Resistance. *ACI Structural Journal*, V.100, No.6:785-794.

Lamanna, A.J., Bank, L.C., and Scott, D.W. 2001. Flexural Strengthening of Reinforced Concrete Beams using Fasteners and Fiber-Reinforced Polymer Strips. *ACI Structural Journal*, V.98, No.3:368-376.

Lee, J., Filippou, F.C., and Fenves, G.L. 1999. Simulation of the Hysteretic Behaviour of Reinforced Concrete Members. Structural Engineering in the 21st Century

Proceedings of the 1999 Structural Congress, New Orleans, Louisiana, April 18-21, 1999:119-202.

Lee, D.H. and Elnashai, A.S. 2002. Inelastic Seismic Analysis of RC Bridge Piers Including Flexural-Shear-Axial Interaction. *Structural Engineering and Mechanics,* V.13, No.3:241-260.

Lehman, D., Moehle, J., Mahin, S., Calderone, A., and Henry, L. 2004. Experimental Evaluation of the Seismic Performance of Reinforced Concrete Bridge Columns. *ASCE Journal of Structural Engineering,* V.130, No.6:869-879.

Li, Q., Duan, Y., and Wang, G. 2002. Behaviour of Large Concrete Specimens in Uniaxial Tension. *Magazine of Concrete Research*, V.54, No.5:385-391.

Li, Y.F. and Sung, Y.Y. 2003. Seismic Repair and Rehabilitation of a Shear-Failure Damaged Circular Bridge Column Using Carbon Fibre Reinforced Plastic Jacketing. *Can. J. Civ. Eng.,* V.30:819-829.

Li, Y.F. and Sung, Y.Y. 2004. A Study on the Shear-Failure of Circular Sectioned Bridge Column Retrofitted by Using CFRP Jacketing. *Journal of Reinforced Plastics and Composites,* Vol.23, No.8:811-830.

Lynn, A.C., Moehle, J.P., Mahin, S.A., and Holmes, W.T. 1996. Seismic Evaluation of Existing Reinforced Concrete Building Columns. *Earthquake Spectra,* V.12, No.4:715-739.

Lubliner, J., Oliver, J., Oller, S., and OÑate, E. 1989. A Plastic-Damage Model for Concrete. *Int. J. Solids Structures,* V.25, No.3:229-326.

Ma, R., Xiao, Y., and Li, K.N. 2000. Full-Scale Testing of a Parking Structure Column Retrofitted with Carbon Fiber Reinforced Composites. *Construction and Building Materials,* Vol.14: 63-71.

MacGregor, J.M. and Bartlett, F.M. 2000. Reinforced Concrete-Mechanics and Design (*First Canadian Edition*). Prentice Hall Canada Inc., Scarborough, Ontario.

Maekawa, K. and An, X. 2000. Shear Failure and Ductility of RC Columns After Yielding of Main Reinforcement. *Engineering Fracture Mechanics,* Vol.65: 335-368.

Mander, J.B., Priestley, M.J.N., and Park, R. 1988. Theoretical Stress-Strain Model for Confined Concrete. *ASCE Journal of Structural Engineering*, V. 114, No.8:1804-1826.

Marti, P. 1985. Basic Tools of Reinfroced Concrete Beam Design. *ACI Journal, Proceedings* V. 82, Jan.-Feb. 1985 No.1:46-56.

Massicotte, B, Elwi, A.E., and MacGregor, J.G. 1988. Analysis of Reinforced Concrete Panels Loaded Axially and Transversely. *Structural Engineering Report 161*, Department of Civil & Environmental Engineering, University of Alberta. 1988.

Melek M. and Wallace, W. 2004. Cyclic Behavior of Columns with Short Lap Splices. *ACI Structural Journal*, V.101, No.6:802-811.

Memon, M.S., and Sheikh, S.A. 2005. Seismic Resistance of Square Concrete Columns Retrofitted with Glass Fiber-Reinforced Polymer. *ACI Structural Journal*, V.102, No.5:774-783.

Mirmiran, A., Samaan, M., Cabrera S., and Shahawy, M. 1998. Design, Manufacture and Testing of a New hybrid Column. *Construction and Building materials,* V.12, No.1:39-49.

Moehle, J. P. 2000. State of Research on Seismic Retrofit of Concrete Building Structures in the U.S." *US-Japan Symposium and Workshop on Seismic Retrofit of Concrete Structures.*

Moretti, M.L., and Tassios, T.P. 2006. Behavior and Ductility of RC Short Columns Using Global Truss Model. *ACI Structural Journal*, V.103, No.3:319-327.

Nanni, A. and Norris, M.S. 1995. FRP Jacketed Concrete Under Flexural and Combined Flexural-Compression. *Construction and Building Materials,* Vol. 9, No.5: 273-281.

NBCC. 1995. National Building Code of Canada. National Research Council of Canada, Ottawa, Ontatio.

Nesheli, K.N., Yamakawa, T., and Satoh, H. 2004. Experimental Study on Retrofitting of Shear Critical RC Columns Using Pre-Tensioned Aramid Fiber Belts. *Proceedings of the First Conference on Application of FRP Composite in Construction and Rehabilitation of Structures*, May 4, Tehran, Iran: 95-104.

Nezamian, A., Setunge, S., and Chandler, L. 2004. Comparisons Between ACI 440 and FIB 14 Design Guidelines in Using CFRP for Strengthening of a Concrete Bridge Headstock. *Proceedings of the Fourth International Conference on Advanced Composite Materials in Bridges and Structures*, July 20-23, 2004, Calgary, Canada.

Nielsen, M. P. 1999. Limit Analysis and Concrete Plasticity *(Second Edition)*. CRC Press. Washington D.C.

Noguchi, H. and Uchida, K. 2004. Finite Element Method Analysis of Hybrid Structural Frames with Reinforced Concrete Columns and Steel Beams. *ASCE Journal of Structural Engineering,* V.130, No.2:328-335.

Ožbolt, J. and Li, Y.J. 2001. Three-Dimensional Cyclic Analysis of Compressive Diagonal Shear Failure. *Finite Element Analysis of Reinforced Concrete Structures,* American Concrete Institute (ACI) SP-205:61-80.

Parent, S. and Labossière, P. 2000. Finite Element Analysis of Reinforced Concrete Columns Confined with Composite Materials. *Can. J. Civ. Eng.,* V.27:400-411.

Park, S. W., Xia, Q., and Zhou, M. 2001. Dynamic behavior of concrete at high strain rates and pressures: II. numerical simulation. *International Journal of Impact Engineering*, 25:887-910.

Parvin, A. and Wang, W. 2001. Behavior of FRP Jacketed Concrete Columns under Eccentric Loading. *ASCE Journal of Composites for Construction,* V.5, No.3:146-152.

Parvin, A. and Wang, W. 2002. Concrete Columns Confined by Fiber Composite Wraps under Combined Axial and Cyclic Lateral Loads. *Composite Structures*, No.58:539-549.

Priestley, M.J.N., Seible, F., Xiao, Y., and Verma, R. 1994a. Steel Jacket Retrofit of Reinforced Concrete Bridge Columns for Enhanced Shear Strength—Part 1: Theoretical Considerations and Test Design. *ACI Structural Journal*, Vol.91, No.4:394-404.

Priestley, M.J.N., Seible, F., Xiao, Y., and Verma, R. 1994b. Steel Jacket Retrofit of Reinforced Concrete Bridge Columns for Enhanced Shear Strength—Part 2: Test Results and Comparison with Theory. *ACI Structural Journal*, Vol.91, No.5:537-551.

Priestley, M.J.N., Verma, R., and Xiao, Y. 1994c. Seismic Shear Strength of Reinforced Concrete Columns. *ASCE Journal of Structural Engineering,* V.120, No.8:2310-2329.

Priestley, M.J.N. and Seible, F. 1995. Design of Seismic Retrofit Measures for Concrete and Masonry Structures. *Construction and Building Materials,* Vol. 9, No. 6:365-377.

Rodriguez, M. and Park, R. 1994. Seismic Load Tests on Reinforced Concrete Columns Strengthened by Jacketing. *ACI Structural Journal*, V. 91, No.2:150-159.

Rusinowski, P. 2005. Two-way Concrete Slabs With Openings-Experiments, Finite Element Analyses and Design. *Master Thesis,* Department of Civil Engineering, Lulea University of Technology, June 2005, 118pp.

Saatcioglu, M. 1996. Design of Seismic Resistant Concrete Columns for Confinement. *Worldwide Advances in Structural Concrete and Masonry, Proceedings of the CCMS Symposium held in Conjunction with Structures Congress XIV,* Chicago, Illinois, April 15-18, 1996:233-244.

Saatcioglu, M. and Baingo, D. 1999. Circular High-Strength Concrete Columns under Simulated Seismic Loading. *ASCE Journal of Structural Engineering,* V.125, No.3:272-280.

Saatcioglu, M. and Yalcin, C. 2003. External Prestressing Concrete Columns for Improved Seismic Shear Resistance. *ASCE Journal of Structural Engineering,* V.129, No.8:1057-1070.

Saiidi, M.S., Martinovic, F., McElhaney, B., Sanders, D., and Gordaninejad, F. 2004. Assessment of Steel and Fiber Reinforced Plastic Jackets for Seismic Retrofit of

Reinforced Concrete Columns with Structural Flares. *ASCE Journal of Structural Engineering,* V.130, No.4:609-617.

Saito, S. and Higai, T. 2001. Spring Network Models for Analysis of Reinforced Concrete Columns Under Cyclic loading. *Finite Element Analysis of Reinforced Concrete Structures,* American Concrete Institute (ACI) SP-205:97-120.

Sause, R., Harries, K.A., Walkup, S.L., Pessiki, S., and Ricles, J.M. 2004. Flexural Behavior of Concrete Columns Retrofitted with Carbon Fiber-Reinforced Polymer Jackets. *ACI Structural Journal*, Vol.101, No.5:708-716.

Schlaich, J., Schäfer, K., and Jennewein, M. 1987. Toward a Consistent Design of Structural Concrete. *PCI Journal*, V. 32, No.3:74-150.

Sheikh, S.A. 2002. Performance of Concrete Structures Retrofitted with Fibre Reinforced Polymers. *Engineering Structures*, V.24:869-879.

Su, P.K.L. and Zhu, Y. 2005. Experimental and Numerical Studies of External Steel Plate Strengthened RC Coupling Beams. *Engineering Structures,* V.27:1537-1550.

Takiguchi, K. and Abdullah. 2001. Shear Strengthening of Reinforced Concrete Columns Using Ferrocement Jacket. *ACI Structural Journal*, V. 98, No.5:696-704.

Todeschini, C.E., Bianchini, A.C., and Kesler, C.E. 1964. Behaviour of Concrete Columns Reinforced with High Strength Steels. *ACI Journal, Proceedings,* V. 61, No.6:701-716.

Triantafillou, T.C., Papanicolaou, C.G., Zissimopoulos, P., and Laourdekis, T. 2006. Concrete Confinement with Textile-Reinforced Mortar Jackets. *ACI Structural Journal*, V. 103, No.1:28-37.

Valluvan, R., Kreger, M. E., and Jirsa, J.O. 1993. Strengthening of Column Splices for Seismic Retrofit of Nonductile Reinforced Concrete Frames. *ACI Structural Journal*, V.90, No.4:432-440.

Vecchio, F.J. and Collins, M.P. 1986. The Modified Compression-Field Theory for Reinforced Concrete Elements Subjected to Shear. *ACI Structural Journal,* V.83, No.2:219-231.

Vecchio, F.J. and Collins, M.P. 1988. Predicting the Response of Reinforced Concrete Beams Subjected to Shear Using Modified Compression Field. *ACI Structural Journal,* V.85, No.3:258-268.

Vecchio, F.J. 1989. Nonlinear Finite Element Analysis of Reinforced Concrete Membranes. *ACI Structural Journal,* V.86, No.1:26-35.

Wong, Y.L., Paulay, T. and Priestley, M.J.N. 1993. Response of Circular Reinforced Concrete Columns to Multi-Directional Seismic Attack. *ACI Structural Journal,* V.90, No.2:180-191.

Woodward, K.A. 1980. Behavior of Short R/C Columns Subjected to Cyclic Bilateral Deformation. *Proceedings of the Seventh World Conference on Earthquake Engineering*, Istanbul, Turkey: 347-354.

Woodward, K.A. and Jirsa, J.O. 1984. Influence of Reinforcement on RC Short Column Lateral Resistance. *ASCE Journal of Structural Engineering,* V.110, No.1:90-104.

Xiao, Y. and Ma, R. 1997. Seismic Retrofit of RC Circular Columns Using Prefabricated Composite Jacketing. *ASCE Journal of Structural Engineering,* V.123, No.10:1357-1364.

Xiao, Y., Priestley, M.J. and Seible, F. 1993. Steel Jacket Retrofit for Enhancing Shear Strength of Short Rectangular RC Columns. *Structural System Research Project SSRP-92/*07. Department of Applied Mechanics and Engineering Sciences, University of California, San Diego, La Jolla, California.

Xiao, Y. and Wu, H. 2003. Retrofit of Reinforced Concrete Columns Using Partially Stiffened Steel Jackets. *ASCE Journal of Structural Engineering,* V.129, No.6:725-732.

Xiao, Y., Wu, H. and Martin, G.R. 1999. Prefabricated Composite Jacketing of RC Columns for Enhanced Shear Strength. *ASCE Journal of Structural Engineering,* V.125, No.30:255-264.

Yamakawa, T., Banazadeh, M., and Fujikawa, S. 2004. Emergency Retrofit of Damaged RC columns Right after Seismic Attack Using Pre-tensioned Aramid Fibre Belts. *1st Conference on Application of FRP Composites in Construction and Rehabilitation of Structures.* May 4, 2004, Tehran. Iran: 15-28.

Yan, Z. and Pantelides, C.P. 2006. Fibre-Reinforced Polymer Jacketed and Shape-Modified Compression Members: II—Model. *ACI Structural Journal,* V.103, No.6:894-903.

Youakim, S.A. and Ghali, A. 2003. Behavior of Concrete Columns with Double-Head Studs under Earthquake Loading: Parametric Study. *ACI Structural Journal,* V.100, No.6:785-794.

Appendix A—Photos for specimens during tests

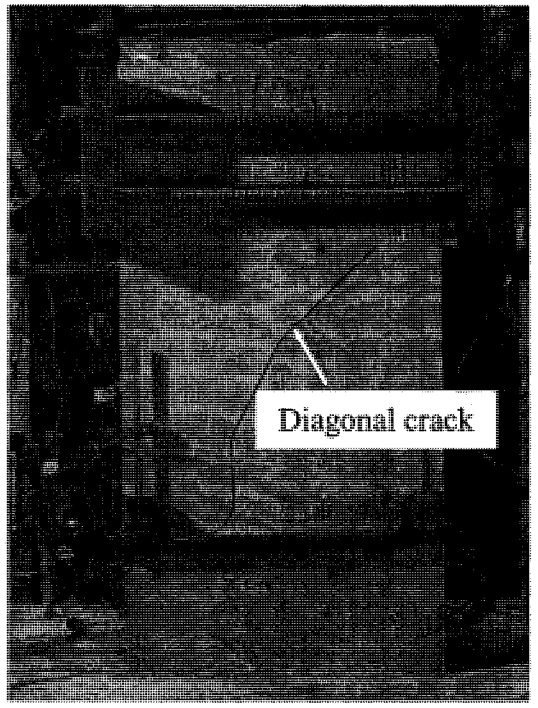

(a) At cycle 16 (μ =2.3) (West side)

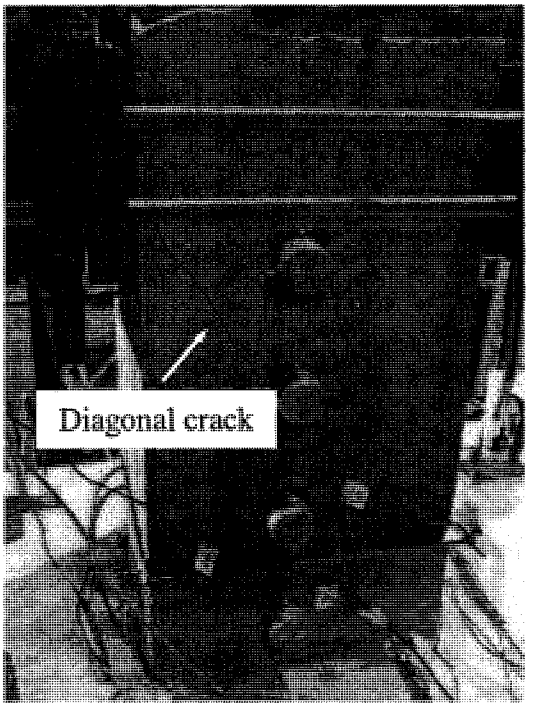

(b) At cycle 16 (μ =2.3) (East side)

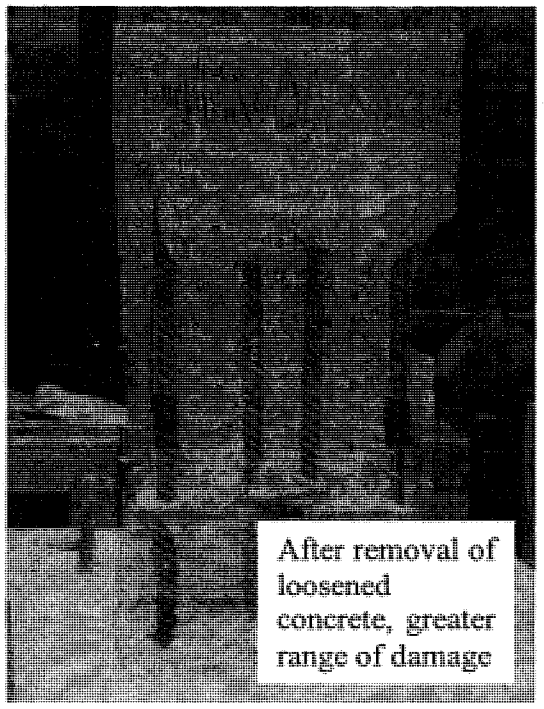

(c) At end of test (North side)

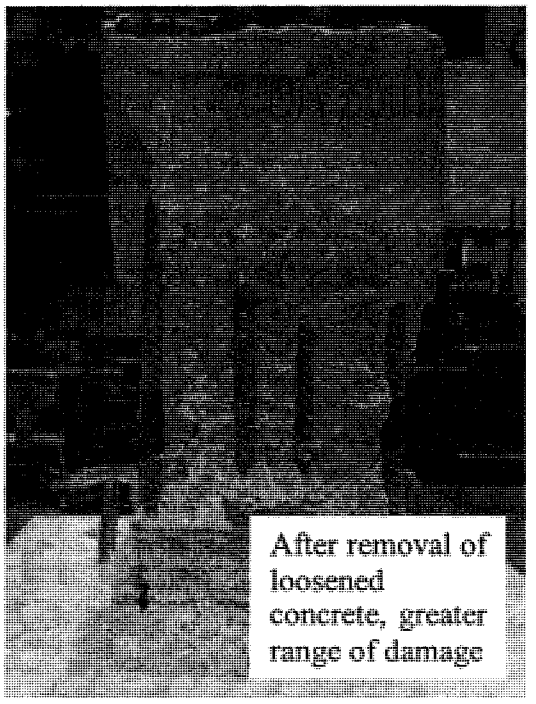

(d) At end of test (South side)

Figure A-1 Specimen CV0A

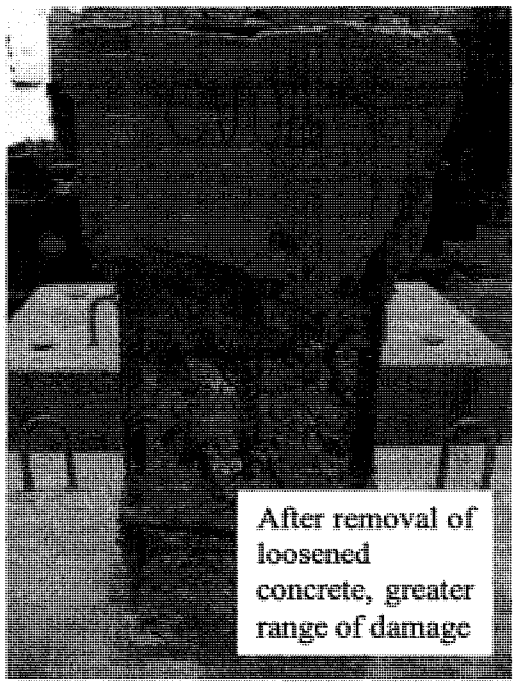

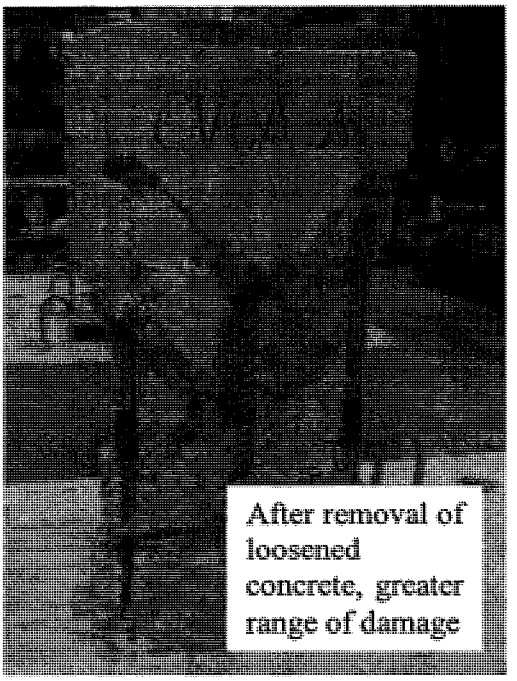

(e) At end of test (West side) (f) At end of test (East side)

Figure A-1 Specimen CV0A (Cont')

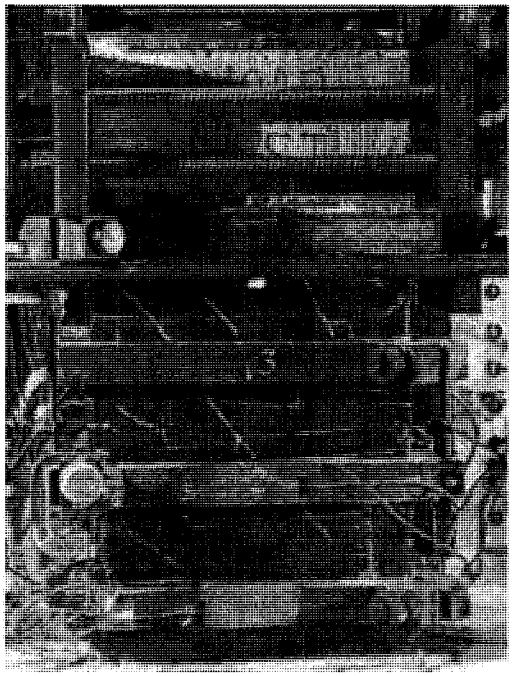

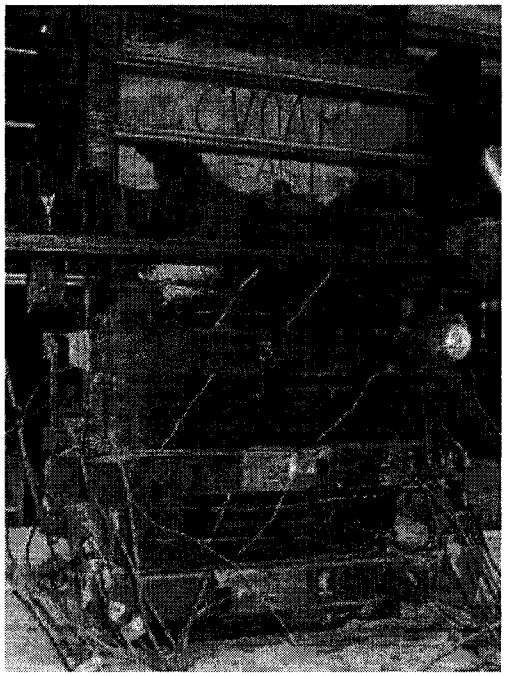

(a) Cracks at cycle 16 (μ =2) (West side) (b) Cracks at cycle 16 (μ =2) (East side)

Figure A-2 Specimen CV0AR

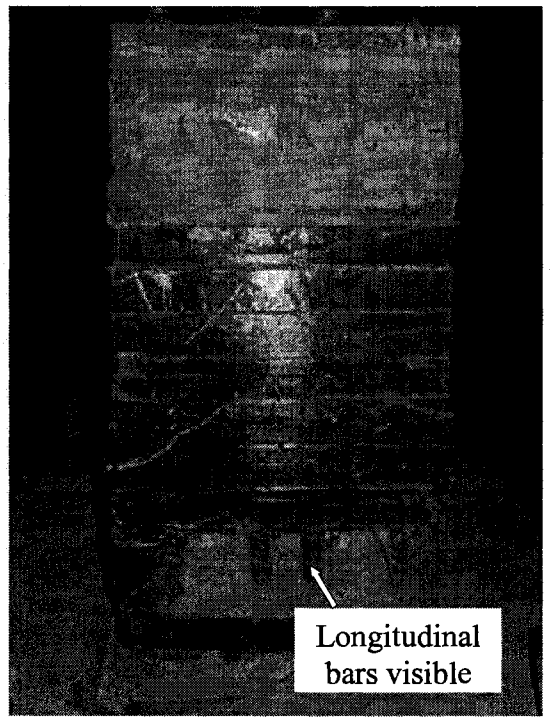

(c) At end of test (North side)

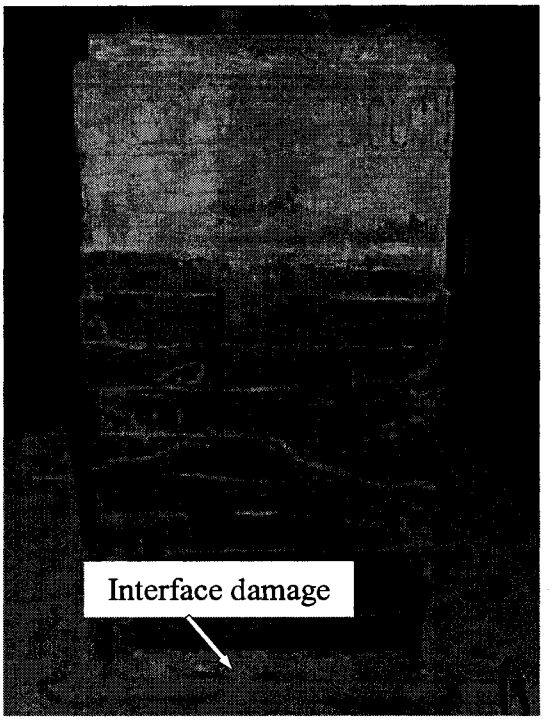

(d) At end of test (South side)

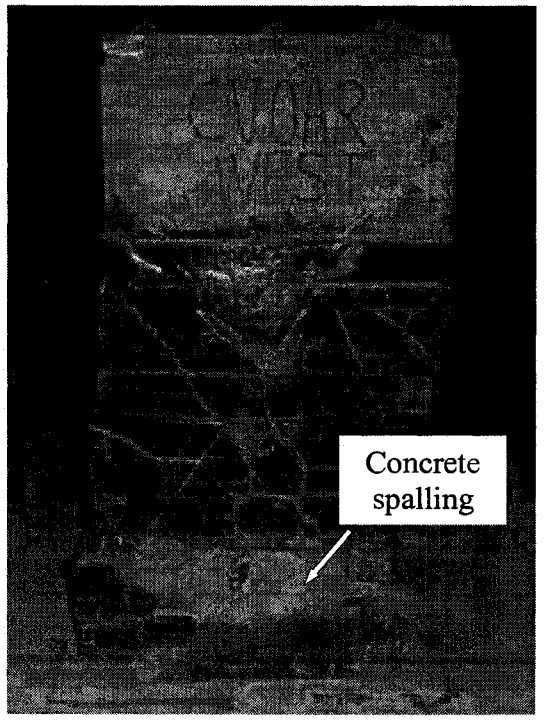

(e) At end of test (West side)

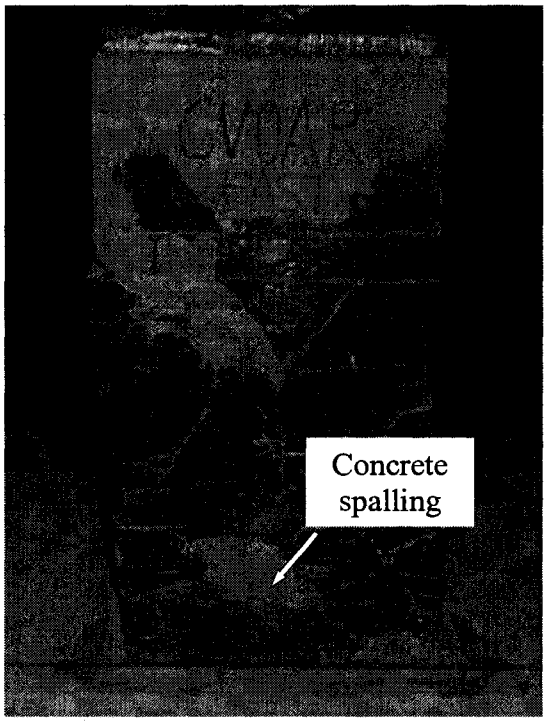

(f) At end of test (East side)

Figure A-2 Specimen CV0AR (Cont')

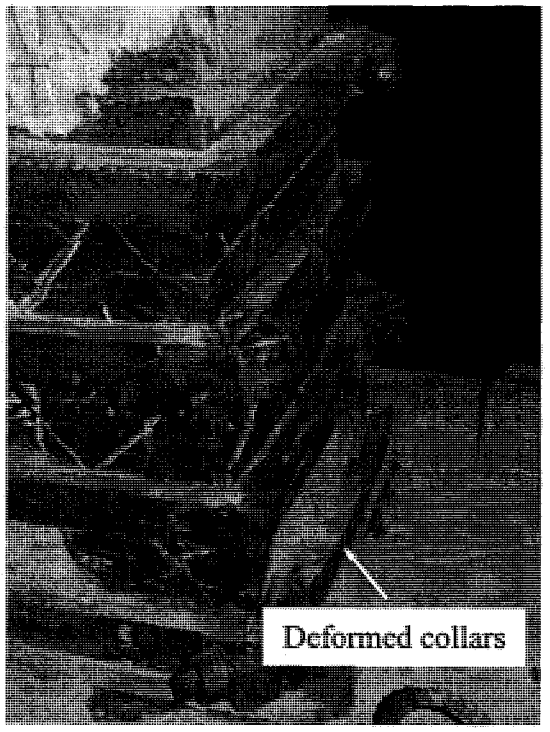

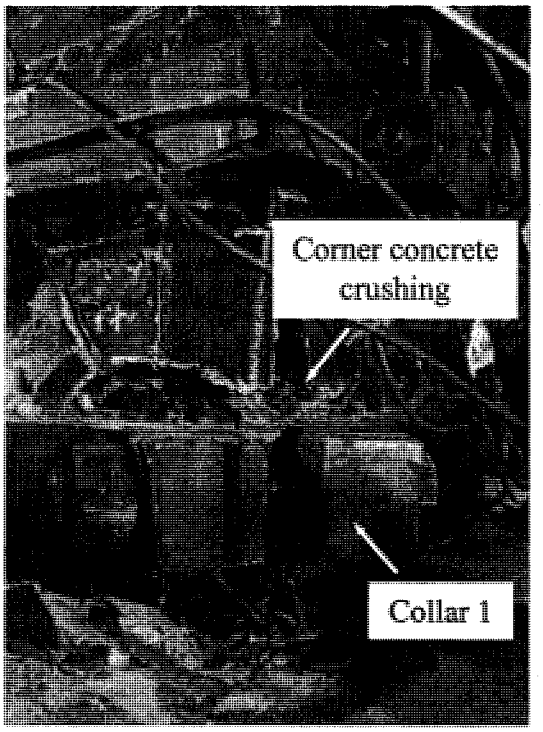

(g) End of test-bending of collars (South side) (h) Crushing (Southwest corner at cycle 52)

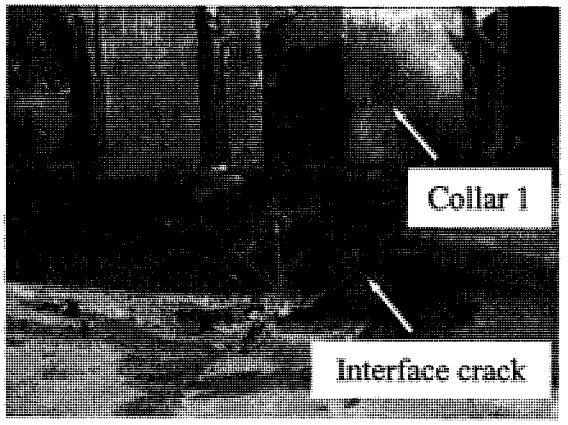

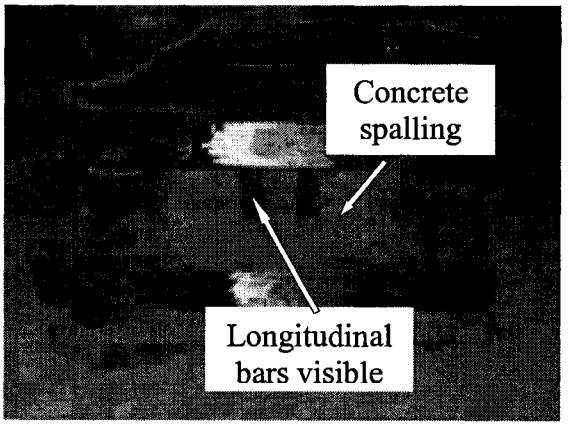

(i) Wide crack in interface (At cycle 31) (j) Visible of bars end of test (North side)

Figure A-2 Specimen CV0AR (Cont')

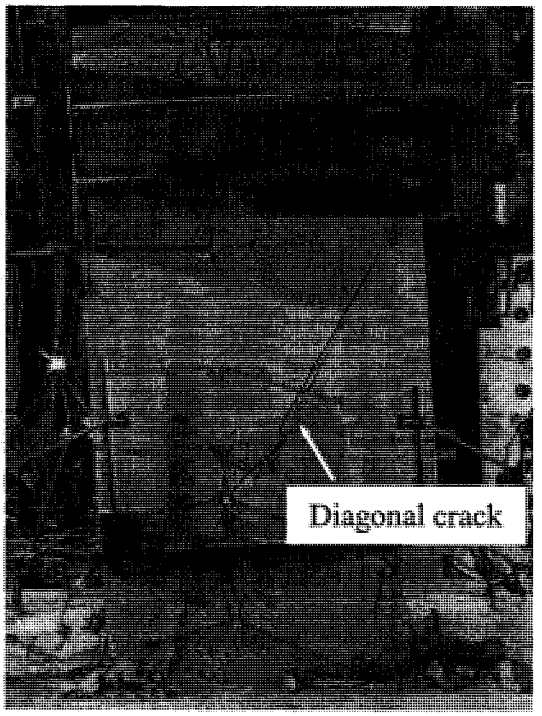

(a) Cracks at cycle 16 (μ =4) (West side)

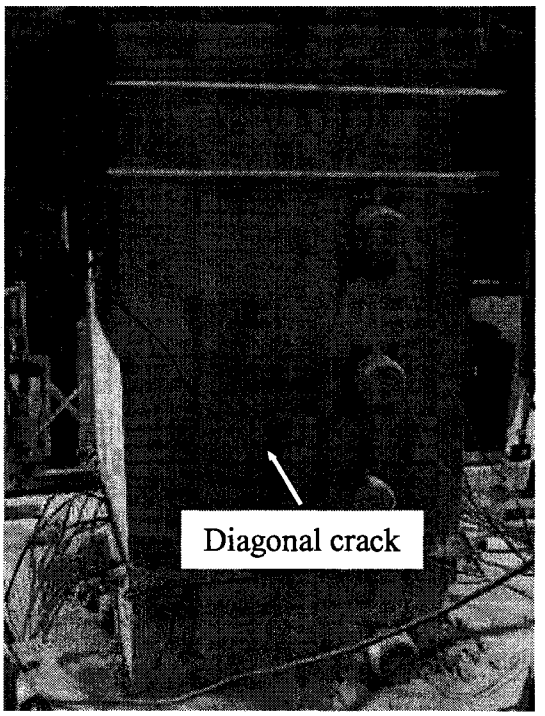

(b) Cracks at cycle 16 (μ =4) (East side)

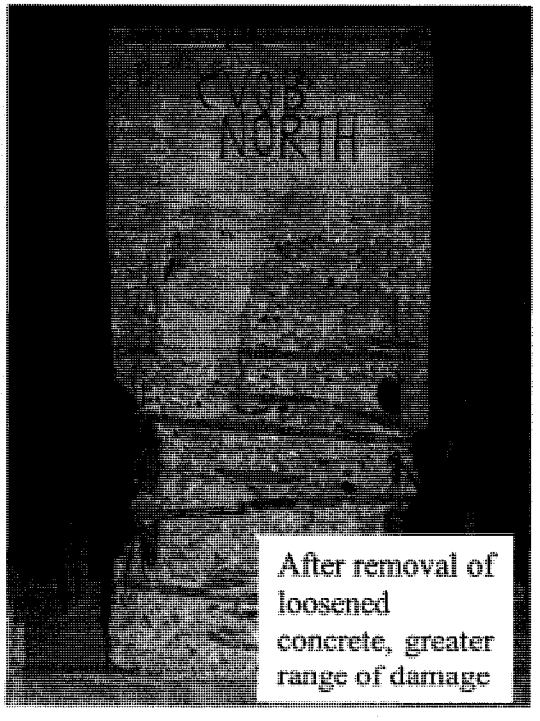

(c) At end of test (North side)

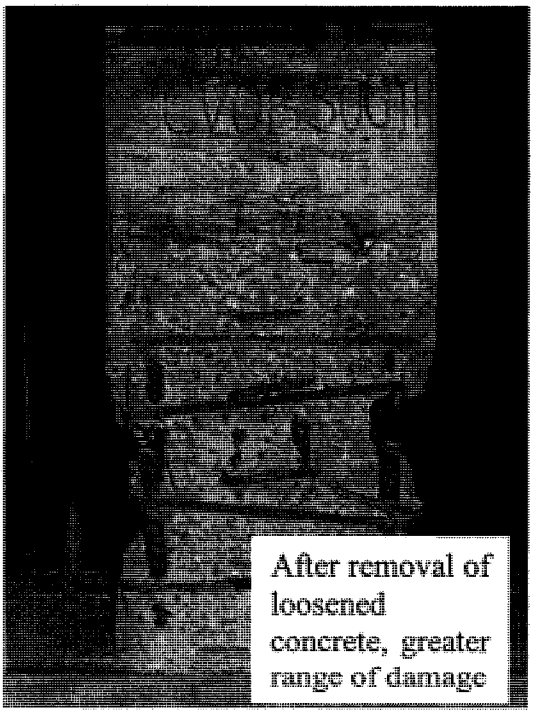

(d) At end of test (South side)

Figure A-3 Specimen CV0B (Cont')

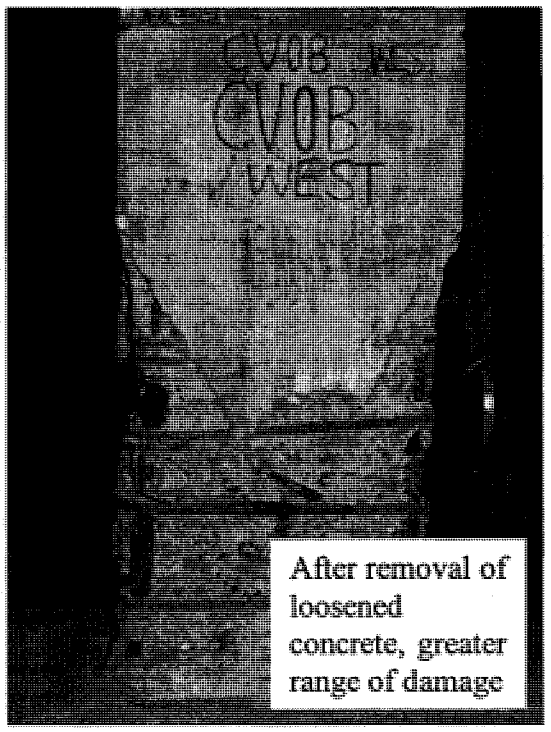

(e) At end of test (West side)

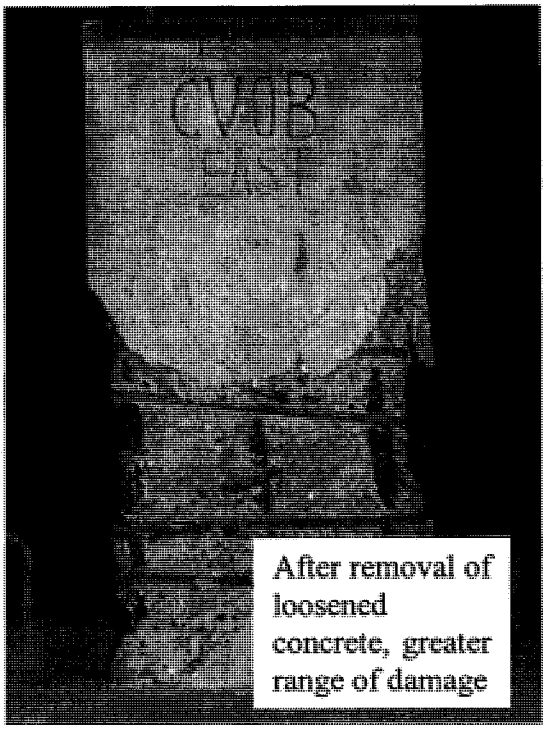

(f) At end of test (East side)

Figure A-3 Specimen CV0B (Cont')

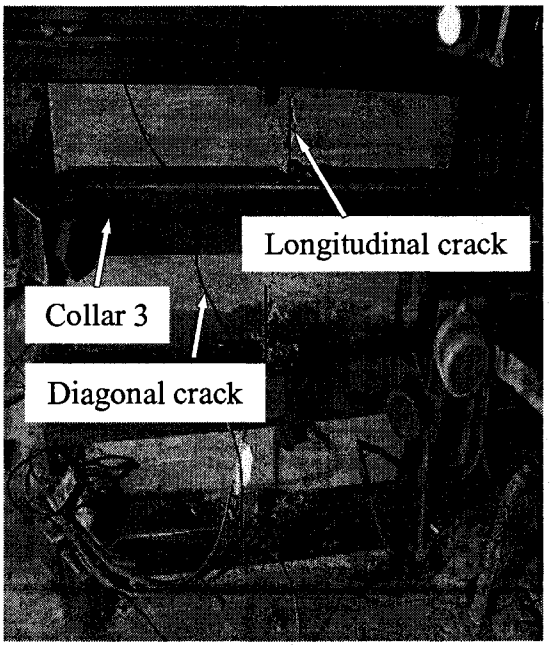

(a) Cracks at cycle 16 (μ =4)

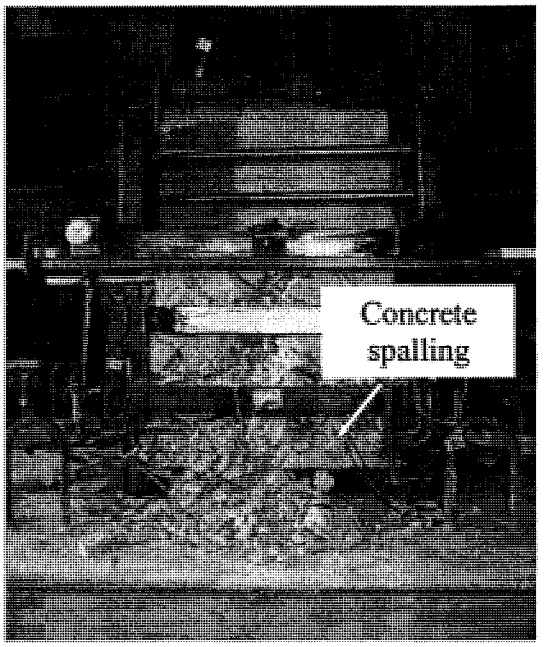

(b) At end of test (μ =8) (West side)

Figure A-4 Specimen CV1

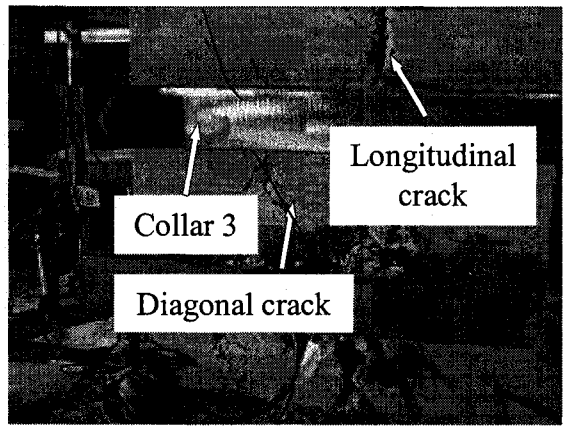

(c) At cycle 21 (μ =6) (West side)

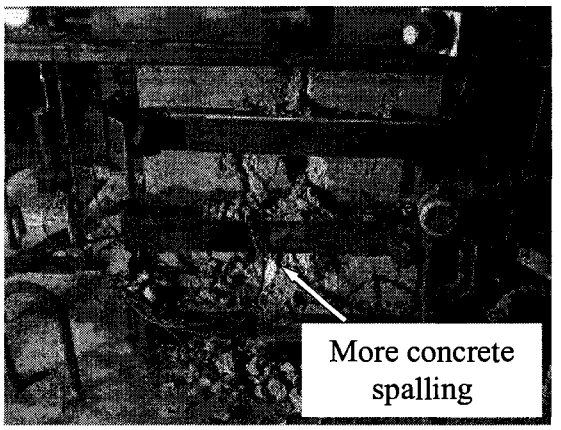

(d) At cycle 25 (μ =6) (West side)

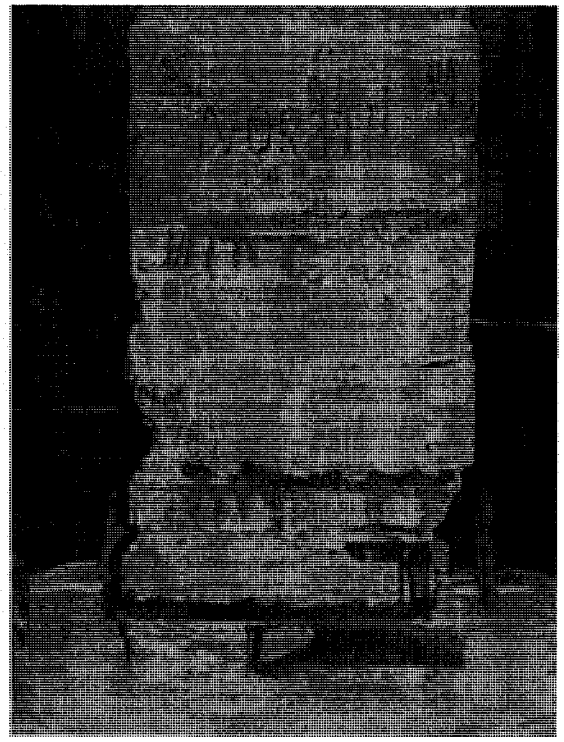

(e) At end of test (North side)

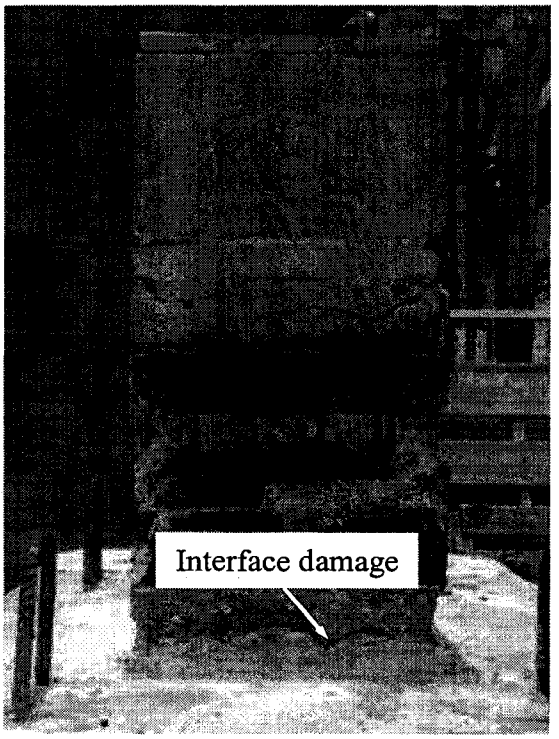

(f) At end of test (South side)

Figure A-4 Specimen CV1 (Cont')

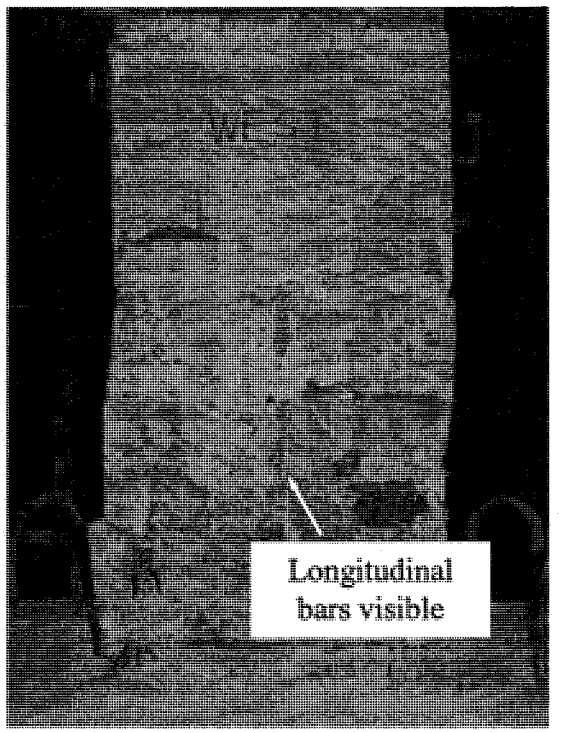

(g) At end of test (West side)

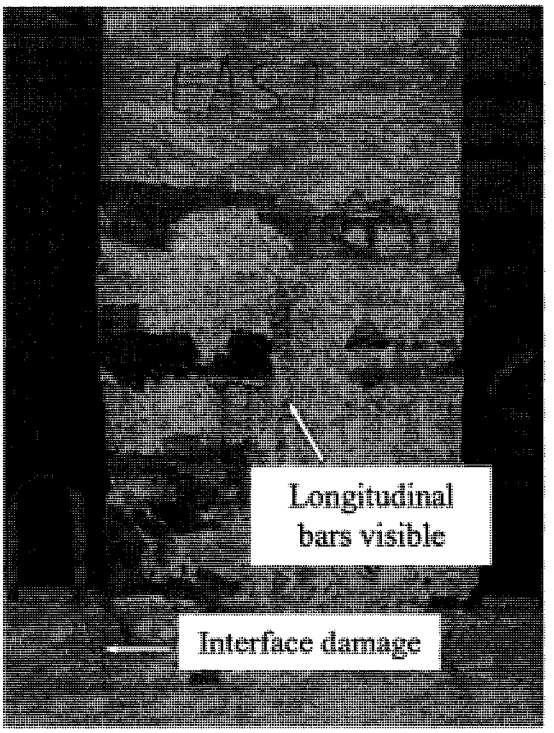

(h) At end of test (East side)

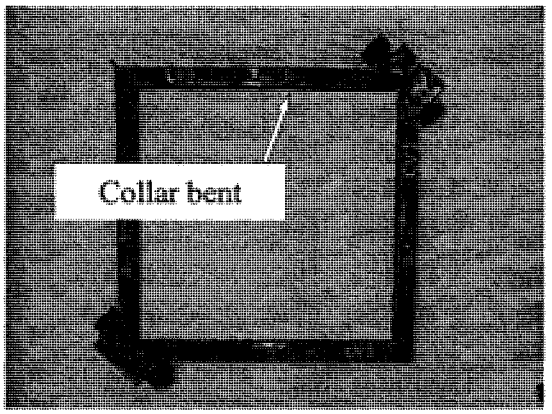

(i) Collars after test (collar 1)

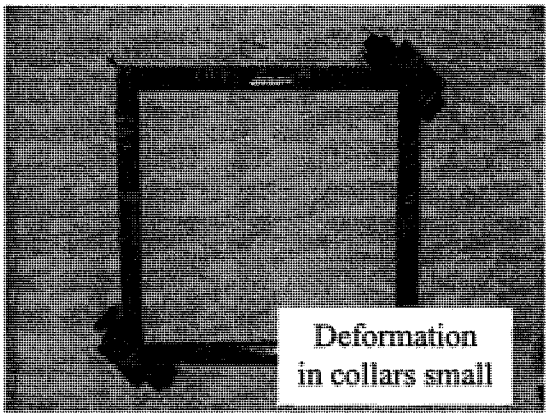

(j) Collars after test (collar 2)

Figure A-4 Specimen CV1 (Cont')

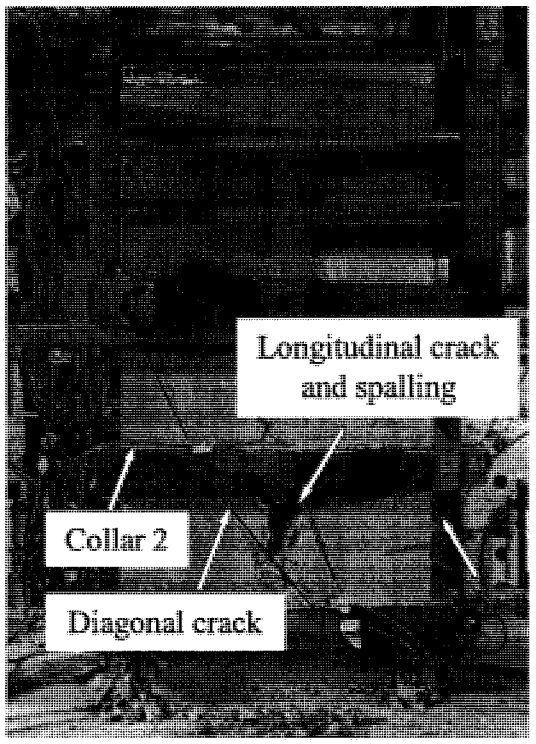

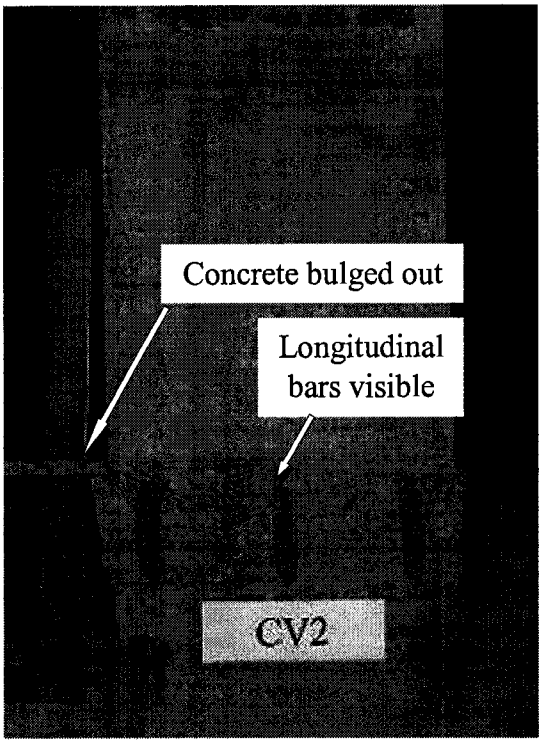

(a) Diagonal and longitudinal cracks (West side) (b) At the end of test (West side)

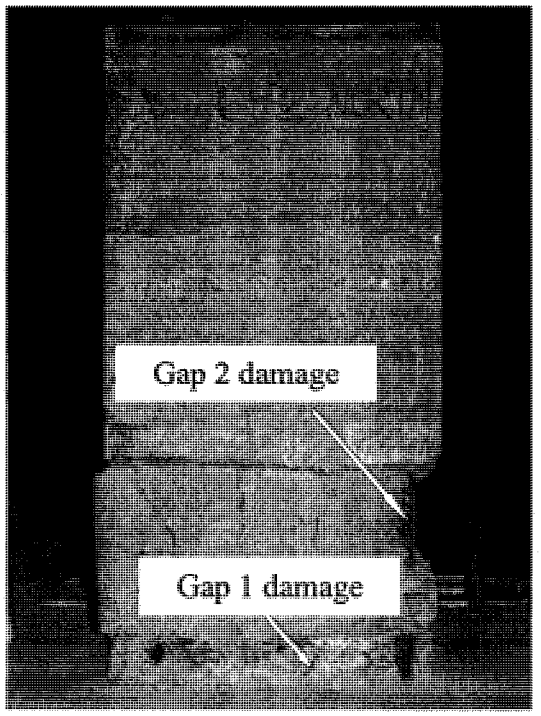

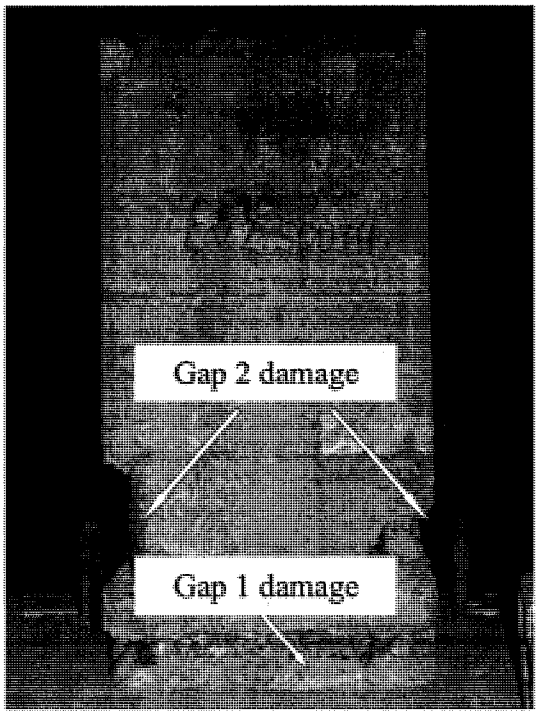

(c) At end of test (North side) (d) At end of test (South side)

Figure A-5 Specimen CV2

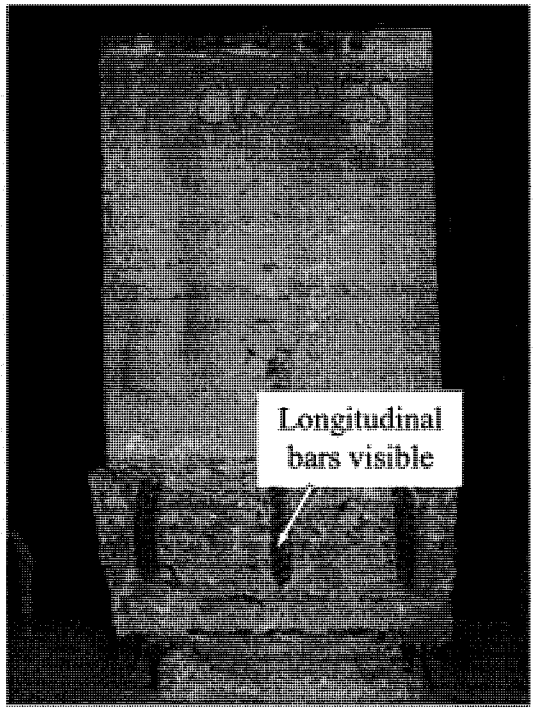

(e) At end of test (West side)

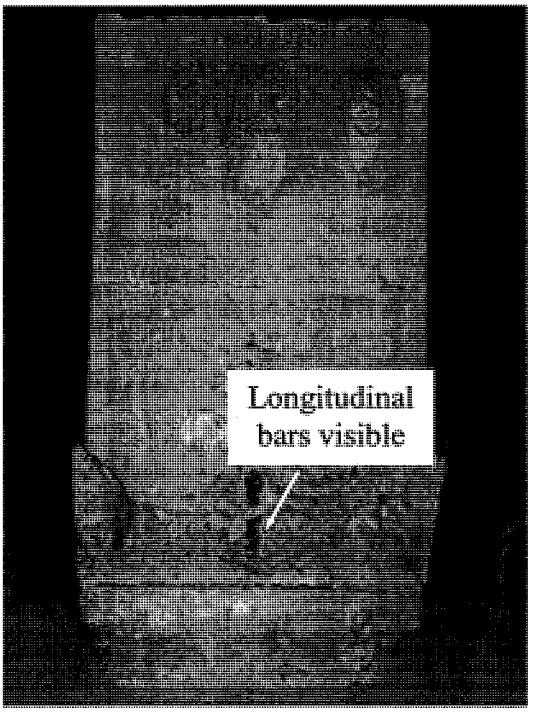

(f) At end of test (East side)

Figure A-5 Specimen CV2 (cont')

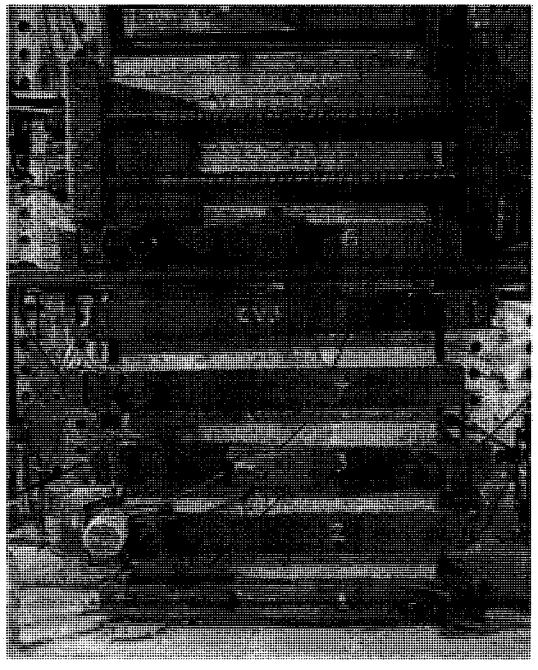

(a) At cycle 16 (μ =4) (West side)

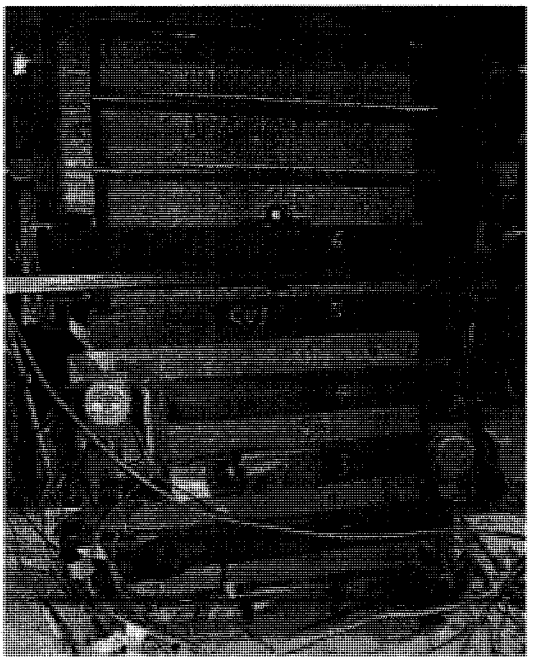

(b) At cycle 16 (μ =4) (East side)

Figure A-6 Specimen CV3

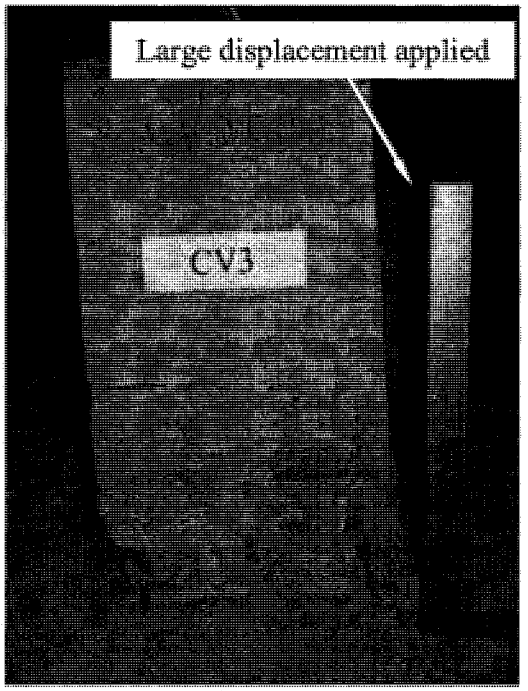

(c) Column sustained large displacement

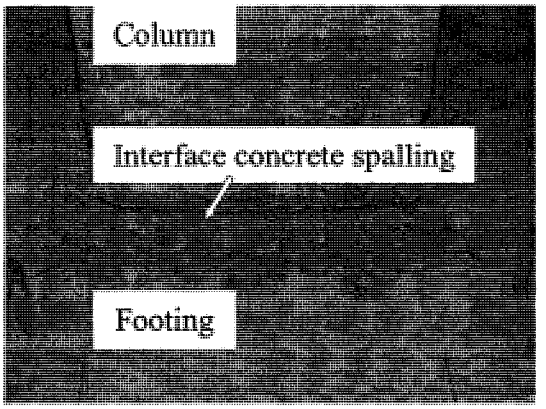

(d) Damage at the interface (North side)

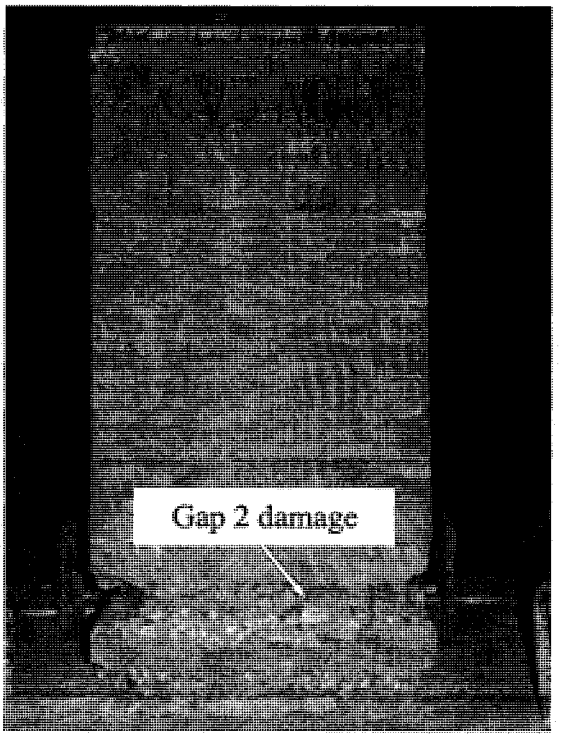

(e) At end of test (North side)

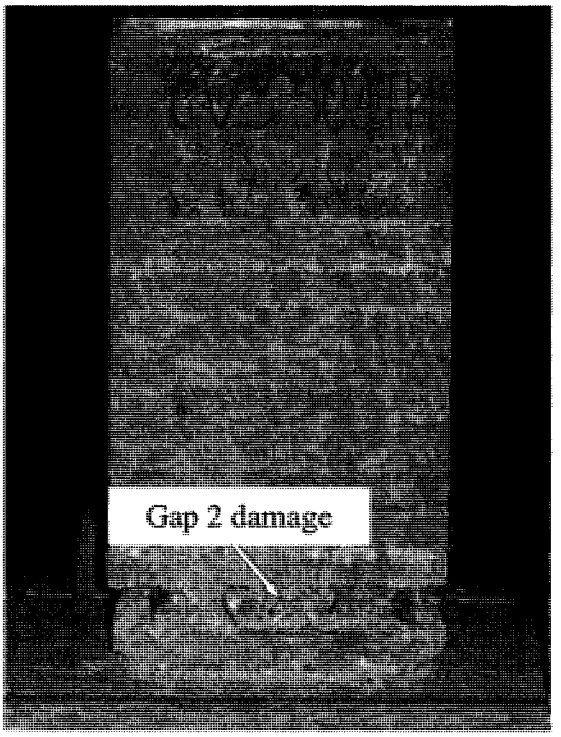

(f) At end of test (South side)

Figure A-6 Specimen CV3 (Cont')

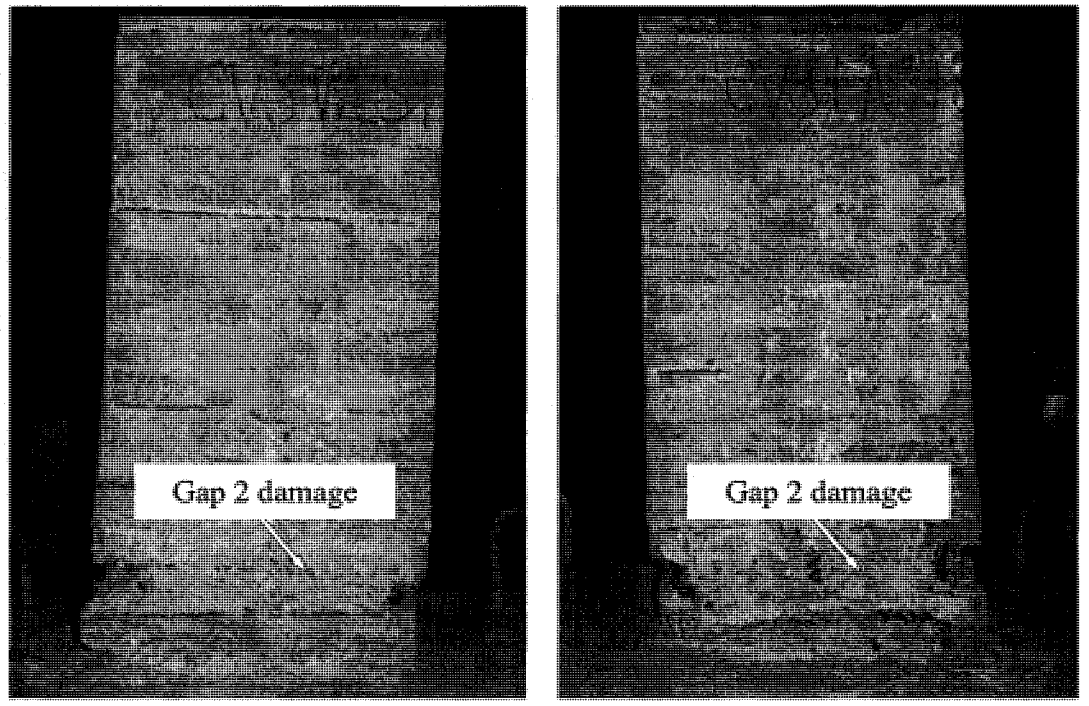

(g) At end of test (West side) (h) At end of test (East side)

Figure A-6 Specimen CV3 (Cont')

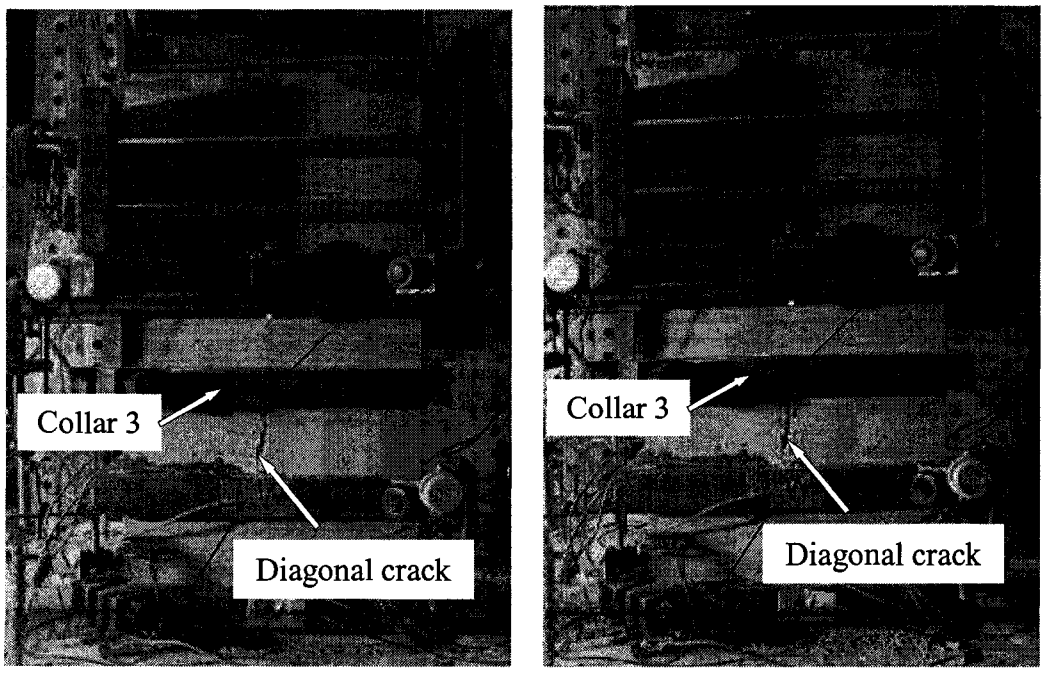

(a) Cracks at cycle 16 (μ =4) (West side) (b) Cracks at cycle 21 (μ =6) (East side)

Figure A-7 Specimen CV4

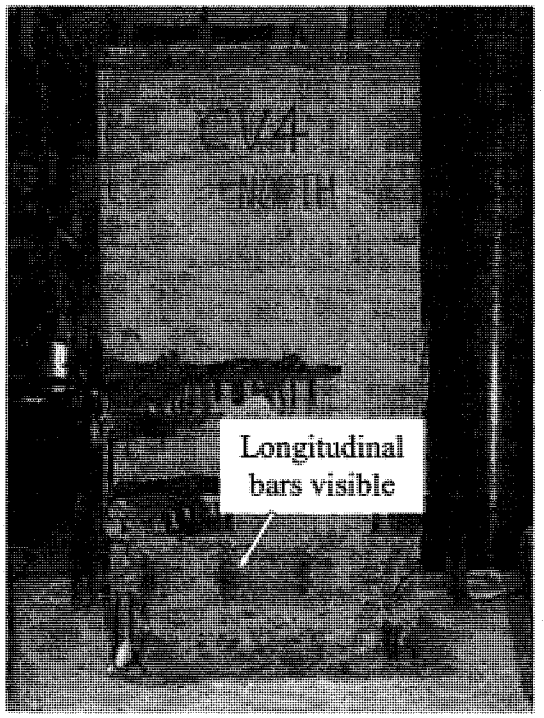

(c) At end of test (North side)

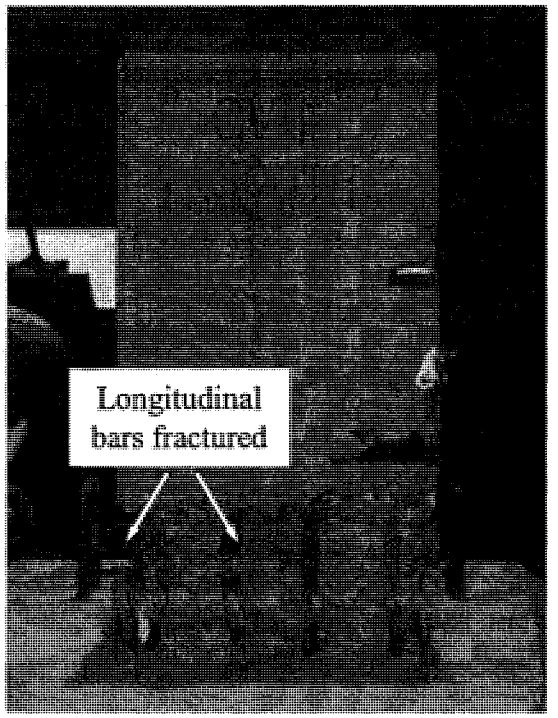

(d) At end of test (South side)

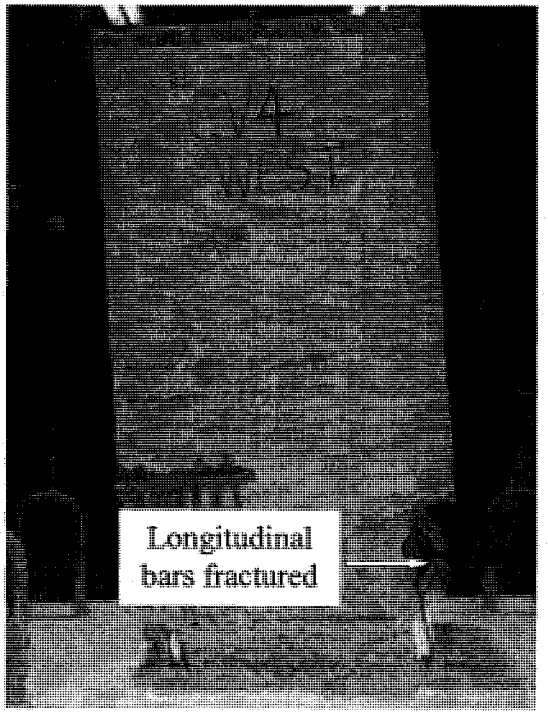

(e) At end of test (West side)

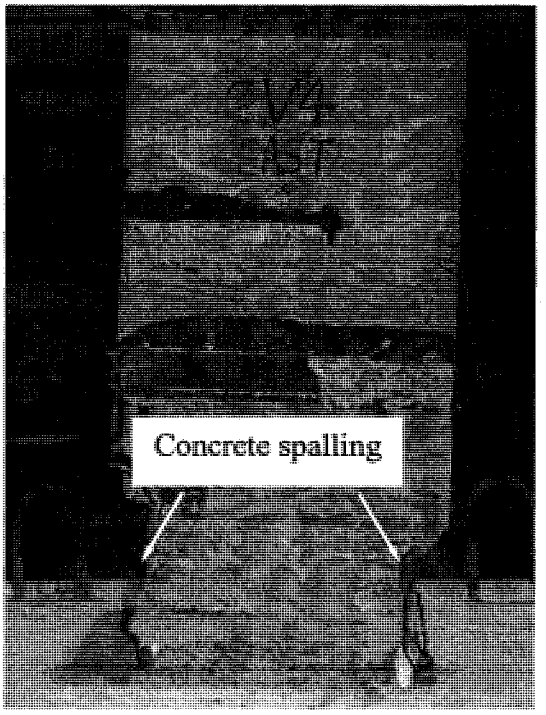

(f) At end of test (East side)

Figure A-7 Specimen CV4 (Cont')

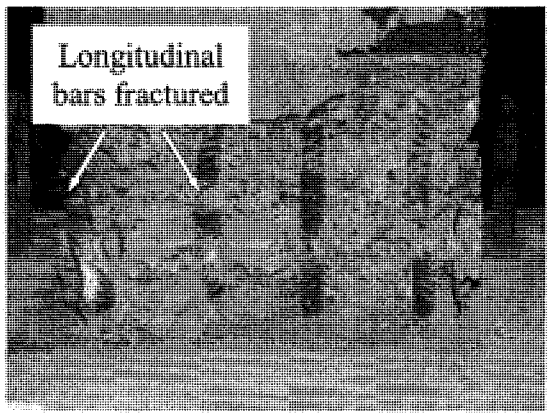

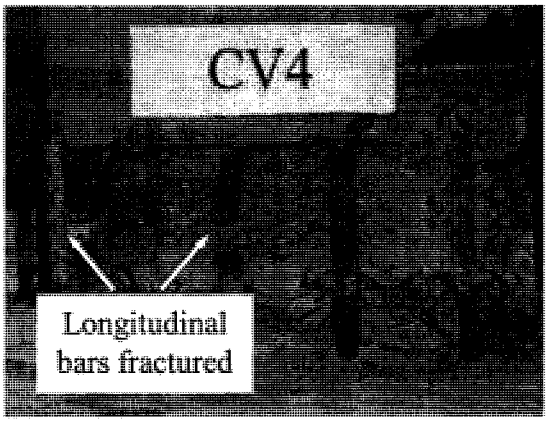

(g) Fracture of bars (South side)

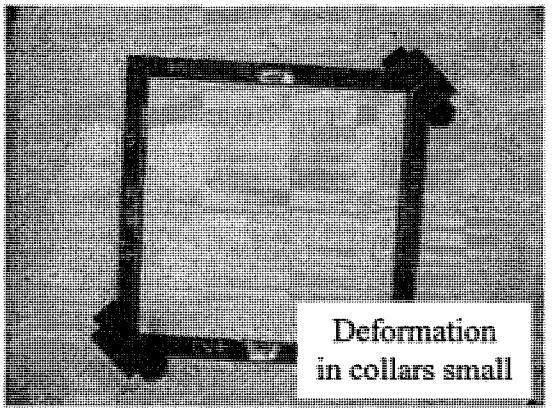

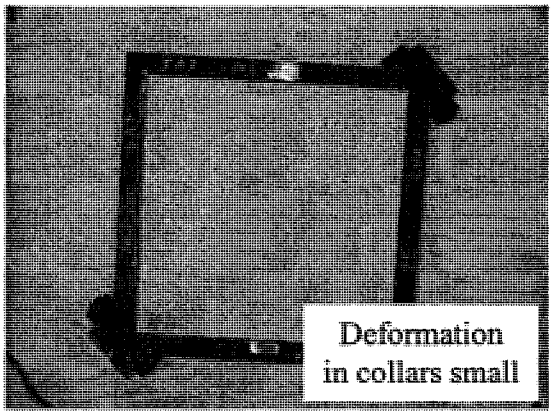

(h) Collar after test (collar 1)

(i) Collar after test (collar 2)

Figure A-7 Specimen CV4 (Cont')

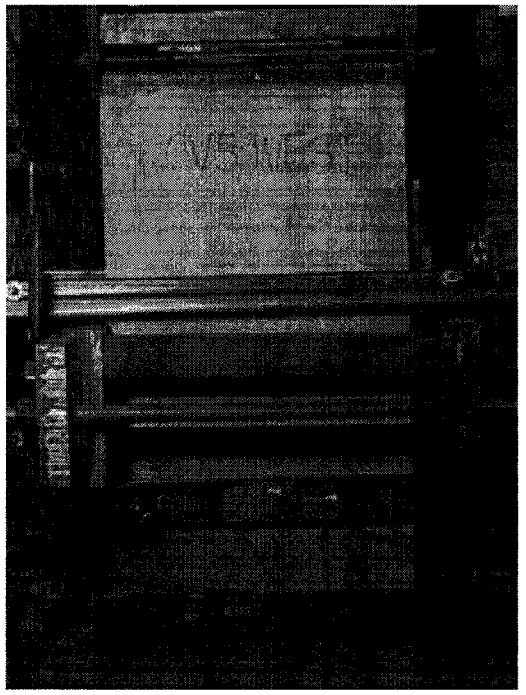

(a) At cycle 16 (μ =2.26) (West side)

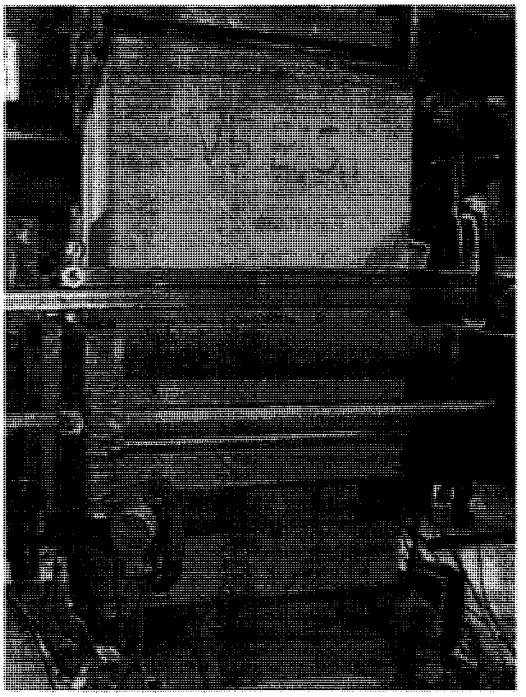

(b) At cycle 16 (μ =2.26) (East side)

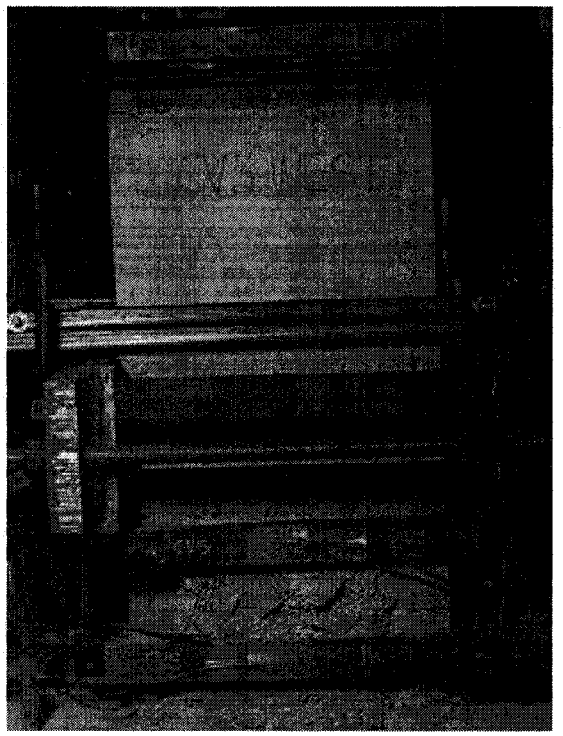

(c) Damage at cycle 26 (μ =4.52) (West side)

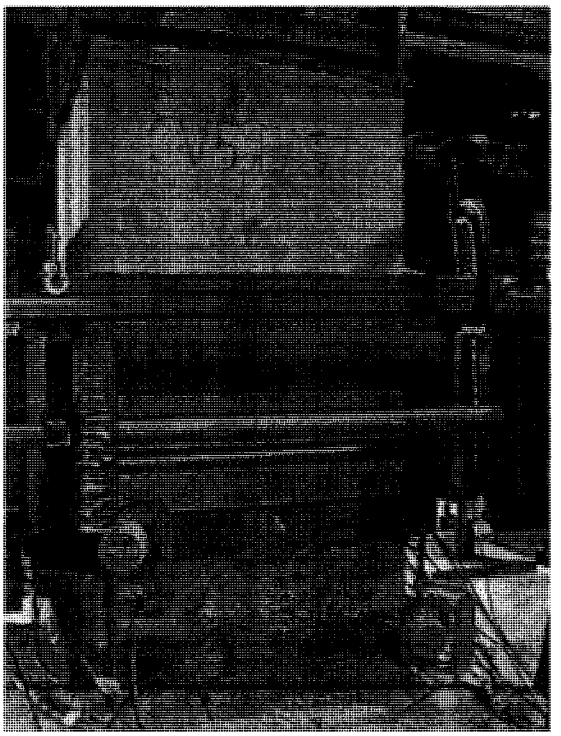

(d) At cycle 26 (μ =4.52) (East side)

Figure A-8 Specimen CV5

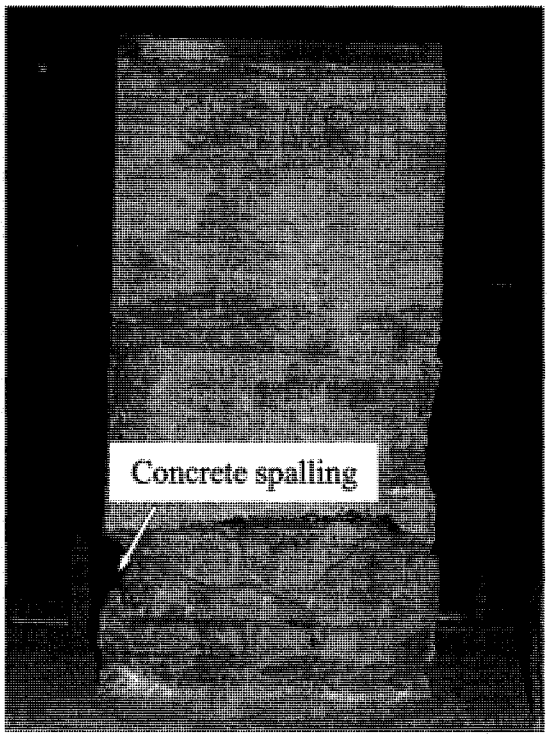

(e) At end of test (North side)

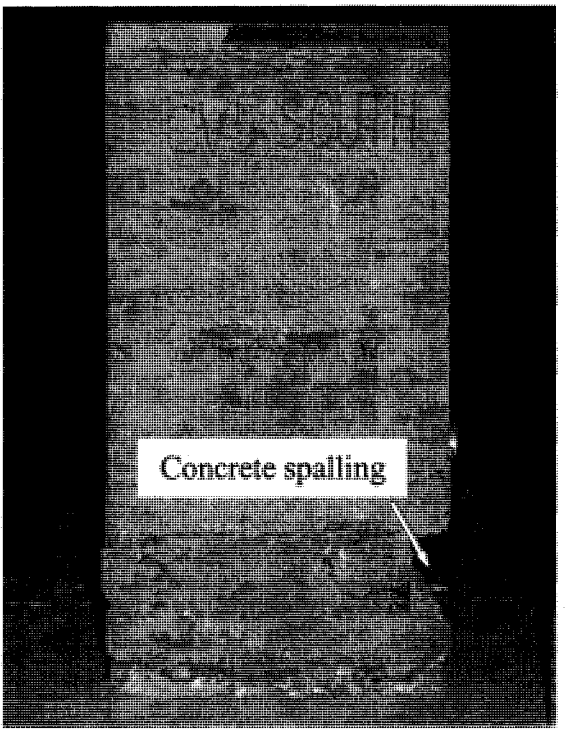

(f) At end of test (South side)

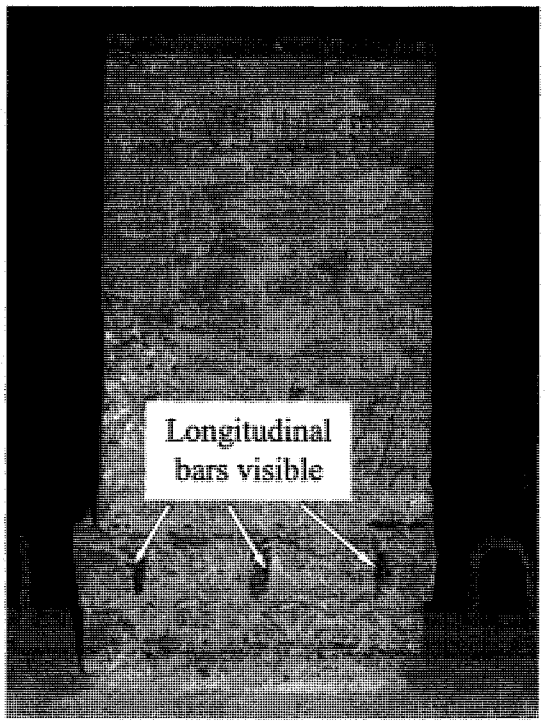

(g) At end of test (West side)

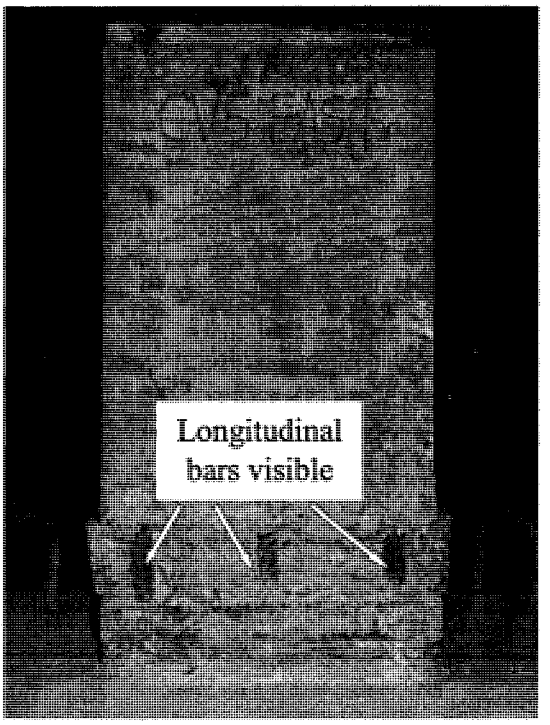

(h) At end of test (East side)

Figure A-8 Specimen CV5 (Cont')

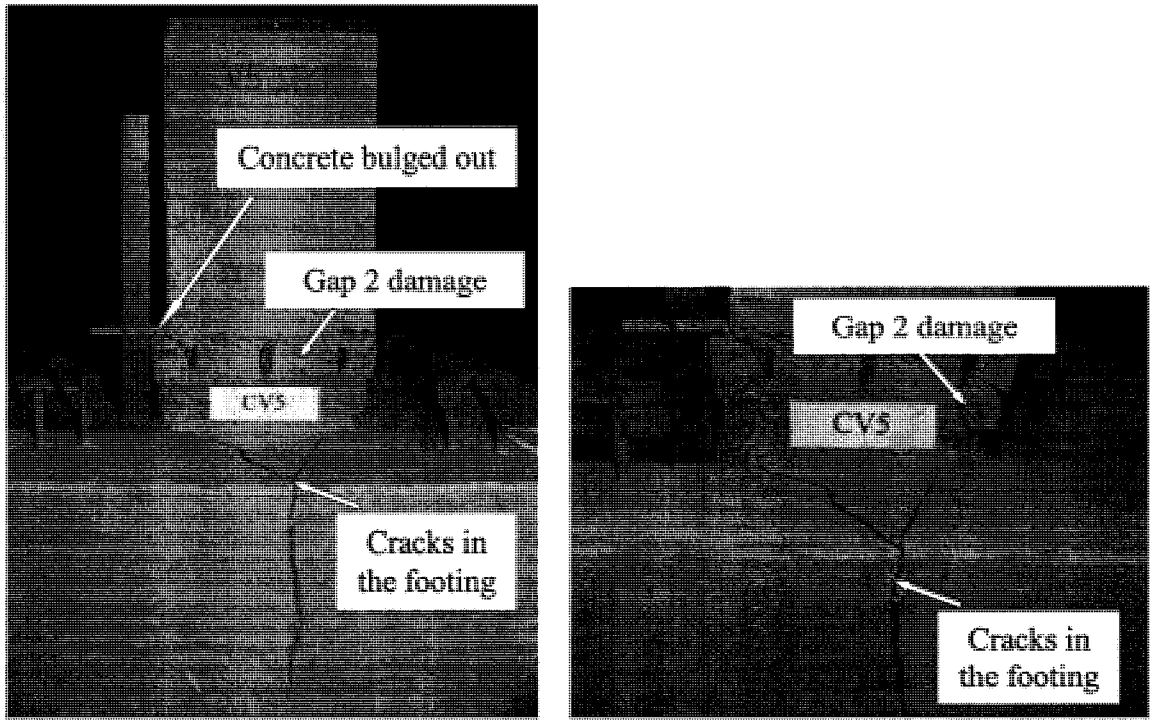

(i) Cracks in footing

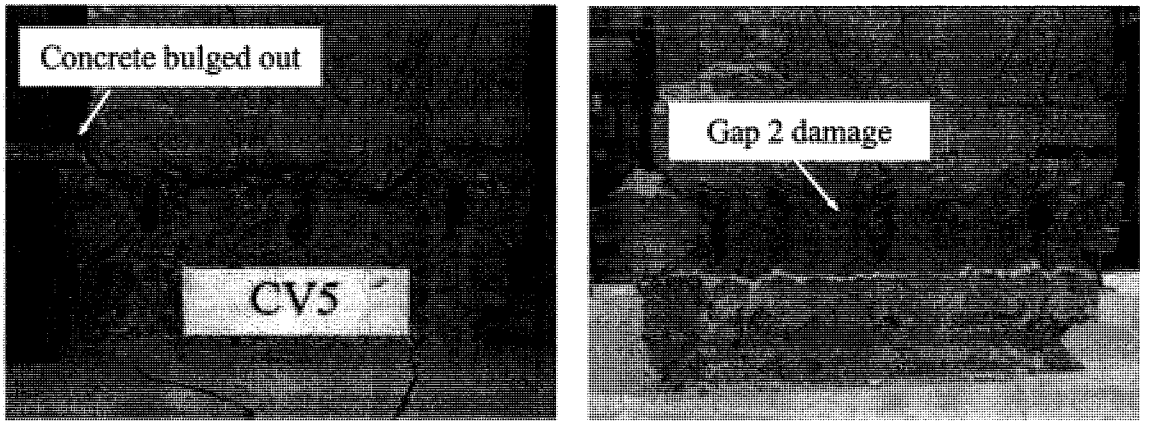

(j) Shear displacement

Figure A-8 Specimen CV5 (Cont')

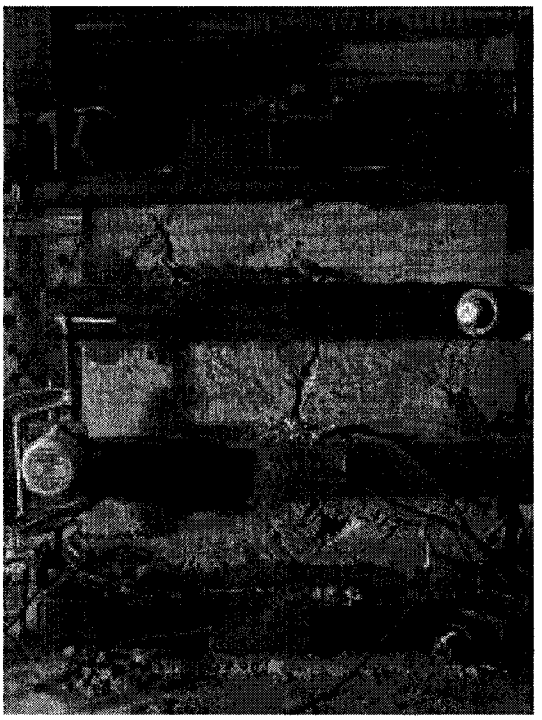

(a) Cracks at cycle 16 (μ =4) (West side)

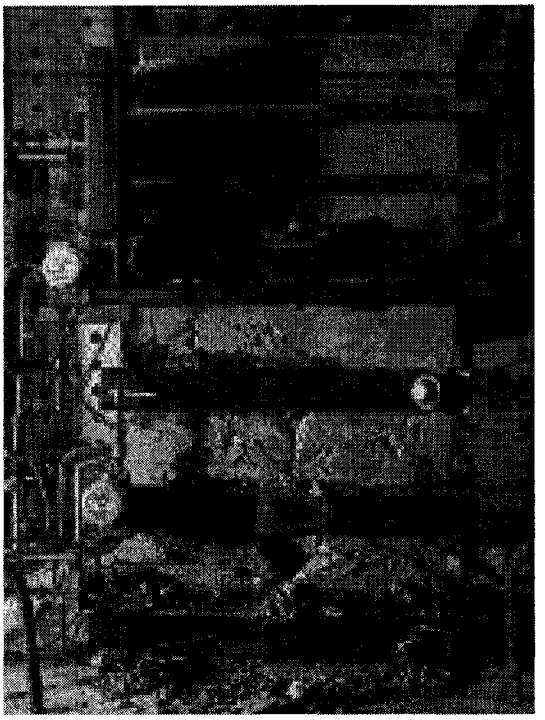

(b) Damage at cycle 18 (μ =4) (West side)

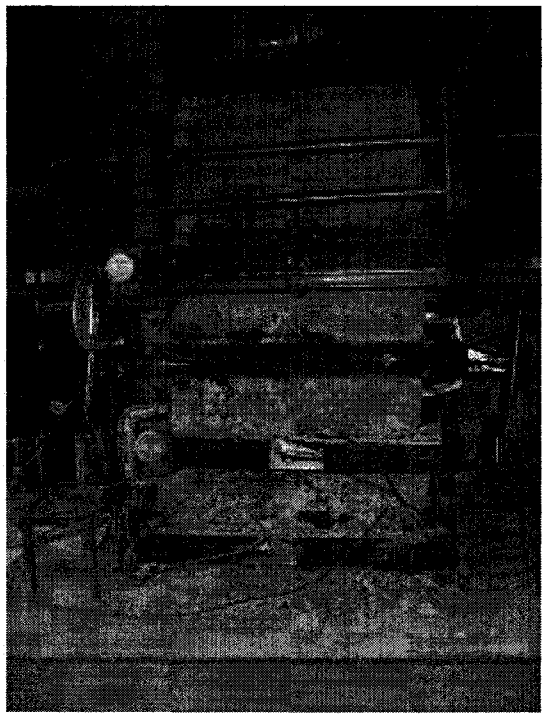

(c) Damage at cycle 21 (μ =6) (West side)

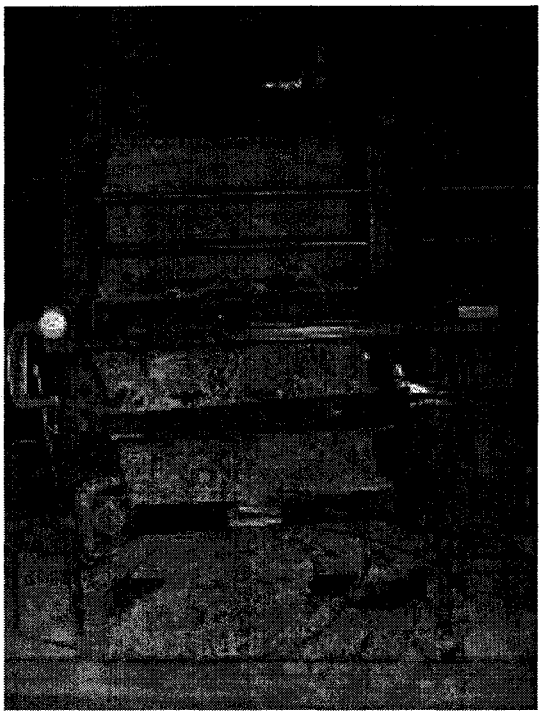

(d) Damage at cycle 26 (μ =7) (West side)

Figure A-9 Specimen CV6

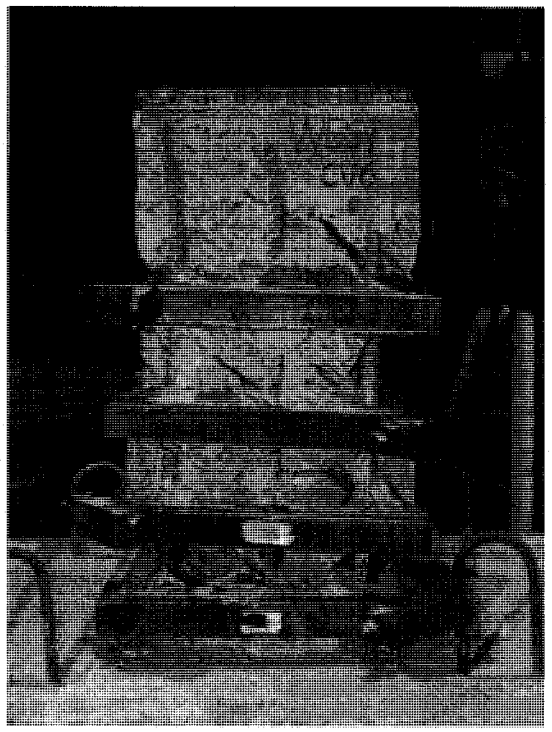
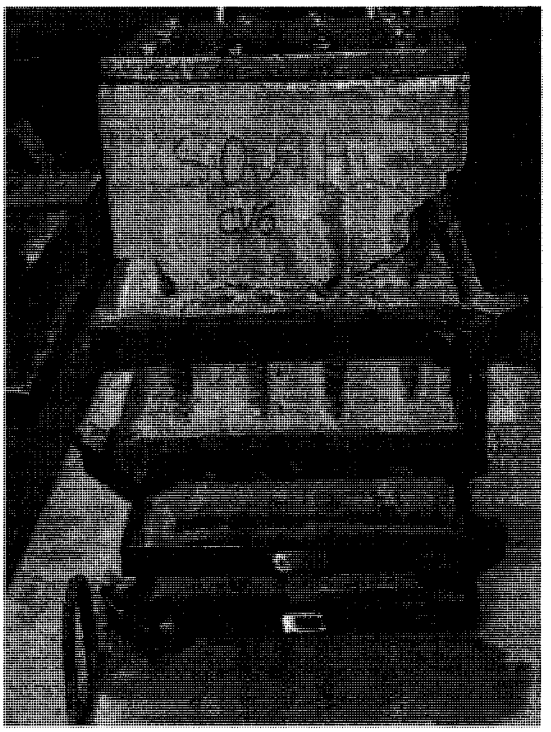

(e) At end of test (No slippage of collars even under significant concrete spalling)

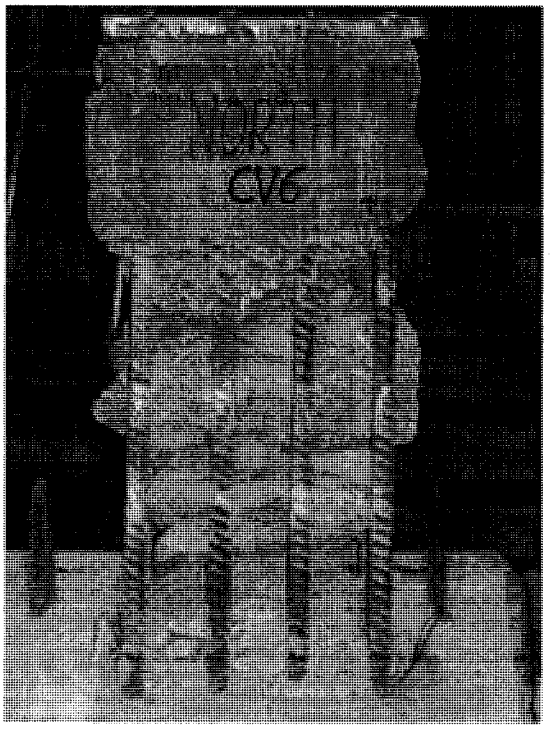

(f) At end of test (North side)

(g) At end of test (South side)

Figure A-9 Specimen CV6 (Cont')

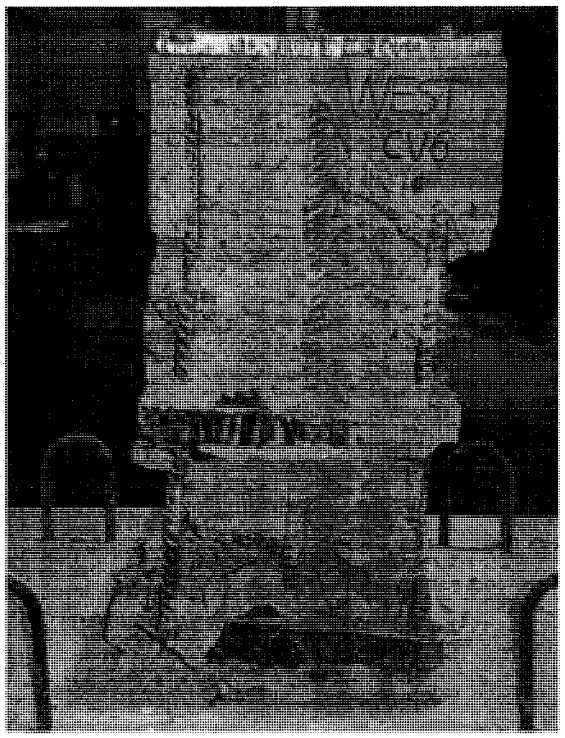

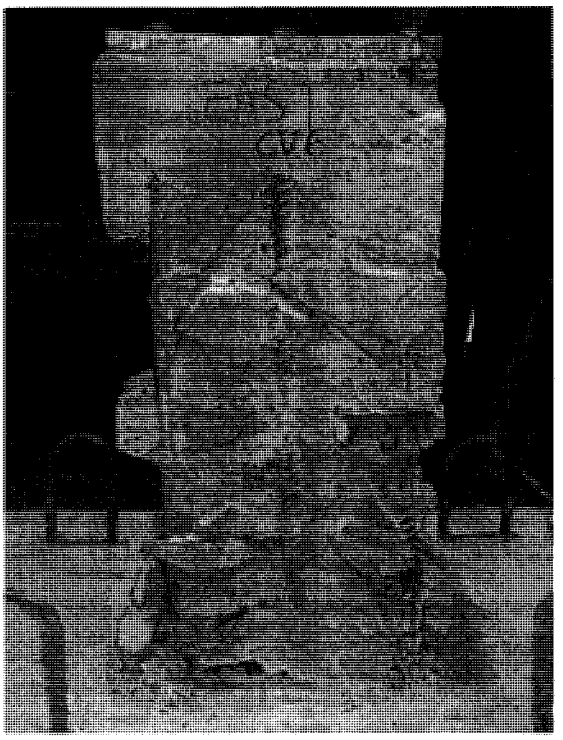

(h) At end of test (West side)

(i) At end of test (East side)

Figure A-9 Specimen CV6 (Cont')

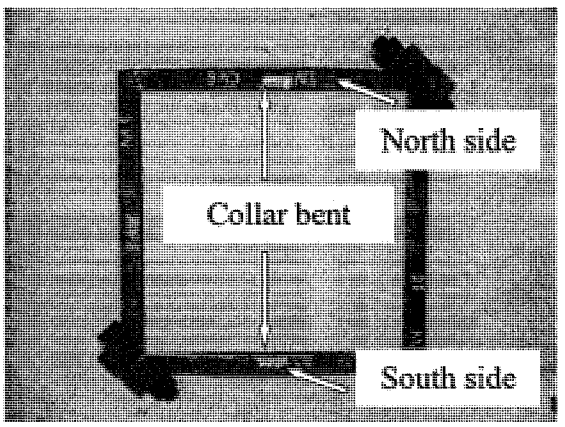

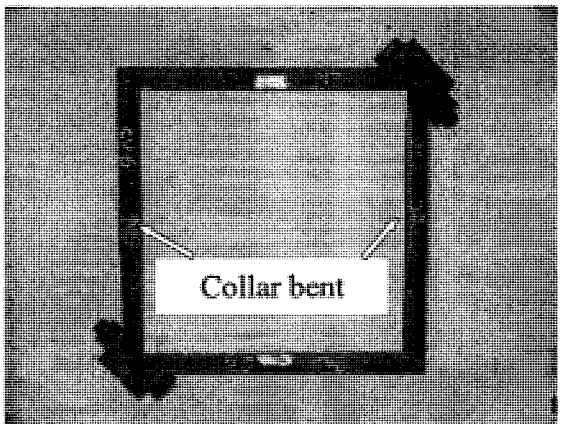

(j) Collar after test (collar 1)

(k) Collar after test (collar 2)

Figure A-9 Specimen CV6 (Cont')

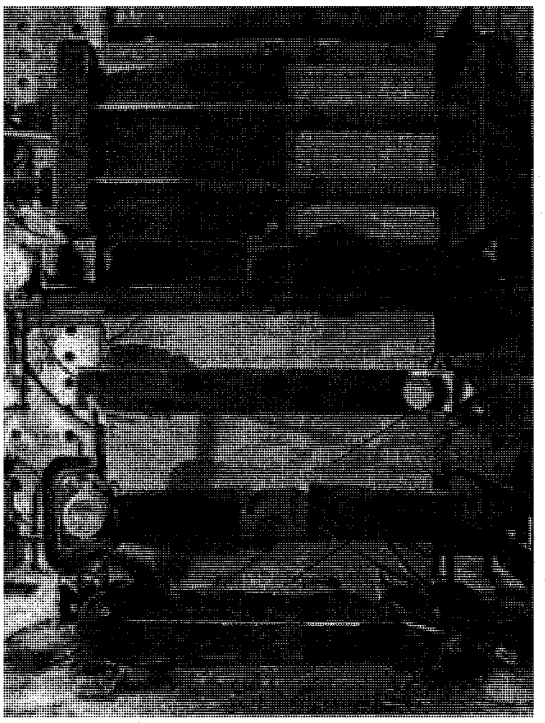

(a) At cycle 16 (μ =4) (West side)

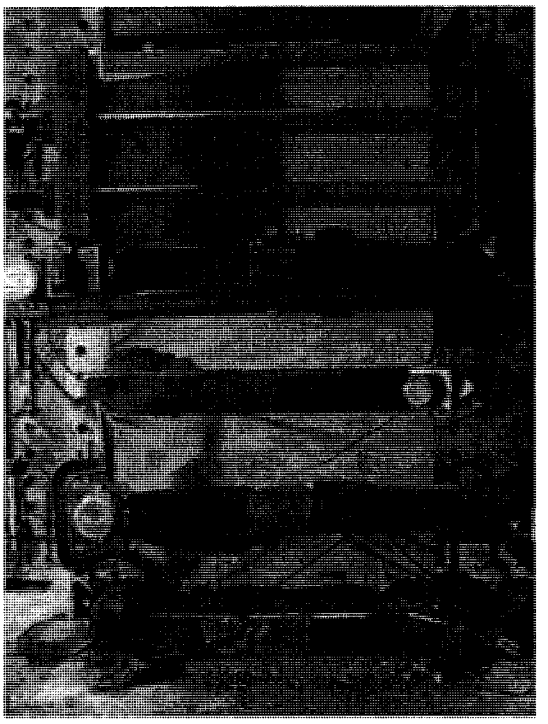

(b) At cycle 21 (μ =6) (West side)

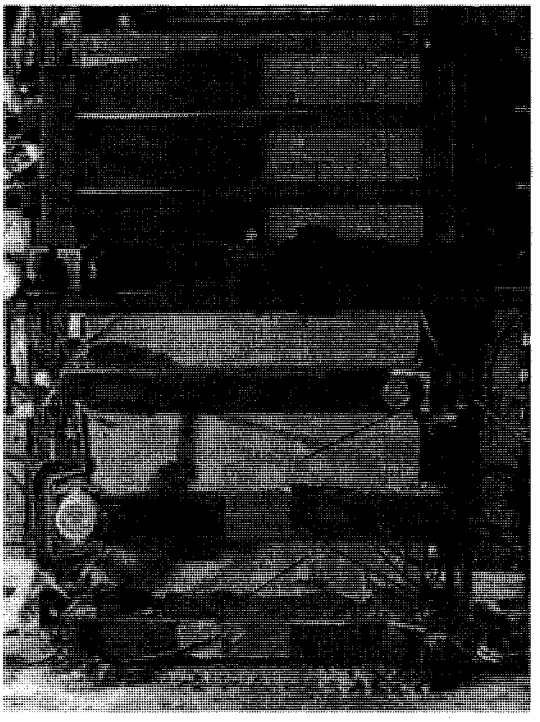

(c) At cycle 26 (μ =8) (West side)

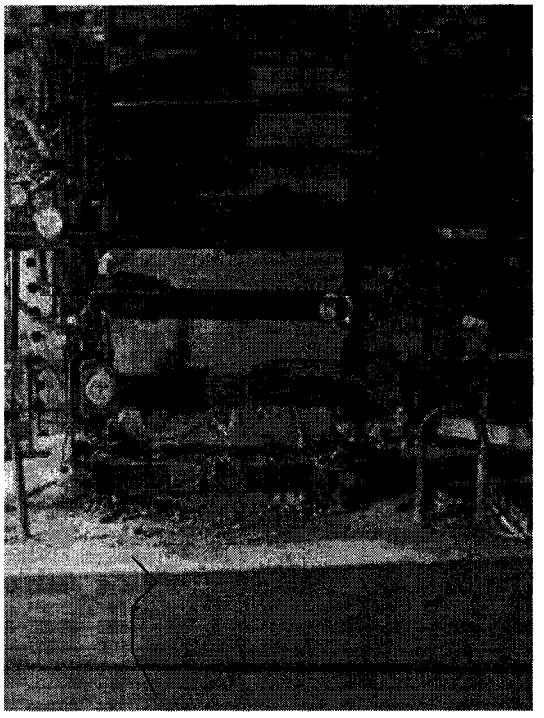

(d) At cycle 29 (μ =8) (West side)

Figure A-10 Specimen CV7

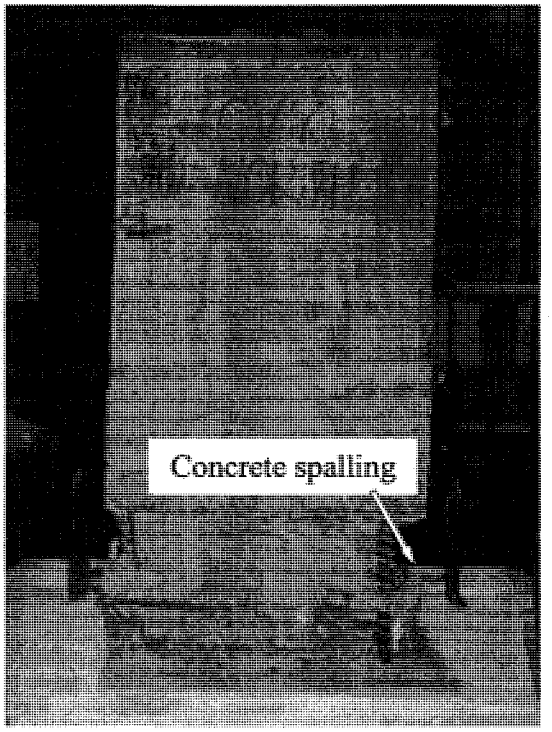

(e) At end of test (North side)

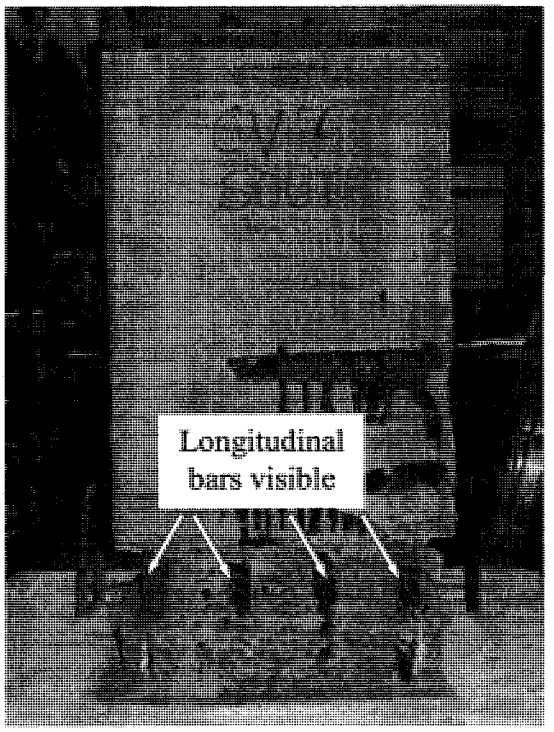

(f) At end of test (South side)

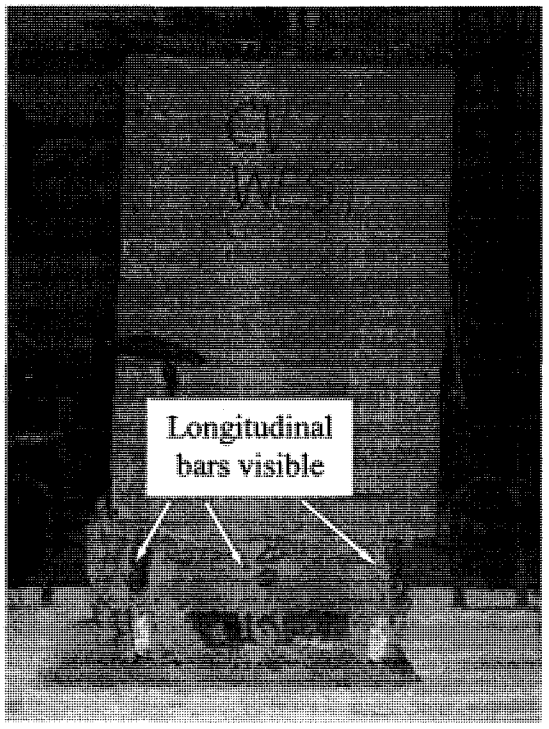

(g) Minor damage except at the bottom (West side)

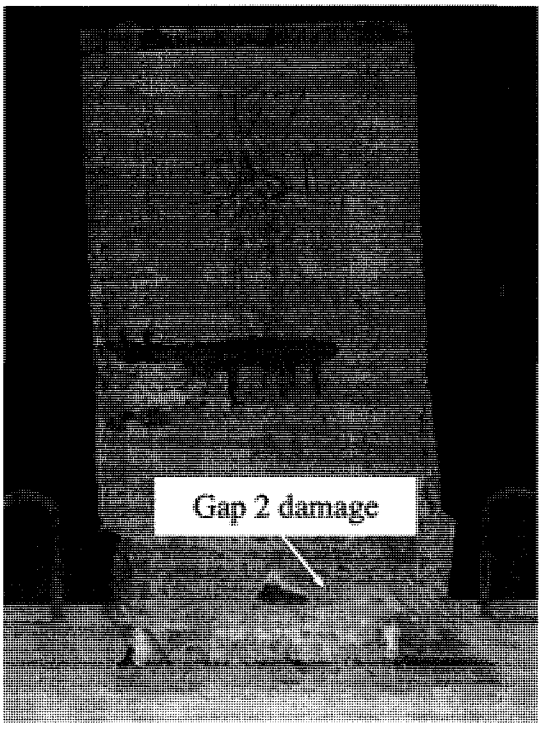

(h) At end of test (East side)

Figure A-10 Specimen CV7 (Cont')

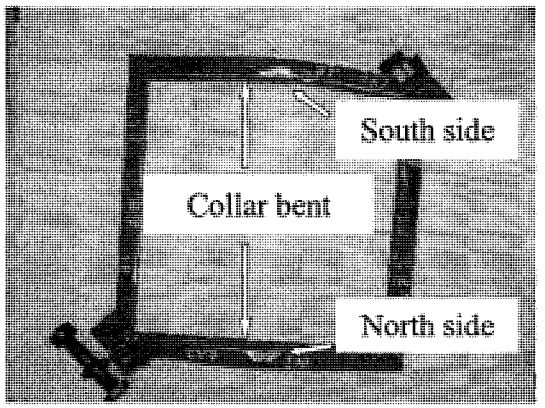

(i) Collar after test (collar 1)

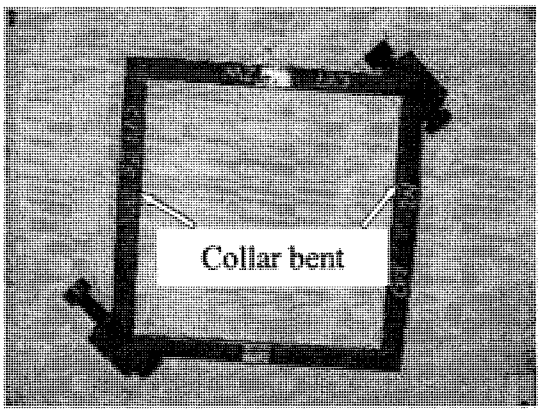

(j) Collar after test (collar 2)

Figure A-10 Specimen CV7 (Cont')

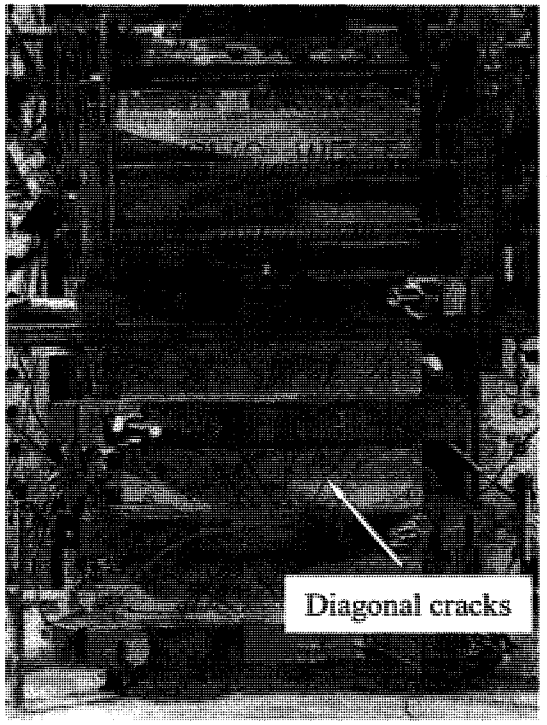

(a) Cracks at cycle 16 (μ =4) (West side)

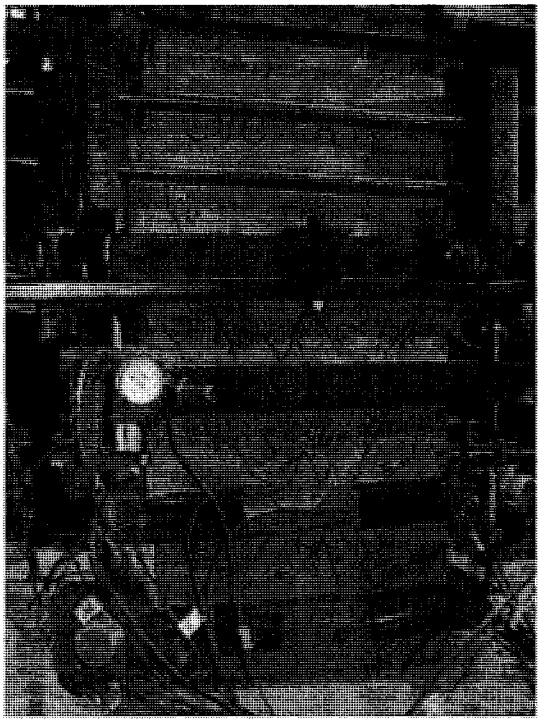

(b) At cycle 16 (μ =4) (East side)

Figure A-11 Specimen CV8

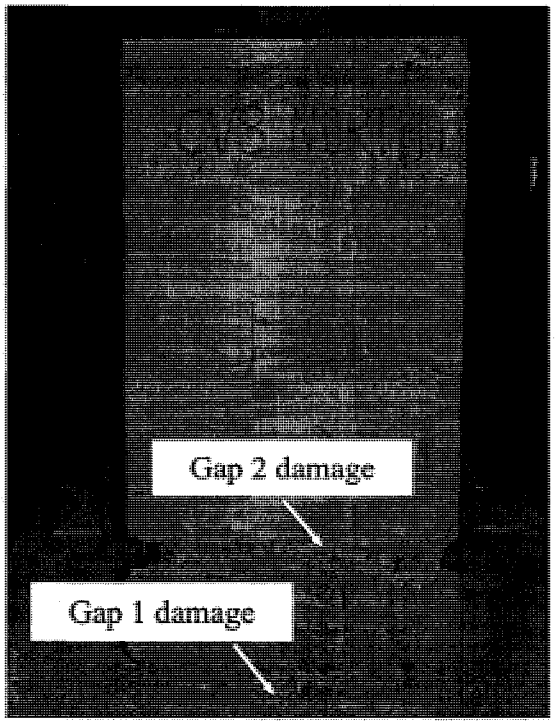

(c) At end of test (North side)

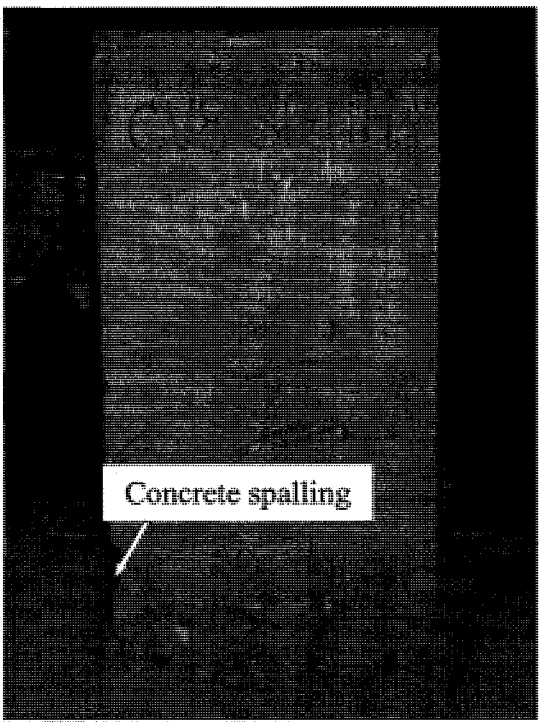

(d) At end of test (South side)

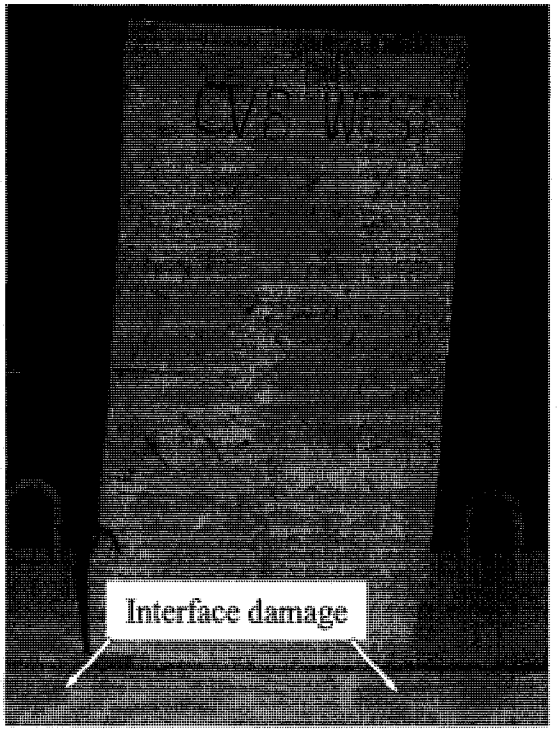

(e) At end of test (West side)

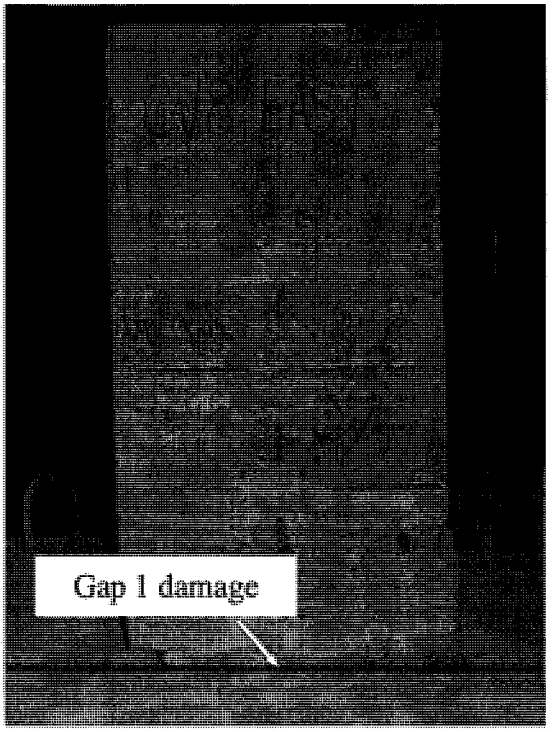

(f) At end of test (East side)

Figure A-11 Specimen CV8 (Cont')

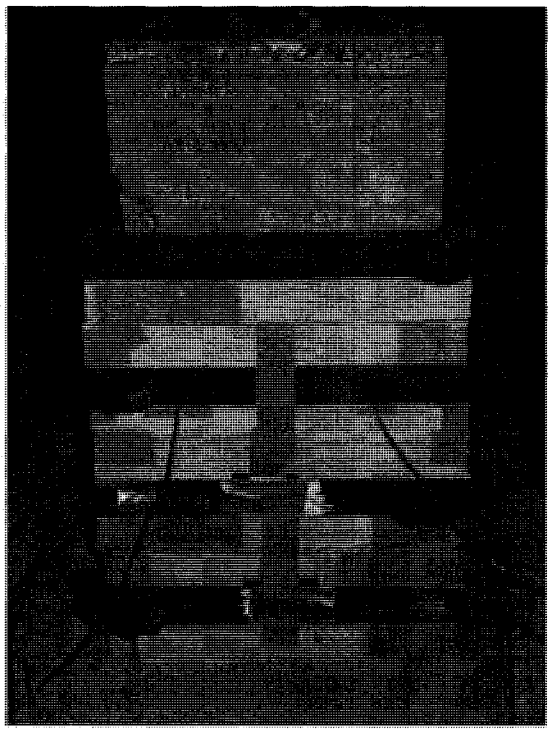

(a) Form for grout

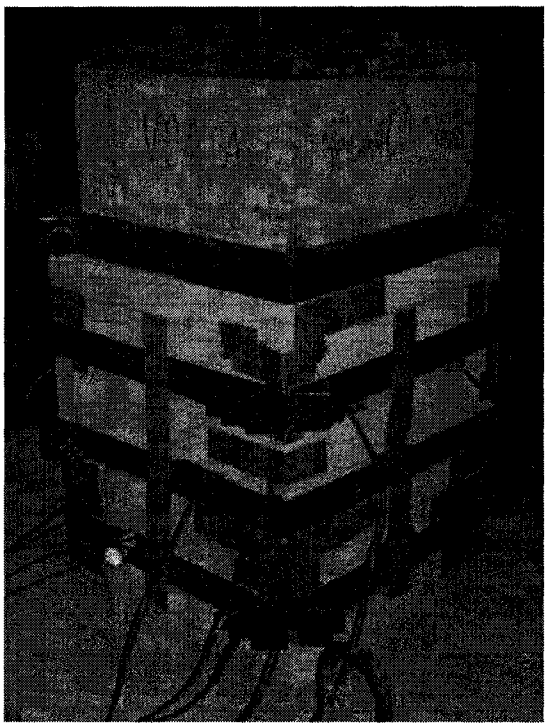

(b) Form for grout

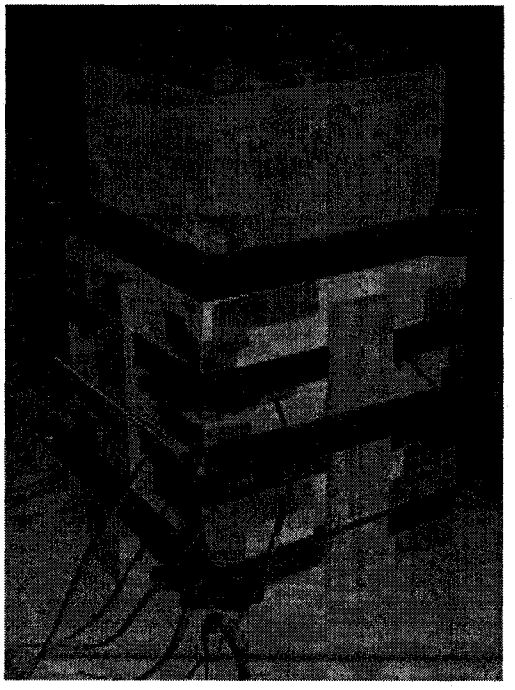

(c) Brace system for form

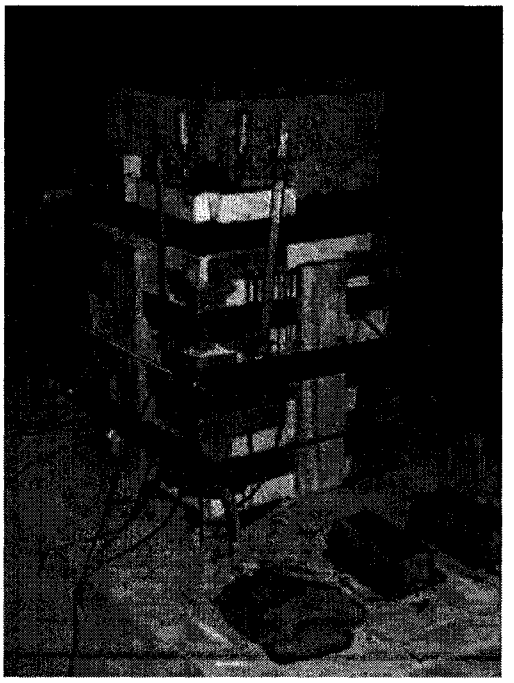

(d) After grout

Figure A-12 Repair of damaged specimen

Appendix B—Moment-drift hysteresis curves for test specimens

As mentioned in the Chapter 4 Section 4.3, the moment at the base, where the critical section is, accounts for the geometry, lateral loads, and axial loads within the system, including the $P-\Delta$ effect. Moment is calculated by Eq. 4-1. Lateral drift, expressed in percentage, is defined as the lateral displacement at the point of application (Δ_2) of the horizontal load divided by the vertical distances from the base of the column to the horizontal loading position (H_1), and calculated as follow:

$$Drift = \Delta_2 / H_1 \times 100\% \qquad \text{[B-1]}$$

where H_1 is 650 mm for all the test specimens except specimen CV5 which is 350 mm.

Figure B-1 to Figure B-11 show the moment-drift hysteretic response for the test specimens.

A moment-drift envelope for each column was obtained by connecting the peak points for the initial hysteresis loop obtained at each displacement level. The moment-drift envelopes for the test specimens are shown in Figure B-12.

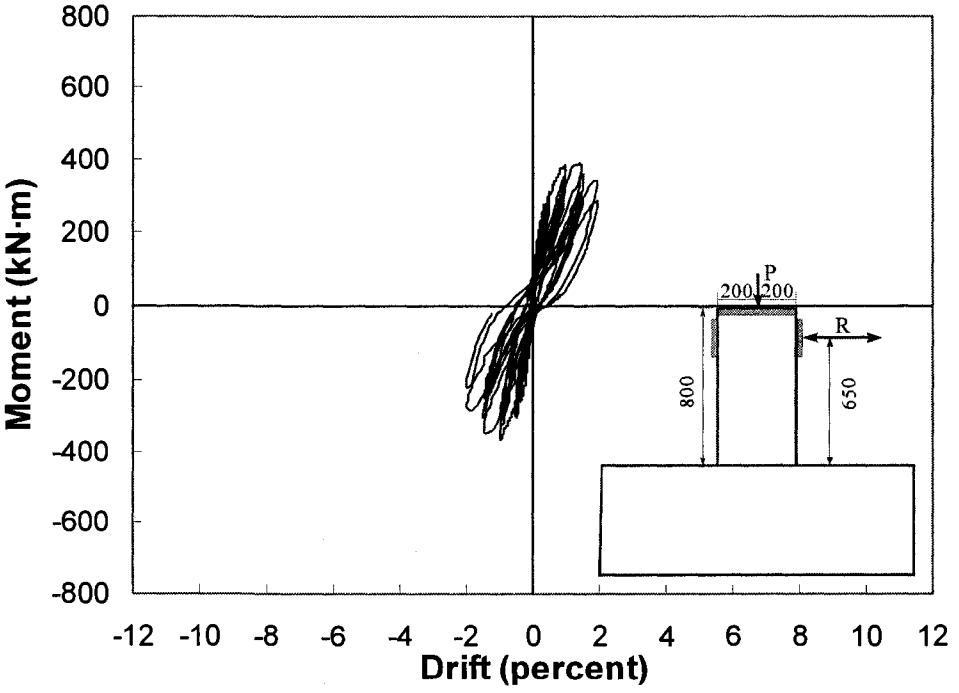

Figure B-1 Moment–drift hysteresis loops for specimen CV0A

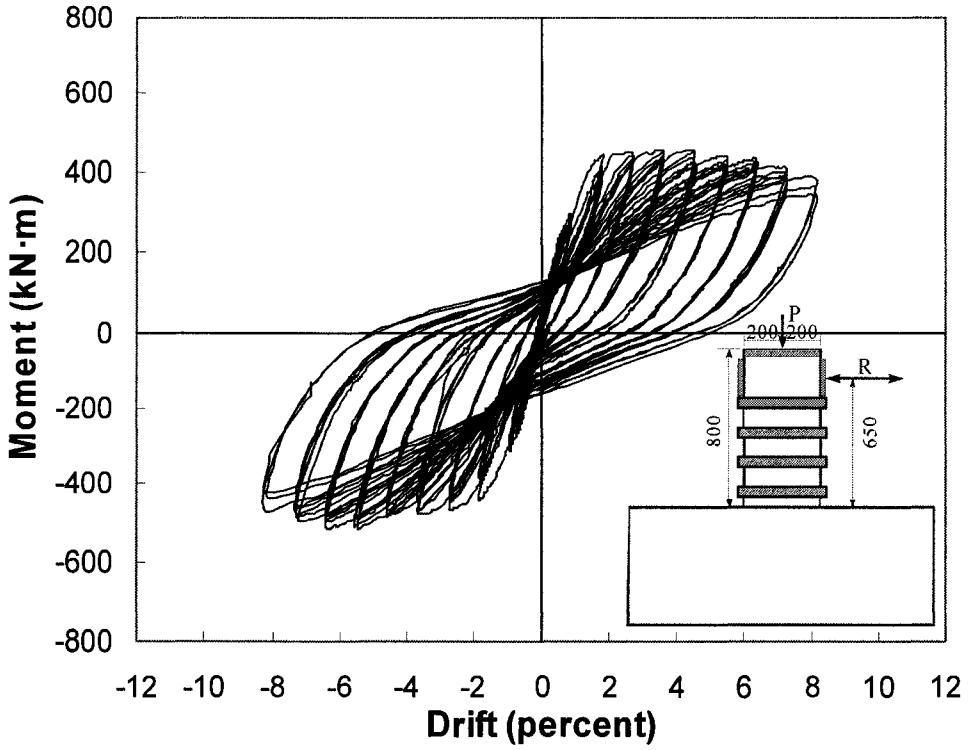

Figure B-2 Moment–drift hysteresis loops for specimen CV0AR

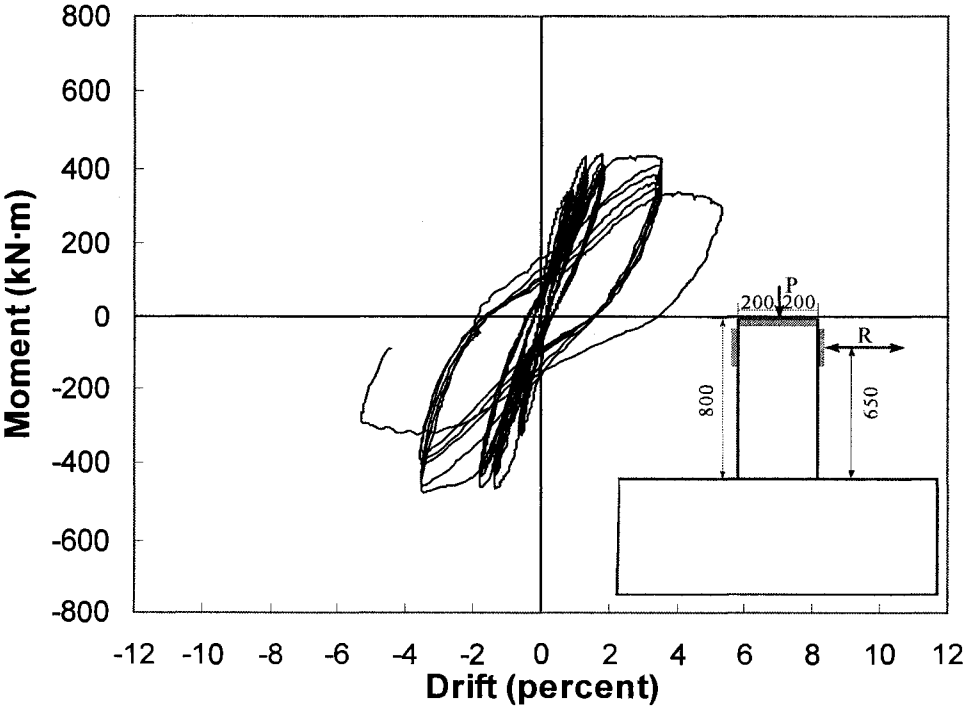

Figure B-3 Moment–drift hysteresis loops for specimen CV0B

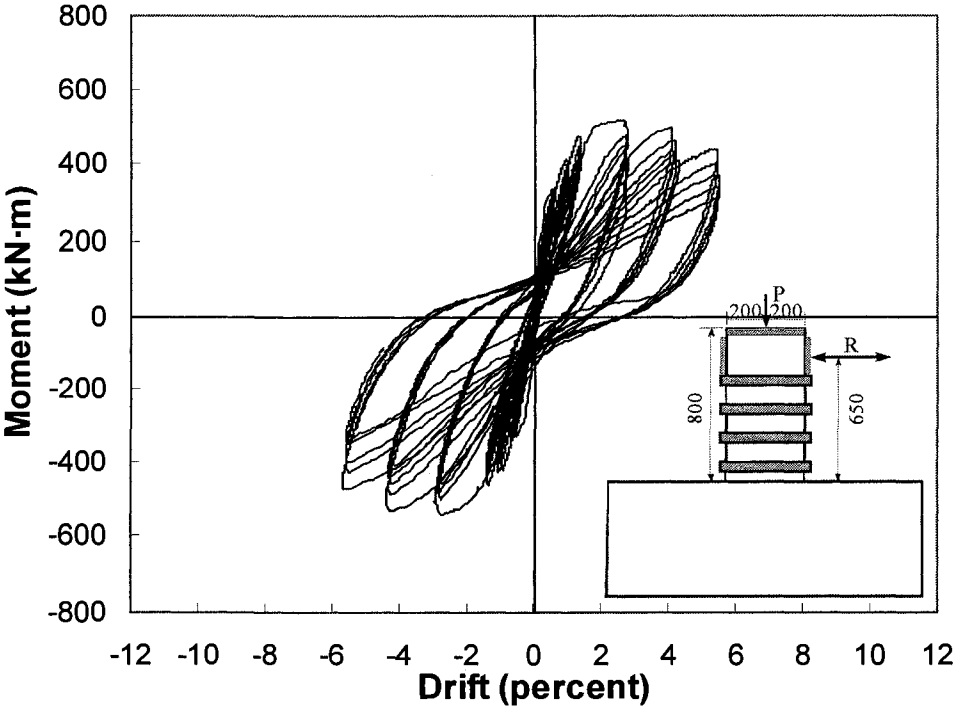

Figure B-4 Moment–drift hysteresis loops for specimen CV1

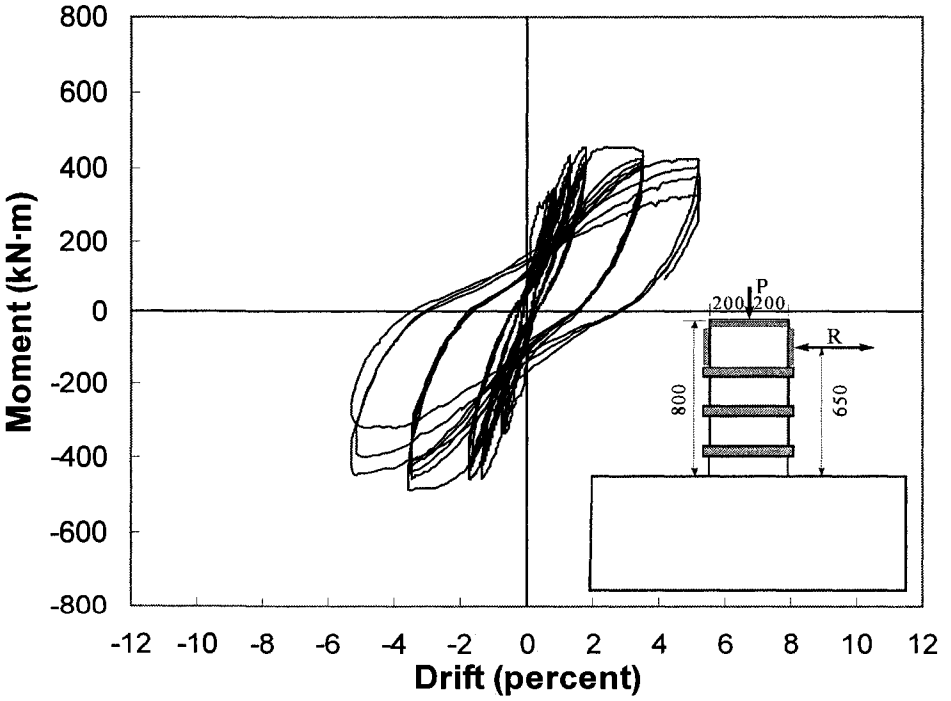

Figure B-5 Moment–drift hysteresis loops for specimen CV2

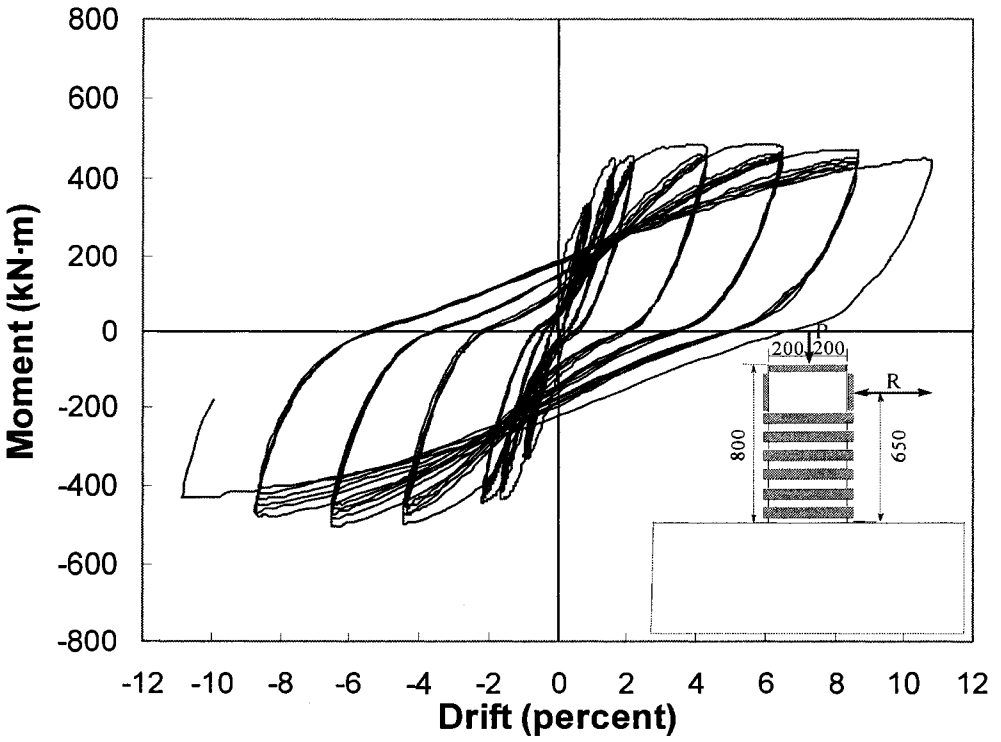

Figure B-6 Moment–drift hysteresis loops for specimen CV3

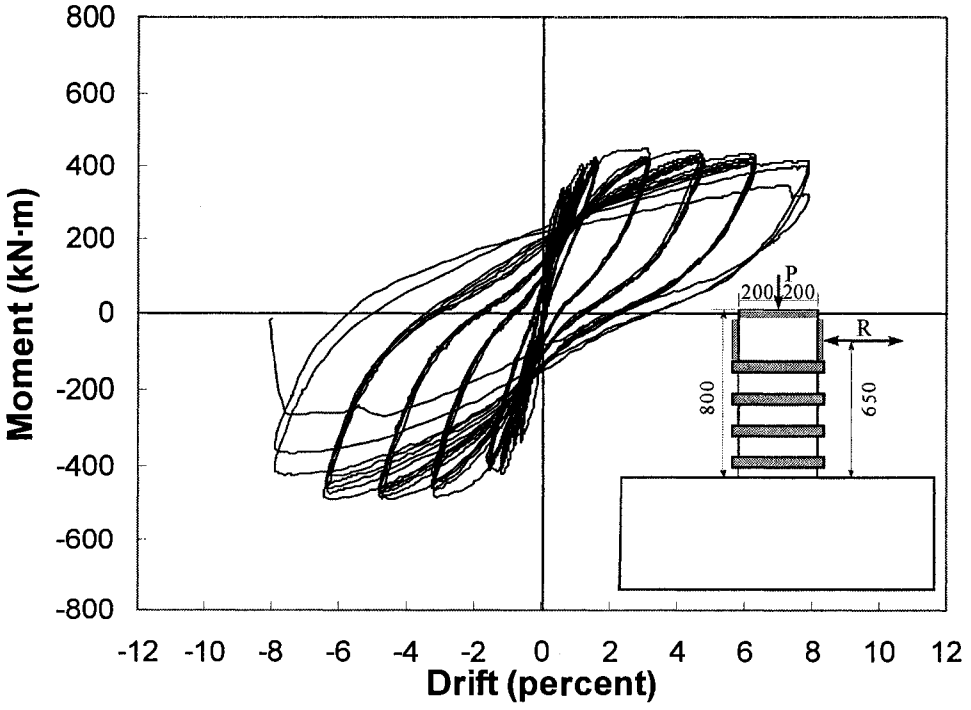

Figure B-7 Moment–drift hysteresis loops for specimen CV4

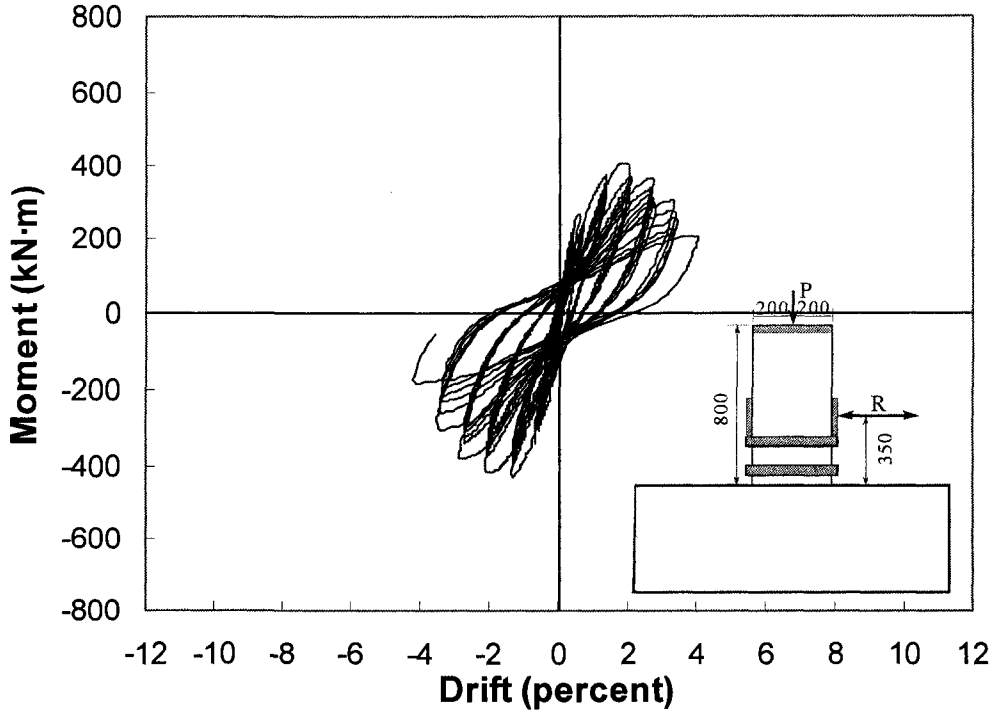

Figure B-8 Moment–drift hysteresis loops for specimen CV5

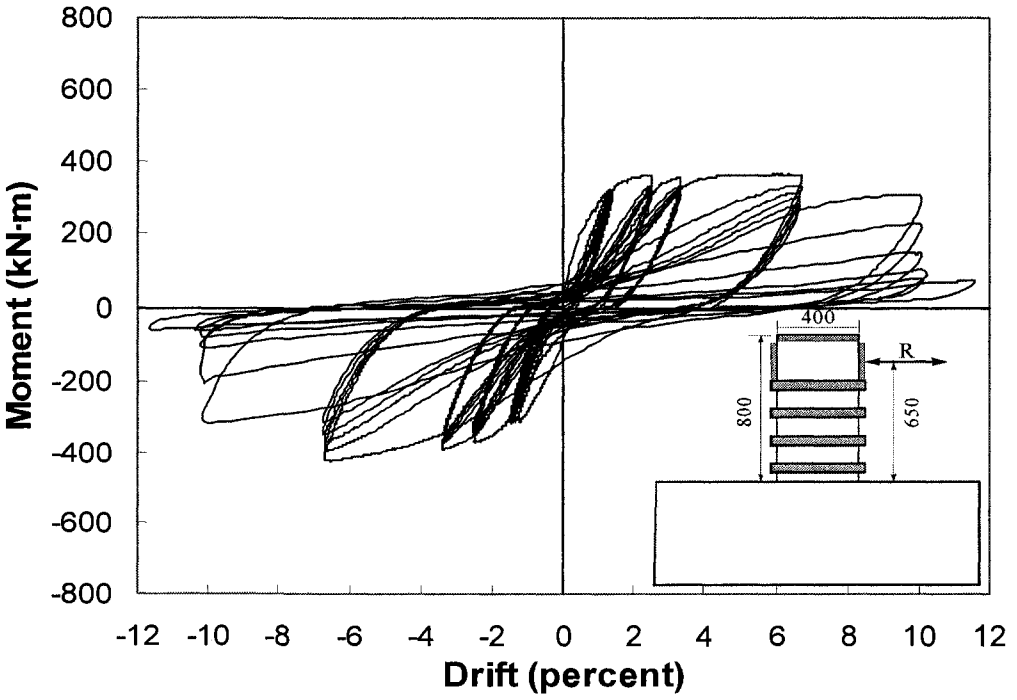

Figure B-9 Moment–drift hysteresis loops for specimen CV6

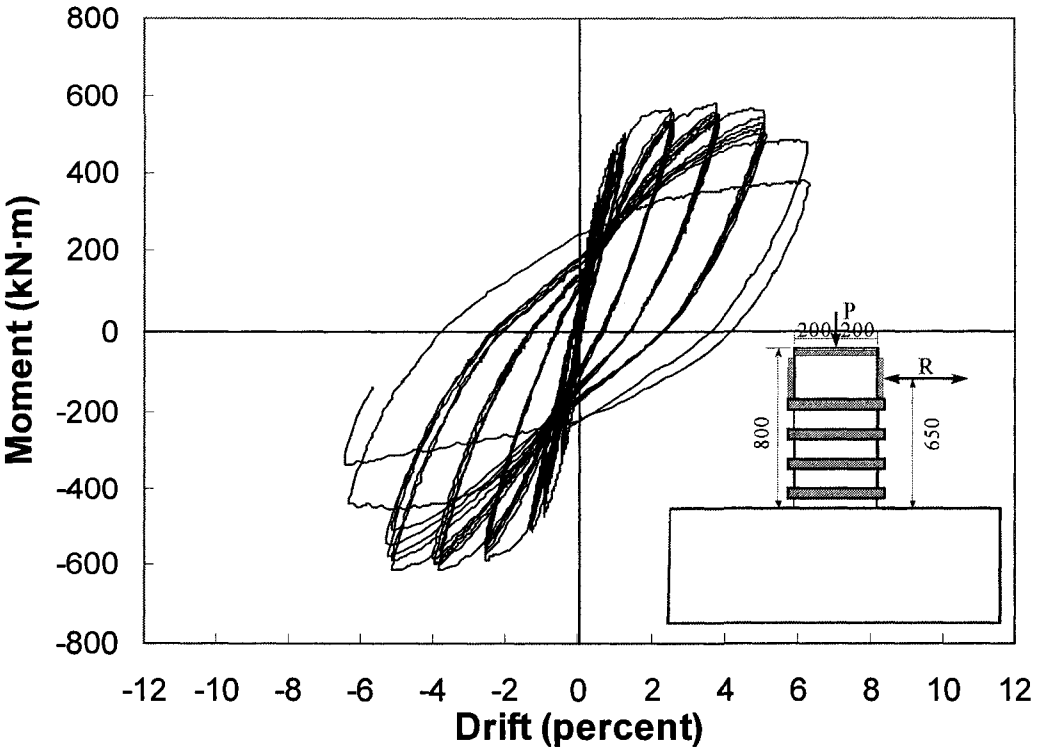

Figure B-10 Moment–drift hysteresis loops for specimen CV7

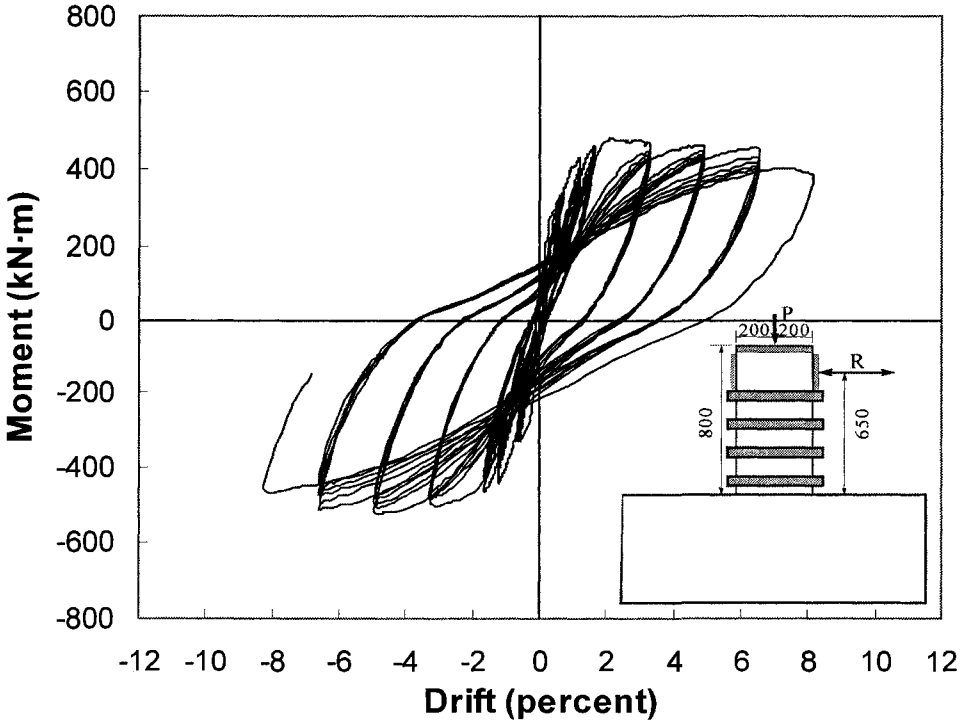

Figure B-11 Moment–drift hysteresis loops for specimen CV8

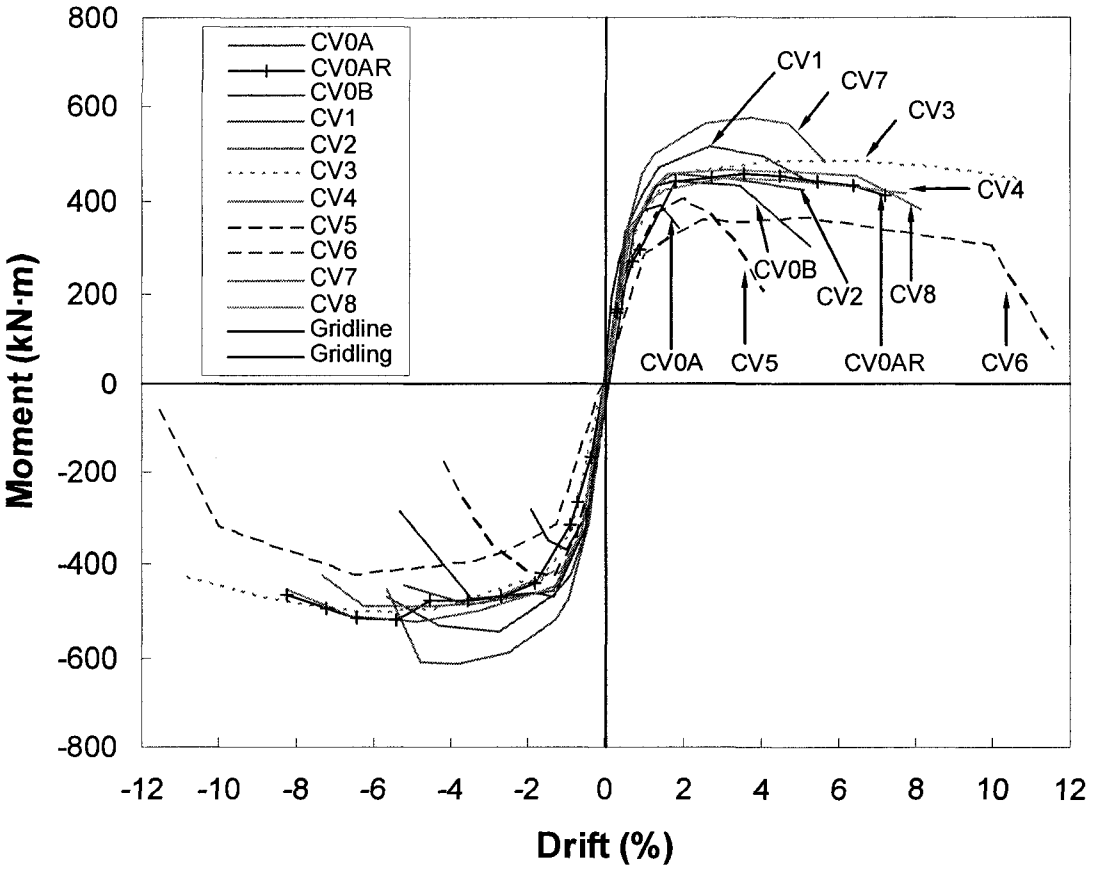

Figure B-12 Moment–drift envelopes for test specimens

Appendix C—Peak lateral force comparisons between finite element analysis results and proposed model evaluations for columns with parameter variations

As discussed in the Chapter 6 Section 6.4.4, Tables 6-7 and 6-8 show the range of the comparison between the finite element analysis result and the proposed model evaluation for 400×400×800 mm and 600×600×1225 mm columns with parameters varied. Parameters considered include collar spacing and collar stiffness, bolt pretension, longitudinal reinforcement ratio, aspect ratio, axial compression index, concrete compressive strength. Detailed values for finite element result and proposed model evaluations are shown in Tables C-1 (a) through C-1 (u) and Tables C-2 (a) through C-2 (u).

For the 400×400×800 mm columns, the specimen CV1 was taken as the standard case reference collared column in the parametric study for convenience, with variations of the parameters reported in the corresponding tables: 30×50 mm external steel collar with centre-to-centre spacing of 150 mm, concrete compressive strength of 33.3 MPa, ten 25M longitudinal bars, shear span of 650 mm, no pretension applied to the collar connection bolts, and axial compression index of 0.3. Similarly, for the 600×600×1225 mm columns, the standard case reference collared column has the following features (identical to CV1 except for the shear span): 30×50 mm external steel collar with centre-to-centre spacing of 150 mm, concrete compressive strength of 33.3 MPa, ten 25M longitudinal bars, shear span of 1100 mm, no pretension applied to the collar connection bolts, and axial compression index of 0.3.

$V_{lsa,flexure}$ is the lateral force corresponding to flexural strength from layered sectional analysis; $V_{lsa,shear}$ is the shear strength from layered sectional analysis; $V_{esa,flexure}$ is the lateral force corresponding to flexural strength from equivalent rectangular stress block sectional analysis; $V_{esa,shear}$ is the shear strength from equivalent rectangular stress block sectional analysis; $V_{max,fea}$ is the peak lateral force from finite element analysis; $V_{max,esa}$ is the maximum lateral force from equivalent rectangular stress block sectional analysis, which is taken as the smaller value of $V_{esa,flexure}$ and $V_{esa,shear}$; $V_{max,lsa}$ is the maximum lateral force from layered sectional analysis, which is taken as the smaller value of $V_{lsa,flexure}$ and $V_{lsa,shear}$.

Table C-1 (a) Peak lateral force comparisons between finite element analysis results and proposed model evaluations (400×400×800 mm columns with collar spacing varied)

Collar c/c spacing (mm)	$V_{lsa,flexure}$ (kN)	$V_{lsa,shear}$ (kN)	$V_{esa,flexure}$ (kN)	$V_{esa,shear}$ (kN)	$V_{max,fea}$ (kN)	$V_{max,lsa}$ (kN)	$V_{max,esa}$ (kN)	$V_{max,fea}$ /$V_{max,lsa}$	$V_{max,fea}$ /$V_{max,esa}$
100	777	1243	818	1242	846	777	818	1.09	1.03
150	770	977	777	977	768	770	777	1.00	0.99
200	768	825	748	825	736	768	748	0.96	0.98
250	767	728	734	728	704	728 *	728	0.97	0.97
300	762	661	725	661	668	661	661	1.01	1.01
Mean								**1.00**	**1.00**
C. O. V.								**0.05**	**0.03**

* Shaded cell in the following tables indicates the peak lateral force is governed by the shear strength instead of the flexural strength

Table C-1 (b) Peak lateral force comparisons between finite element analysis results and proposed model evaluations (400×400×800 mm columns with bolt pretension varied)

Bolt pretens-ion (kN)	$V_{lsa,flexure}$ (kN)	$V_{lsa,shear}$ (kN)	$V_{esa,flexure}$ (kN)	$V_{esa,shear}$ (kN)	$V_{max,fea}$ (kN)	$V_{max,lsa}$ (kN)	$V_{max,esa}$ (kN)	$V_{max,fea}$ /$V_{max,lsa}$	$V_{max,fea}$ /$V_{max,esa}$
0	770	977	777	977	768	770	777	1.00	0.99
41	777	981	792	980	786	777	792	1.01	0.99
82	785	985	808	984	782	785	808	1.00	0.97
123	793	988	821	988	807	793	821	1.02	0.98
143	797	990	827	989	828	797	827	1.04	1.00
Mean								**1.01**	**0.99**
C. O. V.								**0.02**	**0.01**

Table C-1 (c) Peak lateral force comparisons between finite element analysis results and proposed model evaluations (400×400×800 mm columns with longitudinal reinforcement varied)

Long. reinfor. and ratio	$V_{lsa,flexure}$ (kN)	$V_{lsa,shear}$ (kN)	$V_{esa,flexure}$ (kN)	$V_{esa,shear}$ (kN)	$V_{max,fea}$ (kN)	$V_{max,lsa}$ (kN)	$V_{max,esa}$ (kN)	$V_{max,fea}$ /$V_{max,lsa}$	$V_{max,fea}$ /$V_{max,esa}$
Ten 10M-0.63%	430	585	440	977	581	430	440	1.35	1.32
Ten 15M-1.25%	516	792	525	977	697	516	525	1.35	1.33
Ten 20M-1.88%	601	873	609	977	754	601	609	1.25	1.24
Ten 25M-3.13%	770	977	777	977	768	770	777	1.00	0.99
Ten 30M-4.38%	939	1045	943	977	729	939	943	0.78	0.77
Mean								**1.15**	**1.13**
C. O. V.								**0.22**	**0.21**

Table C-1 (d) Peak lateral force comparisons between finite element analysis results and proposed model evaluations (400×400×800 mm columns with aspect ratio varied)

Aspect ratio, shear span	$V_{lsa,flexure}$ (kN)	$V_{lsa,shear}$ (kN)	$V_{esa,flexure}$ (kN)	$V_{esa,shear}$ (kN)	$V_{max,fea}$ (kN)	$V_{max,lsa}$ (kN)	$V_{max,esa}$ (kN)	$V_{max,fea}$ /$V_{max,lsa}$	$V_{max,fea}$ /$V_{max,esa}$
0.5625, 225 mm	2230	1353	2245	977	1694	1353	977	1.25	1.73
0.9375, 375 mm	1331	1166	1347	977	1096	1166	977	0.94	1.12
1.3125, 525 mm	952	925	962	977	743	925	962	0.80	0.77
1.625, 650 mm	770	977	777	977	769	770	777	1.00	0.99
1.875, 750 mm	667	930	673	977	706	667	673	1.06	1.05
Mean								**1.01**	**1.13**
C. O. V.								**0.16**	**0.32**

Table C-1 (e) Peak lateral force comparisons between finite element analysis results and proposed model evaluations (400×400×800 mm columns with collar dimension varied)

Collar (mm× mm)	$V_{lsa,flexure}$ (kN)	$V_{lsa,shear}$ (kN)	$V_{esa,flexure}$ (kN)	$V_{esa,shear}$ (kN)	$V_{max,fea}$ (kN)	$V_{max,lsa}$ (kN)	$V_{max,esa}$ (kN)	$V_{max,fea}$ /$V_{max,lsa}$	$V_{max,fea}$ /$V_{max,esa}$
20×20	763	507	728	507	666	507	507	1.31	1.31
20×30	761	598	734	598	691	598	598	1.16	1.16
20×40	762	687	741	687	707	687	687	1.03	1.03
20×50	763	774	750	774	721	763	750	0.94	0.96
20×60	765	858	761	858	727	765	761	0.95	0.96
Mean								**1.08**	**1.08**
C. O. V.								**0.15**	**0.14**

Table C-1 (f) Peak lateral force comparisons between finite element analysis results and proposed model evaluations (400×400×800 mm columns with collar dimension varied)

Collar (mm× mm)	$V_{lsa,flexure}$ (kN)	$V_{lsa,shear}$ (kN)	$V_{esa,flexure}$ (kN)	$V_{esa,shear}$ (kN)	$V_{max,fea}$ (kN)	$V_{max,lsa}$ (kN)	$V_{max,esa}$ (kN)	$V_{max,fea}$ /$V_{max,lsa}$	$V_{max,fea}$ /$V_{max,esa}$
30×20	763	598	735	598	690	598	598	1.15	1.15
30×30	767	731	746	731	727	731	731	0.99	0.99
30×40	769	858	759	857	758	769	759	0.99	1.00
30×50	770	977	777	977	768	770	777	1.00	0.99
30×60	771	1087	786	1087	812	771	786	1.05	1.03
30×70	774	1191	801	1191	825	774	801	1.07	1.03
30×80	776	1289	818	1288	836	776	818	1.08	1.02
Mean								**1.05**	**1.03**
C. O. V.								**0.05**	**0.05**

Table C-1 (g) Peak lateral force comparisons between finite element analysis results and proposed model evaluations (400×400×800 mm columns with collar dimension varied)

Collar (mm× mm)	$V_{lsa,flexure}$ (kN)	$V_{lsa,shear}$ (kN)	$V_{esa,flexure}$ (kN)	$V_{esa,shear}$ (kN)	$V_{max,fea}$ (kN)	$V_{max,lsa}$ (kN)	$V_{max,esa}$ (kN)	$V_{max,fea}$ /$V_{max,lsa}$	$V_{max,fea}$ /$V_{max,esa}$
40×20	768	688	744	688	699	688	688	1.02	1.02
40×30	770	858	759	857	760	770	759	0.99	1.00
40×40	772	1014	774	1013	820	772	774	1.06	1.06
40×50	773	1156	790	1155	851	773	790	1.10	1.08
40×60	774	1287	807	1286	866	774	807	1.12	1.07
40×70	778	1409	826	1408	874	778	826	1.12	1.06
40×80	781	1521	846	1520	884	781	846	1.13	1.04
Mean								**1.08**	**1.05**
C. O. V.								**0.04**	**0.02**

Table C-1 (h) Peak lateral force comparisons between finite element analysis results and proposed model evaluations (400×400×800 mm columns with collar dimension varied)

Collar (mm× mm)	$V_{lsa,flexure}$ (kN)	$V_{lsa,shear}$ (kN)	$V_{esa,flexure}$ (kN)	$V_{esa,shear}$ (kN)	$V_{max,fea}$ (kN)	$V_{max,lsa}$ (kN)	$V_{max,esa}$ (kN)	$V_{max,fea}$ /$V_{max,lsa}$	$V_{max,fea}$ /$V_{max,esa}$
50×20	767	774	750	774	754	767	750	0.98	1.01
50×30	770	975	768	975	791	770	768	1.03	1.03
50×40	772	1155	785	1155	844	772	785	1.09	1.07
50×50	774	1317	804	1316	862	774	804	1.11	1.07
50×60	778	1464	824	1463	898	778	824	1.15	1.09
50×70	782	1598	844	1597	871	782	844	1.11	1.03
50×80	788	1722	868	1720	880	788	868	1.12	1.01
Mean								**1.09**	**1.05**
C. O. V.								**0.05**	**0.03**

Table C-1 (i) Peak lateral force comparisons between finite element analysis results and proposed model evaluations (400×400×800 mm columns with collar dimension varied)

Collar (mm× mm)	$V_{lsa,flexure}$ (kN)	$V_{lsa,shear}$ (kN)	$V_{esa,flexure}$ (kN)	$V_{esa,shear}$ (kN)	$V_{max,fea}$ (kN)	$V_{max,lsa}$ (kN)	$V_{max,esa}$ (kN)	$V_{max,fea}$ /$V_{max,lsa}$	$V_{max,fea}$ /$V_{max,esa}$
60×20	768	857	755	857	756	768	755	0.99	1.00
60×30	774	1085	775	1084	839	774	775	1.08	1.08
60×40	771	1285	794	1284	897	771	794	1.16	1.13
60×50	780	1463	815	1461	907	780	815	1.16	1.11
60×60	783	1622	836	1620	908	783	836	1.16	1.09
60×70	787	1766	858	1764	918	787	858	1.17	1.07
60×80	794	1898	880	1896	920	794	880	1.16	1.05
Mean								**1.13**	**1.08**
C. O. V.								**0.06**	**0.04**

Table C-1 (j) Peak lateral force comparisons between finite element analysis results and proposed model evaluations (400×400×800 mm columns with collar dimension varied)

Collar (mm× mm)	$V_{lsa,flexure}$ (kN)	$V_{lsa,shear}$ (kN)	$V_{esa,flexure}$ (kN)	$V_{esa,shear}$ (kN)	$V_{max,fea}$ (kN)	$V_{max,lsa}$ (kN)	$V_{max,esa}$ (kN)	$V_{max,fea}$ /$V_{max,lsa}$	$V_{max,fea}$ /$V_{max,esa}$
70×30	773	1187	780	1187	865	773	780	1.12	1.11
70×40	776	1404	801	1403	904	776	801	1.17	1.13
70×50	780	1595	823	1594	916	780	823	1.17	1.11
70×60	786	1764	845	1763	923	786	845	1.17	1.09
70×70	792	1916	868	1915	927	792	868	1.17	1.07
70×80	799	2055	890	2053	930	799	890	1.16	1.05
Mean								**1.16**	**1.09**
C. O. V.								**0.02**	**0.02**

Table C-1 (k) Peak lateral force comparisons between finite element analysis results and proposed model evaluations (400×400×800 mm columns with collar dimension varied)

Collar (mm× mm)	$V_{lsa,flexure}$ (kN)	$V_{lsa,shear}$ (kN)	$V_{esa,flexure}$ (kN)	$V_{esa,shear}$ (kN)	$V_{max,fea}$ (kN)	$V_{max,lsa}$ (kN)	$V_{max,esa}$ (kN)	$V_{max,fea}$ /$V_{max,lsa}$	$V_{max,fea}$ /$V_{max,esa}$
80×30	776	1283	784	1282	888	776	784	1.14	1.13
80×40	779	1515	806	1514	912	779	806	1.17	1.13
80×50	784	1716	848	1715	926	784	848	1.18	1.09
80×60	789	1894	852	1892	930	789	852	1.18	1.09
80×70	796	2053	875	2051	937	796	875	1.18	1.07
80×80	804	2321	897	2321	934	804	897	1.16	1.04
Mean								**1.17**	**1.09**
C. O. V.								**0.01**	**0.03**

Table C-1 (l) Peak lateral force comparisons between finite element analysis results and proposed model evaluations (400×400×800 mm columns with concrete strength varied)

Collar, concrete (mm× mm, MPa)	$V_{lsa,flexure}$ (kN)	$V_{lsa,shear}$ (kN)	$V_{esa,flexure}$ (kN)	$V_{esa,shear}$ (kN)	$V_{max,fea}$ (kN)	$V_{max,lsa}$ (kN)	$V_{max,esa}$ (kN)	$V_{max,fea}$ /$V_{max,lsa}$	$V_{max,fea}$ /$V_{max,esa}$
20x20, 20 MPa	627	427	613	427	391	427	427	0.92	0.92
20x20, 30 MPa	730	487	700	486	596	487	486	1.22	1.22
20x20, 40 MPa	801	520	784	550	788	520	550	1.52	1.43
20x20, 50 MPa	925	619	865	619	1010	619	619	1.63	1.63
20x20, 60 MPa	1023	695	944	691	1217	695	691	1.75	1.76
Mean								**1.41**	**1.39**
C. O. V.								**0.24**	**0.24**

Table C-1 (m) Peak lateral force comparisons between finite element analysis results and proposed model evaluations (400×400×800 mm columns with concrete strength varied)

Collar, concrete (mm× mm, MPa)	$V_{lsa,flexure}$ (kN)	$V_{lsa,shear}$ (kN)	$V_{esa,flexure}$ (kN)	$V_{esa,shear}$ (kN)	$V_{max,fea}$ (kN)	$V_{max,lsa}$ (kN)	$V_{max,esa}$ (kN)	$V_{max,fea}$ /$V_{max,lsa}$	$V_{max,fea}$ /$V_{max,esa}$
30×50, 20 MPa	638	911	652	910	505	638	652	0.79	0.77
30×50, 30 MPa	736	960	743	959	713	736	743	0.97	0.96
30×50, 40 MPa	835	1010	829	1009	878	835	829	1.05	1.06
30×50, 50 MPa	926	1061	910	1061	1094	926	910	1.18	1.20
30×50, 60 MPa	1032	1115	988	1115	1286	1032	988	1.25	1.30
Mean								**1.05**	**1.06**
C. O. V.								**0.17**	**0.19**

Table C-1 (n) Peak lateral force comparisons between finite element analysis results and proposed model evaluations (400×400×800 mm columns with concrete strength varied)

Collar, concrete (mm× mm, MPa)	$V_{lsa,flexure}$ (kN)	$V_{lsa,shear}$ (kN)	$V_{esa,flexure}$ (kN)	$V_{esa,shear}$ (kN)	$V_{max,fea}$ (kN)	$V_{max,lsa}$ (kN)	$V_{max,esa}$ (kN)	$V_{max,fea}$ /$V_{max,lsa}$	$V_{max,fea}$ /$V_{max,esa}$
60×60, 20 MPa	652	1305	701	1305	556	652	701	0.85	0.79
60×60, 30 MPa	731	1604	804	1602	804	731	804	1.10	1.00
60×60, 40 MPa	847	1658	899	1657	1008	847	899	1.19	1.12
60×60, 50 MPa	941	1713	989	1712	1194	941	989	1.27	1.21
60×60, 60 MPa	1035	1769	1075	1767	1400	1035	1075	1.35	1.30
Mean								**1.15**	**1.08**
C. O. V.								**0.17**	**0.18**

Table C-1 (o) Peak lateral force comparisons between finite element analysis results and proposed model evaluations (400×400×800 mm columns with concrete strength varied)

Collar, concrete (mm× mm, MPa)	$V_{lsa,flexure}$ (kN)	$V_{lsa,shear}$ (kN)	$V_{esa,flexure}$ (kN)	$V_{esa,shear}$ (kN)	$V_{max,fea}$ (kN)	$V_{max,lsa}$ (kN)	$V_{max,esa}$ (kN)	$V_{max,fea}$ /$V_{max,lsa}$	$V_{max,fea}$ /$V_{max,esa}$
70×70, 20 MPa	661	1558	727	1558	594	661	727	0.90	0.82
70×70, 30 MPa	761	1897	835	1896	821	761	835	1.08	0.98
70×70, 40 MPa	855	1955	933	1954	1034	855	933	1.21	1.11
70×70, 50 MPa	949	2012	1016	2011	1218	949	1016	1.28	1.20
70×70, 60 MPa	1040	2072	1113	2071	1407	1040	1113	1.35	1.26
Mean								**1.16**	**1.07**
C. O. V.								**0.15**	**0.17**

Table C-1 (p) Peak lateral force comparisons between finite element analysis results and proposed model evaluations (400×400×800 mm columns with concrete strength varied)

Collar, concrete (mm× mm, MPa)	$V_{lsa,flexure}$ (kN)	$V_{lsa,shear}$ (kN)	$V_{esa,flexure}$ (kN)	$V_{esa,shear}$ (kN)	$V_{max,fea}$ (kN)	$V_{max,lsa}$ (kN)	$V_{max,esa}$ (kN)	$V_{max,fea}$ /$V_{max,lsa}$	$V_{max,fea}$ /$V_{max,esa}$
80×80, 20 MPa	675	1843	745	1843	618	675	745	0.92	0.83
80×80, 30 MPa	773	2318	863	2318	838	773	863	1.08	0.97
80×80, 40 MPa	869	2328	964	2328	1044	869	964	1.20	1.08
80×80, 50 MPa	960	2336	1057	2336	1247	960	1057	1.30	1.18
80×80, 60 MPa	1051	2343	1146	2343	1440	1051	1146	1.37	1.26
Mean								**1.17**	**1.06**
C. O. V.								**0.15**	**0.16**

Table C-1 (q) Peak lateral force comparisons between finite element analysis results and proposed model evaluations (400×400×800 mm columns with axial compression varied)

Collar, axial compression index (mm×mm)	$V_{lsa,flexure}$ (kN)	$V_{lsa,shear}$ (kN)	$V_{esa,flexure}$ (kN)	$V_{esa,shear}$ (kN)	$V_{max,fea}$ (kN)	$V_{max,lsa}$ (kN)	$V_{max,esa}$ (kN)	$V_{max,fea}$ /$V_{max,lsa}$	$V_{max,fea}$ /$V_{max,esa}$
20×20, 0.0	540	393	532	393	487	393	393	1.24	1.24
20×20, 0.1	655	426	634	425	543	426	425	1.28	1.28
20×20, 0.2	722	463	688	463	608	463	463	1.31	1.31
20×20, 0.3	763	507	728	507	671	507	507	1.32	1.32
20×20, 0.4	793	601	736	559	710	601	559	1.18	1.27
20×20, 0.5	755	607	686	599	787	607	599	1.30	1.31
20×20, 0.6	710	633	632	599	823	633	599	1.30	1.37
20×20, 0.7	661	599	570	599	838	599	570	1.40	1.47
Mean								**1.29**	**1.32**
C. O. V.								**0.05**	**0.05**

Table C-1 (r) Peak lateral force comparisons between finite element analysis results and proposed model evaluations (400×400×800 mm columns with axial compression varied)

Collar, axial compression index (mm×mm)	$V_{lsa,flexure}$ (kN)	$V_{lsa,shear}$ (kN)	$V_{esa,flexure}$ (kN)	$V_{esa,shear}$ (kN)	$V_{max,fea}$ (kN)	$V_{max,lsa}$ (kN)	$V_{max,esa}$ (kN)	$V_{max,fea}$ /$V_{max,lsa}$	$V_{max,fea}$ /$V_{max,esa}$
30×50, 0.0	541	856	540	855	597	541	540	1.11	1.11
30×50, 0.1	657	894	648	894	641	657	648	0.98	0.99
30×50, 0.2	729	935	724	934	701	729	724	0.96	0.97
30×50, 0.3	769	977	777	977	768	769	777	1.00	0.99
30×50, 0.4	802	947	810	1022	827	802	810	1.03	1.02
30×50, 0.5	770	1003	808	1070	904	770	808	1.17	1.12
30×50, 0.6	709	1087	764	1062	942	709	764	1.33	1.23
30×50, 0.7	680	893	716	892	967	680	716	1.42	1.35
Mean								**1.12**	**1.10**
C. O. V.								**0.14**	**0.11**

Table C-1 (s) Peak lateral force comparisons between finite element analysis results and proposed model evaluations (400×400×800 mm columns with axial compression varied)

Collar, axial compression index (mm×mm)	$V_{lsa,flexure}$ (kN)	$V_{lsa,shear}$ (kN)	$V_{esa,flexure}$ (kN)	$V_{esa,shear}$ (kN)	$V_{max,fea}$ (kN)	$V_{max,lsa}$ (kN)	$V_{max,esa}$ (kN)	$V_{max,fea}$ /$V_{max,lsa}$	$V_{max,fea}$ /$V_{max,esa}$
60×60, 0.0	543	1466	553	1464	665	543	553	1.22	1.20
60×60, 0.1	660	1517	667	1515	715	660	667	1.08	1.07
60×60, 0.2	738	1569	769	1567	801	738	769	1.09	1.04
60×60, 0.3	783	1622	836	1620	907	783	836	1.16	1.09
60×60, 0.4	820	1676	893	1675	979	820	893	1.19	1.10
60×60, 0.5	801	1330	932	1730	1069	801	932	1.33	1.15
60×60, 0.6	724	1788	951	1787	1114	724	951	1.54	1.17
60×60, 0.7	719	1846	919	1845	1161	719	919	1.61	1.26
Mean								**1.28**	**1.14**
C. O. V.								**0.14**	**0.06**

Table C-1 (t) Peak lateral force comparisons between finite element analysis results and proposed model evaluations (400×400×800 mm columns with axial compression varied)

Collar, axial compression index (mm×mm)	$V_{lsa,flexure}$ (kN)	$V_{lsa,shear}$ (kN)	$V_{esa,flexure}$ (kN)	$V_{esa,shear}$ (kN)	$V_{max,fea}$ (kN)	$V_{max,lsa}$ (kN)	$V_{max,esa}$ (kN)	$V_{max,fea}$ /$V_{max,lsa}$	$V_{max,fea}$ /$V_{max,esa}$
70×70, 0.0	544	1791	560	1791	673	544	560	1.24	1.20
70×70, 0.1	662	1801	677	1799	737	662	677	1.11	1.09
70×70, 0.2	743	1858	785	1857	819	743	785	1.10	1.04
70×70, 0.3	790	1917	869	1915	926	790	869	1.17	1.07
70×70, 0.4	828	1976	931	1974	1023	828	931	1.23	1.10
70×70, 0.5	816	1791	984	2034	1096	816	984	1.34	1.11
70×70, 0.6	779	1915	1023	2095	1156	779	1023	1.48	1.13
70×70, 0.7	739	2085	1030	2157	1214	739	1030	1.64	1.18
Mean								**1.29**	**1.12**
C. O. V.								**0.13**	**0.04**

Table C-1 (u) Peak lateral force comparisons between finite element analysis results and proposed model evaluations (400×400×800 mm columns with axial compression varied)

Collar, axial compression index (mm×mm)	$V_{lsa,flexure}$ (kN)	$V_{lsa,shear}$ (kN)	$V_{esa,flexure}$ (kN)	$V_{esa,shear}$ (kN)	$V_{max,fea}$ (kN)	$V_{max,lsa}$ (kN)	$V_{max,esa}$ (kN)	$V_{max,fea}/V_{max,lsa}$	$V_{max,fea}/V_{max,esa}$
80×80, 0.0	546	2322	567	2322	688	546	567	1.26	1.21
80×80, 0.1	665	2322	687	2322	769	665	687	1.16	1.12
80×80, 0.2	755	2322	799	2322	831	755	799	1.10	1.04
80×80, 0.3	804	2322	899	2322	936	804	899	1.16	1.04
80×80, 0.4	847	2322	966	2322	1038	847	966	1.23	1.07
80×80, 0.5	853	2322	1029	2322	1111	853	1029	1.30	1.08
80×80, 0.6	819	2322	1079	2322	1183	819	1079	1.44	1.10
80×80, 0.7	782	2775	1118	2322	1230	782	1118	1.57	1.10
Mean								**1.28**	**1.10**
C. O. V.								**0.11**	**0.05**

Table C-2 (a) Peak lateral force comparisons between finite element analysis results and proposed model evaluations (600×600×1225 mm columns with collar spacing varied)

Collar c/c spacing (mm)	$V_{lsa,flexure}$ (kN)	$V_{lsa,shear}$ (kN)	$V_{esa,flexure}$ (kN)	$V_{esa,shear}$ (kN)	$V_{max,fea}$ (kN)	$V_{max,lsa}$ (kN)	$V_{max,esa}$ (kN)	$V_{max,fea}/V_{max,lsa}$	$V_{max,fea}/V_{max,esa}$
100	1092	1793	1130	1792	1466	1092	1130	1.34	1.30
150	1089	1478	1070	1477	1457	1089	1070	1.34	1.36
200	1090	1298	1045	1297	1434	1090	1045	1.32	1.37
250	1084	1183	1031	1182	1454	1084	1031	1.34	1.41
300	1084	1105	1023	1104	1412	1084	1023	1.30	1.38
Mean								**1.33**	**1.36**
C. O. V.								**0.01**	**0.03**

Table C-2 (b) Peak lateral force comparisons between finite element analysis results and proposed model evaluations (600×600×1225 mm columns with bolt pretension varied)

Bolt pretens -ion (kN)	$V_{lsa,flexure}$ (kN)	$V_{lsa,shear}$ (kN)	$V_{esa,flexure}$ (kN)	$V_{esa,shear}$ (kN)	$V_{max,fea}$ (kN)	$V_{max,lsa}$ (kN)	$V_{max,esa}$ (kN)	$V_{max,fea}$ /$V_{max,lsa}$	$V_{max,fea}$ /$V_{max,esa}$
0	1089	1478	1070	1477	1457	1089	1070	1.34	1.36
41	1102	1485	1107	1484	1466	1102	1107	1.33	1.32
82	1114	1491	1139	1490	1485	1114	1139	1.33	1.30
123	1126	1496	1164	1496	1494	1126	1164	1.33	1.28
143	1129	1499	1175	1498	1498	1129	1175	1.33	1.27
Mean								**1.33**	**1.31**
C. O. V.								**0.00**	**0.03**

Table C-2 (c) Peak lateral force comparisons between finite element analysis results and proposed model evaluations (600×600×1225 mm columns with longitudinal reinforcement varied)

Long. reinfor. and ratio	$V_{lsa,flexure}$ (kN)	$V_{lsa,shear}$ (kN)	$V_{esa,flexure}$ (kN)	$V_{esa,shear}$ (kN)	$V_{max,fea}$ (kN)	$V_{max,lsa}$ (kN)	$V_{max,esa}$ (kN)	$V_{max,fea}$ /$V_{max,lsa}$	$V_{max,fea}$ /$V_{max,esa}$
Ten 15M-0.56%	842	1771	829	1477	1116	842	829	1.33	1.35
Ten 25M-1.39%	1088	1486	1070	1477	1227	1088	1070	1.13	1.15
Ten 30M-1.89%	1250	1594	1229	1477	1310	1250	1229	1.05	1.07
Ten 35M-2.78%	1493	1710	1466	1477	1457	1493	1466	0.98	0.99
Ten 45M-4.17%	1896	1841	1857	1477	1528	1841	1477	0.83	1.03
Mean								**1.06**	**1.12**
C. O. V.								**0.17**	**0.12**

Table C-2 (d) Peak lateral force comparisons between finite element analysis results and proposed model evaluations (600×600×1225 mm columns with aspect ratio varied)

Aspect ratio, shear span	$V_{lsa,flexure}$ (kN)	$V_{lsa,shear}$ (kN)	$V_{esa,flexure}$ (kN)	$V_{esa,shear}$ (kN)	$V_{max,fea}$ (kN)	$V_{max,lsa}$ (kN)	$V_{max,esa}$ (kN)	$V_{max,fea}$ /$V_{max,lsa}$	$V_{max,fea}$ /$V_{max,esa}$
0.8333, 500 mm	2393	2119	2354	2103	2104	2119	2103	0.99	1.00
1.0833, 650 mm	1841	1882	1811	1869	2048	1841	1811	1.11	1.13
1.3333, 800 mm	1496	1421	1471	1705	1760	1421	1471	1.24	1.20
1.5333, 950 mm	1259	1588	1239	1578	1581	1259	1239	1.26	1.28
1.8333, 1100 m m	1088	1486	1070	1477	1457	1088	1070	1.34	1.36
Mean								**1.19**	**1.19**
C. O. V.								**0.11**	**0.12**

Table C-2 (e) Peak lateral force comparisons between finite element analysis results and proposed model evaluations (600×600×1225 mm columns with collar dimension varied)

Collar (mm× mm)	$V_{lsa,flexure}$ (kN)	$V_{lsa,shear}$ (kN)	$V_{esa,flexure}$ (kN)	$V_{esa,shear}$ (kN)	$V_{max,fea}$ (kN)	$V_{max,lsa}$ (kN)	$V_{max,esa}$ (kN)	$V_{max,fea}$ /$V_{max,lsa}$	$V_{max,fea}$ /$V_{max,esa}$
20×20	1081	1156	1023	1156	1393	1081	1023	1.29	1.36
20×30	1083	1395	1030	1395	1410	1083	1030	1.30	1.37
20×40	1085	1133	1034	1133	1421	1085	1034	1.31	1.37
20×50	1085	1236	1043	1235	1428	1085	1043	1.32	1.37
20×60	1086	1336	1054	1335	1430	1086	1054	1.32	1.36
Mean								**1.31**	**1.37**
C. O. V.								**0.01**	**0.01**

Table C-2 (f) Peak lateral force comparisons between finite element analysis results and proposed model evaluations (600×600×1225 mm columns with collar dimension varied)

Collar (mm× mm)	$V_{lsa,flexure}$ (kN)	$V_{lsa,shear}$ (kN)	$V_{esa,flexure}$ (kN)	$V_{esa,shear}$ (kN)	$V_{max,fea}$ (kN)	$V_{max,lsa}$ (kN)	$V_{max,esa}$ (kN)	$V_{max,fea}$ /$V_{max,lsa}$	$V_{max,fea}$ /$V_{max,esa}$
30×20	1088	1395	1029	1394	1406	1088	1029	1.29	1.37
30×30	1087	1185	1041	1185	1424	1087	1041	1.31	1.37
30×40	1085	1336	1054	1335	1448	1085	1054	1.33	1.37
30×50	1089	1478	1070	1477	1457	1089	1070	1.34	1.36
30×60	1088	1610	1087	1609	1457	1088	1087	1.34	1.34
30×70	1092	1733	1109	1732	1464	1092	1109	1.34	1.32
30×80	1096	1848	1132	1847	1473	1096	1132	1.34	1.30
Mean								**1.33**	**1.35**
C. O. V.								**0.01**	**0.02**

Table C-2 (g) Peak lateral force comparisons between finite element analysis results and proposed model evaluations (600×600×1225 mm columns with collar dimension varied)

Collar (mm× mm)	$V_{lsa,flexure}$ (kN)	$V_{lsa,shear}$ (kN)	$V_{esa,flexure}$ (kN)	$V_{esa,shear}$ (kN)	$V_{max,fea}$ (kN)	$V_{max,lsa}$ (kN)	$V_{max,esa}$ (kN)	$V_{max,fea}$ /$V_{max,lsa}$	$V_{max,fea}$ /$V_{max,esa}$
40×20	1088	1134	1040	1134	1418	1088	1040	1.30	1.36
40×30	1093	1337	1057	1336	1440	1093	1057	1.32	1.36
40×40	1094	1523	1077	1523	1455	1094	1077	1.33	1.35
40×50	1097	1693	1100	1692	1470	1097	1100	1.34	1.34
40×60	1093	1847	1125	1846	1484	1093	1125	1.36	1.32
40×70	1103	1988	1152	1976	1496	1103	1152	1.36	1.30
40×80	1102	2358	1181	1896	1506	1102	1181	1.37	1.27
Mean								**1.34**	**1.33**
C. O. V.								**0.02**	**0.02**

Table C-2 (h) Peak lateral force comparisons between finite element analysis results and proposed model evaluations (600×600×1225 mm columns with collar dimension varied)

Collar (mm× mm)	$V_{lsa,flexure}$ (kN)	$V_{lsa,shear}$ (kN)	$V_{esa,flexure}$ (kN)	$V_{esa,shear}$ (kN)	$V_{max,fea}$ (kN)	$V_{max,lsa}$ (kN)	$V_{max,esa}$ (kN)	$V_{max,fea}$ /$V_{max,lsa}$	$V_{max,fea}$ /$V_{max,esa}$
50×20	1088	1238	1051	1237	1439	1088	1051	1.32	1.37
50×30	1095	1479	1076	1478	1443	1095	1076	1.32	1.34
50×40	1096	1694	1102	1692	1481	1096	1102	1.35	1.34
50×50	1097	1884	1131	1882	1499	1097	1131	1.37	1.33
50×60	1102	2346	1160	1877	1516	1102	1160	1.38	1.31
50×70	1103	2364	1191	2061	1536	1103	1191	1.39	1.29
50×80	1107	2346	1223	2341	1551	1107	1223	1.40	1.27
Mean								**1.36**	**1.32**
C. O. V.								**0.02**	**0.03**

Table C-2 (i) Peak lateral force comparisons between finite element analysis results and proposed model evaluations (600×600×1225 mm columns with collar dimension varied)

Collar (mm× mm)	$V_{lsa,flexure}$ (kN)	$V_{lsa,shear}$ (kN)	$V_{esa,flexure}$ (kN)	$V_{esa,shear}$ (kN)	$V_{max,fea}$ (kN)	$V_{max,lsa}$ (kN)	$V_{max,esa}$ (kN)	$V_{max,fea}$ /$V_{max,lsa}$	$V_{max,fea}$ /$V_{max,esa}$
60×20	1089	1338	1064	1337	1433	1089	1064	1.32	1.35
60×30	1095	1611	1094	1610	1459	1095	1094	1.33	1.33
60×40	1098	1848	1126	1846	1508	1098	1126	1.37	1.34
60×50	1102	1782	1158	1833	1528	1102	1158	1.39	1.32
60×60	1104	2364	1190	2115	1636	1104	1190	1.48	1.37
60×70	1107	2450	1223	2449	1558	1107	1223	1.41	1.27
60×80	1114	2785	1247	2785	1566	1114	1247	1.41	1.26
Mean								**1.39**	**1.32**
C. O. V.								**0.04**	**0.03**

Table C-2 (j) Peak lateral force comparisons between finite element analysis results and proposed model evaluations (600×600×1225 mm columns with collar dimension varied)

Collar (mm× mm)	$V_{lsa,flexure}$ (kN)	$V_{lsa,shear}$ (kN)	$V_{esa,flexure}$ (kN)	$V_{esa,shear}$ (kN)	$V_{max,fea}$ (kN)	$V_{max,lsa}$ (kN)	$V_{max,esa}$ (kN)	$V_{max,fea}$ /$V_{max,lsa}$	$V_{max,fea}$ /$V_{max,esa}$
70×30	1100	1734	1112	1733	1489	1100	1112	1.35	1.34
70×40	1099	1987	1146	1968	1536	1099	1146	1.40	1.34
70×50	1102	2364	1180	2058	1553	1102	1180	1.41	1.32
70×60	1107	2447	1215	2447	1561	1107	1215	1.41	1.28
70×70	1112	2837	1242	2837	1569	1112	1242	1.41	1.26
70×80	1120	3228	1264	3228	1580	1120	1264	1.41	1.25
Mean								**1.40**	**1.30**
C. O. V.								**0.02**	**0.03**

Table C-2 (k) Peak lateral force comparisons between finite element analysis results and proposed model evaluations (600×600×1225 mm columns with collar dimension varied)

Collar (mm× mm)	$V_{lsa,flexure}$ (kN)	$V_{lsa,shear}$ (kN)	$V_{esa,flexure}$ (kN)	$V_{esa,shear}$ (kN)	$V_{max,fea}$ (kN)	$V_{max,lsa}$ (kN)	$V_{max,esa}$ (kN)	$V_{max,fea}$ /$V_{max,lsa}$	$V_{max,fea}$ /$V_{max,esa}$
80×30	1100	1847	1126	1846	1512	1100	1126	1.38	1.34
80×40	1101	1891	1162	1891	1547	1101	1162	1.40	1.33
80×50	1106	2335	1199	2335	1565	1106	1199	1.42	1.30
80×60	1112	2779	1233	2779	1570	1112	1233	1.41	1.27
80×70	1121	3223	1255	3223	1578	1121	1255	1.41	1.26
80×80	1127	3670	1278	3670	1578	1127	1278	1.40	1.24
Mean								**1.40**	**1.29**
C. O. V.								**0.01**	**0.03**

Table C-2 (l) Peak lateral force comparisons between finite element analysis results and proposed model evaluations (600×600×1225 mm columns with concrete strength varied)

Collar, concrete (mm× mm, MPa)	$V_{lsa,flexure}$ (kN)	$V_{lsa,shear}$ (kN)	$V_{esa,flexure}$ (kN)	$V_{esa,shear}$ (kN)	$V_{max,fea}$ (kN)	$V_{max,lsa}$ (kN)	$V_{max,esa}$ (kN)	$V_{max,fea}$ /$V_{max,lsa}$	$V_{max,fea}$ /$V_{max,esa}$
20x20, 20 MPa	815	724	791	724	880	724	724	1.22	1.22
20x20, 30 MPa	1018	1122	966	677	1267	1018	677	1.24	1.87
20x20, 40 MPa	1215	1219	1138	830	1599	1215	830	1.32	1.93
20x20, 50 MPa	1408	1305	1305	1071	1893	1305	1071	1.45	1.77
20x20, 60 MPa	1607	1382	1466	1382	2178	1382	1382	1.58	1.58
Mean								**1.36**	**1.67**
C. O. V.								**0.11**	**0.17**

Table C-2 (m) Peak lateral force comparisons between finite element analysis results and proposed model evaluations (600×600×1225 mm columns with concrete strength varied)

Collar, concrete (mm× mm, MPa)	$V_{lsa,flexure}$ (kN)	$V_{lsa,shear}$ (kN)	$V_{esa,flexure}$ (kN)	$V_{esa,shear}$ (kN)	$V_{max,fea}$ (kN)	$V_{max,lsa}$ (kN)	$V_{max,esa}$ (kN)	$V_{max,fea}$ /$V_{max,lsa}$	$V_{max,fea}$ /$V_{max,esa}$
30×50, 20 MPa	823	1179	837	1315	960	823	837	1.17	1.15
30×50, 30 MPa	1024	1437	1013	1436	1310	1024	1013	1.28	1.29
30×50, 40 MPa	1220	2528	1184	1563	1641	1220	1184	1.35	1.39
30×50, 50 MPa	1410	2627	1350	1030	1943	1410	1030	1.38	1.89
30×50, 60 MPa	1617	2702	1511	1133	2239	1617	1133	1.38	1.98
Mean								**1.31**	**1.54**
C. O. V.								**0.07**	**0.24**

Table C-2 (n) Peak lateral force comparisons between finite element analysis results and proposed model evaluations (600×600×1225 mm columns with concrete strength varied)

Collar, concrete (mm× mm, MPa)	$V_{lsa,flexure}$ (kN)	$V_{lsa,shear}$ (kN)	$V_{esa,flexure}$ (kN)	$V_{esa,shear}$ (kN)	$V_{max,fea}$ (kN)	$V_{max,lsa}$ (kN)	$V_{max,esa}$ (kN)	$V_{max,fea}$ /$V_{max,lsa}$	$V_{max,fea}$ /$V_{max,esa}$
60×60, 20 MPa	842	2089	931	2089	1116	842	931	1.33	1.20
60×60, 30 MPa	1039	2109	1128	2109	1418	1039	1128	1.37	1.26
60×60, 40 MPa	1235	2554	1310	2126	1713	1235	1310	1.39	1.31
60×60, 50 MPa	1429	2875	1484	2141	2008	1429	1484	1.41	1.35
60×60, 60 MPa	1622	3252	1653	2154	2347	1622	1653	1.45	1.42
Mean								**1.39**	**1.31**
C. O. V.								**0.03**	**0.06**

Table C-2 (o) Peak lateral force comparisons between finite element analysis results and proposed model evaluations (600×600×1225 mm columns with concrete strength varied)

Collar, concrete (mm× mm, MPa)	$V_{lsa,flexure}$ (kN)	$V_{lsa,shear}$ (kN)	$V_{esa,flexure}$ (kN)	$V_{esa,shear}$ (kN)	$V_{max,fea}$ (kN)	$V_{max,lsa}$ (kN)	$V_{max,esa}$ (kN)	$V_{max,fea}$ /$V_{max,lsa}$	$V_{max,fea}$ /$V_{max,esa}$
70×70, 20 MPa	855	2809	956	2809	1153	855	956	1.35	1.21
70×70, 30 MPa	1049	2831	1173	2831	1450	1049	1173	1.38	1.24
70×70, 40 MPa	1243	2849	1373	2849	1739	1243	1373	1.40	1.27
70×70, 50 MPa	1433	2864	1553	2864	2051	1433	1553	1.43	1.32
70×70, 60 MPa	1623	3027	1726	2877	2375	1623	1726	1.46	1.38
Mean								**1.41**	**1.28**
C. O. V.								**0.03**	**0.05**

Table C-2 (p) Peak lateral force comparisons between finite element analysis results and proposed model evaluations (600×600×1225 mm columns with concrete strength varied)

Collar, concrete (mm× mm, MPa)	$V_{lsa,flexure}$ (kN)	$V_{lsa,shear}$ (kN)	$V_{esa,flexure}$ (kN)	$V_{esa,shear}$ (kN)	$V_{max,fea}$ (kN)	$V_{max,lsa}$ (kN)	$V_{max,esa}$ (kN)	$V_{max,fea}$ /$V_{max,lsa}$	$V_{max,fea}$ /$V_{max,esa}$
80×80, 20 MPa	868	3639	977	3638	1166	868	977	1.34	1.19
80×80, 30 MPa	1065	3663	1205	3663	1463	1065	1205	1.37	1.21
80×80, 40 MPa	1256	3681	1420	3681	1755	1256	1420	1.40	1.24
80×80, 50 MPa	1443	3698	1617	3698	2078	1443	1617	1.44	1.29
80×80, 60 MPa	1632	3712	1795	3712	2398	1632	1795	1.47	1.34
Mean								**1.40**	**1.25**
C. O. V.								**0.04**	**0.05**

Table C-2 (q) Peak lateral force comparisons between finite element analysis results and proposed model evaluations (600×600×1225 mm columns with axial compression varied)

Collar, axial compression index (mm×mm)	$V_{lsa,flexure}$ (kN)	$V_{lsa,shear}$ (kN)	$V_{esa,flexure}$ (kN)	$V_{esa,shear}$ (kN)	$V_{max,fea}$ (kN)	$V_{max,lsa}$ (kN)	$V_{max,esa}$ (kN)	$V_{max,fea}$ /$V_{max,lsa}$	$V_{max,fea}$ /$V_{max,esa}$
20×20, 0.0	525	598	521	594	650	525	521	1.24	1.25
20×20, 0.1	781	687	761	684	963	687	684	1.40	1.41
20×20, 0.2	975	797	935	794	1214	797	794	1.52	1.53
20×20, 0.3	1082	1164	1021	722	1395	1082	722	1.29	1.93
20×20, 0.4	1152	1164	1057	982	1540	1152	982	1.34	1.57
20×20, 0.5	1116	1164	978	1154	1626	1116	978	1.46	1.66
20×20, 0.6	1044	1164	872	1154	1671	1044	872	1.60	1.92
20×20, 0.7	942	1164	728	1154	1654	942	728	1.76	2.27
Mean								**1.45**	**1.69**
C. O. V.								**0.11**	**0.18**

Table C-2 (r) Peak lateral force comparisons between finite element analysis results and proposed model evaluations (600×600×1225 mm columns with axial compression varied)

Collar, axial compression index (mm×mm)	$V_{lsa,flexure}$ (kN)	$V_{lsa,shear}$ (kN)	$V_{esa,flexure}$ (kN)	$V_{esa,shear}$ (kN)	$V_{max,fea}$ (kN)	$V_{max,lsa}$ (kN)	$V_{max,esa}$ (kN)	$V_{max,fea}$ /$V_{max,lsa}$	$V_{max,fea}$ /$V_{max,esa}$
30×50, 0.0	526	1159	525	1152	733	526	525	1.39	1.40
30×50, 0.1	782	1260	770	1253	983	782	770	1.26	1.28
30×50, 0.2	979	1369	969	1361	1243	979	969	1.27	1.28
30×50, 0.3	1088	1486	1070	1477	1457	1088	1070	1.34	1.36
30×50, 0.4	1161	2527	1132	1007	1616	1161	1007	1.39	1.61
30×50, 0.5	1131	2527	1102	949	1751	1131	949	1.55	1.85
30×50, 0.6	1062	2527	1019	1048	1854	1062	1019	1.75	1.82
30×50, 0.7	965	2527	905	1280	1888	965	905	1.96	2.09
Mean								**1.49**	**1.58**
C. O. V.								**0.15**	**0.17**

Table C-2 (s) Peak lateral force comparisons between finite element analysis results and proposed model evaluations (600×600×1225 mm columns with axial compression varied)

Collar, axial compression index (mm×mm)	$V_{lsa,flexure}$ (kN)	$V_{lsa,shear}$ (kN)	$V_{esa,flexure}$ (kN)	$V_{esa,shear}$ (kN)	$V_{max,fea}$ (kN)	$V_{max,lsa}$ (kN)	$V_{max,esa}$ (kN)	$V_{max,fea}$ /$V_{max,lsa}$	$V_{max,fea}$ /$V_{max,esa}$
60×60, 0.0	527	2125	535	2114	704	527	535	1.34	1.32
60×60, 0.1	785	2125	791	2114	1009	785	791	1.29	1.28
60×60, 0.2	990	2125	1016	2114	1304	990	1016	1.32	1.28
60×60, 0.3	1104	2364	1187	2114	1547	1104	1187	1.40	1.30
60×60, 0.4	1186	2125	1294	2114	1783	1186	1294	1.50	1.38
60×60, 0.5	1172	2517	1370	2114	1916	1172	1370	1.64	1.40
60×60, 0.6	1112	3068	1384	2114	2025	1112	1384	1.82	1.46
60×60, 0.7	1026	3816	1331	2114	2116	1026	1331	2.06	1.59
Mean								**1.55**	**1.38**
C. O. V.								**0.16**	**0.07**

Table C-2 (t) Peak lateral force comparisons between finite element analysis results and proposed model evaluations (600×600×1225 mm columns with axial compression varied)

Collar, axial compression index (mm×mm)	$V_{lsa,flexure}$ (kN)	$V_{lsa,shear}$ (kN)	$V_{esa,flexure}$ (kN)	$V_{esa,shear}$ (kN)	$V_{max,fea}$ (kN)	$V_{max,lsa}$ (kN)	$V_{max,esa}$ (kN)	$V_{max,fea}$ /$V_{max,lsa}$	$V_{max,fea}$ /$V_{max,esa}$
70×70, 0.0	528	2848	541	2837	710	528	541	1.34	1.31
70×70, 0.1	786	2848	802	2837	1015	786	802	1.29	1.26
70×70, 0.2	995	2848	1039	2837	1317	995	1039	1.32	1.27
70×70, 0.3	1115	2848	1242	2837	1569	1115	1242	1.41	1.26
70×70, 0.4	1201	2848	1377	2837	1830	1201	1377	1.52	1.33
70×70, 0.5	1198	2848	1480	2837	2037	1198	1480	1.70	1.38
70×70, 0.6	1144	2848	1554	2837	2204	1144	1554	1.93	1.42
70×70, 0.7	1065	2931	1561	2837	2364	1065	1561	2.22	1.51
Mean								**1.59**	**1.34**
C. O. V.								**0.19**	**0.06**

Table C-2 (u) Peak lateral force comparisons between finite element analysis results and proposed model evaluations (600×600×1225 mm columns with axial compression varied)

Collar, axial compression index (mm×mm)	$V_{lsa,flexure}$ (kN)	$V_{lsa,shear}$ (kN)	$V_{esa,flexure}$ (kN)	$V_{esa,shear}$ (kN)	$V_{max,fea}$ (kN)	$V_{max,lsa}$ (kN)	$V_{max,esa}$ (kN)	$V_{max,fea}$ /$V_{max,lsa}$	$V_{max,fea}$ /$V_{max,esa}$
80×80, 0.0	529	3680	547	3668	705	529	547	1.33	1.29
80×80, 0.1	788	3680	812	3668	1021	788	812	1.30	1.26
80×80, 0.2	1001	3680	1058	3668	1322	1001	1058	1.32	1.25
80×80, 0.3	1126	3680	1275	3668	1580	1126	1275	1.40	1.24
80×80, 0.4	1218	3680	1443	3668	1855	1218	1443	1.52	1.29
80×80, 0.5	1227	3680	1568	3668	2078	1227	1568	1.69	1.33
80×80, 0.6	1178	3680	1668	3668	2292	1178	1668	1.94	1.37
80×80, 0.7	1107	3680	1740	3668	2504	1107	1740	2.26	1.44
Mean								**1.60**	**1.31**
C. O. V.								**0.20**	**0.05**